INTERNATIONAL MARITIME ORGANIZATION

4 ALBERT EMBANKMENT
LONDON SE1 7SR
Telephone: +44 (0)20 7735 7611 Fax: +44 (0)20 7587 3210

E

MSC.1/Circ.1652
26 April 2023

EXPLANATORY NOTES TO THE INTERIM GUIDELINES ON THE SECOND GENERATION INTACT STABILITY CRITERIA

1 The Maritime Safety Committee, at its 102nd session (4 to 11 November 2020) approved the *Interim guidelines on the second generation intact stability criteria* (MSC.1/Circ.1627) (Interim Guidelines). In approving the Interim Guidelines, the Committee recognized the necessity of developing associated explanatory notes to ensure uniform interpretation and application.

2 To this end, the Committee, at its 105th session (20 to 29 April 2022), approved the *Explanatory notes to the Interim guidelines on second generation intact stability criteria* (Explanatory Notes), set out in the annex, as prepared by the Sub-Committee on Ship Design and Construction, at its eighth session (17 to 21 January 2022).

3 The Explanatory Notes are intended to provide Administrations and the shipping industry with specific guidance to assist in the uniform interpretation and application of the Interim Guidelines.

4 Member Governments are invited to bring the annexed Explanatory Notes to the attention of all parties concerned, in particular shipbuilders, shipmasters, shipowners, ship operators and shipping companies, and recount their experience gained through their use to the Organization.

***

ANNEX

EXPLANATORY NOTES TO THE INTERIM GUIDELINES ON THE SECOND GENERATION INTACT STABILITY CRITERIA

CONTENTS

Appendix 5 Theoretical background, validation, and application examples to guidelines on operational measures

1 Background information
- 1.1 Ships and loading conditions used in background studies
- 1.2 Preparation of operational measures
- 1.3 Preparation of operational guidance in design phase
- 1.4 Probabilistic operational guidance
- 1.5 Deterministic operational guidance
- 1.6 Definition of thresholds
- 1.7 Simplified operational guidance
- 1.8 When operational measures are not suitable
- 1.9 Influence of propulsion, steering and seakeeping

2 Application examples
- 2.1 Operational guidance based on DSA for parametric and synchronous roll
- 2.2 Operational guidance for parametric roll
- 2.3 DSA-based operational limitations related to areas or routes and season
- 2.4 DSA-based operational limitations related to maximum significant wave height
- 2.5 Simplified operational guidance for surf-riding/broaching failure mode
- 2.6 Simplified operational guidance from level 2 vulnerability assessment for parametric roll
- 2.7 Level 2-based operational limitations related to maximum wave height

3 Wave cases for preparation of operational limitations using level 1 and level 2 vulnerability assessment

4 Supplementing information on preparation of simplified operational guidance for surf-riding/broaching failure mode

Appendix 6 Application examples of treatment of loading conditions

- 1.1 Cruise ship
- 1.2 1,700 TEU container ship

PART A

INTRODUCTION TO THE EXPLANATORY NOTES TO THE INTERIM GUIDELINES ON THE SECOND GENERATION INTACT STABILITY CRITERIA (MSC.1/CIRC.1627)

1 The Maritime Safety Committee (MSC), at its 102nd session (4 to 11 November 2020), approved the *Interim guidelines on the second generation intact stability criteria* (MSC.1/Circ.1627), hereinafter referred to as "Interim Guidelines". These Explanatory Notes to the Interim Guidelines are intended as a support in the application of the Interim Guidelines by providing further clarifications and explanations to the elements therein.

2 These Explanatory Notes should be consulted for an improved understanding and uniform application of the Interim Guidelines. The paragraph numbers used in part B directly correspond to the numbering in the Interim Guidelines.

3 Because the approach taken in the Interim Guidelines is new for many Administrations and the industry, these Explanatory Notes have been developed to assist the users. Some of the concepts employed in the Interim Guidelines are relatively easy to grasp, others may require more consideration, explanation and in-depth discussion. In view of this, the structure of the Explanatory Notes follows that of the Interim Guidelines and provides comments and explanations for those paragraphs of the Interim Guidelines that have been identified as most benefiting from additional discussion, clarification or explanation.

4 The appendices provide additional information that is pertinent to the Interim Guidelines. Beginning with the description of the stability failure modes addressed by the Interim Guidelines in appendix 1, examples are provided of how the Interim Guidelines may be applied and the process by which assessments of ship's vulnerability are made in appendix 2. Appendix 3 is devoted to providing detailed explanation of the process by which certain elements that are essential to proper assessment of the vulnerability criteria are performed and the considerations that the user should take into account when performing the calculations associated with those elements.

5 Because of their complexity and the considerations that should be employed in performing a direct stability assessment, appendix 4 is devoted to this subject. This appendix provides the background of direct stability assessment, gives detailed description of the validation of the computer software to be used for direct stability assessment, and presents examples of the application of direct stability assessment.

6 In a similar manner, appendix 5 presents the background of operational measures, gives a description of the validation of the preparation of operational measures, and presents examples of the preparation of operational measures, based on different data sources and purposes.

7 The resources and effort required for a direct stability assessment and the preparation of operational measures require that some economy be achieved by limiting the number of loading conditions for a ship for which these activities will be performed. Therefore, the choice of the loading conditions to be used for these purposes should be carefully considered. For this reason, appendix 6 is prepared to aid the users in the selection of loading conditions.

8 Finally, the scientific community that has supported the development of the Interim Guidelines published its research outcomes associated with the second generation intact stability criteria in major scientific journals, conferences and book chapters. Some of these publications discuss and provide further reading related to the underlying basis for the second

generation intact stability criteria. The contents of the external references included in these Explanatory Notes are not to be considered as part of, or as an extension of, the text of these Explanatory Notes. These are included only for respecting the copyrights or investigating the background of the criteria. It is also noteworthy to mention here that several other contributions to other literature were also relevant to the second generation intact stability criteria.[1]

[1] Including, but not limited to:
Spyrou, K. J., Belenky, V. L., Katayama, T., Bačkalov, I., and Francescutto, A., eds., Contemporary Ideas on Ship Stability: From Dynamics to Criteria, Springer, 2023, ISBN: 978-3-031-16328-9; and
Belenky, V., Spyrou, K., van Walree F., Neves, M.A.S., and Umeda, N., eds., Contemporary Ideas on Ship Stability. Risk of Capsizing, Springer, 2019, ISBN: 978-3-030-00514-6.

PART B

GUIDANCE ON INDIVIDUAL SECTIONS OF THE INTERIM GUIDELINES[2]

1 GENERAL

1.1 Introduction

1.1.1 *Purpose*

1.1.1.1 Motivation for and modes of stability failure covered by the second generation intact stability criteria

The motivation for the development of performance-based criteria for intact stability is derived from the appearance of new types of vessels and modes of operation. This is discussed, in part, in the preamble to the 2008 Intact Stability Code, as adopted by resolution MSC.267(85):

> "…in view of a wide variety of types, sizes of ships and their operating and environmental conditions, problems of safety against accidents related to stability have generally not been solved. In particular, the safety of a ship in a seaway involves complex hydrodynamic phenomena which up to now have not been fully investigated and understood. Motion of ships in a seaway should be treated as a dynamical system and relationships between ship and environmental conditions such as wave and wind excitations are recognized as extremely important elements. Based on hydrodynamic aspects and stability analysis of a ship in a seaway, stability criteria development poses complex problems that require further research."

Part A of the 2008 Intact Stability Code explains further: "It is recognized by the Organization that performance-oriented criteria for the identified phenomena listed in this section (righting lever variation, resonant roll in dead ship condition, and broaching and other manoeuvring-related phenomena) need to be developed and implemented to ensure a uniform international level of safety." Responding to this need, the Organization pursued the development of second generation intact stability criteria for the identified phenomena as well as the hazard associated with excessive accelerations.

1.1.1.2 As the framework for the development explains, the intact stability regulations contained in the 2008 Intact Stability Code provide deterministic criteria associated with physical typologies and sizes of ships operated in the 1960s. Ships that have typologies or sizes outside the scope of those for which those regulations were developed, as well as some ships that fully satisfy the 2008 Intact Stability Code, may be susceptible to different modes of stability failures. These ships may have non-conventional hull geometry, modes of operation, or loading conditions neither envisioned by nor within the applicability limits of the first generation criteria. As a result, second generation intact stability criteria are considered as a complement to the first generation criteria.

The aim of the second generation intact stability criteria is to establish recommendations for ship design, applicable to all types of ships vulnerable to major dynamic modes of stability failures.

[2] This part was prepared to realize paragraph-to-paragraph comparisons with the Interim Guidelines. Thus, the section and paragraph numbers are based on the Interim Guidelines.

1.1.2 *Framework*

1.1.2.1 The second generation intact stability criteria involve stability assessment using methods aligned with physics of the phenomena under consideration. To facilitate this, definitions, terminology and nomenclature specific to the second generation intact stability criteria were developed.

1.1.3 *Application logic*

1.1.3.1 At least one design assessment option (level 1 or level 2 vulnerability criteria or direct stability assessment) or operational measures should be applied to each considered loading condition. The loading conditions to which the design assessment or operational measures are applied should be based on actual loading during standard operation, depending on the actual layout of cargo hold, the purpose of voyages and the expected weather, and could include special loading for delivery voyages, additional securing of fishing net, heavy weather ballast adjustment and so on.

1.1.4 *Testing*

1.1.4.1 With reference to item .3 that addresses the level 2 vulnerability criterion for the pure loss of stability failure mode, it is noted that the dynamics of water on deck may significantly affect the stability in waves for ships with low freeboard. The vulnerability criteria do not take into account the dynamics of water on deck; therefore this may lead to very conservative results.

1.1.5 *Feedback*

1.1.5.1 The feedback solicited in the Interim Guidelines can be separated into three types:

.1 the results of application of the Interim Guidelines;

.2 comments on the Interim Guidelines or Explanatory Notes, including requests for increased clarity and explanation; and

.3 suggestions of alternatives or improvements/refinements of the criteria contained in the Interim Guidelines.

Submissions of feedback on any of these types should be submitted to the Organization by electronic means to sdc@imo.org as directed by the following:

Feedback on results (.1 above) should be formatted similar to that provided by the examples given in appendix 2 to the Explanatory Notes.

Feedback on the Interim Guidelines or the Explanatory Notes that comment on or request clarity of the Interim Guidelines or Explanatory Notes should identify the element of the Interim Guidelines or Explanatory Notes for which comment is given and the reason for which it is given.

Feedback of a suggestion of an alternative or an improvement should include an analysis of the basis for the suggestion and a comparison with the criterion given in the Interim Guidelines that provides a comprehensive assessment of the basis for the comparison including all intermediate results that compare the criteria on a common basis. Examples of such comparison may be discovered in relevant publications.

1.1.6 ***Relationship with mandatory criteria***

1.1.6.1 The second generation intact stability criteria establish minimum recommendations for ship design, applicable to all types of ships and major dynamic modes of stability failures. Verification of the ship vulnerability to the major dynamic modes of stability failures is regarded as a complementary assessment and shall not be used as an alternative to the 2008 Intact Stability Code criteria.

1.1.7 ***Notes for application***

1.1.7.1 A ship with an extended low weather deck means a vessel which is engaged primarily in the transport of stores, materials and equipment to offshore installations and designed with accommodation and bridge erections in the forward part of the vessel and an exposed cargo deck in the after part for the handling of cargo at sea.

1.2 Definitions

1.2.1 The term "environmental condition" that is used in the Interim Guidelines is to be intended as synonymous with "sea state", unless additional information is necessary to characterize the environment for specific applications.

1.3 Nomenclature

1.3.2 General ship characteristics

"A_k = total overall area of the bilge keels (no other appendages) (m^2);"

The total overall area of the bilge keels means the sum of the projected area of the bilge keel normal to the hull on both the port and starboard sides. Only for the dead ship stability level 1 criterion, the projected area of a bar keel, if fitted, can be added.

1.3.4 Loading condition characteristics

"GM = metacentric height of the loading condition in calm water (m), with or without correction for free surface effect, as required;"

The free surface effect should be taken into account for calculating GM and righting lever in calm water and in waves, except for the excessive acceleration failure mode.

"T_r = linear natural roll period in calm water (s)"

The free surface effect should be taken into account for calculating T_r, except for the excessive acceleration failure mode.

2 Guidelines on vulnerability criteria

2.1 Preface

Vulnerability criteria are intended to distinguish between vulnerable and non-vulnerable loading conditions of a ship; a ship's loading condition that satisfies the standard of any assessment level of a stability failure mode is considered to have an acceptable level of safety with reference to that stability failure mode.

2.2 Assessment of ship vulnerability to the dead ship condition failure mode

2.2.1 *Application*

2.2.1.4 The application of stability limit information is additional to the stability limits that are obtained from application of the 2008 Intact Stability Code, part A. One should keep in mind that resonance effects for these failure modes may create areas showing vulnerability within the allowed GM limits obtained from applying the criteria in part A. It is therefore recommended to perform these second generation stability calculations for different GMs for each draught and trim to reveal these vulnerable areas.

2.2.2 *Level 1 vulnerability criterion for the dead ship condition*

2.2.2.1 For the purpose of level 1 vulnerability assessment for dead ship stability failure, the method of assessment included in the "Severe wind and rolling criterion (weather criterion)" in section 2.3 of part A of the 2008 Intact Stability Code is used, but the steepness factor s in table 2.3.4-4 of section 2.3 of part A is substituted with the steepness factor s specified in table 4.5.1 of the *Interim guidelines for alternative assessment of the weather criterion* (MSC.1/Circ.1200) (see figure 2.2.1).

2.2.2.4

"φ_1 = angle of roll to windward due to wave action (deg)."

Refer to the Explanatory Notes to the International Code on Intact Stability, 2008 (2008 Intact Stability Code) (MSC.1/Circ.1281), section 3.5.4.

Table 2.2.2.4-4 of the Interim Guidelines is imported from MSC.1/Circ.1200 as shown in figure 2.2.1.

Table 2.3.4-4 – Values of factor s

T	s
≤ 6	0.100
7	0.098
8	0.093
12	0.065
14	0.053
16	0.044
18	0.038
≥ 20	0.035

2008 IS Code – Part A

To be substituted by

Table 4.5.1: Wave steepness as a function of the full scale natural roll period

Ship roll period T_ϕ [s]	Wave steepness $s = H / \lambda$
<6	0.100
6	0.100
7	0.098
8	0.093
12	0.065
14	0.053
16	0.044
18	0.038
20	0.032
22	0.028
24	0.025
26	0.023
28	0.021
30	0.020
>30	0.020

MSC.1/Circ.1200 – Chapter 4

Figure 2.2.1 Explanation to table 2.2.2.4-4 of the Interim Guidelines

2.2.3 *Level 2 vulnerability criterion for the dead ship condition*

2.2.3.1 The objective of the level 2 vulnerability assessment methodology is to provide a simplified conservative probabilistic measure of vulnerability of the ship, in the considered loading condition, to the dead ship stability failure mode.

Several assumptions are required to provide a suitable tool for level 2 vulnerability assessment. Some of such assumptions are described in the relevant sections of these Explanatory Notes. However, the fundamental set of underlying assumptions is as follows:

.1 the ship is assumed to be in dead ship condition in irregular waves and gusty wind for a specified exposure time;

.2 wind and waves are assumed to blow/propagate in the same direction and the water depth is sufficiently large (water depth is larger than half the wavelength) to allow an assumption of infinite water depth;

.3 the ship is assumed to remain beam to wind and waves;

.4 the wind state is characterized by a mean wind speed and a gustiness spectrum;

.5 the sea state is characterized by a wave elevation spectrum and waves are assumed to be long-crested; and

.6 the roll motion of the vessel can be modelled as a one-degree of freedom (1-DOF) system.

The measure, indicated as C, is a long-term probability index ranging from 0.0 (good) to 1.0 (bad), which is obtained as a weighted average of short-term indices C_S.

2.2.3.2 The weighting factor W_i should be obtained from the wave scatter table such as table 2.7.2.1.2 of the Interim Guidelines as the ratio of the value described in the cell to the sum of the values in all cells, which represents the relative frequency of occurrence of short-term environmental condition specified with the significant wave height and the mean zero-crossing wave period.

The total number of short-term environmental conditions corresponds to the number of cells with non-zero frequency of occurrences in the wave scatter table such as table 2.7.2.1.2 of the Interim Guidelines because the short-term environmental conditions can be specified with the significant wave height and mean zero-crossing wave period.

2.2.3.2.1 The short-term dead ship failure index, C_S, depends on the characteristics of the ship in the considered loading condition and the short-term environmental conditions of a given duration. This is obtained by a simplified calculation methodology which takes into account characteristics of roll in the considered short-term environmental condition.

For ships which are not port/starboard symmetric, the short-term dead ship failure index C_S is to be determined as the average between the index calculated for wind and waves coming from both port and starboard sides.

A conceptual scheme of the assumed underlying simplified physical modelling of the phenomenon is shown in figure 1.1 of appendix 1. The overview of the logic of the short-term modelling is as follows:

.1 ship characteristic parameters are assumed to be available (displacement, righting lever, roll damping, windage area characteristics, etc.);

.2 the environmental conditions are specified in terms of wind and waves;

.3 the wind state is provided as a mean wind speed and a wind gustiness spectrum;

.4 the mean heeling moment due to wind is determined starting from the mean wind speed;

.5 the spectrum of the roll moment due to the wind gust is determined starting from the wind gustiness spectrum;

.6 the sea state is provided in terms of a sea elevation spectrum, from which a wave slope spectrum is directly determined;

.7 the spectrum of roll moment due to the waves is determined starting from the wave slope spectrum;

.8 the total spectrum of roll moment is assumed to be given by the sum of the spectrum of roll moment due to wind gustiness and the spectrum of roll moment due to waves; and

.9 the dynamics of roll is then assumed to be modelled by means of a linear 1-DOF equation of motion, which takes into account the ship characteristics (roll restoring, roll natural period, roll damping), the mean heeling moment due to the mean wind speed, and the irregular roll moment due to the combined effect of gust and waves.

In this assessment, heeling angles to the leeward side are implicitly assumed to be positive, whereas heeling angles to the windward side are assumed to be negative.

"T_{exp} = exposure time, to be taken as equal to $3600\ s$;"

For the purpose of this assessment, the ship is conventionally assumed to be exposed to each short-term environmental condition for one hour (3,600s).

2.2.3.2.2 A set of standard environmental conditions is assumed that refers to both the short- and the long-term. The short-term characterization is given in terms of mean wind speed, spectrum of wind gust and spectrum of sea elevation. The long-term characterization is given in terms of a wave scatter diagram. A deterministic relation is assumed between the mean wind speed and the significant wave height. The wave conditions are described in section 2.7.2 of the Interim Guidelines. The mean wind speed is considered to be correlated only with the significant wave height.

The wind is assumed to fluctuate around the mean wind velocity. The total wind speed is given by the sum of the mean wind speed U_W (m/s) and the gust fluctuation speed v (m/s).

2.2.3.2.3 Once the roll motion equation is set up, it needs to be solved in order to provide the necessary information for the estimation of the short-term failure index C_S. To this end, a simplified approximate methodology is used in order to obtain an estimation of the short-term roll motion resulting from the 1-DOF modelling. From this information, the short-term failure index C_S can be determined.

$S_v(\omega)$: The spectrum of the gust, S_v ((m/s)^2/(rad/s)), is of the Davenport type, and it depends on the mean wind speed U_W (m/s). This represents a distribution of power of the fluctuating wind velocity around the mean wind velocity in the range of the fluctuation circular frequency ω (rad/s). In addition, the coefficient, K, is a typical frictional drag coefficient of sea surfaces.
μ_e: For explanation of the equivalent linear roll damping coefficient, μ_e, see paragraph 9.3.5 of appendix 3 for details.

2.2.3.2.4 For further details and considerations for the assessment of the estimated effective wave slope function, refer to appendix 3, section 8.

2.3 Assessment of ship vulnerability to the excessive acceleration failure mode

2.3.1 *Application*

2.3.1.2 The location where passengers or crew unprotected by a safety device such as seat belts and harness may be present refers to spaces, such as the navigation bridge, and other spaces designated for use by passengers that may normally be occupied in service. Locations where passengers or crew may occasionally be present, and typically not in heavy weather, should not be considered (e.g. areas to which access is provided by vertical means of access only).

2.3.2 *Level 1 vulnerability criterion for the excessive acceleration failure mode*

2.3.2.1

$$"\varphi \cdot k_L \cdot \left(g + \frac{4\pi^2 h_r}{T_r^2}\right) \le R_{EA1}"$$

The natural roll period, T_r, should be evaluated following paragraph 2.7.1.2 of the Interim Guidelines.

"φ = characteristic roll amplitude (rad) = $4.43\ r\ s\ /\ \delta_\varphi^{0.5}$;"

The characteristic roll amplitude is determined under the assumption that the roll variance is predominantly determined by frequencies close to the natural roll frequency.

"δ_φ = non-dimensional logarithmic decrement of roll decay;"

The non-dimensional logarithmic decrement coefficient δ_φ should be calculated as

$$\delta_\varphi = 0.5 \cdot \pi \cdot R_{PR}$$

where R_{PR} is determined according to paragraph 2.5.2.1 of the Interim Guidelines.

2.3.3 *Level 2 vulnerability criterion for the excessive acceleration failure mode*

2.3.3.2

$$"C = \sum_{i=1}^{N} W_i\, C_{S,i}"$$

This measure, indicated as C, is a long-term probability index ranging from 0.0 (good) to 1.0 (bad), which is obtained as a weighted average of short-term indices $C_{S,i}$.

"W_i = weighting factor for the short-term environmental condition, as specified in 2.7.2 of the Interim Guidelines;"

The weighting factor W_i should be obtained from the wave scatter table such as table 2.7.2.1.2 of the Interim Guidelines as the ratio of the value described in the cell to the sum of the values in all cells, which represents the relative frequency of occurrence of short-term environmental condition specified with the significant wave height and the mean zero-crossing wave period.

"N = total number of short-term environmental conditions, according to 2.7.2 of the Interim Guidelines;"

The total number of short-term environmental conditions corresponds to the number of cells with non-zero frequency of occurrences in the wave scatter table such as table 2.7.2.1.2 of the Interim Guidelines because the short-term environmental conditions can be specified with the significant wave height and mean zero-crossing wave period.

2.3.3.2.2 For a more realistic assessment of excessive accelerations, the wave spreading is taken into account by multiplication with the reduction factor 3/4 (= 0.75).

"N = number of intervals of wave frequency in the evaluation range, not to be taken less than 100;"

This number is different from the total number of short-term environmental conditions in paragraph 2.3.3.2 of the Interim Guidelines.

"a, b = cosine and sine components, respectively, of the Froude-Krylov roll moment in regular beam waves of unit amplitude ($kN \cdot m / m$), calculated directly or using an appropriate approximation;"

See section 8.3 of appendix 3.

"B_e = equivalent linear roll damping factor (kN m s), with $B_e = 2J_{T,roll}\,\mu_e$ where μ_e (1/s) is the equivalent linear roll damping coefficient;"

See section 9.3 of appendix 3.

2.4 Assessment of ship vulnerability to the pure loss of stability failure mode

2.4.1 *Application*

2.4.1.1 The assessment of vulnerability to pure loss of stability is carried out only for ships with relatively high service speed. If the speed is low, the duration over which the ship is exposed to decreased stability (reduced righting lever) is generally too short for a large heel angle to develop.

2.4.2 *Level 1 vulnerability criterion for the pure loss of stability failure mode*

2.4.2.1 The level 1 criterion is a simplified version of the level 2 criteria. While the level 2 criteria evaluate the vulnerability using the righting lever curve in waves, the level 1 criterion assesses on the metacentric height, including free surface correction, in waves.

"$GM_{min} \geq R_{PLA}$ and $\frac{\nabla_D - \nabla}{A_W(D-d)} \geq 1.0$"

Paragraph 2.4.2 should be used for hull forms that do not feature significant tumblehome, which is represented when the following guideline is met:

$$"\frac{\nabla_D - \nabla}{A_W(D - d)} < 1.0"$$

For such vessels, level 2 vulnerability assessment, direct stability assessment, or development of operational measures may be applied.

"GM_{min} = minimum value of the metacentric height (m) calculated as provided in 2.4.2.2 of the Interim Guidelines;"

The level 1 assessment of the vulnerability to pure loss of stability is performed using a conservative approximation of the smallest GM value during the wave pass.

2.4.2.2 The calculation of GM in waves should be based on the simplified formula for GM_{min} that requires only hydrostatic data.

$$"GM_{min} = KB + \frac{I_{TL}}{\nabla} - KG"$$

Use of this simplified formula may be recommended for relatively full ships, where significant variation of stability while the wave overtakes the ship is not expected. Usually, the simplified formula produces a more conservative result.

"I_{TL} = transverse moment of inertia of the waterplane at the draught d_L (m^4);"

A conservative, simplified formula of GM_{min} on a wave evaluates the second moment of the area of the waterplane at an artificial low draught to calculate a GM_{min}. If the hydrostatic data available for the ship includes data for this low draught, this calculation should be able to be performed without using stability software to calculate the GM_{min}.

2.4.3 *Level 2 vulnerability criteria for the pure loss of stability failure mode*

Although the initial stability represented by GM used in the level 1 criterion explains an onset of stability failure, the final occurrence of stability failure itself should be judged using the righting lever GZ as the level 2 criteria. Thus, the level 2 criteria are normally expected to be less conservative than the level 1 criterion. On the other hand, the calculation of GZ in waves requires more computational effort than that of GM.

2.4.3.1 The level 2 assessment requires evaluation of two criteria in the condition under the reduced righting lever due to a wave.

$$"\max(CR_1, CR_2) \le R_{PL0}"$$

The ship is considered not to be vulnerable if the largest value among $CR1$ and $CR2$ does not exceed the standard (i.e. 0.06).

2.4.3.2

"W_i = weighting factor for the short-term environmental condition as specified in 2.4.3.2.2 of the Interim Guidelines;"

The weighting factor W_i should be obtained from the wave scatter table such as table 2.7.2.1.2 of the Interim Guidelines as the ratio of the value described in the cell to the sum of the values in all cells, which represents the relative frequency of occurrence of short-term environmental condition specified with the significant wave height and the mean zero-crossing wave period.
2.4.3.2.1 The level 2 vulnerability assessment for pure loss of stability is based on the calculation of weighted criteria CR_1 and CR_2 on the basis of criteria $C1_i$ and $C2_i$ determined for

each calculation wave as defined in 2.4.3.2.2 and 2.4.3.2.3 of the Interim Guidelines. In order to reduce the calculation effort, criteria $C1$ and $C2$ are pre-computed for the set of 11 waves defined in 2.4.3.2.1 (where the case i = 0 corresponds to calm water) of the Interim Guidelines. Criteria $C1_i$ and $C2_i$ are then linearly interpolated from the pre-calculated data, as indicated in 2.4.3.2.2 of the Interim Guidelines.

The software used for calculation of the GZ curves in waves should be capable of balancing the ship in sinkage and trim for each position of the wave crest and each heel angle. The free surface correction, corresponding to the loading condition under consideration, has to be applied.

Calculations are carried out for 11 locations of the waves crest for each wave height: with the wave crest located at the amidships and 0.1L, 0.2L, 0.3L, 0.4L and 0.5L forward, and 0.1L, 0.2L, 0.3L, 0.4L and 0.5L aft thereof.

2.4.3.2.2 Refer to section 2.7.2 of these Explanatory notes for further details.

2.4.3.2.3 See appendix 3, section 7.

2.4.3.3 ***Criterion 1***

Criterion 1 is an evaluation of the angle of vanishing stability, φ_V. If φ_V is less than a standard value (30 degrees), the loading condition is considered to be vulnerable in the wave case under consideration.

For each *GZ* curve, the angle of vanishing stability has to be evaluated. The smallest value of the angle of vanishing stability $\varphi_{V\min}$ for each wave height is used for further calculations.

2.4.3.4 ***Criterion 2***

Criterion 2 is an evaluation of the stable heel angle under the action of a heeling lever, φ_S, due to an external heeling force which is related to the Froude number. If φ_S is greater than a standard value (15 degrees for passenger ships and 25 degrees for other ships), the loading condition is considered to be vulnerable in the wave case under consideration.

$$"C2_\mathrm{i} = \begin{cases} 1 & \varphi_\mathrm{sw} > K_{PL2} \\ 0 & otherwise \end{cases}"$$

For each wave height H_i, the heel angle φ_{sw} is the maximum static heel angle in a wave pass.

$$"l_{PL2} = 8\left(\frac{H_i}{\lambda}\right) dFn^2 (\mathrm{m});"$$

For each wave height H_i, an arm of a heeling moment l_{PL2i} is computed as given in 2.4.3.4 of the Interim Guidelines.

For each value of the arm of a heeling moment l_{PL2i} and each position of the wave crest, a static angle φ_S is computed; if the computation is not possible (l_{PL2i} exceeds maximum of the GZ curve), the conventional value of 180 degrees is used.

2.5 Assessment of ship vulnerability to the parametric rolling failure mode

2.5.2 *Level 1 vulnerability criterion for the parametric rolling failure mode*

The background of the vulnerability level 1 criterion is available in section 6 of appendix 3. The definition of sharp bilge is provided in paragraph 5.2 of appendix 3.

2.5.3 *Level 2 vulnerability criteria for the parametric rolling failure mode*

2.5.3.1 $C1$ is also referred to as the "first check" and $C2$ is also referred to as the "second check". For the background of the level 2 criteria, refer to section 6 of appendix 3. The standard for the second check of the level 2 criterion was determined with the reports of a major large heel incident of a containership. The containership encountered a severe storm in the North Pacific which resulted in rolling of up to 40 degrees port and starboard in bow seas and the loss overboard or destruction through collapse of more than 800 deck stowed containers. The model experiment and numerical simulation revealed that the cause of the accident was parametric rolling in head seas without the forward velocity. The sample calculation result used to determine the standard of the level 2 criterion is provided in section 5.4 of appendix 2 as an application example.[3]

2.5.3.2.1 For further details and considerations for the assessment of $GM(H_i, \lambda_i)$, refer to appendix 3, paragraphs 7.4 and 7.5.

2.5.3.2.3 Details regarding the procedure for the determination of wave cases in table 2.5.3.2.3 of the Interim Guidelines are reported in section 10 of appendix 3.

2.5.3.3 The factors K_i in table 2.5.3.3 were derived from an original idea where the ship speed was considered equal to the service speed and the heading of the vessel with respect to the waves was sampled from longitudinal to beam waves, leading to an orthogonal projection of ship service speed on the wave direction $V_s{\cdot}K_i$ with $K_i = cos((i - 1)\ \pi/2N)$ i=1,2,…,N. However, in the final version of the criterion in the Interim Guidelines, for realizing a simple and conservative estimation, the waves are considered to be purely longitudinal and the forward ship speed used in the calculations is varied on the basis of factors K_i in table 2.5.3.3. The amplitude of restoring variation due to waves decreases when the ship heading is deviated from the condition of longitudinal waves and the roll damping decreases when the ship speed is smaller than the service speed. Thus, calculating the restoring variation in purely longitudinal waves and the roll damping at a forward speed corresponding to $V_s{\cdot}K_i$ realizes a conservative estimation. When the value of N is sufficiently large, the $C2$ index is expected to converge to a certain value. Fig. 2.5.3.3 indicates the case of the C11 class containership shown in appendix 2. In this case, $N = 12$ is sufficient. The formula in the Interim Guidelines uses $N = 12$.

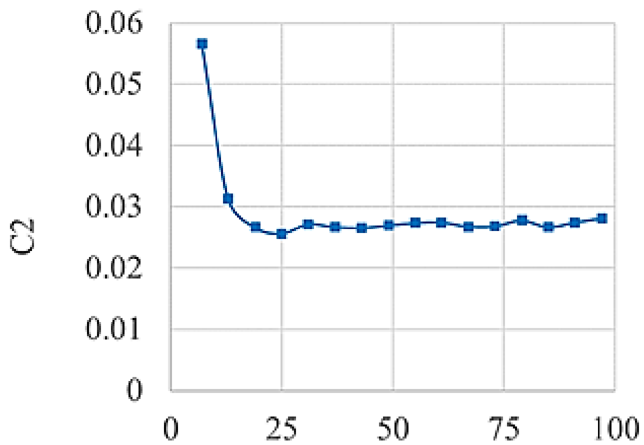

The number of speeds that were sampled, 2*N*+1

[3] Note: The information of the accident is taken from the document SLF45/6/7 "Head-sea parametric rolling and its influence on container lashing systems" submitted by the United States in 2002.

Fig. 2.5.3.3 The relationship between the $C2$ index and the number of wave heading for the C11 class containership

2.5.3.3.1 The equation of motion takes into account forces acting on the ship. The simplest mathematical model that is capable of evaluating the maximum roll angle includes four moments:

.1 inertia, including added inertia (or added mass) as a part of hydrodynamic forces;

.2 roll damping, which expresses energy loss from roll motions in creating waves, vortices and skin friction;

.3 roll restoring (stiffness) is determined from calculation of GZ in waves as specified in 2.5.3.4.1 of the Interim Guidelines; and

.4 transverse wave forces are absent for a ship in exact following or head long-crested seas.

Proper estimation of these four components is explained in greater detail in appendix 3, sections 1 and 2.

2.5.3.4 The maximum roll angle to which reference is made in paragraph 2.5.3.4 of the Interim Guidelines corresponds to the maximum roll angle when roll motion has reached a steady state. The parametric roll response includes the initial transition from the initial conditions to a steady state in which roll amplitudes are similar. Different criteria for "similarity" can be used: relative (the difference is less than 3 - 5%) or absolute (less than one degree). Following these criteria, the steady state portion of the response can be extracted (see figure 2.5.3.4.1) and the resultant maximum roll angle can be found as an average of steady state roll amplitudes.

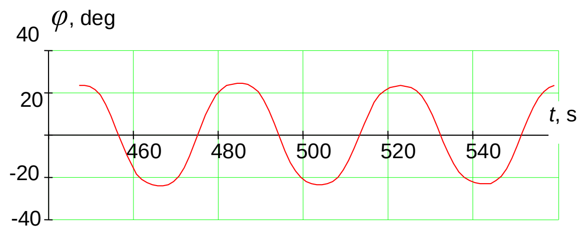

Figure 2.5.3.4.1 – Steady state portion of the roll motion in parametric resonance conditions

The steady state parametric rolling is not the only possible type of roll response. If parametric rolling is not possible for the given wave conditions, the response could be represented by decaying roll oscillations – as shown in figure 2.5.3.4.2. The response is not expected to look like a decaying sine function because of both the parametric excitation and non-linearity of the equation of motion. In some cases, the roll angle may initially increase and then damp out.

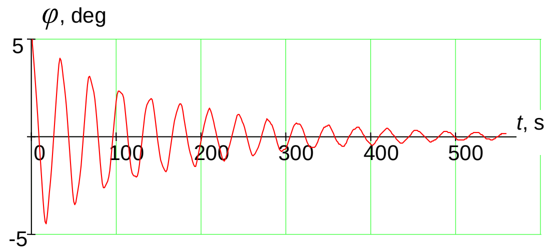

Figure 2.5.3.4.2 – Roll response in absence of parametric rolling

Another possible response may include "capsizing" (see figure 2.5.3.4.3) if the GZ curve was computed for the entire range of 180 degrees (like in figure 2.1 of appendix 3). If the GZ curve is not computed for the full range, the calculation should be explicitly stopped once the roll angle exceeds the cut-off roll angle.

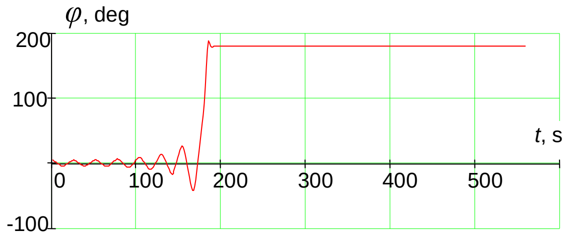

Figure 2.5.3.4.3 – Roll response with parametric roll and capsizing

2.5.3.4.1 For further details and considerations for the assessment of the roll angle, refer to section 4 of appendix 3.

2.5.3.4.2 Refer to section 7 of appendix 3 for further details.

2.6 Assessment of ship vulnerability to the surf-riding/broaching failure mode

2.6.2 *Level 1 vulnerability criteria for the surf-riding/broaching failure mode*

2.6.2.1 The criterion and the standard for the Froude number in the level 1 criterion were adopted as a part of the MSC/Circ.707 in 1995 and then superseded by MSC.1/Circ.1228. This guidance concludes that, under the appropriate wave conditions, surf-riding may occur when the ship speed is higher than:

$$\mathrm{V_S} \geq \frac{1.8\sqrt{\mathrm{L}}}{\cos(180^\circ - \beta)}$$

where V_S is the speed of the ship in knots and β is the angle of wave encounter in degrees. Assuming following seas $\beta = 180^\circ$ and transforming the formulae to be based on the Froude number yields:

$$F_n \geq \frac{1.8 \cdot 0.5144}{\sqrt{g}} = 0.296 \approx 0.3$$

This is regarded as the lower limit of threshold for surf-riding under any initial condition for conventional ships in the worst waves. It is compared with examples of such thresholds calculated for some sample ships with the Melnikov analysis, which was used in the level 2 criterion, as shown in figure 2.6.1. This result also indicates that the worst wavelength for surf-riding is comparable to the ship length. This means that longer ships require longer waves for surf-riding but the lengths of steep ocean waves have certain limits so that a small possibility for surf-riding exists for very long ships. Thus, the level 1 vulnerability criteria also require a threshold of ship length, i.e. 200 m.

Systematic calculation results of the stability failure due to broaching by using the critical wave method, which is specified in section 5.2 of appendix 4, and geometrical scaled ship hulls shown in figures 2.6.2 and 2.6.3 indicate that, if the ship length exceeds 200 m, the danger of broaching could be regarded as very small.

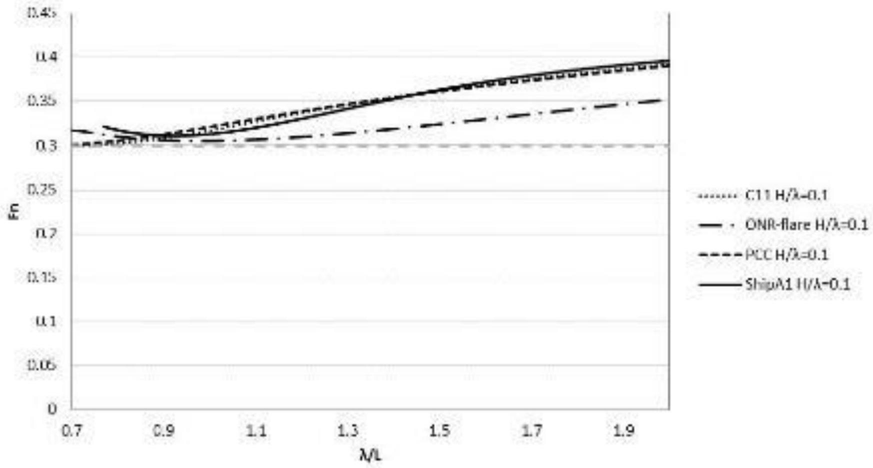

Figure 2.6.1 – Thresholds of surf-riding under any initial condition for some sample ships in the wave steepness (H/λ) of 1/10 with different wave length to ship length ratio (λ/L) compared with the nominal Froude numbers (Fn) of 0.3

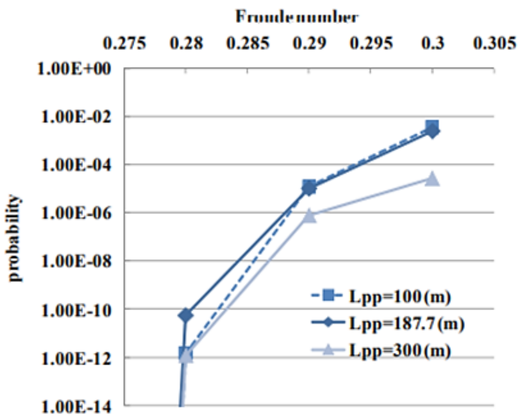

Figure 2.6.2 – Broaching-induced stability failure probability per hour for geometrically scaled ro-ro ship hulls with different sizes in the North Atlantic

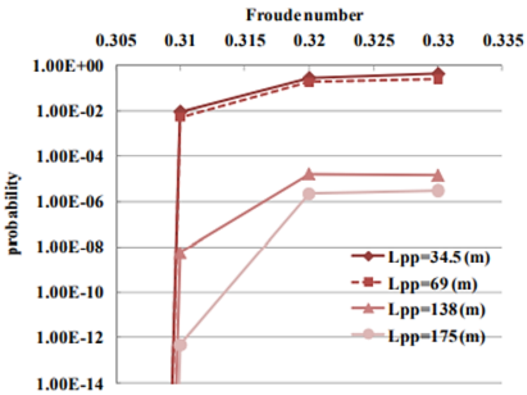

Figure 2.6.3 – Broaching-induced stability failure probability per hour for geometrically scaled fishing vessel hulls, which is used in section 6 of appendix 2, with different sizes in the North Atlantic

2.6.3 *Level 2 vulnerability criterion for the surf-riding/broaching failure mode*

2.6.3.2

"$W2(H_s, T_z)$ = weighting factor of short-term sea state specified in 2.7.2.1 as a function of the significant wave height, H_S, and the zero-crossing wave period, T_Z, in which $W2(H_s, T_z)$ is equal to the number of occurrences of the combination divided by the total number of occurrences in the table, and it corresponds to the factor W_i specified in 2.7.2 of the Interim Guidelines;"

The weighting factor $W2$ should be obtained from the wave scatter table such as table 2.7.2.1.2 of the Interim Guidelines as the ratio of the value described in the cell to the sum of the values in all cells, which represents the relative frequency of occurrence of short-term environmental condition specified with the significant wave height and the mean zero-crossing wave period.

2.6.3.2.1 The calculation formula of, W_{ij}, in paragraph 2.6.3.3 of the Interim Guidelines is the joint probability density function of local wave steepness and local wavelength under the stationary wave state with Bretschneider wave spectrum.

The envelope of an irregular wave time history is described with the slowly varying amplitude and phase. Then the joint probability density of the envelope amplitude, phase and their time derivatives can be calculated as the Gaussian process. If the wave spectrum is reasonably narrow, the envelope amplitude can be regarded as one half of the local wave height and the time derivative of the envelope phase can be related to the local wave period because of the wave dispersion relation. Thus, the joint probability density function of the local wave height and the local wave period can be obtained by transforming the envelope amplitude, phase, and their time derivatives.

2.6.3.2.2 Further details on the assessment of the regular wave are provided in section 5.4 of appendix 1.

2.6.3.2.3 Because the level 1 criterion is a simple assessment of Froude number, no resistance or thrust data is needed. However, the level 2 vulnerability criteria require the use of reliable estimates of resistance and thrust. Before a ship is completed and sea trials are performed, this data comes from model tests or other resistance estimation techniques. With respect to model tests, not all ship designs are tested to the high Froude numbers that correspond to the speeds at which surf-riding could be expected to occur. Therefore, an accurate procedure is required for prediction of the resistance at high Froude numbers, based on measured resistance data only extending to modest Froude numbers.

The calm water resistance, $R(u)$, can be estimated either by using results of geometrically scaled model tests and the standard scaling law or by using a numerical method with the agreement of the approval authority. The ship's resistance should be estimated to a ship speed up to 20% over the maximum service speed or the phase velocity (celerity) of the fastest wave under consideration.

The calm water resistance curve, $R(u)$, is constructed based on the available resistance data using a polynomial approximation which may, but need not, include terms up to the 5th power:

$$R(u) \approx \sum_{i=1}^{5} r_i u^i = r_1 u + r_2 u^2 + r_3 u^3 + r_4 u^4 + r_5 u^5$$

where, u speed of the ship (m/s) in calm water and r_1, r_2, r_3, r_4, r_5 approximation coefficients for the calm water resistance.

The polynomial fit should be appropriate to ensure the resistance is continuously increasing as a function of speed in the appropriate range. The polynomial fit to approximate resistance curve requires caution. Available data points may not extend to the phase velocity (celerity) of the fastest wave under consideration. If this is the case, the following condition should be verified for all values of ship speeds, u, up to the phase velocity of the fastest wave in consideration, u_{max}:

$$r_1 + 2r_2 u + 3r_3 u^2 + 4r_4 u^3 + 5r_5 u^4 > 0$$

where,

$$u_{\max} = \sqrt{\frac{3gL}{2\pi}}$$

2.6.3.2.4 The propeller thrust should be estimated using geometrically scaled model tests and standard scaling law or using a numerical method that is agreeable to the approval authority. The propeller advance ratio range should cover the whole positive range of propeller thrust coefficient.

The thrust deduction, t_p, should be evaluated using geometrically scaled model tests and standard scaling law. In absence of ship-specific model test data, the following approximations can be made:

$t_p = 0.1$, *for single screw ships; and*

$t_p = 0.325 \cdot C_B - 0.1185 \frac{D_P}{\sqrt{B \cdot d}}$, *for twin screw ships;*

The wake fraction, w_P, should be evaluated using geometrically scaled model tests and standard scaling law. In absence of ship-specific model test data, a conservative assumption of the wake fraction w_P as 0.1 can be made.

Alternative methods can be used with the agreement of the approval authority.

For ships using propulsor(s) other than open propeller(s) or are using unconventional propulsion arrangement, the propulsor thrust may be evaluated with a method appropriate to the propulsor used and with the agreement of the approval authority.

Podded propulsion: With podded propulsion, the underwater body of the unit affects the propeller thrust considerably, and therefore the K_T curve of the whole pod unit in open water should be used. Otherwise, the same method for the conventional propeller can be used.

2.6.3.2.5 The critical number of revolutions of the propulsor corresponding to the surf-riding threshold, n_{cr} (r_j, s_i), (rps) in paragraph 2.6.3.4.6, can be calculated by solving the equation by using an appropriate method. In the case that the resistance in calm water is approximated with the 5th power polynomial, the critical number of revolutions, n_{cr}, corresponding to the second surf-riding threshold may be calculated as follows for each wave case:

$$n_{cr} = \frac{-m_1 + \sqrt{m_1^2 - 4m_0 m_2}}{2m_0}$$

where

$$m_2 = -2\pi \frac{\tau_0}{f_{ij}};\ \ m_1 = 2\pi \frac{\tau_1 c_i}{f_{ij}} + 8a_0$$

$$m_0 = 2\pi \frac{\tau_2 c_i^2 - R(c_i)}{f_{ij}} + 8a_1 - 4\pi a_2 + \frac{64}{3} a_3 - 12\pi a_4 + \frac{1024}{15} a_5$$

The coefficients a_1, a_2, a_3, a_4 and a_5 do not have indexes of the wave cases in order to keep the formulae simple; however, c_i and k_i depend on the wave length and f_{ij} depends on both wavelength and height. The complete amplitude for the wave force with the wave length, λ_i, and wave height, H_{ij}, is calculated by formulae from paragraph 2.6.3.4.5.

Coefficients r_i that are not used in the fitting of the calm water resistance curve shall be taken equal to 0.

2.7 Parameters common to stability failure mode assessments

2.7.1 *Inertial properties of a ship and natural period of roll motion*

2.7.1.1 The factor 1000 appearing in the formula for $J_{T,roll}$ in paragraph 2.7.1.1 of the Interim Guidelines is related to the fact that $J_{T,roll}$ is measured in t·m^2.

2.7.1.2 For ships carrying containers, the following formula can be used alternatively for the natural roll period:

$$T_r = 2\pi\sqrt{(I_{xx} + A_{44})/(mgGM)}$$

where,

$$I_{xx} + A_{44} = 1.1 m_0 \left(\frac{B}{3}\right)^2 + 1.1 m_0 H_{SH}^2 + 1.1 \sum_{i=1}^{N_c} \left\{ m_i\left(y_i^2 + (z_i - z_T)^2\right) + \frac{\left(b_i^2 + h_i^2\right) m_i}{12} \right\}$$

where,

m is the mass of ship in kilograms, H_{SH} is the distance from the centre of mass of ship to the centre of mass of the ship without containers on deck in metres, m_i is the mass of each container loaded on deck in kilograms, y_i and z_i in metres, are the transverse and vertical coordinates of the container centre of mass, respectively, b_i and h_i in metres, are the breadth and height of the container, respectively, z_T is the vertical height of the ship centre of gravity in metres, N_c is the number of containers and m_0 is the mass of the ship without containers on deck in kilograms.

2.7.1.3 For all ships, the following formula can be alternatively used for $I_{xx} + A_{44}$:

$$I_{xx} + A_{44} = mK^2$$

where,

$$\left(\frac{K}{B}\right)^2 = 0.125\left\{C_u \cdot C_b + 1.10C_u\,(1 - C_b)\left(\frac{H_{sp}}{d} - 2.20\right) + \left(\frac{H_s}{B}\right)^2\right\}$$

$$c_u = \frac{A_u}{L_u B}$$

$$H_{sp} = D + \left(\frac{A'}{L_{pp}}\right)$$

c_u = upper deck area coefficient
A_u = projected area of upper deck
L_u = overall length of upper deck
H_{sp} = effective depth
A' = $A + A_c$
A' = lateral projected area of the forecastle and deck house (A) and on-deck cargoes (A_c) .

2.7.2 *Environmental data*

2.7.2.1 This wave scatter table is taken from IACS Recommendation No.34 (Corr.1 Nov. 2001). It is based on data collected from the 1960s through the 1980s; it was revised slightly in 2001. Wave data collected since 2001 is not represented in this table.

The sum of all numbers of occurrences for the given range of T_z and H_s out is 100,000. Therefore, the number of occurrences for one cell divided by 100,000 is the likelihood or probability of these combinations of T_z and H_s to be a short-term environment for a ship in a given loading condition.

While the table does not explicitly state, the number of occurrences out of 100,000 presented in each combination or cell of T_z and H_s reflect occurrences that are within ±0.5s of the given T_z and within ±0.5m of the given H_s. Hence, the values of T_z and H_s for a given cell are the centre values, respectively, of T_z and H_s, but not necessarily the mean values. The relationship between peak wave period and mean zero-crossing wave period can be calculated for Bretschneider wave energy spectrum as $T_z = 0.710\ T_p$.

3 Guidelines for direct stability failure assessment

3.1 Objective

3.1.2 The criteria and assessment procedures are detailed in these explanatory notes; the background of the standard of $2.6 \cdot 10^{-3}$ stability failures per ship per year is explained in paragraph 4.6.3, section 4.7 of appendix 4.

3.1.4 The dynamics of water on deck may significantly contribute to stability in waves for ships with an extended low weather deck. Since modelling of the effect of water on deck is difficult even with numerical methods that are employed in the direct stability assessment, it is not addressed in the present guidelines. However, if the effect of water on deck is ignored in numerical simulations, the results may be too conservative for the dead ship condition and pure loss of stability failure modes.

3.2 Requirements

3.2.1 The present guidelines consider the occurrence of excessive roll angles or excessive rigid-body accelerations as intact stability failures. The former may result in capsizing while both may impair normal operation of the ship and could be dangerous to crew, passengers, cargo or ship equipment. As excessive roll angles, the following limits are considered: 40 degrees, exceedance of which may lead to malfunctioning of the ship's engine or to a major shift of cargo, and thus static heel angle, which reduces freeboard; angle of vanishing stability in calm water, exceedance of which is associated with capsizing; and angle of submergence of unprotected openings in calm water, exceedance of which is associated with possible water ingress in internal compartment, and thus significant change in ship stability characteristics. In the direct stability assessment, the smallest of these three values should be used. As excessive lateral acceleration, the value of 9.81 m/s^2 is employed. These definitions of stability failures imply rather severe consequences. Depending on the particular case, stricter requirements may be applied if necessary.

3.2.2 Direct stability assessment should be performed with empty anti-roll tanks and retracted anti-roll fins. If anti-roll fins are not retractable, they should be considered as fixed in neutral position.

3.3 Requirements for a method that adequately predicts ship motions

3.3.2 *General requirements*

3.3.2.1 *Modelling of waves*

3.3.2.1.1 Several methods are available in engineering practice for modelling of irregular waves: they include, for example, computing the wave elevation as a sum of harmonic components with random phases and band-pass filtering the pseudo-white noise generated by maximum-length sequence.

3.3.2.1.2 Modelling irregular waves as a finite sum of harmonic components with random phases is a simple method, which computes the time history of wave elevation $\zeta(t)$ as

$$\zeta(t) = \sum_{i=1}^{M} a_i cos\,(\omega_i t + \epsilon_i)$$

where $a_i = \{2S_{ZZ}(\omega_i)\, D(\mu_i)\, \Delta\omega_i\, \Delta\mu_i\}^{1/2}$ are amplitudes, ω_i frequencies, μ_i directions and ϵ_i phases of harmonic components, S_{ZZ} is the wave energy spectrum and D is the wave energy angular spreading function. The phases of harmonic components ϵ_i are randomly selected in the interval $[0,2\pi)$; their frequencies ω_i, directions μ_i and amplitudes a_i may also be randomly varied. To generate random values, pseudo-random number generators can be used. In this method, if more than one of ratios between different two component frequencies are rational, the time history has a self-repetition period. If so, the duration of each simulation should be limited, to avoid self-repetition effects, using the following requirements:

.1 absence of self-repetition of waves, which can be checked by computing the autocovariance function of the free surface elevation using the wave energy spectrum,

$$R(t) = \sum_{i=1}^{M} S_{ZZ}(\omega_i)\, D(\mu_i)\, \cos(\omega_{ei} t)\, \Delta\omega_{ei}\, \Delta\mu_i$$

where $\omega_{ei} = \omega_i - \omega_i^2\, g^{-1}\, V_S\, \cos(\mu_i)$ is the encounter frequency. Until the peaks of the autocovariance function do not increase with increasing simulation time t, the duration of the simulation is still sufficiently small to ensure the absence of self-repetition of waves; and

.2 absence of self-repetition of roll motion, for which the absence of self-repetition of waves may not be sufficient due to narrow-banded nature of roll excitation. To verify the absence of self-repetition effects of roll motion, quantile plots can be used (see section 3.7 of appendix 4 for details).

3.3.2.1 *Modelling of roll damping: avoiding duplication*

3.3.2.2.2 Regarding item .2 addressing CFD computations, refer to the ITTC recommended guidelines 7.5-03-02-03 (issued in 2014 or amended).

3.3.3 *Requirements for particular stability failure modes*

3.3.3.5 For excessive acceleration stability failure mode, the minimum requirements to the resolved degrees of freedom do not include the sway motion. Since sway contributes to lateral acceleration, special consideration should be given to accurate (or, at least, conservative) reproduction of lateral acceleration if sway motion is not explicitly modelled.

In these cases, a proof should be provided that the error in the lateral acceleration is either conservative or, if non-conservative, does not exceed 10% or 0.05g, whichever is larger.

3.4 Requirements for validation of software for numerical simulation of ship motions

3.4.2 *Qualitative validation requirements*

Examples for the backbone curve and the roll response curve are shown in figures 3.4.1 and 3.4.2.

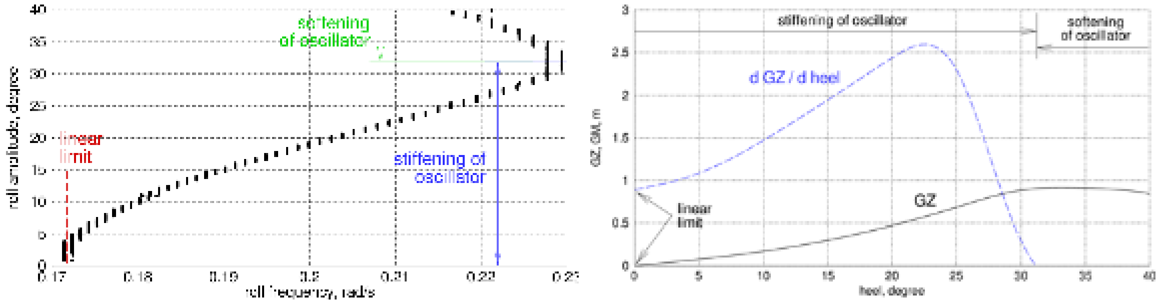

Figure 3.4.1 – Left: backbone curve (roll amplitude vs. roll frequency from roll decay simulation); Right: righting lever curve (GZ) and derivative of GZ with respect to heel angle vs. heel angle

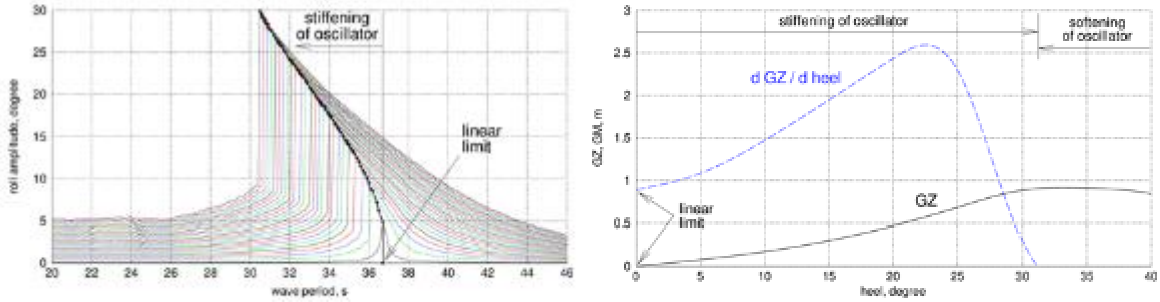

Figure 3.4.2 – Left: roll amplitude in regular waves vs. wave frequency (one line per wave height) and line through peak roll response (solid black line with circles); Right: righting lever curve (GZ) and derivative of GZ with respect to heel angle vs. heel angle

With reference to the change of stability in waves, see example in section 2.3 of appendix 4. The background for this phenomenon is presented in chapter 3 of appendix 1.

With respect to the response curve for parametric roll in regular waves, additional information is presented in section 2.4 of appendix 4. The background for this phenomenon is presented in chapter 4 of appendix 1.

With reference to surf-riding equilibrium, the background for these phenomena is presented in chapter 5 of appendix 1.

3.4.3 *Quantitative validation requirements*

3.5.5.3 Examples for the roll response curves are shown in figures 3.4.3 and 3.4.4.

With reference to the change of stability in waves, see example in section 2.3 of appendix 4. The background for this phenomenon is presented in chapter 3 of appendix 1.

With respect to the response curve for parametric rolling in regular waves, additional information is presented in section 2.5 of appendix 4.

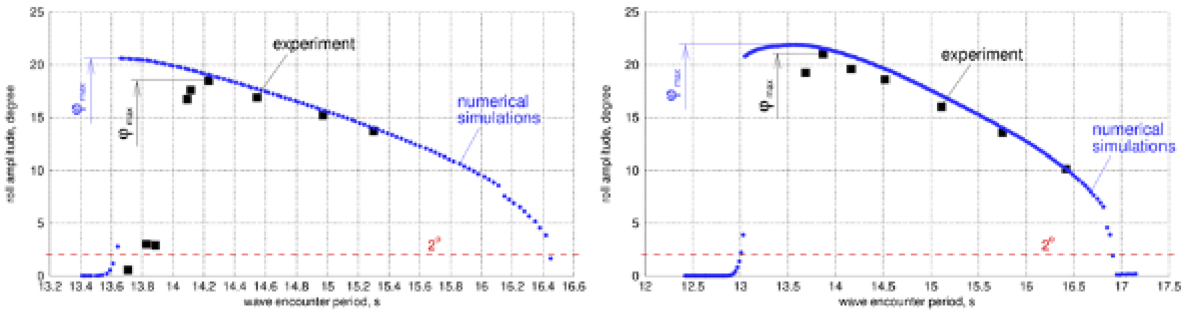

Figure 3.4.3 – Computed and measured amplitude of roll in regular head waves

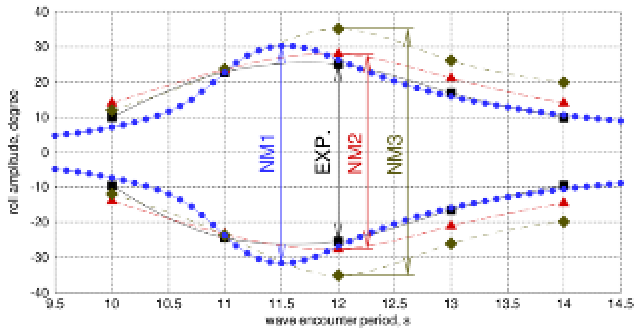

Figure 3.4.4 – Measured (EXP.) and computed with three numerical methods (NM1, NM2, NM3) double amplitude of roll in regular beam waves

3.5 Procedures for direct stability assessment

3.5.2 *Verification of failure modes*

3.5.2.1 The physical background of stability failure modes is explained in appendix 1.

Verification of a failure mode in a direct stability assessment means identification of the observed failure with one of the five modes addressed. Unambiguous identification of stability failure mode may be difficult. Identification is needed to exclude an irrelevant failure from the count, e.g. case of heel caused by broaching from assessment addressing parametric roll.

Relevant definitions are given below:

- *Local roll period* is the zero-crossing period of the roll motion, containing the stability failure event.
- *Local heave period* is the zero-crossing period of the heave motion, containing the stability failure event.
- *Local pitch period* is the zero-crossing period of the pitch motion, containing the stability failure event.
- *Local wave encounter period* is the zero-crossing period of the wave elevation at the centre of gravity of the ship, containing the stability failure event.
- *Natural roll period* is defined in calm water for the maximum roll amplitude during the roll period containing the stability failure. Due to the non-linearity of roll motion, the wave encounter frequency corresponding to the largest roll response may significantly differ from the linear natural roll frequency, as shown in figures 2.1.1, 2.2.3 and 4.3.1 of appendix 4.

Chapter 7 of appendix 4 shows application examples of the verification of failure mode.

3.5.2.2 The background for verification of the pure loss of stability failure mode is presented in chapter 3 of appendix 1. An example of a verification of the failure mode is presented in appendix 4, section 7.2.

3.5.2.3 The background for verification of the parametric roll stability failure mode is presented in chapter 4 of appendix 1. Particular attention is directed to figure 4.2 of appendix 1. Examples of verifications of the failure mode are presented in appendix 4 and section 7.1.

3.5.2.4 The background for verification of the surf-riding/broaching stability failure mode is presented in chapter 5 of appendix 1. An example of a verification of the failure mode is presented in appendix 4, section 7.3.

3.5.2.5 The background for verification of the dead ship condition and the excessive acceleration stability failure modes are presented in chapters 1 and 2, respectively, of appendix 1. An example of a verification of the failure mode is presented in appendix 4, section 7.4.

3.5.3 *Environmental and sailing conditions*

3.5.3.1 *General approaches for selection of environmental and sailing conditions*

3.5.3.1.3 For short-crested irregular waves, wave energy is spread with respect to the mean wave direction. The cosine-squared wave energy spreading is given by

$$D(\mu',\mu)=\left(\frac{2}{\pi}\right)\left\{max\left(0, cos\left(\mu'-\mu\right)\right)\right\}^2$$

where μ' is the wave direction and μ is the mean wave direction. For long-crested irregular waves, $D(\mu',\mu) = 1$, when $\mu' = \mu$ and 0 otherwise.

Since short-crested waves provide more realistic representation of sea state compared to long-crested waves, this model can be used both in numerical simulations and model tests for any stability failure mode. At the same time, the use of long-crested waves in numerical simulations or model tests may be less expensive and is, in many cases, more conservative. In such cases, the long-crested wave model can be used if it is more practicable for the particular stability failure mode and numerical simulation method or model test.

If assessment employs irregular short-crested waves, the numerical method used should be validated in model experiments in irregular short-crested waves or using a sufficient number of wave directions in irregular long-crested waves.

3.5.3.2 *Full probabilistic assessment*

3.5.5.3.1 The estimate of the mean long-term rate of stability failures is a random variable subject to uncertainty. To take this into account, the employed practical criterion is the upper boundary $\bar{r}_U$ of the 95%-confidence interval of the average "long-term" stability failure rate, paragraph 3.3.5 of appendix 4. This criterion can be conservatively calculated (for each addressed loading condition) as a weighted average, over relevant sea states (H_s, T_z) and sailing conditions (v_s, μ), of the upper boundary $r_U(H_s,T_z,\mu,v_s)$ of the 95%-confidence interval of the "short-term" stability failure rate:

$$\bar{r}_U = \sum_s \sum_\mu \sum_{v_s} f_s(H_s,T_z) \cdot f_\mu(\mu) \cdot f_v(v_s) \cdot r_U(H_s,T_z,\mu,v_s) \Delta H_s \Delta T_z \Delta v_s \Delta\mu$$

where $f_s(H_s, T_z)$ is the probability density of sea states, equal to $w_i / (\Delta H_s \Delta T_z)$, where W_i are the weights provided in the scatter table, ΔH_s, ΔT_z are ranges of significant wave height and zero-crossing wave period of cells in the scatter table, $f_\mu(\mu)$ is the probability density of wave directions, and $f_v(v_s)$ is the probability density of forward speeds; note that $\sum_\mu f_\mu(\mu) \Delta\mu = 1$, $\sum_{v_s} f_v(v_s) \Delta v_s = 1$ and $\sum_s f_s(H_s,T_z)\, \Delta h\, H_s\, \Delta T_z = 1$.

In the assessment, the resolution of significant wave heights ΔH_s should be at least 1.0 m, the zero-crossing wave periods ΔT_z should be at least 1.0 s and the mean wave directions $\Delta\mu$ should be at least 15 degrees. The range of ship forward speeds from zero to full service speed should be divided into at least 6 intervals Δv_s.

The upper boundary $r_U(H_s, T_z, \mu, v_s)$ of the 95%-confidence interval of the "short-term" stability failure rate is obtained for each combination (H_s, T_z, μ, v_s), by either direct counting, an extrapolation of $r_U(H_s, T_z, \mu, v_s)$ over the significant wave height H_s or another statistical extrapolation method.

The stability failure rate, evaluated with direct stability assessment, is the statistical estimate. Statistical estimates have a natural variability, i.e. different numerical simulations or model tests may produce different values due to random reasons. This variability is characterized by a confidence interval, as shown in figure 3.5.1. The confidence interval contains a true value of the failure rate with the confidence probability that is usually taken as 95%. The upper boundary r_U of the 95%-confidence interval of stability failure rate is used in direct stability assessment in section 3.5.3.2 of the Interim Guidelines. This boundary is obtained for each combination (H_s, T_z, μ, v_s) by either direct counting, extrapolation of failure rate over significant wave height or another statistical extrapolation method.

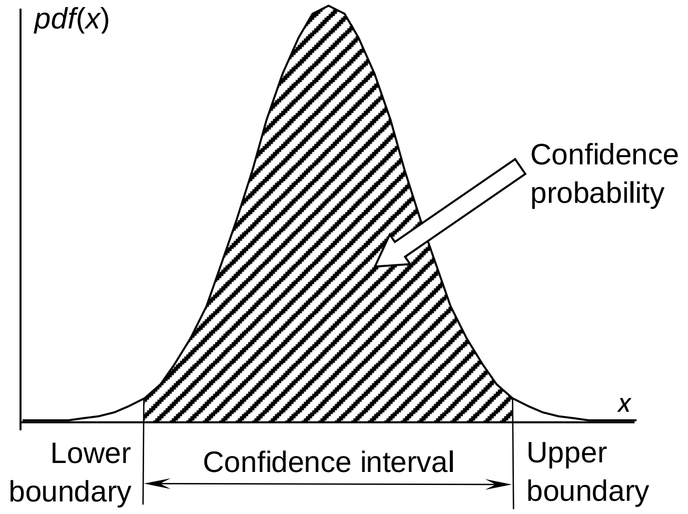

Figure 3.5.1 – Confidence interval of normally distributed estimate

3.5.3.2.2 See paragraph 4.6.4 of appendix 4.

3.5.3.3 *Assessment in design situations using probabilistic criteria*

3.5.5.3.1 Whereas the full probabilistic assessment requires evaluation of stability failure rate for a large (of the order of magnitude 10^4) number of combinations of sea state parameters (H_s, T_z) and sailing conditions (v_s, μ), the idea of the direct stability assessment in design situations, see section 4.4 of appendix 4, is to reduce the evaluation of stability failure rate to few (up to 20) combinations (H_s, T_z, v_s, μ), referred to as design situations; the employed sea states are rather steep to increase the stability failure rate and thus minimize the total simulation or testing time required for the assessment. The design situations are specific for stability failure modes.

3.5.3.3.2 Example procedure for probabilistic assessment in design situations is described in section 4.7.10 of appendix 4.

3.5.3.3.3 The threshold λ in paragraph 3.5.3.3.2 is equal to $1.389 \cdot 10^{-4}$ 1/s ($= 1/(3600s \times 2)$) because it represents one stability failure every two hours.

3.5.3.3.4 Explanations to table 3.5.3.3.4 of the Interim Guidelines – Design situations for each stability failure mode:

.1 range of zero-crossing wave periods T_z is specified for the dead ship condition and excessive acceleration stability failure modes in terms of its ratio, 0.7 to 1.3, to the natural roll period T_r. To define the natural roll period, free roll decay simulations or tests should be performed before the assessment;

.2 for pure loss of stability and surf-riding/broaching stability failure modes, the appropriate assumption for the forward speed should be the maximum attainable speed in waves considering added resistance due to wind and waves, propulsion system and engine diagram; however, as a conservative simplification, the assessment is performed at maximum nominal service speed, i.e. at the forward speed that is attained in waves at the propeller rotation speed equal to the propeller rotation speed at the maximum ship service speed in calm water;

.3 for pure loss of stability and surf-riding/broaching stability failure modes, the wave period is given in terms of peak wave period corresponding to specified wave lengths (1.0L for pure loss of stability and from 1.0L to 1.5L for surf-riding/broaching); peak wave period corresponding to wave length λ is defined as T_p = $(2\pi\lambda/g)^{1/2}$ and the mean zero-crossing wave period can be calculated for Bretschneider wave energy spectrum as $T_z = 0.710\, T_p$; and

.4 for parametric roll stability failure mode, assessment is performed in head and following waves at zero forward speed; in model tests, soft spring arrangement can be used to keep ship's position and heading at zero speed.

3.5.3.3.5 One significant wave height Hs is used per mean zero-crossing wave period Tz. This wave height corresponds to the probability density of sea state f_s = 10^{-5} 1/(m·s). The probability densities of sea states are defined as $f_s(H_s, T_z) = W_i / (\Delta H_s \Delta T_z)$, where W_i are the weights provided in the scatter table and ΔH_s, ΔT_z are the ranges of significant wave height and zero-crossing wave period of cells in the scatter table. To define the probability density of a sea state with significant wave height H_s between significant wave heights H_{s1} and H_{s2}, corresponding to centres of the ranges in the scatter table, linear logarithmic interpolation can be used:

$f_s = f_{s1}^{\gamma} f_{s2}^{1-\gamma}$ with $\gamma=(H_{s2} - H)/(H_{s2} - H_{s1})$ (similarly for interpolation between wave periods).

3.5.4 *Direct counting procedure*

3.5.4.1 The proposed example procedures are based on simulations of ship motions in multiple independent realizations of the same irregular seaway. The seaway is modelled as a sum of harmonic components. Independent realizations are produced by random variation of the phases and, possibly, frequencies, directions and amplitudes of the components. To generate random values, pseudo-random number generators are used.

3.5.4.2 The background and application examples of direct counting procedures to estimate the upper boundary of the 95%-confidence interval of stability failure rate are described in sections 3.3, 3.4 and 3.5 of appendix 4.

3.5.4.3 Since the available direct counting procedures assume that the occurrence of stability failure can be described as a Poisson process, they should prevent self-repetition effects, transient hydrodynamic effects at the beginning of simulations and autocorrelation of large roll motions. To neutralize the effect of self-repetition, duration of each simulation is limited. The effect of autocorrelation of big roll motions can be neutralized by stopping or ignoring a simulation after an encountered stability failure. The effect of transient hydrodynamic effects at the beginning of simulations can be neutralized by either switching off the counter of stability failures and simulation timer during initial transients or by random variation of initial conditions for each realization.

3.5.4.4 Regarding items .1 and .2:

.1 Numerical simulations or model tests are carried out for arbitrary (e.g. constant) simulation time, which is limited by the maximum duration or first stability failure, whichever happens earlier. After each simulation, the number of stability failures encountered in the simulation ΔN (1 or 0) and duration of simulation Δt (time to failure if realization ended with a stability failure or full duration of simulation otherwise) are recorded, and

.1 N^* is calculated as N before the last simulation plus one;
.2 total number of failures N is increased by ΔN;
.3 total simulation time t_t is increased by Δt;
.4 maximum likelihood estimate of failure rate is updated as $\hat{r} = N/t_t$;
.5 conservative estimate of maximum likelihood estimate of the failure rate is calculated as $\hat{r}^*=N^*/t_t$; and
.6 upper and lower boundaries of 95%-confidence interval of the failure rate are updated as $r_U=0.5\chi^2_{1\text{-}0.05/2,2N^*}\hat{r}^*/N^*$ and $r_L=0.5\chi^2_{0.05/2,2N}\hat{r}/N$, respectively, where $\chi^2_{p,f}$ denotes the p·100%-quantile of χ^2-distribution with f degrees of freedom (details can be found in section 3.3 of appendix 4).

.2 Numerical simulations are carried out with a common predefined maximum exposure time t_{exp} for each single realization. If a stability failure is encountered in a simulation, further time history does not need to be considered, and the simulation can also be stopped before t_{exp} for that realization. After each simulation, the total number of carried out realizations, M, and the total number of realizations during which at least one stability failure has been observed, N, are recorded. The increase of the counter N from the previous realization is ΔN, with $\Delta N = 1$ if at least one stability failure occurred during the present simulation and $\Delta N = 0$ otherwise. The maximum likelihood estimate of the probability of at least one stability failure in an exposure time t_{exp} is calculated as $p^* = N / M$ and the corresponding failure rate is calculated as $r^* = -ln(1-p^*)/t_{exp}$. The lower and upper boundaries of the 95%-confidence interval for the probability of at least one stability failure in an exposure time t_{exp} are then calculated. The lower boundary is calculated as $p_L = \nu_1 \cdot F_{\nu_1,\nu_2;0.05/2}/(\nu_2 + \nu_1 \cdot F_{\nu_1,\nu_2;0.05/2})$ with $\nu_1 = 2 \cdot N$ and $\nu_2 = 2 \cdot (M - N + 1)$, for $N > 0$; in case $N = 0$, then $p_L = 0$. The upper boundary is calculated as $p_U = \nu_1 \cdot F_{\nu_1,\nu_2;1-0.05/2}/(\nu_2 + \nu_1 \cdot F_{\nu_1,\nu_2;1-0.05/2})$ with $\nu_1 = 2 \cdot (N+1)$ and $\nu_2 = 2 \cdot (M - N)$, for $N < M$; in case $N = M$, then $p_U = 1$. The corresponding lower and upper boundaries of the 95%-confidence interval for the failure rate are finally calculated as $r_L = -ln(1-p_L)/t_{exp}$ and $r_U = -ln(1-p_U)/t_{exp}$, respectively. The symbol $F_{\nu_1,\nu_2;x}$ (with $x = 0.05/2$ or $x = 1 - 0.05/2$) indicates the inverse cumulative F-distribution with ν_1 and ν_2 degrees of freedom, calculated at the specified value x. The same approach can be used in case model tests are carried out instead of numerical simulations.

3.5.4.5 Full probabilistic direct stability assessment requires evaluation of the upper boundary $r_U(H_s, T_z, \mu, v_s)$ of the 95%-confidence interval of the "short-term" stability failure rate for each relevant combination of significant wave height H_s, mean zero-crossing wave period T_z, ship forward speed v_s, and mean wave direction μ with respect to the ship heading. For non-vulnerable ships and loading conditions, for combinations of wave periods and directions away from roll resonance and for moderate significant wave heights, the stability failure rate may be very low, so that application of direct counting is impractical. Therefore, direct counting should be used for such combinations (H_s, T_z, μ, v_s) for which this is affordable, otherwise statistical extrapolation can be used, section 3.5.5.

Direct stability assessment in design situations does not require statistical extrapolation, thus the use of direct counting is sufficient. However, statistical extrapolation still can be used when this seems practicable.

Preparation of operational guidance using only direct counting is, in principle, possible, but may be rather time-consuming. Use of statistical extrapolation may significantly accelerate the preparation of operational guidance: in the same way as for the full probabilistic direct stability assessment, direct counting is used to define the upper boundary of 95%-confidence interval of stability failure rate for such combinations (H_s, T_z, μ, v_s) for which this is affordable, otherwise statistical extrapolation is used.

3.5.5 *Extrapolation procedures*

3.5.5.3 *Extrapolation over wave height*

3.5.5.3.1 Extrapolation of the mean time to stability failure or mean rate of stability failures over significant wave height significantly reduces required simulation time since numerical simulations or model tests are conducted at greater significant wave heights than those required in the assessment, where stability failure rate is greater, and results are extrapolated to lower significant wave heights. This method is especially useful for the full probabilistic direct stability assessment and probabilistic operational measures, which require evaluation of stability failure rate for all possible combinations of sailing conditions (v_s, μ) and sea states (H_s, T_z): direct counting is used to define stability failure rate for such combinations (v_s, μ, H_s, T_z) where this is affordable, and extrapolation over significant wave height is applied to these results to define the stability failure rate for the remaining combinations.

3.5.5.3.2 The extrapolation can be performed either in the form

$$ln\,T = A + B / H_s^2$$

or, equivalently, in the form

$$ln\,r = A + B / H_s^2$$

since $r = 1/T$; here T *(s)* is the mean time to stability failure, r (1/s) is the stability failure rate, and A *and* B are coefficients which do not depend on the significant wave height but depend on the ship loading condition, forward speed, zero-crossing wave period and mean wave direction. Coefficients A and B can be obtained by, for example, linear regression of $ln(r)$, or $ln(T)$, with respect to $1/H_s^2$. Information regarding this extrapolation procedure is provided in section 5.1 of appendix 4, which contains validation and application examples of this procedure to parametric and synchronous roll and pure loss of stability.

3.5.5.3.3 If r_k are the maximum likelihood estimates of the stability failure rate obtained by direct counting at significant wave heights H_{sk}, $k = 1,\dots,K$, and N_k are the numbers of stability failures that were encountered to estimate r_k, use at least three values of r_k for extrapolation, which were obtained for a range of significant wave heights not less than 2 m. Each of these values should not exceed 5% of the reciprocal natural roll period of the ship, i.e. $r_k < 0.05/T_r$ (or $T_k > 20T_r$). The values used should be checked for outliers and possible non-conservative extrapolation; if necessary, points used for extrapolation should be added or removed.

The extrapolated stability failure rate r_e is defined by linear extrapolation of $\ln \hat{r}_k$ over $1/H_{sk}^2$ as

$$ln\, r_e = \sum_{k=1}^{K} b_k\, ln\, \hat{r}_k$$

The coefficients b_k can be obtained by several methods, e.g. least-squares method, see section 5.1.4 of appendix 4. Note that in any case, $\sum_{k=1}^{K} b_k = 1$.

Details for the calculation of the upper boundary of the 95%-confidence interval of the extrapolated stability failure rate, r_{eU}, are provided in section 5.1.3 of appendix 4.

3.5.5.4 Other extrapolation procedures

3.5.5.4.1For more details on these other extrapolation procedures, refer to appendix 4.

.1 Theoretical background, example and statistical validation for the envelope peaks over threshold (EPOT) extrapolation procedure is described in section 5.4 of appendix 4. An applicable failure mode includes roll in the dead ship condition and in pure loss of stability. Applicability may be extended to the parametric roll failure mode after adjustment is made of the de-clustering procedure and a proper statistical validation.

.2 Theoretical background and example for the Split-time/motion perturbation method (MPM) extrapolation procedure is described in section 5.3 of appendix 4. The Split-time/MPM can be applied for excessive acceleration failure mode. The metric for excessive acceleration failure mode is formulated on condition of exceedance of the target lateral acceleration.

.3 The critical wave method for surf-riding and broaching is described in section 5.2 of appendix 4.

4 Guidelines for operational measures

4.1 General principles

4.1.1 These Guidelines consider the following operational measures, see paragraph 4.3.1 of the Interim Guidelines: operational limitations related to areas or routes and season; operational limitations related to maximum significant wave height; and operational guidance. The applicability of these measures for each of the five stability failure modes is explained in table 4.1.1.

Table 4.1.1 Applicability of the operational measures for five stability failure modes

Stability failure mode	Operational measures		
	Operational limitations related to areas or routes and season	Operational limitations related to maximum significant wave height	Operational guidance
Dead ship condition	applicable	not applicable	not applicable
Excessive acceleration	applicable	applicable	applicable
Pure loss of stability	applicable	applicable	applicable
Parametric rolling	applicable	applicable	applicable
Surf-riding/broaching	applicable	applicable	applicable

For four stability failure modes (excessive acceleration, pure loss of stability, parametric rolling and surf-riding/broaching), any operational measure can be used. For the dead ship condition failure mode, operational limitations related to maximum significant wave height and operational guidance are not applicable since this stability failure mode assumes inoperable main propulsion plant and auxiliaries. Such ships cannot avoid heavy weather and, once in heavy weather, cannot control speed and course to follow operational recommendations.

4.1.2 The aim of operational measures is to provide the same level of safety, quantified by the upper boundary $\bar{r}_U$ of the 95%-confidence interval of the average "long-term" stability failure rate, as the level provided by the criteria, procedures and standards provided by the guidelines for vulnerability criteria in chapter 2 of the Interim Guidelines or the direct stability assessment in chapter 3; for

.1 operational limitations related to areas or routes and season, this means that the ship is subject to the design assessment procedures in chapter 2 or chapter 3 with a different wave scatter table and corresponding wind statistics, which correspond to a specified area or route during a specified season;

.2 operational limitations related to maximum significant wave height, this means that the ship is subject to design assessment procedures in chapter 2 of the Interim Guidelines or chapter 3 of the Interim Guidelines with a wave scatter table which is considered up to a specified significant wave height; wind statistics are correspondingly modified; and

.3 operational guidance, this means that acceptable combinations of ship forward speed and wave height, period and direction with respect to ship heading are defined so that the level of safety, provided by operation in these combinations, is the same as provided by the design assessment procedures in chapter 2 of the Interim Guidelines or chapter 3 of the Interim Guidelines.

4.2 Stability failures

4.2.1 For ships with an extended low weather deck, motions in waves may lead to accumulation of water on deck. Dynamics of water on deck may significantly contribute to stability in waves for such ships. Since modelling of the effect of water on deck is difficult even with numerical methods that are employed in the direct stability assessment, it is not addressed in the present guidelines. However, if the effect of water on deck is ignored in numerical simulations, then the results may not be sufficiently conservative for the dead ship condition and pure loss of stability failure modes.

4.3 Operational measures

4.3.2 The amount of information, preparation and planning significantly differs between operational measures:

.1 operational limitations related to areas or routes and season are based on design assessment combined with wave scatter table and corresponding wind statistics that correspond to a specified area or route during a specified season, therefore the application of these operational limitations does not require weather data during the operation of the ship or any specific information and planning; however, actual data should be always available for the loading condition to ensure that the parameters of the loading condition are within the applicability range of the operational limitations. An estimate of the actual draught, trim, displacement, metacentric height, longitudinal position of the centre of gravity and natural roll period should be available at departure from the port and during the voyage, together with the estimated change of these parameters until the arrival in the next port;

.2 operational limitations related to maximum significant wave height are based on design assessment combined with a wave scatter table that is considered up to a specified significant wave height and correspondingly modified wind statistics. Therefore, application of these operational limitations requires a weather forecast, containing at least the significant wave height, and an actual passage plan which accounts for the most recent weather forecast and actual loading condition. To ensure that the ship does not encounter a situation when no acceptable sailing conditions are available, the passage plan should be available for the next three days to allow for enough time for routing adjustment. An estimate of the actual draught, trim, displacement, metacentric height, longitudinal position of the centre of gravity and natural roll period should be available at departure from the port and during the voyage, together with the estimated change of these parameters until the arrival in the next port; and

.3 operational guidance identifies for each sea state acceptable and unacceptable combinations of ship forward speed and wave direction with respect to ship heading, therefore it requires detailed forecast information about wave energy spectrum (which contains, at least, significant wave height, mean zero-crossing period and mean direction of wind sea and swell) and wind characteristics, together with means for indicating unacceptable combinations of ship speed and heading relative to mean wave direction. To ensure that the ship does not encounter a situation when no acceptable sailing conditions are available, the passage plan should be available for the next three days to allow for enough time for routing adjustment. An estimate of the actual draught, trim, displacement, metacentric height, longitudinal position of the centre of gravity and natural roll period should be available at departure from the port and during the voyage, together with the estimated change of these parameters until the arrival in the next port.

4.4 Acceptance of operational measures

4.4.3 Operational measures can reduce the stability failure rate to any low level by application of sufficiently strict operational measures. However, if operational limitations related to maximum significant wave height or operational guidance excludes too many sailing conditions in too many sea states, including moderate sea states, as not acceptable for some loading condition, such loading condition cannot be considered as sufficiently safe in routine practical operation even when operational measures are provided. Therefore, a loading condition cannot be considered as acceptable if the ratio of the total duration of all situations which should be avoided to the total operational time is greater than 0.2, section 1.8 of appendix 5. This restriction relates to operational limitations related to maximum significant wave height and operational guidance since operational limitations related to areas or routes and season do not impose any restrictions on sailing conditions or sea states.

4.4.5 Acceptable sailing conditions may be unattainable in some sea states due to limits of propulsion and steering systems of the ship or undesirable due to other problems, e.g. excessive vertical motions, accelerations and slamming. Neglecting this contradiction may lead to misleading guidance or even put the ship in danger if in some sea state all acceptable sailing conditions are unattainable, dangerous or unfeasible.

For example, for parametric roll in bow waves, roll motions may decrease with increasing forward speed, but high speeds could be either unattainable or could lead to excessive vertical motions or loads. Therefore, if practicable, it is suggested for wave directions from head waves to 60 degree off-bow to define the maximum attainable forward speed taking into account the added resistance in seaway and the ship's propulsion system, as well as maximum suitable forward speed from the point of view of absolute and relative motions, vertical accelerations and slamming.

The maximum attainable and maximum suitable forward speeds in bow waves can be defined from model tests. In cases where this is not practicable, proven conservative estimates can be used. A conservative alternative for parametric roll in bow waves is to evaluate roll motions at zero forward speed.

In sea states where heading into seaway is necessary to avoid excessive lateral accelerations, the ability of the ship to keep a sufficient forward speed in head waves is required. The sufficient forward speed to keep heading into bow waves can be defined from model tests; in cases where this is not practicable, proven conservative estimates can be used. As a conservative assumption, 20% of the full service speed in calm water could be considered as a general indication.

4.5 Preparation procedures

4.5.1 *Operational limitations related to areas or routes and season*

4.5.1.3 Preparation of operational limitations using some level 1 and level 2 vulnerability assessment procedures requires definition of regular wave cases based on a modified wave scatter table. Definition of such wave cases is detailed in section 10 of appendix 3.

4.5.2 *Operational limitations related to maximum significant wave height*

4.5.2.3 Preparation of operational limitations using some level 1 and level 2 vulnerability assessment procedures requires definition of regular wave cases based on a modified wave scatter table. Such wave cases are defined in the same way as for operational limitations related to areas or routes and season, see details in section 10 of appendix 3.

4.5.3 *General principles of preparation of operational guidance*

4.5.3.2 Operational guidance can be prepared using any of three equivalent approaches which are recommended for the preparation of operational guidance. The theoretical background and application examples are included in sections 1 and 2, respectively, of appendix 5 of these explanatory notes.

4.5.3.3 Operational guidance should clearly indicate acceptable and unacceptable sailing conditions for each relevant sea state. A possible form of presentation of operational guidance is a polar diagram, see an example in figure 4.5.1 and more examples in section 2 of appendix 5.

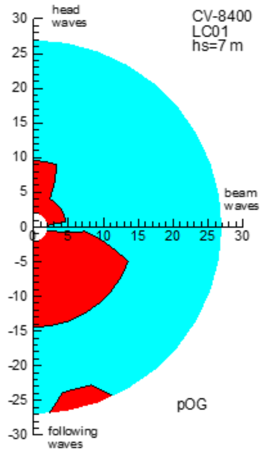

Figure 4.5.1 – Unacceptable sailing situations (combinations of ship forward speed and wave direction with respect to ship heading, red) for 8400 TEU container ship in axes ship speed (knots, radial coordinate) - mean wave direction (circumferential coordinate) for significant wave height 7.0 m.

4.5.3.4 Other forms of operational guidance, different from polar diagrams, can be used; in any case, for presentation of operational guidance it is recommended that:

.1 operational guidance is available for all loading conditions subject to operational guidance;

.2 acceptable and unacceptable sailing conditions (combinations of mean wave direction and ship forward speed) are easily and clearly identifiable for each relevant sea state;

.3 resolution of mean wave directions is at least 15 degrees and the range of ship forward speeds extends from zero to full service speed in at least six intervals; and

.4 sea states cover all non-zero entries of the applicable wave scatter table with discretization intervals not exceeding 1.0 m for significant wave heights and 1.0 s for zero-crossing wave periods.

4.5.4 *Probabilistic operational guidance*

4.5.4.1 Operational guidance indicates unacceptable sailing conditions, i.e. combinations (v_s, μ) that should be avoided, for each range of sea states (H_s, T_z) in the relevant wave scatter table. A probabilistic operational guidance uses the upper boundary r_U of the 95%-confidence interval of the "short-term" stability failure rate $r_U(H_s, T_z, \mu, v_s)$ as the criterion to distinguish between acceptable and unacceptable sailing conditions.

4.5.4.2 See paragraph 1.6.2 of appendix 5. Additional levels may be added for augmented guidance; levels corresponding to lower failure rates may serve as a warning. Additional levels, corresponding to larger failure rates, may be helpful for finding the best way of exiting the unacceptable sailing condition, in case the guidance is used in real time.

4.5.4.3 The upper boundary $r_U(H_s, T_z\ \mu, v_0)$ of the 95%-confidence interval of the stability failure rate should be defined for combinations (H_s, T_z, μ, v_0) with a resolution of at least 1.0 m for significant wave heights, 1.0 s for zero-crossing wave periods and 15 degrees for mean wave headings; the range of ship forward speeds from zero to full service speed should be divided into at least six intervals. This boundary can be obtained by either direct counting, extrapolation of r_U over significant wave height or another statistical extrapolation method:

.1 direct counting, see paragraph 3.5.4.4 of the Interim Guidelines and corresponding explanatory notes, is time-consuming when stability failure rate is low. If direct counting procedure in paragraph 3.5.4.4.1 is used, computational time can be reduced using acceptance check during simulation following example procedure in paragraph 4.7.10 of appendix 4 with an acceptance threshold $\lambda = 10^{-6}$ 1/s. Numerical simulations should be carried out for each combination (H_s, T_z), μ, v_0) in multiple independent realizations of the sea state according to recommendations in the explanatory text to paragraph 3.5.4.3 of the Interim Guidelines; and

.2 combination of direct counting with statistical extrapolation may significantly accelerate the preparation of operational guidance: direct counting is used to define the upper boundary of 95%-confidence interval of stability failure rate r_U for such combinations (H_s, T_z, v_0, μ) for which it is affordable, otherwise statistical extrapolation is used.

4.5.4.4 If a certain situation is assessed as unacceptable, all situations with greater H_s and the same v_s, μ and T_z are considered unacceptable, whereas if a certain situation is found acceptable, all situations with lower h_s and the same v_s, μ and T_z are considered acceptable.

4.5.6 ***Simplified operational guidance***

4.5.6.2 Regarding items .3 and .4:

.3 caution should be exercised, as a mathematical model of roll motions with 1 degree of freedom may not be always conservative in prediction of parametric roll occurrences for all speed and headings. (See sections 1.7 and 2.6 of appendix 5); and

.4 refer to section 2.5 of appendix 5.

4.6 Application

4.6.3 For seaway consisting of two wave systems (e.g. wind sea and swell) with significant wave heights h_{s1} and h_{s2}, zero-crossing wave periods T_{z1} and T_{z2} and mean wave directions μ_1 and μ_2, the ship responses can be approximated by theoretical modelling of wave systems and overlapping their effects, section 1.3 of appendix 5.

Ship responses to these two wave systems are defined separately, using pre-computed databases of ship responses to wave systems with parameters (H_{s1}, T_{z1}, μ_1) and (H_{s2}, T_{z2}, μ_2) with theoretical wave energy spectra: upper boundary r_{U1} and r_{U2} of the 95%-confidence interval of the "short-term" stability failure rate when using probabilistic operational guidance; mean three-hour maximum roll φ_{3h1} and φ_{3h2} or lateral acceleration a_{y3h1} and a_{y3h2} amplitude when using deterministic operational guidance; and unacceptable sailing conditions (v_s, μ) for each of these wave systems when using simplified operational guidance.

Unacceptable sailing conditions (v_s, μ) are defined for the combination of these wave systems as those for which $r_{U1} + r_{U2} > 10^{-6}\ s^{-1}$ for probabilistic operational guidance; $\alpha(\varphi_{3h1} + \varphi_{3h2}) > x_{\lim}$ or $\alpha(a_{y3h1} + a_{y3h2}) > x_{\lim}$ for deterministic operational guidance ($\alpha = 2$ is the scaling factor and $x_{\lim}$ is the corresponding stability failure threshold, paragraph 3.2.1 of the Interim Guidelines for direct stability assessment); and sailing conditions which are unacceptable in any of these two wave systems for simplified operational guidance.

4.6.4 The master of a vessel operating under operational limitations related to maximum significant wave height or operational guidance should always have an actual passage plan which accounts for the most recent weather forecast and actual loading condition. To ensure that the ship does not encounter a situation when all acceptable sailing conditions are unattainable or unfeasible, the passage plan should be always available for the next three days to allow for enough time to avoid a storm. As accurate as practicable data should be available for the loading condition at departure from the port, including draught, trim, displacement, metacentric height, longitudinal position of the centre of gravity, and natural roll period. An estimate of the current state of these parameters should be always available during the voyage together with the estimated change of these parameters for the time until the arrival in the next port.

APPENDIX 1

PHYSICAL DESCRIPTION OF THE STABILITY FAILURE MODES ADDRESSED BY SECOND GENERATION INTACT STABILITY CRITERIA

1 Physical background of stability failure related to the dead ship condition

1.1 Modelling in the level 1 criterion for the dead ship condition

1.1.1 Dead ship condition was the first mode of stability failure addressed by the physics-based severe wind-and-roll criterion, also known as the "weather criterion", which was adopted by IMO in 1985 (resolution A.562(14)) and is now embodied in section 2.3 of part A of the 2008 Intact Stability Code. The scenario of the weather criterion is shown in figure 1.1. This scenario assumes that a ship has lost its power and has turned into beam seas, where it is rolling under the action of waves as well as heeling and drifting under the action of wind. Drift-related heel is a result of action of a pair of forces: wind aerodynamic force and hydrodynamic reaction caused by transverse motion of the ship.

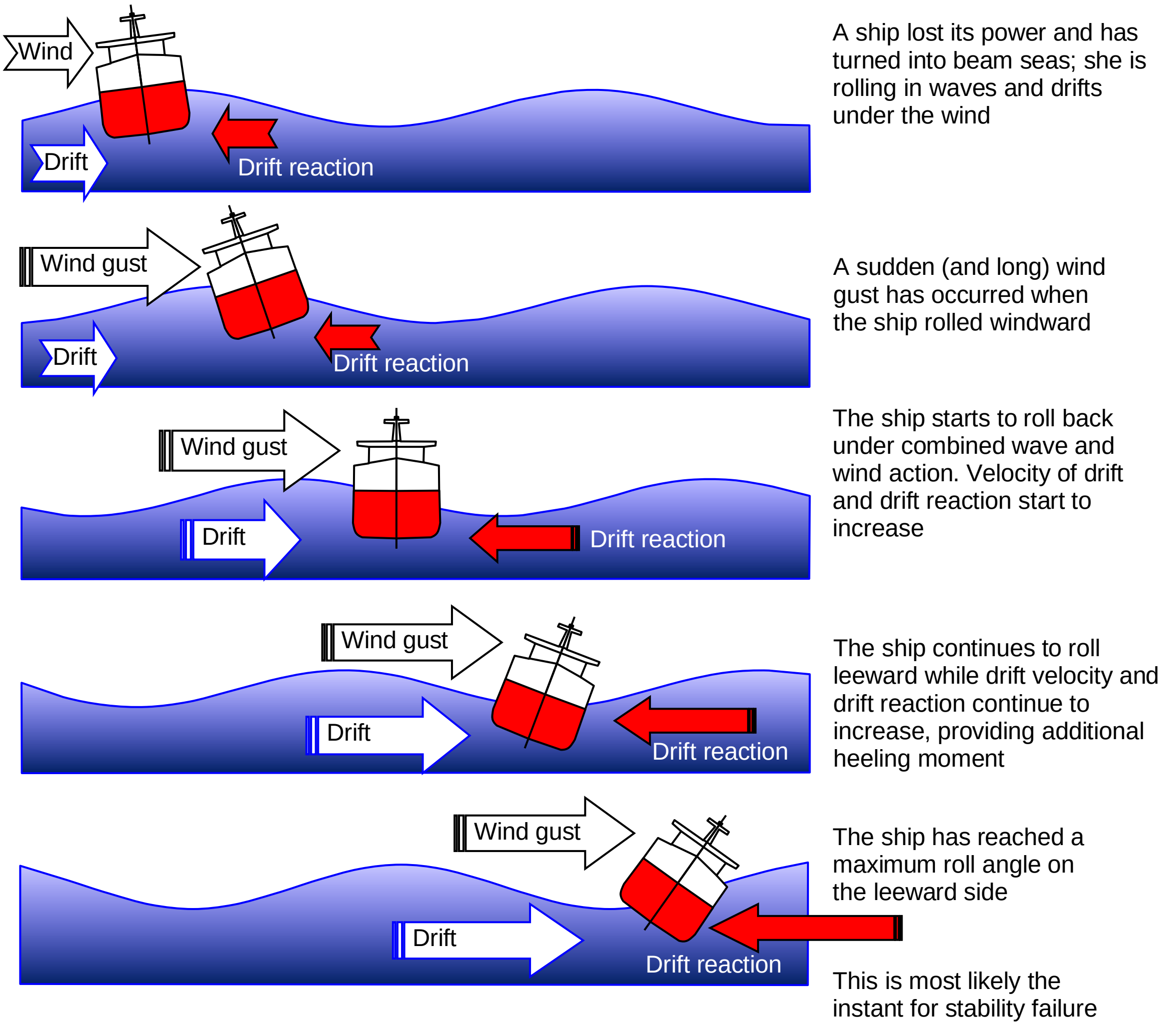

Figure 1.1 Scenario of stability failure in dead ship conditions

1.1.2 Next, a sudden and long gust of wind occurs. The worst possible instant for this is when the ship is rolled at the maximum windward angle; in this case, action of wind is added to the action of waves. The strengthening wind increases drift velocity, and this leads to an increase of the hydrodynamic drift reaction. The increase of the drift velocity leads to the increase of the hydrodynamic reaction and, therefore, to the increase of the heeling moment by the pair of aerodynamic and hydrodynamic forces. The gust is assumed to last long enough so the ship can roll to the other side completely; the achieved leeward roll angle is the base of the criterion. If it is too large, or some openings may be flooded, the stability of the ship is considered insufficient.

2 Physical background of stability failure related to excessive accelerations

2.1 Accelerations caused by ship motions

2.1.1 When a ship is rolling, the objects in higher locations travel longer distances. A period of roll motions is the same for all the locations on board the ship. To cover longer distance during the same time, the linear velocity must be larger. As the velocity changes its direction every half a period, larger linear velocity leads to larger linear accelerations. Large linear acceleration means larger inertial force (see figure 2.1).

2.1.2 Inertial forces acting in a horizontal plane are more dangerous for a human than vertical inertial forces. The vertical inertia forces cause brief overloading, while horizontal inertial forces cause humans to lose their balance, fall or even be thrown against walls, bulkheads or and other structures. Large accelerations are mostly caused by roll motions so they have predominantly lateral direction.

2.1.3 If the GM value is larger, the period of roll motion is smaller. Thus, for the same roll amplitude the changes of linear velocity occur faster, so accelerations are larger.

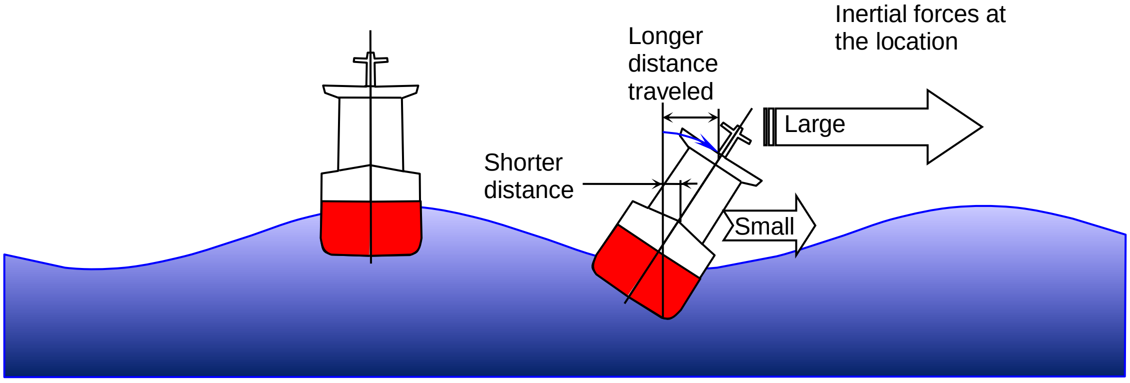

Figure 2.1 Scenario of stability failure related to excessive accelerations

2.2 Synchronous resonance in ship motions

2.2.1 A large angle of roll may be caused by different physical mechanisms. Some of them are already included as a part of vulnerability assessment of the second generation of IMO stability criteria: pure loss of stability, parametric rolling and broaching. Among these phenomena, parametric rolling is known to cause excessive accelerations. However, synchronous resonance is not covered by other vulnerability criteria.

2.2.2 Synchronous resonance is a phenomenon of amplification of motion response when the natural frequency of the ship motion is close to the frequency of the wave excitation.

2.2.3 The frequency of wave excitation depends on wave frequency, ship heading relative to waves and ship speed. When a ship sails against the waves (between head and beam wave encounter angles) the frequency of encounter is higher than the frequency of waves. This effect is the strongest in head waves, weakens in bow quartering seas and completely disappears in beam seas. When a ship sails in the same direction as the waves, the frequency of encounter decreases. This effect is the strongest in following seas, weakens in stern quartering seas and completely disappears in beam seas. Higher speed increases this effect.

2.2.4 The motion amplification effect of the synchronous resonance is the strongest when the encounter frequency is close to natural roll frequency (see figure 2.2). An increase of the amplitude of excitation (angle of wave slope) leads to an increase of resonance effect at all frequencies; however, the strongest increase is around the natural roll frequency (see figure 2.2a).

2.2.5 An increase of roll damping leads to decrease of motion amplitude; the effect is noticeable around natural frequency (see figure 2.2b). Thus, an increase of roll damping helps to mitigate the effects of the synchronous resonance.

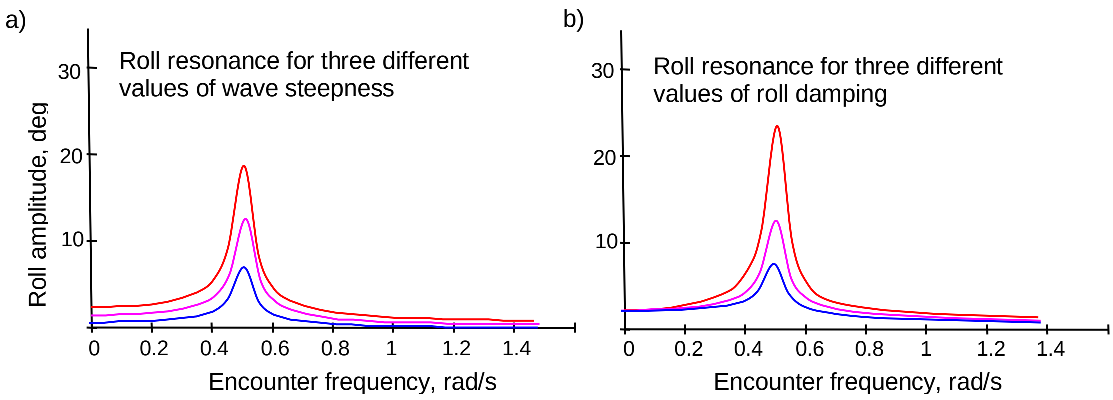

Figure 2.2 Synchronous roll resonance: a) influence of wave slope and b) roll damping

3 Physical background and scenario of pure loss of stability

3.1 Righting lever variation in waves

3.1.1 When a ship is under way through longitudinal waves, the submerged part of the hull changes. These changes may become significant if the length of the wave is comparable to the length of the ship. As a first example, one may observe the changes that occur when the trough of a wave is located amidships (see figure 3.1). For many ships, the upper part of the bow section is usually wide, due to bow flare. Bow flare provides protection from spray and green water shipping, and provides opportunity for deck cargo stowage. The bow flare makes the waterplane larger, if the upper part of the bow section becomes partially submerged. The upper part of the aft section of the hull may be wider. Cargo stowage considerations often mandate wide afterbodies. Therefore, the after part of the waterplane also increases, once the upper part of the aft section becomes submerged. Unlike the bow and aft sections, the midship section of most ships is often nearly wall-sided (see figure 3.1a). These characteristics mean that very little change occurs in the waterplane width with variations in draught. When the wave trough is amidships, the draught at the midship section is low, but as the hull is wall-sided in this region, there is little waterplane change. As a result, when the wave trough is located around the midship section, the overall waterplane area is increased (see figure 3.1b).

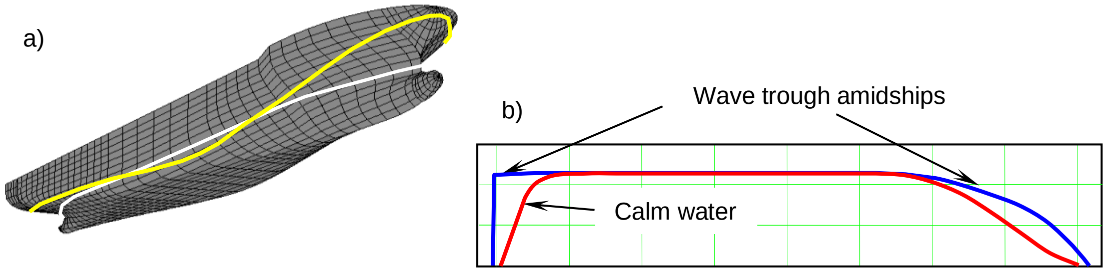

Figure 3.1 Changes in hull geometry when a wave trough is amidships: a) 3D view and b) waterplane

3.1.2 When the wave crest is located near amidships, the situation changes dramatically (figure 3.2). The underwater part of the bow section is usually quite narrow, especially around the waterline. Even for a bulbous bow, it is still narrower than for the section with bow flare. The reason for this is the consideration of resistance. The faster the ship is, the finer its underwater bow section tends to be. If the wave crest is amidships and the wave has a length similar to a ship length, the wave trough is located around the bow section. This makes the draught at the bow quite shallow. As a result, the waterplane becomes very narrow in this region. The underwater part of the aft section is also very narrow. The main design consideration is to provide the propulsor with enough water to efficiently power the ship. Consideration of energy efficiency impels a designer towards a buttock flow stern design. When the wave crest is located amidships, another wave trough is located near the aft section. The draught at the stern becomes smaller, which tends to make the waterplane very narrow in the aft part (see figure 3.2a). As mentioned previously, the midship section is typically more wall-sided, so it does not significantly affect the waterplane. Figure 3.2b shows the effect of the wave crest amidships, where the overall waterplane is reduced in area.

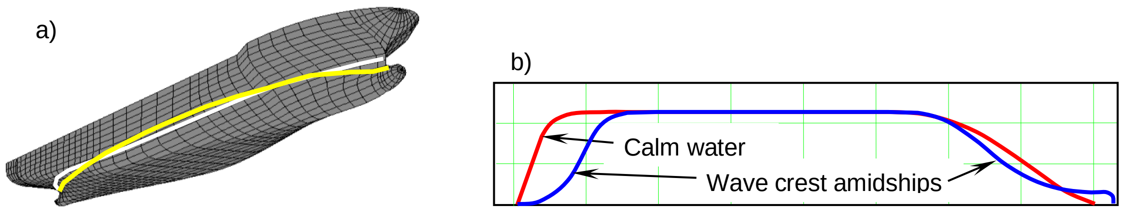

Figure 3.2 Changes in hull geometry when a wave crest is amidships: a) 3D view and b) waterplane

3.1.3. The waterplane area has a significant effect on ship stability, which is well known from ship hydrostatics. If the waterplane area is reduced, then the righting lever (GZ) curve is reduced as well (see figure 3.3). The change of stability in waves, as examined above, is the physical basis for the stability failure mode known as pure loss of stability. The dynamics of pure loss of stability are different from that of parametric rolling, but are also closely related to the severity and duration of waterplane changes. A possible scenario for the development of a stability failure caused by pure loss of stability is shown in figure 3.4.

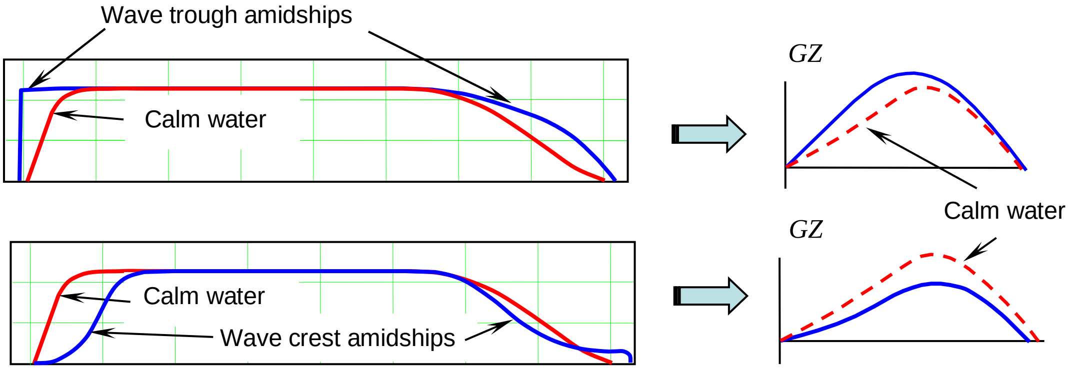

Figure 3.3 Stability, represented by righting lever curves, corresponding to waterplane changes with the midship located on the wave trough (top) and the wave crest (bottom)

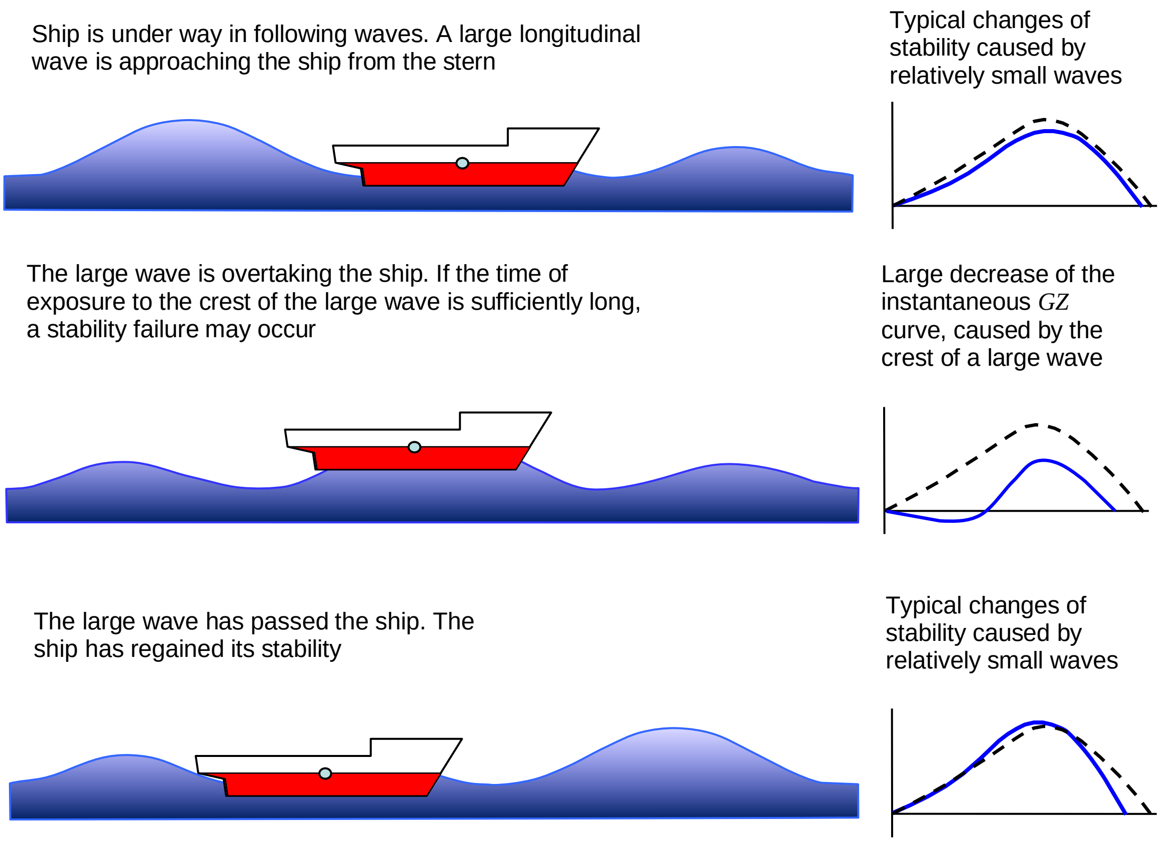

Figure 3.4 A possible scenario for the development of pure loss of stability

3.1.4 The case diagrammed in figure 3.4 shows a large wave approaching the ship from the stern while the ship is under way with relatively high speed in following seas. If the celerity (speed) of the large wave is just slightly above the ship speed, the duration needed for the large wave to pass or overtake the ship may be long ("long" here means at least an order of magnitude greater than the natural roll period). Once the crest of the large wave is near the midship section of the ship, the righting lever may be significantly decreased. Further, because of the significant duration that this condition may exist, a large heel angle may develop, which could lead to capsize. Once the large wave overtakes the ship, the righting lever is restored and the ship will return to the upright position, if a significant heel did not already occur.

3.1.5 A significantly reduced righting lever curve due to a relative wave profile does not necessarily result in a total or partial stability failure. An external heel moment is required for stability failure to occur. If no external heel moment exists, the upright condition will be retained except for cases in which the metacentric height in waves becomes negative, which allows an angle of loll. As the external moments to be relevant, wave exciting roll moment due to oblique wave heading and heel moment induced by a hydrodynamic force due to ship manoeuvring motions are candidates. Several existing model experiments using freely running ship models in stern-quartering waves indicate that coupling with manoeuvring motion is essential to explaining the forward speed effect on the stability failures of pure loss of stability. An example is shown in figure 3.5. If we take account of only surge-roll coupled motion, the pure loss of stability does not drastically depend on the forward speed. If we take account of also coupling with manoeuvring motions, however, the drastic forward speed effect on pure loss of stability can be explained. Thus, the heel moment induced by the hydrodynamic force due to ship manoeuvring motions should be included.

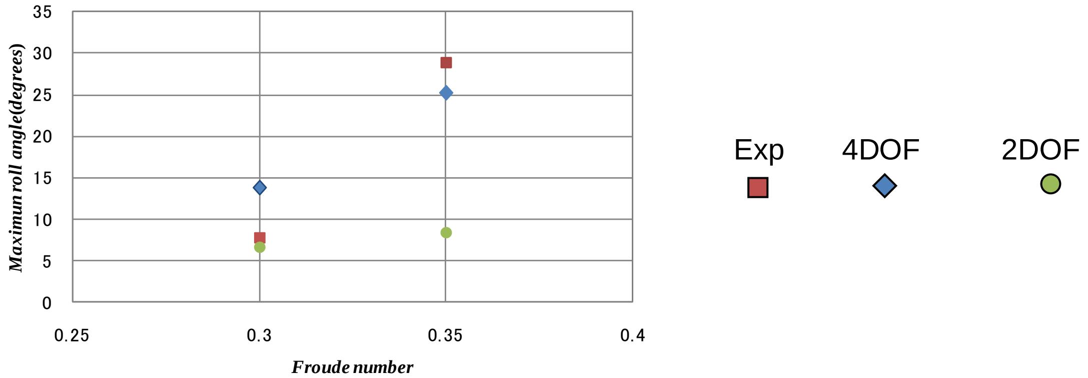

Figure 3.5 Forward speed effect on pure loss of stability in irregular stern-quartering waves for a containership model in a model basin (here, 2 DOF and 4 DOF mean surge-roll and surge-sway-yaw-roll coupled simulation models, respectively)[4]

4 Physical background of parametric rolling

4.1 Development of parametric rolling

4.1.1 Parametric rolling (a shortening of the formal term "parametric roll resonance") is a dynamic stability phenomenon in which an amplification of roll motion is caused by periodic variation of transverse stability in waves. The phenomenon of parametric rolling is predominantly observed in head, following, bow and stern-quartering seas when the ship's encounter frequency is approximately twice that of the ship's roll natural frequency and the ship's roll damping is insufficient to dissipate additional energy (accumulated because of parametric resonance).

4.1.2 Figure 4.1 shows the process by which parametric rolling develops. If the ship rolls while in the wave trough, increased stability (i.e. righting lever) provides stronger restoring, or restoring moment. As the ship returns to the upright position, its roll motion rate is increased, since there was an additional restoring from the increased stability. If at that time, however, the ship has the wave crest at midship, the stability is decreased and the ship will roll further to the opposite side because of the greater roll motion rate and less resistance to heeling. Then, if the wave trough reaches the midship section when the ship reaches its maximum

4 Kubo. H., Umeda. N., Yamane. K., Matsuda. A., 2012, *Pure Loss of Stability in Astern Seas: Is it Really Pure?*, Proceedings of the 6th Asia Pacific Workshop on Marine Hydrodynamics, Johor, pp. 307-312.

amplitude roll, stability increases again and the cycle starts again. Note that there was one half of the roll cycle associated with the passing of an entire wave. So, there are two waves that pass during each roll period. That means the roll period is generally equivalent to twice that of the wave period, as diagrammed in figure 4.2.

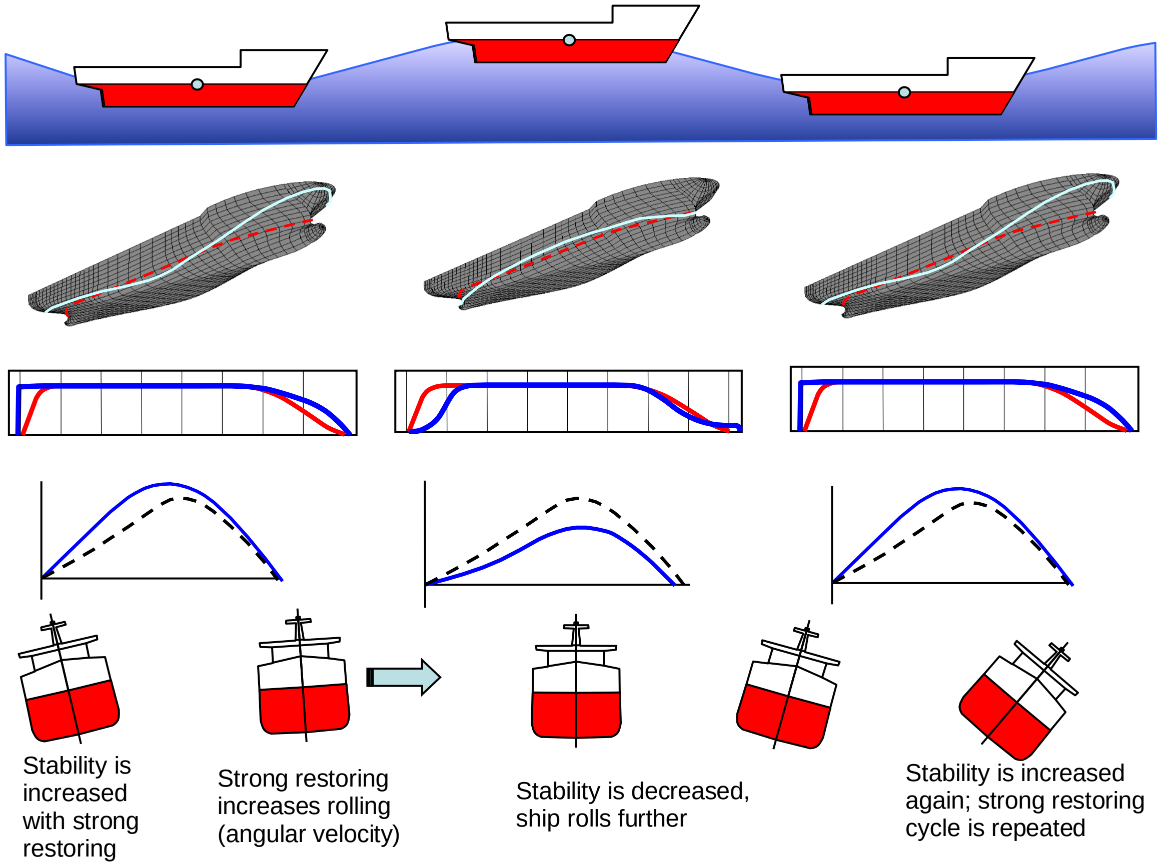

Figure 4.1 Development of parametric roll resonance

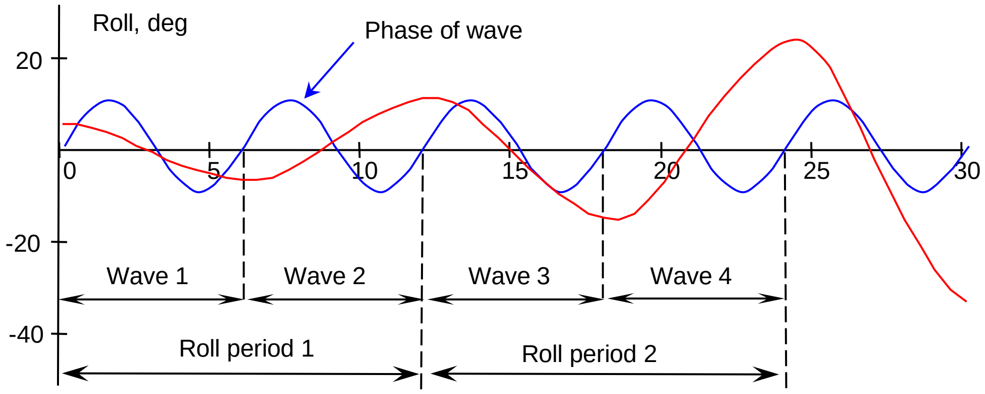

Figure 4.2 Time histories plots of parametric roll resonance

4.2 Frequency characteristics of parametric rolling

4.2.1 Parametric rolling is a resonance phenomenon and, similar to roll resonance in beam waves (see figure 4.3a), parametric rolling has a limited frequency range (see figure 4.3b). The principal difference between the two phenomena is that the span of the frequency range for parametric rolling depends on the magnitude of stability change, while the frequency range for roll resonance depends on wave height (see figure 4.3c). Also, if the beam waves are far from the resonance frequency, the ship only rolls with very small amplitude. Parametric rolling does not exist (the amplitude is equal to zero) outside of the frequency range.

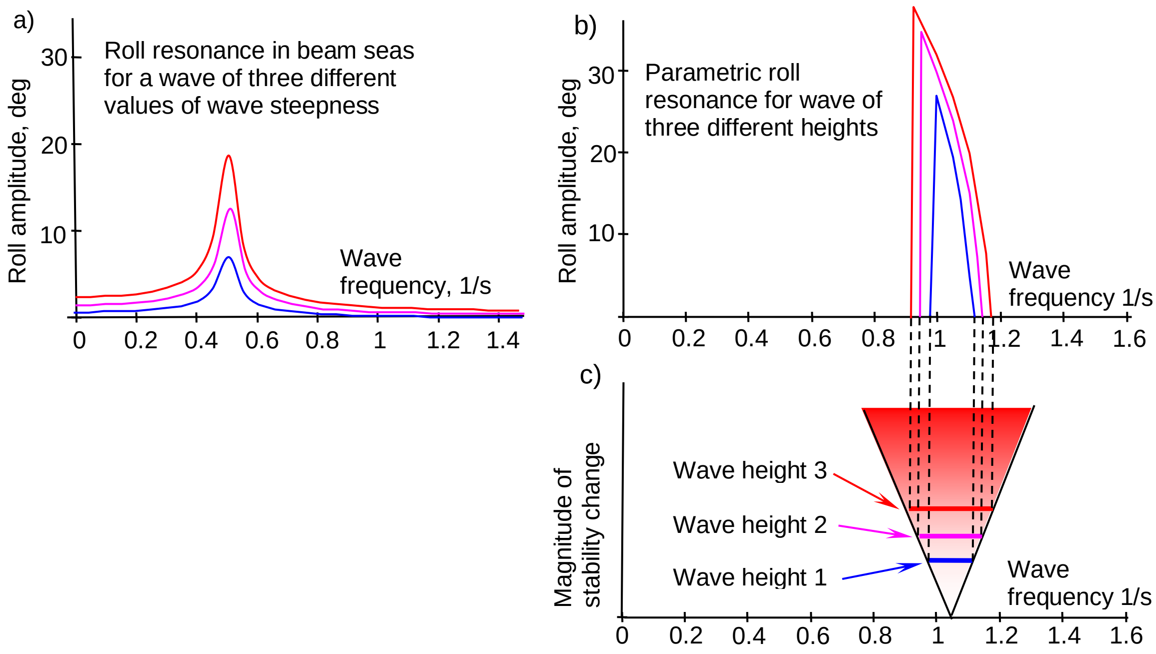

**Figure 4.3 a) roll resonance in beam seas; b) parametric roll resonance;
c) frequency range of parametric roll resonance**

4.3 Influence of roll damping

4.3.1 When a ship rolls in calm water after being disturbed, the roll amplitudes decrease successively due to roll damping (see figure 4.4). A rolling ship generates waves and eddies, and experiences frictional drag. All of these processes contribute to roll damping. Roll damping may play a critical role in the development of parametric roll resonance. If the "loss" of energy per cycle caused by damping is more than the energy "gain" caused by the changing stability in longitudinal seas, the roll angles will not increase and the parametric resonance will not develop. Once the energy "gain" per cycle is more than the energy "loss" due to damping, the amplitude of the parametric rolling starts to grow.

4.3.2 There is then a roll damping threshold for parametric roll resonance. If the roll damping moment is higher than the threshold, then parametric roll resonance is not possible. If the roll damping moment is below the threshold, then the parametric roll resonance can take place. During the parametric roll resonance, the combination of harder restoring due to the increased stability on the wave trough and larger achieved roll angles due to the decreased stability on the wave crest, which occur generally equivalent to twice during the roll period, makes the roll angle grow significantly. The only other condition that has to be met is that the energy loss due to roll damping is not large enough to completely consume the increase of energy caused by parametric roll resonance – the roll damping is below the threshold value.

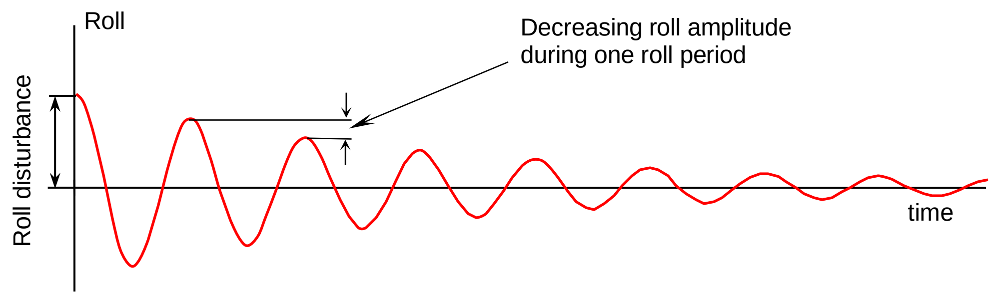

Figure 4.4 Successively decreasing roll amplitudes due to roll damping in calm water

4.4 Influence of speed and wave direction

4.4.1 The frequency of encounter with waves changes when a ship is in motion. When a ship is sailing in following or stern-quartering seas, the direction of waves and the ship heading are similar (see figure 4.5a). As a result, the relative speed is small and a ship encounters fewer waves during the same time period (compared to a zero-speed case). The encounter period is increased (and the encounter frequency is decreased) in following or stern-quartering waves.

4.4.2 When a ship is sailing in head or bow-quartering seas, the direction of waves and the ship heading are opposite (see figure 4.5b). As a result, the relative speed is large and a ship encounters more waves during the same time (compared with the zero-speed case). The encounter period is decreased (and the encounter frequency is increased) in head or bow-quartering waves.

4.4.3 The inception of parametric rolling depends on the frequency of encounter being in the frequency range where the parametric rolling is possible (see figure 4.3c). Therefore, the development of parametric rolling depends on speed and heading.

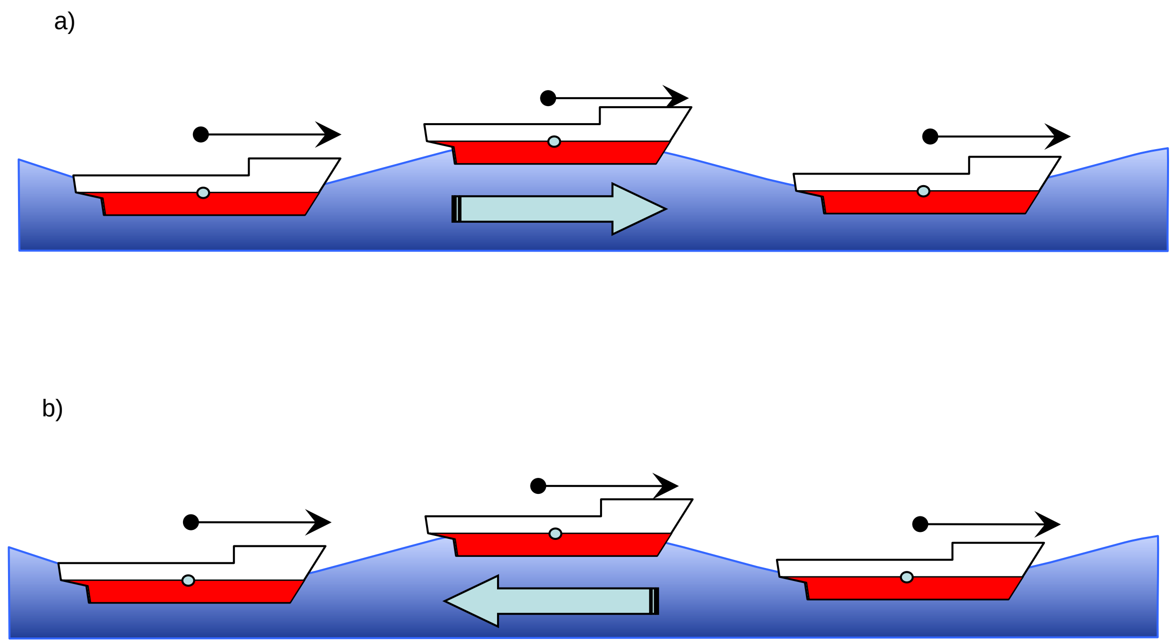

Figure 4.5 Influence of speed and wave direction on parametric resonance: a) following and stern-quartering seas: the encounter period is longer than the wave period; and b) head and bow-quartering seas: the encounter period is shorter than the wave period

5 Physical background of surf-riding and broaching

5.1 General description of surf-riding/broaching failure mode

5.1.1 Broaching (a shortening of "broaching-to") is a violent uncontrollable turn that occurs despite maximum steering efforts to maintain course. As with any other sharp turn event, broaching is accompanied by a large heel angle, which has the potential effect of a partial or total stability failure. Broaching is usually preceded by surf-riding, which occurs when a wave, approaching from the stern, "captures" a ship and accelerates the ship to the speed of the wave (i.e. the wave celerity). Surf-riding is a single wave event in which the wave profile does not vary relative to the ship. Because most ships are directionally unstable in the surf-riding condition, this manoeuvring yaw instability could lead to an uncontrollable turn – termed "broaching."

5.1.2 Because surf-riding usually precedes broaching, the likelihood of surf-riding occurrence can be used to formulate vulnerability criteria for broaching. In order for surf-riding to occur, several conditions need to be satisfied:

.1 the wavelength should be comparable to the ship length or larger;

.2 the wave should be sufficiently steep to produce sufficient wave surfing force; and

.3 the ship speed and course should be comparable to the wave celerity and direction, respectively.

5.1.3 When a ship proceeds in following waves, three main forces act in the axial direction. Thrust is the force produced by the ship's propulsor to propel the ship forward. Resistance (or drag) is the force that opposes the forward ship motion. The surging wave force is the force imparted by a wave to either push the ship forward or back depending on whether the ship is on the face or back of a wave, respectively. These forces are represented in figure 5.1.

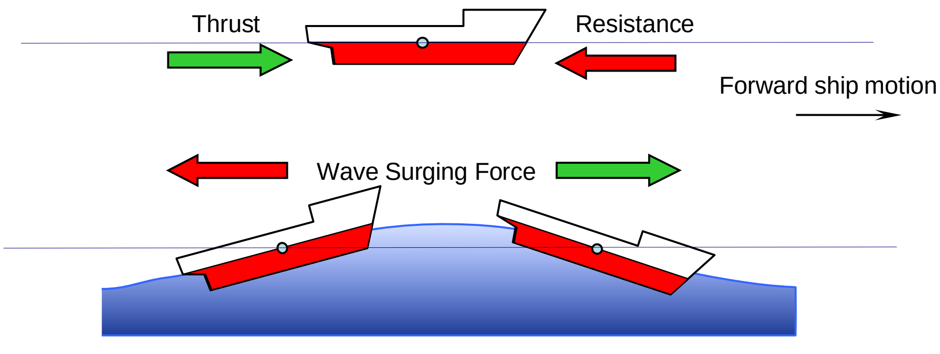

Figure 5.1 Forces acting on a ship in following waves

5.1.4 When a surging wave force is present, three conditions are possible in periodic waves:

.1 *Surging motion*. This condition occurs when the wave surge force is insufficient to overcome the difference between the thrust of the ship's propulsor and the resistance of the ship at the wave celerity. In this case, the ship oscillates from increasing speed when on the front side of the wave to decreasing speed when on the back side of the wave – an oscillatory motion.

5.1.5 The other two conditions involve the two ship speed thresholds that can cause surf-riding and that are directly related to the thrust the ship's propulsor delivers to maintain a given speed.

.1 Surf-riding under certain initial condition (*first threshold of surf-riding).* This is the situation that the ship shall run with the wave phase speed only for certain combinations of initial ship speed and position along the wave, and in particular when the ship speed is sufficiently close to the wave celerity. Under this condition, the forward surge force of the wave at a particular point on the wave exceeds the difference between the thrust of the ship's propulsor and the resistance of the ship at the wave celerity. In this case, surf-riding could occur if the ship is sufficiently accelerated by an instantaneous external force.

.2 Surf-riding under any initial condition (*second threshold of surf-riding)*. This is the situation that the ship is forced to run with the wave irrespective of the initial ship speed. Under this condition, the ship cannot be overtaken by waves so that the periodic surging motion beyond one wavelength cannot exist.

5.1.6 To explain these three conditions more fully and since surf-riding occurs when the ship speed is equal to the wave celerity, locating the position of reference on the wave crest allows a convenient way to understand surf-riding. In this view, when the ship surf-rides, it appears to remain stationary because the reference position moves with the wave.

5.1.7 In the case of surging motion, the thrust delivered by the ship's propulsor is not sufficient to propel the ship to a speed equal to the wave celerity in calm water, which is depicted in figure 5.2a. Figure 5.2b shows the difference between the thrust and resistance in calm water for the ship located at different positions on a wave; this difference is negative when the resistance is greater than the thrust. Because there is no position on the wave in which the thrust – resistance difference is fully compensated by wave force, the only motion occurring is surging forward and backward depending on the ship's position on the wave.

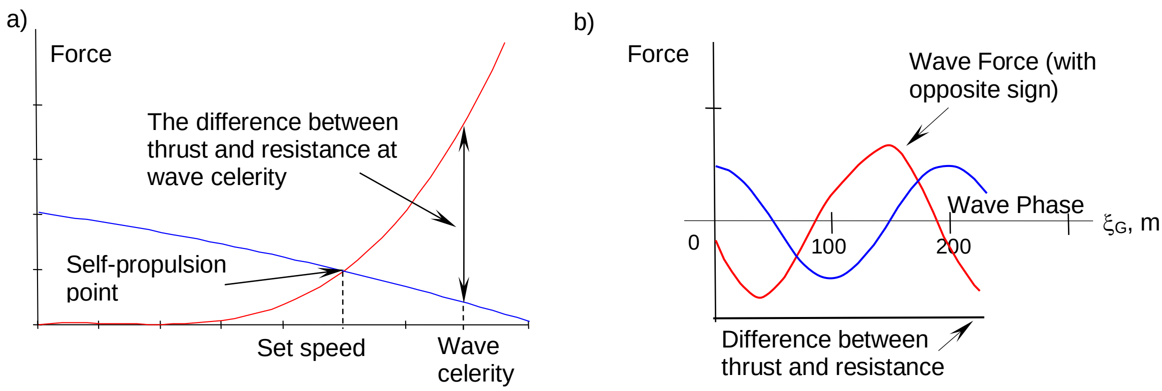

Figure 5.2 a) resistance and propulsion showing self-propulsion point and thrust-resistance difference, and b) wave forces and balance between thrust and resistance shown for different ship positions on a wave

5.1.8 The mechanics of surging can be illustrated using the curves of thrust and resistance as shown in figure 5.3. When the ship is on the back side of the wave, the surging force pushes the ship backwards, which causes the instantaneous speed to decrease and the resistance to become less than the thrust. This difference is directed forward, against the surging force. When the ship is on the face of the wave, the surging force pushes the ship forward causing the instantaneous speed to increase and the resistance to exceed the thrust. As the wave passes the ship, these two conditions recur.

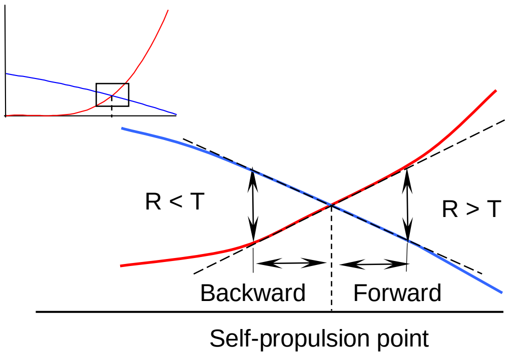

Figure 5.3 Small surging motions around self-propulsion point

5.2 Description of surf-riding equilibrium

5.2.1 The value of the wave force depends on the location of the ship on the wave as well as the wave height and wavelength. The face of the wave pushes a ship forward – hence, the forward wave or surge force; while the back slope does the opposite. Indeed, there are neutral points near the wave crest and wave trough. If the wave has appropriate length and height, the surge force is sufficient to offset the negative difference between the thrust and resistance. This creates two points of equilibrium as shown in figure 5.4. This figure superimposes the surge force with the difference between thrust and resistance (the horizontal line below the abscissa) and shows the intersections with the wave force curve to mark the two points of equilibrium on the wave. The stable equilibrium marks the first threshold of surf-riding.

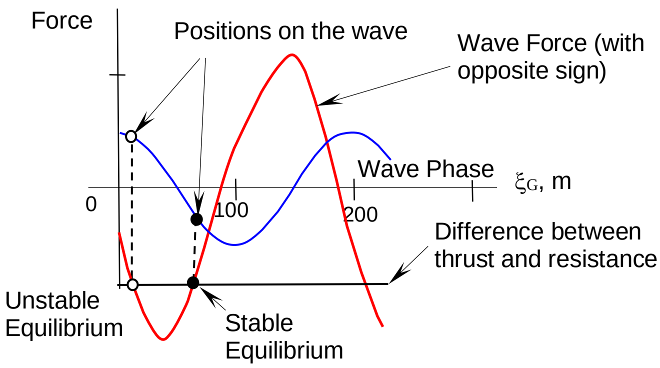

Figure 5.4 Wave forces and balance between thrust and resistance for different positions of a ship on a wave showing the first threshold of surf-riding

5.3 Stability of surf-riding equilibrium

5.3.1 Figure 5.5 provides an example of the two points of equilibrium referred to as stable and unstable. If a ship is considered to be surf-riding in which midship is located about 70 m forward of the wave crest (marked as stable equilibrium near wave trough in figure 5.4 and figure 5.5), the ship speed will be equal to the wave celerity. If the ship is disturbed from this location forward and toward the wave trough, the surge force decreases. Therefore, the difference between thrust and resistance will cause a decrease in the instantaneous ship speed and the wave will start to overtake the ship. As the ship moves back on the wave face toward the wave crest, the wave surge force increases and pushes the ship back to the stable equilibrium.

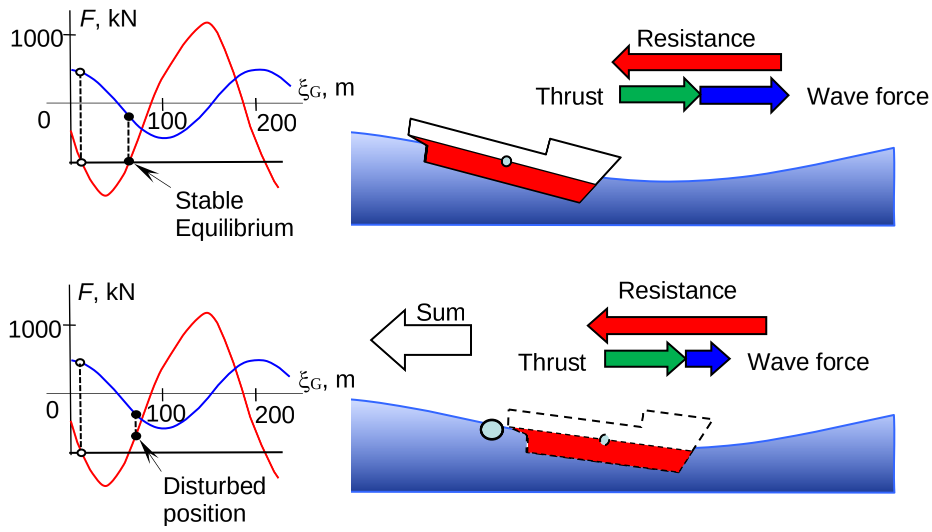

Figure 5.5 A disturbance forward from the stable equilibrium

5.3.2 Conversely to the case shown by figure 5.5, figure 5.6 considers the ship to be disturbed from the equilibrium backwards and towards the wave crest. In this case, the wave force becomes larger than the difference between thrust and resistance. Thus, the ship speed will increase and move on the wave forward to the surf-riding equilibrium (trough). Therefore, in either case (i.e. a disturbance forward or backward), the ship will tend to move toward the equilibrium near the wave trough, which makes this equilibrium stable.

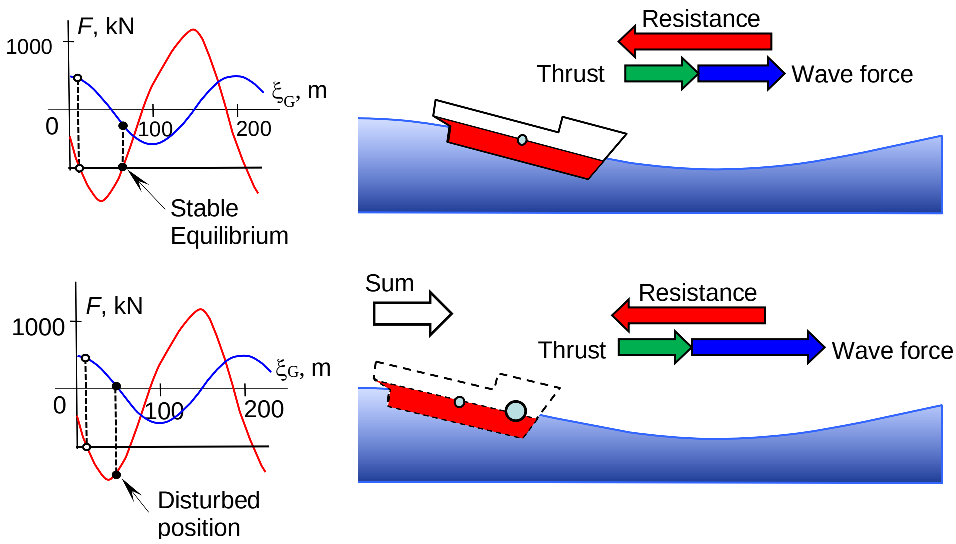

Figure 5.6 A disturbance backwards from the stable equilibrium

5.3.3 If a ship is now considered to be surf-riding with the midship located about 30 m forward of the wave crest (marked as unstable equilibria near wave crest in figure 5.4), the ship speed will be equal to the wave celerity. If the ship is disturbed from this location forward (towards the wave trough as shown in figure 5.7), the wave force increases and will cause the ship speed to increase and move the ship further forward on the wave until it arrives at the stable equilibrium near the wave trough.

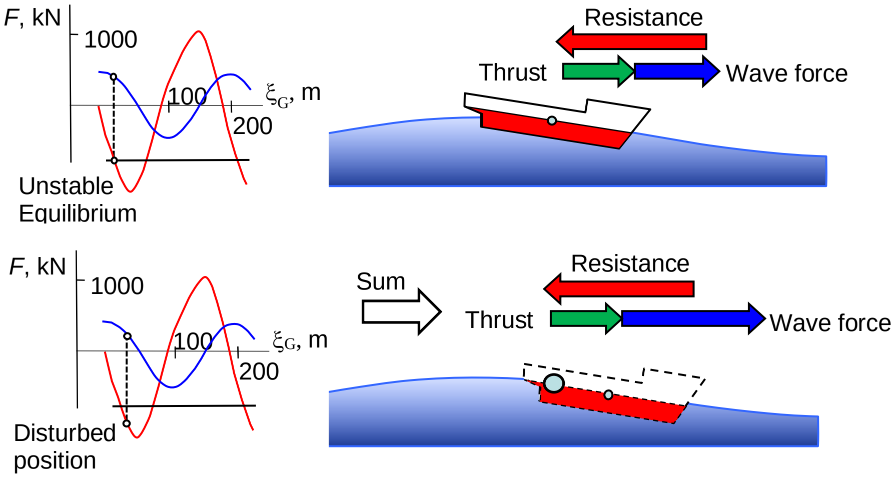

Figure 5.7 Disturbance forward from the unstable equilibrium

5.3.4 Conversely, if the ship is disturbed from this location backward, towards the wave crest as shown in figure 5.8, the wave force decreases and the instantaneous speed also starts to decrease. In this case, difference between thrust and resistance will cause a decrease in the instantaneous ship speed which causes the wave to start to overtake the ship. There are several scenarios that consider what may happen next, but in no case does the ship return back to this equilibrium, which makes the equilibrium near the wave crest unstable.

5.3.5 If there is no surf-riding equilibrium, surf-riding is not possible and the ship will simply surge. That means that all the combinations of instantaneous speed and position on the wave lead to the same outcome. However, once points of equilibrium appear at certain positions on the wave, not all the combinations of the wave position and instantaneous speed lead to the same response. If a ship is "placed" exactly at the location of the stable equilibrium near the wave trough and accelerated to the wave celerity, the ship will surf-ride. Any small disturbance from this position will return the ship back to equilibrium. If a ship is placed at the unstable equilibrium near the wave crest, accelerated to the wave celerity and then disturbed towards the wave trough, it will end up at the stable surf-riding equilibrium as well. Thus, there is a set of combinations of wave positions and instantaneous speeds that will lead to surf-riding. One can say that these combinations form a "domain of attraction to surf-riding equilibrium." Outside of this domain, two options are possible: surging or surf-riding. So, in principle, once outside of the attraction domain, the ship either continues to surge or is attracted to surf-riding equilibrium on some other wave.

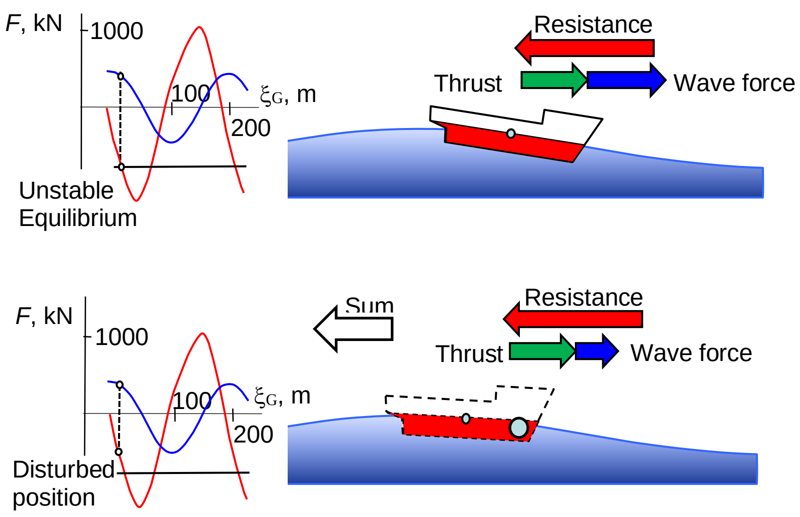

Figure 5.8 Disturbance backward from the unstable equilibrium

5.4 Transition from surging motion to surf-riding

5.4.1 When the energy/work balance of the wave surging force and the difference between thrust and resistance is considered, the latter disperses the kinetic energy obtained from the wave. When these two works are balanced, the ship's response is surging motion. However, if a wave provides the ship with more kinetic energy than the difference between thrust and resistance can disperse, this excessive kinetic energy eventually leads to acceleration and to attraction to the surf-riding equilibrium. The surf-riding becomes a new energy balance between the works of wave surging force and the difference between thrust and resistance. The ship surf-rides because of the excessive kinetic energy imparted to the ship.

5.4.2 The face of the wave provides more chances for surf-riding because the wave surging force is directed forward. If the ship is on the back side of the wave, the wave surging force is directed backward but a surging energy balance still may occur because both surging and surf-riding may co-exist for the same speed setting and wave parameters. If the initial kinetic energy level can be dispersed by the difference between thrust and resistance, surging will occur; if not, surf-riding will occur. If the wave parameters are such that the wave adds too much kinetic energy (steep waves) to ship motions that it cannot be dispersed by the difference between thrust and resistance, then surging motions are no longer possible. Even when the ship starts with low initial kinetic energy level on the back slope of the wave with the ship's propulsor delivering a set thrust, each sequential wave will add a bit of kinetic energy that cannot be dispersed; then inevitably surf-riding will occur as the ship moves towards stable equilibrium. This is referred to as the "surf-riding under any initial condition" of surf-riding which is the basis used for the surf-riding vulnerability criteria. The "surf-riding under certain initial condition" is not used for these criteria.

5.4.3 For a particular wave, the thrust at the surf-riding under any initial condition identifies the critical setting of the ship's propulsor in the vulnerability criterion for which surf-riding becomes inevitable. For example, consider energy balance during the time that one wave overtakes the ship. The Melnikov analysis or the systematic phase plane analysis can be used to identify the surf-riding under any initial condition. The level 2 vulnerability criterion directly uses the Melnikov analysis for many possible combinations of wave height and wavelength.

The level 1 vulnerability criteria are empirical estimates based on many calculated results of such analysis assuming a wave steepness of 0.1, which is widely accepted as the practical limit of stable gravity deep water waves.

APPENDIX 2

EXAMPLES OF ASSESSMENTS USING VULNERABILITY CRITERIA ACCORDING TO THE SECOND GENERATION INTACT STABILITY CRITERIA

1 Example input data set

1.1 The data for a ship's loading condition that is needed to complete the assessments contained in the Second generation intact stability criteria varies and depends upon which vulnerability criteria and which levels of each are to be assessed. Table 1.1 below indicates what data for the ship and the respective loading condition is needed for the particular vulnerability assessment to be performed.

Table 1.1 – Ship and loading condition data needed for vulnerability assessments associated with each stability failure mode and level that is additional to that needed to demonstrate compliance with section 2.2 of part A of the 2008 Intact Stability Code

Stability Failure Mode	Dead Ship Condition		Pure Loss of Stability		Parametric Rolling		Surf-riding/ Broaching		Excessive Acceleration	
	Level 1	Level 2	Level 1	Level 2	Level 1	Level 2	Level 1	Level 2	Level 1	Level 2
Ship data:										
Hull form (offsets)	X	X		X		X		X		X
Hydrostatic data	X		X		X					
Bilge keel data	X	X			X	X			X	X
Hull and Cargo forms above waterline	X	X								
Loading condition data:										
Righting lever curve, calm water	X	X								
Righting lever curve, in waves				X		X				
Roll radius of gyration		X				X				X
Vertical centre of gravity	X	X	X	X	X	X			X	X
Propulsion data:										
Operational speed							X	X		
Calm-water resistance								X		
Propulsor thrust								X		

Specific examples of input values for and outcomes of assessments using vulnerability criteria for both levels 1 and 2 and for each stability failure mode is presented in sections 2 through 6.

1.2 Input Data

One subject ship is the C11 class post-Panamax containership. The input was based on the data made available to the Intact Stability Correspondence Group (ISCG) presented by ITTC and available at (http://www.naoe.eng.osaka-u.ac.jp/imo/ssdp1.htm). The hull form is in figure 1.1, while principal dimensions, basic hydrostatic table, and relevant input parameters are in table 1.2. Note that the KG value adjusted to account for the free-surface correction, which results in an upright GM = 1.40 m. The GZ curve is shown in figure 1.2.

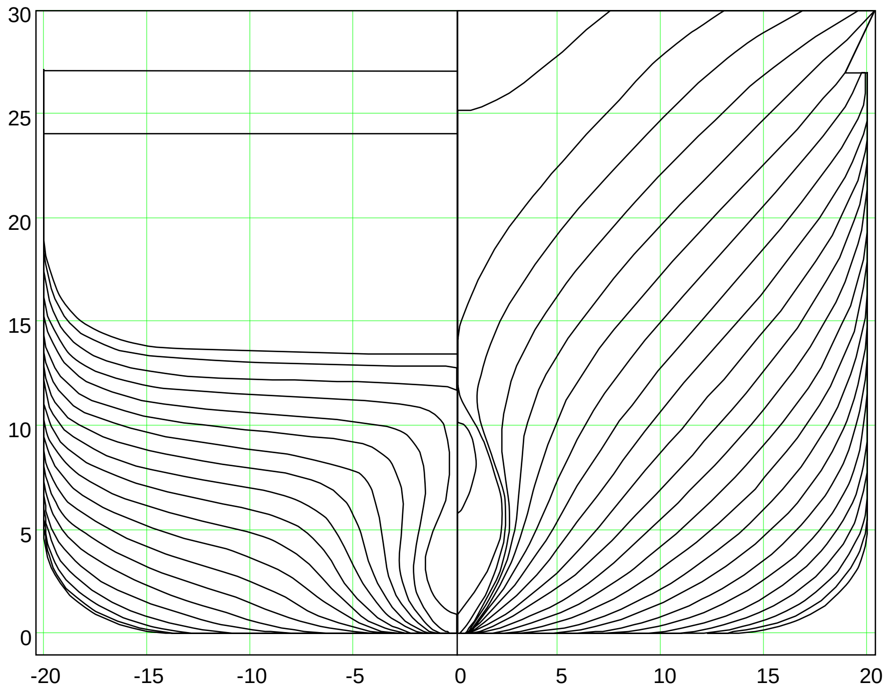

Figure 1.1 Hull form of C11 class containership

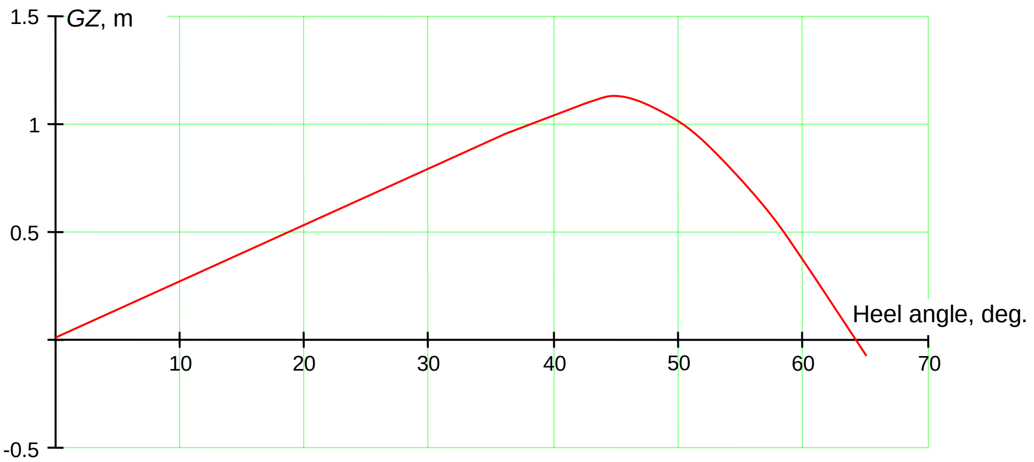

Figure 1.2 *GZ* curve computed for a *KG* corresponding to a *GM* = 1.4 m

Table 1.2 Principal dimensions, basic hydrostatic data and other relevant input parameters

Length, bp, m	262.00	Bilge keel length ratio (l_{BK}/L_{bp})		0.2921
Beam, m	40.00	Bilge keel height ratio (h_{BK}/B)		0.010
Draught amidships, m	11.50	Down flooding angle, °		50
Trim, °	0.0	Lateral windage area, m^2		7,887
KG, m	18.976	Height of centroid above WL, m		14.73
Volumetric displacement, m^3	67,504	Wind heeling moment coefficient		1.17
Block coefficient	0.56	Natural roll period, s		30.35
Midship section coefficient	0.959	Natural frequency, s^{-1}		0.21
GM, m	1.40	Number of propellers		1
Diameter of propeller, m	8.4	Propeller expanded area ratio		0.590
Propeller pitch ratio	0.743	Propeller number of blades		6
Location of excessive acceleration assessment		x = -50 m	y = 20 m	z = 40 m

2 Example of assessment of ship vulnerability to the dead ship condition failure mode

2.1 The subject ship used here is the C11 class containership.

2.2 The subject ship used in this section (section 2) is slightly different from the one in the sections 4 and 5. There are two differences: First, the natural roll frequency is normally computed by approximation formula from the 2008 Intact Stability Code. In this section, direct calculation was used. As a result, the period of roll used here is 30 s (table 1.2) while 23 s was used in the 2008 Intact Stability Code. The second difference is the GM value adjustment priority.[5]

2.3 A level 1 vulnerability assessment in dead ship condition failure mode is described in section 2.2.2 of the Interim Guidelines. This assessment is essentially the weather criterion with the table of roll periods extended to 30 s. With this change in mind, one gets the following results:

- Area a = 0.0428
- Area b = 0.389
- Angle of heel under action of steady wind = 4.90 degrees
- Angle of roll to windward due to wave action = 13.46 degrees
- effective slope coefficient r =1.12

These results clearly indicate that the subject ship is not vulnerable to a stability failure in the dead ship condition.

2.4 A level 2 vulnerability assessment for stability failure in the dead ship condition is described in section 2.2.3 of the Interim Guidelines. The effective wave slope function is calculated with the standard methodology described in paragraph 2.2.3.2.5 of the Interim Guidelines and section 8.2 of the appendix 3. The obtained value is 0.723, which is compared with the direct Froude-Krylov calculation, which is based on paragraph 8.1.1.4 of appendix 3, and the weather criterion as shown in figure 2.1. The roll damping coefficient was calculated by the methods of 9.2 of appendix 3 as the effective linear roll damping coefficient as a function

5 There could be some difference between GM computed from the moment of inertia of the waterplane area and the value evaluated from the GZ curve. The GZ curves were adjusted so as to match the GM obtained from waterplane calculations. In this section, the KG was adjusted to produce the desirable GM as assessed by the GZ curve.

of the roll amplitude and then linear and cubic damping coefficients by the method of paragraph 9.3.7 of appendix 3 are used for the stochastic linearization specified in paragraph 9.3.5 of appendix 3.

Figure 2.1 Effective wave coefficient function for the C11 class containership

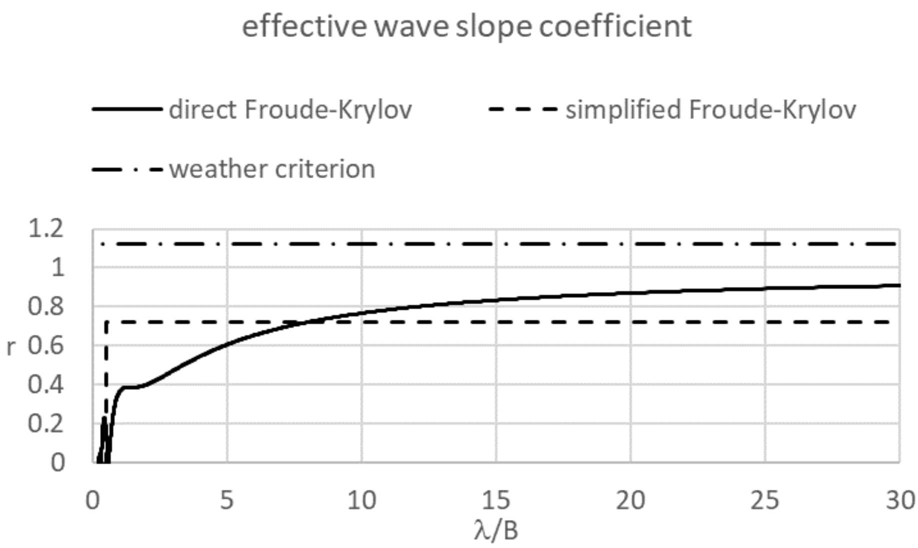

2.5 The product of the short-term failure index, which can be calculated with paragraph 2.2.3.2.1 of the Interim Guidelines, and the weighted factor of short-term environmental condition, which is available in section 2.7.2 of the Interim Guidelines, for each short-term environmental condition, $W_iC_{s,i}$, is shown in table 2.1 for checking the calculation results.

Table 2.1 The value of W_iC_{si} as the function of the significant wave height and mean zero crossing wave period

		Tz(s)																	
		1.5	2.5	3.5	4.5	5.5	6.5	7.5	8.5	9.5	10.5	11.5	12.5	13.5	14.5	15.5	16.5	17.5	18.5
	0.5	0	0	0	0	0	0	0	0	0	0	0	0	0	0	0	0	0	0
	1.5	0	0	0	0	0	0	0	0	0	0	0	0	0	0	0	0	0	0
	2.5	0	0	0	0	0	0	0	0	0	0	0	0	0	0	0	0	0	0
	3.5	0	0	0	1.95E-20	0	0	0	0	0	0	0	0	0	0	0	0	0	0
	4.5	0	0	0	0	1.26E-16	0	0	0	0	0	0	0	0	0	0	0	0	0
	5.5	0	0	0	0	2.53E-12	8.83E-15	5.53E-19	0	0	0	0	0	0	0	0	0	0	0
	6.5	0	0	0	0	3.7E-10	2.9E-11	9.92E-14	3.3E-17	0	0	0	0	0	0	0	0	0	0
	7.5	0	0	0	0	0	2.53E-09	1.05E-10	5.68E-13	8.87E-16	7.81E-19	0	0	0	0	0	0	0	0
Hs(m)	8.5	0	0	0	0	0	3.69E-08	9.07E-09	3.43E-10	4.01E-12	3.3E-14	5.5E-16	3.35E-17	4.57E-18	6.15E-19	5.6E-20	2.44E-21	0	0
	9.5	0	0	0	0	0	1.52E-07	1.03E-07	1.5E-08	6.88E-10	2.01E-11	8.49E-13	8.04E-14	1.23E-14	1.76E-15	1.76E-16	1.11E-17	4.4E-19	1.43E-20
	10.5	0	0	0	0	0	0	3.7E-07	1.39E-07	1.71E-08	1.22E-09	9.83E-11	1.28E-11	2.21E-12	3.51E-13	4.16E-14	3.41E-15	1.88E-16	1.15E-17
	11.5	0	0	0	0	0	0	5.74E-07	5.23E-07	1.37E-07	1.96E-08	2.66E-09	4.63E-10	9.28E-11	1.66E-11	2.3E-12	2.13E-13	1.65E-14	1.96E-15
	12.5	0	0	0	0	0	0	6.03E-07	1.04E-06	4.96E-07	1.26E-07	2.61E-08	5.94E-09	1.38E-09	2.81E-10	4.44E-11	4.89E-12	3.9E-13	0
	13.5	0	0	0	0	0	0	0	1.28E-06	1.16E-06	4.97E-07	1.58E-07	4.72E-08	1.33E-08	3.04E-09	5.66E-10	6.3E-11	1.12E-11	0
	14.5	0	0	0	0	0	0	0	8.36E-07	1.25E-06	9.48E-07	4.02E-07	1.49E-07	4.84E-08	1.23E-08	2.41E-09	3.43E-10	0	0
	15.5	0	0	0	0	0	0	0	0	7.19E-07	1.18E-06	6.59E-07	3.31E-07	1.15E-07	3.47E-08	5.64E-09	2.6E-09	0	0
	16.5	0	0	0	0	0	0	0	0	0	6.48E-07	6.52E-07	3.27E-07	1.74E-07	4.69E-08	2.45E-08	0	0	0

2.6 The long-term probability index is obtained by summing up the above values following paragraph 2.2.3.2 of the Interim Guidelines. The result of vulnerability assessment is as follows:

$$C = 0.0000161 < R_{DS0} = 0.06 \qquad (2.1)$$

The result of level 2 vulnerability assessment is consistent with level 1 criterion and has indicated no vulnerability of the considered ship to stability failure in the dead ship condition.

3 Example of assessment of ship vulnerability to the excessive acceleration failure mode

3.1 The subject ship is the C11 class container ship and details are shown in section 1.2. Additional data of the assessment condition required for vulnerability assessment to the excessive acceleration failure mode are shown in table 3.1. The considered location is the navigational deck, based on paragraph 2.3.1.2.

Table 3.1 Assessment condition of C11 class container ship

$h_k(\mathrm{m})$	Height of the navigational deck above the keel	48.72
$x(\mathrm{m})$	Longitudinal distance of the location where passenger or crew may be present from the aft perpendicular	177.41
$GM(\mathrm{m})$	Metacentric height without free-surface correction	8.00
$KG(\mathrm{m})$	Height of the centre of gravity above the keel	12.75

3.2 Example of level 1 vulnerability assessment to the excessive acceleration

3.2.1 Calculation for Level 1 based on section 2.3.2 of the Interim Guidelines

.1 Factor K_L, taking into account simultaneous action of roll, yaw and pitch motions:

$$x > 0.65L,\ K_L = 0.527 + 0.727x/L = 1.019 \quad (3.1)$$

.2 Natural roll period T_r based on paragraph 2.7.1.2 of the Interim Guidelines:

$$T_r = 2CB/\sqrt{GM} = 9.63\ (s) \quad (3.2)$$
$$C = 0.373 + 0.023(B/d) - 0.043(L/100) = 0.340 \quad (3.3)$$

.3 Effective wave slope coefficient r:

$$r = \frac{K_1 + K_2 + OG \cdot F}{\frac{B^2}{12C_B d} - \frac{C_B d}{2} - OG} = 0.689 \quad (3.4)$$
$$\tilde{B} = 2\pi^2 B/(gT_r^2) = 0.869 \quad (3.5)$$
$$\tilde{T} = 4\pi^2 C_B d/(gT_r^2) = 0.280 \quad (3.6)$$
$$\beta = sin(\tilde{B})/\tilde{B} = 0.879 \quad (3.7)$$
$$\tau = exp(-\tilde{T})/\tilde{T} = 2.698 \quad (3.8)$$
$$F = \beta(\tau - 1/\tilde{T}) = -0.766 \quad (3.9)$$
$$K_1 = g\beta T_r^2(\tau + \tau\tilde{T} - 1/\tilde{T})/(4\pi^2) = -2.356 \quad (3.10)$$
$$K_2 = g\beta T_r^2(\beta - cos\,\tilde{B})/(4\pi^2) = 14.479 \quad (3.11)$$

.4 Wave steepness s:

Wave steepness s is determined according to the natural roll period T_r.

$$s = 0.082 \quad (3.12)$$

.5 Non-dimensional logarithmic decrement of roll decay δ_φ based on paragraph 9.3.1 of appendix 3 and paragraph 2.5.2.1 of the Interim Guidelines:

$$\delta_\varphi = 0.5\pi R_{PR} = 0.651 \quad (3.13)$$

$$\begin{aligned} R_{PR} &= 1.87, \textit{ if the ship has a sharp bilge; otherwise,} \\ &= 0.17 + 0.425(100A_k/(LB)), \quad \textit{if} C_m \geq 0.96, \\ &= 0.17 + (10.625C_m - 9.755)(100A_k/(LB)), \quad \textit{if} 0.94 < C_m < 0.96 \end{aligned}$$

$= 0.17 + 0.2125(100A_k/(LB)),$ $\quad if C_m \leq 0.94, and$
$(100A_k/(LB))$ *should not exceed 4*

$where\, C_m \geq 0.96,$

$$R_{PR} = 0.17 + 0.425(100A_k/(LB)) = 0.414 \qquad (3.14)$$

.6 Roll amplitude φ :

$$\varphi = 4.43rs/\delta_\varphi^{0.5} = 0.311(rad) \qquad (3.15)$$

.7 Lateral acceleration:

$$\varphi K_L(g + 4\pi^2 h_r T_r^2) = 8.048\ (m/s^2)\ > R_{EA1} = 4.64\ (m/s^2) \qquad (3.16)$$

Height above the roll axis to the navigational deck

$$h_r = h_k - (KG + d)/2 = 36.59(m) \qquad (3.17)$$

Thus, this loading condition is possibly vulnerable to excessive accelerations.

3.3 Example of level 2 vulnerability assessment to the excessive accelerations

3.3.1 In level 2 vulnerability assessment for the excessive acceleration, simplified 1 degree of freedom model is adopted for the amplitude of roll. For the calculation of the roll response, the equivalent linear roll damping coefficient can be defined at the 15 degree of roll amplitude, which is based on paragraph .9.3.8 of appendix 3, figure 3.1 shows the non-dimensional roll damping coefficient $\hat{B}_{44}$ at the 15 degree of roll amplitude calculated by Ikeda's simplified formula, which is based on section 9.2 and paragraph 9.3.2 of appendix 3.

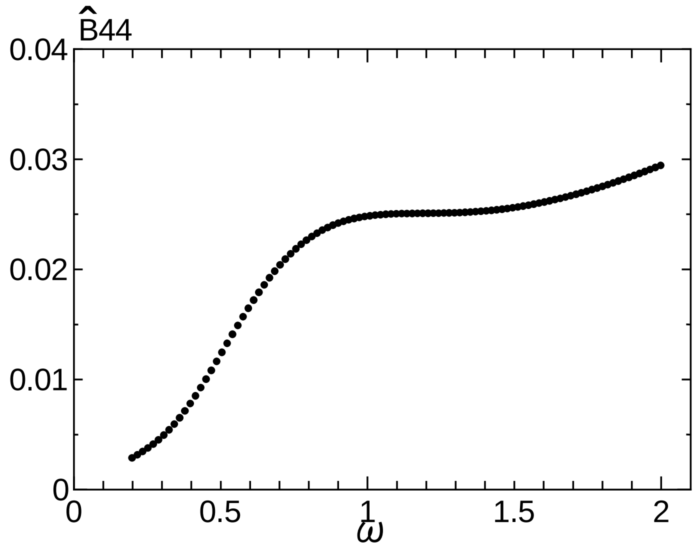

Figure 3.1 Non-dimensional roll damping coefficient $\hat{B}_{44}$(φ_a=15deg.)

3.3.2 Froude-Krylov roll moment is calculated using the effective wave slope coefficient, based on section 8.3 of appendix 3, as shown in figure 3.2.

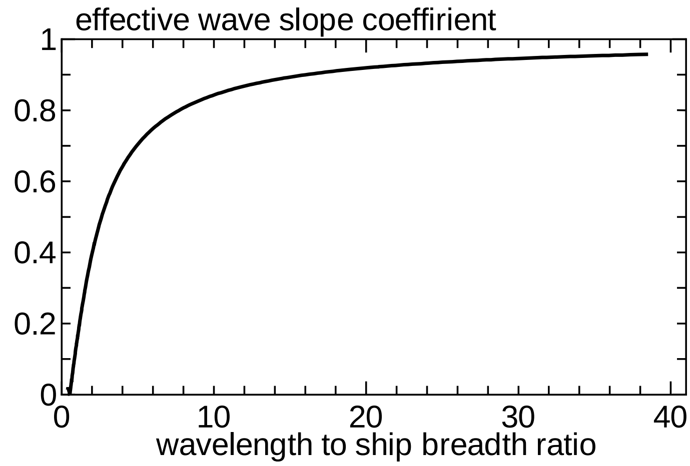

Figure 3.2 Effective wave slope coefficient

3.3.3 The lateral acceleration is calculated taking into account roll motion and vertical acceleration. The standard deviation of lateral acceleration at zero speed and in beam seaway σ_{LAi} is obtained using the frequency spectrum of the seaway and reduction factor 0.75 for influence of short-crestedness, based on paragraph 2.3.3.2.2 of the Interim Guidelines. The considered wave scattering diagram is table 2.7.2.1.2 of the Interim Guidelines. Table 3.2 shows the standard deviation of lateral acceleration σ_{LAi} for each wave condition.

Table 3.2 Standard deviation of lateral acceleration σ_{LAi}

σ_{LAi}	average zero-crossing period Tz (s)																	
Hs(m)	1.5	2.5	3.5	4.5	5.5	6.5	7.5	8.5	9.5	10.5	11.5	12.5	13.5	14.5	15.5	16.5	17.5	18.5
0.5	0.0005	0.0145	0.0528	0.1081	0.1851	0.2333	0.2395	0.2229	0.1987	0.1742	0.1520	0.1327	0.1164	0.1026	0.0910	0.0811	0.0726	0.0654
1.5	0.0016	0.0434	0.1585	0.3243	0.5553	0.6999	0.7184	0.6686	0.5961	0.5225	0.4559	0.3982	0.3493	0.3078	0.2729	0.2432	0.2179	0.1962
2.5	0.0027	0.0724	0.2642	0.5406	0.9255	1.1666	1.1975	1.1145	0.9935	0.8709	0.7598	0.6637	0.5821	0.5130	0.4548	0.4053	0.3632	0.3270
3.5	0.0038	0.1013	0.3699	0.7569	1.2958	1.6331	1.6763	1.5601	1.3910	1.2194	1.0640	0.9292	0.8149	0.7183	0.6366	0.5674	0.5083	0.4578
4.5	0.0049	0.1303	0.4756	0.9731	1.6658	2.0998	2.1552	2.0057	1.7883	1.5675	1.3678	1.1946	1.0479	0.9235	0.8185	0.7295	0.6536	0.5886
5.5	0.0060	0.1592	0.5812	1.1895	2.0362	2.5663	2.6342	2.4515	2.1856	1.9160	1.6715	1.4601	1.2806	1.1287	1.0005	0.8916	0.7989	0.7194
6.5	0.0071	0.1882	0.6869	1.4057	2.4062	3.0330	3.1130	2.8972	2.5830	2.2643	1.9756	1.7257	1.5133	1.3338	1.1824	1.0536	0.9441	0.8501
7.5	0.0082	0.2171	0.7926	1.6217	2.7765	3.5000	3.5917	3.3437	2.9804	2.6127	2.2795	1.9912	1.7461	1.5392	1.3642	1.2157	1.0895	0.9809
8.5	0.0093	0.2461	0.8983	1.8382	3.1467	3.9661	4.0706	3.7881	3.3779	2.9609	2.5834	2.2568	1.9791	1.7444	1.5463	1.3780	1.2345	1.1118
9.5	0.0104	0.2750	1.0040	2.0543	3.5171	4.4328	4.5497	4.2344	3.7749	3.3091	2.8874	2.5221	2.2118	1.9496	1.7280	1.5401	1.3799	1.2426
10.5	0.0115	0.3040	1.1095	2.2707	3.8872	4.8990	5.0289	4.6797	4.1725	3.6579	3.1906	2.7877	2.4446	2.1548	1.9100	1.7021	1.5251	1.3733
11.5	0.0126	0.3330	1.2153	2.4870	4.2568	5.3656	5.5082	5.1254	4.5706	4.0062	3.4957	3.0532	2.6775	2.3601	2.0919	1.8644	1.6703	1.5040
12.5	0.0137	0.3619	1.3210	2.7031	4.6271	5.8327	5.9867	5.5714	4.9679	4.3543	3.7987	3.3181	2.9103	2.5653	2.2738	2.0263	1.8155	1.6349
13.5	0.0148	0.3909	1.4265	2.9194	4.9980	6.2992	6.4653	6.0175	5.3647	4.7032	4.1037	3.5847	3.1431	2.7706	2.4556	2.1886	1.9609	1.7658
14.5	0.0159	0.4198	1.5323	3.1356	5.3675	6.7654	6.9448	6.4630	5.7619	5.0507	4.4068	3.8497	3.3764	2.9757	2.6374	2.3505	2.1062	1.8966
15.5	0.0170	0.4488	1.6380	3.3526	5.7385	7.2326	7.4236	6.9087	6.1595	5.3991	4.7106	4.1146	3.6083	3.1812	2.8194	2.5128	2.2514	2.0273
16.5	0.0181	0.4777	1.7438	3.5679	6.1082	7.6987	7.9025	7.3546	6.5574	5.7480	5.0150	4.3806	3.8419	3.3867	3.0013	2.6749	2.3967	2.1580

3.3.4 The short-term excessive acceleration failure index $C_{s,i}$, which is the probability that the ship will exceed a specified lateral acceleration, is calculated using the standard deviation of lateral acceleration σ_{LAi}, based on paragraph 2.3.3.2.1 of the Interim Guidelines. The long-term probability index C is calculated as a weighted average by weighting factor for the short-term condition W_i, and $C_{s,i}$, based on paragraph 2.3.3.2 of the Interim Guidelines. Table 3.3 shows the value of $W_i C_{s,i}$ for each wave condition.

Table 3.3 The value of $W_i C_{s,i}$ for each wave condition

$W_i C_{s,i}$	average zero-crossing period Tz (s)																	
Hs(m)	1.5	2.5	3.5	4.5	5.5	6.5	7.5	8.5	9.5	10.5	11.5	12.5	13.5	14.5	15.5	16.5	17.5	18.5
0.5	0.00E+00	0.00E+00	0.00E+00	0.00E+00	0.00E+00	0.00E+00	0.00E+00	0.00E+00	0.00E+00	0.00E+00	0.00E+00	0.00E+00	0.00E+00	0.00E+00	0.00E+00	0.00E+00	0.00E+00	0.00E+00
1.5	0.00E+00	0.00E+00	0.00E+00	7.21E-203	1.67E-70	1.09E-44	2.50E-42	9.93E-49	3.67E-61	2.04E-79	4.60E-104	5.22E-136	2.36E-176	2.42E-226	1.96E-287	0.00E+00	0.00E+00	0.00E+00
2.5	0.00E+00	0.00E+00	0.00E+00	6.97E-77	7.91E-28	9.48E-18	1.65E-16	1.10E-18	3.27E-23	5.78E-30	4.11E-39	5.87E-51	7.03E-66	2.59E-84	9.69E-107	1.19E-133	0.00E+00	0.00E+00
3.5	0.00E+00	0.00E+00	0.00E+00	6.64E-43	1.25E-16	1.02E-10	1.18E-09	1.47E-10	8.05E-13	2.48E-16	3.80E-21	2.12E-27	2.86E-35	5.71E-45	9.67E-57	7.35E-71	1.38E-87	0.00E+00
4.5	0.00E+00	0.00E+00	0.00E+00	0.00E+00	1.77E-12	3.57E-08	4.29E-07	2.10E-07	1.13E-08	8.41E-11	8.59E-14	1.04E-17	1.20E-22	1.00E-28	4.46E-36	7.02E-45	2.43E-55	0.00E+00
5.5	0.00E+00	0.00E+00	0.00E+00	0.00E+00	9.10E-11	3.42E-07	4.85E-06	5.34E-06	1.00E-06	4.07E-08	3.74E-10	7.33E-13	2.72E-16	1.62E-20	1.28E-25	1.09E-31	7.20E-39	4.13E-47
6.5	0.00E+00	0.00E+00	0.00E+00	0.00E+00	4.92E-10	6.74E-07	1.17E-05	2.24E-05	9.28E-06	1.07E-06	3.65E-08	3.72E-10	1.06E-12	7.62E-16	1.23E-19	3.78E-24	1.80E-29	1.22E-35
7.5	0.00E+00	0.00E+00	0.00E+00	0.00E+00	0.00E+00	5.90E-07	1.25E-05	3.64E-05	2.64E-05	6.10E-06	4.99E-07	1.48E-08	1.57E-10	5.55E-13	6.03E-16	1.83E-19	1.47E-23	1.92E-28
8.5	0.00E+00	0.00E+00	0.00E+00	0.00E+00	0.00E+00	3.29E-07	8.44E-06	3.43E-05	3.77E-05	1.45E-05	2.20E-06	1.38E-07	3.58E-09	3.76E-11	1.52E-13	2.17E-16	9.75E-20	1.24E-23
9.5	0.00E+00	0.00E+00	0.00E+00	0.00E+00	0.00E+00	1.73E-07	4.21E-06	2.27E-05	3.48E-05	1.98E-05	4.74E-06	5.15E-07	2.59E-08	5.95E-10	6.12E-12	2.63E-14	4.23E-17	2.91E-20
10.5	0.00E+00	0.00E+00	0.00E+00	0.00E+00	0.00E+00	0.00E+00	1.79E-06	1.19E-05	2.39E-05	1.85E-05	6.36E-06	1.05E-06	8.70E-08	3.60E-09	7.47E-11	7.36E-13	3.11E-15	8.31E-18
11.5	0.00E+00	0.00E+00	0.00E+00	0.00E+00	0.00E+00	0.00E+00	6.14E-07	5.29E-06	1.33E-05	1.33E-05	6.11E-06	1.42E-06	1.73E-07	1.13E-08	4.02E-10	6.80E-12	6.47E-14	5.79E-16
12.5	0.00E+00	0.00E+00	0.00E+00	0.00E+00	0.00E+00	0.00E+00	2.61E-07	2.12E-06	6.26E-06	7.83E-06	4.56E-06	1.39E-06	2.32E-07	2.20E-08	1.18E-09	3.26E-11	4.58E-13	0.00E+00
13.5	0.00E+00	0.00E+00	0.00E+00	0.00E+00	0.00E+00	0.00E+00	0.00E+00	7.94E-07	2.63E-06	3.97E-06	2.87E-06	1.09E-06	2.38E-07	3.03E-08	2.40E-09	8.67E-11	3.67E-12	0.00E+00
14.5	0.00E+00	0.00E+00	0.00E+00	0.00E+00	0.00E+00	0.00E+00	0.00E+00	3.16E-07	9.39E-07	1.82E-06	1.51E-06	7.00E-07	1.91E-07	3.06E-08	2.97E-09	1.65E-10	0.00E+00	0.00E+00
15.5	0.00E+00	0.00E+00	0.00E+00	0.00E+00	0.00E+00	0.00E+00	0.00E+00	0.00E+00	2.81E-07	7.68E-07	6.86E-07	4.08E-07	1.24E-07	2.58E-08	2.35E-09	4.90E-10	0.00E+00	0.00E+00
16.5	0.00E+00	0.00E+00	0.00E+00	0.00E+00	0.00E+00	0.00E+00	0.00E+00	0.00E+00	0.00E+00	2.33E-07	2.95E-07	1.63E-07	7.67E-08	1.51E-08	4.79E-09	0.00E+00	0.00E+00	0.00E+00

3.3.5 Based on paragraph 2.3.3.1 of the Interim Guidelines, the result of level 2 vulnerability assessment to excessive acceleration is as follows:

$$C = \sum_{i=1}^{N} W_i C_{s,i} = 0.00047 > R_{EA2} = 0.00039 \quad (3.18)$$

Thus, this loading condition is possibly vulnerable to excessive accelerations.

4 Example of assessment of ship vulnerability to the pure loss of stability failure mode

4.1 As an example, the following data of a containership at the full load condition are used:

L_{BP}	*262.0 m*	*ship length between perpendiculars*
L	*262.0m*	*ship length defined in 2008 Intact Stability Code*
B	*40.0 m*	*moulded ship breadth*
D	*24.45 m*	*moulded ship depth*
d	*11.5 m*	*moulded mean ship draught*
τ	*0 m*	*initial trim*
LCG	*125.52 m*	*longitudinal centre of gravity from aft perpendicular*
C_B	*0.559*	*block coefficient*
GM	*1.965 m*	*metacentric height with free surface correction*
VCG	*18.4 m*	*vertical centre of gravity above baseline*
KB	*6.54 m*	*vertical centre of buoyancy above baseline*
Vs	*12.165 m/s*	*ship service speed*

4.2 Level 1 based on section 2.4.2 of the Interim Guidelines

4.2.1 Firstly, the Froude number, Fn, is calculated.

$$F_n = V_s/\sqrt{gL} = 12.165/\sqrt{9.81 \times 262} = 0.240 \quad (4.1)$$

Thus, the criteria for pure loss of stability should be applied to the ship.

4.2.2 Secondly, the lower draught is calculated:

$$\delta d_L = Min\{d - 0.25 d_{full}, LS_w/2\} = Min\{0.75 \text{ x } 11.5, 262 \text{ x } 0.0334/2\} = Min\{8.625, 4.3754\} = 4.3754 \text{ m} \quad (4.2)$$

$$d_L = d - \delta d_L = 11.5 - 4.3754 = 7.125 \text{ m} \quad (4.3)$$

so that, according to the hydrostatic data as shown in Figure4.1, the relevant I_L is 665,500m^4.

4.2.3 Thirdly, GM_{min} is calculated as follows:

$$GM_{min} = KB + (I_L/V) - VCG = KB + (I_L/(C_B \text{ x } L_{BP} \text{ x } B \text{ x } d) - VCG = 6.54 + (665{,}500/(0.559 \text{ x } 262 \text{ x } 40 \text{ x } 11.5) - 18.4 = -1.982 \text{ m} \quad (4.4)$$

Therefore, GM_{min}(= -1.982) < R_{LA}(= 0.05) so that the ship is judged as possibly vulnerable to pure loss of stability.

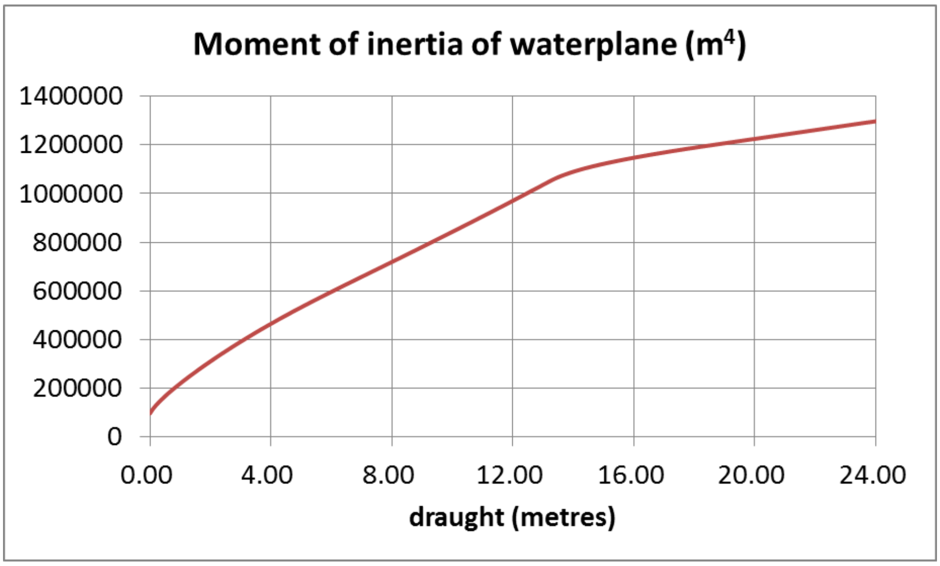

Figure 4.1 Relationship between draught and the moment of inertia of the waterplane for the sample ship

4.3 Level 2 based on section 2.4.3 of the Interim Guidelines

4.3.1 Firstly, GZ curves for the ship with the wave steepness ranging from 0 to 0.1 are calculated. Examples are shown in figure 4.2.

4.3.2 Secondly, criteria 1 and 2 are applied to the ship. The results are as follows:

CR_1 = 0.000, where the critical wave steepness for the angle of vanishing stability of 30 degrees is 0.07291.

CR_2 = 0.003821, where the critical wave steepness for the angle of heel of 25 degrees is 0.03941.

Thus: $Max\{CR_1,CR_2\} = 0.003821$. (4.5)

Since this is smaller than 0.06, the ship is not judged as vulnerable to pure loss of stability.

4.3.3 Figure 4.2 shows the GZ curves in waves at wave crest amidships under different wave steepness. In case of a wave steepness of 0.04, the GM in waves is almost zero. On the other hand, the level 1 criterion uses the wave steepness of 0.0334. Thus, this figure indicates the possibility of negative GM for the ship exists as the level 1 criterion suggests with some margin. The level 2 criterion explains that, if the ship meets a certain wave crest, significant heel could occur under the riding on crest situation where the ship is slowly overtaken by a wave crest. However, the level 2 criterion also indicates that the ship rarely meets such waves, even in the North Atlantic. This is a physical explanation based on the vulnerability criteria for the pure loss of stability failure of the ship.

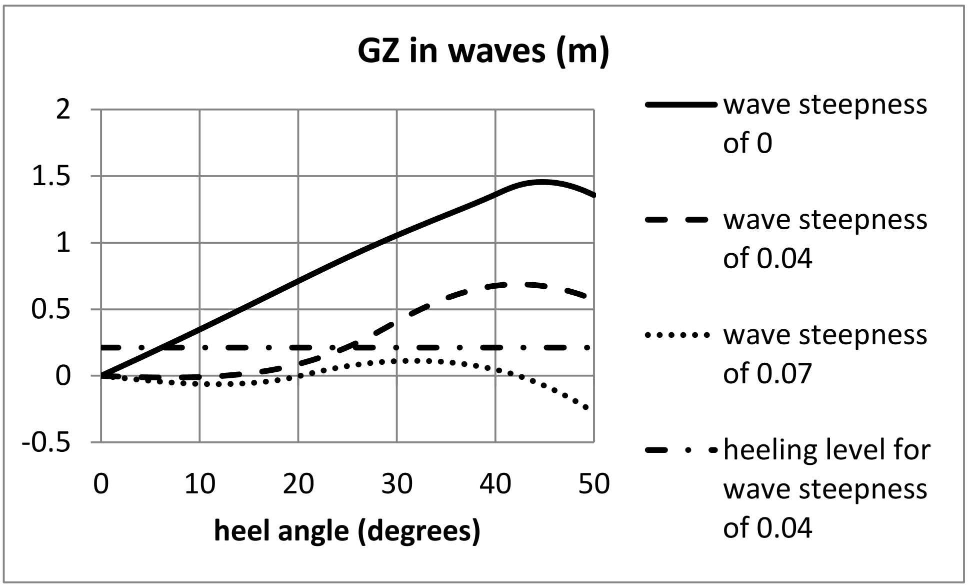

Figure 4.2 *GZ* curves for the ship in waves at wave crest amidships

5 Example of assessment of ship vulnerability to parametric rolling

5.1 As an example, the following data of a containership at the full load condition are used:

L_{BP}	*262.0 m*	*ship length between perpendiculars*
L_{f}	*262.0 m*	*ship length defined in 2008 Intact Stability Code*
B	*40.0 m*	*moulded ship breadth*
D	*24.45 m*	*moulded ship depth*
d	*12.34 m*	*moulded mean ship draught*
τ	*0 m*	*trim*
LCG	*124.7 m*	*longitudinal centre of gravity from aft perpendicular*
C_{B}	*0.576*	*block coefficient*
C_{m}	*0.962*	*midship section coefficient*
GM	*1.965 m*	*metacentric height with free surface correction*
$T_{\square}$	*25.7 s*	*ship natural roll period*
VCG	*18.37 m*	*vertical centre of gravity above baseline*
l_{BK}/L_{BP}	*0.292*	*bilge keel length normalized with ship length between perpendiculars*
b_{BK}/B	*0.0100*	*bilge keel width normalized with moulded ship breadth*
V_{S}	*12.861 m/s*	*ship service speed*

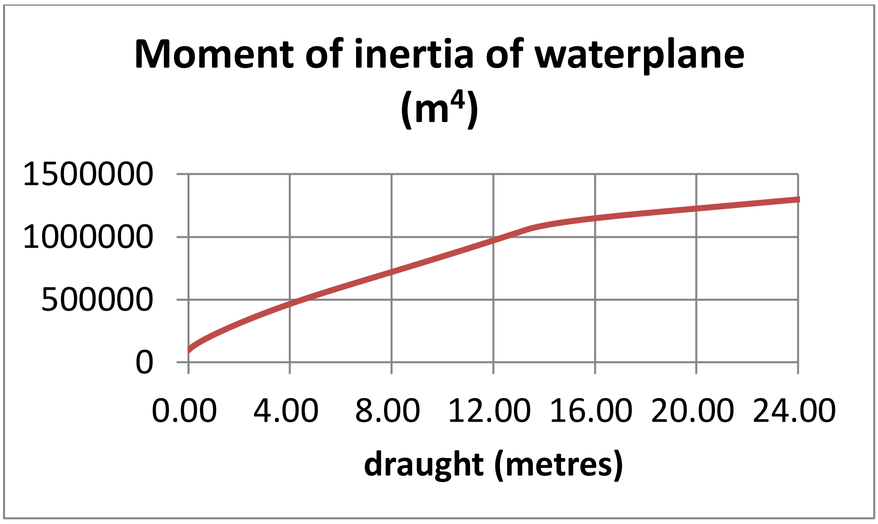

Figure 5.1 The moment of inertia of the waterplane vs. draught for the subject ship

5.2 Level 1 based on section 2.5.2 of the Interim Guidelines

5.2.1 Firstly, the bilge keel area ratio, $100A_K/(L_{BP}B)$, is calculated:

$$100A_K/(L_{BP}B) = 100 \times (l_{BK}/L_{BP}) \times (b_{BK}/B) \times 2 = 100 \times 0.292 \times 0.01 \times 2 = 0.584 \quad (5.1)$$

5.2.2 Secondly, considering C_m = 0.962 at the full load condition, the standard, R_{PR}, is calculated:

$$R_{PR} = 0.17 + 0.425(100A_K/(L_{BP}B)) = 0.17 + 0.425 \times 0.584 = 0.4182 \quad (5.2)$$

5.2.3 Thirdly, the lower draught is calculated:

$$\delta d_L = Min\{d - 0.25d_{full}, LS_w/2\} = Min\{0.75 \times 12.34, 262 \times 0.0167/2\} = Min\{9.255, 2.188\} = 2.188 \text{ m} \quad (5.3)$$

$$d_L = d - \delta d_L = 12.34 - 2.188 = 10.152 \text{ m} \quad (5.4)$$

so that, according to the hydrostatic data, the relevant I_L is 847,948 m^4.

5.2.4 Fourthly, the higher draught is calculated:

$$\delta d_H = Min\{D - d, LSw/2\} = Min\{24.45 - 12.34, 262 \times 0.0167/2\} = Min\{12.11, 2.188\} = 2.188 \text{ m} \quad (5.5)$$

$$d_H = d + \delta d_H = 12.34 + 2.188 = 14.528 \text{ m} \quad (5.6)$$

so that, according to the hydrostatic data shown in figure 5.1, the relevant I_H is 1,106,866 m^4.

5.2.5 Fifthly, $\delta GM/GM$ is calculated as follows:

$$\delta GM/GM = (I_H - I_L)/(2V)/GM = (I_H - I_L)/(2 \times C_B \times L_{BP} \times B \times d)/GM = (1106866 - 847948)/(2 \times 0.576 \times 262 \times 40 \times 12.34)/1.965 = 0.8844 \quad (5.7)$$

Therefore, $\delta GM/GM$(= 0.8844) > R_{PR}(= 0.4182) so that the ship is judged as possibly vulnerable to parametric roll. The reason of this judgement is explained in paragraph 6.1 of appendix 3.

5.3 First check of level 2 based on section 2.5.3 of the Interim Guidelines

5.3.1 Firstly, GM values in longitudinal waves are calculated for the 16 wave cases specified in table 2.5.3.2.3 of the Interim Guidelines. As an example, the GM variation for the wave case no.9, in which the wave height is 3.625m and the wavelength is 243.705m, are shown in figure 5.2. In this case, the maximum GM, GM_{max}, is 3.306m: the minimum GM, GM_{min}, is 0.807m. Thus, GM = (GM_{max} + GM_{min})/2 = 2.057m: δGM = (GM_{max} - GM_{min})/2 = 1.250m. Therefore, $\delta GM/GM$ = 0.6077.

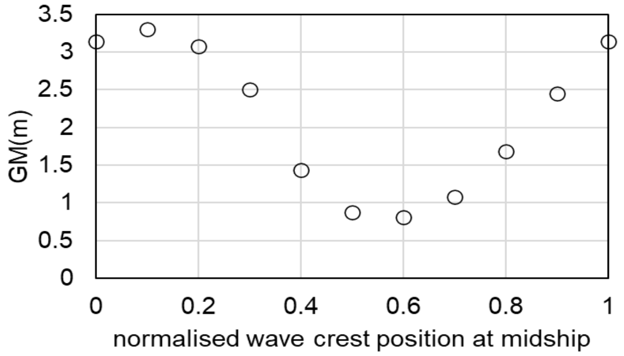

Figure 5.2 GM variation in longitudinal waves for the wave case no. 9

On the other hand, R_{PR} was already calculated in paragraph 5.2.2 as 0.4182: V_{PR} is calculated by the formula in paragraph 2.5.3.2.2 of the Interim Guidelines so that V_{PR} = 0.1044m/s. Thus, the requirement in paragraph 2.5.3.2.1 of the Interim Guidelines is not satisfied because GM = 2.057m > 0 but $\delta GM/GM$ (= 0.6077) > R_{PR} (= 0.4182). The requirement in paragraph 2.5.3.2.2 of the Interim Guidelines is also not satisfied because V_{PR} (= 0.1044m/s) < V_S (= 12.861 m/s). Therefore, the C value defined in paragraph 2.5.3.2 of the Interim Guidelines shall be 0. Repeating the same calculations for other wave cases, the dangerous wave cases among 16 are identified as shown in table 5.1.

Table 5.1 Judgement for wave cases

wave case number	W	λ(m)	H(m)	$\delta GM/GM$	V_{PR}(m/s)	C_i	W_iC_i
1	0.000013	22.574	0.35	0.0169	4.189	0	0
2	0.00165	37.316	0.495	0.0322	4.747	0	0
3	0.0209	55.734	0.857	0.0774	5.030	0	0
4	0.0928	77.857	1.295	0.1210	5.038	0	0
5	0.199	103.655	1.732	0.2410	4.630	0	0
6	0.249	133.139	2.205	0.1908	4.102	0	0
7	0.209	166.309	2.697	0.4336	3.215	1	0.209
8	0.129	203.164	3.176	0.5860	1.859	1	0.129
9	0.0625	243.705	3.625	0.6077	0.104	1	0.0625
10	0.0248	287.931	4.04	0.5793	1.852	1	0.0248
11	0.00837	335.843	4.421	0.5414	3.964	1	0.00837
12	0.00247	387.44	4.769	0.5014	6.272	1	0.00247
13	0.000658	442.723	5.097	0.4632	8.852	1	0.000658
14	0.000158	501.691	5.37	0.4130	11.757	0	0
15	0.000034	564.345	5.621	0.3594	14.963	0	0
16	0.000007	630.684	5.95	0.3157	18.398	0	0

Then, by summing up W_iC_i, the final index, $C1$, is calculated as follows:

$$C1 = 0.4368. \tag{5.8}$$

Since $C1$ is larger than the standard of 0.06, the ship is judged as possibly vulnerable to parametric roll.

5.4 Second check of level 2 based on section 2.5.3 of the Interim Guidelines

5.4.1 First, the maximum roll angles should be calculated for the effective waves having the different effective wave height h_j =0.01*j (j = 1 …10) by calculating the time series. As a case example, the results for the Froude number of 0.0 in head waves are shown in figure 5.3.

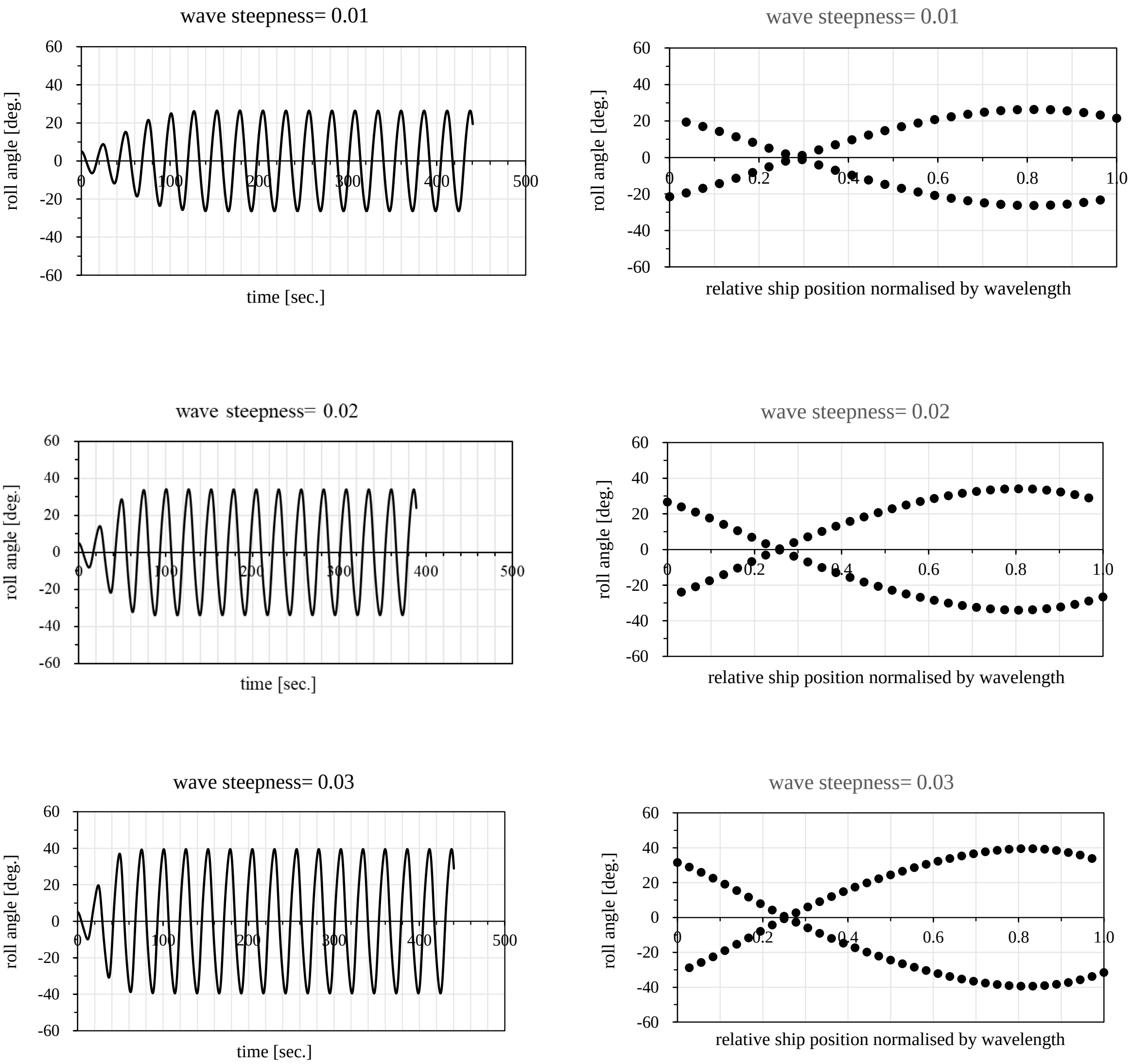

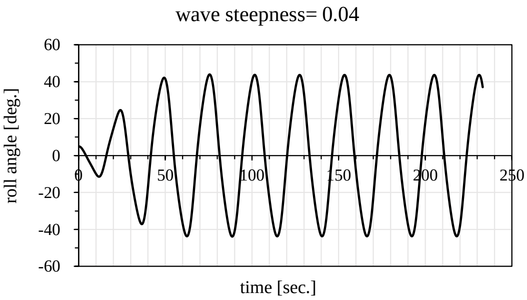
wave steepness= 0.04
roll angle [deg.]
time [sec.]

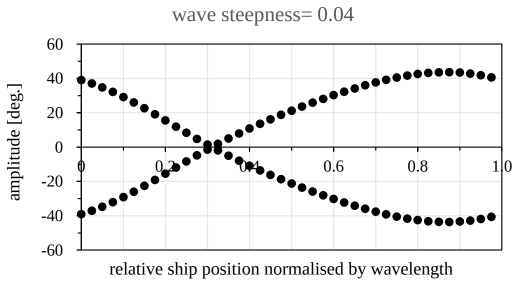
wave steepness= 0.04
amplitude [deg.]
relative ship position normalised by wavelength

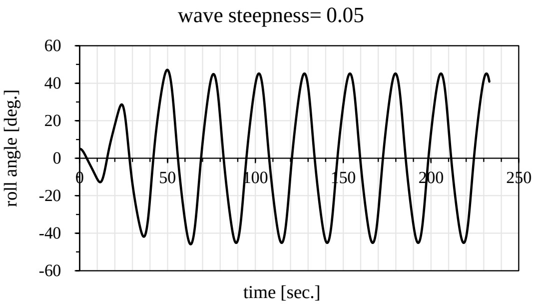
wave steepness= 0.05
roll angle [deg.]
time [sec.]

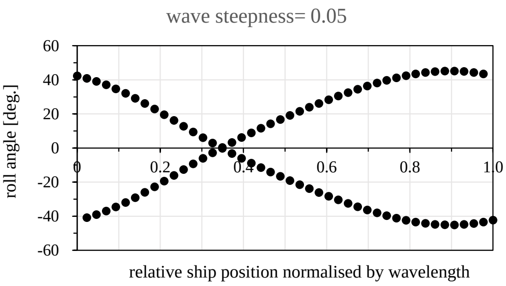
wave steepness= 0.05
roll angle [deg.]
relative ship position normalised by wavelength

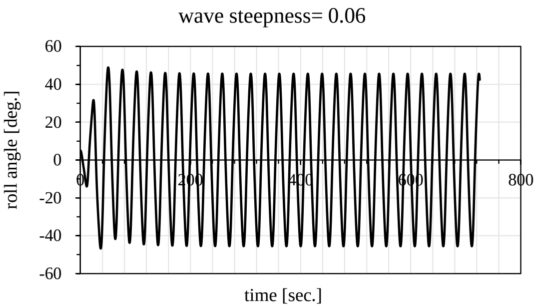
wave steepness= 0.06
roll angle [deg.]
time [sec.]

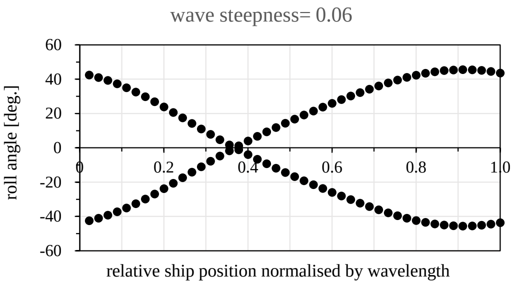
wave steepness= 0.06
roll angle [deg.]
relative ship position normalised by wavelength

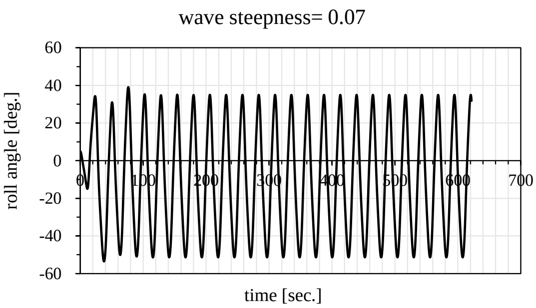
wave steepness= 0.07
roll angle [deg.]
time [sec.]

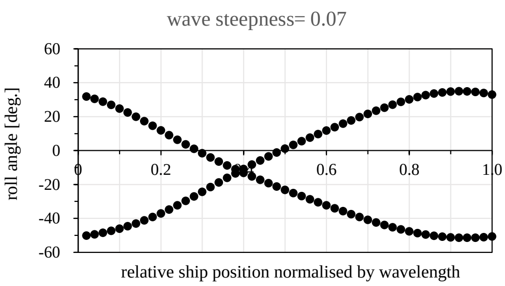
wave steepness= 0.07
roll angle [deg.]
relative ship position normalised by wavelength

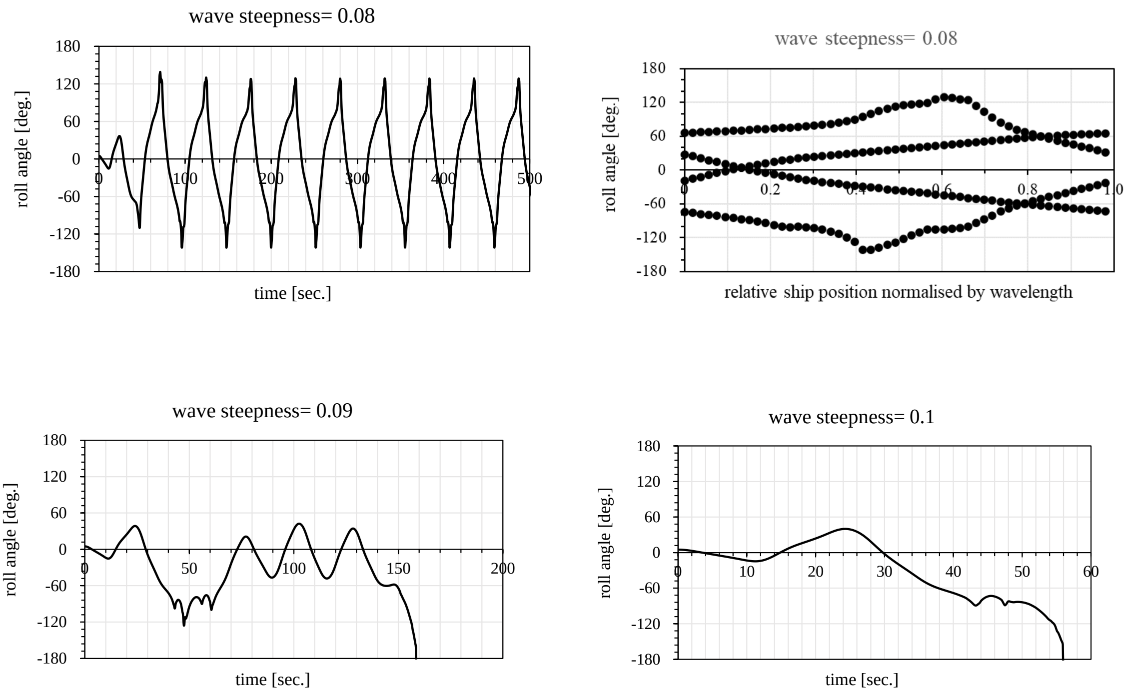

Figure 5.3 Time series of roll angle from the initial state (left) and steady states of roll angle during two encounter wave cycles (right) as functions of the relative longitudinal ship position to a wave trough, which is normalized with the wavelength.

5.4.2 The time series from the initial states include some transient behaviours so that the steady states should be identified by checking the convergence towards periodic states. In figure 5.3 it should be underlined that the cases for the wave steepness ranging from 0.05 to 0.07 show overshoot responses so that the maximum roll angle in the overall time series is not the maximum angle to be used for the calculation of the $C2$ index. While the transient response depends on the initial wave phase, the steady-state does not. In the cases for the wave steepness ranging from 0.01 to 0.07, each steady-state includes two lines within one encounter wave cycle. This means that the encounter wave cycle is exactly half the roll period so that this steady roll motion can be regarded as the parametric rolling that the level 1 criterion deals with. In the case of the wave steepness of 0.08, four lines exist within one encounter wave cycle so that this periodic motion is not relevant to the phenomenon to be evaluated here. In other words, one roll occurs during four encounter waves. In the cases for the wave steepness ranging from 0.09 to 0.1, the roll angle exceeds 180 degrees so that this transient behaviour is also not the phenomenon to be evaluated here.

5.4.3 The relationship between the wave steepness and maximum roll angle during the steady motion can be obtained as shown in figure 5.4 by using the results shown in figure 5.3. In this case, the critical wave steepness under which the maximum roll angle is equal to the threshold of 25 degrees can be calculated by using the linear interpolation as 0.00948. It is noteworthy here that the maximum roll angle under the wave steepness of 0.07 is smaller than that of 0.06. Not only the amplitude of restoring moment variation but also the mean of the restoring moment variation increases with the wave steepness. Thus, the condition for parametric rolling could be violated with larger wave steepness often in regular waves but not so often in irregular waves because of its spectrum of the incident waves. Thus, the requirement in paragraph 7.5 of appendix 3 is indispensable for excluding the drawback due to the approximation using the regular waves.

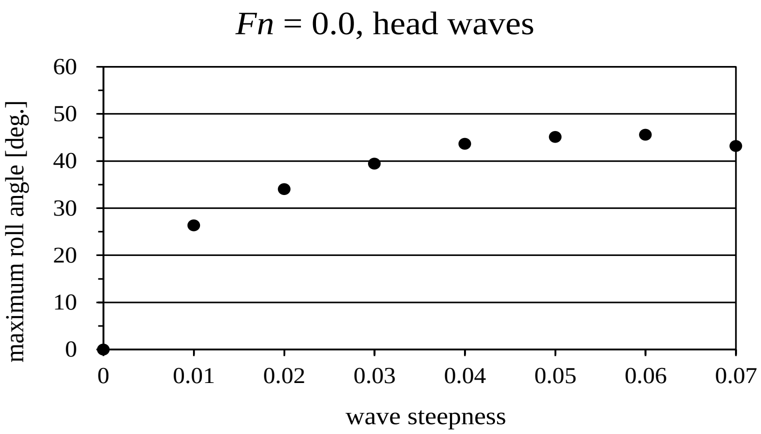

Figure 5.4 Relationship between the wave steepness and the maximum roll angle for the Froude number of 0.0 in head waves.

5.4.4 Repeating the same procedure for different ship speeds and heading, the critical wave steepness can be determined as shown in table 5.2. Here, if the largest value of the maximum roll angle cannot be determined up to the wave steepness of 0.1, the critical wave steepness is at least larger than 0.1. On the other hand, the 1/3 largest steepness of the effective wave can be calculated from the wave scatter table as shown in table 5.3. Here, the shaded cells indicate the effective wave steepnesses are larger than the critical wave steepness for the Froude number of 0.0 in head waves so that the index $C_{s,i}$ for the relevant cell should be 1. Thus, the $C2$ (F_n = 0.0, β_h) value for the Froude number of 0.0 in head waves can be calculated as 0.00948.

Table 5.2 Critical wave steepness

F_n / *heading*	Critical wave steepness
0.254 / head	> 0.1000
0.252 / head	> 0.1000
0.245 / head	> 0.1000
0.234 / head	> 0.1000
0.220 / head	> 0.1000
0.201 / head	> 0.1000
0.179 / head	> 0.1000
0.154 / head	0.05760
0.127 / head	0.04457
0.097 / head	0.03367
0.066 / head	0.02357
0.033 / head	0.01451
0.000 / head	0.00948
0.000 / follow	0.00924
0.033 / follow	0.01720
0.066 / follow	0.03589
0.097 / follow	> 0.1000
0.127 / follow	> 0.1000
0.154 / follow	> 0.1000
0.179 / follow	0.09294
0.201 / follow	> 0.1000
0.220 / follow	> 0.1000
0.234 / follow	> 0.1000
0.245 / follow	> 0.1000
0.252 / follow	> 0.1000
0.254 / follow	> 0.1000

Table 5.3 The 1/3 largest steepness of the effective wave

Effective wave steepness	averaging zero-crossing period Tz(s)																	
Hs(m)	1.5	2.5	3.5	4.5	5.5	6.5	7.5	8.5	9.5	10.5	11.5	12.5	13.5	14.5	15.5	16.5	17.5	18.5
0.5	1.40E-09	2.74E-05	1.06E-04	2.01E-04	3.83E-04	7.33E-04	1.07E-03	1.29E-03	1.38E-03	1.38E-03	1.33E-03	1.26E-03	1.17E-03	1.08E-03	9.91E-04	9.09E-04	8.34E-04	7.65E-04
1.5	4.19E-09	8.22E-05	3.17E-04	6.04E-04	1.15E-03	2.20E-03	3.21E-03	3.86E-03	4.13E-03	4.14E-03	4.00E-03	3.77E-03	3.51E-03	3.24E-03	2.97E-03	2.73E-03	2.50E-03	2.30E-03
2.5	6.99E-09	1.37E-04	5.28E-04	1.01E-03	1.92E-03	3.66E-03	5.35E-03	6.43E-03	6.88E-03	6.90E-03	6.66E-03	6.28E-03	5.84E-03	5.39E-03	4.96E-03	4.55E-03	4.17E-03	3.83E-03
3.5	9.79E-09	1.92E-04	7.39E-04	1.41E-03	2.68E-03	5.13E-03	7.50E-03	9.00E-03	9.64E-03	9.66E-03	9.33E-03	8.79E-03	8.18E-03	7.55E-03	6.94E-03	6.36E-03	5.84E-03	5.36E-03
4.5	1.26E-08	2.47E-04	9.51E-04	1.81E-03	3.45E-03	6.60E-03	9.64E-03	1.16E-02	1.24E-02	1.24E-02	1.20E-02	1.13E-02	1.05E-02	9.71E-03	8.92E-03	8.18E-03	7.50E-03	6.89E-03
5.5	1.54E-08	3.01E-04	1.16E-03	2.22E-03	4.21E-03	8.06E-03	1.18E-02	1.41E-02	1.51E-02	1.52E-02	1.47E-02	1.38E-02	1.29E-02	1.19E-02	1.09E-02	1.00E-02	9.17E-03	8.42E-03
6.5	1.82E-08	3.56E-04	1.37E-03	2.62E-03	4.98E-03	9.53E-03	1.39E-02	1.67E-02	1.79E-02	1.79E-02	1.73E-02	1.63E-02	1.52E-02	1.40E-02	1.29E-02	1.18E-02	1.08E-02	9.95E-03
7.5	2.10E-08	4.11E-04	1.58E-03	3.02E-03	5.75E-03	1.10E-02	1.61E-02	1.93E-02	2.06E-02	2.07E-02	2.00E-02	1.88E-02	1.75E-02	1.62E-02	1.49E-02	1.36E-02	1.25E-02	1.15E-02
8.5	2.38E-08	4.66E-04	1.80E-03	3.42E-03	6.51E-03	1.25E-02	1.82E-02	2.18E-02	2.34E-02	2.35E-02	2.26E-02	2.14E-02	1.99E-02	1.83E-02	1.69E-02	1.55E-02	1.42E-02	1.30E-02
9.5	2.66E-08	5.21E-04	2.01E-03	3.83E-03	7.28E-03	1.39E-02	2.03E-02	2.44E-02	2.62E-02	2.62E-02	2.53E-02	2.39E-02	2.22E-02	2.05E-02	1.88E-02	1.73E-02	1.58E-02	1.45E-02
10.5	2.94E-08	5.76E-04	2.22E-03	4.23E-03	8.04E-03	1.54E-02	2.25E-02	2.70E-02	2.89E-02	2.90E-02	2.80E-02	2.64E-02	2.45E-02	2.26E-02	2.08E-02	1.91E-02	1.75E-02	1.61E-02
11.5	3.22E-08	6.30E-04	2.43E-03	4.63E-03	8.81E-03	1.69E-02	2.46E-02	2.96E-02	3.17E-02	3.18E-02	3.06E-02	2.89E-02	2.69E-02	2.48E-02	2.28E-02	2.09E-02	1.92E-02	1.76E-02
12.5	3.49E-08	6.85E-04	2.64E-03	5.04E-03	9.58E-03	1.83E-02	2.68E-02	3.21E-02	3.44E-02	3.45E-02	3.33E-02	3.14E-02	2.92E-02	2.70E-02	2.48E-02	2.27E-02	2.08E-02	1.91E-02
13.5	3.77E-08	7.40E-04	2.85E-03	5.44E-03	1.03E-02	1.98E-02	2.89E-02	3.47E-02	3.72E-02	3.73E-02	3.60E-02	3.39E-02	3.15E-02	2.91E-02	2.68E-02	2.46E-02	2.25E-02	2.07E-02
14.5	4.05E-08	7.95E-04	3.06E-03	5.84E-03	1.11E-02	2.13E-02	3.11E-02	3.73E-02	3.99E-02	4.00E-02	3.86E-02	3.64E-02	3.39E-02	3.13E-02	2.87E-02	2.64E-02	2.42E-02	2.22E-02
15.5	4.33E-08	8.50E-04	3.27E-03	6.24E-03	1.19E-02	2.27E-02	3.32E-02	3.98E-02	4.27E-02	4.28E-02	4.13E-02	3.89E-02	3.62E-02	3.34E-02	3.07E-02	2.82E-02	2.59E-02	2.37E-02
16.5	4.61E-08	9.04E-04	3.49E-03	6.65E-03	1.26E-02	2.42E-02	3.53E-02	4.24E-02	4.54E-02	4.56E-02	4.40E-02	4.15E-02	3.86E-02	3.56E-02	3.27E-02	3.00E-02	2.75E-02	2.53E-02

5.4.5 Repeating the same procedure for different ship speeds and heading, the $C2$ (F_n, β) values can be determined as table 5.4.

Table 5.4 $C2$ (F_n, β) values for different ship speeds and heading

F_n / *heading*	$C2(F_{ni}, \beta)$
0.254 / head	0.00000
0.252 / head	0.00000
0.245 / head	0.00000
0.234 / head	0.00000
0.220 / head	0.00000
0.201 / head	0.00000
0.179 / head	0.00000
0.154 / head	0.00000
0.127 / head	0.00000
0.097 / head	0.00039
0.066 / head	0.01016
0.033 / head	0.15082
0.000 / head	0.39110
0.000 / follow	0.40224
0.033 / follow	0.08247
0.066 / follow	0.00018
0.097 / follow	0.00000
0.127 / follow	0.00000
0.154 / follow	0.00000
0.179 / follow	0.00000
0.201 / follow	0.00000
0.220 / follow	0.00000
0.234 / follow	0.00000
0.245 / follow	0.00000
0.252 / follow	0.00000
0.254 / follow	0.00000

5.4.6 By using the formula in paragraph 2.5.3.3 of the Interim Guidelines, the final value of $C2$ is obtained as follows:

$$C2 = 0.02563 \tag{5.9}$$

Since $C2$ > 0.025, the ship is judged as vulnerable to parametric roll.

5.5 Level 1 as shown in section 5.2 and the first check of level 2 as shown in table 5.1 indicate that parametric roll could occur for the ship under the wave steepness of about 0.009 or larger. However, these do not provide any information about the magnitude. Table 5.2 shows that the parametric roll amplitude could be more than 25 degrees, which could induce cargo damage and so on, only when the ship is at zero or very low forward velocity. It also indicates the ship could often meet such sea states in the North Atlantic. Therefore, the level 2 criterion judges the ship as vulnerable to parametric roll. At the same time, table 5.2 also suggests that a ship can be operated without vulnerability to parametric rolling, provided that the ship service speed is maintained in the specified sea states.

6 Example of assessment of ship vulnerability to surf-riding/broaching

6.1 As an example, the following data of a fishing vessel is used:

L_{BP}	34.5 m
B	7.6 m
d	2.65 m
trim	0.30 m
LCB	1.31 m aft from the midship
C_B	0.597
Service Fn	0.40
D_{p}	2.60 m
t_{p}	0.142
w_p	0.156
M_X/M	0.0667
r_0	0
r_1	-4273.53 [Ns/m]
r_2	7491.11 [Ns^2/m^2]
r_3	-2668.12 [Ns^3/m^3]
r_4	408.20 [Ns^4/m^4]
r_5	-17.005 [Ns^5/m^5]
κ_0	0.2244
κ_1	-0.2283
κ_2	-0.1373

The local breadth B (m), local draught d (m) and sectional area A (m^2) are provided below as a function of the longitudinal section position (m) measured from the midship as shown in table 6.1:

Table 6.1 Sectional areas, local breadth and local draught of the fishing vessel

x =	-21.65	A =	0.00E+00	B =	0	d =	0
x =	-20.55	A =	1.85E+00	B =	7.1555	d =	0.448703
x =	-19.45	A =	2.61E+00	B =	7.4162	d =	0.539137
x =	-18.35	A =	3.28E+00	B =	7.57	d =	0.629572
x =	-17.25	A =	3.88E+00	B =	7.57	d =	0.715006
x =	-15.53	A =	5.40E+00	B =	7.5857	d =	1.275049
x =	-13.8	A =	7.82E+00	B =	7.58	d =	3.255005
x =	-12.075	A =	1.04E+01	B =	7.5851	d =	3.175004
x =	-10.35	A =	1.28E+01	B =	7.58	d =	3.105004
x =	-6.9	A =	1.61E+01	B =	7.57	d =	2.955002
x =	-3.45	A =	1.76E+01	B =	7.59	d =	2.800001
x =	0	A =	1.71E+01	B =	7.59	d =	2.65
x =	3.45	A =	1.58E+01	B =	7.6	d =	2.499999
x =	6.9	A =	1.38E+01	B =	7.4916	d =	2.354998
x =	10.35	A =	1.04E+01	B =	6.4367	d =	2.199996
x =	12.075	A =	8.00E+00	B =	5.3209	d =	2.134996
x =	13.8	A =	5.24E+00	B =	3.672	d =	2.044995
x =	15.525	A =	2.86E+00	B =	1.9245	d =	1.959995
x =	17.25	A =	1.17E+00	B =	0.91	d =	1.794994

The fitting qualities of resistance and thrust coefficient, based on paragraphs 2.6.3.4.6 and 2.6.3.4.4 of the Interim Guidelines, are shown in figures 6.1 and 6.2, respectively.

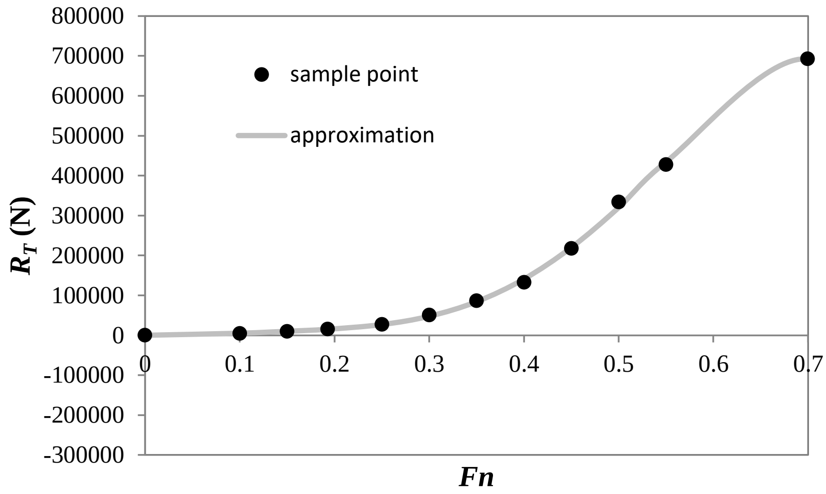

Figure 6.1 Ship resistance curve and its approximation using the fifth power polynomial

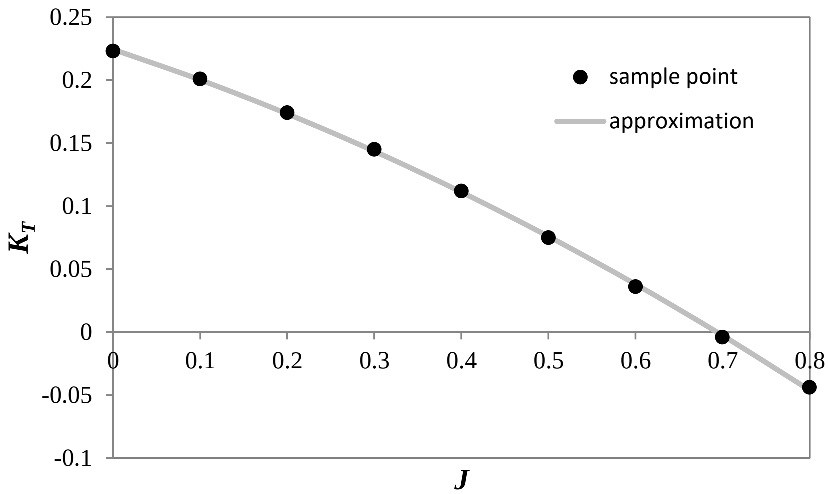

Figure 6.2 Propeller thrust coefficient curve and its approximation using the second power polynomial

6.2 This ship is judged as possibly vulnerable in the level 1 check, based on section 2.6.2 of the Interim Guidelines, because its service Froude number is larger than 0.3 and the ship length is smaller than 200 m.

6.3 Thus, it is necessary to check the vulnerability with the level 2. Firstly, the critical Froude number for surf-riding needs to be calculated under any initial condition using the Melnikov analysis, based on paragraph 2.6.3.4.6 of the Interim Guidelines. Examples of the calculated critical Froude numbers for typical local waves are as shown in table 6.2.

Table 6.2 Example of critical Froude numbers for surf-riding under some wave cases

	Critical Froude number with linear wave celerity
λ/L=1.250, H/λ=0.0504	0.3296
λ/L=1.500, H/λ=0.0396	0.3563
λ/L=1.500, H/λ=0.0504	0.3428
λ/L=1.500, H/λ=0.0600	0.3325
λ/L=1.750, H/λ=0.0504	0.3577

6.4 Secondly, the probability index C values are calculated as a function of the nominal Froude number, F_n, based on paragraph 2.6.3.2 of the Interim Guidelines, as shown in table 6.3.

Table 6.3 Probability index C values for some nominal Froude number

Fn	C with linear wave celerity
0.30	7.88E-04
0.35	2.31E-02
0.40	5.91E-02
0.45	8.77E-02
0.50	9.19E-02

This means that this subject ship is judged as vulnerable for surf-riding/broaching stability failure in the level 2 check because the C value at designed Froude number of 0.4 is larger than the standard of 0.005.

APPENDIX 3

ELEMENTS FOR NUMERICAL MODELLING OF ROLL MOTION IN THE VULNERABILITY CRITERIA OF THE SECOND GENERATION INTACT STABILITY CRITERIA

1 Equation of motion

1.1 This section on the equation of motion is provided because it is used or referenced in more than one of the stability failure mode vulnerability criteria. For level 2 of the vulnerability criteria for parametric roll, the user is expected to solve this equation numerically. To do so, the elements of the equation, especially the coefficients of the terms require some discussion to provide the user with appropriate assessment. Other failure modes use these elements in their assessments.

1.2 The equation of motion takes into account forces acting on the ship. The simplest mathematical model that is capable of evaluating the maximum roll angle includes four moments:

.1 inertia, including added inertia (or added mass) as a part of hydrodynamic forces;

.2 roll damping, which expresses energy loss from roll motions in creating waves, vortices and skin friction;

.3 roll restoring (stiffness) is modelled with the GZ curve with relative wave elevation taken into account only for parametric rolling and pure loss of stability failure modes; and

.4 transverse wave forces are absent for a ship in exact following or head long-crested seas.

1.3 The roll inertia of a ship as a solid body is measured by the transverse moment of inertia I_{xx}. Inertial forces are proportional to accelerations. There are also hydrodynamic forces acting on a ship, subject to accelerated motion that are also proportional to the accelerations. These hydrodynamic forces are usually expressed as an additional mass or a moment of inertia and referred to as "added mass" in roll A_{44}. The roll inertia is expressed as:

$$M_{IN} = (I_{xx} + A_{44}) \cdot W_{\varphi} \tag{1.1}$$

where W_{φ} is the angular acceleration in roll; calculation of the moment of inertia as well as added inertia is provided in section 2.7.1 of the Interim Guidelines.

1.4 Damping of roll motions is essentially a transfer of kinetic energy of a moving ship to the environment. It is a complex process because this energy transfer occurs through different physical phenomena. Skin friction causes the layers of water nearest to the hull to move. The moving surface of the hull leads to formation of vortices; the kinetic energy of the water moving in those vortices is taken from the ship. Due to its motion, the ship also makes waves on water surface that also dissipate energy. The complexity of these physical phenomena is the reason why a model test is the most reliable source of information on roll damping. However, recent developments in computational fluid dynamics (CFD) hold good promise for the availability of this computational method in the future. In the absence of ship-specific or prototype data, the simplified Ikeda method can be applied (see section 9.2). A moment of roll damping is presented in the following form:

$$M_D = (I_{xx} + A_{44}) \cdot \left(\delta_0 V_\varphi + \delta_1 V_\varphi \left|V_\varphi\right| + \delta_2 V_\varphi^3\right) \quad (1.2)$$

where δ_0, δ_1 and δ_2 are coefficients computed with the simplified Ikeda method and V_φ is the angular velocity of roll motions.

The simplified Ikeda method contains some empirical elements and, for this reason, the range of its applicability should be observed.

1.5 Alternatively, numerical simulations can be used for the estimation of roll damping, based on the solution of viscous hydrodynamic equations with the guidance of CFD for roll damping. In this case, validation of simulations should be performed for selected loading conditions to the satisfaction of Administration. Validation should be performed in comparison with model tests performed according to the procedures in MSC.1/Circ.1200 or alternative test procedures.

2 Equation of motion with respect to parametric rolling

2.1 Roll restoring

2.1.1 A proper representation of roll restoring is very important for the correct representation of parametric rolling. The variation of stability in waves is a primary mechanism of development of parametric rolling (an explanation is provided in chapter 4 of appendix 1). The calculation of the instantaneous roll restoring, while straightforward if disturbance due to the ship hull is ignored, may be too complex for the level 2 vulnerability check. Hence, a quasi-static approach can be used instead.

2.2 Evaluation of metacentric height and righting lever curve in longitudinal waves

2.2.1 The quasi-static approach means that the GZ curve for the ship on a wave is calculated using the hydrostatic algorithm (in which forces and moments are balanced in heave and pitch), but the waterplane is not flat – it is determined from the intersection of a wave and the hull surface. Known also as "wave-pass" calculations, the capability for this calculation is provided by a number of commercially available hydrostatic software packages. For the assessment of parametric rolling, calculation of the GZ curve up to 180 degrees is recommended if the superstructures including down-flooding opening are properly modelled; it sets a natural maximum and prevents the numerical solution from growing too large and causing a numerical error. Alternatively, a maximum cut-off angle can be used. Exceedance of the cut-off roll angle stops the calculation. Practical value of the cut-off roll angle may be set equal to the largest available angle in the GZ curve calculation and is expected to be around 50 to 90 degrees. Figures 2.1a and 2.1b show the GZ variation in waves as a series of curves. Each curve is calculated for a particular position of the wave crest relative to the midship which results in a surface shown in figure 2.1c. For the intermediate values of heel angle and of the wave crest position, a bilinear or bi-cubic spline interpolation can be used.

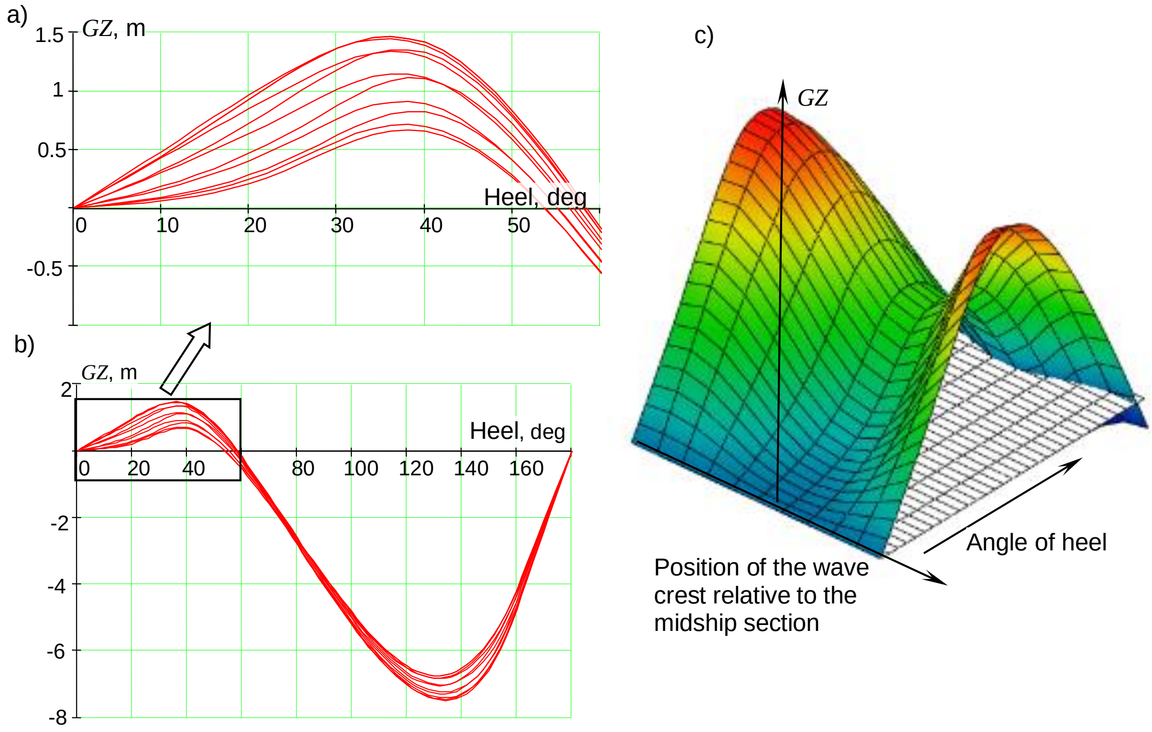

Figure 2.1 The *GZ* curve in waves (steepness 0.02, C11 class containership, full load): a) positive range, b) full range and c) as a surface

2.2.2 The definition of wave crest position is illustrated in figure 2.2. The position of the wave crest is a function of time:

$$X_C(t) = 0.5\lambda\, sin(\omega_e t) \tag{2.1}$$

where,

ω_e = the wave frequency of encounter = $\omega_e = \omega - \frac{\omega^2}{g} V_S \cos\psi$, and

ψ = is the relative wave heading (0 degrees – following waves, 180 degrees – head waves).

Thus, the value of the *GZ* curve in waves can be presented as a function of time and angle of heel, φ:

$$GZ = GZ(t, \varphi) \tag{2.2}$$

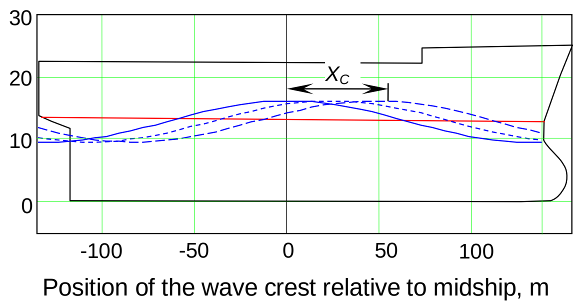

Figure 2.2 Definition of the position of the wave crest relative to the midship section

2.2.3 For the symmetric GZ curve, the total restoring moment is expressed as:

$$M_R = \mathrm{sign}(\varphi) \cdot \rho \nabla g \cdot GZ(t, |\varphi|) \tag{2.3}$$
$$\mathrm{sign}(\varphi) = \begin{cases} 1 & \varphi \geq 0 \\ -1 & \varphi < 0 \end{cases}$$

For the asymmetric GZ curve, the calculations are to be done for starboard and portside separately and the total restoring moment is expressed as:

$$M_R = \rho \nabla g \cdot GZ_B(t, \varphi) \tag{2.4}$$
$$GZ_B(t, \varphi) = \begin{cases} GZ_S(t, \varphi) & \varphi \geq 0 \\ GZ_P(t, \varphi) & \varphi < 0 \end{cases}$$

Where $GZ_B(t,\phi)$ = complete righting curve (m);

$GZ_S(t,\phi)$ = righting curve for starboard (m); and

$GZ_P(t,\phi)$ = righting curve for port side (m).

Restoring action of the righting lever curve is assumed to be described by a positive value while rolling to the starboard and a negative value while rolling to the port side.

2.3 Assessment of the equation of motion in terms of inertia

2.3.1 Following Newton's second law, the equation of roll motion is expressed as the inertial force equal to the sum of all other forces. Since the ship is in longitudinal waves, there is negligible or no direct forcing that comes from the waves:

$$M_{IN} = -M_D - M_R \tag{2.5}$$

2.3.2 In the equation in the previous paragraph, the negative sign is inserted because both damping and restoring forces are directed against the roll motion or the rate of motion. The equation of roll motion can be rewritten with each force as a function of motion parameters or time:

$$M_{IN}(W_\varphi = \ddot{\varphi}) + M_D(V_\varphi = \dot{\varphi}) + M_R(t, \varphi) = 0 \tag{2.6}$$

This equation relates the roll motion with the roll rate and the angular roll acceleration. These quantities are related through differentiation: the angular velocity is a derivative of roll and the angular acceleration is a derivative of angular velocity. Thus, this equation is a differential equation. The solution of this differential equation is a time history of roll motions, similar to that shown in figure 2.3, which shows parametric rolling. As the ship is sailing in longitudinal waves, there is no forcing in the transversal plane, so the observed rolling motion in periodic waves is usually a result of parametric resonance if the roll period is twice the encounter wave period.

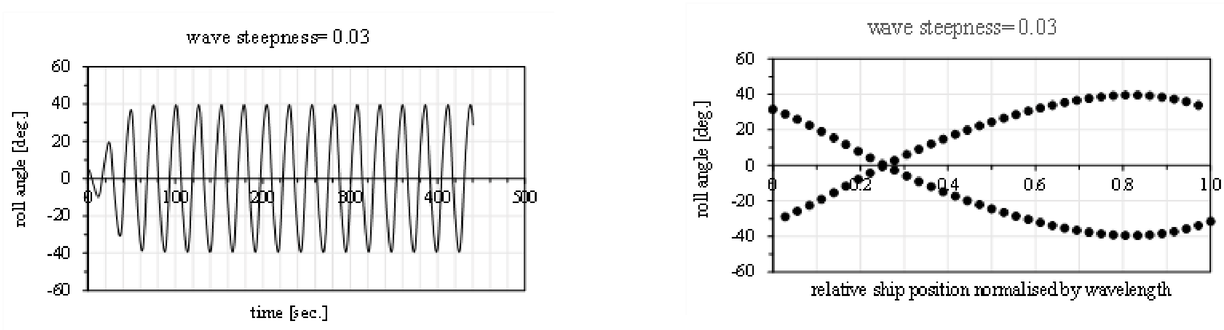

Figure 2.3 Time history of parametric rolling from the initial state (left) and steady states of roll angle during two encounter wave cycles (right) as functions of the relative longitudinal ship position to a wave trough, which is normalized with the wavelength.

2.3.3 The equation in the previous paragraph can be solved with an appropriate numerical method. For this purpose, the equation is presented in a form of a vector-valued equation:

$$\begin{pmatrix} \dot{\varphi} \\ \dot{V}_\varphi \end{pmatrix} = \begin{pmatrix} V_\varphi \\ \frac{1}{I_X + A_{44}} \left(-M_D(V_\varphi) - M_R(t, \varphi) \right) \end{pmatrix} \quad (2.7)$$

If V_φ and φ at the specified time, t, the V_φ and φ at the next time step can be determined. Thus, the time series starting from an initial state can be determined.

2.3.4 The vector-valued equation in paragraph 2.3.3 can be integrated with a reliable algorithm such as the fourth-order Runge-Kutta method with the initial conditions for the calculations, i.e. values of roll angle and roll rate at the beginning (or at time step t = 0). The solution, as illustrated in figure 2.3, was computed with assumed initial conditions (φ = 5 degrees and V_φ = 0 degrees/s). While the calculation can assume zero for both φ and V_φ, the development of parametric rolling may not occur until a much longer duration is calculated.

2.3.5 To complete the inputs necessary for the calculation, two more parameters are needed: the time step Δt and the total simulation time T_{sim}. The time step Δt should be sufficiently small to achieve numerical convergence, and the total simulation time T_{sim} should be sufficiently long to achieve a steady state or a capsize.

3 Information regarding level 2 vulnerability criterion for the dead ship condition

3.1 Roll modelling in beam waves and wind

3.1.1 Roll in the dead ship condition is represented by the uncoupled roll model in beam waves and wind. Roll motion is due to the forcing of wind and waves. The wave exciting moment is proportional to the effective wave slope, which is the product of the wave slope and the effective wave slope coefficient at each wave frequency. The wind moment is due to the time-independent mean wind speed and the time-varying component of the wind velocity, i.e. the gust. The time dependent wind exciting moment is related to the time-varying component of the wind velocity. Since the relative roll angle is responsible for vanishing stability and down flooding in beam waves, the Interim Guidelines use the effective relative roll angle in its paragraph 2.2.3.2.3.

3.1.2 The effective wave slope angle can be defined by the product of the wave slope angle and the effective wave slope function. The wave slope angle can be calculated by the product of the wave number and the wave elevation. Thus, the wave slope spectrum shall be obtained by the product of the wave energy spectrum and the square of the wave number as shown in paragraph 2.2.3.2.3 of the Interim Guidelines.

3.1.3 The wind velocity consists of the constant component and the time-varying component. The wind-induced roll moment is proportional to the square of the wind velocity. Since the time-varying component is usually much smaller than the constant component, the time-varying roll moment is proportional to the product of the constant wind velocity and the time-varying component of the wind velocity. Thus, the wind loading spectrum can be obtained by the product of the wind velocity power spectrum and the square of the mean wind velocity as shown in paragraph 2.2.3.2.3 of the Interim Guidelines.

3.2 Roll damping, natural roll frequency and the effective wave slope function

3.2.1 Paragraph 2.2.3.2.3 of the Interim Guidelines requires the stochastic linearization method for equivalent roll damping, which is described in paragraph 9.3.5. In this method, it is necessary to calculate the standard deviation of the roll angular velocity. Since the roll angular velocity is the derivative of the roll angle with respect to time, the power spectrum of the roll angular velocity is the product of the roll power spectrum and the square of the circular frequency. Thus, the standard deviation of the roll angular velocity can be evaluated as the area of power spectrum of the roll angular velocity.

3.2.2 The spectrum of roll angular velocity, $S_{d\phi}(\omega)$ ((rad/s)^2/(rad/s)), which is necessary for the determination of the equivalent linear roll damping coefficient μ_e (1/s), is calculated as follows:

$$S_{d\phi}(\omega) = \omega^2 \cdot H^2(\omega) \cdot \frac{S_M(\omega)}{(\rho g \nabla GM)^2} \tag{3.1}$$

where

$$S_M(\omega) = S_{M_{waves}}(\omega) + S_{\delta M_{wind,tot}}(\omega) \tag{3.2}$$

$$S_{M_{waves}}(\omega) = (\rho g \nabla GM_{res})^2 \cdot r^2(\omega) \cdot S_{\alpha\alpha}(\omega) \tag{3.3}$$

In equation (3.1), $S_M(\omega)$ ((N m)^2/(rad/s)) is the spectrum of total roll moment due to waves and wind gustiness, while the other quantities appearing in equation (3.1) are defined in section 2.2.3 of the Interim Guidelines.

3.2.3 The natural roll frequency can be determined mainly with the slope of the righting arm with respect to the heel angle. In case of the ship roll motion around the upright condition, the slope is the metacentric height. In case of the ship with beam wind, it should be corrected with the heel angle due to the constant wind velocity as shown in the paragraph 2.2.3.2.3 of the Interim Guidelines.

3.2.4 The effective wave slope function for a conventional mono-hull vessel can be evaluated as described in section 8.2. For multi-hull vessels or ships having very short natural roll periods, alternative methods described in section 8.1 are available.

4 Calculation of maximum roll angle for assessment of parametric rolling in check 2 of level 2 of the vulnerability criteria

4.1 The numerical simulation for the parametric roll response should start with the initial condition specified in paragraph 2.3.4. The simulated response could resolve to either the upright condition, a periodic steady-state, a non-periodic oscillatory behaviour or the exceedance of 180 degrees. If parametric rolling is not possible for the given wave conditions, the response is represented by decaying roll oscillations, as shown in figure 4.1. In this case, the maximum roll angle occurs during the transient stage and it could depend on the initial wave phase. Thus, it should be ignored. Thus, the maximum roll angle here should be regarded as zero. When the wave steepness is zero, a simple roll decay curve is obtained so that the maximum roll angle should be regarded as zero in place of the initial roll angle of 5 degrees.

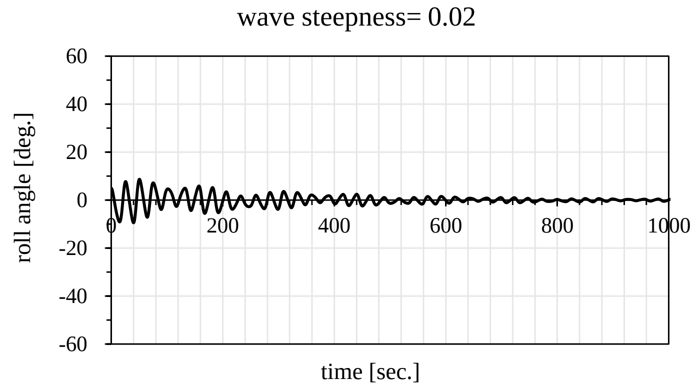

Figure 4.1 An example of roll response in absence of parametric rolling

4.2 A typical example of the simulated periodic response is shown in figure 4.2. In this case, the maxim transient roll angle is about 47.3 degrees but the steady-state amplitude is about 43.6 degrees. Since the transient behaviour depends on the initial wave phase, the maximum roll angle should be determined only from the steady-state. The steady-state can be identified if the difference of the roll angle at every two wavelengths converges to a negligibly small value. If the steady-state roll angles during the two encounter wave cycle are plotted as a function of the relative longitudinal ship position to a wave trough, in other words, the phase difference to waves, figure 4.3 can be drawn. Here, the two lines can be found. This means that one roll cycle occurs when the ship meets two encounter wave cycles. Thus, this rolling behaviour is the parametric rolling that the level 1 criterion deals with.

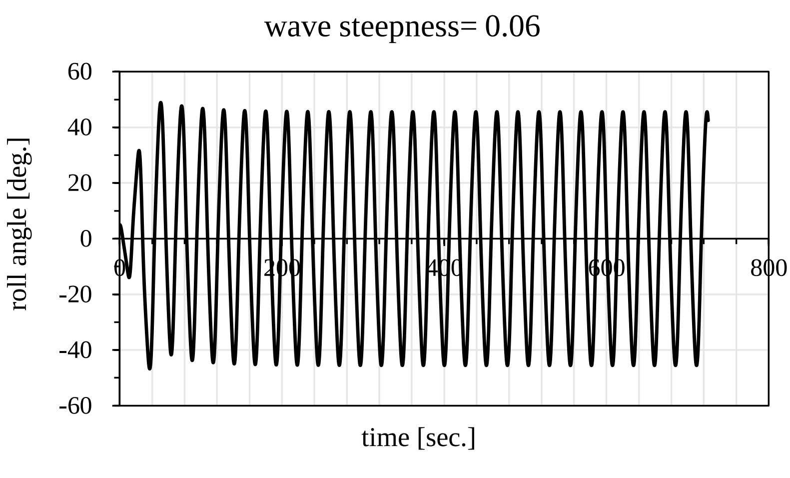

Figure 4.2 An example of periodic roll response with the overshoot

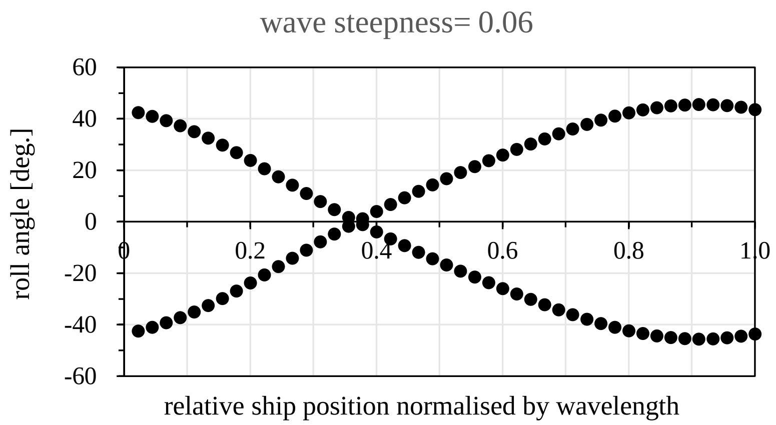

Figure 4.3 The periodic steady-state roll during one wavelength

4.3 If we slightly increase the wave steepness in the above case, the symmetry of steady roll motion breaks as shown in figure 4.4. The absolute value of the maximum roll angle is smaller than that of the minimum roll angle. This is one of the typical non-linear phenomena. In the case of asymmetric roll, the average of two absolute values should be used as the maximum roll angle to be used for the calculation of the $C2$ value.

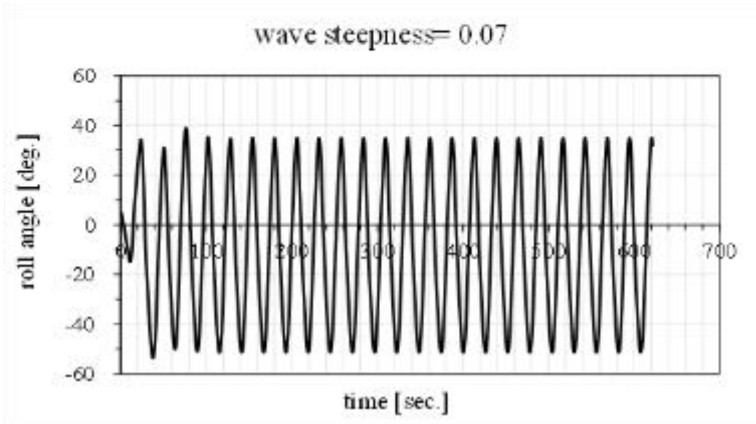

Figure 4.4 An example of asymmetric periodic roll response

4.4 Another type of periodic steady roll response is shown in figure 4.5. This roll cycle occurs within one wave encounter cycle so that this is not the parametric roll that the level 1 criterion deals with. For avoiding the inconsistency between the two levels, this response should be dealt with outside the framework of the multi-layered criteria structure.

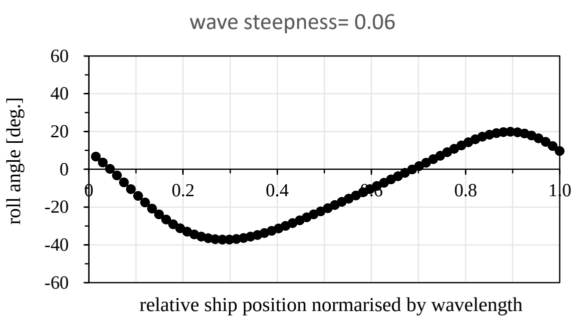

Figure 4.5 An example of another type of period roll response

4.5 More complicated response sometimes occurs as shown in figure 4.6. In this case, the roll motion seems to consist of one larger roll cycle together with two smaller roll cycles. However, it is not a simple repeat. If we draw a phase portrait as figure 4.7, where the abscissa is the roll angle and the ordinate is the roll angular velocity, it can be confirmed this is not a periodic motion. This response should be dealt with outside the framework of the multi-layered criteria structure.

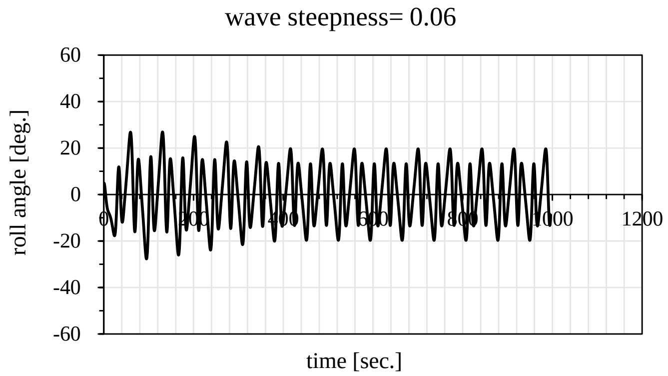

Figure 4.6 An example of non-periodic roll response

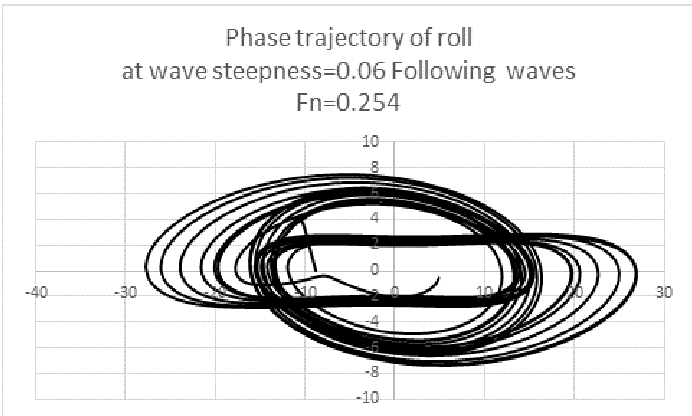

Figure 4.7 The phase trajectory of non-periodic roll response

4.6 When the calculated roll angle leaves the entire range of the given GZ curve, such as ± 180 degrees, the calculation should be explicitly stopped as the occurrence of capsizing. The obtained roll behaviour is just transient so that the maximum roll angle cannot be determined. Its example is shown in figure 4.8. The periodic parametric rolling occurs with the wave steepness of 0.08 and the capsizing occurs if the wave steepness is slightly increased.

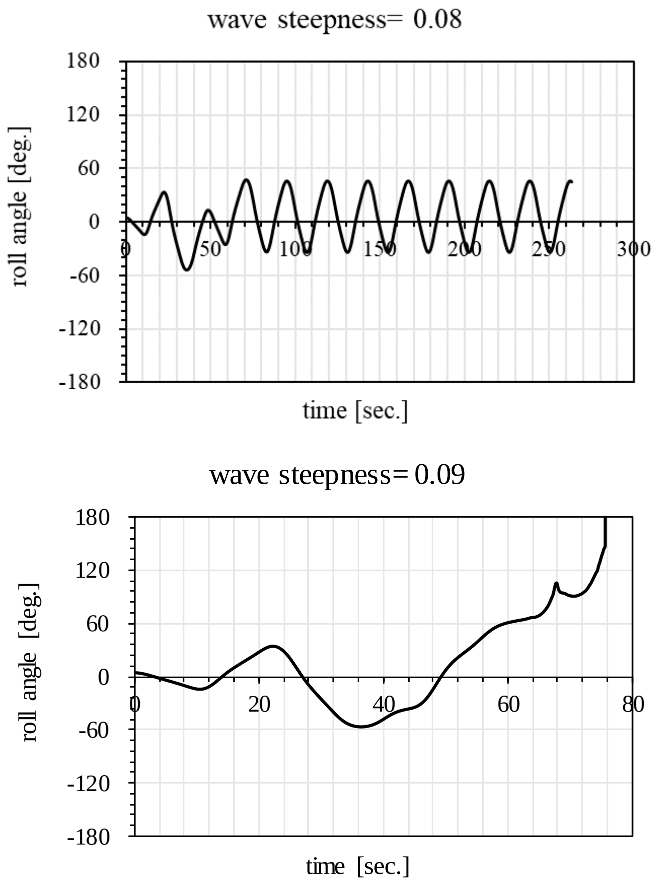

Figure 4.8 Examples of roll response with parametric rolling and capsizing

5 Supplementing information on calculation for checking vulnerability to parametric rolling

5.1 For the calculation of the bilge keel area to be used in paragraph 2.5.2.1 of the Interim Guidelines, the fin stabilizers may be regarded as a kind of bilge keel if they are non-retractable and calculated as a part of total bilge keel area. On the other hand, the centre skeg should not be included unless the midship section coefficient is less than 0.9. This is because existing model experiments indicate that the increase of the roll damping due to a centre skeg is almost zero for the case of small rise of floor. This may be because the pressure created by the skeg on the bottom works as a negative roll damping.

5.2 The "sharp bilge" in paragraph 2.5.2.1 of the Interim Guidelines means that bilge radius is smaller than 1% of the ship's breadth and the angle between piece-wise lines representing the bilge is smaller than 120° as shown in figure 5.1.

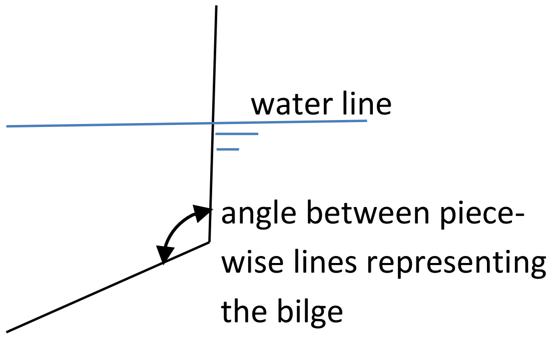

Figure 5.1 Definition of the angle between piece-wise lines representing the bilge

a. The value of s_w in paragraph 2.5.2.2 of the Interim Guidelines can be corrected if operational limitations are implemented. In this case, a wave scatter table should be provided that is consistent with the implemented operational limitations, in accordance with section 2.7.2 of the Interim Guidelines, and s_W can be determined as specified in section 10.1.

5.4 For the calculation in paragraph 2.5.3.2.1 of the Interim Guidelines, a sinusoidal wave should be used without hydrodynamic disturbance due to the ship. The water pressure due to the wave may include the effect of wave particle velocity assuming that water depth is larger than the wavelength or a hydrostatic pressure profile starting from the actual free surface should be used.

6 Discussion on the relationship between level 1 and 2 vulnerability criteria for parametric rolling

6.1 The vulnerability level 1 criterion and the first check of level 2 criteria represent a simplification of the second check of level 2 criteria. By simplifying equation (2.7) and examining steady solutions, the occurrence condition for parametric roll is obtained as follows:

$$\frac{\delta GM_1}{GM} > \frac{2\delta_0}{\omega_r} \tag{6.1}$$

The right-hand side of this equation indicates the normalized roll damping coefficient multiplied by 2. These vulnerability criteria apply the empirical formulae for the equivalent roll damping as the function of bilge keel area and the midship coefficient, which was developed using Ikeda's simplified estimation method. This outcome is used for the vulnerability level 1 criterion and the first check of the level 2 criteria. Therefore, these requirements are a simplification of the second check of the level 2 criteria.

6.2 In the level 1 criterion a wavelength equal to the ship length is considered as a typical worst-case condition. In the level 2 first check criterion, wavelengths and corresponding wave steepnesses of the calculation "wave cases" are determined from the considered wave scatter table. The steepness used in the level 1 criterion is defined as the maximum wave steepness among those in the wave cases of the level 2 first check criterion. The procedure for the determination of the wave cases from the relevant wave scatter table is described in section 10 of this appendix. For unrestricted service, the relevant wave scatter table is table 2.7.2.1.2 of the Interim Guidelines. The wave scatter diagram can be different in case operational limitations are implemented. In that case, wave cases for the level 2 first check criterion and the steepness in the level 1 criterion are modified following the procedure in section 10.

6.3 The difference between the level 1 criterion and the first check of the level 2 criteria are as follows. While the level 2 uses 16 different reference waves for calculating the metacentric height variation, the level 1 uses the wave having the worst wavelength, i.e. the wavelength to ship length ratio of 1 and a wave steepness which is the maximum among those of the wave cases used for level 2 first check. Thus, the level 1 criterion is expected to be more conservative than the first check of the level 2 criteria.

6.4 While both the level 1 criterion and the first check of the level 2 criteria judge the danger of parametric roll with its occurrence condition, the second check of level 2 criterion judges with the magnitude of parametric roll. This means that, if parametric roll occurs with small amplitude, the second check of level 2 criteria could conclude that the ship is not vulnerable to stability failure due to parametric roll. Thus, the second check of level 2 criteria is less conservative in principle.

7 Method to establish equivalence between regular and irregular waves as provided in vulnerability criteria, level 2 for both pure loss of stability and parametric roll stability failure modes (Grim's effective wave approach) to assess the change of stability in longitudinal irregular waves

7.1 Although actual ocean waves are irregular, it is practical to simplify the irregular waves as a regular wave. Since the restoring variation due to waves has the non-linear relationship with the incident waves, the response amplitude operator approach used for the dead ship condition and excessive acceleration stability failure modes cannot be applied to the pure loss and parametric rolling failure modes. To overcome this situation, one traditional approach was developed in Germany, which is known as Grim's effective wave (see figure 7.1).

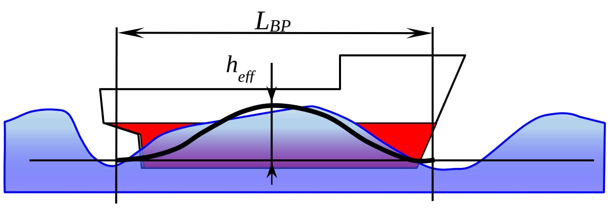

Figure 7.1 A concept of Grim's effective wave

7.2 This approach is based on the concept that an irregular wave spatial profile around the ship can be substituted by a longitudinal regular wave with the wavelength equal to the ship length and with the wave crest or trough situated at the longitudinal centre of gravity. If we calculate the righting arm GZ with this regular wave, the relationship between GZ and its wave height can be regarded as non-linear but non-frequency-dependence so that stochastic estimation of GZ in irregular waves is possible. A comparison of the application of effective wave concept with direct stability calculations has well verified this approach as shown in figure 7.2.

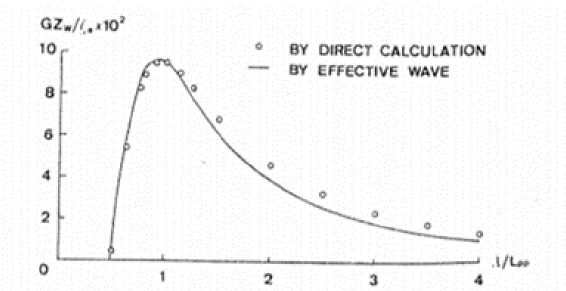

Figure 7.2 Verification of Grim's effective wave by using a direct calculation of the GZ in longitudinal waves with the wave crest amidships and a heel angle of 30 degrees and the wave height of 5% L for a trawler[6]

6 Umeda, N. and Yamakoshi, Y. *Probability of Ship Capsizing due to Pure Loss of Stability in Quartering Seas*. Naval Architecture and Ocean Engineering, The Society of Naval Architects of Japan, Vol. 30, pp. 73–85, 1994.

7.3 In the level 2 vulnerability criteria for pure loss of stability, for determining the indices for each H_i in paragraph 2.4.3.2.2 of the Interim Guidelines, the relationship between h in paragraph 2.4.3.2.1 of the Interim Guidelines and the index should be obtained by calculation. Here, if the index has a peak at the certain wave height h_p, the peak value of the index should be used when the wave height is larger than h_p. When local peaks are present, this conservative approach is used with reference to each local peak up to a wave height where direct calculations are more conservative.

7.4 For the level 2 vulnerability criteria for pure loss of stability, the 3% largest effective wave height, H_i, in paragraph 2.4.3.2.3 of the Interim Guidelines should be calculated as follows:

$$H_i = 5.9725\sqrt{m_0} \tag{7.1}$$

$$m_0 = \int_{0.01\omega_L}^{\omega_L} \left\{ \frac{\frac{\omega^2 L}{g} sin\left(\frac{\omega^2 L}{2g}\right)}{\pi^2 - \left(\frac{\omega^2 L}{2g}\right)^2} \right\}^2 S_{ZZ}(\omega)d\omega + \int_{\omega_L}^{3\omega_L} \left\{ \frac{\frac{\omega^2 L}{g} sin\left(\frac{\omega^2 L}{2g}\right)}{\pi^2 - \left(\frac{\omega^2 L}{2g}\right)^2} \right\}^2 S_{ZZ}(\omega)d\omega] \tag{7.2}$$

where

$$\omega_L = \sqrt{\frac{2g\pi}{L}} \tag{7.3}$$

If $H_i > 0.1L$, H_i should be set as $H_i = 0.1L$.

7.5 In the level 2 vulnerability criteria for parametric rolling, for determining the maximum roll angle, for each H_{ri} in paragraph 2.5.3.4.2 of the Interim Guidelines, the relationship between h_j in paragraph 2.5.3.4 of the Interim Guidelines and the maximum roll angle should be obtained by calculation. Here, if the maximum roll angle has a peak at the certain wave height h_p, the peak value of the maximum roll angle should be used when the wave height is larger than h_p. When local peaks are present, this conservative approach is used with reference to each local peak up to a wave height where direct calculations are more conservative.

7.6 For the level 2 vulnerability criteria for parametric rolling, the representative wave height, H_{ri}, in paragraph 2.5.3.4.2 of the Interim Guidelines, which corresponds to the 1/3 largest effective wave height, should be calculated as follows:

$$H_{ri} = 4.0043\sqrt{m_0} \tag{7.4}$$

If $H_{ri} > 0.1L$, H_{ri} should be set as $H_{ri} = 0.1L$.

8 Determination of roll moment due to waves and effective wave slope function

8.1 Methods for evaluating the effective wave slope function

8.1.1 The use of uncoupled roll model for beam waves can be justified from the viewpoint of coupled ship dynamics but only when the wavelength is sufficiently longer than the ship breadth and the wave exciting roll moment is calculated by integrating incident wave pressure on its own as described in paragraph 3.5.4 of the explanatory notes to the 2008 Intact Stability Code, MSC.1/Circ. 1281. The amplitude of wave exciting roll moment is conveniently expressed as a linear slope of a wave across the transverse sections of the ship. There are a number of methods that can be applied to determine this function, $r(\omega)$:

.1 a linear strip theory of coupled sway-yaw-roll motions with the non-linear roll damping in regular beam waves, in which the amplitude of roll motion under the synchronous condition, φ_m, in radians, can be determined. By using the roll damping moment, the amplitude of the wave exciting roll moment for the uncoupled roll motion can be calculated. Then the effective wave slope coefficient can be determined by equation (8.1.1).

$$r(\omega_r) = \frac{2 \cdot (a \cdot \varphi_m + b \cdot \varphi_m^2 + c \cdot \varphi_m^3)}{\pi^2 \cdot s} \qquad (8.1.1)$$

where a, b and c are the Froude extinction coefficients defined in paragraph 9.3.4 of appendix 3. The obtained value of r can be used for all frequencies, in which the ratio of wavelength to ship breadth is larger than 0.5: $r(\omega)$ should be assumed to be 0 for ratios of wavelength to the ship moulded breadth less than 0.5. Alternatively, the above procedure can be applied to the case where the synchronous roll amplitude of coupled motions can be determined with a model test in regular beam waves according to MSC.1/Circ.1200.

.2 a station simplified method in which the sectional area curve along the ship length is kept constant, but the geometry of each station is assumed to be rectangular. This allows the calculation of the distribution of incident wave pressure caused by the wave elevation across the transverse section to be performed analytically. The value of $r(\omega)$ should be evaluated at the natural roll frequency for the wavelength to ship's breadth ratio of 0.5 or larger; $r(\omega)$ should be assumed to be 0 for ratios of wavelength to the ship moulded breadth less than 0.5.

.3 a direct pressure integration of the incident wave pressure over the submerged hull surface up to the level of the incident wave profile.

.4 a direct pressure integration method of the incident wave pressure over the submerged hull surface up to the level of mean waterline without the ship motions.

8.1.2 For the latter two methods, $r(\omega)$ should be calculated using the following equation:

$$r(\omega) = \frac{M_{FK}(\omega)}{W \cdot GM \cdot \alpha_0(\omega)} \qquad (8.1.2)$$

where

M_{FK} = the amplitude of the Froude-Krylov roll moment, calculated by integrating wave pressures on the ship hull;

W = the weight of displacement;

GM = the metacentric height without free surface correction; and

α_0 = is the amplitude of the angle of wave slope at the centreline.

8.1.3 Since the vulnerability criteria is required to be applied with minimal computational efforts, the method described in 8.1.1.2 is recommended as standard method. It requires only sectional breadth, sectional draught and sectional area as well as the longitudinal position of the transverse sections and the vertical height of ship gravitational centre.

8.1.4 The standard method for the estimation of the effective wave slope is applicable only to standard mono-hull vessels. For a ship which does not fall in this category, other prediction methods described in 8.1.1.1, 8.1.1.3 and 8.1.1.4 should be applied. For a ship having very short natural roll period, the method described in 8.1.1.1 is desirable.

8.2 Standard methodology for the estimation of the effective wave slope function

8.2.1 The standard methodology for the estimation of the wave slope function is based on the following assumptions and approximations:

.1 The underwater part of each transverse section of the ship is substituted by an "equivalent underwater section" having, in general, the same breadth at waterline and the same underwater area of the original section; however:

.1 sections having zero breadth at waterline, such as those in the region of the bulbous bow, are neglected; and

.2 the draught of the "equivalent underwater section" is limited to the ship sectional draught.

.2 The effective wave slope coefficient for each wave frequency is determined by using the "equivalent underwater sections" considering only the undisturbed linear wave pressure.

.3 For each section, a formula is applied which is exact for rectangles.

8.2.2 For each longitudinal position x along the vessel, the draught $T_{eq}(x)$ (m), the breadth $B_{eq}(x)$ (m) and the underwater sectional area $A_{eq}(x)$ (m^2) of the "equivalent vessel" are to be calculated as follows:

$$\begin{cases} \text{if } A(x) > 0 \text{ and } B(x) > 0: \begin{cases} \text{if } \frac{A(x)}{B(x)} \le T(x) \text{ then } \begin{cases} A_{eq}(x) = A(x) \\ B_{eq}(x) = B(x) \\ T_{eq}(x) = \frac{A(x)}{B(x)} \end{cases} \\ \text{if } \frac{A(x)}{B(x)} > T(x) \text{ then } \begin{cases} T_{eq}(x) = T(x) \\ B_{eq}(x) = B(x) \\ A_{eq}(x) = B_{eq}(x) \cdot T_{eq}(x) \end{cases} \end{cases} \\ \text{otherwise: } \begin{cases} A_{eq}(x) = 0 \\ B_{eq}(x) = 0 \\ T_{eq}(x) = 0 \end{cases} \end{cases} \tag{8.2.1}$$

where $A(x)$, $B(x)$ and $T(x)$ are, respectively, the underwater sectional area, the sectional breadth at waterline and the sectional draught of the ship.

8.2.3 The underwater volume ∇_{eq} (m^3), the transverse metacentric radius $BM_{T,eq}$ (m), the vertical position of the centre of buoyancy KB_{eq} (m) and the vertical position of centre of gravity KG_{eq} (m) of the "equivalent vessel" are to be calculated as follows:

$$\begin{cases} \nabla_{eq} = \displaystyle\int_{x_{AE}}^{x_{FE}} A_{eq}(x)dx \\ BM_{T,eq} = \dfrac{1}{\nabla_{eq}} \cdot \displaystyle\int_{x_{AE}}^{x_{FE}} \dfrac{1}{12} \cdot B_{eq}^{3}(x)dx \\ KB_{eq} = T + \dfrac{1}{\nabla_{eq}} \cdot \displaystyle\int_{x_{AE}}^{x_{FE}} \dfrac{-T_{eq}(x)}{2} \cdot A_{eq}(x)dx \\ KG_{eq} = KB_{eq} + BM_{T,eq} - \overline{GM} \end{cases} \quad (8.2.2)$$

where $\overline{GM}$ is the upright metacentric height (m), T is the draught amidships (m), and x_{AE} and x_{FE} correspond to the longitudinal coordinates of the aft end and forward end of the ship, respectively. The vertical positions KB_{eq} and KG_{eq} are defined with respect to the base line of the ship.

$$\begin{cases} r(\omega) = \left| \dfrac{\int_{x_{AE}}^{x_{FE}} C(x)dx}{\nabla_{eq} \cdot \overline{GM}} \right| \\ \text{where} \\ C(x) = \begin{cases} 0 \quad \text{if } A_{eq}(x) = 0 \text{ and } B_{eq}(x) = 0 \\ A_{eq}(x) \cdot \left[K_1(x) + K_2(x) + F_1(x) \cdot OG_{eq}\right] \quad \text{otherwise} \end{cases} \\ \text{and} \\ k_w = \omega^2/g \quad ; \quad OG_{eq} = KG_{eq} - T \\ K_1(x) = \dfrac{sin\left(k_w \cdot \dfrac{B_{eq}(x)}{2}\right)}{\left(\dfrac{k_w \cdot B_{eq}(x)}{2}\right)} \cdot \dfrac{\left(1 + k_w \cdot T_{eq}(x)\right) \cdot e^{-k_w \cdot T_{eq}(x)} - 1}{k_w^2 \cdot T_{eq}} \\ K_2(x) = -\dfrac{e^{-k_w \cdot T_{eq}(x)}}{k_w^2 \cdot T_{eq}(x)} \cdot \left[cos\left(k_w \cdot \dfrac{B_{eq}(x)}{2}\right) - \dfrac{sin\left(k_w \cdot \dfrac{B_{eq}(x)}{2}\right)}{\left(\dfrac{k_w \cdot B_{eq}(x)}{2}\right)}\right] \\ F_1(x) = -\dfrac{1 - e^{-k_w \cdot T_{eq}(x)}}{k_w \cdot T_{eq}(x)} \cdot \dfrac{sin\left(k_w \cdot \dfrac{B_{eq}(x)}{2}\right)}{\left(\dfrac{k_w \cdot B_{eq}(x)}{2}\right)} \end{cases} \quad (8.2.3)$$

8.3 Direct calculation of the Froude-Krylov roll moment used in the level 2 criterion for excessive acceleration failure mode

8.3.1 The parameters a and b in paragraph 2.3.3.2.2 of the Interim Guidelines are the cosine and sine components, respectively, of the Froude-Krylov roll moment in regular beam waves of unit amplitude (kN·m/m).

8.3.2 The parameters a and b can be calculated by integration of the undisturbed linear wave pressure over the mean wetted hull surface of the ship, S_H, with the following formulae:

$$a = \frac{1}{1000}\rho g \iint_{S_H} e^{k_w z} cos(k_w y)\, n_4 dS\,,\ b = -\frac{1}{1000}\rho g \iint_{S_H} e^{k_w z} sin(k_w y)\, n_4 dS \quad (8.3.1)$$

where g is the acceleration due to gravity (m/s^2), ρ is the density of sea water (kg/m^3), $k_w=\omega^2/g$ is the wave number (rad/m), (x, y, z) are the coordinates of a generic point over S_H (m^3), with the x-axis directed longitudinally from stern to bow, the y-axis directed transversally from starboard to port side and the z-axis directed upwards. The quantity n_4 (m) is defined as follows:

$$n_4 = (z - z_G) \cdot n_y - (y - y_G) \cdot n_z \tag{8.3.2}$$

where y_G (m) and z_G (m) are, respectively, the transversal and vertical coordinates of the centre of gravity (without correction for free surface), n_y (-) and n_z (-) are, respectively, the transversal and vertical components of the unit normal vector to the hull pointing towards the fluid.

8.3.3 For laterally symmetric ship hulls, the parameters a and b can also be determined as follows:

$$a = 0, \;\; b = \frac{1}{1000} m \cdot g \cdot GM \cdot r \cdot \frac{\omega^2}{g} \tag{8.3.3}$$

where m (kg) is the ship mass, GM (m) is the metacentric height, and r (-) is the effective wave slope function calculated according to the linear Froude-Krylov approach.

9 Estimation of roll damping

9.1 General

9.1.1 There are a number of ways by which roll damping data can be obtained for the purpose of determining damping coefficients for use in the level 2 vulnerability criteria assessments. These methods include, but are not limited to, model experiments, the ITTC recommended procedure (7.5-02-07-04.5) approved in 2021 or amended, and the simplified Ikeda method. The procedure for determining roll damping coefficients is presented in the following sections.

9.2 The simplified Ikeda method [7]

9.2.1 *General considerations*

9.2.1.1 The equivalent linear roll damping coefficient, $B_{44}(\varphi_a)$ as a function of the roll amplitude, φ_a, can be obtained by the following prediction method. Here, the roll damping coefficient B_{44} and the circular roll frequency $\omega = 2\pi/T_r$ are non-dimensionalized using the following equations:

$$\hat{B}_{44} = \frac{B_{44}}{\rho \nabla B^2}\sqrt{\frac{B}{2g}} \qquad\qquad \hat{\omega} = \omega\sqrt{\frac{B}{2g}} \tag{9.2.1}$$

The prediction method used here separates the roll damping into five damping components: the skin-friction damping component, B_F, the wave-making damping component, B_W, the eddy-making damping, B_E, the bilge keel damping component, B_{BK}, and the lift component, B_L, which is added for forward speeds.[8] This allows the roll damping coefficient B_{44} to be

---

7 Kawahara, Y., Maekawa, K., Ikeda, Y. *A Simple Prediction Formula of Roll Damping of Conventional Cargo Ships on the Basis of Ikeda's Method and Its Limitation*. Chapter 26 of Contemporary Ideas on Ship Stability and Capsizing in Waves, Neves, M.A.S., Belenky V.L., de Kat, J.O., Spyrou, K. and Umeda, N., eds., Springer, ISBN 978-94-007-1481-6, pp. 465-486, 2011.

8 If the simplified Ikeda method is used for individual components as opposed to the total roll damping coefficient, due caution should be exercised and validation should be carried out on the basis of experimental data.

expressed, in dimensional form, as follows:

$$B_{44} = B_F + B_W + B_E + B_L + B_{BK} \quad (9.2.2).$$

9.2.1.2 For each component, a prediction formula was developed based on hydrodynamics together with the parameters adjusted with systematic model experimental results and validated with many merchant ships. As a result, the obtained formula uses hull geometry offset and bilge keel details. Then, for simplicity, regression analyses for the systematically calculated results of the established prediction method were executed. As a result, a simplified prediction method, which only uses the ship principal particulars and the bilge keel dimensions, was obtained. Users are cautioned that all digits of coefficients in the formulae must be used.

9.2.1.3 The formulae for the respective components in 9.2.2, 9.2.3, 9.2.4, 9.2.5, or 9.2.6 are applicable for ranges of certain vessel parameters, which derive from the regression analysis on which they are based. Because of the nature of the regression analysis, if a ship's parameter exists outside its applicable range, the parameter value should be kept at the corresponding maximum or minimum limit value for the use of the associated formula.

The parameters C_B, B/d, OG/d, and C_m have the associated application limits for the B_W, B_E, *and* B_{BK} damping components:

$0.5 \leq C_B \leq 0.85$; $2.5 \leq B/d \leq 4.5$; $-1.5 \leq OG/d \leq 0.2$; and $0.9 \leq C_m \leq 0.99$. (9.2.3)

$\hat{\omega} \leq 1.0$ is applicable only for the B_W damping component.

For the B_{BK} damping component, additional application limits apply:

$0.01 \leq b_{BK}/B \leq 0.06$ and $0.05 \leq l_{BK}/L_{BP} \leq 0.4$,

where b_{BK} and l_{BK} indicate the width and length of each bilge keel, respectively.

There are no application limits for both the B_F and the B_L damping components. For the application of the method, the length between perpendiculars, L_{BP} , should be taken equal to L.

9.2.2 *Skin-friction damping component*

9.2.2.1 The skin-friction damping component is given by the following equation:

$$B_F = \frac{4}{3\pi}\rho s_f r_f^3 \varphi_a \omega c_f \quad (9.2.4)$$

where c_f is the frictional coefficient, r_f is the average radius from the axis of rolling, s_f is the wetted surface area, and the roll amplitude, φ_a, is expressed in radians. These parameters are given as follows:

$$c_f = \left(\frac{1.328}{\sqrt{3.22}}\right)\frac{\sqrt{T_r \nu}}{r_f \varphi_a} \quad (9.2.5)$$

$$r_f = \frac{(0.887+0.145C_B)\cdot(1.7d+C_B B)-2\cdot OG}{\pi} \quad (9.2.6)$$

$$s_f = L_{BP}(1.75d+C_B B) \quad (9.2.7)$$

where φ_a denotes roll amplitude (radians), ν is the coefficient of dynamic viscosity, OG is the distance from calm water surface to the centre of gravity (downward direction is positive), L_{BP} is the ship length between perpendiculars, and d *is the* draught. In the present method, therefore, $OG = d - KG$.

9.2.3 *Wave-making damping component*

9.2.3.1 The non-dimensionalized wave-making damping component is given by the following equation:

$$\hat{B}_W = \frac{A_1}{\hat{\omega}} \cdot exp\left(\frac{-1}{1.44} A_2 (log(\hat{\omega}) - A_3)^2\right) \qquad (9.2.8)$$

where

$$x_1 = B/d \;;\; x_2 = C_b \;;\; x_3 = C_m \;;\; x_4 = 1 - OG/d \;;$$
$$A_1 = AA_1 \cdot \sum_{i=1}^{3} \sum_{j=1}^{4} \sum_{k=1}^{5} Q1_{j+4(i-1),k} x_1^{5-k} x_2^{4-j} x_4^{3-i}$$
$$AA_1 = 1.0 + (1 - x_4) \cdot \sum_{i=1}^{2} \sum_{j=1}^{3} \sum_{k=1}^{5} Q1_{j+3(i-1)+12,k} x_1^{5-k} x_2^{3-j} x_3^{2-i}$$
$$A_2 = \sum_{i=1}^{5} Q2_i x_4^{5-i} \;;$$

Table 9.1 presents the factors of $Q1$ that includes two indices: the first index refers to the row number and the second index refers to the column number.

Table 9.1 – Factors $Q1$ and $Q2$

Factor $Q1$					
column→ / row↓	1	2	3	4	5
1	0.00000	0.00000	0.00000	0.00000	0.00000
2	0.00000	-0.002222	0.040871	-0.286866	0.599424
3	0.00000	0.010185	-0.161176	0.904989	-1.641389
4	0.00000	-0.015422	0.220371	-1.084987	1.834167
5	-0.0628667	0.4989259	0.52735	-10.7918672	16.616327
6	0.1140667	-0.8108963	-2.2186833	25.1269741	-37.7729778
7	-0.0589333	0.2639704	3.1949667	-21.8126569	31.4113508
8	0.0107667	0.0018704	-1.2494083	6.9427931	-10.2018992
9	0.00000	0.192207	-2.787462	12.507855	-14.764856
10	0.00000	-0.350563	5.222348	-23.974852	29.007851
11	0.00000	0.237096	-3.535062	16.368376	-20.539908
12	0.00000	-0.067119	0.966362	-4.407535	5.894703
13	0.00000	17.945	-166.294	489.799	-493.142
14	0.00000	-25.507	236.275	-698.683	701.494
15	0.00000	9.077	-84.332	249.983	-250.787
16	0.00000	-16.872	156.399	-460.689	463.848
17	0.00000	24.015	-222.507	658.027	-660.665
18	0.00000	-8.56	79.549	-235.827	236.579
Factor $Q2$					
Index	1	2	3	4	5
$Q2$	0.00000	-1.402	7.189	-10.993	9.45

$$A_3 = AA_3 + \sum_{i=1}^{7} \sum_{j=1}^{7} Q3_{i,j} x_2^{7-j} x_4^{7-i} \quad ; \text{and}$$

$$AA_3 = \sum_{i=1}^{4} Q4_{1,i} x_1^{4-i} \cdot \sum_{j=1}^{2} \sum_{k=1}^{4} Q4_{j+1,k} x_2^{4-k} x_4^{2-j} \cdot \left(\sum_{i=1}^{9} Q5_i \left(x_4 - \sum_{j=1}^{4} Q4_{4,j} x_1^{4-j} \right)^{10-i} + \sum_{i=1}^{3} Q5_{i+9} x_1^{3-i} \right)$$

Table 9.2 presents the factors of $Q3$ that includes two indices: the first index, i, refers to the row number and the second index, j, refers to the column number.

Table 9.2 – Factors $Q3$

Factor $Q3$							
column→ row↓	1	2	3	4	5	6	7
1	-7686.0287	30131.5678	-49048.9664	42480.7709	-20665.147	5355.2035	-577.8827
2	61639.9103	-241201.0598	392579.5937	-340629.4699	166348.6917	-43358.7938	4714.7918
3	-130677.4903	507996.2604	-826728.7127	722677.104	-358360.7392	95501.4948	-10682.8619
4	-110034.6584	446051.22	-724186.4643	599411.9264	-264294.7189	58039.7328	-4774.6414
5	709672.0656	-2803850.2395	4553780.5017	-3888378.9905	1839829.259	-457313.6939	46600.823
6	-822735.9289	3238899.7308	-5256636.5472	4500543.147	-2143487.3508	538548.1194	-55751.1528
7	299122.8727	-1175773.1606	1907356.1357	-1634256.8172	780020.9393	-196679.7143	20467.0904

Table 9.3 presents the factors of $Q4$ that includes two indices: the first index refers to the row number and the second index refers to the column number. Table 9.3 also presents the factors of $Q5$ that includes one index ranging from 1 to 12 and is obtained from the cell below the index in table 9.3.

Table 9.3 – Factors $Q4$ and $Q5$

Factor $Q4$				
column→ row↓	1	2	3	4
1	-0.3767	3.39	-10.356	11.588
2	-17.102	41.495	-33.234	8.8007
3	36.566	-89.203	71.8	-18.108
4	0	-0.0727	0.7	-1.2818
Factor $Q5$				
Index	1	2	3	4
$Q5$	-1.05584	12.688	-63.70534	172.84571
Index	5	6	7	8
$Q5$	-274.05701	257.68705	-141.40915	44.13177
Index	9	10	11	12
$Q5$	-7.1654	-0.0495	0.4518	-0.61655

9.2.4 *Eddy-making damping component*

9.2.4.1 The non-dimensionalized eddy-making damping component is given by the following equation:

$$\hat{B}_E = \frac{4\hat{\omega}\varphi_a}{3\pi x_2 \cdot {x_1}^3} C_R \tag{9.2.9}$$

Where,

roll amplitude, φ_a, is expressed in radians;

$x_1 = B/d$; $x_2 = C_B$; $x_3 = C_m$;
$C_R = A_E \cdot exp(B_{E1} + B_{E2} \cdot {x_3}^{B_{E3}})$;

$A_E = (-0.0182x_2 + 0.0155) \cdot (x_1 - 1.8)^3 + \sum_{i=1}^{5} Q6_{1,i} x_2^{5-i}$;
$B_{E1} = (-0.2x_1 + 1.6) \cdot (3.98x_2 - 5.1525) \frac{OG}{d} \left(\frac{OG}{d} \sum_{i=1}^{3} Q6_{2,i} x_2^{3-i} + \sum_{i=1}^{2} Q6_{2,i+3} x_2^{2-i} \right)$;

$B_{E2} = (0.25 \frac{OG}{d} + 0.95) \cdot \frac{OG}{d} + \sum_{i=1}^{5} Q6_{3,i} x_2^{5-i}$; and

$$B_{E3} = (46.5 - 15x_1) \cdot x_2 + 11.2x_1 - 28.6;$$

Table 9.4 presents the factors of $Q6$ that includes two indices: the first index refers to the row number and the second index refers to the column number.

Table 9.4 – Factors $Q6$

Factor $Q6$					
column→ row↓	1	2	3	4	5
1	-79.414	215.695	-215.883	93.894	-14.848
2	0.9717	-1.55	0.723	0.04567	0.9408
3	0	-219.2	443.7	-283.3	59.6

9.2.5 *Bilge keel damping component*

9.2.5.1 The non-dimensionalized bilge keel damping component is given by the following equation:

$$\hat{B}_{BK} = A_{BK} \cdot \hat{\omega} \cdot exp(B_{BK1} + B_{BK2} \cdot {x_3}^{B_{BK3}}) \tag{9.2.10}$$

where

$$x_1 = B/d \;\; ; \;\; x_2 = C_B \;\; ; \;\; x_3 = C_m;$$

$$x_6 = \varphi_a \;(deg) \;\; ; \;\; x_7 = \frac{b_{BK}}{B} \;\; ; \;\; x_8 = \frac{l_{BK}}{L_{BP}};$$

$$A_{BK} = f_1 \cdot f_2 \cdot f_3;$$

$$f_1 = (x_1 - 2.83)^2 \sum_{i=1}^{3} Q7_{1,i} x_2^{3-i} + \sum_{i=1}^{3} Q7_{2,i} x_2^{3-i};$$

$$f_2 = \sum_{i=1}^{3} Q7_{3,i} x_6^{3-i};$$

$$f_3 = \sum_{i=1}^{2} \sum_{j=1}^{3} Q7_{3+i,j} x_7^{3-j} x_8^{3-i};$$

$$B_{BK1} = \frac{OG}{d} \cdot \left(5x_7 + 0.3x_1 - 0.2x_8 + \sum_{i=1}^{3} Q7_{6,i} x_6^{3-i}\right)$$

$$B_{BK2} = -15x_7 + 1.2x_2 - 0.1x_1 + \sum_{i=1}^{3} Q7_{7,i} \left(\frac{OG}{d}\right)^{3-i}; \text{ and}$$

$$B_{BK3} = 2.5\frac{OG}{d} + 15.75.$$

Table 9.5 presents the factors of $Q7$ that includes two indices: the first index refers to the row number and the second index refers to the column number.

Table 9.5 – Factors $Q7$

Factor $Q7$			
column→ row↓	1	2	3
1	0	-0.3651	0.3907
2	0	-2.21	2.632
3	0.00255	0.122	0.4794
4	-0.8913	-0.0733	0
5	5.2857	-0.01185	0.00189
6	0.00125	-0.0425	-1.86
7	-0.0657	0.0586	1.6164

9.2.6 *Lift damping component* [9]

9.2.6.1. The non-dimensionalized lift damping component is given by the following equation:

$$\hat{B}_L = \frac{S_L U K_n l_0 l_R}{2\nabla B^2}\left(1 - 1.4\frac{OG}{l_R} + 0.7\frac{OG^2}{l_0 l_R}\right)\sqrt{\frac{B}{2g}} \quad (9.2.11)$$

where

$$K_n = \frac{2\pi d}{L_{BP}} + \kappa\left(4.1\frac{B}{L_{BP}} - 0.045\right);$$

$S_L = L_{BP} d,\ l_0 = 0.3d\ ,\ \ l_R = 0.5d,\ U = F_n\sqrt{L_{BP} g}$; and

$$\kappa = \begin{cases} 0 & C_m \leq 0.92 \\ 0.1 & 0.92 < C_m \leq 0.97 \\ 0.3 & 0.97 < C_m \end{cases}$$

9.3 Equivalent linear roll damping coefficients for the dead ship and excessive acceleration failure modes

9.3.1 In level 1 vulnerability assessment for the excessive acceleration stability failure mode, the non-dimensional logarithmic decrement of roll decay δ_ϕ is calculated as

$$\delta_\varphi = 0.5 \cdot \pi \cdot R_{PR} \quad (9.3.1)$$

where R_{PR} is determined according to paragraph 2.5.2.1 of the Interim Guidelines.

9.3.2 In the level 2 vulnerability assessments for the excessive acceleration stability failure mode and the dead ship stability failure modes, the linear, quadratic and cubic roll damping coefficients can be determined from the equivalent linear roll damping coefficients $B_{44}(\varphi_a)$ (Nm/(rad/s)), which can be obtained with the simplified Ikeda method, for some different roll amplitude by a least square method or equivalent.

$$\frac{2\pi^2 B_{44}(\varphi_a)}{WGMT_r^2} = \frac{\delta_0}{2} + \frac{4}{3\cdot\pi}\cdot\delta_1\cdot\omega_r\cdot\varphi_a + \frac{3}{8}\cdot\delta_2\cdot\omega_r^2\cdot{\varphi_a}^2 \quad (9.3.2)$$

where $W = \rho \cdot g \cdot \nabla$(N). Here, one or more roll damping coefficients can be set a priori to zero, provided that the final fitting is sufficiently accurate.

9.3.3 Alternatively, these roll damping coefficients, δ_0, δ_1 and δ_2, can be determined with roll decay test of the scaled ship model in calm water. The model is initially inclined up to a certain heel angle. This initial angle should be larger than about 25°. If the mean roll angle between the initial angle and the next peak angle is smaller than 20°, the initial angle should be increased to obtain a mean angle of 20° or over. When the initial roll angle is given to the model, additional sinkage and trim should be minimum. The model should be released from an initial angle with zero roll angular velocity. During this test, no disturbance including waves propagating in the longitudinal direction of the basin and reflected by its end should be given to the model. At least four tests with different initial angles are required. If the roll damping is very large, the number of tests should be increased to obtain a sufficient number of peaks of the roll angle. Recording of the roll time history should start before the release of the model to confirm that no angular velocity is given when releasing. Recording should continue until the

[9] Ikeda, Y. *Prediction Methods of Roll Damping of Ships and Their Application to Determine Optimum Stabilization Devices*. Marine Technology, 41(02), 89-93, 2004.

model has reached rolling angles smaller than 0.5°. This eventually requires that the length of the basin should be sufficiently large.

9.3.4 Assuming that the absolute values of measured consecutive extremes (one maximum and following minimum or vice versa) of roll angle during roll decay are φ_1, φ_2 , …. (radians), the mean roll angle $\varphi_{mi} = \frac{\varphi_i+\varphi_{i+1}}{2}$ and the decrement $\Delta\varphi = \varphi_i - \varphi_{i+1}$are calculated. Then Froude's extinction coefficients, a, b and c are determined by fitting these data with equation (9.3.3).

$$\Delta\varphi = a\varphi_m + b\varphi_m^2 + c\varphi_m^3 \tag{9.3.3}$$

Here, one or more extinction coefficients can be set a priori to zero, provided that the final fitting is sufficiently accurate. Then, the roll damping coefficients, by using the energy conservation law, are calculated as follows:

$$\frac{\delta_0}{2} = \frac{2a}{T_r} \tag{9.3.4}$$

$$\delta_1 = \frac{3b}{4} \tag{9.3.5}$$

$$\delta_2 = \frac{4c}{3\pi^2} T_r \tag{9.3.6}$$

9.3.5 The evaluation of ship motions for vulnerability assessment for dead ship condition and excessive acceleration requires linearized roll damping coefficient μ_e (1/s), using statistical linearization. The linearized roll damping coefficient μ_e can be calculated from the following algebraic equation:

$$\mu_e = \frac{\delta_0}{2} + \sqrt{\frac{2}{\pi}} \cdot \delta_1 \cdot \sigma_{d\varphi}(\mu_e) + \frac{3}{2} \cdot \delta_2 \cdot \sigma_{d\varphi}^2(\mu_e) \tag{9.3.7}$$

where $M_D = 2\mu_e(I_{xx} + A_{44})\dot{\varphi}$ and $\sigma_{d\varphi}$ is the standard deviation of roll angular velocity.
As both parts of the equation contain the unknown damping coefficient μ_e, the equation is solved numerically using any appropriate iterative algorithm.

9.3.6 The evaluation of ship motion for the vulnerability assessment for parametric rolling could be based on the following procedure:

.1 The roll motion in calm water can be modelled as follows:

$$(I_{xx} + A_{44})\ddot{\varphi} + (I_{xx} + A_{44})(\delta_0\dot{\varphi} + \delta_1\dot{\varphi}^2 + \delta_2\dot{\varphi}^3) + WGM\varphi = 0 \tag{9.3.8}$$

where

$\ddot{\varphi}$ = roll angular acceleration;

$\dot{\varphi}$ = roll angular velocity; and

W = ship weight.

.2 If the equivalent linear damping coefficient, ($B_{44}(\varphi_a)$, is introduced, the following is obtained:

$$(I_{xx} + A_{44})\ddot{\varphi} + B_{44}(\varphi_a)\dot{\varphi} + WGM\varphi = 0 \tag{9.3.9}$$

then,

$$\ddot{\varphi} + 2\alpha_e\dot{\varphi} + \omega_r^2\varphi = 0 \qquad (9.3.10)$$

where,

$2\alpha_e = \frac{B_{44}(\varphi_a)}{I_{xx}+J_{xx}}$; and

$\omega_r = \sqrt{\frac{WGM}{I_{xx}+J_{xx}}}$.

.3 On the other hand, the solution of equation (9.3.10) is given by $\varphi = \varphi_a e^{-\alpha_e t} cos(\omega_r t - \varepsilon)$ and the extinction curve is given by

$$\Delta\varphi = a\varphi_m + c\varphi_m^3 = (a + c\varphi_m^2)\varphi_m = a_e\varphi_m \qquad (9.3.11).$$

.4 Thus,

$$a_e = \frac{\alpha_e T_r}{2} = \frac{\alpha_e \pi}{\omega_r} = \frac{B_{44}(\varphi_a)}{2(I_{xx}+A_{44})}\frac{\pi}{\omega_r} \qquad (9.3.12).$$

9.3.7 Using the above relationship, a procedure to determine linear and cubic damping coefficients is as follows:

.1 First, B_{44} is obtained with the roll amplitude, φ_a, of 1 degree using the simplified Ikeda method. Using equation (9.3.12) and assuming $a = a_e$, the value of a is obtained.

.2 Then, B_{44} is obtained with the roll amplitude of 25 degrees using the simplified Ikeda method. Using equation (9.3.12), the value of a_e is obtained.

.3 Then, c is determined with the following equation and the value of a determined at the step .1:

$$a_e = a + c\varphi_m^2 \qquad (9.3.13)$$

where φ_m corresponds to 25 degrees.

.4 Using equations (9.3.4) and (9.3.6), linear and cubic roll damping coefficients can be calculated as follows:

$$\frac{1}{2}\delta_0 = \frac{\omega_\varphi}{\pi}a \qquad (9.3.14)$$

$$\delta_3 = \frac{4c}{3\pi^2}\left(\frac{2\pi}{\omega_\varphi}\right) \qquad (9.3.15)$$

9.3.8 For the level 2 criterion for the excessive acceleration failure mode, the following two alternative methods can be used to estimate the roll damping. In the stochastic linearization method for equivalent roll damping, the roll amplitude can be alternatively approximated as follows:

$$\varphi_a = 0.3T_r\sigma_{d\varphi} \qquad (9.3.16)$$

Alternatively, the equivalent linear roll damping coefficient can be defined at 15 degrees of roll amplitude.

10 Methods for determining wave cases for vulnerability criteria

10.1 The selection of the waves to be used in vulnerability criteria is based on the following:

.1 A wave scatter table is selected (the basis for unrestricted service is considered to be IACS Recommendation No.34 (Corr.1 Nov. 2001);

.2 For each spectral period reported in the wave scatter table (typically the zero crossing period) the "reference significant wave height" is selected as the conditional mean significant wave height. This provides a "reference significant wave height" for each spectral period of the wave scatter diagram. Eventually we obtain a series of "reference environmental conditions" $\left(T_{ref,i}, H_{1/3,ref,i} = H_{1/3,ref}\left(T_{ref,i}\right)\right)$ with $i = 1,\ldots,N$ and N being the number of periods in the wave scatter diagram and T_{ref} being the mean period of the spectrum. Each environmental condition has an associated probability $W_i = Pr\{\left(T_{ref,i}, H_{1/3,ref,i}\right)\}$ which is obtained from the wave scatter table as the probability associated to the spectral period $T_{ref,i}$.

.3 The set of N "calculation waves" ("wave cases") are selected separately for parametric roll and pure loss of stability starting from the obtained set of "reference environmental conditions". The following equivalence is used (in the formulae, g is the acceleration due to gravity equal to 9.81m/s^2):

For parametric roll:

$$\begin{cases} \text{Wavelength: } \lambda_i = \frac{g \cdot T_{ref,i}^2}{2\pi} \\ \text{Wave height: } H_i = k_{PR} \cdot H_{1/3,ref,i} \\ \text{Weighting factor: } W_i \\ \text{with } k_{PR} = 0.70 \end{cases} \qquad (10.1.1)$$

For pure loss of stability:

$$\begin{cases} \text{Wavelength: } \lambda_i = \frac{g \cdot T_{ref,i}^2}{2\pi} \\ \text{Wave height: } H_i = k_{PL} \cdot H_{1/3,ref,i} \\ \text{Weighting factor: } W_i \\ \text{with } k_{PR} = 1.40 \end{cases} \qquad (10.1.2)$$

.1 The first check of level 2 vulnerability calculation for parametric rolling are carried out using waves defined in equation (10.1.1).

.2 Level 1 vulnerability calculations are carried out using the following conservative value for the wave steepness parameter:

For parametric roll:

$$s_W = max\left(k_{PR} \cdot \frac{H_{1/3,ref,i}}{\lambda_i}\right) \quad i = 1,\ldots,N \qquad (10.1.3)$$

For pure loss of stability:

$$s_W = max\left(k_{PL} \cdot \frac{H_{1/3,ref,i}}{\lambda_i}\right) \quad i = 1,\ldots,N \qquad (10.1.4)$$

10.2 Application example based on reference wave scatter table

10.2.1 An example application of the procedure is reported in the following. The standard reference environmental conditions in paragraph 2.7.2 of the Interim Guidelines are used, and the corresponding wave scatter table is table 2.7.2.1.2, which refers to IACS Recommendation No.34 (Corr. Nov.2001). Assuming a Bretschneider sea spectrum, the zero-crossing period, T_Z, presented in table 2.7.2.1.2 can be converted to the mean period, T_{mean}, as follows:

$$\text{Bretschneider sea spectrum:} \quad T_{mean} = 1.0864 \cdot T_z \tag{10.2.1}$$

If the sea spectrum to be used has a spectral shape that is different from the shape of the Bretschneider spectrum, then the equation 10.2.1 should be modified appropriately.

10.2.2 The reference period to be used for the determination of the wavelength in the "wave cases" is assumed to be the mean spectral period defined, starting from the zero-crossing period provided by the wave scatter table (table 2.7.2.1.2).

If P_{ij} is defined to be the probability associated with the sea state $\left(T_{z,i}, H_{1/3,j}\right)$ characterized by period $T_{z,i}$ and significant wave height $H_{1/3,j}$ the conditional average significant wave height $E\left\{H_{1/3}\middle|T_{z,i}\right\}$ is determined as follows:

$$E\left\{H_{1/3}\middle|T_{z,i}\right\} = \frac{1}{W_i}\sum_{j=1}^{M} P_{ij} \cdot H_{1/3,j} \quad \text{where} \quad W_i = \sum_{j=1}^{M} P_{ij} \tag{10.2.2}$$

Then, the reference significant wave height is assumed to be equal to the conditional average significant wave height obtained in equation (10.2.2), i.e.:

$$H_{1/3,ref,i} = E\left\{H_{1/3}\middle|T_{z,i}\right\} \tag{10.2.3}$$

The wavelength λ_i is determined as:

$$\lambda_i = \frac{g \cdot T_{ref,i}^2}{2 \cdot \pi} = \frac{g \cdot T_{mean,i}^2}{2 \cdot \pi} = \frac{g \cdot (1.0864 \cdot T_{z,i})^2}{2 \cdot \pi} \tag{10.2.4}$$

10.2.3 The conditional average significant wave height as a function of the zero-crossing period is presented in table 10.1.

Table 10.1 Conditional average significant wave height as a function of the zero-crossing period

Zero crossing period T_z [s]	Conditional average significant wave height $E\left\{H_{1/3}\middle|T_z\right\}$ [m]
3.5	0.500
4.5	0.707
5.5	1.225
6.5	1.850
7.5	2.474
8.5	3.150
9.5	3.852

Zero crossing period T_z [s]	Conditional average significant wave height $E\{H_{1/3}\|T_z\}$ [m]
10.5	4.537
11.5	5.179
12.5	5.771
13.5	6.315
14.5	6.813
15.5	7.281
16.5	7.671
17.5	8.029
18.5	8.500

10.2.4 On the basis of the reference wave scatter table and of the results in table 10.1:

.1 The wave steepness s_W in paragraph 2.4.2.2 of the Interim Guidelines can be determined using (10.1.2), (10.1.4) and (10.2. 4);

.2 The wave steepness s_W in paragraph 2.5.2.2 of the Interim Guidelines can be determined using (10.1.1), (10.1.3) and (10.2.4);

.3 The wave cases reported in table 2.5.3.2.3 of the Interim Guidelines can be determined using (10.1.1) and (10.2.4).

APPENDIX 4

THEORETICAL BACKGROUND, VALIDATION, AND APPLICATION EXAMPLES FOR GUIDELINES ON DIRECT STABILITY ASSESSMENT

1 Introduction

1.1 In a probabilistic direct stability assessment and probabilistic operational measures, probability of stability failure is used directly as a safety measure (criterion); therefore, these options require counting of stability failures, which is described below in sections concerning direct counting.

1.2 Direct counting means that stability failures need to be encountered in simulations, which leads to a problem of rarity since stability failures are very rare for relevant ships and loading conditions; therefore, very long simulations are required. Besides, accurate estimation of the stability failure probability requires encounter of a sufficiently large number of stability failures, which further increases the required simulation time.

1.3 At the same time, direct stability assessment should enable the most accurate assessment within second generation intact stability criteria (SGISC), taking into account as much relevant physics as possible and in the most accurate way. This means that the simulation tools employed are rather slow and require much more computational time than tools used in level 1 and level 2 vulnerability assessment.

1.4 Therefore, some methods to accelerate assessment are required in the probabilistic procedures used. Several such methods are used in the Interim Guidelines: assessment in design situations, statistical extrapolation and deterministic assessment.

2 Validation of numerical methods for simulation of ship motions

2.1 Qualitative validation: Backbone curve

2.1.1 Qualitative validation requirements are summarized in table 3.4.2 of the Interim Guidelines. A demonstration of consistency between the calculated roll backbone curve and the GZ curve in calm water is required for software where the hydrostatic and Froude-Krylov forces are calculated with a body-exact formulation. The roll backbone curve is a dependency of the roll frequency in calm water on the initial roll amplitude.

2.1.2 To serve the purpose of the qualitative validation, the roll backbone curve provided by the calculation code should be computed in the same software configuration that is used for the direct stability assessment. Figure 2.1.1 illustrates calculations of the backbone curve. The backbone curve, computed with a potential flow code, suggests an initial increase of GM as the backbone curve shows an initial hardening, which is confirmed by the local GM (derivative of GZ) shown in figure 2.1.2.

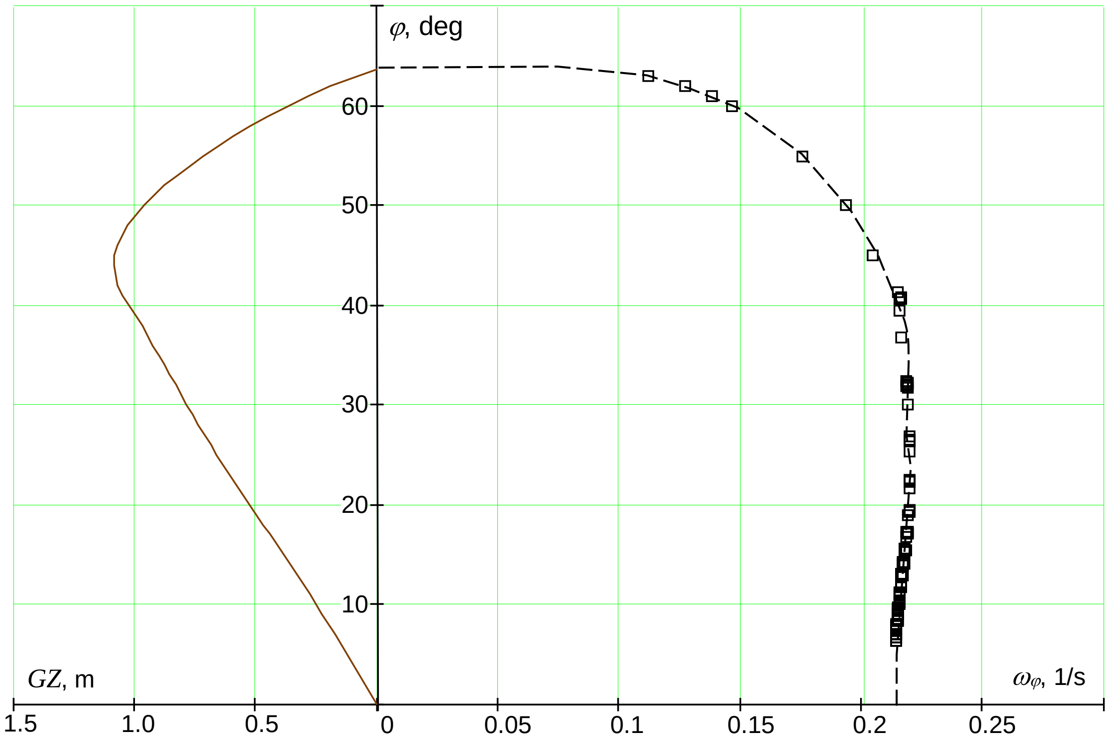

Figure 2.1.1: The roll backbone curve and the *GZ* curve

2.1.3 As expected, the backbone curve "bends" towards zero with the softening of the dynamical system around 40° of the initial amplitude. An unstable equilibrium at the angle of vanishing stability slows down the dynamical system causing the roll period to grow.

2.1.4 The calculations of the backbone curve were done by series of simulations in calm water. All initial conditions except for the roll angle are set to zero. The initial roll angle is set close to the angle of vanishing stability. In total, 4 to 6 simulations are recommended with different initial roll angles. The difference between roll angles can be taken as 0.1 º. In general, it may not always be possible to perform roll decays starting very close to the angle of vanishing stability. In such cases, the roll decay should start from large enough initial angles.

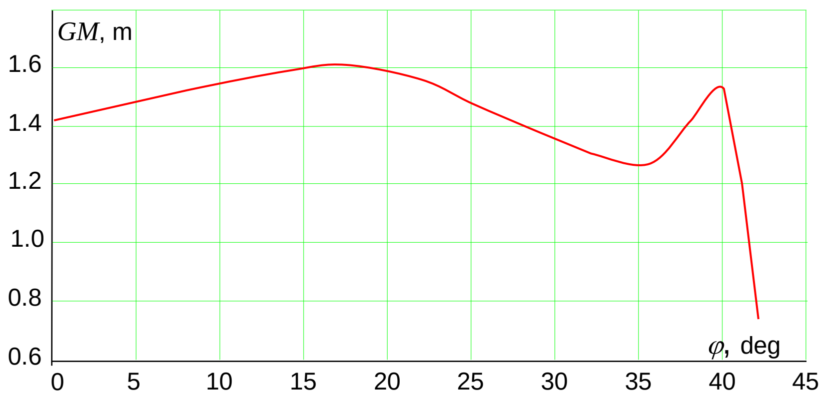

Figure 2.1.2: local *GM* (derivative of *GZ*) vs. heel angle

2.1.5 A calculation of the natural frequency is performed on a half-oscillation basis: $\omega_\varphi(A_i) = \pi/(t_{i+1} - t_i)$, where an amplitude A_i occurs between the zero-crossings at t_{i+1} and t_i, shown in figure 2.1.3.

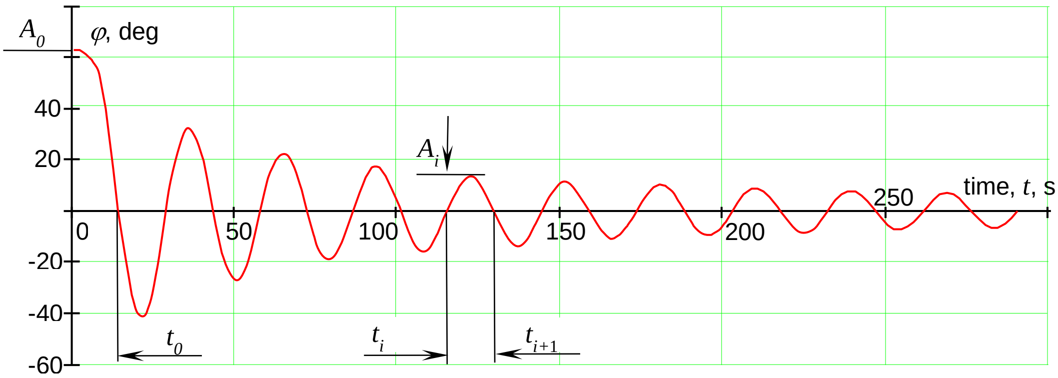

Figure 2.1.3: Roll motion computed with potential flow code

2.1.6 The largest amplitude is the initial roll angle, A_0, as shown in figure 2.1.3. The lowest frequency on the backbone curve is computed with a quarter of an oscillation, $\omega_\varphi(A_0) = 0.5\pi/t_0$.

2.2 Qualitative validation: Response curve

2.2.1 The qualitative validation from table 3.4.2 of the Interim Guidelines contains a requirement for the demonstration of consistency between the calculated roll backbone curve and the roll response curve. The roll response curve is a dependence of roll amplitude in regular waves on the frequency of those waves.

2.2.2 Calculation of the roll response curve was done by a series of simulations in regular waves with frequencies in a range from 0.7 to 1.2 of the roll natural frequency. Two sets of simulations were performed: one set from low frequency to high frequency and the other set from high frequency to low.

2.2.3 Each simulation was carried out until a steady state was achieved. Duration of the simulation was at least 30 roll periods. A criterion of a steady state was the observation of a periodic solution where the difference between the successive amplitudes was within 1%. The reported amplitude was computed as an average of five successive amplitudes satisfying this steady state requirement.

2.2.4 The steady state initial conditions were computed for a time instant of a wave zero-crossing during one of five roll oscillations where amplitudes satisfy the steady state requirement of 2.2.3. Initial conditions for the first simulation were set to zero; steady state initial conditions from previous simulations were used for the second and further simulations.

2.2.5 The consistency between the roll response curve and the backbone curve is observed when the response curves bend together with the backbone curve as can be seen in the example described in paragraphs 2.2.6-2.2.10.

2.2.6 Example calculations[10] are presented for a fishing vessel, for which a panel model is shown in figure 2.2.1 (without a forecastle), the principal characteristics are given in table 2.2.1, and the GZ curve, used for the single degree of freedom (1-DOF) response curve calculation, is shown in figure 2.2.2.

Table 2.2.1 Principal dimensions of a fishing vessel

Length BP, m	22.00
Breadth moulded, m	6.62
Draught amidships, m	2.70
KG, m	2.78
Displacement, t	197.00
GM, m	0.22

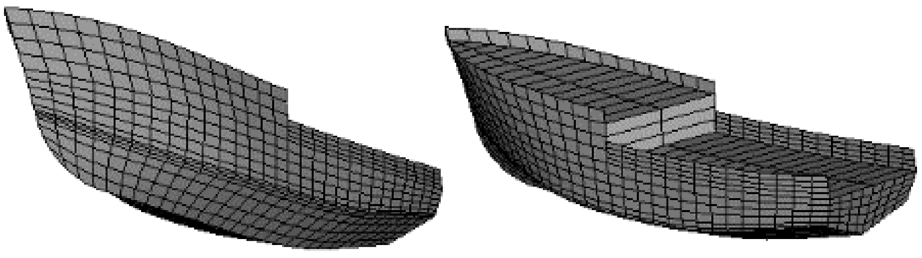

Figure 2.2.1 Hull geometry of a fishing vessel

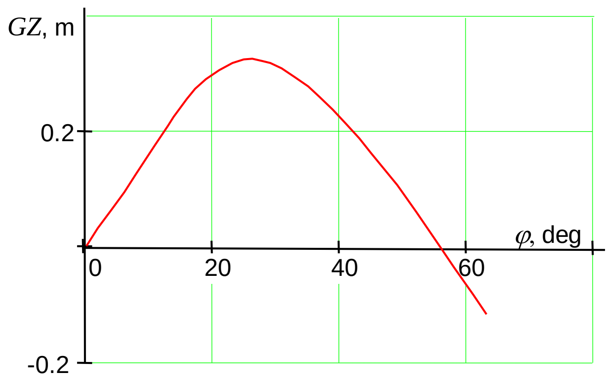

Figure 2.2.2: Righting arm (GZ) curve of fishing vessel for response curve calculation

2.2.7 Calculations were carried out with a 3D potential flow code and consisted of a series of simulations in regular beam waves. After the initial transient, positive and negative peaks were measured, shown in figure 2.2.3 (⊡ for positive peaks and + for negative peaks). Simulation started from high and then from low wave frequencies. Initial conditions were assigned using the steady state response, achieved for the previous wave frequency.

2.2.8 The roll response amplitudes computed by the 3D potential flow code are located on both sides of the backbone curve, showing an expected "bending pattern". The consistency between backbone curve and roll response curve has been demonstrated.

[10] Shin, Y. S, Belenky, V. L., Lin, W. M., Weems, K. M. and Engle, A. H. *Nonlinear time domain simulation technology for seakeeping and wave-load analysis for modern ship design*. *SNAME Trans*. Vol. 111, pp. 557-578, 2003.

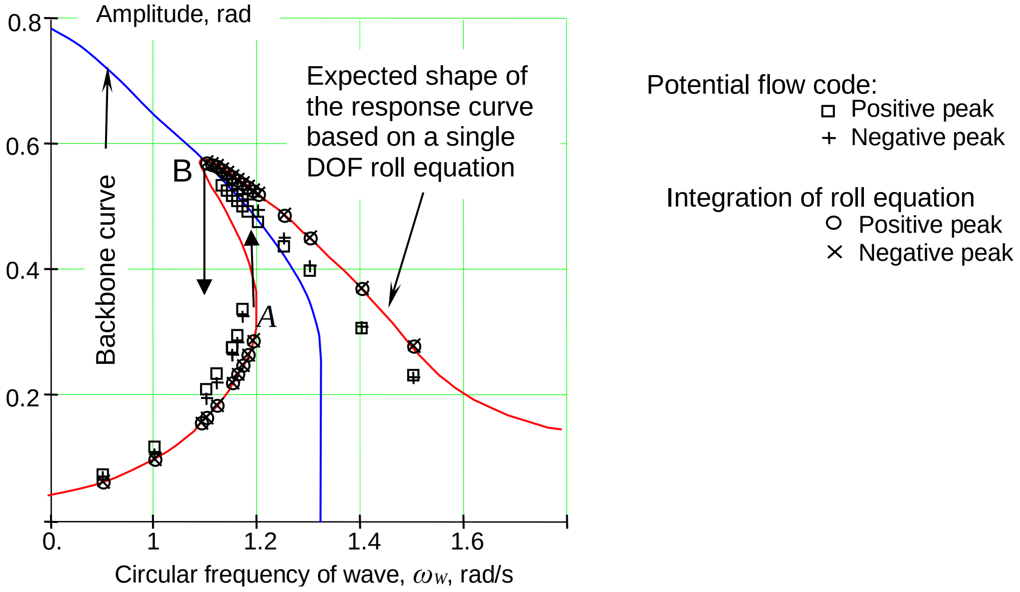

Figure 2.2.3:Response curve of roll, based on 3D potential flow simulations; circular frequency range from 0.9 to 1.18 rad/s, wave amplitude 0.4 m

2.2.9 To reveal expected shape of the roll response curve, 3D potential flow simulations were supplemented with a direct numerical integration of the approximate differential equation for roll, using the actual GZ curve and approximate Froude-Krylov wave excitation:

$$\ddot{\varphi} + \delta_0\dot{\varphi} + f(\varphi) = \alpha_m\omega_{\varphi 0}^2\sin(\omega_W t) \qquad (2.2.1)$$

where $\omega_{\varphi 0}$ is the natural roll frequency, δ_0 is the roll damping coefficient, α_m is the effective amplitude of the wave slope, ω_W is the wave frequency, and $f(\varphi)$ is the stiffness function, expressed through the GZ curve as $f(\varphi) = mgGZ(\varphi)/(I_x + A_{44})$, where m is mass displacement, I_x the transverse moment of inertia of ship mass and A_{44} is added mass in roll. Numerical integration of the ordinary differential equation was done in the same way as in 3D potential flow simulations: the steady state condition of the previous frequencies was used as initial conditions for the next wave frequency. The results are shown in figure 2.2.3 (○ for positive and × for negative peaks).

2.2.10 As expected, the bending of the backbone curve causes a response curve to fold, forming a range of frequencies where two stable steady state responses are possible; identified by points A and B in figure 2.2.3. The observation of the folding of the 3D potential flow response demonstrates consistency between the backbone curve and the response curve that satisfies the requirement in line 2 of table 3.4.2 of the Interim Guidelines. However, the regions of frequency with multiple steady states are not always present, and the response curve may still bend and show only one single steady state for each forcing frequency.

2.3 Qualitative validation: Change of stability in waves

2.3.1 The qualitative validation, table 3.4.2 of the Interim Guidelines, requires demonstration of a capability to reproduce the wave pass effect. The objective is to verify that the stability decreases when the wave crest is located near the midship sections. An example of a possible procedure can be found in the literature.[11] Verification of the variation of instantaneous stability in waves with a numerical simulation is carried out as follows:

.1 Set the wave length equal to the ship length.

.2 Set the simulation in following waves at a ship forward speed equal to the wave celerity.

.3 Set an initial position of a ship to have a wave trough near the midship section. The ship is expected to remain stationary relative to the wave.

.4 Apply a constant external heeling moment.

.5 Record the ship motions until the transition is completed and an equilibrium state is achieved; then, extract the equilibrium heel angle.

.6 Repeat the procedure for different values of the external heeling moment.

.7 Repeat the procedure for an initial position of the ship corresponding to a location of the wave crest near the midship section.

2.3.2 Example calculations were carried out for the ONR tumblehome top configuration;[12] principal characteristics are given in table 2.3.1. The wave length is equal to the ship length (154 m) and the wave height is 6 m. Two wave positions were used for qualitative validation, with a wave crest midships and wave trough midships.

Table 2.3.1 Principal dimensions of ONR tumblehome top configuration

Length BP, m	154.00
Breadth moulded, m	18.00
Draught midships, m	5.50
KG, m	8.32
Displacement, t	8,675.60
GM, m	1.50

2.3.3 Figure 2.3.1 shows the achieved heel angles under the external heeling moment (heeling lever curves), computed with a 3D potential flow code for the wave crest and the wave trough located midships. The figure demonstrates the change of stability in waves: the achieved heel angle under the same heeling moment is significantly larger when wave crest is located near midships, compared to when the wave trough is located near midships. The figure also shows that the stability on a wave trough is better, while stability on a wave crest is worse in comparison with calm water.

11 Belenky, V. and Weems, K.M. *Probabilistic Qualities of Stability Change in Waves*. Proc. 10th Intl. Ship Stability Workshop, Daejeon, Korea, pp. 95-108, 2008.

12 Bishop, R. C., Belknap, W., Turner, C., Simon, B. and Kim, J. H. *Parametric Investigation on the Influence of GM, Roll Damping, and Above-Water Form on the Roll Response of Model 5613*. Report NSWCCD-50-TR-2005/027, 2005.

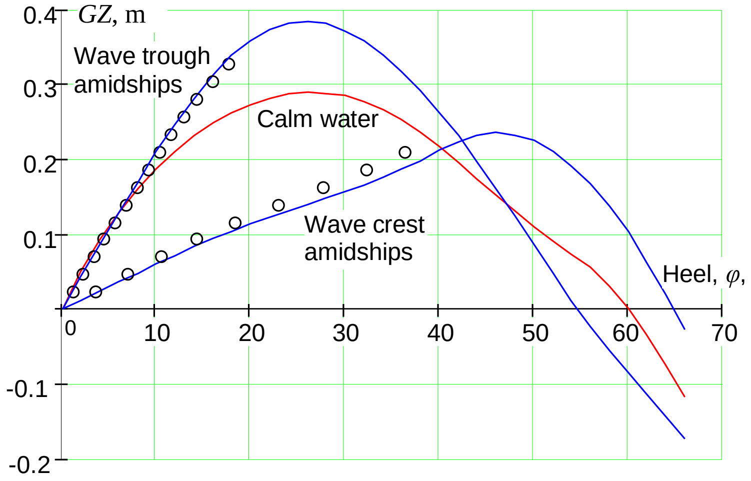

Figure 2.3.1: ***GZ* curves from both static calculations in waves (solid lines) and heeling lever curves (circles) computed with a 3D potential flow code**

2.4 Qualitative validation: Principal parametric roll resonance

2.4.1 The qualitative validation, as shown in table 3.4.2 of the Interim Guidelines, requires demonstration of a capability to reproduce a principal parametric roll resonance. The objective is to observe an increase and stabilization of amplitudes in following or head waves at an encounter frequency that is about twice the natural roll frequency (which is termed principal parametric roll resonance).

2.4.2 Figure 2.4.1 shows a time history from 3D potential flow code simulations in following waves for the C11 class container ship at zero forward speed. The draught is 12.7 m, the KG is 19.0 m, the GM is 1.29 m and the natural roll frequency is 0.199 rad/s. The wave height was 2 m and the wave frequency was 0.42 rad/s (equal to the encounter frequency at zero forward speed). Figure 2.4.2 shows the entire frequency range of the principle parametric resonance computed for these conditions.

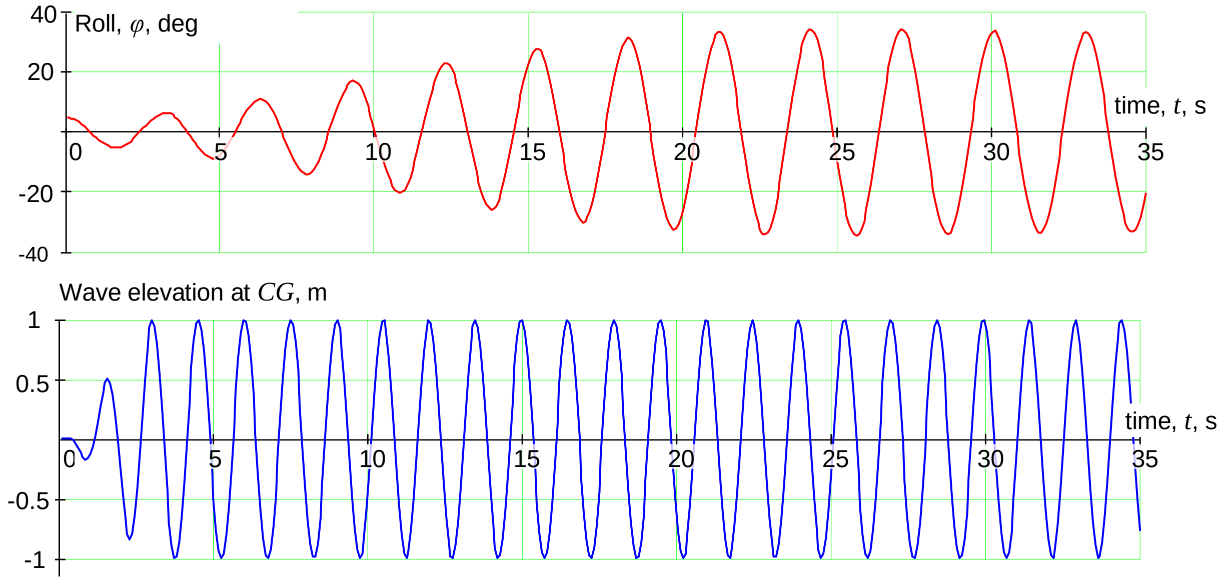

Figure 2.4.1: Time history of the principle parametric resonance computed with a 3D potential flow code for the C11 class container ship with a natural roll period of 0.199 rad/s at zero forward speed, a wave height of 2 m and a wave frequency of 0.42 rad/s

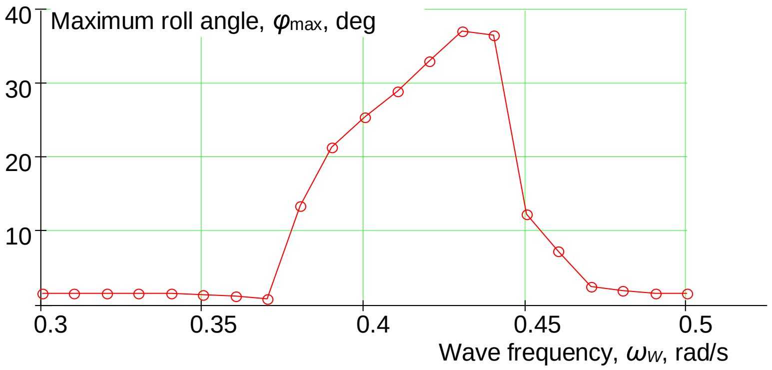

Figure 2.4.2: The frequency range of the principle parametric resonance computed with 3D potential flow code for the C11-class container ship with a natural roll period of 0.199 rad/s at zero forward speed and a wave height of 2 m

2.4.3 Since there is no direct roll excitation in following waves, parametric resonance is the only reason for increasing roll amplitude; a non-zero amplitude response is grouped around a wave encounter frequency that is twice the roll frequency. Thus, it is the principle parametric resonance.

2.5 Quantitative validation requirements

2.5.1 Indicative requirements and acceptance criteria for the quantitative validation of numerical methods for the simulation of ship motions for direct stability assessment are summarized in table 3.4.3 of the Interim Guidelines; rows 1, 2 and 4 are relevant for the parametric roll stability failure mode.

2.5.2 Row 1 of table 3.4.3 of the Interim Guidelines contains requirements for the response curve of parametric roll: the maximum (over encounter frequency) roll amplitude should not be underpredicted by more than 10% if the amplitude is less than the angle of the maximum GZ and 20% otherwise. At the same time, an underprediction of less than two degrees can be disregarded. A comparison of 3D potential flow code results with a model test on parametric roll[13] is shown in figure 2.5.1. The model test included all six DOF and was run at a fixed speed of 10 knots in a wave with full-scale height of 8.4 m and period of 14.0 s. The difference between the measured and the computed parametric roll amplitude was within one degree. However, the comparison is available for one frequency and one can accept partial satisfaction of the requirements in the first row.

13 France, W. N., Levadou, M., Treakle, T.M., Paulling, J.R., Michel, R W.K and Moore, C. *An Investigation of Head-Sea Parametric Rolling and its Influence on Container Lashing Systems*, Marine Technology, 40(1): 1-19, 2003.

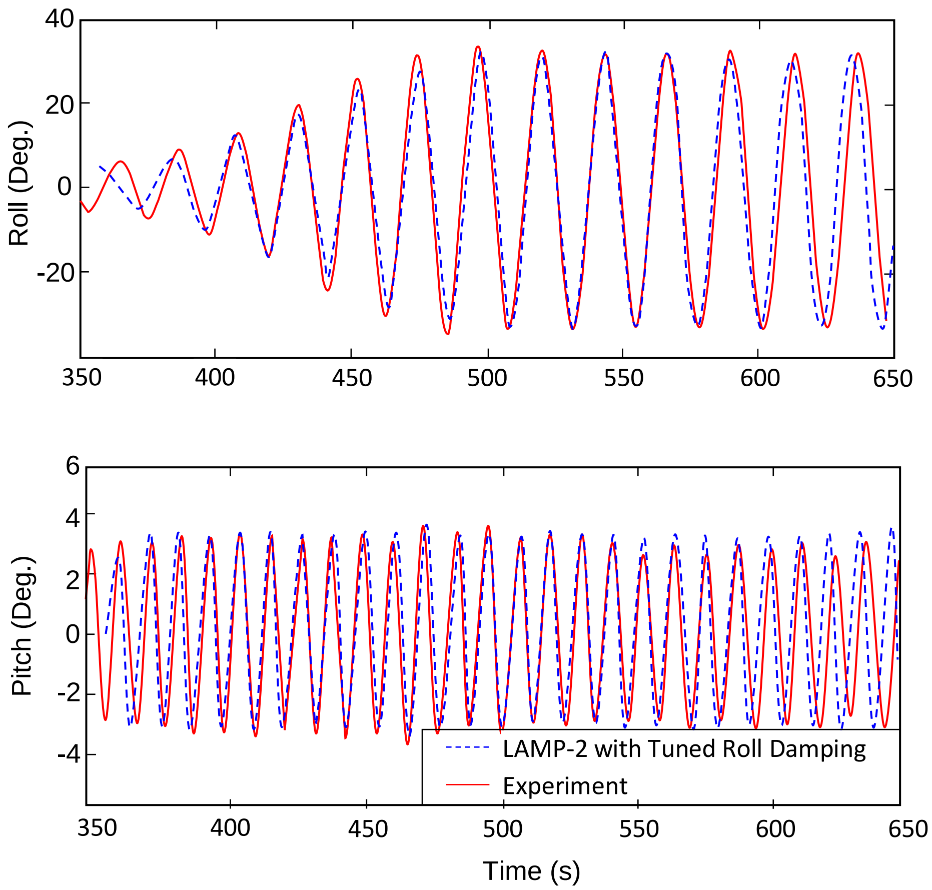

Figure 2.5.1:A comparison in a time series of parametric rolling between the experiment and a 3D potential flow code

2.5.3 Row 4 of table 3.4.3 of the Interim Guidelines contains requirements for the variance testing for parametric roll. The objective is to demonstrate a correct, in terms of statistics, modelling of roll response in irregular waves. An example using the C11 class post-Panamax containership, whose details are available in appendix 2, is shown in figures 2.5.2 and 2.5.3.[14] Here, the model experiment was conducted at a towing tank: the ship model was towed by a towing carriage using soft elastic ropes. The measuring time durations of the experiments were 4,200, 2,400 and 1,200 s in full scale for the Froude numbers of 0.0, 0.05, 0.1, respectively. The numerical model used here is a heave-roll-pitch coupled model. The non-linear Froude-Krylov forces are directly calculated by integrating the wave pressure up to an irregular wave surface profile. The 2D hydrodynamic forces used for the radiation and diffraction forces are calculated for the submerged hull by the integral equation method with an instantaneous roll angle taken into account. The radiation forces in roll are calculated for the natural roll frequency and those in vertical motion (heave and pitch) are done for the peak of mean wave frequency. The linear and quadratic roll damping coefficients are used in the mathematical model: they are determined from an experimental result of roll decay tests. The numbers of realizations for both the experiment and the simulation are 10 for the Froude number of 0.0 and 0.05 and are 5 for the Froude number of 0.1. In all cases, the confidence intervals of the ensemble average of variance of roll angle from the simulation are overlapped with those from the experiment or more conservative than the experiment. Thus, this numerical code complies with the row 4 of table 3.4.3 of the Interim Guidelines.

14 Hashimoto, H. and Umeda, N. (2019) "Prediction of Parametric Rolling in Irregular Head Waves" Chapter 16 of *Contemporary Ideas on Ship Stability. Risk of Capsizing*, Belenky, V., Spyrou, K., van Walree F., Neves, M.A.S., and Umeda, N. *eds*., Springer, ISBN 978-3-030-00514-6, pp. 275-289.

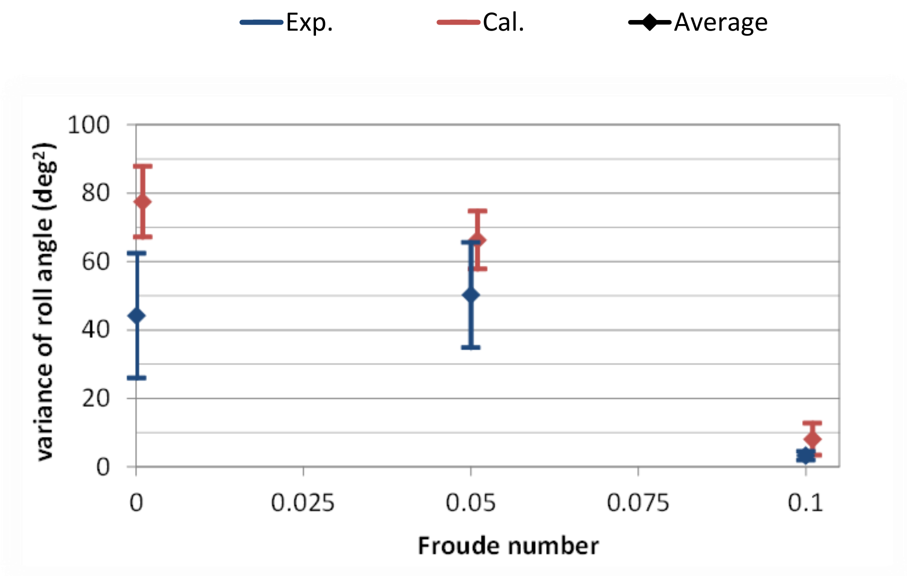

Figure 2.5.2: The variance of the parametric roll angle in irregular head waves for several Froude numbers with T_{01} = 9.99s and H_s = 7.82m

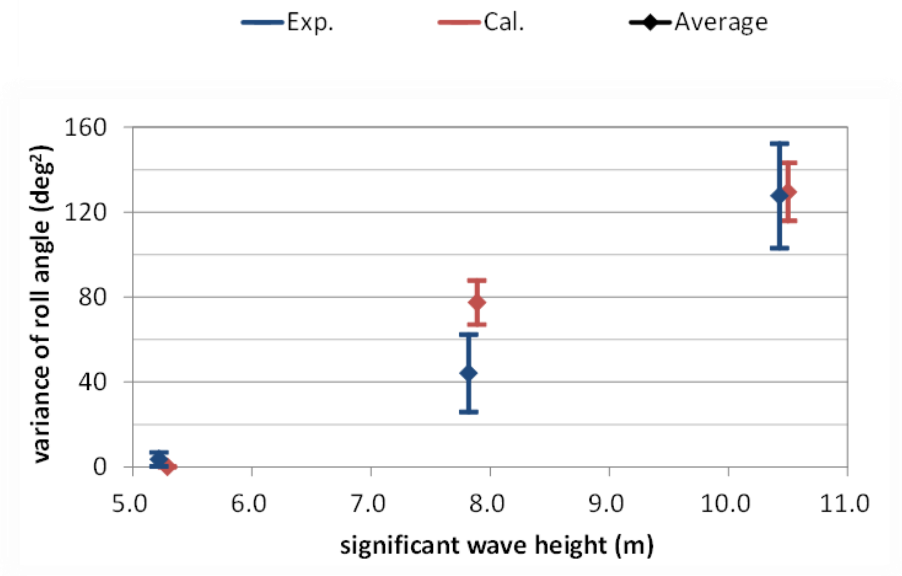

Figure 2.5.3: Variance of parametric roll angle in irregular head waves for several significant wave heights with T_{01} = 9.99s and F_n = 0.0

2.5.4 Row 5 of table 3.4.3 of the Interim Guidelines contains requirements for conditions for surf-riding/broaching. For broaching, figure 5.2.2 in appendix 4 is an example of the relevant validation using the ONR flare topside vessel. The differences between the model experiment and the coupled surge-sway-yaw-roll simulation are 15% for the critical wave steepness at the nominal Froude number of 0.4 and 1% for the speed setting at the wave steepness of 0.05. Thus, this numerical model is quantitatively validated under these conditions.

2.6 Validation example for dead ship condition stability failure mode

2.6.1 An example of validation of numerical method is provided for a large cruise ship; table 2.6.1 shows its principal particulars and figure 2.6.1 shows its GZ curve.

Table 2.6.1: Principal particulars of a cruise ship

Length between perpendiculars	246.00 m
Breath	37.50 m
Draught	8.21 m
Metacentric height (*GM*)	2.50 m
Natural roll period	23.55 s

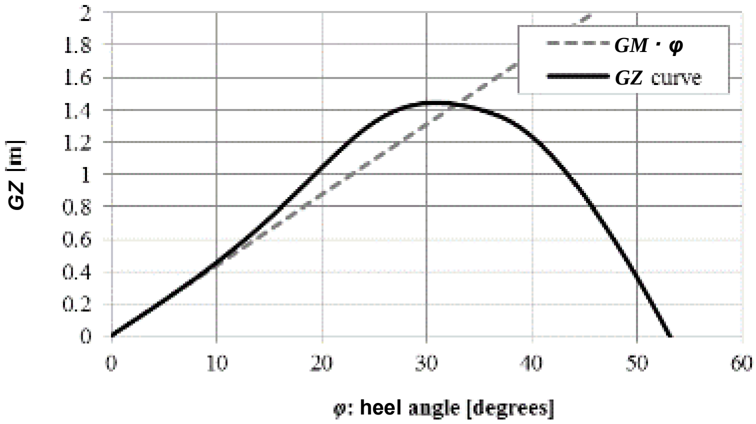

Figure 2.6.1: *GZ* curve of cruise ship

2.6.2 A coupled sway-heave-roll-pitch model was applied in long-crested irregular beam waves. Radiation and diffraction forces and moment were calculated using strip theory, and the roll damping moment was estimated from the roll decay test for a scaled model.

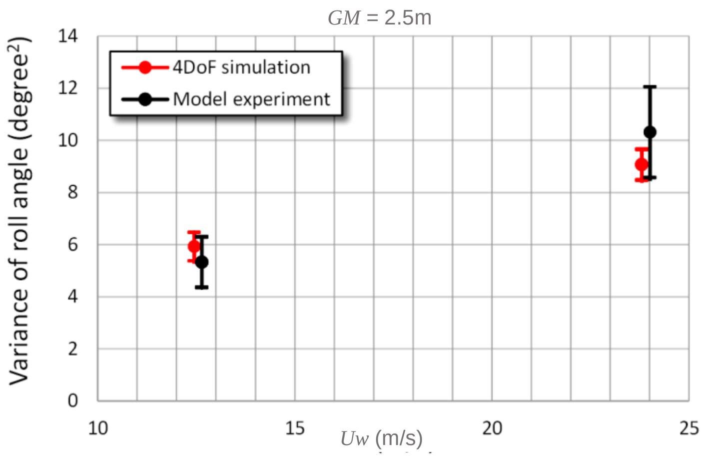

Figure 2.6.2: The variance of the roll angle of the cruise ship in beam wind and waves

2.6.3 For the validation, model experiments using a scaled model were used. The sway motion was softly constrained, and the yaw motion was fixed by a cable system. A comparison of the roll variance in figure 2.6.2 indicates that the 95% confidence intervals of the simulation and the experiment are overlapped so that the numerical code explains the model experiments.

2.7 Validation example of linear method for excessive acceleration failure mode

2.7.1 A ship motion prediction based on linear potential hydrodynamics, otherwise referred to as the ”linear superposition method” in the following, can be used for direct stability assessment for the excessive acceleration failure mode, if it is quantitatively validated based on paragraph 3.4.3 of the Interim Guidelines for a ship and its loading conditions similar to those to be assessed. This is because excessive accelerations can be assessed with sufficient accuracy even with a linear theory if the effect of nonlinear damping can be approximated by using stochastically equivalent linearization (paragraph 9.3.5 of appendix 3) or by using linearized damping at 15º (paragraph 9.3.8 of appendix 3).

2.7.2 To validate this method, numerical results are compared with model experiments[15] conducted according to the ITTC recommended procedure 7.5-02-07-04 for intact stability model tests. An example of the validation is provided for a container ship of which the principal particulars are shown in table 2.7.1. First, the numerical code for the Response Amplitude Operators is validated. Here, the Salvesen-Tuck-Faltinsen method based on strip theory is used. The ship motions were calculated with five degrees of freedom; hydrodynamic forces were calculated by two-dimensional source distribution method. The roll damping coefficient was estimated from a roll decay test. The comparison of lateral acceleration in regular beam waves between numerical and experimental results in figure 2.7.1 shows a good agreement.

Table 2.7.1: Principal particulars of the container ship

Length between perpendiculars	320.00 m
Breadth	42.80 m
Draught at aft perpendicular	9.073 m
Draught at midship section	8.08 m
Draught at forward perpendicular	7.083 m
Metacentric height, GM	8.54 m
Height of bilge keel	0.60 m
Length of bilge keel	96.00 m
Longitudinal distance of bridge from aft perpendicular	77.70 m
Height of bridge from baseline	50.00 m

[15] Kuroda, T., Hara, S., Houtani, H. and Ota, D. *Direct Stability Assessment for excessive acceleration failure mode and validation by model test*. Ocean Engineering, Vol.187, 106137, 2019.

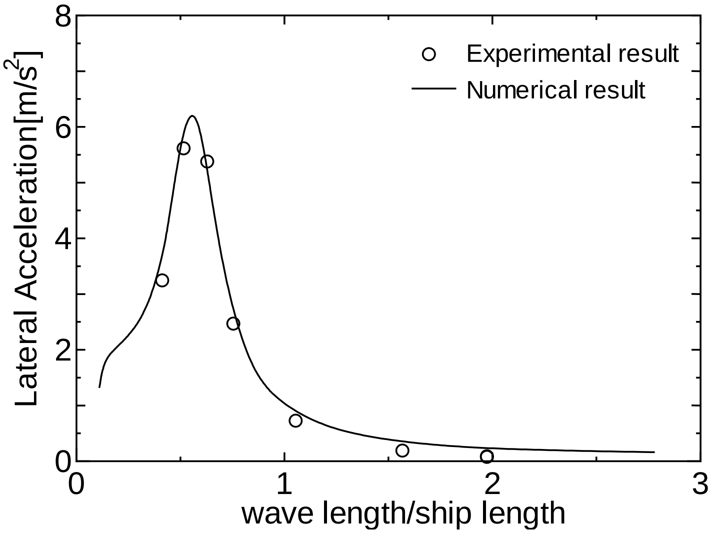

Figure 2.7.1:
A comparison of the lateral acceleration in regular beam waves between numerical and experimental results

2.7.3 Second, the linear superposition method is validated. The mean of one-third largest amplitudes of lateral acceleration in short-crested irregular beam waves is compared between level 2 vulnerability criterion, linear superposition method and experiments in figure 2.7.2 at significant wave height 5.5 m and mean zero-crossing wave period 9.5 s. Short-crested irregular waves are modelled where the frequency spectrum is the ITTC recommended unlimited fetch spectrum (1978) and the wave energy spreading is the fourth power of the cosine function. Seven model test runs of three-hours duration (in full scale) were carried out, with randomly varied phases and directions of harmonic wave components discretizing the wave energy spectrum. The comparison shows that the linear superposition method is close to the experiments and provides conservative estimates; further, the level 2 vulnerability criterion is consistent with respect to the linear superposition method.

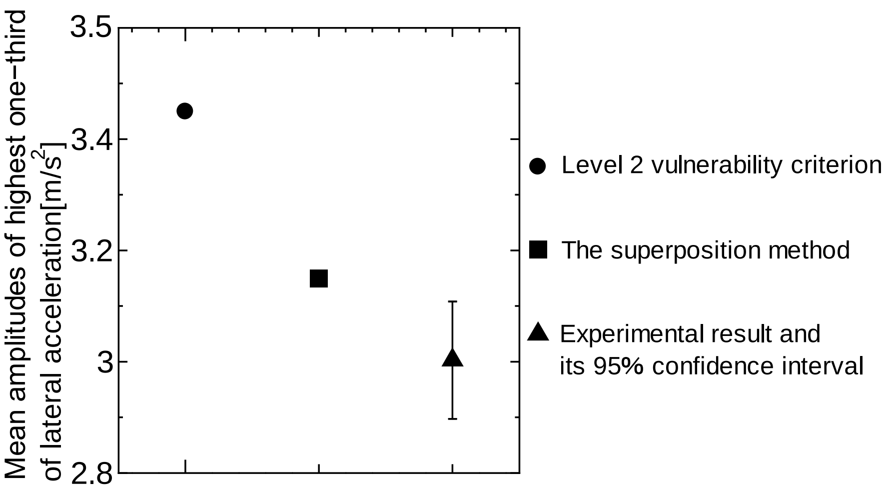

Figure 2.7.2:
A comparison of the mean of the one-third largest lateral acceleration amplitudes in an irregular short-crested beam waves between the level 2 vulnerability criterion, linear superposition method and experiment

2.7.4 These results indicate that the linear superposition method with transfer functions of ship motions obtained with frequency-domain calculations is feasible for the direct stability assessment for the excessive acceleration failure mode.

3 Direct counting

3.1 Introduction

3.1.1 *Direct counting* is counting of the number of stability failures per given exposure time. Direct counting is used in the probabilistic design stability assessment in design situations as well as in the full probabilistic direct stability assessment and in operational measures. It can be used in combination with statistical extrapolation, which itself uses direct counting.

3.1.2 Counting the number of stability failures per given exposure time assumes a stationary Poisson process. The stationarity assumption is justified since both the design assessment and operational measures consider ensemble statistics over a large number of ships, each of which operates in stationary conditions for unlimited time. The Poisson process assumption requires, in addition, that stability failures happen independently, i.e. the occurrence of one failure does not affect the probability of occurrence of a second failure. The validity of this assumption is based on two heuristic considerations: *clumping heuristic* (although large roll motions tend to appear in groups, the occurrence of such groups may be independent), and *rarity heuristic* (rare events tend to be independent).

3.1.3 To ensure that numerical simulations or model tests also satisfy the requirements of a stationary Poisson process, special procedures are required that are considered below.

3.2 Definition and characteristics of Poisson process

3.2.1 A *counting process* is defined as a stochastic process, when a random variable N counts the number of events (stability failures for the Interim Guidelines) in a time interval from 0 to t. For a stationary Poisson process, the failures are *independent* (the numbers of failures in non-overlapping time intervals are independent) and *stationary* (the number of failures depends only on the length of a time interval and not on its location in time).

3.2.2 There are several equivalent definitions of a Poisson process; the following[16] is used here: Poisson process with a constant rate $r > 0$ is a counting process where the number of events $N(t)$ in a time interval of length t satisfies the Poisson distribution with the mean rt, i.e.

$$p\{N(t) = k\} = (rt)^k \cdot e^{-rt}/k! \text{ for } k = 0, 1, \ldots \qquad (3.2.1)$$

3.2.3 The probability mass function of Poisson distribution, $f(k) = p\{N(t) = k\}$, eq. (3.2.1), is equal to the probability that the number of events during a time interval t is equal to k.

3.2.4 The useful properties of a Poisson process include:

.1 the *superposition property*: sum of independent Poisson processes N_1, …, N_k, i.e. $N_1 + \cdots + N_k$, is a Poisson process with the rate $r_1 + \cdots + r_k$. This means that failure rates can be found separately for different stability failure modes and summed to give the total stability failure rate; conversely, if the sum of two independent random variables is Poisson distributed, so are each of these two variables;

.2 the *random split property*: if each event in a Poisson process $N(t)$ with rate r is randomly tagged as either process $N_1(t)$, with probability p, or $N_2(t)$, with probability $1 - p$, then the two resulting processes $N_1(t)$ and $N_2(t)$ are independent Poisson processes with rates rp and $r(1 - p)$, respectively;

16 Ross, Sheldon M. *Stochastic Processes*. Wiley, 1996.

.3 the *thinning property*: if each event of a Poisson process with rate r is randomly marked, with probability p, then the marked process is a Poisson process with rate rp;

.4 the *mean* of a Poisson process, equal to the mean number of events per interval t (i.e. the rate is equal to the expected number of events per unit time), is given by:

$$E\{N(t)\} = \int_0^\infty t f(t) dt = rt \tag{3.2.2}$$

.5 the *variance* of the Poisson process is equal to the mean, Var$\{N(t)\} = rt$.

3.2.5 A special case of eq. (3.2.1) is $k = 0$, which provides the probability p that *no stability failures* occur from time 0 to time t:

$$p \equiv p\{N(t) = 0\} = e^{-rt} \tag{3.2.3}$$

3.2.6 From eq. (3.2.3), the probability p^* can be defined as:

$$p^* \equiv p\{N(t) > 0\} = 1 - p\{N(t) = 0\} = 1 - p = 1 - e^{-rt} \tag{3.2.4}$$

which means that at least one stability failure occurs during the time interval t, i.e. that $k > 0$ ("probability of stability failure during time t").

3.2.7 The linearization of eq. (3.2.4) with respect to rt leads to a popular approximation (note, however, that this approximation is valid only for small values of product rt):

$$p^* \approx rt \tag{3.2.5}$$

3.2.8 A Poisson process can also be seen as a sequence of time intervals T_1 (from $t = 0$ to the first failure), T_2 (between the first and second failures), etc. These time intervals are also random variables. The probability that the time until the first failure exceeds t, i.e. $p\{T_1 > t\}$, is the same as the probability that no failures occur before time t, i.e. $p\{N(t) = 0\} = e^{-rt}$, eq. (3.2.3). Therefore, $p\{T_1 > t\} = e^{-rt}$, which means that T_1 is an exponentially distributed random variable. Similarly, all time intervals T_i are exponentially distributed random variables with the rate r.

3.2.9 Therefore, a Poisson process can also be defined as a counting process in which the time intervals between events are independent random variables, which are exponentially distributed with rate r (note that this definition automatically ensures independent and stationary increments):

$$p\{T>t\} = e^{-rt} \text{ for } t > 0 \text{ and } 0 \text{ otherwise} \tag{3.2.6}$$

3.2.10 An important property of the exponential distribution is its *memoryless property*: if a failure has not occurred until time t, the distribution of the remaining waiting time is the same as the distribution of the original waiting time, i.e. the remaining waiting time has no memory of the previous waiting time. The exponential distribution is the only continuous distribution with this property: if the time intervals between arrivals are not exponential, the process will not be a Poisson process.

3.2.11 Other useful properties of the exponential distribution include:

.1 corresponding to sum of Poisson processes, if $T_1,\ldots,T_k$ are independent exponentially distributed random variables with rates $r_1,\ldots,r_k$, then $\min(T_1,\ldots,T_k)$ is exponentially distributed with the rate $r_1+\cdots+r_k$, and the index of the variable that achieves the minimum is distributed according to the law $p\{i \mid T_i = \min(T_1,\ldots,T_k)\} = r_i/(r_1+\cdots+r_k)$;

.2 according to eq. (3.2.4), cumulative distribution function of time to failure is

$$F(t) \equiv p\{T < t\} = 1 - p\{T > t\} = 1 - e^{-rt} \text{ for } t > 0 \text{ and } 0 \text{ otherwise} \tag{3.2.7}$$

.3 probability density function of exponential distribution, i.e. of time intervals between events in a Poisson process, is

$$f(t) = \mathrm{d}F(t)/\mathrm{d}t = re^{-rt} \text{ for } t > 0 \text{ and } 0 \text{ otherwise} \tag{3.2.8}$$

.4 the mean of exponentially distributed random variable T (i.e. mean time between stability failures) is

$$E\{T\} \equiv \bar{T} = \int_0^\infty tre^{-rt}dt = 1/r \text{ , and} \tag{3.2.9}$$

.5 the second moment $E\{T^2\} = \int_0^\infty t^2re^{-rt}dt = 2/r^2$, then the variance of the time between failures is $Var\{T\} \equiv E\{T^2\} - E^2\{T\} = 2\bar{T}/r - \bar{T}^2 = 1/r^2 = \bar{T}^2$, and the standard deviation of time between failures is then equal to

$$\sigma_T = (Var\{T\})^{1/2} = 1/r = \bar{T}. \tag{3.2.10}$$

3.2.12 Since the rate r is the only parameter defining a Poisson process, any statistical characteristic of the exponential distribution, including the variance and the standard deviation, is known once the stability failure rate is known. To confirm eq. (3.2.10), figure 3.2.1 shows the ratio $\sigma\{T\}/\bar{T}$ equal to 1 according to eq. (3.2.10), as a function of the number of counted failures N, and figure 3.2.2 shows the estimate of the standard deviation $\sigma\{T\}$ as a function of the estimate of the mean time to failure $\bar{T}$ after N = 200 counted failures.

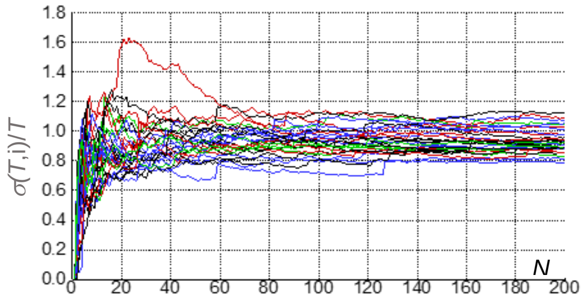

Figure 3.2.1: The ratio of the estimate of the standard deviation of the time to failure to the estimate of mean time to failure vs. number of failures

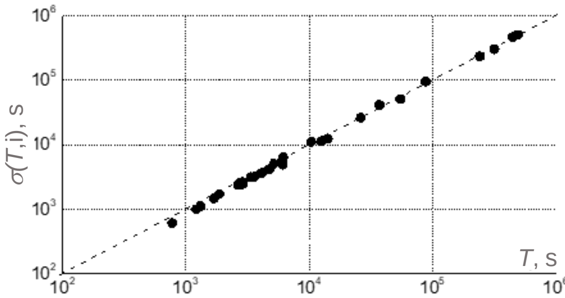

Figure 3.2.2: The estimate of the standard deviation of the time to failure vs. the estimate of the mean time to failure from 200 simulated failures

3.3 Definition of failure rate from sample data using exponential distribution

3.3.1 Both the Poisson distribution and the corresponding exponential distribution are defined by a single parameter, the stability failure rate r. To define it from a series of numerical simulations or model tests, consider time intervals T_i between failures and define the *sample mean time to failure* after N failures as:

$$\hat{T} = (1/N)\sum_{i=1}^{N} T_i \quad (3.3.1)$$

3.3.2 To estimate the stability failure rate:

.1 the joint probability density function L_r of all individual time intervals T_i is defined: since T_i are independent, then eq. (3.2.8) leads to

$$L_r(T_1, T_2, \cdots, T_N; r) = \prod_{i=1}^{N} re^{-rT_i} \quad (3.3.2);$$

.2 the most probable value of *r*, called the *maximum likelihood estimate*, is the value that maximizes L_r (i.e. the value of *r* that is most probable for a given measured data set T_1, T_2, $\cdots$, T_{N}). To do this, it is more convenient to maximize $\ln(L_r) = \sum_{i=1}^{N}(\ln r - rT_i)$, which is possible as a logarithm is a monotonously increasing function, i.e. L_r and $\ln(L_r)$ have maximum at the same r. Hence, the maximum of $\ln(L_r)$ can be defined from the condition $d \ln(L_r)/dr = 0$, i.e.

$$\mathrm{d} \ln L_r / \mathrm{d}r = \sum_{i=1}^{N}(1/r - T_i) = N/r - \sum_{i=1}^{N} T_i = N/r - N\hat{T} = 0 \quad (3.3.3);$$

.3 from eq. (3.3.3), the maximum likelihood estimate of the stability failure rate can be calculated simply as:

$$\hat{r} = 1/\hat{T}. \quad (3.3.4).$$

3.3.3 The total simulation time (or total model testing time) t_{t} is defined as

$$t_{\mathrm{t}} = \sum_{i=1}^{N} T_i \quad (3.3.5)$$

3.3.4 Using eq. (3.3.1), eq. (3.3.4) and the definition (3.3.5), the maximum likelihood estimate of the stability failure rate $\hat{r}$ can be calculated simply as the total number of failures divided by the total simulation (or model testing) time:

$$\hat{r} = N/t_{\mathrm{t}} \quad (3.3.6)$$

3.3.5 Since the estimate of the stability failure rate is a random variable, it varies between different series of simulations or model tests and, thus, it can be defined only with uncertainty, which decreases with an increasing duration of numerical simulations or model tests. To account for this uncertainty, direct stability assessment and operational measures use as a practical criterion the upper boundary of the 95%-confidence interval of the stability failure rate. The $(1 - \alpha)\cdot 100$%-confidence interval for the stability failure rate, where α is a small value (e.g. for 95%-confidence interval, $\alpha = (1 - 95/100) = 0.05$, is calculated as the confidence interval of the rate parameter of an exponential distribution:[17]

$$\frac{2N}{\hat{r}\chi^2_{1-\alpha/2,2N}} < \frac{1}{r} < \frac{2N}{\hat{r}\chi^2_{\alpha/2,2N}} \quad (3.3.7)$$

3.3.6 Here, $\chi^2_{p,f}$ denotes the $p\cdot 100$%-quantile (corresponding to a lower tail area, equal to the cumulative probability *p*) of the χ^2-distribution with *f* degrees of freedom, figure 3.3.1. The function $\chi^2_{p,f}$ is available in many software packages. For a small N, table 3.3.1 may be used, providing $\chi^2_{p,f}$ values for $p = 1 - \alpha/2$ and $p = \alpha/2$ (at $\alpha = 0.05$) and $f = 2N$.

[17] Ross, Sheldon M. *Introduction to probability and statistics for engineers and scientists*. 4th ed., Associated Press, p. 267, 2009.

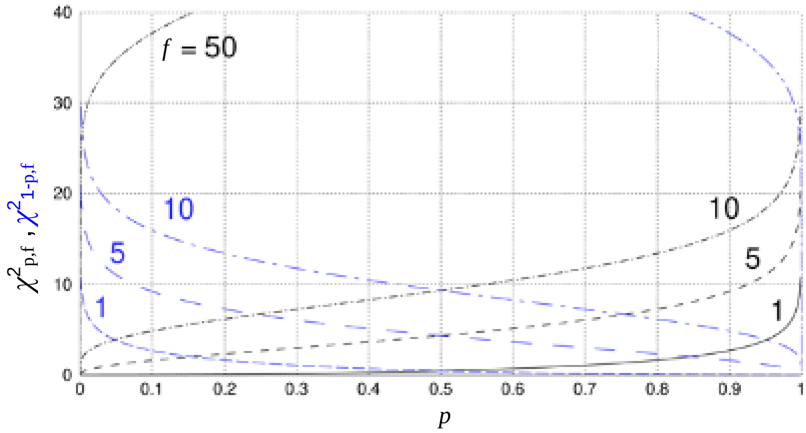

Figure 3.3.1: Examples of the functions $\chi^2_{p,f}$ and $\chi^2_{1-p,f}$ for f = 1, 5, 10 and 50 degrees of freedom vs. the cumulative probability p

Table 3.3.1. Functions $\chi^2_{1-\alpha/2,2N}$ and $\chi^2_{\alpha/2,2N}$ for α = 0.05 and N = 1, 2, …, 24

N	$\chi^2_{1-\alpha/2,2N}$	$\chi^2_{\alpha/2,2N}$	N	$\chi^2_{1-\alpha/2,2N}$	$\chi^2_{\alpha/2,2N}$	N	$\chi^2_{1-\alpha/2,2N}$	$\chi^2_{\alpha/2,2N}$
1	7.3778	0.0506	9	31.5264	8.2307	17	51.9660	19.8063
2	11.1433	0.4844	10	34.1696	9.5908	18	54.4373	21.3359
3	14.4494	1.2373	11	36.7807	10.9823	19	56.8955	22.8785
4	17.5345	2.1797	12	39.3641	12.4012	20	59.3417	24.4330
5	20.4832	3.2470	13	41.9232	13.8439	21	61.7768	25.9987
6	23.3367	4.4038	14	44.4608	15.3079	22	64.2015	27.5746
7	26.1189	5.6287	15	46.9792	16.7908	23	66.6165	29.1601
8	28.8454	6.9077	16	49.4804	18.2908	24	69.0226	30.7545

3.3.7 For a large N ($N \geq 25$ is sufficient for practical purposes), the χ^2 distribution converges to a normal distribution (which is also available in many software packages): $\chi^2_{p,2N} \to 2N + 2\sqrt{N} \cdot \aleph_{0,1}(p)$, where $\aleph_{0,1}(p)$ is the p·100%-percentile of the standard normal distribution.

3.3.8 Solving eq. (3.3.7) with respect to r gives:

$$0.5\hat{r}\chi^2_{\alpha/2,2N}/N < r < 0.5\hat{r}\chi^2_{1-\alpha/2,2N}/N \qquad (3.3.8)$$

3.3.9 From eq. (3.3.8), the upper r_U and lower r_L boundaries of a (1 – α)·100%-confidence interval for the stability failure rate can be calculated as:

$$r_U = 0.5\hat{r}\chi^2_{1-\alpha/2,2N}/N \qquad (3.3.9)$$
$$r_L = 0.5\hat{r}\chi^2_{\alpha/2,2N}/N \qquad (3.3.10)$$

3.3.10 The upper r_U and lower r_L boundaries of a 95%-confidence interval for the stability failure rate are then $r_U = 0.5\hat{r}\chi^2_{0.975,2N}/N$ and $r_L = 0.5\hat{r}\chi^2_{0.025,2N}/N$, respectively; the normal distribution approximation, paragraph 3.3.7, gives $r_U = \hat{r}(1 + 1.96N^{-1/2})$ and $r_L = \hat{r}(1 - 1.96N^{-1/2})$ for a 95%-confidence interval.

3.3.11 Using these estimates, any other characteristic of the process can be calculated with formulae from section 3.2. For example, the upper p_U and lower p_L boundaries of the (1 – α)·100%-confidence interval of probability of stability failure during time interval t (i.e. probability that at least one stability failure happens during time interval t) can be calculated according to eq. (3.2.4) as:

$p_{\mathrm{U}} = 1 - \exp(- r_U t)$ (3.3.11)
$p_{\mathrm{L}} = 1 - \exp(- r_{\mathrm{L}} t)$ (3.3.12)

3.4 Definition of failure rate from sample data from analysis of probability of failure

3.4.1 Alternatively, the probability $\hat{p}$ that at least one failure happens within a given exposure time t_{exp} can be defined directly from the results of M simulations, each of the same duration t_{exp}. Denoting as N the total number of simulations in which at least one stability failure was encountered, the maximum likelihood estimate of this probability can be calculated as:

$$\hat{p} \approx N/M \quad (3.4.1)$$

3.4.2 Note that since eq. (3.4.1) requires only the number of such simulations in which at least one stability failure was observed, the continuation of simulations after the first encountered stability failure is not necessary. Accordingly, the actual total simulation time for a simulation with a stability failure can be shorter than the reference exposure time t_{exp}.

3.4.3 The substitution of eq. (3.4.1) in eq. (3.2.4) leads to $N/M = 1 - \exp(- rt_{exp})$, and then to the following estimate of the failure rate:

$$r = - \ln(1 - N/M)/t_{exp} \quad (3.4.2)$$

3.4.4 Three items should be noted:

.1 the estimate given by eq. (3.4.2) converges to the result given by eq. (3.3.6) when M increases to infinity while the total simulation time t_t is kept constant (i.e. when $t_{exp} = t_t / M \rightarrow 0$). Thus, eq. (3.3.6) provides better accuracy than eq. (3.4.2) for the same total simulation time;

.2 eq. (3.4.2) cannot be used if every simulation contains at least one failure (i.e. $M = N$). To avoid this issue and, besides, improve accuracy of the estimate (3.4.2), the results can be post-processed by separating the simulations into intervals shorter than t_{exp} but longer than the decorrelation time described in section 3.8 of this appendix. The length of these shorter intervals should be the same for all simulations; this length should be used instead of t_{exp} in eq. (3.4.2). If such post-processing does not resolve this issue, post-processing of the results can be performed using the procedures described in sections 3.3 and 3.5; and

.3 the treatment of stability failures that occur during initial transients while keeping the exposure time t_{exp} constant requires special care when using the approach based on eq. (3.4.2).

3.4.5 For the determination of the confidence interval for the probability $\hat{p}$ that at least one failure happens within the specified exposure time t_{exp}, the Clopper-Pearson method can be used, according to which the lower and upper boundaries of a (1 - α)·100%-confidence interval for p^* can be found as:

.1 the lower boundary of the (1 - α)·100%-confidence interval:

$$p_L = 0 \text{ for } N = 0 \text{ or } p_L = \frac{\nu_1 \cdot F_{\nu_1,\nu_2;\alpha/2}}{\nu_2 + \nu_1 \cdot F_{\nu_1,\nu_2;\alpha/2}} \text{ otherwise} \quad (3.4.3)$$

where $\nu_1 = 2N$ and $\nu_2 = 2(M - N + 1)$; and

.2 the upper boundary of the (1 - α)·100%-confidence interval:

$p_U = 1$ for $N = M$ or $p_U = \frac{\nu_1 \cdot F_{\nu_1,\nu_2;1-\alpha/2}}{\nu_2 + \nu_1 \cdot F_{\nu_1,\nu_2;1-\alpha/2}}$ otherwise (3.4.4)

where $\nu_1 = 2(N + 1)$ and $\nu_2 = 2(M - N)$.

3.4.6 In equations (3.4.3) and (3.4.4), $F_{\nu_1,\nu_2;x}$ (with $x = \alpha/2$ or $1 - \alpha/2$) is the inverse cumulative F-distribution with ν_1 and ν_2 degrees of freedom, calculated at a value x. This function is available in many software packages.

3.4.7 The upper r_U and lower r_L boundaries of the $(1 - \alpha)\cdot 100\%$-confidence interval of the failure rate estimate can be calculated from the assumed relation $p = 1 - exp(-r \cdot t_{exp})$, as

$$r_U = -\ln(1 - p_U)/t_{exp} \quad (3.4.5)$$
$$r_L = -\ln(1 - p_L)/t_{exp} \quad (3.4.6)$$

3.4.8 A 95%-confidence interval corresponds to a significance level $\alpha = 0.05$.

3.4.9 The value of the maximum exposure time t_{exp} is specified by the user and it may depend on the considered conditions.

3.5 Definition of failure rate from sample data using binomial distribution

3.5.1 This procedure is based on the assumption of a binomial distribution of the failure rate estimate.[18] This distribution is equivalent to the Poisson process assumption for failure events and the exponential distribution of the time before and between failures, which is essential for a direct counting procedure.

3.5.2 The binomial distribution describes the probability that there will be N_{aU} independent up-crossing events of a level *a* or down-crossing events of a level $-a$, associated with stability failure, out of a total $N_a = \sum_{k=1}^{Nr} N_k$ instances of observation of roll motion or lateral acceleration. The data set of observation consists of N_r records. Each record contains N_k observations, $k = 1,\ldots N_r$; i.e. the records may contain different numbers of observations and may be of different durations.

3.5.3 The first up-crossing (or down-crossing) after the initial transition time is an independent event. The next independent up-crossing (or down-crossing) is counted only after decorrelation time T_{dc} has passed. The total number of independent up-crossings and down-crossings is $N_{aU} = \sum_{k=1}^{Nr} N_{Uk}$, where N_{Uk} is the number of independent up-crossings and down-crossings observed during the k-th record.

3.5.4 The failure rate is estimated as $\hat{r} = N_{aU}\Delta t / T_a$, where Δt is the time increment used in the simulation, $T_a = \sum_{k=1}^{Nr}(N_k \Delta t - T_{\mathrm{ramp}})$ is the total time of all records with a ramp time T_{ramp} excluded to account for initial transients.

3.5.5 The number of independent up-crossings or down-crossings N_{aU} is a random variable with a binomial distribution. The binomial distribution has only one parameter, the probability that the event will occur at any particular instant of time. This probability can be estimated as $\hat{p} = N_{aU}\Delta t / T_a$.

18 Leadbetter, M.R., Rychlik, I. and Stambaugh, K. *Estimating Dynamic Stability Event Probabilities from Simulation and Wave Modeling Methods*. Chapter 22 of *Contemporary Ideas on Ship Stability. Risk of Capsizing*, Belenky, V., Spyrou, K., van Walree F., Neves, M.A.S., and Umeda, N., eds., Springer, ISBN 978-3-030-00514-6, pp. 381-391, 2019.

3.5.6 The variance of a variable N_{aU} that satisfies a binomial distribution can be estimated as $\hat{V}_{NU} = T_a\hat{p}(1-\hat{p}))/\Delta t \approx N_{aU}$ since Δt and $\hat{p}$ are small values. Since Δt is small, also $\hat{p}$ is small, therefore $\hat{V}_{NU}$ can be determined as $\hat{V}_{NU} = N_{aU}$.

3.5.7 $r_{U,L} = \hat{r} \cdot \left(1 \pm \frac{Q_N\left(0.5\cdot(1+P_\beta)\right)}{\sqrt{N_{aU}}}\right)$ with $\hat{r} = \frac{N_{aU}}{T_a}$ (3.5.1)

where Q_N is the quantile of the standard normal distribution and $P_ß$ is the accepted confidence probability. For $P_ß$ = 0.95, $Q_N\left(0.5(1+P_\beta)\right) = 1.96$.

3.5.8 For the total number of failures N_{aU} = 25 and less, it is recommended to use a binomial distribution directly for the evaluation of the boundaries of confidence interval. Using a normal approximation for the binomial distribution may be inaccurate for a small number of events due to the practical limits of applicability of the Central Limit Theorem:

$$r_U = Q_B\,(1-\alpha/2, T_a/\Delta t, \hat{p})/T_a \qquad (3.5.2)$$

$$r_L = Q_B\,(\alpha/2, T_a/\Delta t, \hat{p})/T_a \qquad (3.5.3)$$

where $Q_B(P,N,p)$ is a quantile of the binomial distribution for probability P, the number of trials (time steps) N, and parameter p.

3.6 Long-term statistics

3.6.1 The long-term operation can be considered as a sum of stationary Poisson processes, each of which has a constant rate r_i and occurs in a stationary situation which is encountered with a probability p_i. Then, applying the *sum property* and *tagging property* of a stationary Poisson process, the long-term operation can be considered to be a stationary Poisson process with a constant rate $\bar{r}$, which is equal to:

$$\bar{r} = \sum_i r_i p_i \qquad (3.6.1)$$

3.6.2 All the properties of a Poisson process remain applicable by using the mean rate $\bar{r}$, for example:

.1 the distribution of the number of failures in a time interval from t to $t + \tau$, i.e. the probability that k failures occur in time interval from t to $t + \tau$, is equal to:

$$p\{N(t+\tau) - N(t) = k\} = (\bar{r}\tau)^k \exp(-\bar{r}\tau)/k! \qquad (3.6.2)$$

.2 the probability that no failures occur from time t to time $t + \tau$ is:

$$p \equiv p\{N(t+\tau) - N(t) = 0\} = \exp(-\bar{r}\tau) \qquad (3.6.3)$$

.3 the probability that at least one failure happens from time t to time $t + \tau$ ("probability of failure during time τ") is:

$$p^* \equiv p\{N(t+\tau) - N(t) > 0\} = 1 - \exp(-\bar{r}\tau) \qquad (3.6.4)$$

3.6.3 Therefore, the problem reduces to the definition of a constant rate r_i in each stationary situation from either the numerical simulations or model tests in such a way that ensures that the process is a stationary Poisson process.

3.7 Cautions in numerical simulations or model tests

3.7.1 Numerical simulations (or model tests) and the counting procedure used should ensure the stationarity of the process and the independence of the counted stability failures. The following straightforward procedure may seem suitable: run a single simulation of roll motion of sufficient duration and, after each encountered stability failure, increase the number N of failures by 1. Then, increase the total simulation time t_t by the simulation time from the previous failure and update the estimate of the failure rate $\hat{r} = N/t_t$, eq. (3.3.6), and the estimate of the upper boundary of its (1 − α)·100%-confidence interval $r_{\mathrm{U}} = 0.5\hat{r}\chi^2_{1-\alpha/2,2N}/N$, eq. (3.3.9). Once r_U is less than the acceptance standard, the simulations can be stopped and the loading condition can be considered acceptable.

3.7.2 However, the collection of sufficient statistics in a single simulation run of sufficient duration may be impossible in practice since the duration of numerical simulations or model tests is limited because:

.1 the duration of model tests is limited by tank size and wave reflection effects;

.2 the duration of numerical simulations and model tests is limited by self-repetition effects if the sea state is modelled as a finite sum of harmonic components:

$$\zeta(t) = \sum_{i=1}^{M} a_i \cos(\omega_i t + \varepsilon_i) \tag{3.7.1}$$

where $a_i = \{2S_{ZZ}(\omega_i)D(\mu_i)\Delta\omega_i\Delta\mu_i\}^{1/2}$ are amplitudes, ω_i are frequencies, μ_i are headings and ε_i are phases of harmonic components, randomly selected in the interval [0,2π], S_{ZZ} is the wave energy spectrum and D is the wave energy angular spreading function; and

.3 for resonance phenomena, such as parametric roll and synchronous roll, the bandwidth of significant roll response is narrow. This narrow bandwidth of encounter frequencies may lead to a self-repetition effect and may further limit the duration of a roll numerical simulation.

3.7.3 A solution is to generate multiple independent *realizations* of the same sea state, by a random variation of phases ε_i for each realization, and to simulate ship motions in each such realization for a limited time. The frequencies ω_i, headings μ_i and perhaps also amplitudes a_i of components can also be randomly varied. To generate random values, pseudo-random number generators can be used.

3.7.4 For a set of simulations in multiple realizations of the same sea state, eq. (3.3.6) is still applicable; in this equation, N and t_t should be taken as the total number of stability failures and the total simulation time, respectively, over all realizations.

3.7.5 Transient hydrodynamic effects that occur at the beginning of each simulation lead to the violation of the stationarity requirement and thus reduce the accuracy of the failure rate estimation. These effects may also lead to numerical instabilities in time-domain numerical simulation codes. To address this problem, the following possibilities (or their combination) can be used:

.1 Exclude a certain period of time after the start of each simulation from post-processing. For this purpose, 50 roll periods is suggested for stability failure modes dominated by roll motion. The initial transients are excluded from t_{t} (section 3.3), t_{exp} (section 3.4) or T_{a} (section 3.5). If a stability failure occurs during the initial transient, it is not counted in the number of failures N and simulation timer is set again to zero after such stability failure.

.2 Smoothly (e.g. linearly) increase the wave (or forces acting on the ship) from zero to the nominal value during a specified *ramp time*, the duration of which for stability failure modes dominated by roll is recommended to be set equal to 10 roll periods. This time is excluded from the post-processing.

.3 Randomly vary the initial conditions for each realization.

3.7.6 The independence of stability failures may also be violated by the autocorrelation of large roll motions since large roll amplitudes, caused by resonance, tend to appear in groups. If the direct counting approach in section 3.4 is used, this effect is automatically neutralized since occurrence of the second, etc. stability failures in the same simulation does not change the result. If the direct counting approaches in sections 3.3 or 3.5 are used, neglecting this effect may lead to overestimation of the stability failure rate estimate and underestimation of the size of the confidence interval. To neutralize this effect, a simple solution is to stop a simulation if a stability failure is encountered. Another possibility is to switch off the simulation timer t_t and stability failure counter N after an encountered failure for the decorrelation time; an example procedure for that approach is provided in section 3.8.

3.7.7 Stopping a simulation after an encountered failure and switching off the post-processing for the decorrelation time have a similar amount of unused data. In the former method, this is due to transient effects that occur at the start of a new simulation. In the latter method, this is due to the decay of the autocorrelation function of roll motion. However, the former method is simpler. Another benefit of the former method is that restarting also handles self-repetition effects because, for relevant durations of simulations and stability failure rates, a stability failure is not encountered in each simulation. Therefore, after the first encountered failure, there is no benefit in waiting for a second failure in the same simulation.

3.7.8 After removing portions of the time histories of roll motion affected by self-repetition effects, initial transients and autocorrelation of stability failures, the remaining pieces represent a single stationary Poisson process: the removed pieces can be disregarded due to the memoryless property, the durations of the remaining pieces may be arbitrary (in particular, equal), and whether a failure was encountered in each simulation or not, figure 3.7.1, can be disregarded. This means that eq. (3.3.6) can be used for the maximum likelihood estimate of the failure rate, with N and t_t representing sums over all remaining pieces of the simulations. Similarly, a sample mean time to failure is $\hat{T} = t_t/N$, and all formulae from sections 3.2, 3.3, 3.4 and 3.5 can be directly applied.

3.7.9 To define the maximum duration of simulations to avoid self-repetition effects, two requirements should be checked: first, there should be an absence of self-repetition of waves and, second, an absence of self-repetition of roll motion, for which the absence of self-repetition of waves may not be sufficient due to a narrow-banded roll response.

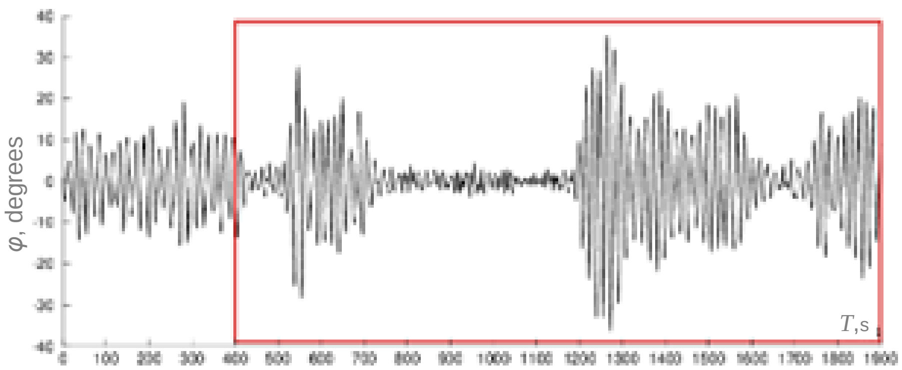

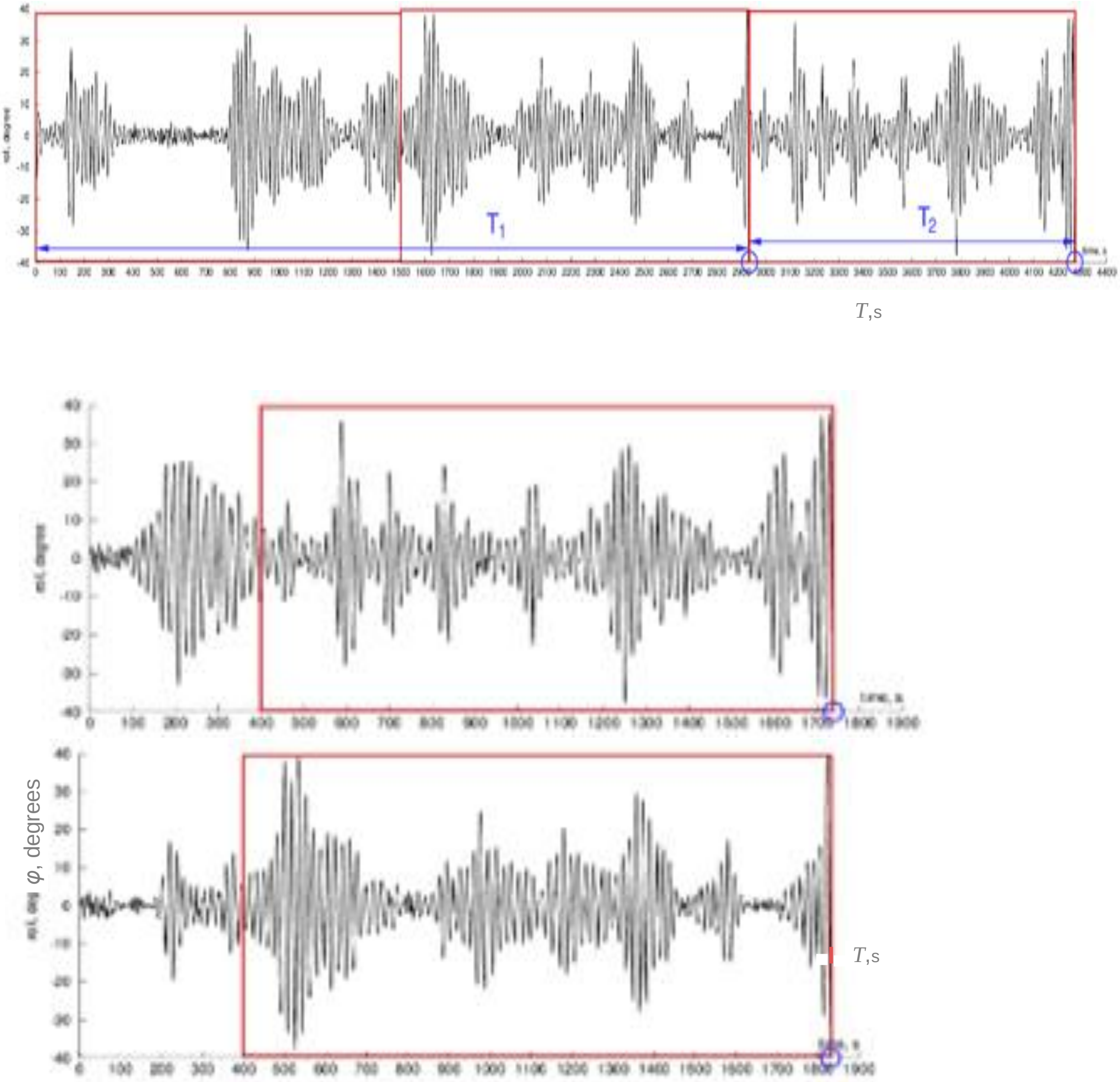

(a)
(b)
Figure 3.7.1: A roll motion in multiple realizations of a sea state (a) and the resulting Poisson process (b)

3.7.10 To check for the absence of the self-repetition of waves, the autocovariance function $R_{\mathrm{w}}(\tau)$ of wave elevation is computed as

$$R_{\mathrm{w}}(\tau) = \int_0^{\infty} S_{ZZ}(\omega)\cos(\omega\tau)d\omega \approx \sum_{i=1}^{N} S_{ZZi}\cos(\omega_{\mathrm{w}i}\tau) \qquad (3.7.2)$$

where τ is time lag.

3.7.11 The autocorrelation function $r_{\mathrm{w}}(\tau)$ is normalized by the variance or $R_{\mathrm{w}}(\tau = 0)$:

$$r_w(\tau) = R_w(\tau)/R_w(0) \qquad (3.7.3)$$

3.7.12 The autocorrelation function, computed using eq. (3.7.2) for long-crested waves and using a discretization with 210 frequencies for 30 minutes of the target record length, is shown in figure 3.7.2. No increases of the autocorrelation function are observed; thus, no self-repetition effect should be expected.

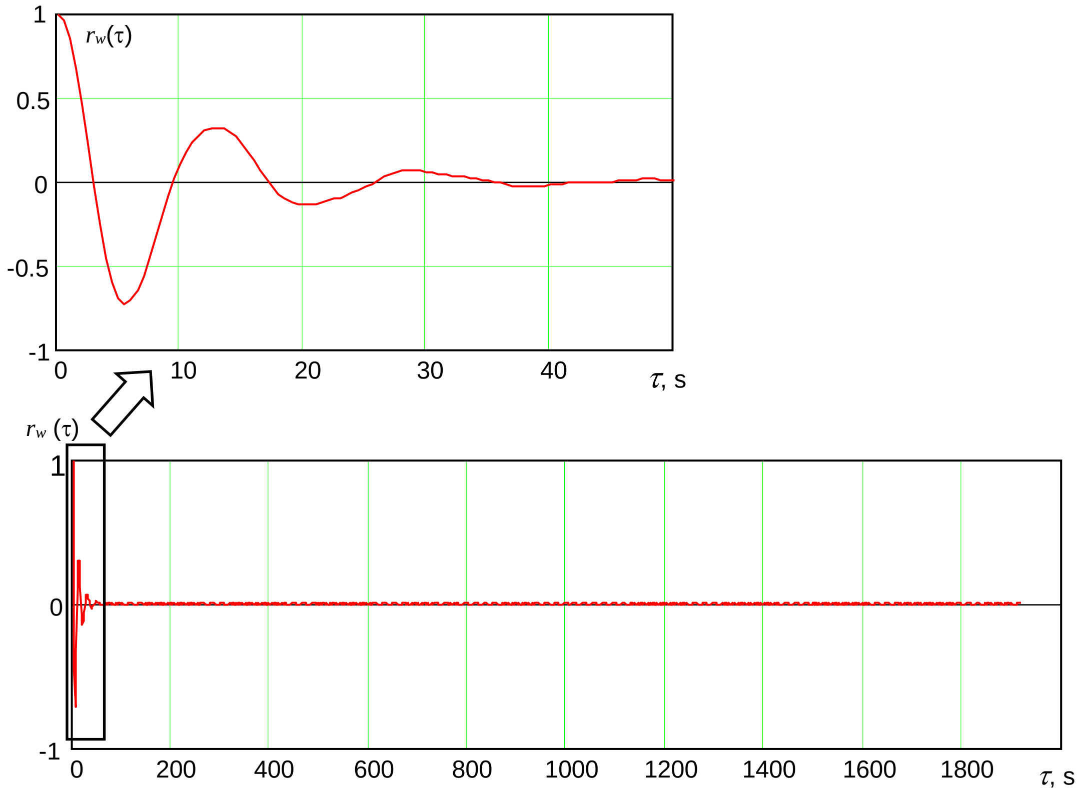

Figure 3.7.2: The autocorrelation function for 210 frequencies

3.7.13 The described check for the self-repetition effect was performed for a fixed location. If a ship is moving forward in head or bow-quartering waves, the rate of wave encounter is greater compared to the fixed location, so the actual check of the self-repetition effect is done for each speed and heading combination, using encounter frequency ω_{ei}, instead of the wave frequency:

$$\omega_{\mathrm{ei}} = \omega_{\mathrm{wi}} - k_{\mathrm{wi}} v_s \cos\mu : k_{wi} = \omega_{wi}^2 / g \qquad (3.7.4)$$

3.7.14 The autocovariance and the autocorrelation function were computed as follows:

$$R_{\mathrm{we}}(\tau) \approx \sum_{i=1}^{N} S_{wei} \cos(\omega_{\mathrm{ei}}\tau) \Delta\omega_{wei},\ r_{\mathrm{we}}(\tau) = R_{\mathrm{we}}(\tau) / R_{\mathrm{we}}(0) \qquad (3.7.5)$$

where S_{wei} is the spectrum of the encounter waves.

3.7.15 Figure 3.7.3 shows the autocorrelation function, computed for forward speed of 20 knots in head seas. The growth of the autocorrelation function indicates a self-repetition effect.

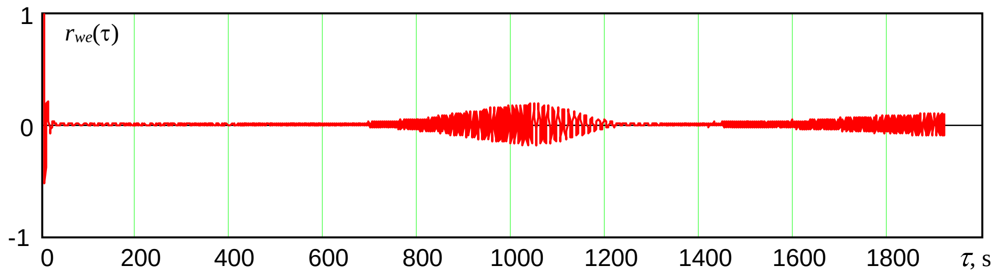

Figure 3.7.3: The autocorrelation function for 210 frequencies at 20 knots in head seas

3.7.16 Figure 3.7.3 indicates the beginning of self-repetition effects at about 650 s. However, for massive computations, such as those required in a direct stability assessment, the search for the self-repetition effect needs to be done automatically. For this purpose a peak-based envelope of the autocorrelation function is used, see figure 3.7.4.

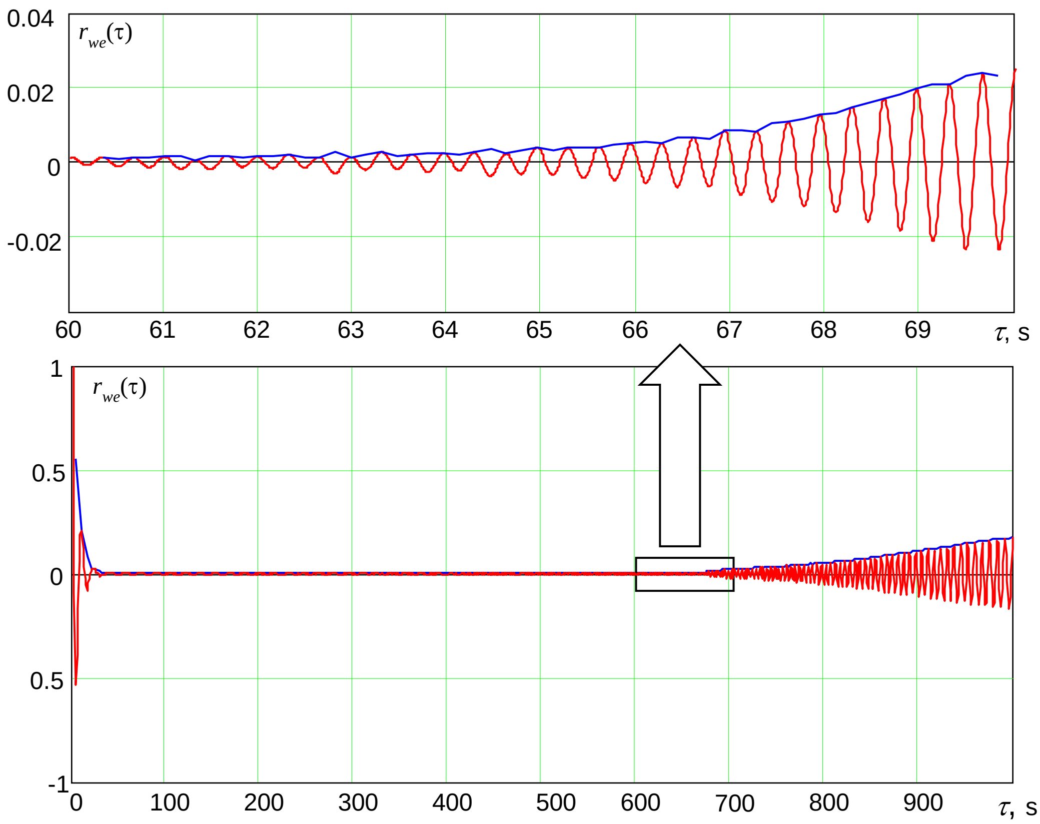

Figure 3.7.4: Use of an envelope to detect the inception of a self-repetition effect

3.7.17 A natural criterion for a time of inception of the self-repetition effect is when the envelope starts to increase. However, implementation of this criterion may encounter a problem due to small amplitude oscillations which may be observed on the envelope; for an example, see the zoomed-in portion of the autocorrelation plot in figure 3.7.4. Averaging over every three values seems to remediate this problem, figure 3.7.5.

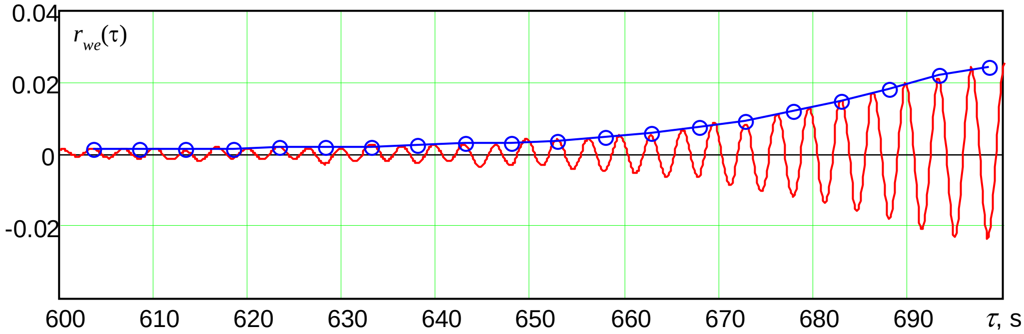

Figure 3.7.5: On the detection of the inception of a self-repetition effect

3.7.18 To prevent the criterion of self-repetition from being too sensitive, a threshold of 0.005 is introduced. The search for an increase in the averaged envelope starts only when it exceeds the threshold. The times where the self-repetition effect was detected are shown in table 3.7.1. For the initial frequency discretization with 210 frequencies and for these combinations of speed and heading, the wave model (3.7.1) is statistically valid up to the time durations in table 3.7.1. To increase the time duration of the validity of a model in head and bow-quartering seas, the number of frequencies needs to be increased to 560; this provides 30 minutes of validity for all combinations of speeds and headings, see table 3.7.2.

Table 3.7.1: Time until self-repetition occurs for 210 frequencies for a peak wave period of 14 s

	Speed, kn			
Heading, °	5	10	15	20
105	1752	1570	1427	1307
120	1579	1318	1131	988.9
135	1465	1159	962.8	824.6
150	1379	1060	861.3	727.8
165	1335	1005	808.6	677.5
180	1318	988.9	791.1	659.3

Table 3.7.2: Time until self-repetition occurs for 560 frequencies for a peak wave period of 14 s

	Speed, kn			
Heading, °	5	10	15	20
105	1920	1920	1920	1920
120	1920	1920	1920	1920
135	1920	1920	1920	1920
150	1920	1920	1920	1920
165	1920	1920	1920	1847
180	1920	1920	1920	1802

3.7.19 To check for the self-repetition of roll motion, an ensemble-average autocorrelation function of roll motion can be computed; however, such computations are time-consuming and prone to numerical errors. A simpler check is to use quantile plots of time to failure to verify whether the distribution of time to failure deviates from the exponential distribution. To investigate self-repetition effects, parametric roll resonance in head waves and synchronous roll resonance in beam waves were simulated for a systematically varied significant wave height in two types of simulations: in one, denoted "limited", the simulation time was limited to three hours (while simulations were stopped after the first failure in any case); and in the other denoted "unlimited", the simulations were run always until the first failure occurred.

3.7.20 To compare the distribution of time to failure with the exponential distribution, quantile diagrams (QQ diagrams) like those shown in figure 3.7.6 were used. This figure shows QQ diagrams derived from "limited" and "unlimited" simulations. Since the cumulative distribution function of an exponentially distributed time to failure is $F(t) = 1 - e^{-rt}$ for $t > 0$, the ratio $T_i/\bar{T}$ should be equal to $-\ln(1 - F_i)$ (see the blue dashed lines in figure 3.7.6). For comparison, the cumulative distribution function F_i was calculated from the sample data as $i / (N + 1)$, where i is the index of a stability failure when stability failures are sorted in ascending order of T_i. Figure 3.7.6 shows that the "unlimited" simulations overestimate the time to failure compared

to the exponential distribution and compared to the 'limited' simulations for cases with a large time to failure. This can be explained by the presence of self-repetition effects: the same "uncritical" realization (i.e. a realization where a stability failure does not happen soon) repeats itself again and again (since the repetition is not exact, failure may eventually occur but much later than it should).
"

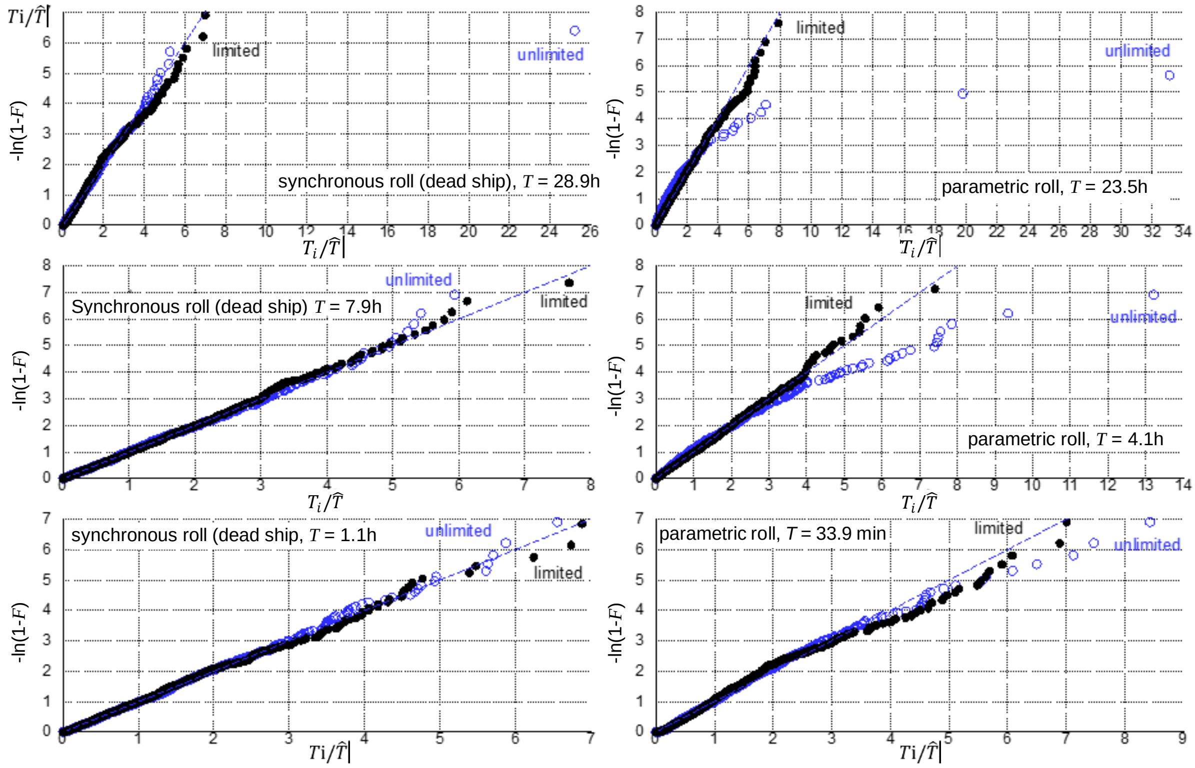

Figure 3.7.6: Quantile diagrams from 'limited' (●) and 'unlimited' (O) simulations for synchronous roll (left) and parametric roll (right) resonance cases

3.7.21 This means the simulations that have a long duration lead to a deviation from the Poisson process, which means that the notion of *failure rate* and the formulae from this section are not applicable. Moreover, using these formulae despite this (i.e. assuming that the process were a Poisson process) would lead to an underestimation of the failure rate, i.e. a non-conservative error which should be avoided. Thus, the maximum duration of simulations should be limited. According to the presented results, when at least $1.9 \cdot 10^4$ frequencies are used, simulations up to three hours are possible. In general, quantile plots can be used to verify absence of self-repetition effects.

3.7.22 To check whether the described measures ensure applicability of the Poisson process assumption, the χ^2 goodness-of-fit test was applied to several cases of parametric roll resonance and synchronous roll resonance in head and beam waves, respectively, at systematically varied significant wave heights. Only "limited" simulations of a three-hour duration (or until failure if it happened) were used. Random realizations of the same sea state were repeated until about 10^3 failures were encountered in each sea state. The observed times to failure were compared with the exponential distribution, which was defined using the maximum likelihood estimate for the failure rate $\hat{r} = 1/\hat{T}$, eq. (3.3.4).

3.7.23 The full range $t \geq 0$ of the time to failure was subdivided into a number of $k \geq 5$ intervals of equal probability $\Delta F = \Delta(1 - e^{-rt}) = 1/k$; the number of intervals was systematically increased up to a maximum $k = N/5$. The number O_i of the observed times to failure within each interval i

was counted, and the expected number E_i was calculated, according to the assumed exponential distribution, as N / k. Subsequently:

.1 the *test statistic* was calculated as

$$x = \sum_{i=1}^{k} (O_i - E_i)^2 / E_i \qquad (3.7.6)$$

.2 the *critical value* of the test statistic at the *significance level* $\alpha = 0.05$ was defined as $c_{5\%} = \chi^2_{1-\alpha,f}$, i.e. the value of the χ^2 distribution, at the cumulative probability 1 - $\alpha = 0.95$ and the number of degrees of freedom $f = k - p - 1$, where $p = 1$ is the number of parameters of the assumed distribution estimated from the sample data; and

.3 the results were presented (see figure 3.7.7) as the ratio x / $c_{5\%}$ depending on the number of intervals k: when x / $c_{5\%} < 1$, the *null hypothesis* that the data follow the assumed distribution cannot be rejected at the significance level of 5%.

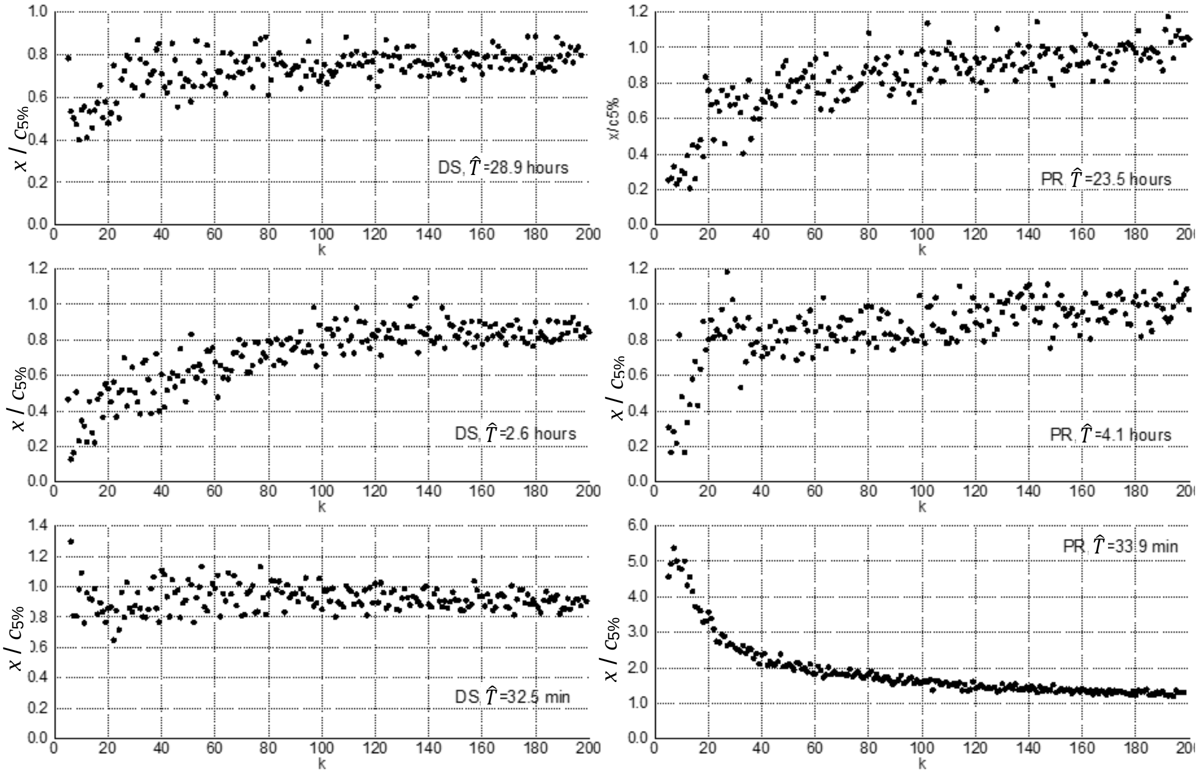

Figure 3.7.7: The ratio of the χ^2-test statistic to the critical value $\chi^2_{1-\alpha,k-2}$ for the significance level α = 5% vs. the number of intervals k of the time to failure for synchronous roll resonance (left) and parametric roll resonance (right) for several values of the sample mean time to failure

3.7.24 Figure 3.7.8 shows the ratio x / $c_{5\%}$ for k = 200 as a function of the sample mean time to failure. For *synchronous roll resonance*, the Poisson process model is acceptable (at the 5% significance level) in all studied cases. On the other hand, for *parametric roll resonance*, the results disagree with the Poisson process assumption: marginally at $\hat{T} \approx 2$ hours and increasingly greater for $\hat{T}$ decreasing below two hours. However, the χ^2 test is considered as very strict when the amount of data is large.

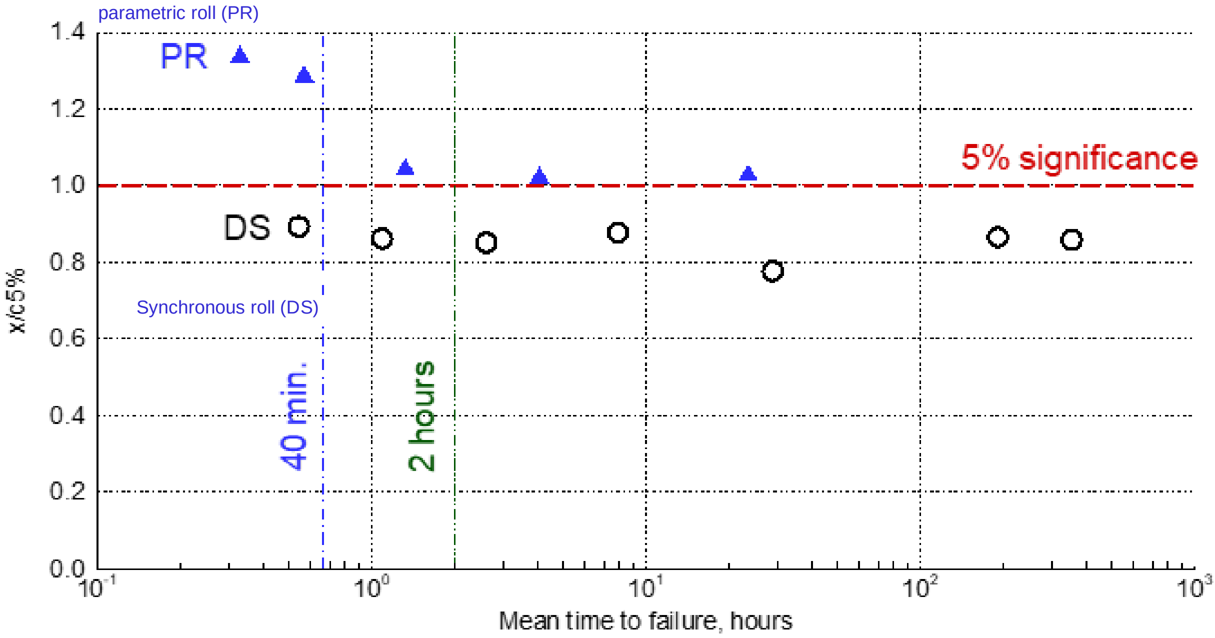

Figure 3.7.8: The ratio $x/c_{5\%}$ for synchronous roll resonance (○) and parametric roll resonance (▲) vs. the sample mean time to failure at k = 200

3.8 Decorrelation

3.8.1 The independence of stability failures may also be violated by the autocorrelation of large roll motions since large roll amplitudes, caused by resonance, tend to appear in groups. Neglecting this effect may lead to an overestimation of the stability failure rate estimate and an underestimation of the size of the confidence interval. One of the possibilities to neutralize this effect is to switch off the simulation timer t_t and the stability failure counter N after an encountered failure until the envelope of the autocorrelation function of roll motion reduces to a specified level; here, an example procedure for that possibility is provided.

3.8.2 A practical way to judge if the events related to a stochastic process are independent is to compare the time between the events with a decorrelation time of the process. The decorrelation time is a duration when the autocorrelation function value becomes insignificant, so that two-time sections of the process are considered uncorrelated. Uncorrelated values are assumed to be independent. This is an assumption since the correlation only indicates a dependence in terms of the second joint moment of the distribution. For example, for a joint PDF of random variables x and y with their respective mean values E_x and E_y, the second joint moment is a covariance, which is defined as $\int_{-\infty}^{\infty}(x-E_x)(y-E_y)pdf(x,y)dxdy$. The decorrelation time can be used as an approximate indicator of the independence of events related to a stochastic process.

3.8.3 The autocovariance function (autocorrelation function is a normalized autocovariance function) of a single realization of an ensemble is estimated as:

$$\hat{R}_{\varphi}(\tau_i) = \frac{1}{N}\sum_{j=1}^{N-i}(\varphi_j - \hat{E}_{a\varphi})(\varphi_{i+j} - \hat{E}_{a\varphi}) \quad (3.8.1)$$

where N is the number of a point in the realization, τ_i is i-th time lag and $\hat{E}_{a\varphi}$ is a mean estimate of the ensemble:

$$\hat{E}_{a\varphi} = \sum_{k=1}^{Nr} W_k \hat{E}_{\varphi k} \tag{3.8.2}$$

where Nr is the number of realizations in an ensemble and W_k is a statistical weight of the k-th realization, $W_k = N_k / \sum_{n=1}^{Nr} N_n$, where N_k is a number of data points in the k-th realization.

3.8.4 $\hat{E}_{\varphi k}$ is a mean estimate of k-th realization:

$$\hat{E}_{\varphi k} = \frac{1}{N_k} \sum_{i=1}^{N_k} \varphi_i \tag{3.8.3}$$

3.8.5 Then, the ensemble estimate of the autocovariance function is expressed as:

$$\hat{R}_{a\varphi}(\tau_i) = \sum_{k=1}^{Nr} W_k \hat{R}_{\varphi k}(\tau_i) \tag{3.8.4}$$

$\hat{R}_{\varphi k}(\tau_i)$ is the autocovariance estimate of the k-th realization. An estimate of the autocorrelation function is obtained by normalizing the estimate of the autocovariance function by its zero-term, which is an ensemble variance estimate in this context:

$$\hat{r}_{a\varphi}(\tau_i) = \hat{R}_{a\varphi}(\tau_i) / \hat{R}_{a\varphi}(0) \tag{3.8.5}$$

3.8.6 The ensemble estimate of the autocorrelation function is shown in figure 3.8.1. The decorrelation time is defined here as the time lag for the reduction of the autocorrelation function below 0.05. Since the estimate of autocorrelation function has an oscillatory character, it makes sense to use its envelope rather than the autocorrelation function itself; see figure 3.8.1.

3.8.7 The decorrelation time, evaluated as the first intersection of the envelope with the threshold level 0.05, was determined to be 759.7 s. This is a rather large value in comparison to the wave elevation or synchronous roll where the decorrelation time is usually around one minute. Large autocorrelation times for parametric roll is generally expected since autocorrelation function of parametric roll decays for a long time.[19]

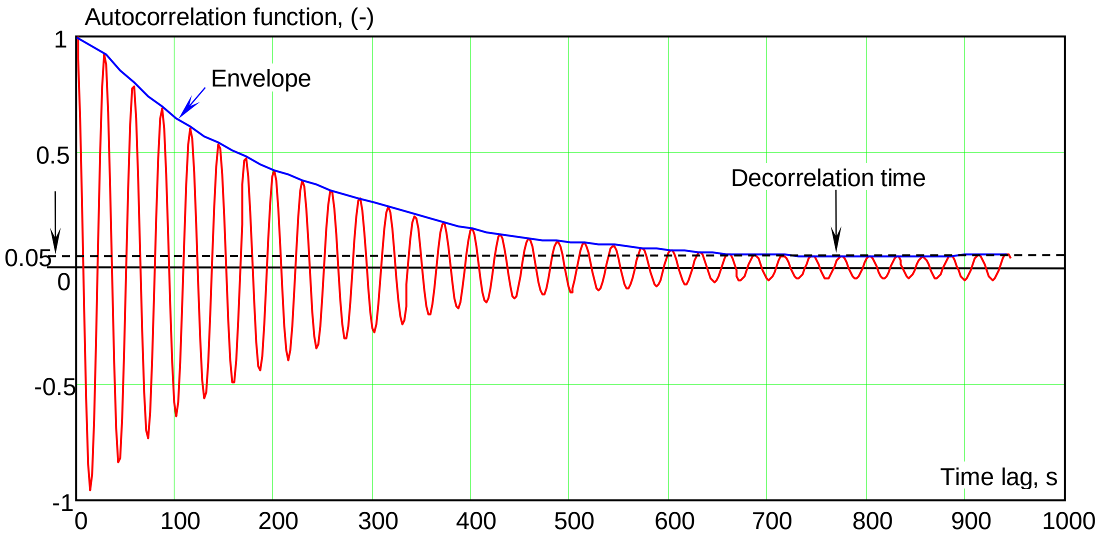

[19] Belenky, V. and Weems, K.M. *Probabilistic Properties of Parametric Roll*. Chapter 6 of *Parametric Resonance in Dynamical Systems*, Fossen, T. I. and Nijmeijer, H., eds., Springer, ISBN 978-1-4614-10423-0, pp. 129-146, 2012.

Figure 3.8.1: The ensemble estimate of the autocorrelation function for a wave heading of 1°, a speed of 5 knots, a significant wave height of 3.5 m, and a mean zero-crossing wave period of 8.5 s

3.8.8 Sometimes, the estimate of autocorrelation function for parametric roll resonance does not reach the threshold level with increasing time lag. One possibility for this is that the envelope has at least one minimum and the lowest minimum is still above the threshold level, which is a result of insufficient data for the estimation of autocorrelation function to the threshold level. The time lag corresponding to the global minimum of the envelope then can be used as a decorrelation time. Another possibility is that the envelope monotonically decreases but does not reach the threshold level, which is likely caused by an insufficient length of the estimate of the autocorrelation function. Since it may be difficult to estimate the autocorrelation function beyond one half of the record length, the conservative solution is to take the decorrelation time as equal to the length of the record.

3.9 Direct counting procedures

3.9.1 The proposed procedures are based on simulations of ship motions in multiple independent realizations of the same irregular seaway and provide the estimate of the upper boundary r_U of the 95%-confidence interval of the rate of stability failures. The procedures can prevent self-repetition effects, transient hydrodynamic effects at the beginning of simulations and autocorrelation of large roll motions.

3.9.2 The sea state is modelled as a sum of harmonic components, see eq. (3.7.1). The phases and, possibly, frequencies, directions and amplitudes of wave components are randomly varied for each realization.

3.9.3 To neutralize the effect of self-repetition, the duration of each simulation is limited. If the direct counting approaches described in sections 3.3 or 3.5 are used to define r_U, the duration of each individual simulation can be arbitrary (in particular, constant). If the approach described in section 3.4 is used, each simulation should have a common exposure time t_{exp}.

3.9.4 With the approaches described in sections 3.3 and 3.5, the effect of the autocorrelation of large roll motions can be neutralized either by stopping a simulation after the first encountered stability failure or by switching off the simulation timer t_{t} and the stability failure counter N after encountered failure until the envelope of the autocorrelation function of roll motion reduces to a specified level. When the approach described in section 3.4 is used, this effect is automatically neutralized since occurrence of the second, etc. stability failures in the same simulation does not change the result (which means that a simulation can be stopped after the first encountered stability failure as well).

3.9.5 The effect of transient hydrodynamic effects at the start of simulations can be neutralized by switching off the counter of stability failures and the simulation timer during initial transients or by random variation of initial conditions for each realization, see paragraph 3.7.5.

3.9.6 Numerical simulations (or model tests) are performed for arbitrary (sections 3.3 and 3.5) or constant (section 3.4) simulation time. If a stability failure is encountered in a simulation, further time history is not considered (thus, the simulation may be stopped). After each simulation, the number of the realization M, the number of stability failures encountered in the simulation ΔN (1 or 0) and duration of simulation Δt are recorded; the total number of failures N is increased by ΔN and the total simulation time t_{t} is increased by Δt.

3.9.7 Based on these parameters, r_{U} is updated after each simulation as follows:

.1 when section 3.3 is used: N^* is calculated as $N + 1$, the maximum likelihood estimate of the failure rate is calculated as $\hat{r} = N/t_{\text{t}}$ and its conservative estimate is calculated as $\hat{r}^* = N^*/t_{\mathrm{t}}$. A conservative estimate of the upper boundary of the 95%-confidence interval of failure rate is calculated as $r_{\mathrm{U}} = 0.5\chi^2_{1-0.05/2,2N^*}\hat{r}^*/N^*$, and the lower boundary is calculated as $r_{\mathrm{L}} = 0.5\chi^2_{0.05/2,2N}\hat{r}/N$;

.2 when section 3.4 is used: the upper boundary of the 95%-confidence interval of failure probability for an exposure time t_{exp} is $p_{\mathrm{U}} = \nu_1 F_{\nu_1,\nu_2;1-0.05/2}/\left(\nu_2 + \nu_1 F_{\nu_1,\nu_2;1-0.05/2}\right)$ with $\nu_1 = 2(N+1)$ and $\nu_2 = 2(M-N)$, for $N < M$; if $N = M$, then $p_{\mathrm{U}} = 1$. The lower boundary is $p_{\mathrm{L}} = \nu_1 F_{\nu_1,\nu_2;0.05/2}/\left(\nu_2 + \nu_1 F_{\nu_1,\nu_2;0.05/2}\right)$ with $\nu_1 = 2N$ and $\nu_2 = 2(M-N+1)$, for $N > 0$; if $N = 0$, then $p_{\mathrm{L}} = 0$. The corresponding lower and upper boundaries of the 95%-confidence interval of the failure rate are calculated as $r_{\mathrm{L}} = -\ln(1-p_{\mathrm{L}})/t_{\mathrm{exp}}$ and $r_{\mathrm{U}} = -\ln(1-p_{\mathrm{U}})/t_{\mathrm{exp}}$, respectively; or

.3 when section 3.5 is used: the decorrelation time T_{dc}.is computed as described in subsection 3.8. The first failure event in each record after the initial transient is always counted; other failure events are counted only if time between them exceeds the decorrelation time. The estimate of the failure rate is computed with the formula in paragraph 3.5.5 and the boundaries of the confidence interval are evaluated as described in paragraph 3.5.7.

3.10 Application examples of direct counting method

3.10.1 *General*

3.10.1 Application examples are based on modelling of ship motions in multiple independent realizations of an irregular seaway and counting the number of stability failures to provide the estimates of the boundaries of the 95%-confidence interval of the stability failure rate for the full probabilistic direct stability assessment.

3.10.2 *Application example based on approach in section 3.3*

3.10.2.1 Numerical simulations (or model tests) are performed for an arbitrary duration. If a stability failure is encountered in a simulation, the simulation is stopped. After each simulation, the number of the realization M, the number of encountered stability failures ΔN (1 or 0) and the duration of simulation Δt (the time to failure if the realization ended with a stability failure or the full duration of simulation otherwise) are recorded. Based on these parameters, the total number of failures N and total simulation time t_{t} are increased by ΔN and Δt, respectively. For a Poisson process, all simulations in which a stability failure did not occur can be treated as one combined simulation; one stability failure is conservatively assumed at the end of the last simulation if it did not end with a stability failure (for this purpose, N^* is set to N+1).

3.10.2.2 The maximum likelihood estimate of the rate of failure is updated as $\hat{r} = N/t_t$, its conservative estimate is updated as $\hat{r}^* = N^*/t_t$, a conservative estimate of both the upper boundary of the 95%-confidence interval of failure rate is updated as $r_{\mathrm{U}} = 0.5\chi^2_{1-0.05/2,2N^*}\hat{r}^*/N^*$ and the lower boundary is updated as $r_{\mathrm{L}} = 0.5\chi^2_{0.05/2,2N}\hat{r}/N$.

3.10.2.3 Table 3.10.1 shows an example of results according to this procedure for parametric roll resonance in a head seaway with a probability density $f_{\mathrm{s}} = 10^{-5}$ $(\mathrm{m{\cdot}s})^{-1}$ in the North Atlantic wave climate of a 1700 TEU container vessel with a GM of 1.8 m using simulations of constant one-hour duration; figure 3.10.1 shows r_{U} and r_{L} depending on the number of simulations M.

Table 3.10.1: Example results of direct counting procedure according to section 3.3

M	ΔN	Δt,s	N^*	N	t_t,s	$\hat{r}$,1/s	r_U,1/s	r_L,1/s	M	ΔN	Δt,s	N^*	N	t_t,s	$\hat{r}$,1/s	r_U,1/s	r_L,1/s
1	1	1682.0	1	1	1682.0	5.945e-4	2.193e-3	1.505e-5	21	1	2235.5	7	7	60990.5	1.148e-4	2.141e-4	4.614e-5
2	0	3600.0	2	1	5282.0	1.893e-4	1.055e-3	4.793e-6	22	1	3505.0	8	8	64495.5	1.240e-4	2.236e-4	5.355e-5
3	1	2270.0	2	2	7552.0	2.648e-4	7.378e-4	3.207e-5	23	1	261.5	9	9	64757.0	1.390e-4	2.434e-4	6.355e-5
4	0	3600.0	3	2	11152.0	1.793e-4	6.478e-4	2.172e-5	24	1	1969.5	10	10	66726.5	1.499e-4	2.560e-4	7.187e-5
5	0	3600.0	3	2	14752.0	1.356e-4	4.897e-4	1.642e-5	25	0	3600.0	11	10	70326.5	1.422e-4	2.615e-4	6.819e-5
6	1	1025.5	3	3	15777.5	1.901e-4	4.579e-4	3.921e-5	26	0	3600.0	11	10	73926.5	1.353e-4	2.488e-4	6.487e-5
7	1	2129.5	4	4	17907.0	2.234e-4	4.896e-4	6.086e-5	27	1	1275.0	11	11	75201.5	1.463e-4	2.445e-4	7.302e-5
8	1	1111.5	5	5	19018.5	2.629e-4	5.385e-4	8.536e-5	28	0	3600.0	12	11	78801.5	1.396e-4	2.498e-4	6.968e-5
9	0	3600.0	6	5	22618.5	2.211e-4	5.159e-4	7.178e-5	29	1	2710.5	12	12	81512.0	1.472e-4	2.415e-4	7.607e-5
10	0	3600.0	6	5	26218.5	1.907e-4	4.450e-4	6.192e-5	30	1	1919.0	13	13	83431.0	1.558e-4	2.512e-4	8.297e-5
11	0	3600.0	6	5	29818.5	1.677e-4	3.913e-4	5.445e-5	31	1	3445.0	14	14	86876.0	1.611e-4	2.559e-4	8.810e-5
12	0	3600.0	6	5	33418.5	1.496e-4	3.492e-4	4.858e-5	32	0	3600.0	15	14	90476.0	1.547e-4	2.596e-4	8.460e-5
13	0	3600.0	6	5	37018.5	1.351e-4	3.152e-4	4.386e-5	33	1	1884.5	15	15	92360.5	1.624e-4	2.543e-4	9.090e-5
14	0	3600.0	6	5	40618.5	1.231e-4	2.873e-4	3.997e-5	34	0	3600.0	16	15	95960.5	1.563e-4	2.578e-4	8.749e-5
15	0	3600.0	6	5	44218.5	1.131e-4	2.639e-4	3.672e-5	35	1	634.0	16	16	96594.5	1.656e-4	2.561e-4	9.468e-5
16	1	136.5	6	6	44355.0	1.353e-4	2.631e-4	4.964e-5	36	0	3600.0	17	16	100194.5	1.597e-4	2.593e-4	9.128e-5
17	0	3600.0	7	6	47955.0	1.251e-4	2.723e-4	4.592e-5	37	0	3600.0	17	16	103794.5	1.542e-4	2.503e-4	8.811e-5
18	0	3600.0	7	6	51555.0	1.164e-4	2.533e-4	4.271e-5	38	0	3600.0	17	16	107394.5	1.490e-4	2.419e-4	8.516e-5
19	0	3600.0	7	6	55155.0	1.088e-4	2.368e-4	3.992e-5	39	0	3600.0	17	16	110994.5	1.442e-4	2.341e-4	8.239e-5
20	0	3600.0	7	6	58755.0	1.021e-4	2.223e-4	3.748e-5	40	1	1801.5	17	17	112796.0	1.507e-4	2.304e-4	8.780e-5

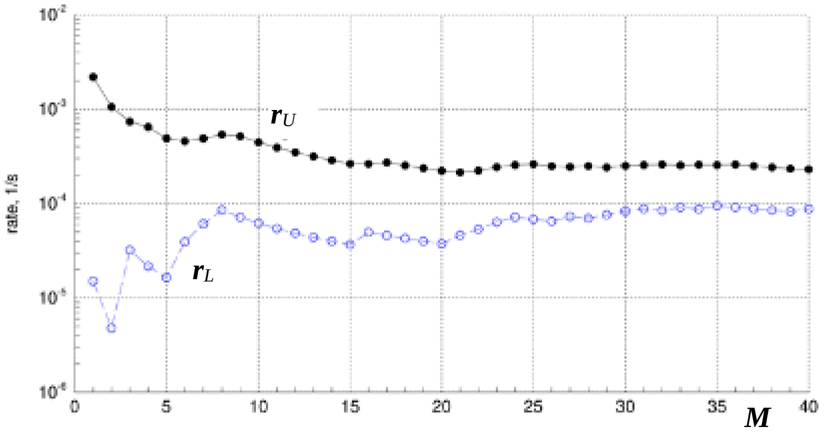

Figure 3.10.1 An example of results of the direct counting procedure according to section 3.3.

4 Direct stability assessment

4.1 Ships and loading conditions used in examples

4.1.1 Five ships were used as examples: a cruise vessel, a RoPax vessel, and three container ships of 1700, 8400 and 14000 TEU capacity. For each ship, five loading conditions were selected: three loading conditions with small GM values and two loading conditions with large GM values. Table 4.1.1 shows the length between perpendiculars, waterline breadth, draught, metacentric height and linear natural roll period for the studied ships and loading conditions (the pitch and yaw radii of inertia, $r_{yy} = \sqrt{I_{yy}/m}$ and $r_{zz} = \sqrt{I_{zz}/m}$, respectively, were set equal to L_{BP} / 4).

Table 4.1.1: Ships and loading conditions used in examples

Ship	L_{BP}, m	B_{wl},m	Loading condition:	LC01	LC02	LC03	LC04	LC05
Cruise vessel	230.9	32.2	d, m	6.9				
			GM, m	1.5	2.0	2.5	3.25	3.75
			T_r, s	19.8	17.2	15.4	13.6	12.6
RoPax vessel	175.0	29.5	d, m	5.5				
			GM, m	3.7	4.5	5.2	5.9	6.6

			T_r, s	11.8	10.7	9.8	9.4	9.0
1700 TEU container ship	159.6	28.1	d, m	9.5			5.5	
			GM, m	0.5	1.2	1.9	5.75	6.75
			T_r, s	29.3	19.4	15.4	8.8	8.2
8400 TEU container ship	317.2	43.2	d, m	13.93	14.44	14.48	11.36	
			GM, m	0.89	1.26	2.01	5.0	6.93
			T_r, s	36.7	31.3	25.7	15.4	13.2
14000 TEU container ship	349.5	51.2	d, m	14.5			8.5	
			GM, m	1.0	2.0	3.0	9.0	12.0
			T_r, s	38.8	27.6	22.6	13.0	11.4

4.2 Examples of full probabilistic direct stability assessment

4.2.1 For each ship and each loading condition, a full probabilistic direct stability assessment was performed using numerical simulations of ship motions in waves to provide a database for the development of simplified procedures. Simulations were performed at six forward speeds, presented in table 4.2.1, for the mean zero-crossing wave periods T_z and significant wave heights H_s covering all entries in the North Atlantic wave scatter table, IACS Recommendation No.34 (Corr.1 Nov. 2001) (table 2.7.2.1.2 of the Interim Guidelines), and for mean wave directions μ from 0 to 180º with an increment of 10º.

Table 4.2.1: Non-dimensional forward speeds used in analysis

Ship	L_{BP}, m	Froude numbers					
Cruise vessel	230.9	0.0	0.0454	0.0908	0.1362	0.1816	0.2270
RoPax vessel	175.0	0.0	0.0546	0.1093	0.1639	0.2185	0.2732
1700 container vessel (CV)	159.6	0.0	0.0481	0.0962	0.1443	0.1924	0.2405
8400 container vessel (CV)	317.2	0.0	0.0452	0.0904	0.1356	0.1808	0.2259
14000 container vessel (CV)	349.5	0.0	0.0427	0.0854	0.1281	0.1708	0.2135

4.2.2 For each combination of sea state (H_s, T_z) and sailing condition (v_0, μ), numerical simulations of ship motions in realizations of the same sea state were performed by using a random variation of frequencies, directions and phases of the wave components comprising each sea state. Each simulation was conducted for a simulation time of two hours or until the first stability failure occurred (a stability failure was defined as the exceedance of a roll angle of 40 º or a lateral acceleration of one g). After this, simulations were repeated in other realizations until N = 200 stability failures were encountered.

4.2.3 Direct counting was used for each "short-term" situation (H_s, T_z, v_0, μ), for which the total simulation time of $3.4 \cdot 10^6$ hours was sufficient to encounter 200 stability failures. The maximum likelihood estimate of stability failure rate was calculated as $r = N/t_t$, eq. (3.3.6), and the upper boundary of its 95%-confidence interval was calculated as $r_U = 0.5 r \chi^2_{1-0.05/2,2N}/N$, eq. (3.3.9); otherwise the extrapolation of the stability failure rate over the significant wave height was used.

4.2.4 A conservative estimate of the upper boundary $\bar{r}_U$ of the 95%-confidence interval of the average "long-term" stability failure rate was calculated according to the explanatory note to paragraph 3.5.3.2.1 of the Interim Guidelines as a weighted average over the sea states (H_s, T_z) and the sailing conditions (v_0, μ), of the upper boundaries r_U of the 95%-confidence intervals of the "short-term" stability failure rate:

$$\bar{r}_U = \sum_s \sum_\mu \sum_{v_s} f_s(H_s, T_z) \cdot f_\mu(\mu) \cdot f_v(v_s) \cdot r_U(H_s, T_z, \mu, v_s) \Delta H_s \Delta T_z \Delta v_s \Delta\mu \qquad (4.2.1)$$

4.2.5 In the calculations performed according to eq. (4.2.1), the mean wave directions μ and ship forward speeds v_s were assumed uniformly distributed between 0 and 360º and between zero and the maximum service speed, respectively.

4.2.6 Table 4.2.2 shows the "long-term" weighted average $\bar{r}_U$ of the upper boundaries of the 95%-confidence intervals of the "short-term" stability failure rate due to parametric and synchronous roll (differentiation between parametric and synchronous roll is described in section 4.4) for all tested ships and loading conditions; the values of $\bar{r}_U$ not satisfying the standard of $2.6 \cdot 10^{-8}$ 1/s are indicated with bold font.

Table 4.2.2: The "long-term" weighted average $\bar{r}_U$, 1/s, of the upper boundaries of the 95%-confidence intervals of the "short-term" stability failure rate for all tested ships and loading conditions

Ship	Parametric roll					Synchronous roll				
	LC01	LC02	LC03	LC04	LC05	LC01	LC02	LC03	LC04	LC05
Cruise vessel	1.67e-06	4.74e-08	3.90e-09	5.28e-10	2.41e-10	4.59e-07	8.01e-09	6.08e-10	1.86e-10	1.23e-10
RoPax vessel	5.47e-10	1.56e-11	1.51e-11	1.15e-11	9.49e-12	5.67e-10	9.90e-12	3.38e-11	4.83e-11	7.01e-11
1700 TEU CV	3.65e-05	9.51e-07	7.50e-09	3.53e-15	2.01e-15	1.41e-05	4.09e-07	3.86e-09	1.36e-12	1.54e-12
8400 TEU CV	4.01e-06	2.44e-06	2.57e-07	9.30e-11	7.31e-13	1.64e-06	9.79e-07	1.17e-07	2.01e-07	7.24e-09
14000 TEU CV	6.47e-05	2.00e-05	1.44e-06	7.95e-19	4.52e-19	5.50e-05	1.49e-05	9.07e-07	3.07e-16	3.46e-16

4.3 Database for the development of direct stability assessment procedures for the parametric roll, pure loss of stability and excessive acceleration failure modes

4.3.1 The example ships demonstrated stability failures due to principal parametric roll resonance in bow waves, principal and fundamental parametric resonance in stern waves (fundamental resonance occurs at an encounter frequency that is about the same as the natural roll frequency) and synchronous roll in beam waves (which is relevant for the dead ship and excessive acceleration stability failure modes). Some of the loading conditions indicated large heel angles in following waves at high forward speeds, although their maximum speeds, while sufficient for vulnerability to the pure loss of stability failure mode, were not sufficiently high for strong pure loss of stability failures. Surf-riding/broaching was not found to be relevant for any of the ships.

4.3.2 To develop and validate procedures for a direct assessment, including an extrapolation of the stability failure rate over the wave height and probabilistic and deterministic assessment in design situations, stability failures that were identified in simulations were separated with respect to the stability failure modes.

4.3.3 Parametric roll (specifically, principal parametric roll resonance) in bow waves was detected in mean wave directions from 180 (head up) to about 70º off-bow. Nevertheless, in all cases where principal parametric roll resonance in bow waves occurred, head waves led to the largest roll motions, figure 4.3.1 (top left and top middle plots). Therefore, for parametric roll in bow waves, an assessment in head waves was expected to detect the worst situations and, moreover, include most relevant stability failure events. To select relevant simulation results from the full database for validation and calibration of simplified methods for parametric roll resonance in bow waves, three sets of reference data were generated: for wave directions from 170 to 180, from 160 to 180, and from 150 to 180.

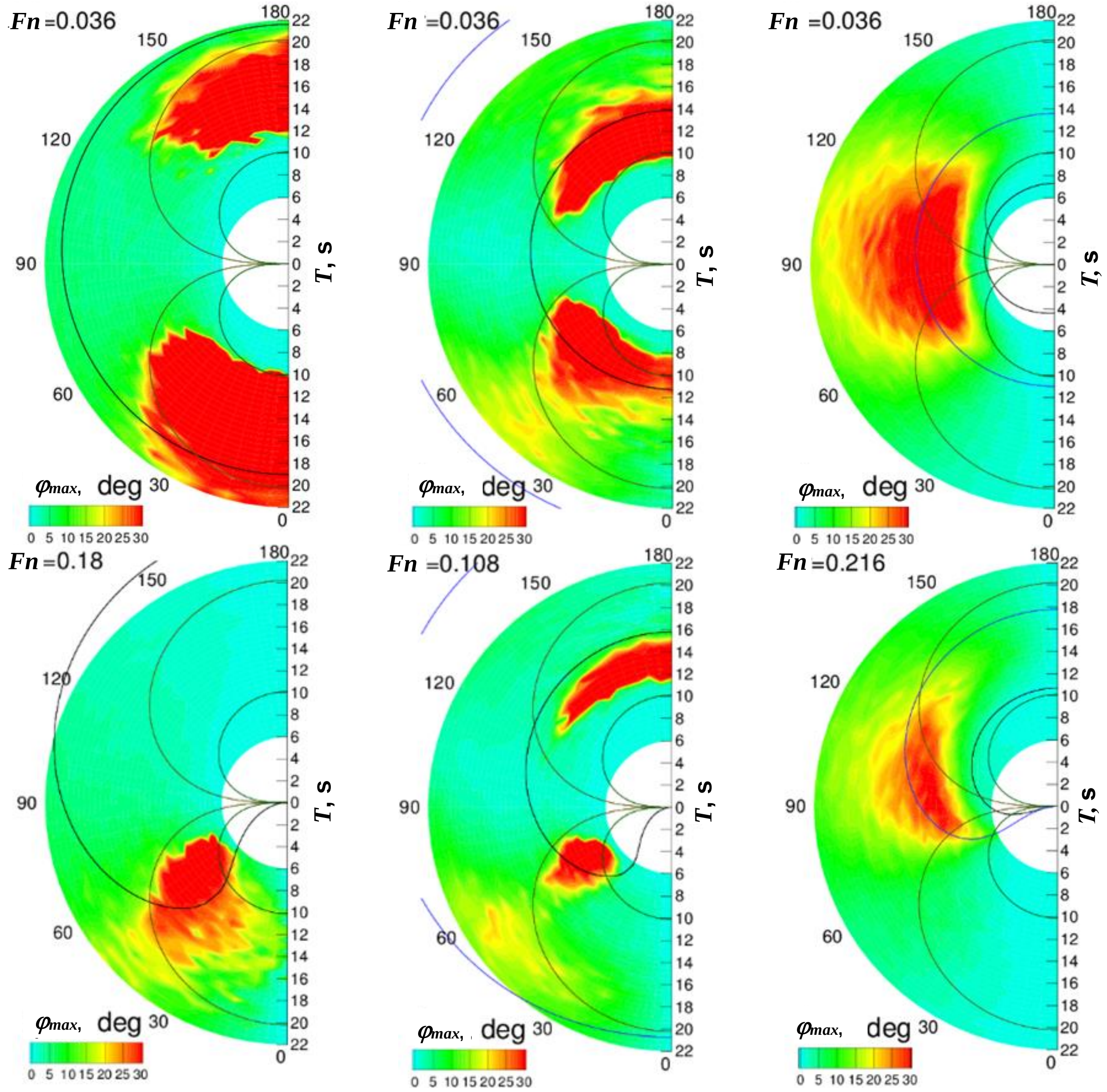

Figure 4.3.1: Colour plots of the mean three-hour maximum roll amplitude vs. the mean wave period (s, radial coordinate) and the mean wave direction (circumferential coordinate, 0, 90 and 180º correspond to following waves, waves from port side and head waves, respectively) for parametric roll resonance at low GM = 0.89 m (left) and medium GM = 2.01 m (middle) and for synchronous roll at high GM = 6.93 m (right) at low (top) and high (bottom) speeds for a 8400 TEU container ship, table 4.1.1. The black and blue lines correspond to the ratio of the peak wave encounter period to the linear natural roll period of 2:1 and 1:1, respectively, and the green lines bound the region with a projected wave length λ / cos μ between 0.5L_{BP} and 2.0L_{BP}.

4.3.4 Parametric roll resonance in stern waves was detected in wave directions from following (0°) up to about 80 off-stern. Unlike for parametric roll in bow waves, for which head waves always represent the worst case, following waves were not always worst (over all stern wave directions) for parametric roll in stern waves. Moreover, for some loading conditions at certain forward speeds, parametric roll did not occur in following waves while it did occur in stern-quartering waves, figure 4.3.1 (bottom left and middle).[20] This means that for some ships in some loading conditions, an assessment in following waves may not detect the possibility of severe parametric roll in stern waves.

4.3.5 This is inconvenient since the need to address parametric roll in stern-quartering waves in a simplified assessment means that the number of required design situations will be significantly increased to include all wave directions from following (0) to 90 off-stern; moreover, this means a significant increase in the number of model tests and much more advanced model testing facilities will be required.

4.3.6 To check whether addressing parametric roll specifically in stern-quartering waves is essential for a direct stability assessment, the results of the full assessment are plotted in figure 4.3.2 as follows: the y-axis corresponds to the total stability failure rate over all wave directions, whereas the x-axis corresponds to the sum of stability failure rates over parametric roll in bow and stern waves (i.e. the sectors from 150 to 180 and 0 to 30, respectively) and synchronous roll in beam waves (i.e. the sector from 60 to 120) for all ships and loading conditions (differentiated by symbol type and colour) and forward speeds. Thus, the x-axis variable neglects parametric roll in stern-quartering waves, which is included in the y-axis variable.

4.3.7 Since the dependency in figure 4.3.2 is monotonous and sharp, the contributions from parametric roll resonance in stern-quartering waves do not need to be additionally addressed in a simplified direct stability assessment (unlike in operational measures): taking into account parametric roll resonance in following waves is sufficient to represent the contributions of parametric roll resonance in all stern wave directions. The reason is that parametric roll resonance in stern-quartering waves becomes important with increasing forward speed (when parametric roll decreases) whereas much larger contributions occur in following waves at low forward speeds. Another contribution to parametric roll resonance in stern-quartering waves comes from fundamental resonance, which is, however, weaker than the principal resonance.

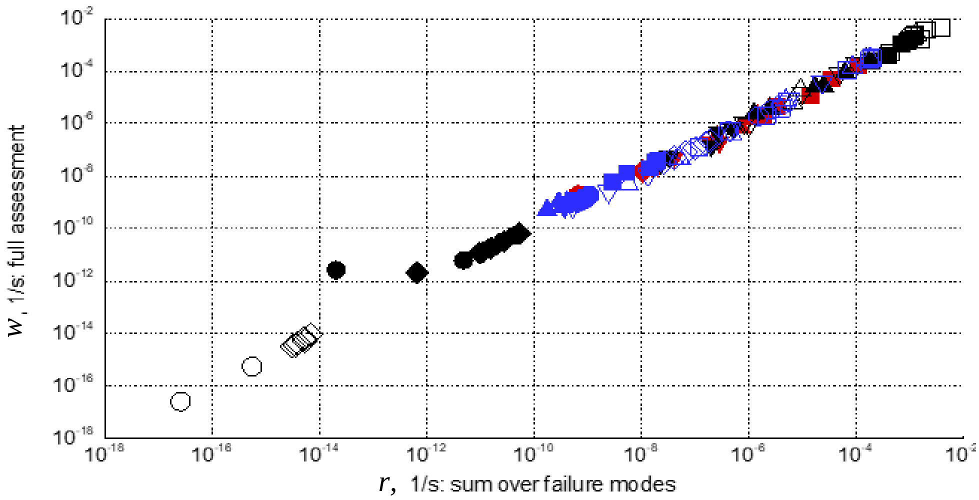

Figure 4.3.2: Total stability faılure rate in all wave directions vs. the sum of the stability failure rates due to parametric roll in bow and stern waves and synchronous roll in beam waves; symbol type and colour differentiate ships and loading conditions

[20] Shigunov, V. el Moctar, O., and Rathje, H. *Conditions of parametric rolling*, Proc. 10th Int. Conf. on Stability of Ships and Ocean Vehicles, 2009.

4.3.8 Therefore, for the development and validation of simplified procedures for parametric roll resonance in stern wave directions, three comparative sets of data were generated from the full database of assessment results, corresponding to wave directions from 0 to 10, 0 to 20 and 0 to 30º.

4.3.9 For synchronous roll in beam waves, the relevant wave directions were found from about 40° off-bow to about 40° off-stern, depending on the forward speed, figure 4.3.1 (top right and bottom right). However, at low forward speeds, the wave directions close to the beam are sufficient to assess synchronous roll. Therefore, to select relevant cases for validation from the full database of assessment results, three comparative sets of reference data were generated, for wave directions from 80 to 100, 70 to 110 and 60 to 120.

4.3.10 Reference data for the pure loss of stability failure mode were also generated, although this stability failure mode was especially difficult to identify since none of the selected ships was expected to undergo severe pure loss of stability due to low maximum speeds (although in the region of vulnerability). Three simple conditions were used: following waves; encounter period (corresponding to peak wave period) exceeding 30 s; and a wave length, corresponding to the peak wave period, close to the ship length.

4.4 Design situations

4.4.1 The full probabilistic direct stability assessment requires averaging of the stability failure rate over all sea states of a relevant wave environment (which is quantified in a wave scatter table) and all relevant sailing conditions and thus a large computational time. It can be proposed to reduce the assessment to few combinations of sea state parameters (wave height and period) and sailing conditions (ship forward speed and relative wave direction), referred to as design situations. The idea is that a simplified safety criterion S can be used for norming if the dependency of the actual criterion W (average stability failure rate) on such a criterion (a) is monotonous and (b) shows little scatter between different ships, loading conditions and forward speeds. The standard for this simplified criterion (further referred to as *threshold* to differentiate it from the standard used for the actual criterion) can be defined using a sufficient number of representative case studies, figure 4.4.1. Note that the exact dependency $W(S)$ does not matter in the practical approval and is not required, as long as it is proven that this dependency satisfies conditions (a) and (b).

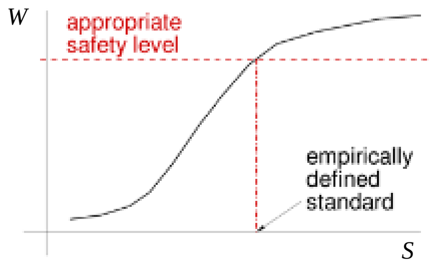

Figure 4.4.1:
The idea of the simplified safety criterion S; W is the "true" safety measure, e.g. a mean long-term probability of stability failure

4.4.2 To verify conditions (a) and (b) in paragraph 4.4.1, the average rate of stability failures was computed using the results of the full probabilistic assessment as given in eq. (4.2.1). However, different forward speeds were applied and evaluated separately because the selection of a suitable speed to be used in design situations was one of the tasks of this investigation:

$$W = \bar{r}(\mathrm{ship}, \mathrm{LC}, v_0) = \sum_s \sum_\mu f_\mathrm{s}(H_\mathrm{s}, T_\mathrm{z}) \cdot f_\mu(\mu) \cdot r(H_\mathrm{s}, T_\mathrm{z}, \mu, v_0) \Delta H_\mathrm{s} \Delta T_\mathrm{z} \Delta\mu \qquad (4.4.1)$$

4.4.3 As the first step, the wave directions for design situations were assumed as 180° for parametric roll in bow waves, 0° for parametric roll in stern waves, 90° for synchronous roll in beam waves and 0° for pure loss of stability.

4.4.4 The second step was the selection of wave height in order to use one significant wave height per wave period. Several approaches to the selection of sea states for design situations were compared in documents SDC 4/5/8 and SDC 4/INF.8, including sea states according to the steepness table from MSC.1/Circ.1200, sea states along constant steepness lines $H_s = \mathrm{const} \cdot T_z^2$, along lines of constant density of sea state occurrence probability, and along lines of constant normed and not normed quantiles of sea state occurrence probability. The results presented in documents SDC 4/5/8 and SDC 4/INF.8, confirmed here, indicate that from these options, sea states selected along the lines of constant density of sea state occurrence probability, figure 4.4.2, provide the best correlation between W and S. Therefore, results are shown here only for such design sea states. The lines of constant density of sea state occurrence probability were defined using a logarithmic interpolation of probabilities (see the explanatory note to paragraph 3.5.3.3.5 of the Interim Guidelines).

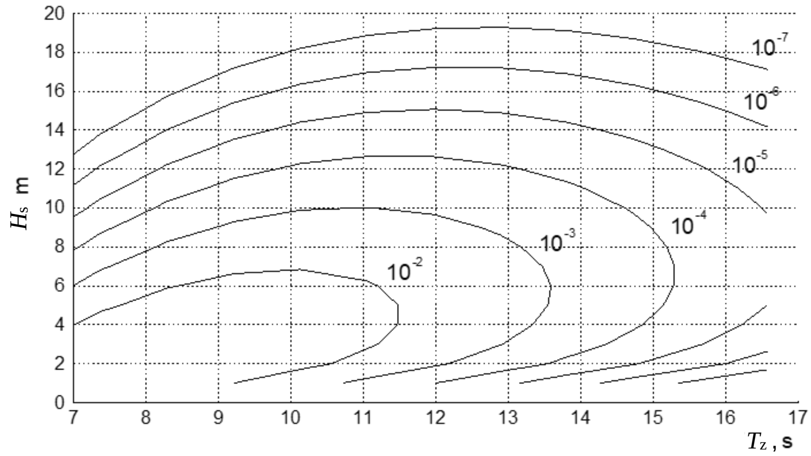

Figure 4.4.2: Contours of constant density of the probability of the occurrence of a particular sea state

4.4.5 As the simplified criterion S in these sea states, the maximum (over design sea states) stability failure rate r was used.

4.4.6 Figures 4.4.3 to 4.4.6 show the "long-term" average stability failure rate W vs. maximum (over design sea states) failure rate in design sea states with probability densities 10^{-7}, 10^{-6}, 10^{-5} and $10^{-4}(\mathrm{m{\cdot}s})^{-1}$ for all failure modes, in which each point corresponds to one ship and combination of loading condition and forward speed. Sharp monotonic dependencies in figure 4.3.2, concerning selection of wave directions for design situations, and in figure 4.4.3 to 4.4.6, at f_S = 10^{-4} $(\mathrm{m{\cdot}s})^{-1}$ and less, concerning the selection of wave heights for design situations, indicate that the accuracy of the simplified criterion S is satisfactory and improves with increasing wave steepness. Note that the required model testing or numerical simulation time quickly reduces with increasing wave height. Therefore, it is more efficient to use design sea states of greater steepness; however, sea states of too large steepness may be difficult to realize in model tests or numerical simulations.

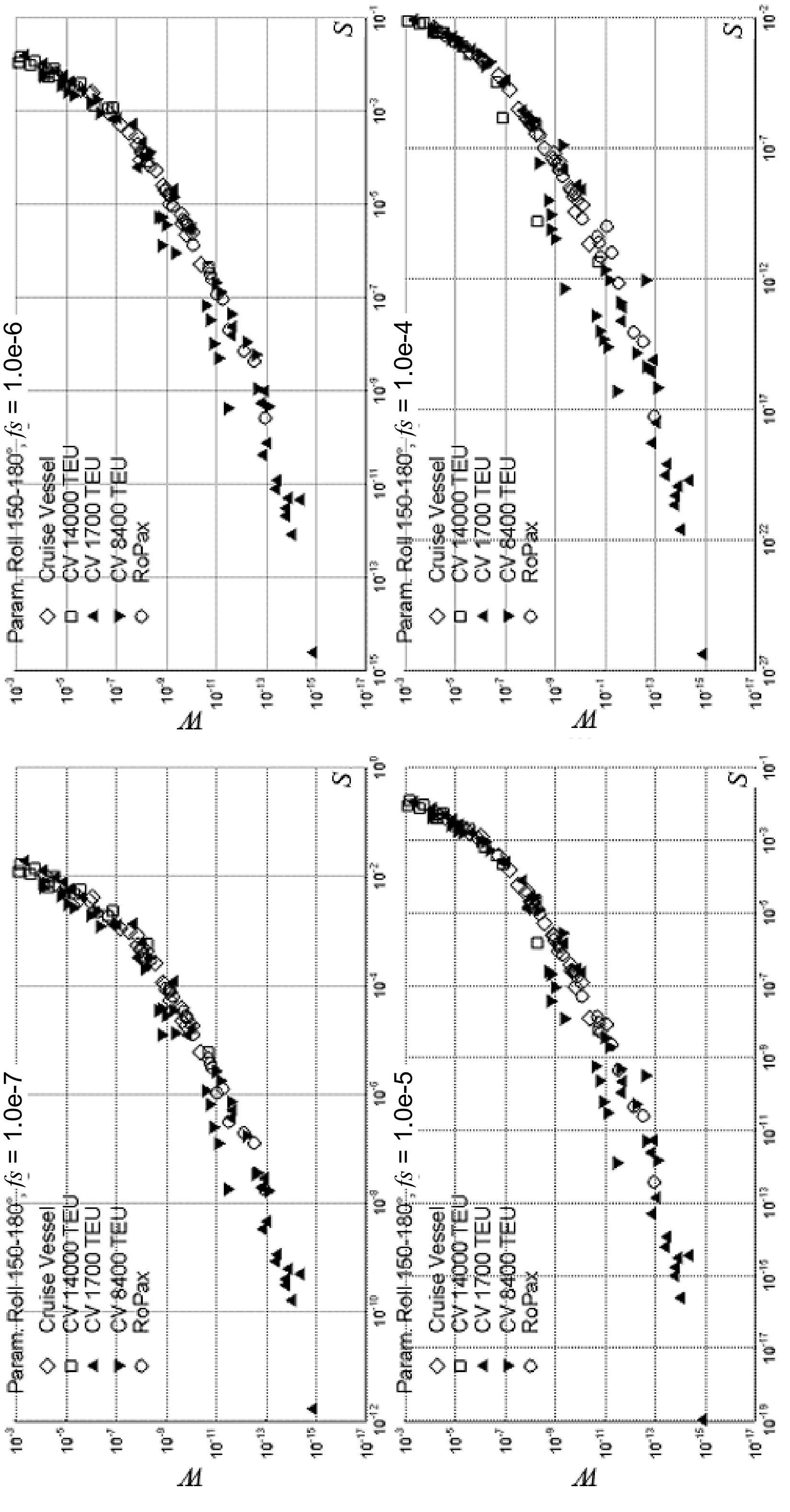

Figure 4.4.3: The *W(S)* for design situations for parametric roll in bow waves: mean long-term stability failure rate *W*(*ship,LC,v*$_0$), 1/s, *y*-axis, in wave directions from 150° to 180° vs. simplified criterion, 1/s, *x*-axis – short-term stability failure rate in head waves, maximum over design sea states along lines with sea state probability density f_s of (top left to bottom right) 10^{-7}, 10^{-6}, 10^{-5} and 10^{-4} (m·s)$^{-1}$

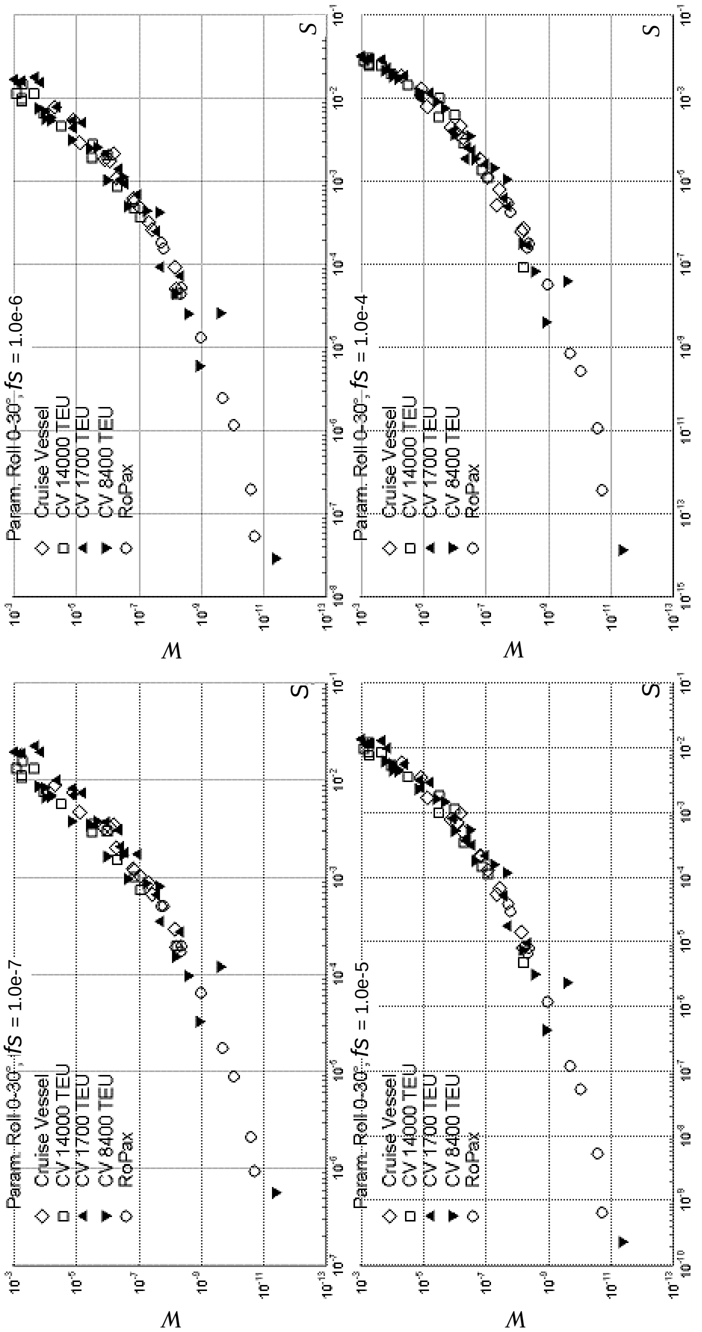

Figure 4.4.4: The $W(S)$ for design situations for parametric roll in stern waves: mean long-term stability failure rate W(*ship*,LC,v_0), 1/s, y-axis, in wave directions 0° to 30° vs. simplified criterion, 1/s, x-axis – short-term stability failure rate in following waves, maximum over design sea states along lines with sea state probability density f_s of (top left to bottom right) 10^{-7}, 10^{-6}, 10^{-5} and 10^{-4} (m·s)$^{-1}$

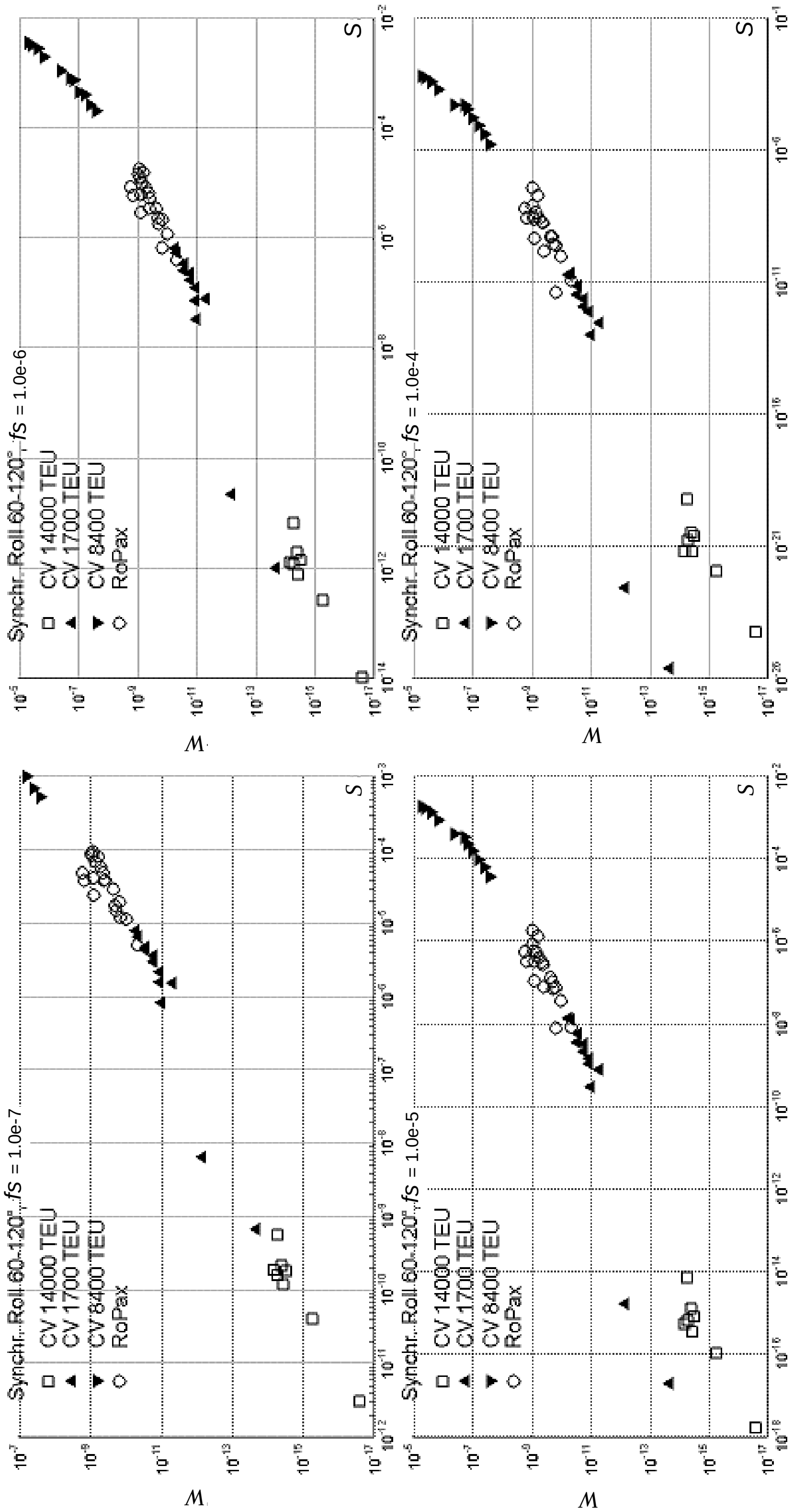

Figure 4.4.5: *W(S)* for synchronous roll in beam waves: mean long-term stability failure rate *W*(*ship,LC,v₀*), 1/s, *y*-axis, in wave directions from 60° to 120° vs. simplified criterion, 1/s, *x*-axis – short-term stability failure rate at μ = 90°, maximum over design sea states along lines with sea state probability density *fs* equal to (from top left to bottom right) 10^{-7}, 10^{-6}, 10^{-5} and 10^{-4} (m·s)$^{-1}$

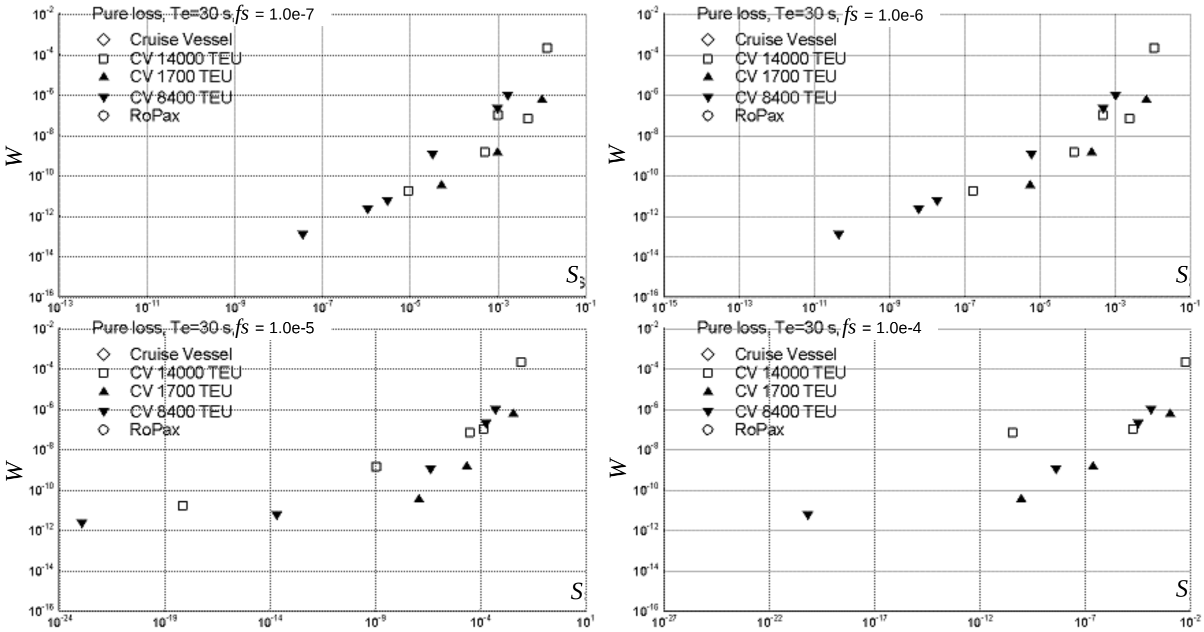

Figure 4.4.6: The $W(S)$ for pure loss of stability: mean long-term stability failure rate W(*ship*,LC,v_0), 1/s, y-axis, vs. simplified criterion, 1/s, x-axis – short-term stability failure rate in following waves, maximum over design sea states with occurrence probability density f_s of (top left to bottom right) 10^{-7}, 10^{-6}, 10^{-5} and 10^{-4} (m·s)$^{-1}$

4.4.7 Results presented above allow a reduction in the number of assessment situations due to using one wave direction per failure mode (which is a reduction factor of about 19) and one wave height per wave period (which is a reduction factor of several orders of magnitude since assessment at low wave heights requires very long simulations, if feasible at all). Another reduction possibility is the selection of a suitable forward speed: if, for example, only one speed needs to be used per failure mode, this will lead to a reduction of the number of assessment situations by about one order of magnitude (for some stability failure modes) and will allow significant simplifications in numerical simulations or the set-up of model tests.

4.4.8 For the dead ship condition and excessive accelerations stability failure modes, only zero forward speed is applied in the full assessment anyway. For the pure loss of stability failure mode, the rate of stability failures increases with increasing speed and, therefore, the maximum speed should be used. To select the forward speed for design situations for the parametric roll stability failure mode, figure 4.4.7 (left) shows the failure rate (maximum over wave periods) due to parametric roll in head waves along the line f_s = 10^{-5} (m·s)$^{-1}$ as a function of Froude number. Each plot corresponds to one ship and each line corresponds to one loading condition.

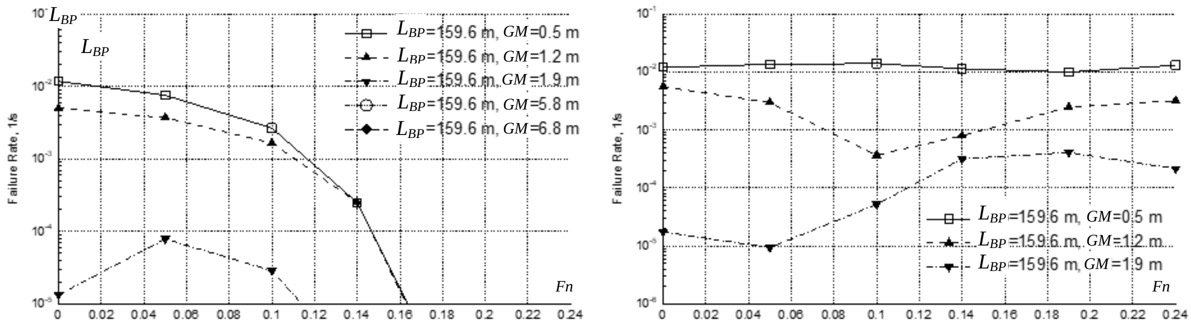

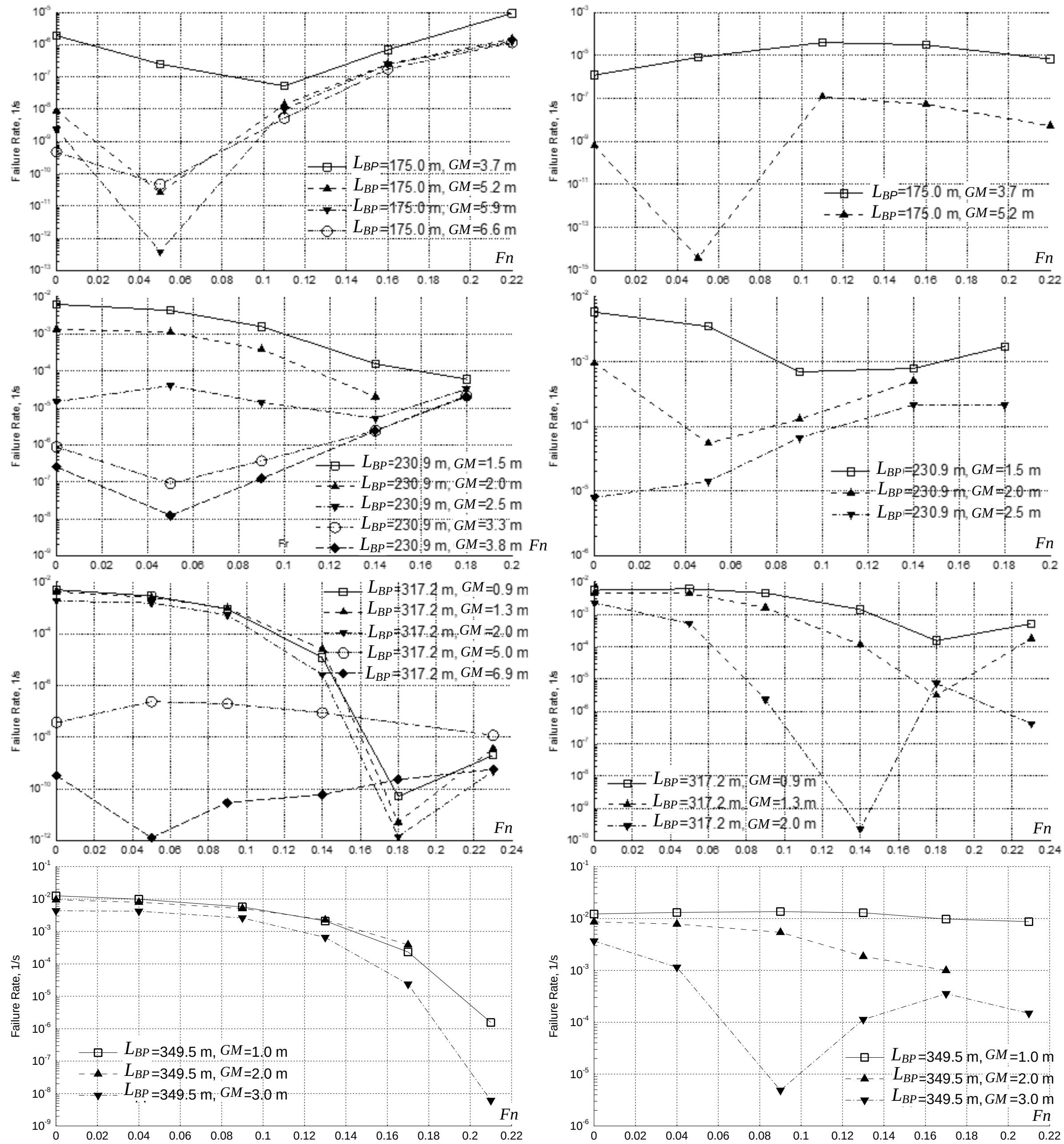

Figure 4.4.7: Maximum (over all wave periods) short-term stability failure rate, 1/s, at a wave height corresponding to sea state probability density f_s = 10^{-5} (m·s)$^{-1}$ (y-axis) vs. Froude number (x-axis) in head (left) and following (right) waves for (from top to bottom) the 1700 TEU container ship, the RoPax vessel, the cruise vessel and the 8400 and 14000 TEU container ships; one line corresponds to one loading condition

4.4.9 The results show that for all loading conditions with a high failure rate, the failure rate due to parametric roll decreases with increasing forward speed, which is due to broadening of the encounter wave spectrum with increasing forward speed in bow waves and increasing roll damping with increasing forward speed (according to operational experience, parametric roll accidents in bow waves have usually happened at low forward speed). For the RoPax vessel in all loading conditions and the cruise vessel in two loading conditions with the largest GM, the stability failure rate increases with increasing forward speed; however, the stability failure rate for these cases is very small anyway. Therefore, it seems appropriate to use only zero forward speed in design situations for parametric roll in bow waves (if zero speed is difficult to implement in simulations or model tests, as low as practicable forward speed can be applied instead).

4.4.10 For parametric roll in stern waves, figure 4.4.7 (right) shows a more complex dependency of the failure rate on the Froude number in design sea states in following waves. This is due to more complex relationship between the wave frequency and the encounter frequency in stern waves and thus a more complex behaviour of the encounter wave spectrum. However, in all cases with a large stability failure rate, a simplified assessment only at zero forward speed will either not introduce any non-conservative error or will be conservative, thus zero (or as low as practicable) forward speed seems appropriate also for parametric roll in following waves.

4.4.11 Zero forward speed in head or following waves may not be realistic in severe seas because of the difficulties for a ship (with a usual steering system) to keep course. However, this assumption is acceptable as a practical simplification for the roll motion assessment procedure (which, however, will require some adjustment of the test set-up).

4.5 Deterministic direct stability assessment

4.5.1 A difficulty of a probabilistic assessment is the need to encounter stability failures in simulations or model tests, which may require long durations of simulations or model tests for relevant cases. An appealing idea is to combine design situations with non-probabilistic criteria, e.g. mean maximum roll amplitude per given exposure time, mean roll amplitude. The idea is still the same as shown in figure 4.4.1: as long as a simplified criterion S is monotonically related to the true safety measure W (average safety failure rate) and the scatter between ships, loading conditions and forward speeds is small, the simplified criterion can be directly used for norming and its acceptance threshold can be defined directly using the results of a deterministic assessment for a sufficient number of representative sample cases.

4.5.2 In documents SDC 4/5/8 and SDC 4/INF.8, this method was verified for roll in beam seas to address dead ship condition and excessive acceleration stability failures. Two deterministic criteria (the mean roll amplitude and the mean three-hour maximum roll amplitude) were tested for different ships, loading conditions and forward speeds in irregular beam seas. The latter criterion has shown significantly better results than the former one, therefore, it was used here in combination with design situations to develop the deterministic assessment.

4.5.3 The same ships and loading conditions were used as listed in table 4.1.1. In the first step, different forward speeds were evaluated separately. For each failure mode, one wave direction was used for design situations: for parametric roll in bow waves, 180°; for parametric roll in stern waves, 0°; for synchronous roll in beam waves, 90° (associated with both the dead-ship condition and excessive acceleration failure modes); and for pure loss of stability, 0°. As in the previous section, the sea states selected along the lines of constant density of seaway occurrence probability, f_S, figure 4.4.2, were used as design sea states.

4.5.4 As the simplified criterion S, the maximum (over design sea states) of the mean three-hour maximum roll amplitude was used. To define it, three-hour numerical simulations were performed in 50 realizations of each sea state by a random variation of frequencies, directions and phases of the components of the modelled seaway. The maximum roll amplitude was defined from each simulation and averaged over 50 maxima. An evaluation of the three-hour maximum roll amplitude is impossible in cases with capsizing, since the roll amplitude is not defined. To distinguish such cases in plots, the mean three-hour maximum roll amplitude is shown for these cases as 60° for ease of identification since the mean three-hour maximum roll amplitude never achieved 60° in simulations where capsizing did not occur for the considered ships.

4.5.5 Figures 4.5.1 to 4.5.4 show the average "long-term" stability failure rate W vs. mean three-hour maximum roll amplitude for parametric roll in bow (figure 4.5.1) and stern (figure 4.5.2) waves, synchronous roll in beam waves (figure 4.5.3) and pure loss of stability (figure 4.5.4). The mean three-hour maximum roll amplitude is defined as the maximum over all wave periods in design sea states with the occurrence probability density $f_s = 10^{-7}$, 10^{-6}, 10^{-5} and 10^{-4} $(\text{m}\cdot\text{s})^{-1}$ for wave directions 180° (for parametric roll in bow waves), 0° (parametric roll in stern waves) and 90° (synchronous roll in beam waves), and for combined conditions of 0° wave direction, encounter peak wave period more than 30 s and wave length equal to ship length (for pure loss of stability). Each point corresponds to one ship in one loading condition at one forward speed.

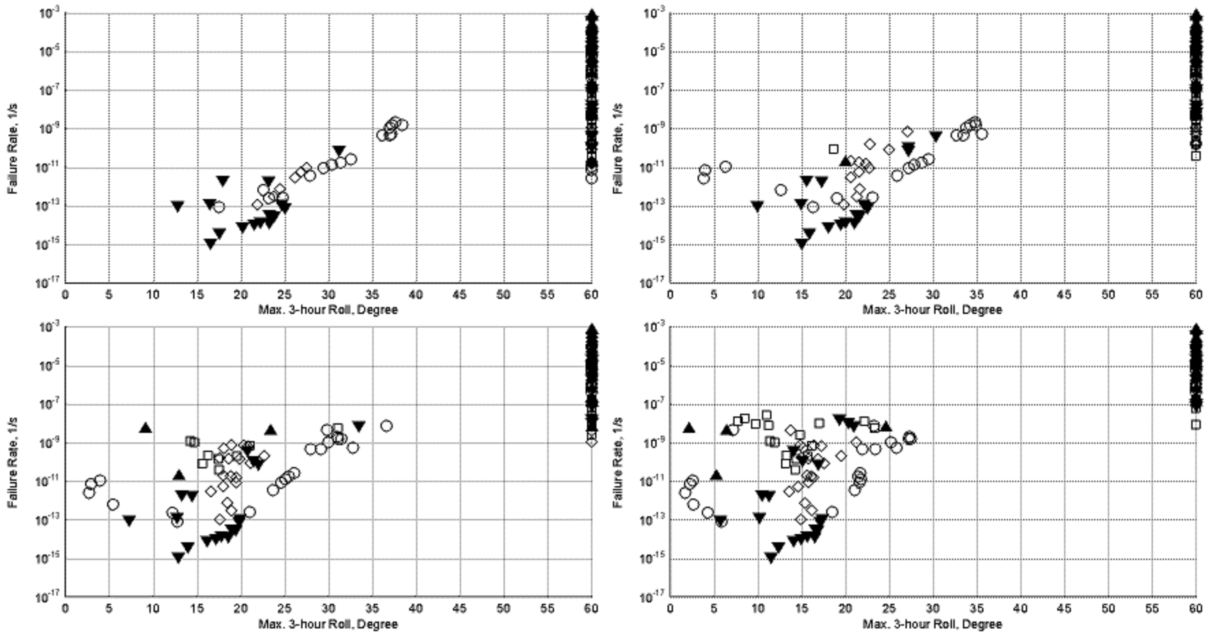

Figure 4.5.1:Parametric roll in bow waves: the long-term average failure rate $W(ship,LC,v_0)$, 1/s, y-axis, in wave directions from 150° to 180° vs. the deterministic criterion, x-axis – mean three-hour maximum roll amplitude in head waves, maximum over design sea states along lines with sea state occurrence probability density f_S (from top left to bottom right) 10^{-7}, 10^{-6}, 10^{-5} and 10^{-4} $(\text{m}\cdot\text{s})^{-1}$; each point means one ship (different symbols), one loading condition and one forward speed; points with mean three-hour maximum roll amplitude 60° indicate capsizing

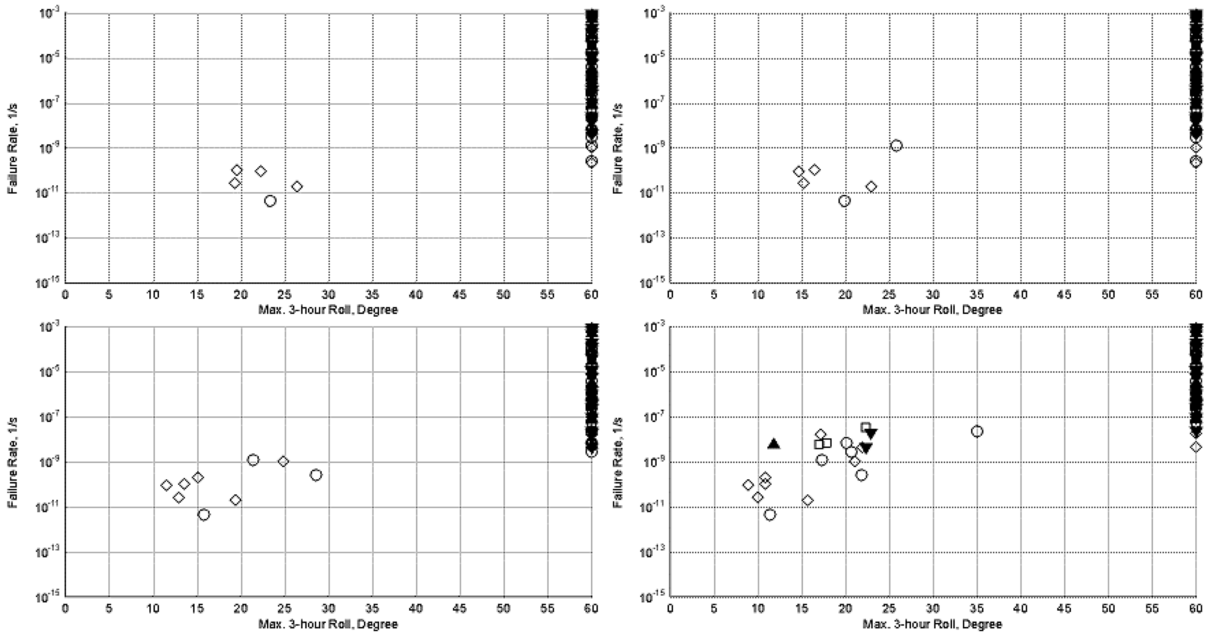

Figure 4.5.2: Parametric roll in stern waves: long-term average stability failure rate $W(\boldsymbol{ship},LC,v_0)$, 1/s, y-axis, in wave directions from 0 to 30° vs. deterministic criterion, x-axis – mean three-hour maximum roll amplitude in following waves, maximum over design sea states along lines with sea state occurrence probability density f_s (from top to bottom) 10^{-7}, 10^{-6}, 10^{-5} and 10^{-4} $(m{\cdot}s)^{-1}$; each point means one ship (different symbols), one loading condition and one forward speed; points with a mean three-hour maximum roll amplitude of 60° indicate capsizing

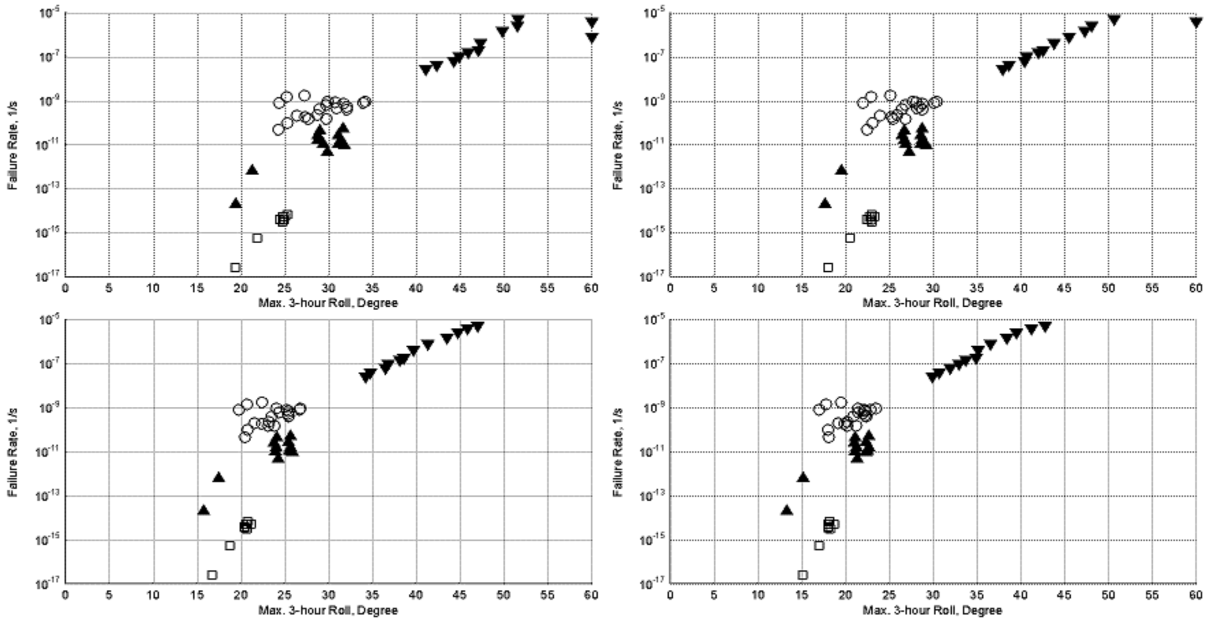

Figure 4.5.3: Synchronous roll in beam waves: long-term average stability failure rate $W(\boldsymbol{ship},LC,v_0)$, 1/s, y-axis, in wave directions from 60 to 120° vs. deterministic criterion, x-axis – mean three-hour maximum roll amplitude at $\mu = 90°$, maximum over design sea states along lines with sea state occurrence probability density f_s (from top left to bottom right) 10^{-7}, 10^{-6}, 10^{-5} and 10^{-4} $(m{\cdot}s)^{-1}$; each point means one ship (different symbols), one loading condition and one forward speed; points with a mean three-hour maximum roll amplitude of 60° indicate capsizing

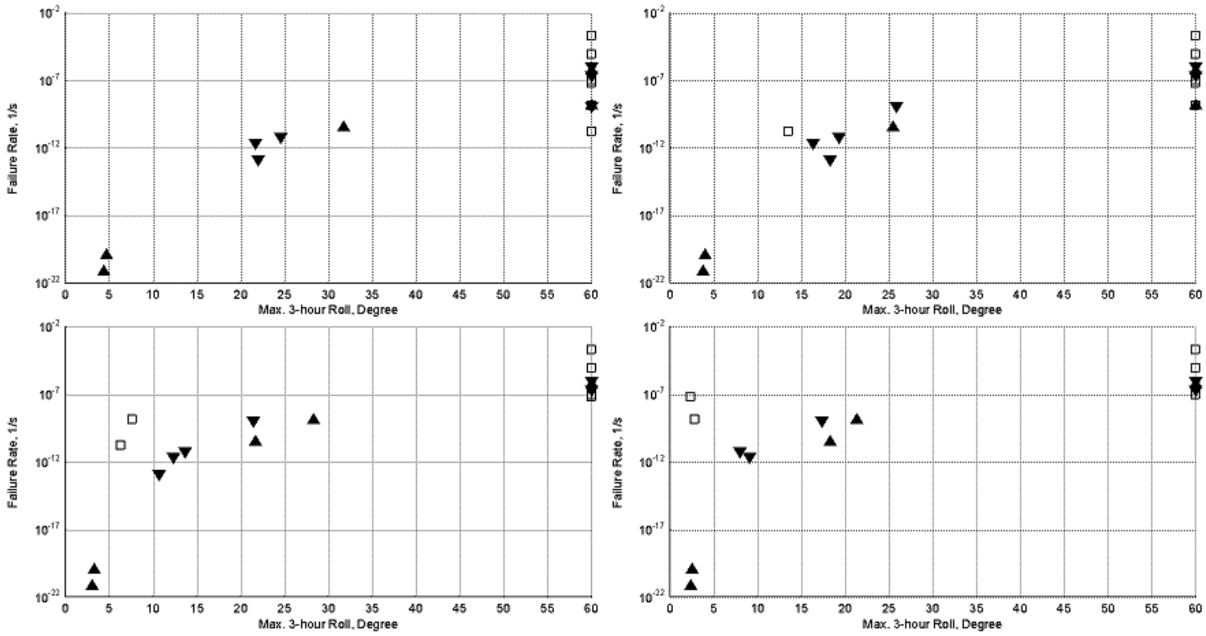

Figure 4.5.4: Pure loss of stability in following waves: long-term average stability failure rate W(*ship*,LC,v_0), 1/s, y-axis, vs. deterministic criterion, x-axis – mean 3h maximum roll amplitude in following waves, maximum over design sea states along lines with sea state occurrence probability density f_s (top left to bottom right) 10^{-7}, 10^{-6}, 10^{-5} and 10^{-4} (m·s)$^{-1}$; each point means one ship (different symbols), one loading condition and one forward speed; points with a mean three-hour maximum roll amplitude equal to 60^o indicate cases with capsizing

4.5.6 The correlation between the average long-term stability failure rate and the mean three-hour maximum roll amplitude in design sea states is very poor, especially in cases with small roll motions. Although increasing roll motions significantly improve this correlation, they also lead to capsizings, which make the evaluation of the deterministic criterion impossible.

4.5.7 To select forward speeds to be used in the design situations, the mean three-hour maximum roll amplitude in head and following (for parametric roll), beam (synchronous roll) and following (pure loss of stability) waves in sea states with a probability density 10^{-5} (m·s)$^{-1}$ is plotted vs. forward speed in figures 4.5.5 to 4.5.8. The results are similar to the speed dependency of the probabilistic criterion: for parametric roll in head waves and for synchronous roll, decreasing forward speed maximizes the three-hour maximum roll amplitude, whereas for pure loss of stability, the greatest roll responses correspond to the maximum forward speed. For parametric roll in following waves, the maximum roll may either decrease or increase with increasing forward speed; however, for the most critical loading conditions, low forward speeds lead to the maximum roll response. Therefore, similar recommendations are given for the selection of forward speed as those given for the probabilistic direct stability assessment in design situations.

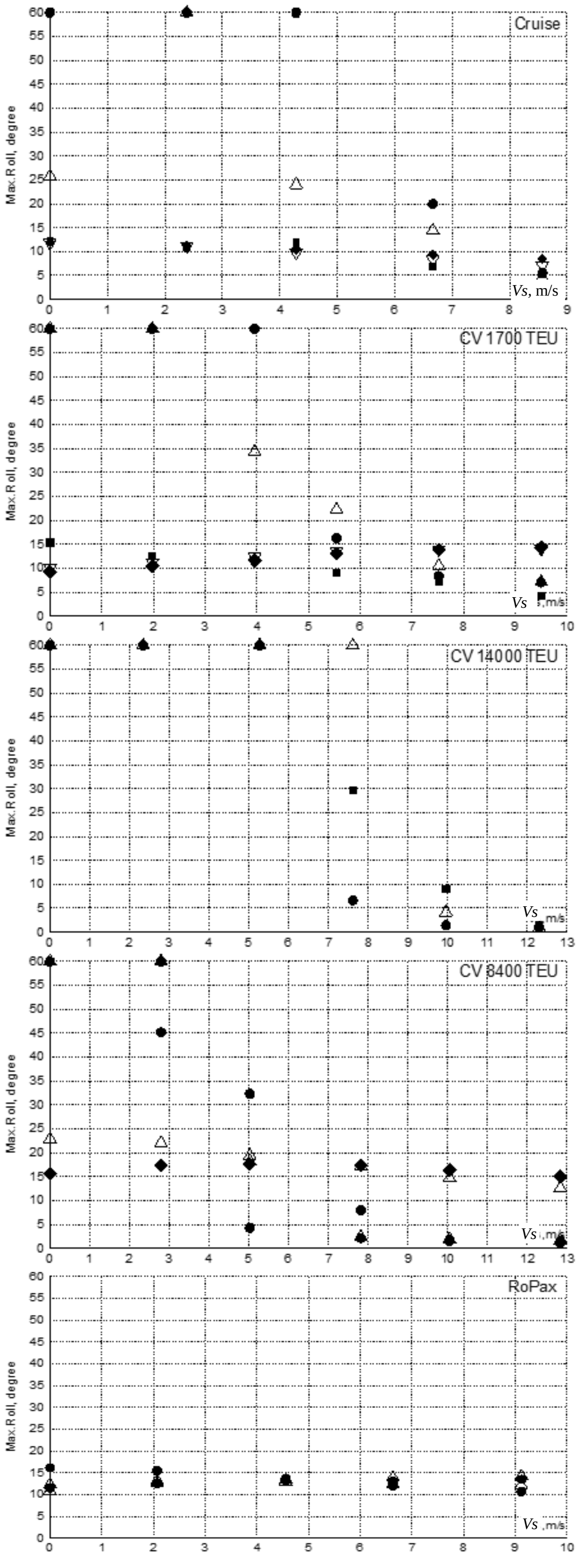

Figure 4.5.5: The mean 3h maximum roll amplitude due to parametric roll in head waves in sea states with f_s=10^{-5} (m·s)$^{-1}$ vs. forward speed. each plot corresponds to one ship; different symbols correspond to different loading conditions.

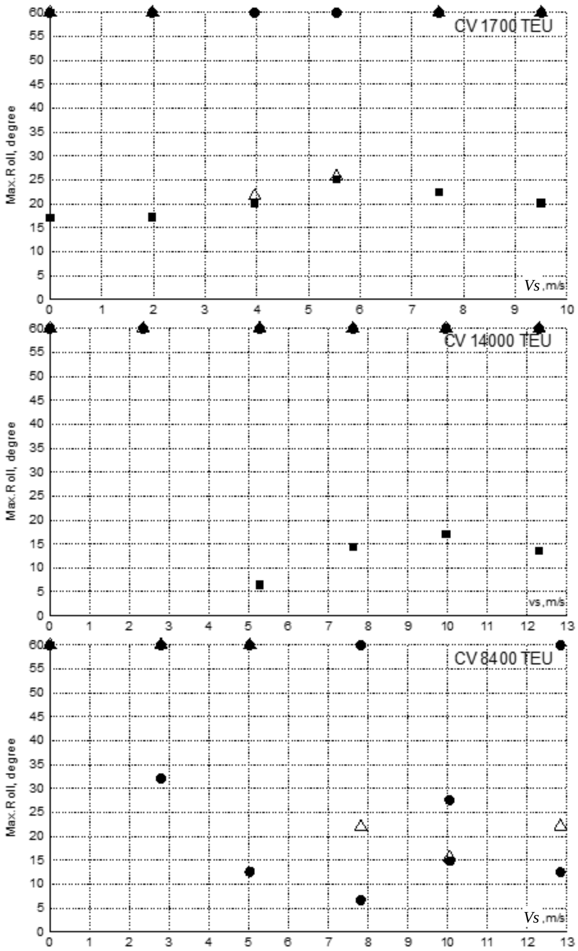

Figure 4.5.6: The mean 3h maximum roll amplitude due to parametric roll in following waves in sea states with f_s=10^{-5} (m·s)$^{-1}$ vs. forward speed. each plot corresponds to one ship; different symbols correspond to different loading conditions.

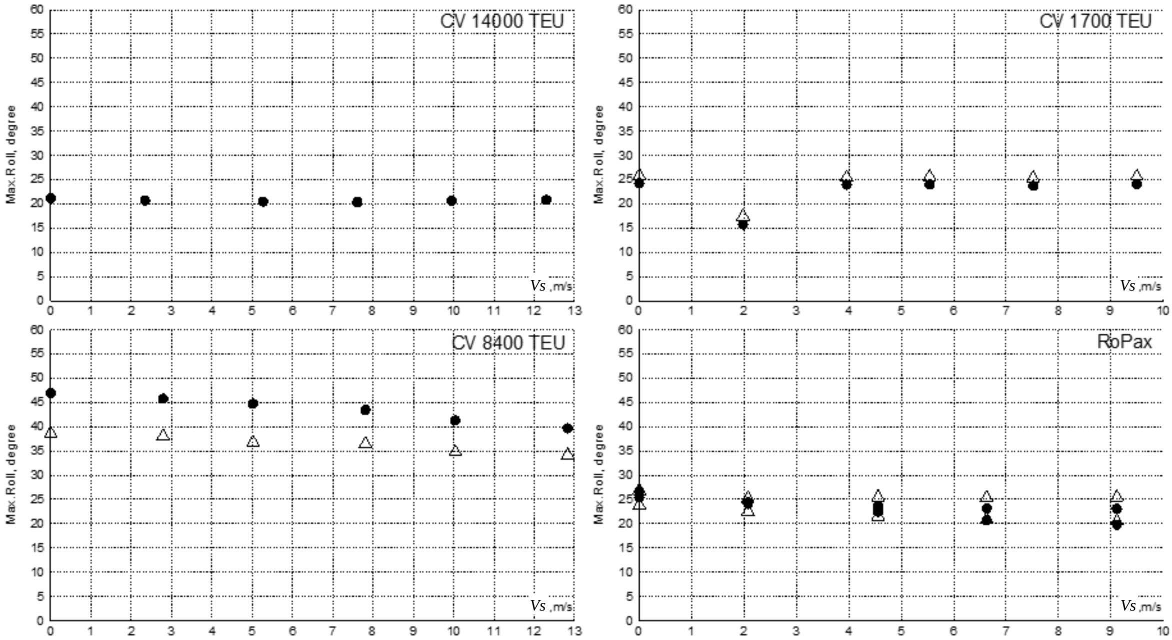

Figure 4.5.7:The mean 3h maximum roll amplitude due to synchronous roll in beam waves in sea states with f_s=10^{-5} (m·s)$^{-1}$ vs. forward speed; each plot corresponds to one ship; different symbols correspond to different loading conditions

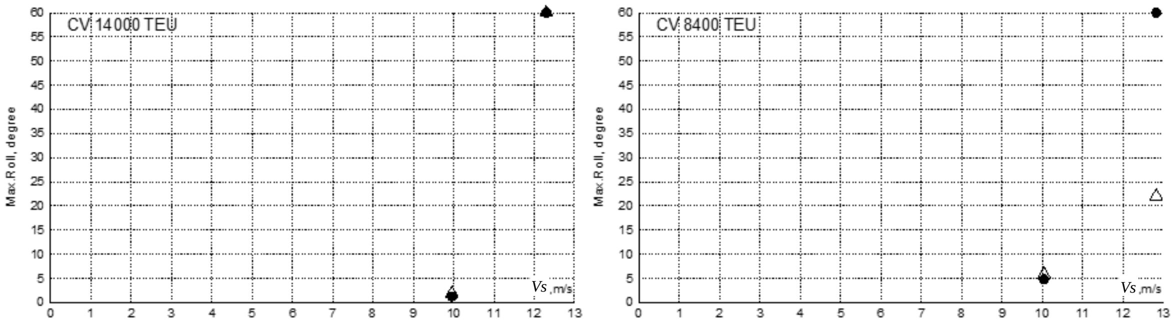

Figure 4.5.8: The mean 3h maximum roll amplitude due to pure loss of stability in following waves in sea states with f_s=10^{-5} (m·s)$^{-1}$ vs. forward speed. each plot corresponds to one ship; different symbols correspond to different loading conditions.

4.6 Definition of standard and thresholds

4.6.1 To distinguish acceptable from not acceptable loading conditions, an acceptance standard should be defined for the average long-term stability failure rate W, as well as consistent acceptance thresholds for the criteria used in the simplified assessment procedures (i.e. for the mean stability failure rate r and the mean 3h maximum roll amplitude φ_{3h} in design situations) for all stability failure modes.

4.6.2 Consider the relationship between the standard for the "long-term" average stability failure rate in the full probabilistic direct stability assessment and the average stability failure rate in the real operation (i.e. the actual safety level). This relationship is uncertain, whereas the average stability failure rate in the full probabilistic direct stability assessment may differ from the average failure rate in real operation by a few orders of magnitude due to several factors:

.1 the full probabilistic direct stability assessment is conducted in a rather severe North Atlantic wave environment while the mean safety level relates to the worldwide operation;

.2 ship routeing and heavy-weather avoidance are not considered;

.3 the assessment is performed separately for each loading condition, thus the worst loading condition (which may never occur in practice) has a dominating effect on the results; and

.4 unsafe forward speeds and courses, avoided in reality in heavy weather, produce dominating (by few orders of magnitude) contributions to the long-term stability failure rate. For example, principal parametric roll resonance in following waves, especially at low speeds, provides dominating contributions to the failure rate for loading conditions with a low *GM*, figure 4.6.1, whereas in reality, such situations are avoided (because of the possibility of stern slamming, low freeboard) or impossible (because of an inability to maintain course).

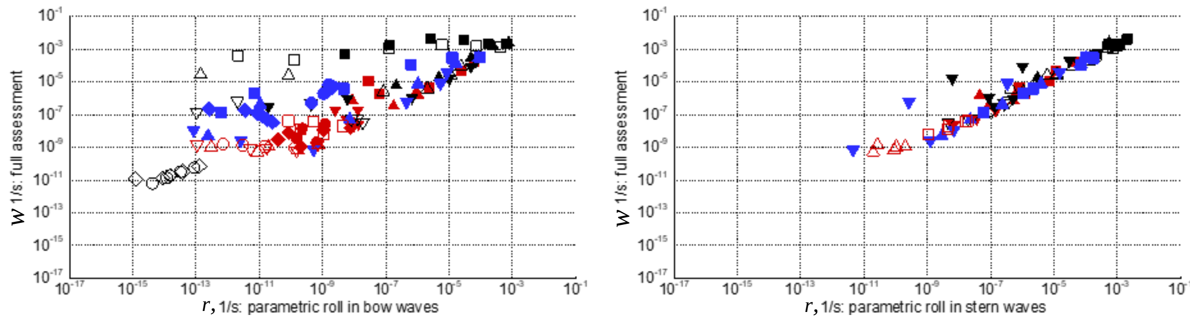

Figure 4.6.1: Contributions to the average long-term stability failure rate *W* (1/s, *y*-axis) from principal parametric roll resonance in bow (left) and stern (right) waves (1/s, *x*-axis); symbol types and colours differentiate ships and loading conditions from table 4.1.1

4.6.3 To estimate the standard for the long-term average stability failure rate for the full probabilistic direct stability assessment, data from FSA studies for container vessels (MSC 83/INF.8), LNG carriers (MSC 83/INF.3), crude oil tankers (MEPC 58/INF.2), cruise ships (MSC 85/INF.2), RoPax vessels (MSC 85/INF.3) and general cargo vessels (MSC 88/INF.8) can be considered. According to the aforementioned FSA studies, losses due to foundering are reported for container ships and general cargo vessels ($9.78{\cdot}10^{-4}$ and $5.10{\cdot}10^{-3}$ losses per ship per year, respectively). Since the second generation intact stability criteria address not only total losses but also other stability failures, another relevant figure is the average frequency of accidents due to heavy weather, which is reported for container ships and LNG carriers as $2.64{\cdot}10^{-3}$ and $3.20{\cdot}10^{-3}$ accidents per ship per year, respectively. The lower of these figures is used here to define the standard, which is $2.64{\cdot}10^{-3}$ stability failures per ship per year.

4.6.4 The value $2.64{\cdot}10^{-3}$ stability failures per ship per year corresponds to the mean time to failure of 378.8 years for one ship. To relate this number to direct stability assessment results, a number of considerations should be taken into account:

.1 the direct stability assessment is performed for each loading condition, even for those in which the ship may rarely sail in reality; to consider this, an assumed factor of 0.1 is applied to the time to stability failure obtained above;

.2 to account for time in port and maintenance, time in port is assumed to be 20% of the total design life; therefore, a factor of 0.8 is applied;

.3 the direct stability assessment is performed for the severe North Atlantic wave environment, whereas the results of the FSAs relate to worldwide service; to consider a reduced time in such a severe wave environment in reality, an assumed reduction factor of 0.2 is applied;

.4 the direct stability assessment assumes that a ship randomly encounters sea states according to their occurrence frequencies in the wave scatter table; however, in reality, ships use weather routeing and heavy-weather avoidance; to account for this, a reduction factor of 0.2 is applied; and

.5 when these factors are applied to the time to stability failure of 378.8 years, a stability failure per ship of 1.2 years is obtained, which means that the standard for the average long-term stability failure rate (that should be ensured by a direct stability assessment and operational measures) $2.6 \cdot 10^{-8}$ 1/s.

4.6.5 A similar study on defining standards for the vertical bending moment[21] shows that setting a standard using results of a numerical analysis as once per the design life in the North Atlantic wave environment leads to too conservative results compared to the existing, sufficiently safe, fleet and rules of classification societies. To harmonize the results of a direct assessment with classification rules, a "routeing factor" of 0.85 was proposed, which should be applied as a multiplication factor to the wave heights. For comparison, the present results of the full probabilistic direct stability assessment were re-evaluated with 0.85-scaled wave heights. This leads to the standard for the average long-term stability failure rate of $1.4 \cdot 10^{-8}$ 1/s, which is close to the estimate given in paragraph 4.6.4.5.

4.6.6 To define the threshold for the short-term stability failure rate r in design situations based on this standard, a number of considerations should be noted:

.1 the results of a direct stability assessment with respect to the dead ship condition stability failure mode in design situations were compared with the results of an assessment of the Weather Criterion of the 2008 Intact Stability Code for reference; this led to the upper and lower estimates for the design-situation threshold for r shown in table 4.6.1;

.2 the threshold for the stability failure rate in design situations should not be too high (otherwise it will be difficult to minimize the influence of initial conditions) or too low (otherwise testing or simulation time will be too large); thus, an appropriate threshold should be between about 10^{-4} 1/s and 10^{-3} 1/s; and

.3 according to paragraph 3.7.24, parametric roll increasingly deviates from the Poisson process assumption for a failure rate exceeding about one failure in two hours, i.e. $1.4 \cdot 10^{-4}$ 1/s.

21 Derbanne, Q., Storhaug, G., Shigunov, V., Xie, G., and Zheng, G. *Rule formulation of vertical hull girder wave loads based on direct computation*, Proc. PRADS 2016, 4-8 September, Copenhagen, 2016.

Table 4.6.1: Estimates of the lower and upper bounds for the design-situation threshold *r* from a comparison with the 2008 IS Code Weather Criterion

f_s, $(m{\cdot}s)^{-1}$	10^{-2}	10^{-3}	10^{-4}	10^{-5}	10^{-6}	10^{-7}
lower	$1.8{\cdot}10^{-34}$	$1.0{\cdot}10^{-15}$	$2.8{\cdot}10^{-10}$	$7.5{\cdot}10^{-8}$	$1.8{\cdot}10^{-6}$	$1.4{\cdot}10^{-5}$
upper	$1.7{\cdot}10^{-9}$	$2.8{\cdot}10^{-5}$	$4.7{\cdot}10^{-4}$	$1.7{\cdot}10^{-3}$	$3.5{\cdot}10^{-3}$	$5.6{\cdot}10^{-3}$

4.6.7 Figure 4.6.2 plots the dependencies of the average long-term stability failure rate W on the short-term stability failure rate in design situations r for parametric roll and synchronous roll and pure loss of stability from figure 4.4.3 to 4.4.6 for $fs = 10^{-2}$ to 10^{-7} $(m{\cdot}s)^{-1}$ together with the bounds for the W-standard and the r-threshold according to the considerations given in paragraph 4.6.4. The bounds for the W-standard are transferred into the bounds for the r-threshold and the other way around using these dependencies. In figure 4.6.2, colours of the bounding rectangles correspond to the FSA studies (red), the comparison with the Weather Criterion (green) and the considerations given in paragraph 4.6.6.2 (blue). The overlapping areas, indicated with arrows in figure 4.6.2 and shown in increased resolution in figure 4.6.3, indicate the possibility of a non-contradicting combination of these bounds if the direct stability assessment in design situations is performed in design sea states with a probability density $fs = 10^{-7}$ to 10^{-5} $(m{\cdot}s)^{-1}$. For greater or lower values of f_s, the areas corresponding to various estimates do not overlap. However, for design sea states with the probability density of 10^{-4} $(m{\cdot}s)^{-1}$, the only limitation is a long simulation time, which is not a crucial problem for some numerical methods.

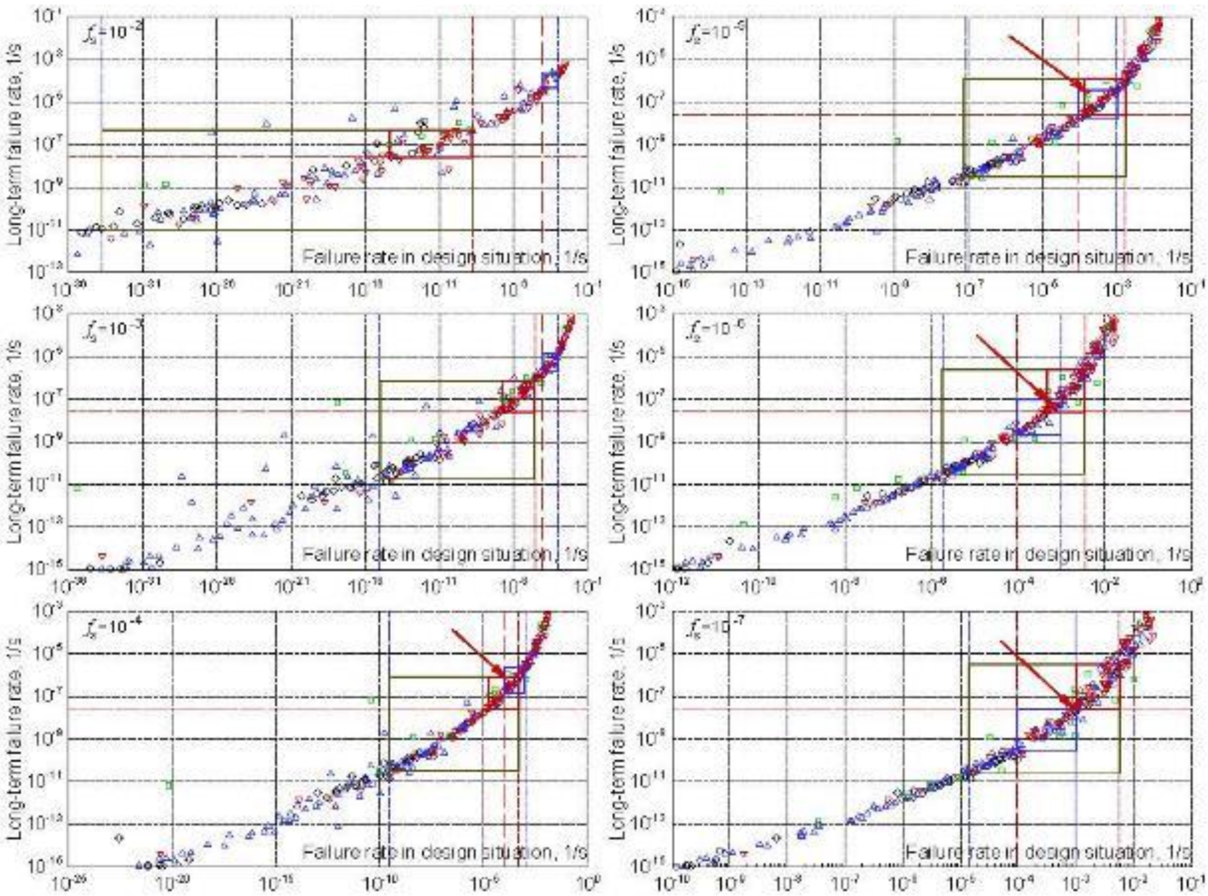

Figure 4.6.2: Combined dependencies of the long-term average stability failure rate W on the short-term design-situation stability failure rate r for all stability failure modes from figure 4.4.3 to 4.4.6 for fs (from top left to bottom right) of 10^{-2} to 10^{-7} $(m{\cdot}s)^{-1}$ together with bounds according to paragraph 4.4.6; the arrows indicate overlapping areas where a non-contradicting combination of bounds is possible

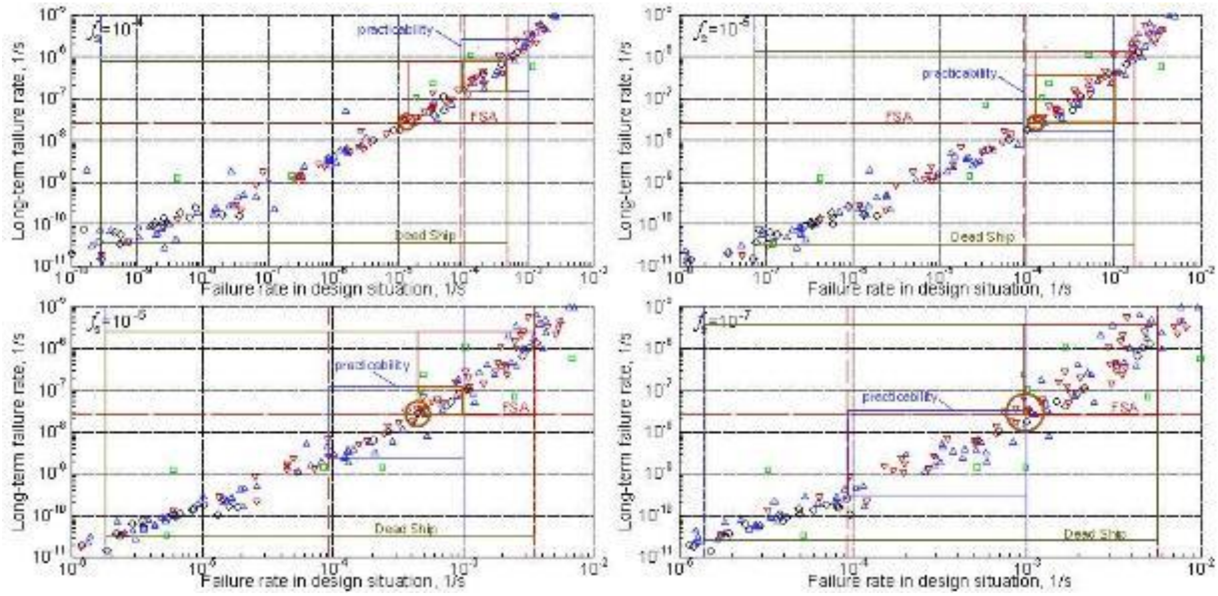

Figure 4.6.3: The definition of the standard and the threshold (increased resolution plots from figure 4.6.2); the thick line rectangle indicates overlapping area

4.6.8 According to the analysis results shown in figure 4.6.3, the value of $2.6 \cdot 10^{-8}$ 1/s seems suitable as a conservative estimate for the standard for the long-term average stability failure rate W in the full probabilistic direct stability assessment.

4.6.9 For the threshold for the mean short-term stability failure rate r in design situations, the following values seem suitable: one stability failure in 20h in design sea states with $f_s = 10^{-4}$ $(m \cdot s)^{-1}$; one stability failure in two hours in design sea states with $fs = 10^{-5}$ $(m \cdot s)^{-1}$; and one stability failure in 40 minutes in design sea states with $fs = 10^{-6}$ $(m \cdot s)^{-1}$. However, one stability failure in 40 minutes contradicts the requirement given in paragraph 4.6.6.3. Therefore, it seems suitable to use as design sea states those with the probability density of occurrence between $fs = 10^{-4}$ $(m \cdot s)^{-1}$ (with the short-term threshold for the mean stability failure rate r equal to one in 20h) and 10^{-5} $(m \cdot s)^{-1}$ (with the threshold of one stability failure in two hours). The latter seems more practicable since it means that there is less simulation time required for the direct stability assessment.

4.6.10 Table 4.6.2 shows the significant wave height vs. the mean zero-crossing wave period at $f_S = 10^{-5}$ for unrestricted service, i.e. wave scatter table from IACS Recommendation No.34 (Corr.1 Nov. 2001) (also presented in the Interim Guidelines, table 2.7.2.1.2).

Table 4.6.2: Significant wave height depending on the mean zero-crossing wave period for sea states with an occurrence probability density of 10-5 (m·s)-1 according to IACS Recommendation No.34 (Corr.1 Nov. 2001)

T_z, s	4.5	5.5	6.5	7.5	8.5	9.5	10.5	11.5	12.5	13.5	14.5	15.5	16.5
H_s, m	2.8	5.5	8.2	10.6	12.5	13.8	14.6	15.1	15.1	14.8	14.1	12.9	10.9

4.6.11 To define the threshold for the mean three-hour maximum roll amplitude φ_{3h} for the deterministic direct stability assessment in design situations, a different approach was used:

.1 the threshold for φ_{3h} was set to one half of the heel angle in the definition of the stability failure to avoid capsizing in model tests or numerical simulations;

.2 the maximum value of the average long-term stability failure rate W was found over all ships, loading conditions and forward speeds satisfying the chosen φ_{3h}-threshold in design situations; and

.3 in this way, the maximum value of the average long-term stability failure rate W becomes a function of the probability density f_s defining the design sea states in which the deterministic direct stability assessment is performed.

4.6.12 Figure 4.6.4 displays a plot of the the resulting average long-term stability failure rate W (y-axis) as a function of the probability density fs defining design sea states (x-axis). To satisfy the selected standard for the average long-term stability failure rate of $2.6{\cdot}10^{-8}$ 1/s (shown as a horizontal dashed line), the design sea states with the probability density $fs = 7{\cdot}10^{-5}$ $(m{\cdot}s)^{-1}$ (circle) should be used. Table 4.6.3 shows the significant wave height vs. the mean zero-crossing wave period for $f_s = 7{\cdot}10^{-5}$ $(m{\cdot}s)^{-1}$ for unrestricted service (IACS Recommendation No.34 (Corr.1 Nov. 2001) wave scatter table and the Interim Guidelines, table 2.7.2.1.2).

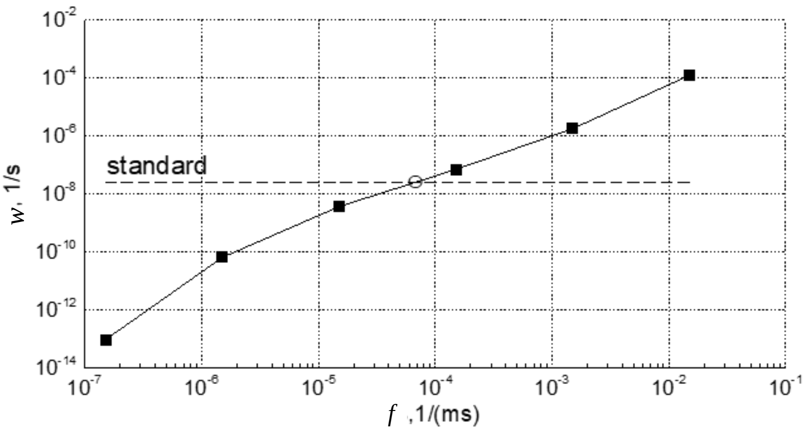

Figure 4.6.4 Definition of design sea states for a deterministic assessment

Table 4.6.3: The significant wave height vs. the mean zero-crossing wave period for a sea state probability density of $7{\cdot}10^{-5}$ $(m{\cdot}s)^{-1}$ in the North Atlantic wave environment

T_z,s	4.5	5.5	6.5	7.5	8.5	9.5	10.5	11.5	12.5	13.5	14.5	15.5
H_s,m	2.0	4.4	6.9	9.1	10.9	12.1	12.8	13.1	13.0	12.5	11.3	9.0

4.6.13 The proposed standard for the average long-term stability failure rate W and the thresholds for the mean short-term failure rate r and the mean three-hour maximum roll amplitude φ_{3h} in design situations can be further adjusted using a full probabilistic direct stability assessment or a direct stability assessment in design situations for ships that have experienced accidents in the loading conditions during those accidents and applying figure 4.6.2 or 4.6.4 to scale the long-term standard into the short-term threshold or vice versa.

4.7 Example procedures for a probabilistic direct stability assessment in design situations

4.7.1 A probabilistic direct stability assessment in design situations does not require statistical extrapolation, therefore this example procedure uses direct counting. Since an assessment in design situations (as well as probabilistic operational guidance) uses a short-term acceptance standard, a more efficient *acceptance check* (i.e. check whether the upper boundary of the 95%-confidence interval of the failure rate does not exceed a standard) can be used with the direct counting procedure in paragraph 3.5.4.4.1 of the Interim Guidelines: namely, a decision on acceptance can be made during a running simulation, see an example procedure in paragraph 4.7.10. The *unacceptance check* is the same as that given in the general direct counting procedure: the lower boundary of the 95%-confidence interval of the failure rate is updated after each encountered failure, and a loading condition is considered as unacceptable once this boundary exceeds the standard in at least one design situation.

4.7.2 An example procedure using the direct counting approach in section 3.3 of this appendix is used for the estimation of the failure rate and its confidence interval. The procedure uses numerical simulations or model tests in multiple independent realizations of the same sea state, which is assumed to be modelled as a sum of harmonic components, eq. (3.6.1). To generate such realizations, the phases ε_i are randomly selected in the interval [0, 2π), whereas the frequencies ω_i and directions μ_i can be either assumed constant in all simulations or randomly selected (within ranges $\Delta\omega_i$ and $\Delta\mu_i$, respectively) for each simulation. The amplitudes a_i can be assumed to be constant or randomly varied. To generate random values, a pseudo-random number generator can be used.

4.7.3 To ensure that stability failures in numerical simulations or model tests satisfy the assumptions of a Poisson process, the procedure neutralizes self-repetition effects (by limiting duration of each simulation), transient hydrodynamic effects at the beginning of simulations (by switching off the counter of stability failures and simulation timer during initial transients) and autocorrelation of large roll motions (by stopping a simulation after the first encountered stability failure). Apart from a limited duration and stopping after the first stability failure, duration of each simulation is arbitrary.

4.7.4 For the *acceptance check*, the upper boundary r_U of the 95%-confidence interval of the failure rate should not exceed a standard λ; combined with eq. (3.3.9) with α = 0.05 and definition $\beta_1(N) = 0.5\chi^2_{1-0.05/2,2N}/N$, this provides the following condition:

$$\hat{T} > \hat{T}_{\mathrm{A}} \equiv \beta_1(N)/\lambda \qquad (4.7.1)$$

4.7.5 Eq. (4.7.1) is not convenient when the stability failure rate is low since it requires the encounter of at least one stability failure while the time until the first failure may be too long for acceptable loading conditions (and even for not acceptable ones away from resonance). Obviously, continuing simulations in such cases is senseless since the absence of a failure during a long time is a sign of an acceptable safety level. To address such cases, eq. (4.7.1) can be used assuming (conservatively) that N = 1 and thus $\hat{T} = t$; this leads to the conclusion that a simulation can be stopped (with the *acceptance* decision) when the simulation time without failure achieves

$$t \geq t_A \equiv \beta_1(1)/\lambda \qquad (4.7.2)$$

4.7.6 To extend this idea on the second and further stability failures, introduce in eq. (4.7.1) the definition eq. (3.3.1), rewritten as $\hat{T} = \hat{T}_{N-1} \cdot (1 - 1/N) + T_N/N$, where $\hat{T}_{N-1}$ is the sample mean time to failure defined from the already encountered $N - 1$ stability failures and assume, conservatively, that $T_N = t$. The result is that a simulation can be stopped with the *acceptance* decision in the considered design situation before the N-th stability failure is encountered when the accumulated simulation time without failure after the $N - 1$-th stability failure achieves

$$t \geq t_{\mathrm{A}} \equiv \beta_1(N) \cdot N/\lambda - \hat{T}_{N-1} \cdot (N-1) \qquad (4.7.3)$$

4.7.7 When $N = 1$, eq. (4.7.3) automatically reduces to $t \geq t_A \equiv \beta_1(1)/\lambda$, i.e. eq. (4.7.2). Therefore, only eq. (4.7.3) is required as an acceptance check for the first and further simulations.

4.7.8 To save simulation time, it is possible to define as *unacceptance,* the check of the requirement that the lower boundary r_{L} of the 95%-confidence interval of the failure rate exceeds the standard λ, which, combined with eq. (3.3.9) with α=0.05 and definition $\beta_2(N) = 0.5\chi^2_{0.05/2,2N}/N$, leads to the following condition:

$$\hat{T} < \hat{T}_{\mathrm{F}} \equiv \beta_2(N)/\lambda \quad (4.7.4)$$

4.7.9 To illustrate the progressive uncertainty reduction with an increasing number of encountered failures, figure 4.7.1 shows β_1 and β_2 vs. N. A calculation of the function $\chi^2_{p,f}$, required to define β_1 and β_2, is described in paragraph 3.3.6 of this appendix.

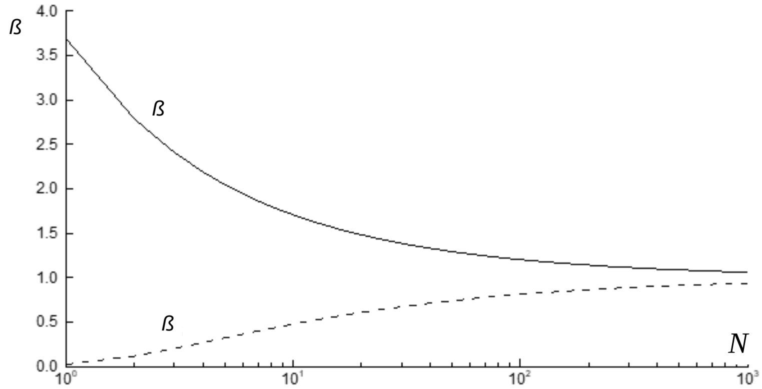

Figure 4.7.1 Functions $\beta_1(N)$ and $\beta_2(N)$

4.7.10 The described example procedure for probabilistic assessment in design situations can be summarized as follows:

.1 numerical simulations or model tests are carried out in multiple independent realizations of the same sea state by a random variation of phases (and, possibly, frequencies, directions and amplitudes) of harmonic waves that discretize the wave energy spectrum. Simulations or tests can be carried out for an arbitrary duration until the maximum duration or first stability failure; the counter of stability failures and the simulation timer are switched off during the initial transients;

.2 after each simulation or test, the total number of failures N is increased by ΔN (1 if ended with a stability failure and 0 otherwise), the total simulation time t_t is increased by the duration of simulation Δt and the sample mean time to failure is updated as $\hat{T} = t_t/N$;

.3 if a simulation achieves time $t_{\mathrm{A}} = \beta_1(N) \cdot N/\lambda - \hat{T}_{N-1} \cdot (N-1)$ without a stability failure with $\beta_1(N) = 0.5\chi^2_{1-0.05/2,2N}/N$, the loading condition can be considered acceptable in the considered design situation without further simulations; and

.4 if the sample mean time to failure after a stability failure satisfies the condition $\hat{T} < \hat{T}_{\mathrm{F}}$, where $\hat{T}_{\mathrm{F}} = \beta_2(N)/\lambda$ and $\beta_2(N) = 0.5\chi^2_{0.05/2,2N}/N$, the loading condition can be considered as not acceptable without further simulations.

4.8 Application examples of probabilistic assessment in design situations

4.8.1 *Parametric roll*

4.8.1.1 The example uses a numerical simulation of ship motions in multiple independent realizations of the sea state and a direct counting of stability failures. The sea state is modelled as a sum of harmonic components that discretize the Bretschneider wave energy spectrum and the cos^2-wave energy angular spreading function into 19 directional ranges $\Delta\mu_i$ and 10^3

frequency ranges $\Delta\omega_i$ per direction. For each realization, the wave energy spectrum was discretized into harmonic components with equal amplitudes, the phases of components were randomly selected in the interval [0, 2π), and their frequencies and directions were randomly selected within the ranges $\Delta\omega_i$ and $\Delta\mu_i$, respectively.

4.8.1.2 To ensure that the stability failures in numerical simulations satisfy Poisson process assumptions, self-repetition effects were avoided by limiting the simulation time in each seaway realization to one hour, the transient hydrodynamic effects at the beginning of each simulation were eliminated by switching off the counter of stability failures and simulation timer during the initial 50 roll periods, and the autocorrelation of large roll motions was avoided by stopping a simulation after the first encountered stability failure.

4.8.1.3 Assessment was performed for a 1700 TEU container ship in loading conditions with GM = 1.7 m, 1.8 m, …, 2.2 m for the parametric roll stability failure mode, using as the criterion the maximum (over all required design situations) of the upper boundary of the 95%-confidence interval of the short-term stability failure rate. For acceptance, this criterion should not exceed the threshold equal to one stability failure in two hours in design sea states with a probability density of 10^{-5} $(\text{m}\cdot\text{s})^{-1}$. The design situations correspond to zero forward speed in head and following mean wave directions. The mean zero-upcrossing wave periods from 4.5 s to 16.5 s with an increment of 1.0 s were used. For each wave period, the significant wave height was selected according to table 4.6.2.

4.8.1.4 Each simulation was run for one hour but stopped after the first stability failure or when a sufficient simulation time for acceptance $t_\text{A} = \beta_1(N) \cdot N/\lambda - \hat{T}_{N-1} \cdot (N-1)$ was achieved with $\beta_1(N) = 0.5\chi^2_{1-0.05/2,2N}/N$. If the sufficient simulation time for acceptance t_A was achieved during a simulation, no further simulations in the considered design situation were conducted and the loading condition was considered as *acceptable* in the considered design situation. Otherwise, after the simulation, the number of failures ΔN (1 or 0) in the simulation and the duration of the simulation Δt (equal to the time to failure if the realization ended with a stability failure or one hour if a stability failure was not encountered) were defined and the total number of failures N and the total simulation time t_t were increased by ΔN and Δt, respectively. The *unacceptance* condition was checked: if $\hat{T} < \hat{T}_\text{F}$, where $\hat{T}_\text{F} = \beta_2(N)/\lambda$, $\beta_2(N) = 0.5\chi^2_{0.05/2,2N}/N$ and $\hat{T} = t_\text{t}/N$ is the sample mean time to failure, no further simulations were conducted for the considered loading condition, which was judged as *unacceptable*.

4.8.1.5 Tables 4.8.1 to 4.8.4 show results for loading conditions with GM = 1.8 m (not acceptable) and 1.9 m (acceptable) together with the required simulation time t_s until each stability failure, cumulative simulation time over all wave periods t_c until the decision. For brevity, the results are shown not after each simulation, but only after stability failures. In these tables, "A" and "F" denote *acceptance* and *not acceptance*, respectively.

Table 4.8.1: Assessment results for GM = 1.8 m in head waves

T_z,s	N	T_i,s	$\hat{T}$,s	t_A,s	A	$\hat{T}_F$,s	F	t_s,s	t_c,s	t_c,hours
7.5	1	9.57e+2	9.57e+2	2.66e+4	-	1.82e+2	-	9.57e+2	9.57e+2	0.3
	2	1.01e+4	5.54e+3	3.92e+4	-	8.72e+2	-	1.01e+4	1.11e+4	3.1
	3	5.02e+2	3.86e+3	4.09e+4	-	1.48e+3	-	5.02e+2	1.16e+4	3.2
	4	7.49e+2	3.08e+3	5.15e+4	-	1.96e+3	-	7.49e+2	1.23e+4	3.4
	5	4.94e+3	3.46e+3	6.14e+4	-	2.34e+3	-	4.94e+3	1.73e+4	4.8
	6	9.50e+2	3.04e+3	6.67e+4	-	2.64e+3	-	9.50e+2	1.82e+4	5.1
	7	1.03e+4	4.08e+3	7.58e+4	-	2.89e+3	-	1.03e+4	2.85e+4	7.9
	8	4.02e+2	3.62e+3	7.53e+4	-	3.11e+3	-	4.02e+2	2.89e+4	8.0
	9	1.28e+3	3.36e+3	8.46e+4	-	3.29e+3	-	1.28e+3	3.02e+4	8.4
	10	7.48e+3	3.77e+3	9.28e+4	-	3.45e+3	-	7.48e+3	3.77e+4	10.5
	11	1.29e+3	3.54e+3	9.47e+4	-	3.59e+3	*F*	1.29e+3	3.90e+4	10.8

Table 4.8.2: Assessment results for *GM* = 1.8 m in following waves

T_z,s	N	T_i,s	$\hat{T}$,s	t_A,s	A	$\hat{T}_F$,s	F	t_s,s	t_c,s	t_c,hours
7.5	1	2.46e+3	2.46e+3	2.66e+4	-	1.82e+2	-	2.46e+3	2.46e+3	0.7
	2	2.65e+3	2.56e+3	3.77e+4	-	8.72e+2	-	2.65e+3	5.11e+3	1.4
	3	3.58e+3	2.90e+3	4.69e+4	-	1.48e+3	-	3.58e+3	8.70e+3	2.4
	4	7.58e+2	2.36e+3	5.44e+4	-	1.96e+3	-	7.58e+2	9.45e+3	2.6
	5	1.44e+3	2.18e+3	6.43e+4	-	2.34e+3	*F*	1.44e+3	1.09e+4	3.0

Table 4.8.3: Assessment results for *GM* = 1.9 m in head waves

T_z,s	N	T_i,s	$\hat{T}$,s	t_A,s	A	$\hat{T}_F$,s	F	t_s,s	t_c,s	t_c,hours
7.5	1	2.11e+2	2.11e+2	2.66e+4	-	1.82e+2	-	2.11e+2	2.11e+2	0.1
	2	3.15e+4	1.59e+4	3.99e+4	-	8.72e+2	-	3.15e+4	3.17e+4	8.8
	3	4.31e+4	2.49e+4	2.03e+4	*A*	1.48e+3	-	2.03e+4	5.20e+4	14.4
8.5	1	4.76e+4	4.76e+4	2.66e+4	*A*	1.82e+2	-	2.66e+4	7.86e+4	21.8
9.5	1	3.01e+4	3.01e+4	2.66e+4	*A*	1.82e+2	-	2.66e+4	1.05e+5	29.2
10.5	1	2.45e+4	2.45e+4	2.66e+4	-	1.82e+2	-	2.45e+4	1.30e+5	36.0
	2	2.04e+4	2.25e+4	1.56e+4	*A*	8.72e+2	-	1.56e+4	1.45e+5	40.3
11.5	1	1.56e+4	1.56e+4	2.66e+4	-	1.82e+2	-	1.56e+4	1.61e+5	44.7
	2	3.49e+4	2.53e+4	2.45e+4	*A*	8.72e+2	-	2.45e+4	1.85e+5	51.5
12.5	1	1.57e+4	1.57e+4	2.66e+4	-	1.82e+2	-	1.57e+4	2.01e+5	55.9
	2	1.99e+4	1.78e+4	2.44e+4	-	8.72e+2	-	1.99e+4	2.21e+5	61.4
	3	6.82e+4	3.46e+4	1.64e+4	*A*	1.48e+3	-	1.64e+4	2.37e+5	65.9
13.5	1	6.05e+3	6.05e+3	2.66e+4	-	1.82e+2	-	6.05e+3	2.43e+5	67.6
	2	8.33e+4	4.47e+4	3.41e+4	*A*	8.72e+2	-	3.41e+4	2.78e+5	77.1

Table 4.8.4: Assessment results for *GM* = 1.9 m in following waves

T_z,s	N	T_i,s	$\hat{T}$,s	t_A,s	A	$\hat{T}_F$,s	F	t_s,s	t_c,s	t_c,hours
7.5	1	2.39e+3	2.39e+3	2.66e+4	-	1.82e+2	-	2.39e+3	2.39e+3	0.7
	2	1.57e+5	7.96e+4	3.77e+4	*A*	8.72e+2	-	3.77e+4	4.01e+4	11.1
8.5	1	5.15e+3	5.15e+3	2.66e+4	-	1.82e+2	-	5.15e+3	4.53e+4	12.6
	2	1.08e+3	3.11e+3	3.50e+4	-	8.72e+2	-	1.08e+3	4.63e+4	12.9
	3	2.78e+4	1.13e+4	4.58e+4	-	1.48e+3	-	2.78e+4	7.41e+4	20.6
	4	6.56e+3	1.01e+4	2.91e+4	-	1.96e+3	-	6.56e+3	8.07e+4	22.4
	5	8.82e+4	2.58e+4	3.32e+4	*A*	2.34e+3	-	3.32e+4	1.14e+5	31.6
9.5	1	1.89e+4	1.89e+4	2.66e+4	-	1.82e+2	-	1.89e+4	1.33e+5	36.9
	2	1.09e+3	9.98e+3	2.12e+4	-	8.72e+2	-	1.09e+3	1.34e+5	37.2
	3	2.78e+3	7.58e+3	3.21e+4	-	1.48e+3	-	2.78e+3	1.37e+5	37.9
	4	1.16e+4	8.59e+3	4.04e+4	-	1.96e+3	-	1.16e+4	1.48e+5	41.2
	5	2.11e+4	1.11e+4	3.94e+4	-	2.34e+3	-	2.11e+4	1.69e+5	47.0
	6	8.16e+3	1.06e+4	2.85e+4	-	2.64e+3	-	8.16e+3	1.78e+5	49.3
	7	2.73e+3	9.49e+3	3.03e+4	-	2.89e+3	-	2.73e+3	1.80e+5	50.1
	8	1.48e+4	1.02e+4	3.74e+4	-	3.11e+3	-	1.48e+4	1.95e+5	54.2
	9	2.48e+4	1.18e+4	3.23e+4	-	3.29e+3	-	2.48e+4	2.20e+5	61.1
	10	8.19e+3	1.14e+4	1.70e+4	-	3.45e+3	-	8.19e+3	2.28e+5	63.4
	11	9.81e+3	1.13e+4	1.82e+4	-	3.59e+3	-	9.81e+3	2.38e+5	66.1
	12	5.55e+4	1.50e+4	1.77e+4	*A*	3.72e+3	-	1.77e+4	2.56e+5	71.0
10.5	1	6.09e+4	6.09e+4	2.66e+4	*A*	1.82e+2	-	2.66e+4	2.82e+5	78.4
11.5	1	2.91e+3	2.91e+3	2.66e+4	-	1.82e+2	-	2.91e+3	2.85e+5	79.2
	2	2.01e+4	1.15e+4	3.72e+4	-	8.72e+2	-	2.01e+4	3.05e+5	84.8
	3	1.97e+3	8.34e+3	2.90e+4	-	1.48e+3	-	1.97e+3	3.07e+5	85.3
	4	1.18e+4	9.21e+3	3.81e+4	-	1.96e+3	-	1.18e+4	3.19e+5	88.6
	5	2.78e+4	1.29e+4	3.69e+4	-	2.34e+3	-	2.78e+4	3.47e+5	96.3
	6	4.75e+3	1.16e+4	1.94e+4	-	2.64e+3	-	4.75e+3	3.51e+5	97.6

	7	4.78e+3	1.06e+4	2.47e+4	-	2.89e+3	-	4.78e+3	3.56e+5	99.0
	8	1.57e+3	9.46e+3	2.97e+4	-	3.11e+3	-	1.57e+3	3.58e+5	99.4
	9	2.96e+4	1.17e+4	3.78e+4	-	3.29e+3	-	2.96e+4	3.87e+5	107.6
	10	1.15e+4	1.17e+4	1.77e+4	-	3.45e+3	-	1.15e+4	3.99e+5	110.8
	11	1.07e+3	1.07e+4	1.57e+4	-	3.59e+3	-	1.07e+3	4.00e+5	111.1
	12	1.81e+4	1.13e+4	2.39e+4	-	3.72e+3	-	1.81e+4	4.18e+5	116.1
	13	2.14e+2	1.05e+4	1.50e+4	-	3.83e+3	-	2.14e+2	4.18e+5	116.2
	14	8.84e+3	1.04e+4	2.39e+4	-	3.94e+3	-	8.84e+3	4.27e+5	118.6
	15	1.97e+4	1.10e+4	2.41e+4	-	4.03e+3	-	1.97e+4	4.47e+5	124.1
	16	2.24e+4	1.17e+4	1.34e+4	*A*	4.12e+3	-	1.34e+4	4.60e+5	127.8

Table 4.8.4 (cont'd): Assessment results for *GM* = 1.9 m in following waves

T_z,s	N	T_i,s	$\hat{T}$,s	t_A,s	*A*	$\hat{T}_F$,s	F	t_s,s	t_c,s	t_c,hours
12.5	1	5.91e+3	5.91e+3	2.66e+4	-	1.82e+2	-	5.91e+3	4.66e+5	129.5
	2	1.42e+4	1.00e+4	3.42e+4	-	8.72e+2	-	1.42e+4	4.80e+5	133.4
	3	1.14e+4	1.05e+4	3.19e+4	-	1.48e+3	-	1.14e+4	4.92e+5	136.6
	4	4.34e+3	8.96e+3	3.16e+4	-	1.96e+3	-	4.34e+3	4.96e+5	137.8
	5	8.40e+3	8.85e+3	3.79e+4	-	2.34e+3	-	8.40e+3	5.05e+5	140.1
	6	4.77e+3	8.17e+3	3.98e+4	-	2.64e+3	-	4.77e+3	5.09e+5	141.5
	7	9.33e+3	8.34e+3	4.50e+4	-	2.89e+3	-	9.33e+3	5.19e+5	144.1
	8	4.89e+3	7.91e+3	4.55e+4	-	3.11e+3	-	4.89e+3	5.24e+5	145.4
	9	1.03e+4	8.17e+3	5.02e+4	-	3.29e+3	-	1.03e+4	5.34e+5	148.3
	10	1.85e+3	7.54e+3	4.95e+4	-	3.45e+3	-	1.85e+3	5.36e+5	148.8
	11	1.44e+4	8.16e+3	5.70e+4	-	3.59e+3	-	1.44e+4	5.50e+5	152.8
	12	9.41e+3	8.27e+3	5.19e+4	-	3.72e+3	-	9.41e+3	5.59e+5	155.4
	13	8.08e+2	7.69e+3	5.17e+4	-	3.83e+3	-	8.08e+2	5.60e+5	155.6
	14	2.15e+4	8.68e+3	6.00e+4	-	3.94e+3	-	2.15e+4	5.82e+5	161.6
	15	1.18e+4	8.89e+3	4.76e+4	-	4.03e+3	-	1.18e+4	5.94e+5	164.9
	16	3.54e+3	8.56e+3	4.48e+4	-	4.12e+3	-	3.54e+3	5.97e+5	165.9
	17	1.49e+4	8.93e+3	5.02e+4	-	4.19e+3	-	1.49e+4	6.12e+5	170.0
	18	2.81e+4	9.99e+3	4.42e+4	-	4.27e+3	-	2.81e+4	6.40e+5	177.8
	19	1.23e+4	1.01e+4	2.50e+4	-	4.33e+3	-	1.23e+4	6.52e+5	181.2
	20	1.68e+4	1.04e+4	2.15e+4	-	4.40e+3	-	1.68e+4	6.69e+5	185.9
	21	7.11e+2	9.98e+3	1.35e+4	-	4.46e+3	-	7.11e+2	6.70e+5	186.1
	22	6.27e+3	9.81e+3	2.15e+4	-	4.51e+3	-	6.27e+3	6.76e+5	187.8
	23	3.55e+4	1.09e+4	2.40e+4	*A*	4.56e+3	-	2.40e+4	7.00e+5	194.5
13.5	1	1.18e+3	1.18e+3	2.66e+4	-	1.82e+2	-	1.18e+3	7.01e+5	194.8
	2	7.55e+4	3.83e+4	3.89e+4	*A*	8.72e+2	-	3.89e+4	7.40e+5	205.6
14.5	1	1.34e+6	1.34e+6	2.66e+4	*A*	1.82e+2	-	2.66e+4	7.67e+5	213.0

4.8.1.6 *Unacceptance* requires much less simulation or testing time than *acceptance* since the exceedance of the threshold in only one situation is sufficient. If simulations in head waves are done first, *unacceptance* requires 87 minutes (if simulations in following waves are done first, only 2.7 minutes) for GM = 1.7 m. For GM = 1.8 m, *unacceptance* requires 10.8h or 3.0h simulation time, respectively. For *acceptance*, significantly more simulation or testing time is required since all design situations must be considered and the failure rate is lower: for GM = 1.9 m, *acceptance* requires 290.1 hours of simulation time (which consist of 77.1 hours in head waves and 213.0 hours in following); for GM = 2.0 m, 262.8 hours are required (69.3 hours in head waves and 193.5 hours in following).

4.8.1.7 The decision and the total required simulation or testing time to make this decision are summarized in table 4.8.5, separately for the assessment in head waves, in following waves and in both head and following waves. For this ship, much less simulation or testing time (bold figures) is required for the *unacceptable* loading conditions in following waves and for *acceptable* loading conditions in head waves. Since the assessment for *acceptable* loading conditions requires much more time than for *unacceptable* loading conditions, for this ship the assessment in head waves requires significantly less time than in following waves.

Table 4.8.5: The decision and the required simulation or testing time if the assessment is done in head, in following or both in head and following waves (results in the second column are shown as "result for head waves + result for following waves = result for both wave directions")

GM, m	Decision (A=acceptable, F=not acceptable)	Total simulation time, hours	Total simulation time, %
1.7	$F + F = F$	1.4 + **0.1** = 1.5	97 + 3 = 100
1.8	$F + F = F$	10.8 + **3.1** = 13.9	78 + 22 = 100
1.9	$A + A = A$	**77.1** + 213.0 = 290.1	27 + 73 = 100
2.0	$A + A = A$	**69.3** + 193.5 = 262.8	36 + 74 = 100
Total		**158.6** + 409.6 = 568.2	28 + 72 = 100

4.8.2 *Dead ship condition*

4.8.2.1 An example of the direct stability assessment in design situations for the dead ship condition is provided for a large cruise ship with the principal particulars and GZ curve shown in table 2.5.1 and figure 2.5.1, respectively.

4.8.2.2 The results of both the level 1 and level 2 vulnerability assessment show that this ship in the considered loading condition is not vulnerable to stability failure in the dead ship condition with a sufficient margin:

.1 Level 1: b/a = 2.171 > 1.0, φ_0 = 6.19º < 16º; and

.2 Level 2: C = 0.001057 < 0.06.

4.8.2.3 A coupled sway-heave-roll-pitch model was applied in changing wind and long-crested irregular beam waves at zero forward speed, which considered the pitch effect in the calculation of the restoring moment. Radiation and diffraction forces and moments were calculated with a strip theory, and the roll damping moment was estimated from a roll decay test. The mean wind velocity was provided using the formula in 2.2.3.2.2 of the Interim Guidelines. The validation of the numerical method without wind and dynamic pitch effects is described in section 2.6 of this appendix.

4.8.2.4 The probabilistic assessment in design situations was executed according to section 3.5.3.3 of the Interim Guidelines, using the direct counting procedure specified in paragraph 3.5.4. The sea states shown in table 3.5.3.3.5 of the Interim Guidelines were used.

4.8.2.5 Table 4.8.6 shows the results: “*A*” and “*F*” indicate acceptance and unacceptance, respectively. In this calculation, the verification of the failure mode was applied: only if the ratio of the instantaneous roll period to the instantaneous heave period or to the instantaneous period of wind velocity fluctuations was between 0.8 and 1.2, the stability failure was judged as a dead ship condition stability failure, which was addressed in this assessment example.

Table 4.8.6: Results of the probabilistic direct stability assessment in design situations for the dead ship condition stability failure mode for cruise ship

T_z (s)	4.5	5.5	6.5	7.5	8.5	9.5	10.5	11.5	12.5	13.5	14.5	15.5	16.5
H_s (m)	2.8	5.5	8.2	10.6	12.5	13.8	14.6	15.1	15.1	14.8	14.1	12.9	10.9
U_w (m/s)	12.0	18.9	24.6	29.2	32.6	34.8	36.2	37.0	37.0	36.5	35.3	33.3	29.8
Judgement	A	A	A	A	A	A	A	A	A	A	A	A	A

4.8.2.6 The results indicate that, if verification of failure modes is used, the considered loading condition is judged as acceptable with respect to the dead ship condition failure mode, which is consistent with the vulnerability assessment. If the verification of failure modes is not used, the effect of parametric roll in beam waves could appear.

5 Statistical extrapolation methods

5.1 Extrapolation of failure rate over wave height

5.1.1 *Background*

5.1.1.1 The extrapolation of the stability failure rate over the significant wave height[22] is based on the following suggestion: rare events happen, with some unknown probability, when a wave or a wave group consisting of a certain (unknown) number of waves is encountered, which exceeds a certain (also unknown) height. Denoting p, n and h as the unknown probability, number of waves and wave height, respectively, the rate of such events can be approximated as $r \sim p \cdot f(h, n : H_s)$, where f is the frequency of encountering rare wave groups with the required characteristics. Since such wave groups are approximately Rayleigh-distributed, $f \sim \exp(-2nh^2/H_s^2)$, and then:

$$\ln r = A + B/H_s^2 \tag{5.1.1}$$

5.1.1.2 In eq. (5.1.1), r is the stability failure rate and the parameters A and B do not depend on H_s but depend on the ship, the loading condition, forward speed and wave period and direction. Since $r = 1/T$, where T is the mean time to failure, the extrapolation can also be performed directly for the mean time to failure:

$$\ln T = A + B/H_s^2 \tag{5.1.2}$$

5.1.1.3 Instead of defining parameters A and B explicitly in terms of unknown quantities p, n and h, the idea of the extrapolation is to define these parameters empirically by direct counting at greater significant wave heights; note, however, that at greater significant wave heights, the events must remain sufficiently rare for this formulation to remain valid. It is also important to emphasize that this method does not imply any assumptions about the relation between exceedance rates of different reaction levels.

5.1.1.4 This method is especially useful for the full probabilistic direct stability assessment and probabilistic operational measures, which are based on the evaluation of the stability failure rate for all possible combinations of sailing conditions (v_s, μ) and sea states (H_s, T_z). First, direct counting is used to define the stability failure rate for such combinations (v_s, μ, H_s, T_z) when resources allow a direct counting calculation. Beyond direct counting, the extrapolation over the significant wave height, eq. (5.1.1), is applied to define the stability failure rate for the remaining combinations.

[22] Tonguć, E. and Söding, H. *Computing capsizing frequencies of ships in seaway*. Proc. 3rd Int. Conf. on Stability of Ships and Ocean Vehicles, 1986.

5.1.1.5 The coefficients A and B can be obtained by, for example, linear regression of $\ln r$, or $\ln T$, with respect to $1/H_s^2$, according to eq. (5.1.1) or (5.1.2), respectively. Data to be used for the linear regression are those at greater significant wave heights, as described in paragraph 5.1.1.3.

5.1.2 *Validation*

5.1.2.1 Document SDC 4/INF.8 shows that results obtained from direct counting can be used for an extrapolation, eq. (5.1.1), if $\ln T > 6$, i.e. $\ln r < -6$, to avoid possible concave portions of the dependency of $\ln T$ on $1/H_s^2$, i.e. a non-conservative extrapolation. In the Interim Guidelines, this condition is formulated as a boundary: the values of the stability failure rate obtained by direct counting can be used for an extrapolation, eq. (5.1.1), when they do not exceed 5% of the reciprocal natural roll period of the ship, i.e. $r < 0.05/T_r$ (or $T > 20T_r$).

5.1.2.2 In documents SDC 4/5/8 and SDC 4/INF.8, the extrapolation of the stability failure rate over the significant wave height in eq. (5.1.1) was validated by comparison with direct counting for synchronous roll in irregular short-crested beam waves (relevant for dead ship condition and excessive acceleration stability failure modes).

5.1.2.3 Here, eq. (5.1.1) is validated for parametric roll in bow and stern waves, synchronous roll in beam waves (associated with both the dead ship condition and excessive acceleration stability failure modes) and pure loss of stability in stern waves for five ships in six loading conditions each: in table 4.1.1, at six forward speeds; in table 4.2.1, in irregular short-crested waves at 14 mean zero-crossing wave periods and systematically varied significant wave heights. To quantify the accuracy of the extrapolation, several variants of extrapolation were tested by varying the number of extrapolation points. For each variant, a specific number of wave heights were selected ranging from 4 to 11 where the minimum wave height in each variant is one for which results can be obtained by direct counting and for which $\ln T > 6$. Excluding this minimum significant wave height, the remaining wave heights were used to perform the extrapolation using eq. (5.1.1) for each variant. The result of direct counting at the minimum significant wave height was used to find the deviation between the extrapolated and directly computed mean time to failure in each variant.

5.1.2.4 Figure 5.1.1 shows validation results as histograms of the ratio of the extrapolated to directly computed estimate of the mean time to failure: y-axis corresponds to the number (normed on 1) of cases in bins and x-axis shows the ratio of the extrapolated mean time to failure T_e to the directly estimated one T.

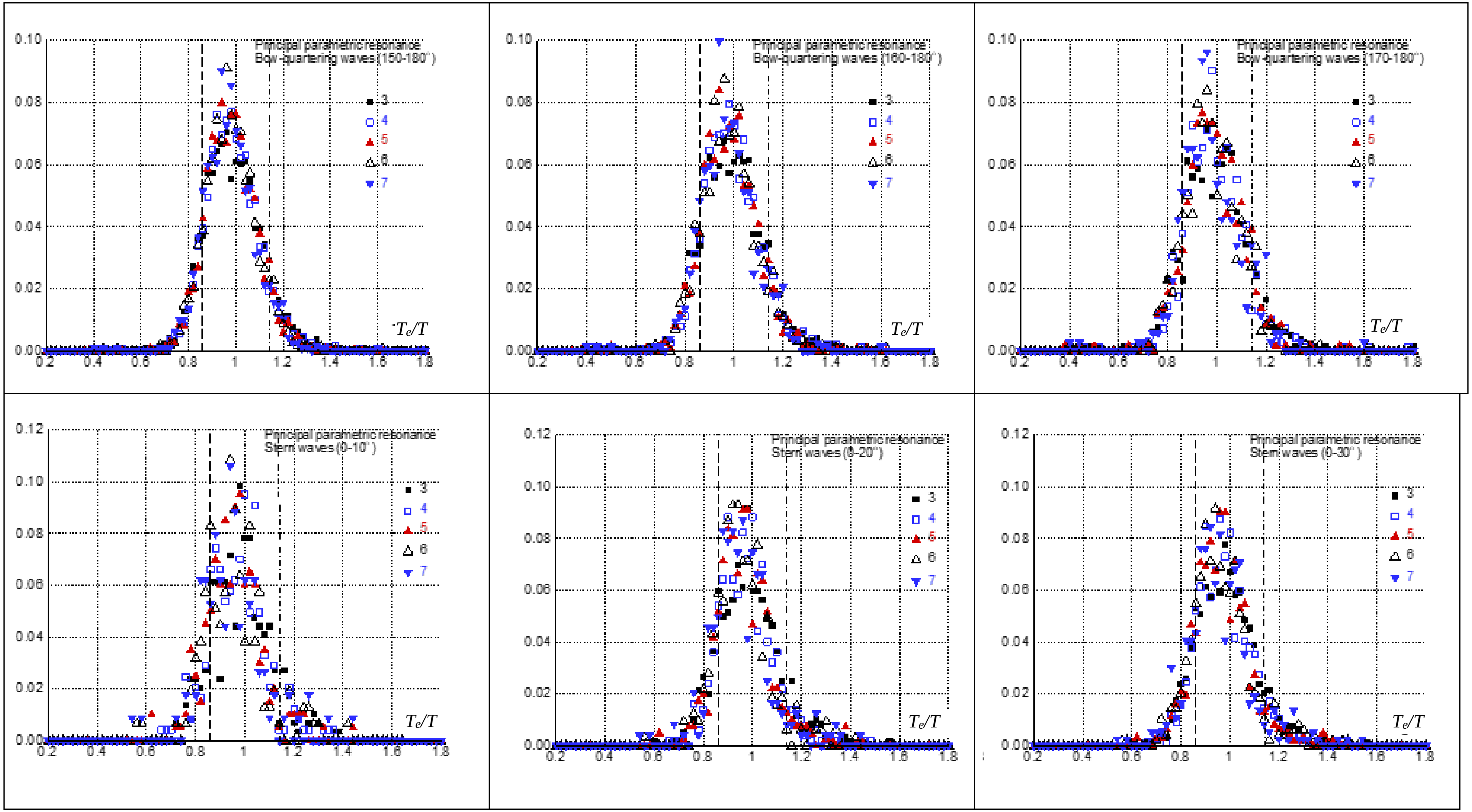
Principal parametric resonance
Bow-quartering waves (150-180°)
Principal parametric resonance
Bow-quartering waves (160-180°)
Principal parametric resonance
Bow-quartering waves (170-180°)
Principal parametric resonance
Stern waves (0-10°)
Principal parametric resonance
Stern waves (0-20°)
Principal parametric resonance
Stern waves (0-30°)
3
4
5
6
7
T_e/T

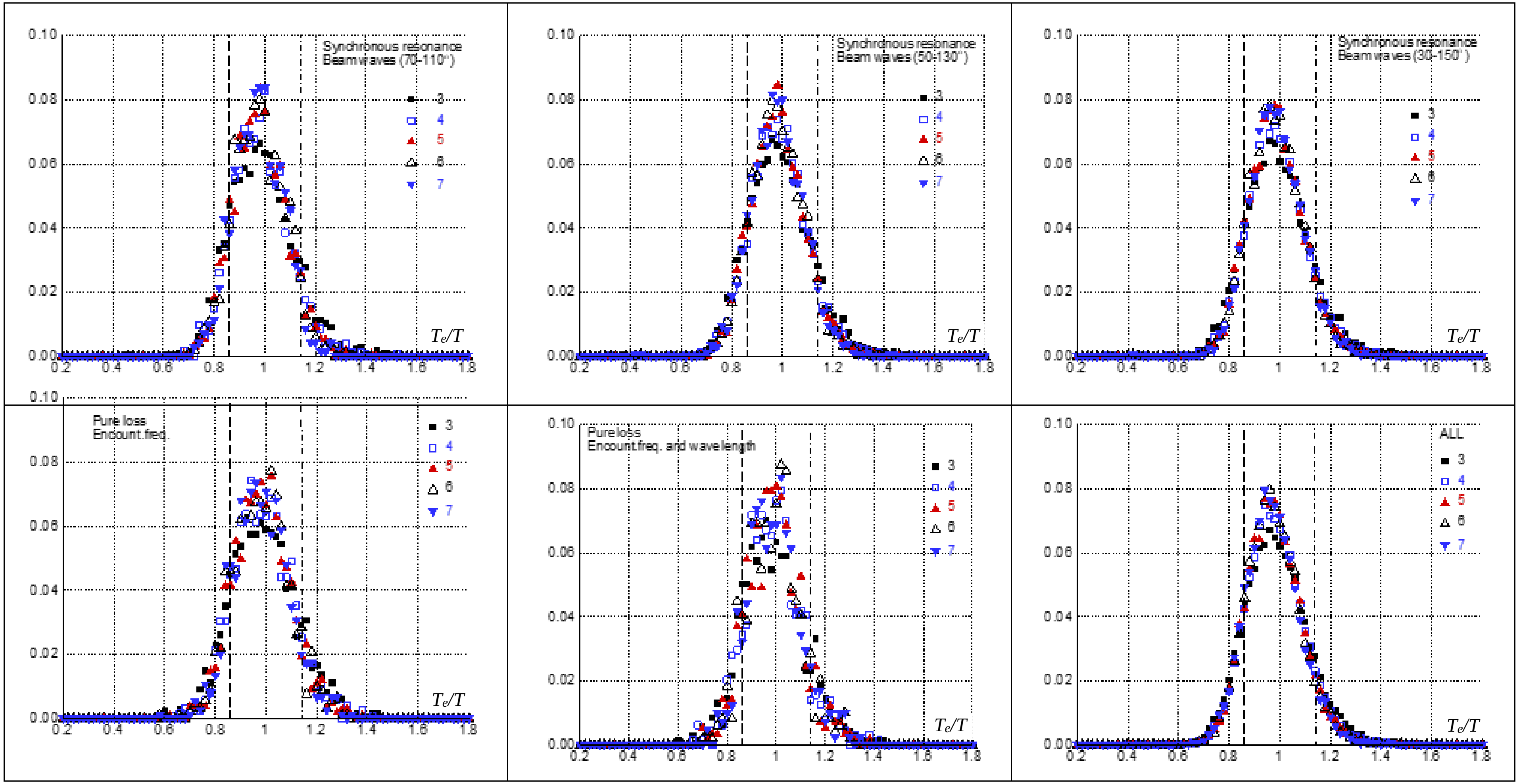

Figure 5.1.1 Histogram (number of cases normalized on 1) of the ratio T_e/T and 95%-confidence interval of directly computed T (vertical lines) for (from top to bottom) parametric roll in bow waves, parametric roll in stern waves, synchronous roll in beam waves, pure loss of stability (bottom left and middle) and all cases together (bottom right). The symbols differentiate the number of points used for the extrapolation.

5.1.2.5 To quantify the accuracy of an extrapolation, the percentage of such extrapolated values that lie within the 95%-confidence interval of the directly computed estimate was calculated, see table 5.1.1. The results show that the extrapolation, eq. (5.1.1), provides sufficiently accurate results and thus is a useful practical tool to accelerate direct stability assessment and the preparation of operational measures.

Table 5.1.1. Percentage of extrapolated values of the time to stability failure within a 95%-confidence interval of a directly computed estimate

Number of wave heights used for extrapolation	3	4	5	6	7	8	9	10
Parametric resonance in bow waves								
Wave directions 150 to 180 degrees	79	83	85	84	83	81	78	81
Wave directions 160 to 180 degrees	79	82	84	82	81	79	77	79
Wave directions 170 to 180 degrees	78	82	83	81	80	78	77	76
Parametric resonance in stern waves								
Wave directions 0 to 10 degrees	79	82	80	76	73	75	71	62
Wave directions 0 to 20 degrees	79	83	84	81	78	80	79	68
Wave directions 0 to 30 degrees	79	82	81	79	76	78	76	68
Synchronous resonance in beam waves								
Wave directions 70 to 110 degrees	77	83	85	87	88	88	85	77
Wave directions 50 to 130 degrees	77	82	83	85	85	85	82	74
Wave directions 30 to 150 degrees	77	82	83	84	84	84	82	78
Pure loss in following waves	77	82	83	84	84	86	87	88
All above cases	**77**	**81**	**82**	**83**	**82**	**81**	**79**	**75**

5.1.3 *Example procedure*

5.1.3.1 Assume that direct counting has provided K maximum likelihood estimates $\hat{r}_k$ of the stability failure rate at significant wave heights H_{sk}, where $k = 1,\dots,K$; where each $\hat{r}_k$ is defined after encountering N_k stability failures (each N_k is not necessarily the same) so that the upper boundaries of the 95%-confidence interval of stability failure rate obtained by direct counting are $r_{\mathrm{U},k} = \hat{r}_k \cdot 0.5\chi^2_{1-\alpha/2,2N_k}/N_k$, eq. (3.3.9), where $\alpha = 0.05$.

5.1.3.2 A linear extrapolation of $\ln \hat{r}_k$ over $1/H_{sk}^2$, eq. (5.1.1), provides the extrapolated failure rate r_e:

$$\ln r_\mathrm{e} = \sum_{k=1}^{K} b_k \ln \hat{r}_k \tag{5.1.3}$$

5.1.3.3 The coefficients b_k, $\sum_{k=1}^{K} b_k = 1$, can be obtained by a least-squares method, see paragraph 5.1.4.3.

5.1.3.4 To define the upper boundary r_eU of the 95%-confidence interval of the extrapolated stability failure rate, the χ^2-distribution can be approximated by use of a normal distribution for a large N (see paragraph 3.3.7) and apply a linear combination of normal distributions to obtain:

$$r_\mathrm{eU} = r_\mathrm{e} \cdot 0.5\chi^2_{1-\alpha/2,2N_\mathrm{e}}/N_\mathrm{e} \tag{5.1.4}$$

5.1.3.5 In eq. (5.1.4), $\alpha = 0.05$, and N_e is defined from:

$$1/N_\mathrm{e} = \sum_{k=1}^{K} b_k^2/N_k \tag{5.1.5}$$

5.1.3.6 When all N_k are the same, i.e. $N_1 = N_2 = \cdots = N_\mathrm{k} = N$, then $N_\mathrm{e} = N/\sum_{k=1}^{K} b_k^2$.

5.1.4 *Application examples*

5.1.4.1 Examples concern loading condition LC01 of the cruise vessel and the 14,000 TEU container ship (see table 4.1.1) in irregular short-crested head and beam waves. The maximum likelihood estimates $\hat{r}_k$ of the stability failure rate, used for the extrapolation, were provided by direct counting for $N = 200$ and, for comparison, 20 stability failures in 1.0 m ranges of significant wave heights H_{sk}, $k = 1, \ldots, K$. The upper boundaries of the 95%-confidence interval of the stability failure rate obtained by direct counting were calculated as $r_{U,k} = \hat{r}_k \cdot 0.5\chi^2_{1-\alpha/2,2N}/N$, where $\alpha = 0.05$. For extrapolation, the results for which $r_k < 0.05/T_r$ were used (see paragraph 5.1.2.1) and the significant wave heights H_{sk} used for the extrapolation were not less than 2.0 m (see paragraph 3.5.5.3.3 of Part B).

5.1.4.2 The extrapolated stability failure rate r_e was obtained by linear extrapolation of $\ln \hat{r}_k$ over $1/H_{sk}^2$, eq. (5.1.2), using least-squares method as:

$$\ln r_e = \sum_{k=1}^{K} b_k \ln \hat{r}_k \tag{5.1.6}$$

5.1.4.3 For the least-squares extrapolation, the coefficients b_k are calculated as:

$$b_k = x/X + (1 - Kx/X)(x_k X - X_2)/(X^2 - KX_2) \tag{5.1.7}$$

where $X = \sum_{k=1}^{K} x_k$, $X_2 = \sum_{k=1}^{K} x_k^2$ and $x_k = 1/H_{sk}^2$; $x = 1/H_s^2$ refers to the significant wave height for which the extrapolation is performed.

5.1.4.4 The upper boundary r_{eU} of the 95%-confidence interval of the extrapolated stability failure rate was calculated as:

$$r_{eU} = r_e \cdot 0.5\chi^2_{1-\alpha/2,2N_e}/N_e \tag{5.1.8}$$

where $\alpha = 0.05$ and, for constant N=200 or N=20, N_e was calculated as $N_e = N/\sum_{k=1}^{K} b_k^2$.

5.1.4.5 Figure 5.1.2 shows the maximum likelihood estimates $\hat{r}_k$ of the failure rate obtained by direct counting ("suitable" points are those with r_k less than 0.05/T_r; "not suitable" points are those with r_k > 0.05/T_r.) and the extrapolated failure rate using three (K = 3) and all suitable points, as well as the upper boundary of the 95%-confidence interval of stability failure rate, obtained by both direct counting and extrapolation, vs. $1/H_s^2$. Note that there is a broadening of the confidence interval of stability failure rate with a decreasing significant wave height due to extrapolation.

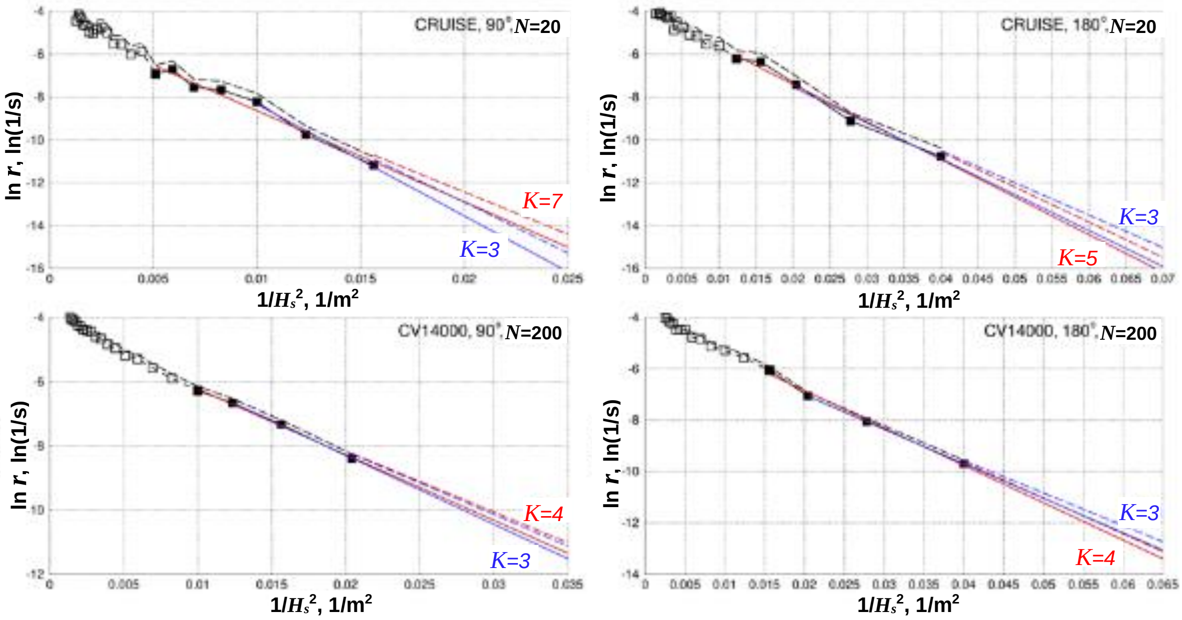

Figure 5.1.2 Examples of extrapolation of failure rate over significant wave height in beam (left) and head (right) waves when direct counting uses 20 (top) and 200 (bottom) stability failures: maximum likelihood estimate of failure rate suitable (■) and not suitable (□) for extrapolation, extrapolated failure rate using three points within H_s range 2.0 m (blue) and all suitable points (red) and corresponding upper boundaries r_U of 95%-confidence interval (dashed lines)

5.2 Critical wave method for surf-riding/broaching failure mode

5.2.1 *Description of method*

5.2.1.1 The critical wave method is one of the statistical extrapolation procedures for the direct stability assessment for the surf-riding/broaching stability failure mode.

5.2.1.2 The critical wave method is a combination of a probabilistic "non-rare" procedure and a deterministic "rare" procedure. The "non-rare" procedure can be regarded as the process of the definition of the initial condition of the "rare" procedure. The "non-rare" procedure is either an evaluation or an estimation of the probability of the encounter of a single large wave that is characterized by the exceedance of values of parameters while the initial conditions belong to a specified range. The "rare" procedure is the determination of the parameters of a single wave and initial conditions that lead to stability failure.

5.2.1.3 For broaching associated with surf-riding, we may assume that broaching is a single wave event, because surf-riding can be regarded as a single wave event. As well established in non-linear dynamics, surf-riding in regular following waves has two different types: one type occurs under any initial state of surge displacement and velocity if the wave and operational conditions satisfy a critical condition and the other type occurs under the limited initial state of surge displacement and velocity. The latter means that, if a ship is initially placed on a stable surf-riding state for example, a ship keeps the surf-riding forever. Because of a two-dimensional nature of the phase plane of dynamics, a self-propelled ship cannot enter the initial state for the latter surf-riding without additional forcing other than assumed waves. Therefore, if a ship keeps a specified propulsor thrust (a specified propeller revolutions for a ship with propellers) with the initial propulsor thrust below the specified thrust, the ship cannot experience the latter type of surf-riding so that the initial condition dependence of surf-riding in regular waves can be excluded. In irregular waves, possibility of the former type of surf-riding may exist but is negligibly small according to existing numerical investigations.

Further investigations also confirmed that broaching probability can be satisfactorily evaluated. Thus, we may ignore the effect of initial conditions. This approach is adopted in the level 2 vulnerability criteria for surf-riding, section 2.6.3 of the guidelines.

5.2.1.4 First, the combinations of the wavelength and wave steepness leading to the first-type surf-riding in regular following waves are determined using the Melnikov analysis, as adopted in the level 2 vulnerability criteria (2.6.3.4.6 of the Interim Guidelines) or its equivalent, under the specified nominal Froude number and the autopilot course from the wave direction.

5.2.1.5 Second, the numerical simulation based on a surge-sway-yaw-roll coupled model with static heave, pitch and an autopilot or equivalent in regular stern-quartering waves should be executed for varied wavelength to ship length ratio and wave steepness inside the region of the first-type surf-riding. Here the initial conditions of the ship motions should be set to be a periodic state under a small Froude number such as 0.1 and a small autopilot course from the wave direction such as 0 degrees. The proportional gain for the autopilot should be set as a practical but reasonably large value, such as 3, and the differential gain should be the minimum for avoiding a directionally unstable phenomenon in calm water (e.g. continued overshooting or zigzag). The integral gain, the non-linear elements and the band pass filter of the autopilot may be excluded.

5.2.1.6 If the instant exists when both the yaw angle and yaw angular velocity increase over time despite the maximum opposite application of rudder deflection, it can be identified as a broaching event. Further, if a failure event (as defined in paragraph 3.2.1 of the Interim Guidelines) occurs during this wave encounter, this combination of the wavelength and the wave steepness should be regarded as a stability failure condition due to broaching in regular waves.

5.2.1.7 Third, the joint probability density function of wavelength and wave height in stationary irregular waves with a cell of a given significant wave height, H_s, and mean zero-crossing wave period, T_z, is integrated within that cell of the stability failure condition due to broaching in regular waves. The obtained value indicates the conditional probability of the stability failure due to broaching per encounter wave in stationary irregular waves of the given significant wave height and mean zero-crossing wave period under the specified nominal Froude number and the autopilot course. The probability density function and the numerical integration method to be used here can be found in paragraphs 2.6.3.2 and 2.6.3.3 of the Interim Guidelines.

5.2.1.8 Repeating the procedures presented in paragraphs 5.2.1.3 to 5.2.1.7 for various significant wave heights and mean wave periods and integrating the product of the conditional probability obtained with the joint probability density function of the significant wave height and mean zero-crossing wave period, the average probability of stability failure due to broaching per encountered wave is found, conditional on the specified nominal Froude number and the autopilot course. The joint probability density function of the significant wave height and mean zero-crossing wave period and the numerical integration method to be used here can be found in 2.6.3.2 of the Interim Guidelines.

5.2.1.9 Repeating the above procedures for various autopilot courses and integrating the product of the conditional probability, obtained above, with the probability density function of the autopilot courses, the average conditional rate of stability failures due to broaching, 1/s, is obtained at the specified nominal Froude number as follows:

$$r = -\ln(1 - p) / T_{\mathrm{we}} \tag{5.2.1}$$

where p is the average probability of stability failure due to broaching per encountered wave, conditional on the specified nominal Froude number, and T_{we} is the mean zero-crossing wave encounter period.

5.2.1.10 Since the critical wave method provides a conservative estimate of the probability of stability failure due to surf-riding/broaching, eq. (5.2.1) can be used to estimate the upper boundary of the 95%-confidence interval of the stability failure rate due to broaching. A further conservative assumption used here is to use as the criterion the product of the stability failure rate r obtained with eq. (5.2.1) with the probability of the specified ship speed and course. The average of this product over the ship speeds and wave heading should not exceed the standard $2.6 \cdot 10^{-8}$ 1/s specified in 3.5.3.2.2 of the Interim Guidelines.

5.2.2 *Application example*

5.2.2.1 Application example of the critical wave method for surf-riding/broaching failure mode based on 5.2.1 concerns the ONR flare topside vessel shown in Figure 5.2.1. Since the ship length is 154 m and the service Froude number is 0.4, this ship is regarded vulnerable to broaching according to the level 1 vulnerability criterion.

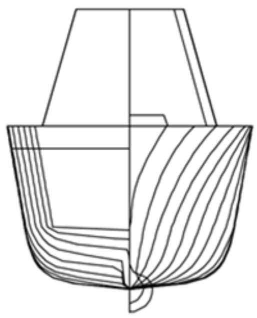

Figure 5.2.1 Body plan of the ONR flare topside vessel.

5.2.2.2 The tool used to calculate the broaching probability in the North Atlantic wave climate is based on a combination of a surge-sway-yaw-roll simulation model with a proportional autopilot in regular waves and stochastic wave theory. First, the simulation model estimates the deterministic broaching zone as a function of wave steepness and wavelength for the given propeller revolution and the autopilot course with respect to wave direction. Second, the broaching probability in stationary sea states specified by the significant wave height, mean wave period and wave energy spectrum is calculated by integrating the probability density function of the local wave height and the wavelength within the deterministic broaching zone. Finally, the average broaching probability per encountered wave in a specified sea area represented by a wave scatter table is obtained by integrating the product of the broaching probability per sea state with the occurrence probability of sea state.

5.2.2.3 The simulation model is based on a non-linear manoeuvring model with the wave-induced forces and moments assuming low encounter frequency. The manoeuvring forces and moments in calm water, including resistance and propeller thrust, are estimated with circular motion captive model tests. The roll damping coefficient is estimated from roll decay tests with a scaled ship model. The wave-induced forces and moments in stern-quartering waves are calculated with a linear slender-body theory under the low encounter frequency assumption as the sum of the Froude-Krylov components and hydrodynamic lift due to wave particle velocity and corrected using captive model tests or viscous-flow computational fluid dynamic methods. The interactions between the manoeuvring forces and waves are ignored under the assumption that the wave steepness and the ship motion normalized with respect to the forward velocity are not large. The stochastic wave theory based on wave envelope theory proposed by Longuet-Higgins is used here, similar to that used in the level 2 vulnerability criteria.

5.2.2.4 Broaching is defined as a phenomenon when the ship cannot keep straight course despite the maximum opposite steering efforts. Based on this definition, the following criteria are used (note that it does not include any quantitative value for course deviation from the autopilot course):

.1 when the rudder deflection reaches its starboard limit, both the ship yaw angular velocity and acceleration have the sign towards port; and

.2 when the rudder deflection reaches its port limit, both the ship yaw angular velocity and acceleration have the sign towards starboard.

5.2.2.5 The broaching probability calculated with the described method is also compared with that measured in model experiments in irregular waves, based on the ITTC recommended procedure 7.5-02-07-04 for intact stability model tests. Examples of the comparison are shown in figures 5.2.2 and 5.2.3.[23] These results indicate that the used prediction procedure can be applied for the direct stability assessment of the ONR flare topside vessel.

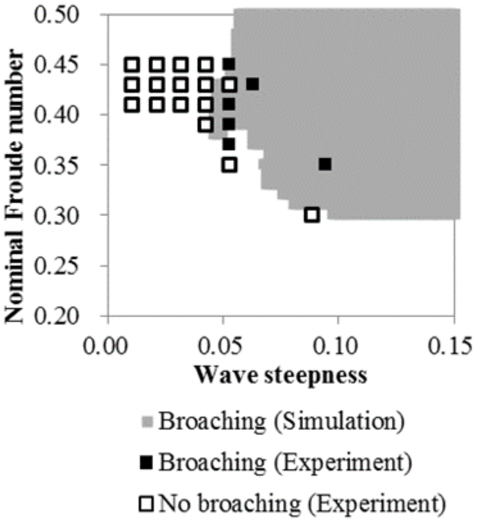

Figure 5.2.2 Comparison of measurement and simulation in broaching region for ONR flare topside vessel in regular waves; wavelength to ship length ratio is 1.25, autopilot course is 15 degrees from wave direction

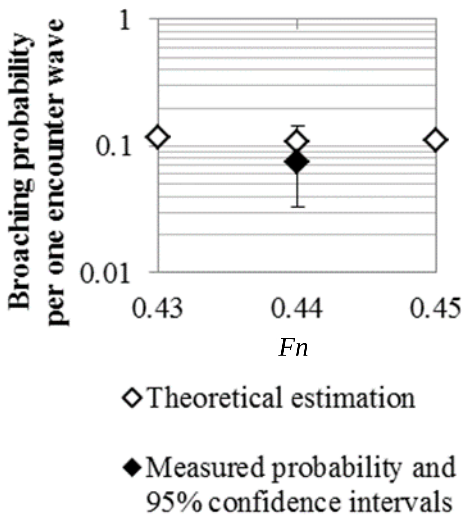

Figure 5.2.3 Comparison of broaching probability between measurement and simulation for ONR flare topside vessel in long-crested irregular waves; significant wave height is 9.65 m, mean wave period 11.11 s, autopilot course 15 degrees from wave direction

5.2.2.6 In addition, example comparison of time series between the model experiment and numerical simulation is shown in figure 5.2.4. Here, two broaching instances occurred, at approximately 67 s and 97 s. The simulation reproduces these two instances and predicts slightly conservatively the roll angle due to broaching.

---

23 Umeda, N., Usada, S., Mizumoto, K., Matsuda, A. *Broaching probability for a ship in irregular stern-quartering waves: theoretical prediction and experimental validation*. Journal of Marine Science and Technology, 21(1), pp. 23-37, 2016.

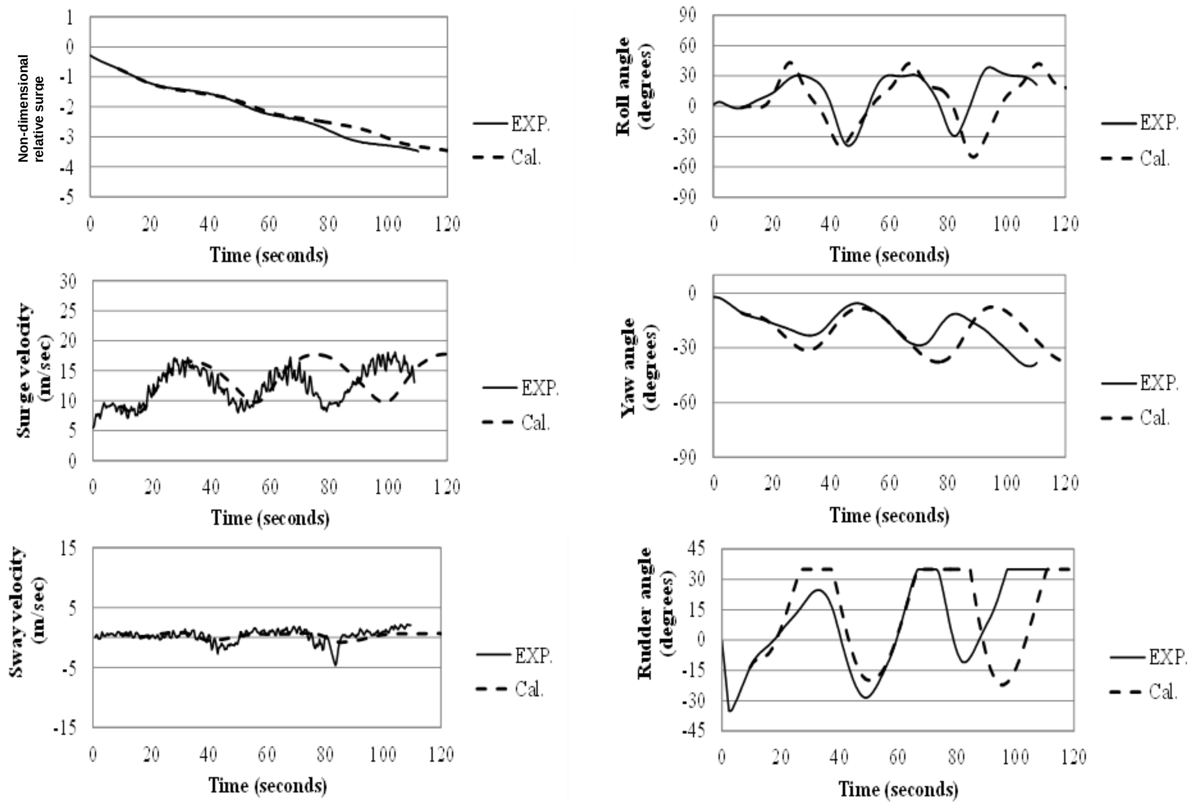

Figure 5.2.4. Comparison between model experiments and numerical calculations

5.2.3 *Results and discussion*

5.2.3.1 Using the described procedure, the probability of exceedance of a 40 degree roll angle due to broaching associated with surf-riding in stationary sea states is obtained, which depends upon the significant wave height H_s, the mean wave period T_{01}, and the autopilot course with respect to the wave direction at a nominal Froude number of 0.4. The results are presented in tables 5.2.1 to 5.2.12. The wave energy spectrum follows the ITTC recommendation (1974) and the wave scatter table, IACS Recommendation No.34 (Corr.1 Nov. 2001) (see the Interim Guidelines, Table 2.7.2.1.2). The Froude number (corresponding to service speed) is 0.4; the rudder gain for the autopilot is 3.

Table 5.2.1. Probability of exceedance of a 40 degree roll angle due to broaching in stationary sea states at an autopilot course of 3.75 degrees and a nominal Froude number of 0.4

Total probability	χ=-3.75																			
3.74E-07			1.5	2.5	3.5	4.5	5.5	6.5	7.5	8.5	9.5	10.5	11.5	12.5	13.5	14.5	15.5	16.5	17.5	18.5
		0.5			0.0000	0.0000	0.0000	0.0000	0.0000	0.0000	0.0000	0.0000	0.0000	0.0000						
		1.5				0.0000	0.0000	0.0000	0.0000	0.0000	0.0000	0.0000	0.0000	0.0000	0.0000	0.0000	0.0000			
		2.5				0.0000	0.0000	0.0000	0.0000	0.0000	0.0000	0.0000	0.0000	0.0000	0.0000	0.0000	0.0000	0.0000		
		3.5				0.0000	0.0000	0.0000	0.0000	0.0000	0.0000	0.0000	0.0000	0.0000	0.0000	0.0000	0.0000	0.0000	0.0000	
		4.5					0.0000	0.0000	0.0000	0.0000	0.0000	0.0000	0.0000	0.0000	0.0000	0.0000	0.0000	0.0000	0.0000	
		5.5					0.0000	0.0000	0.0000	0.0000	0.0000	0.0000	0.0000	0.0000	0.0000	0.0000	0.0000	0.0000	0.0000	0.0000
		6.5					0.0000	0.0000	0.0000	0.0000	0.0000	0.0000	0.0000	0.0000	0.0000	0.0000	0.0000	0.0000	0.0000	0.0000
	H_s (m)	7.5						0.0000	0.0000	0.0000	0.0000	0.0000	0.0000	0.0000	0.0000	0.0000	0.0000	0.0000	0.0000	0.0000
		8.5						0.0000	0.0000	0.0000	0.0000	0.0000	0.0000	0.0000	0.0000	0.0000	0.0000	0.0000	0.0000	0.0000
		9.5						0.0000	0.0000	0.0000	0.0000	0.0000	0.0000	0.0000	0.0000	0.0000	0.0000	0.0000	0.0000	0.0000
		10.5							0.0000	0.0000	0.0000	0.0000	0.0000	0.0000	0.0000	0.0000	0.0001	0.0000	0.0000	0.0000
		11.5							0.0000	0.0000	0.0001	0.0001	0.0000	0.0001	0.0001	0.0001	0.0001	0.0001	0.0001	0.0000
		12.5							0.0000	0.0001	0.0001	0.0002	0.0001	0.0001	0.0002	0.0002	0.0003	0.0002	0.0001	
		13.5								0.0001	0.0003	0.0003	0.0003	0.0002	0.0003	0.0004	0.0005	0.0004	0.0003	
		14.5								0.0002	0.0004	0.0005	0.0005	0.0004	0.0005	0.0006	0.0007	0.0006		
		15.5									0.0006	0.0008	0.0007	0.0006	0.0007	0.0009	0.0009	0.0008		
		16.5										0.0010	0.0010	0.0009	0.0010	0.0011	0.0012			

Table 5.2.2. Probability of exceedance of a 40 degree roll angle due to broaching in stationary sea states at an autopilot course of 7.5 degrees and a nominal Froude number of 0.4

T_{01}(sec)

Total probability	χ=-7.5																			
5.27524E-05			1.5	2.5	3.5	4.5	5.5	6.5	7.5	8.5	9.5	10.5	11.5	12.5	13.5	14.5	15.5	16.5	17.5	18.5
		0.5			0.0000	0.0000	0.0000	0.0000	0.0000	0.0000	0.0000	0.0000	0.0000	0.0000						
		1.5				0.0000	0.0000	0.0000	0.0000	0.0000	0.0000	0.0000	0.0000	0.0000	0.0000	0.0000	0.0000			
		2.5				0.0000	0.0000	0.0000	0.0000	0.0000	0.0000	0.0000	0.0000	0.0000	0.0000	0.0000	0.0000	0.0000		
		3.5				0.0000	0.0000	0.0000	0.0000	0.0000	0.0000	0.0000	0.0000	0.0000	0.0000	0.0000	0.0000	0.0000	0.0000	
		4.5					0.0000	0.0000	0.0000	0.0000	0.0000	0.0000	0.0000	0.0000	0.0000	0.0000	0.0000	0.0000	0.0000	
		5.5					0.0000	0.0000	0.0000	0.0000	0.0000	0.0000	0.0000	0.0000	0.0000	0.0000	0.0000	0.0000	0.0000	0.0000
		6.5					0.0000	0.0000	0.0000	0.0000	0.0000	0.0000	0.0000	0.0000	0.0000	0.0000	0.0000	0.0000	0.0000	0.0000
		7.5						0.0000	0.0000	0.0000	0.0001	0.0002	0.0002	0.0001	0.0000	0.0000	0.0000	0.0000	0.0000	0.0000
	H_s (m)	8.5						0.0000	0.0000	0.0002	0.0006	0.0010	0.0009	0.0005	0.0002	0.0000	0.0000	0.0000	0.0000	0.0000
		9.5						0.0000	0.0002	0.0007	0.0017	0.0026	0.0024	0.0015	0.0006	0.0002	0.0000	0.0000	0.0000	0.0000
		10.5							0.0005	0.0017	0.0037	0.0052	0.0049	0.0031	0.0015	0.0005	0.0001	0.0000	0.0000	0.0000
		11.5							0.0011	0.0032	0.0065	0.0088	0.0082	0.0055	0.0028	0.0011	0.0004	0.0001	0.0000	0.0000
		12.5							0.0020	0.0052	0.0098	0.0129	0.0120	0.0084	0.0046	0.0021	0.0008	0.0003	0.0001	
		13.5								0.0077	0.0135	0.0173	0.0162	0.0117	0.0068	0.0033	0.0014	0.0006	0.0002	
		14.5								0.0102	0.0172	0.0215	0.0204	0.0152	0.0093	0.0049	0.0024	0.0011		
		15.5									0.0207	0.0255	0.0244	0.0187	0.0119	0.0068	0.0036	0.0018		
		16.5										0.0289	0.0279	0.0220	0.0147	0.0089	0.0051			

Table 5.2.3. Probability of exceedance of a 40 degree roll angle due to broaching in stationary sea states at an autopilot course of 11.25 degrees and a nominal Froude number of 0.4

Total probability	χ=-11.25°	T_{01}(sec)																		
0.00068756			1.5	2.5	3.5	4.5	5.5	6.5	7.5	8.5	9.5	10.5	11.5	12.5	13.5	14.5	15.5	16.5	17.5	18.5
		0.5			0.0000	0.0000	0.0000	0.0000	0.0000	0.0000	0.0000	0.0000	0.0000	0.0000						
		1.5				0.0000	0.0000	0.0000	0.0000	0.0000	0.0000	0.0000	0.0000	0.0000	0.0000	0.0000	0.0000			
		2.5				0.0000	0.0000	0.0000	0.0000	0.0000	0.0000	0.0000	0.0000	0.0000	0.0000	0.0000	0.0000	0.0000		
		3.5				0.0000	0.0000	0.0000	0.0000	0.0000	0.0000	0.0000	0.0000	0.0000	0.0000	0.0000	0.0000	0.0000	0.0000	
		4.5					0.0000	0.0000	0.0000	0.0000	0.0000	0.0000	0.0000	0.0000	0.0000	0.0000	0.0000	0.0000	0.0000	
		5.5					0.0000	0.0000	0.0000	0.0000	0.0001	0.0002	0.0001	0.0001	0.0000	0.0000	0.0000	0.0000	0.0000	0.0000
		6.5					0.0000	0.0000	0.0001	0.0003	0.0009	0.0015	0.0014	0.0007	0.0002	0.0000	0.0000	0.0000	0.0000	0.0000
		7.5						0.0001	0.0004	0.0015	0.0038	0.0059	0.0057	0.0036	0.0016	0.0005	0.0001	0.0000	0.0000	0.0000
	H_s (m)	8.5						0.0003	0.0014	0.0046	0.0100	0.0146	0.0147	0.0105	0.0055	0.0021	0.0006	0.0001	0.0000	0.0000
		9.5						0.0009	0.0035	0.0098	0.0197	0.0277	0.0284	0.0219	0.0131	0.0060	0.0021	0.0006	0.0001	0.0000
		10.5							0.0069	0.0173	0.0322	0.0440	0.0455	0.0371	0.0244	0.0129	0.0055	0.0018	0.0005	0.0001
		11.5							0.0115	0.0264	0.0464	0.0619	0.0645	0.0545	0.0384	0.0226	0.0110	0.0043	0.0014	0.0004
		12.5							0.0170	0.0365	0.0612	0.0801	0.0838	0.0728	0.0540	0.0344	0.0186	0.0084	0.0032	
		13.5								0.0467	0.0756	0.0975	0.1024	0.0909	0.0701	0.0475	0.0279	0.0141	0.0060	
		14.5								0.0565	0.0888	0.1133	0.1196	0.1079	0.0859	0.0610	0.0384	0.0210		
		15.5									0.1004	0.1271	0.1347	0.1234	0.1008	0.0744	0.0493	0.0290		
		16.5										0.1385	0.1477	0.1372	0.1144	0.0871	0.0603			

Table 5.2.4. Probability of exceedance of a 40 degree roll angle due to broaching in stationary sea states at an autopilot course of 15 degrees and a nominal Froude number of 0.4

Total probability	χ=-15°	T_{01}(sec)																		
0.002355788			1.5	2.5	3.5	4.5	5.5	6.5	7.5	8.5	9.5	10.5	11.5	12.5	13.5	14.5	15.5	16.5	17.5	18.5
		0.5			0.0000	0.0000	0.0000	0.0000	0.0000	0.0000	0.0000	0.0000	0.0000	0.0000						
		1.5				0.0000	0.0000	0.0000	0.0000	0.0000	0.0000	0.0000	0.0000	0.0000	0.0000	0.0000	0.0000			
		2.5				0.0000	0.0000	0.0000	0.0000	0.0000	0.0000	0.0000	0.0000	0.0000	0.0000	0.0000	0.0000	0.0000		
		3.5				0.0000	0.0000	0.0000	0.0000	0.0000	0.0000	0.0000	0.0000	0.0000	0.0000	0.0000	0.0000	0.0000	0.0000	
		4.5					0.0000	0.0000	0.0000	0.0001	0.0002	0.0002	0.0001	0.0000	0.0000	0.0000	0.0000	0.0000	0.0000	
		5.5					0.0000	0.0000	0.0002	0.0010	0.0022	0.0027	0.0018	0.0007	0.0002	0.0000	0.0000	0.0000	0.0000	0.0000
		6.5					0.0000	0.0003	0.0014	0.0045	0.0088	0.0108	0.0085	0.0044	0.0016	0.0004	0.0001	0.0000	0.0000	0.0000
	H_s (m)	7.5						0.0012	0.0045	0.0118	0.0213	0.0261	0.0225	0.0139	0.0063	0.0021	0.0005	0.0001	0.0000	0.0000
		8.5						0.0031	0.0098	0.0227	0.0385	0.0474	0.0432	0.0301	0.0162	0.0068	0.0022	0.0006	0.0001	0.0000
		9.5						0.0062	0.0168	0.0360	0.0586	0.0722	0.0686	0.0517	0.0314	0.0155	0.0061	0.0020	0.0005	0.0001
		10.5							0.0252	0.0507	0.0800	0.0983	0.0959	0.0764	0.0506	0.0280	0.0129	0.0049	0.0016	0.0004
		11.5							0.0343	0.0658	0.1011	0.1239	0.1232	0.1021	0.0719	0.0434	0.0224	0.0099	0.0037	0.0012
		12.5							0.0436	0.0804	0.1210	0.1477	0.1488	0.1269	0.0937	0.0604	0.0340	0.0167	0.0071	
		13.5								0.0939	0.1388	0.1689	0.1718	0.1498	0.1145	0.0777	0.0468	0.0250	0.0119	
		14.5								0.1060	0.1541	0.1870	0.1917	0.1701	0.1336	0.0943	0.0599	0.0343		
		15.5									0.1666	0.2017	0.2082	0.1874	0.1506	0.1097	0.0728	0.0440		
		16.5										0.2129	0.2213	0.2019	0.1653	0.1236	0.0849			

Table 5.2.5. Probability of exceedance of a 40 degree roll angle due to broaching in stationary sea states at an autopilot course of 18.75 degrees and a nominal Froude number of 0.4

Total probability	χ=-18.75°	T_{01}(sec)																	
0.003325687			1.5	2.5	3.5	4.5	5.5	6.5	7.5	8.5	9.5	10.5	11.5	12.5	13.5	14.5	15.5	16.5	17.5	18.5
		0.5			0.0000	0.0000	0.0000	0.0000	0.0000	0.0000	0.0000	0.0000	0.0000	0.0000						
		1.5				0.0000	0.0000	0.0000	0.0000	0.0000	0.0000	0.0000	0.0000	0.0000	0.0000	0.0000	0.0000			
		2.5				0.0000	0.0000	0.0000	0.0000	0.0000	0.0000	0.0000	0.0000	0.0000	0.0000	0.0000	0.0000	0.0000		
		3.5				0.0000	0.0000	0.0000	0.0000	0.0000	0.0000	0.0000	0.0000	0.0000	0.0000	0.0000	0.0000	0.0000	0.0000	
		4.5					0.0000	0.0000	0.0001	0.0003	0.0007	0.0007	0.0004	0.0001	0.0000	0.0000	0.0000	0.0000	0.0000	
		5.5					0.0000	0.0001	0.0008	0.0025	0.0048	0.0053	0.0035	0.0014	0.0004	0.0001	0.0000	0.0000	0.0000	0.0000
		6.5					0.0001	0.0008	0.0033	0.0088	0.0154	0.0175	0.0133	0.0070	0.0025	0.0006	0.0001	0.0000	0.0000	0.0000
		7.5						0.0026	0.0084	0.0196	0.0323	0.0374	0.0311	0.0190	0.0087	0.0030	0.0008	0.0002	0.0000	0.0000
	H_s (m)	8.5						0.0057	0.0159	0.0339	0.0535	0.0624	0.0548	0.0371	0.0197	0.0083	0.0028	0.0008	0.0002	0.0000
		9.5						0.0100	0.0252	0.0502	0.0768	0.0895	0.0812	0.0588	0.0346	0.0168	0.0068	0.0023	0.0007	0.0002
		10.5							0.0355	0.0673	0.1001	0.1162	0.1078	0.0818	0.0518	0.0278	0.0128	0.0051	0.0018	0.0005
		11.5							0.0463	0.0840	0.1220	0.1412	0.1329	0.1042	0.0696	0.0402	0.0204	0.0091	0.0037	0.0013
		12.5							0.0568	0.0994	0.1416	0.1634	0.1556	0.1252	0.0870	0.0531	0.0290	0.0143	0.0064	
		13.5								0.1129	0.1582	0.1824	0.1755	0.1441	0.1033	0.0660	0.0381	0.0201	0.0098	
		14.5								0.1241	0.1715	0.1978	0.1923	0.1608	0.1183	0.0782	0.0473	0.0264		
		15.5									0.1817	0.2096	0.2058	0.1749	0.1317	0.0897	0.0562	0.0329		
		16.5										0.2181	0.2161	0.1866	0.1434	0.1002	0.0648			

Table 5.2.6. Probability of exceedance of a 40 degree roll angle due to broaching in stationary sea states at an autopilot course of 22.5 degrees and a nominal Froude number of 0.4

Total probability	χ=-22.5°	T_{01}(sec)																	
0.002643946			1.5	2.5	3.5	4.5	5.5	6.5	7.5	8.5	9.5	10.5	11.5	12.5	13.5	14.5	15.5	16.5	17.5	18.5
		0.5			0.0000	0.0000	0.0000	0.0000	0.0000	0.0000	0.0000	0.0000	0.0000	0.0000						
		1.5				0.0000	0.0000	0.0000	0.0000	0.0000	0.0000	0.0000	0.0000	0.0000	0.0000	0.0000	0.0000			
		2.5				0.0000	0.0000	0.0000	0.0000	0.0000	0.0000	0.0000	0.0000	0.0000	0.0000	0.0000	0.0000	0.0000		
		3.5				0.0000	0.0000	0.0000	0.0000	0.0000	0.0000	0.0000	0.0000	0.0000	0.0000	0.0000	0.0000	0.0000	0.0000	
		4.5					0.0000	0.0000	0.0001	0.0002	0.0005	0.0004	0.0002	0.0000	0.0000	0.0000	0.0000	0.0000	0.0000	
		5.5					0.0000	0.0001	0.0006	0.0020	0.0036	0.0037	0.0023	0.0008	0.0002	0.0000	0.0000	0.0000	0.0000	0.0000
		6.5					0.0001	0.0007	0.0027	0.0072	0.0122	0.0132	0.0095	0.0046	0.0015	0.0004	0.0001	0.0000	0.0000	0.0000
	H_s (m)	7.5						0.0022	0.0073	0.0172	0.0275	0.0302	0.0236	0.0135	0.0057	0.0018	0.0004	0.0001	0.0000	0.0000
		8.5						0.0050	0.0146	0.0313	0.0477	0.0524	0.0431	0.0272	0.0135	0.0053	0.0016	0.0004	0.0001	0.0000
		9.5						0.0093	0.0240	0.0475	0.0696	0.0764	0.0650	0.0441	0.0243	0.0111	0.0042	0.0013	0.0003	0.0001
		10.5							0.0345	0.0637	0.0903	0.0992	0.0867	0.0620	0.0370	0.0188	0.0082	0.0031	0.0010	0.0003
		11.5							0.0446	0.0782	0.1081	0.1190	0.1066	0.0795	0.0504	0.0277	0.0134	0.0057	0.0022	0.0007
		12.5							0.0537	0.0901	0.1222	0.1353	0.1240	0.0958	0.0637	0.0372	0.0194	0.0092	0.0039	
		13.5								0.0991	0.1328	0.1480	0.1385	0.1104	0.0764	0.0469	0.0260	0.0132	0.0062	
		14.5								0.1055	0.1403	0.1576	0.1503	0.1231	0.0882	0.0563	0.0327	0.0177		
		15.5									0.1451	0.1642	0.1594	0.1338	0.0987	0.0653	0.0395	0.0223		
		16.5										0.1684	0.1660	0.1424	0.1079	0.0736	0.0461			

Table 5.2.7. Probability of exceedance of a 40 degree roll angle due to broaching in stationary sea states at an autopilot course of 26.25 degrees and a nominal Froude number of 0.4

Total probability	χ=-26.25°	T_{01}(sec)																	
0.000298595			1.5	2.5	3.5	4.5	5.5	6.5	7.5	8.5	9.5	10.5	11.5	12.5	13.5	14.5	15.5	16.5	17.5	18.5
		0.5			0.0000	0.0000	0.0000	0.0000	0.0000	0.0000	0.0000	0.0000	0.0000	0.0000						
		1.5				0.0000	0.0000	0.0000	0.0000	0.0000	0.0000	0.0000	0.0000	0.0000	0.0000	0.0000	0.0000			
		2.5				0.0000	0.0000	0.0000	0.0000	0.0000	0.0000	0.0000	0.0000	0.0000	0.0000	0.0000	0.0000	0.0000		
		3.5				0.0000	0.0000	0.0000	0.0000	0.0000	0.0000	0.0000	0.0000	0.0000	0.0000	0.0000	0.0000	0.0000	0.0000	
		4.5					0.0000	0.0000	0.0000	0.0000	0.0000	0.0000	0.0000	0.0000	0.0000	0.0000	0.0000	0.0000	0.0000	
		5.5					0.0000	0.0000	0.0000	0.0000	0.0001	0.0001	0.0001	0.0000	0.0000	0.0000	0.0000	0.0000	0.0000	0.0000
		6.5					0.0000	0.0000	0.0001	0.0003	0.0008	0.0009	0.0005	0.0002	0.0001	0.0000	0.0000	0.0000	0.0000	0.0000
	H_s (m)	7.5						0.0001	0.0005	0.0016	0.0029	0.0031	0.0021	0.0009	0.0003	0.0001	0.0000	0.0000	0.0000	0.0000
		8.5						0.0004	0.0017	0.0043	0.0069	0.0071	0.0051	0.0026	0.0010	0.0003	0.0001	0.0000	0.0000	0.0000
		9.5						0.0011	0.0037	0.0082	0.0120	0.0126	0.0096	0.0054	0.0023	0.0008	0.0002	0.0001	0.0000	0.0000
		10.5							0.0064	0.0126	0.0178	0.0189	0.0153	0.0095	0.0046	0.0017	0.0006	0.0002	0.0000	0.0000
		11.5							0.0093	0.0169	0.0236	0.0258	0.0221	0.0148	0.0078	0.0033	0.0012	0.0004	0.0001	0.0000
		12.5							0.0120	0.0210	0.0292	0.0329	0.0296	0.0211	0.0120	0.0055	0.0022	0.0007	0.0002	
		13.5								0.0248	0.0347	0.0401	0.0376	0.0282	0.0171	0.0085	0.0036	0.0013	0.0005	
		14.5								0.0283	0.0400	0.0472	0.0455	0.0356	0.0228	0.0122	0.0055	0.0022		
		15.5									0.0448	0.0537	0.0531	0.0429	0.0288	0.0163	0.0079	0.0034		
		16.5										0.0596	0.0599	0.0499	0.0348	0.0207	0.0107			

Table 5.2.8. Probability of exceedance of a 40 degree roll angle due to broaching in stationary sea states at an autopilot course of 30 degrees and a nominal Froude number of 0.4

Total probability	χ=-30°	T_{01}(sec)																		
1.76797E-05			1.5	2.5	3.5	4.5	5.5	6.5	7.5	8.5	9.5	10.5	11.5	12.5	13.5	14.5	15.5	16.5	17.5	18.5
		0.5			0.0000	0.0000	0.0000	0.0000	0.0000	0.0000	0.0000	0.0000	0.0000	0.0000						
		1.5				0.0000	0.0000	0.0000	0.0000	0.0000	0.0000	0.0000	0.0000	0.0000	0.0000	0.0000	0.0000			
		2.5				0.0000	0.0000	0.0000	0.0000	0.0000	0.0000	0.0000	0.0000	0.0000	0.0000	0.0000	0.0000	0.0000		
		3.5				0.0000	0.0000	0.0000	0.0000	0.0000	0.0000	0.0000	0.0000	0.0000	0.0000	0.0000	0.0000	0.0000	0.0000	
		4.5					0.0000	0.0000	0.0000	0.0000	0.0000	0.0000	0.0000	0.0000	0.0000	0.0000	0.0000	0.0000	0.0000	
		5.5					0.0000	0.0000	0.0000	0.0000	0.0000	0.0000	0.0000	0.0000	0.0000	0.0000	0.0000	0.0000	0.0000	0.0000
		6.5					0.0000	0.0000	0.0000	0.0000	0.0000	0.0000	0.0000	0.0000	0.0000	0.0000	0.0000	0.0000	0.0000	0.0000
	H_s (m)	7.5						0.0000	0.0000	0.0000	0.0000	0.0000	0.0000	0.0000	0.0000	0.0000	0.0000	0.0000	0.0000	0.0000
		8.5						0.0000	0.0000	0.0000	0.0001	0.0002	0.0002	0.0001	0.0000	0.0000	0.0000	0.0000	0.0000	0.0000
		9.5						0.0000	0.0001	0.0002	0.0004	0.0007	0.0007	0.0004	0.0001	0.0000	0.0000	0.0000	0.0000	0.0000
		10.5							0.0002	0.0005	0.0011	0.0018	0.0019	0.0012	0.0005	0.0001	0.0000	0.0000	0.0000	0.0000
		11.5							0.0004	0.0011	0.0025	0.0039	0.0039	0.0026	0.0012	0.0004	0.0001	0.0000	0.0000	0.0000
		12.5							0.0008	0.0021	0.0045	0.0067	0.0068	0.0047	0.0023	0.0008	0.0002	0.0000	0.0000	
		13.5								0.0036	0.0072	0.0103	0.0104	0.0075	0.0040	0.0016	0.0005	0.0001	0.0000	
		14.5								0.0054	0.0103	0.0143	0.0144	0.0108	0.0061	0.0027	0.0010	0.0003		
		15.5									0.0136	0.0184	0.0186	0.0143	0.0086	0.0041	0.0016	0.0005		
		16.5										0.0225	0.0227	0.0179	0.0112	0.0058	0.0025			

Table 5.2.9. Probability of exceedance of a 40 degree roll angle due to broaching in stationary sea states at an autopilot course of 33.75 degrees and a nominal Froude number of 0.4

Total probability	χ=-33.75°	T_{01}(sec)																		
0.000151044			1.5	2.5	3.5	4.5	5.5	6.5	7.5	8.5	9.5	10.5	11.5	12.5	13.5	14.5	15.5	16.5	17.5	18.5
		0.5			0.0000	0.0000	0.0000	0.0000	0.0000	0.0000	0.0000	0.0000	0.0000	0.0000						
		1.5				0.0000	0.0000	0.0000	0.0000	0.0000	0.0000	0.0000	0.0000	0.0000	0.0000	0.0000	0.0000			
		2.5				0.0000	0.0000	0.0000	0.0000	0.0000	0.0000	0.0000	0.0000	0.0000	0.0000	0.0000	0.0000	0.0000		
		3.5				0.0000	0.0000	0.0000	0.0000	0.0000	0.0000	0.0000	0.0000	0.0000	0.0000	0.0000	0.0000	0.0000	0.0000	
		4.5					0.0000	0.0000	0.0000	0.0001	0.0000	0.0000	0.0000	0.0000	0.0000	0.0000	0.0000	0.0000	0.0000	
		5.5					0.0000	0.0001	0.0004	0.0005	0.0003	0.0001	0.0000	0.0000	0.0000	0.0000	0.0000	0.0000	0.0000	0.0000
		6.5					0.0001	0.0005	0.0012	0.0017	0.0011	0.0004	0.0001	0.0000	0.0000	0.0000	0.0000	0.0000	0.0000	0.0000
	H_s (m)	7.5						0.0011	0.0024	0.0032	0.0024	0.0011	0.0003	0.0001	0.0000	0.0000	0.0000	0.0000	0.0000	0.0000
		8.5						0.0018	0.0036	0.0046	0.0038	0.0021	0.0008	0.0002	0.0000	0.0000	0.0000	0.0000	0.0000	0.0000
		9.5						0.0025	0.0045	0.0056	0.0050	0.0033	0.0016	0.0006	0.0002	0.0000	0.0000	0.0000	0.0000	0.0000
		10.5							0.0050	0.0063	0.0061	0.0046	0.0027	0.0012	0.0004	0.0001	0.0000	0.0000	0.0000	0.0000
		11.5							0.0054	0.0068	0.0071	0.0060	0.0041	0.0021	0.0008	0.0003	0.0001	0.0000	0.0000	0.0000
		12.5							0.0055	0.0072	0.0081	0.0076	0.0057	0.0033	0.0015	0.0005	0.0002	0.0000	0.0000	
		13.5								0.0076	0.0092	0.0094	0.0075	0.0047	0.0023	0.0009	0.0003	0.0001	0.0000	
		14.5								0.0082	0.0105	0.0113	0.0095	0.0062	0.0033	0.0014	0.0005	0.0002		
		15.5									0.0118	0.0132	0.0115	0.0079	0.0044	0.0021	0.0008	0.0003		
		16.5										0.0150	0.0135	0.0096	0.0056	0.0028	0.0012			

Table 5.2.10. Probability of exceedance of a 40 degree roll angle due to broaching in stationary sea states at an autopilot course of 37.5 degrees and a nominal Froude number of 0.4

Total probability	χ=-37.5°	T_{01}(sec)																		
0.000330052			1.5	2.5	3.5	4.5	5.5	6.5	7.5	8.5	9.5	10.5	11.5	12.5	13.5	14.5	15.5	16.5	17.5	18.5
		0.5			0.0000	0.0000	0.0000	0.0000	0.0000	0.0000	0.0000	0.0000	0.0000	0.0000						
		1.5				0.0000	0.0000	0.0000	0.0000	0.0000	0.0000	0.0000	0.0000	0.0000	0.0000	0.0000	0.0000			
		2.5				0.0000	0.0000	0.0000	0.0000	0.0000	0.0000	0.0000	0.0000	0.0000	0.0000	0.0000	0.0000	0.0000		
		3.5				0.0000	0.0000	0.0000	0.0000	0.0000	0.0000	0.0000	0.0000	0.0000	0.0000	0.0000	0.0000	0.0000	0.0000	
		4.5					0.0000	0.0000	0.0001	0.0002	0.0001	0.0000	0.0000	0.0000	0.0000	0.0000	0.0000	0.0000	0.0000	
		5.5					0.0000	0.0003	0.0011	0.0013	0.0006	0.0001	0.0000	0.0000	0.0000	0.0000	0.0000	0.0000	0.0000	0.0000
		6.5					0.0003	0.0015	0.0036	0.0042	0.0024	0.0007	0.0001	0.0000	0.0000	0.0000	0.0000	0.0000	0.0000	0.0000
	H_s (m)	7.5						0.0035	0.0072	0.0083	0.0055	0.0022	0.0005	0.0001	0.0000	0.0000	0.0000	0.0000	0.0000	0.0000
		8.5						0.0059	0.0110	0.0125	0.0090	0.0043	0.0014	0.0003	0.0001	0.0000	0.0000	0.0000	0.0000	0.0000
		9.5						0.0083	0.0140	0.0159	0.0122	0.0067	0.0027	0.0008	0.0002	0.0000	0.0000	0.0000	0.0000	0.0000
		10.5							0.0160	0.0181	0.0147	0.0090	0.0042	0.0015	0.0004	0.0001	0.0000	0.0000	0.0000	0.0000
		11.5							0.0170	0.0192	0.0165	0.0110	0.0059	0.0025	0.0009	0.0002	0.0001	0.0000	0.0000	0.0000
		12.5							0.0172	0.0195	0.0175	0.0127	0.0075	0.0036	0.0014	0.0005	0.0001	0.0000	0.0000	
		13.5								0.0193	0.0181	0.0141	0.0090	0.0047	0.0021	0.0008	0.0003	0.0001	0.0000	
		14.5								0.0188	0.0184	0.0151	0.0104	0.0059	0.0029	0.0012	0.0005	0.0002		
		15.5									0.0184	0.0159	0.0116	0.0071	0.0037	0.0017	0.0007	0.0003		
		16.5										0.0165	0.0126	0.0081	0.0045	0.0022	0.0010			

Table 5.2.11. Probability of exceedance of a 40 degree roll angle due to broaching in stationary sea states at an autopilot course of 41.25 degrees and a nominal Froude number of 0.4

T_{01}(sec)

Total probability	χ=-41.25																			
0.000467787			1.5	2.5	3.5	4.5	5.5	6.5	7.5	8.5	9.5	10.5	11.5	12.5	13.5	14.5	15.5	16.5	17.5	18.5
		0.5			0.0000	0.0000	0.0000	0.0000	0.0000	0.0000	0.0000	0.0000	0.0000	0.0000						
		1.5				0.0000	0.0000	0.0000	0.0000	0.0000	0.0000	0.0000	0.0000	0.0000	0.0000	0.0000	0.0000			
		2.5				0.0000	0.0000	0.0000	0.0000	0.0000	0.0000	0.0000	0.0000	0.0000	0.0000	0.0000	0.0000	0.0000		
		3.5				0.0000	0.0000	0.0000	0.0000	0.0000	0.0000	0.0000	0.0000	0.0000	0.0000	0.0000	0.0000	0.0000	0.0000	
		4.5					0.0000	0.0001	0.0004	0.0003	0.0001	0.0000	0.0000	0.0000	0.0000	0.0000	0.0000	0.0000	0.0000	
		5.5					0.0002	0.0009	0.0023	0.0023	0.0009	0.0002	0.0000	0.0000	0.0000	0.0000	0.0000	0.0000	0.0000	0.0000
		6.5					0.0008	0.0032	0.0066	0.0066	0.0033	0.0009	0.0001	0.0000	0.0000	0.0000	0.0000	0.0000	0.0000	0.0000
		7.5						0.0067	0.0122	0.0124	0.0073	0.0026	0.0006	0.0001	0.0000	0.0000	0.0000	0.0000	0.0000	0.0000
	H_s (m)	8.5						0.0105	0.0174	0.0179	0.0118	0.0052	0.0016	0.0004	0.0001	0.0001	0.0000	0.0000	0.0000	0.0000
		9.5						0.0137	0.0212	0.0221	0.0158	0.0081	0.0030	0.0009	0.0002	0.0002	0.0000	0.0000	0.0000	0.0000
		10.5							0.0234	0.0247	0.0189	0.0108	0.0048	0.0017	0.0005	0.0005	0.0000	0.0000	0.0000	0.0000
		11.5							0.0241	0.0257	0.0208	0.0130	0.0065	0.0027	0.0009	0.0009	0.0001	0.0000	0.0000	0.0000
		12.5							0.0238	0.0256	0.0216	0.0146	0.0081	0.0037	0.0015	0.0015	0.0002	0.0000	0.0000	
		13.5								0.0247	0.0217	0.0157	0.0094	0.0048	0.0021	0.0021	0.0003	0.0001	0.0000	
		14.5								0.0234	0.0212	0.0161	0.0104	0.0058	0.0028	0.0028	0.0005	0.0002		
		15.5									0.0203	0.0162	0.0111	0.0066	0.0035	0.0035	0.0007	0.0003		
		16.5										0.0159	0.0115	0.0073	0.0041	0.0041	0.0010			

Table 5.2.12. Probability of exceedance of a 40 degree roll angle due to broaching in stationary sea states at an autopilot course of 45 degrees and a nominal Froude number of 0.4

Total probability	χ=-45	T_{01}(sec)																		
0.000599954			1.5	2.5	3.5	4.5	5.5	6.5	7.5	8.5	9.5	10.5	11.5	12.5	13.5	14.5	15.5	16.5	17.5	18.5
		0.5			0.0000	0.0000	0.0000	0.0000	0.0000	0.0000	0.0000	0.0000	0.0000	0.0000						
		1.5				0.0000	0.0000	0.0000	0.0000	0.0000	0.0000	0.0000	0.0000	0.0000	0.0000	0.0000	0.0000			
		2.5				0.0000	0.0000	0.0000	0.0000	0.0000	0.0000	0.0000	0.0000	0.0000	0.0000	0.0000	0.0000	0.0000		
		3.5				0.0000	0.0000	0.0000	0.0000	0.0000	0.0000	0.0000	0.0000	0.0000	0.0000	0.0000	0.0000	0.0000	0.0000	
		4.5					0.0000	0.0004	0.0008	0.0006	0.0001	0.0000	0.0000	0.0000	0.0000	0.0000	0.0000	0.0000	0.0000	
		5.5					0.0005	0.0023	0.0044	0.0034	0.0011	0.0002	0.0000	0.0000	0.0000	0.0000	0.0000	0.0000	0.0000	0.0000
		6.5					0.0019	0.0064	0.0111	0.0092	0.0039	0.0009	0.0001	0.0000	0.0000	0.0000	0.0000	0.0000	0.0000	0.0000
		7.5						0.0119	0.0189	0.0167	0.0086	0.0027	0.0006	0.0001	0.0000	0.0000	0.0000	0.0000	0.0000	0.0000
	H_s (m)	8.5						0.0171	0.0257	0.0238	0.0140	0.0055	0.0016	0.0003	0.0001	0.0000	0.0000	0.0000	0.0000	0.0000
		9.5						0.0211	0.0303	0.0291	0.0190	0.0088	0.0031	0.0008	0.0002	0.0000	0.0000	0.0000	0.0000	0.0000
		10.5							0.0327	0.0322	0.0228	0.0120	0.0049	0.0016	0.0005	0.0001	0.0000	0.0000	0.0000	0.0000
		11.5							0.0331	0.0333	0.0253	0.0148	0.0069	0.0027	0.0009	0.0003	0.0001	0.0000	0.0000	0.0000
		12.5							0.0323	0.0330	0.0264	0.0168	0.0088	0.0038	0.0015	0.0005	0.0002	0.0000	0.0000	
		13.5								0.0318	0.0266	0.0181	0.0103	0.0050	0.0021	0.0008	0.0003	0.0001	0.0000	
		14.5								0.0300	0.0260	0.0188	0.0115	0.0061	0.0029	0.0012	0.0005	0.0002		
		15.5									0.0249	0.0189	0.0124	0.0071	0.0036	0.0017	0.0007	0.0003		
		16.5										0.0186	0.0128	0.0079	0.0043	0.0022	0.0010			

5.2.3.2 The effect of the autopilot course, as shown in Figure 5.2.5, shows that a broaching danger exists in the autopilot course range from 10 to 30 degrees. For a uniform course distribution, the broaching probability in the North Atlantic is $2.02 \cdot 10^{-4}$ (this is a conditional exceedance probability per an encountered wave of a 40-degree roll angle due to broaching associated with surf-riding), which results in the failure rate of $3.22 \cdot 10^{-6}$ 1/s. Since it is greater than the standard of $2.6 \cdot 10^{-8}$ 1/s, this ship can be regarded as vulnerable for broaching if it is operated without operational measures.

5.2.3.3 Since this ship is also judged as vulnerable to broaching failure by the vulnerability level 1 and level 2 criteria, this result can be regarded as consistent.

5.2.3.4 An operational guidance can be developed using tables 5.2.1 to 5.2.12 by specifying the acceptable stability failure probability for each stationary sea state. Figures 5.2.5 and 5.2.6 indicate that reducing the nominal forward speed and increasing the threshold of roll angle are effective for decreasing the stability failure probability due to broaching.

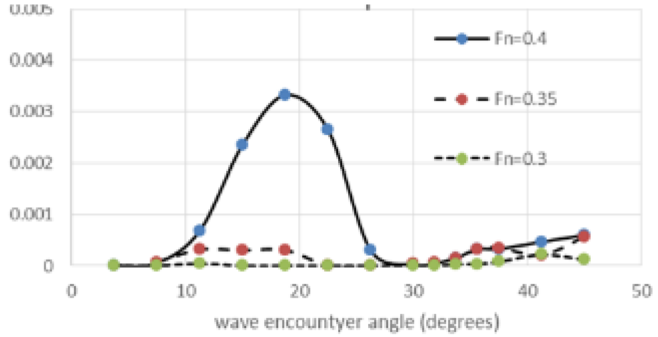

Figure 5.2.5. exceedance probability of a 40 degree roll angle per encountered wave due to broaching associated with surf-riding vs. wave heading for the ONR flare topside vessel in the North Atlantic wave climate

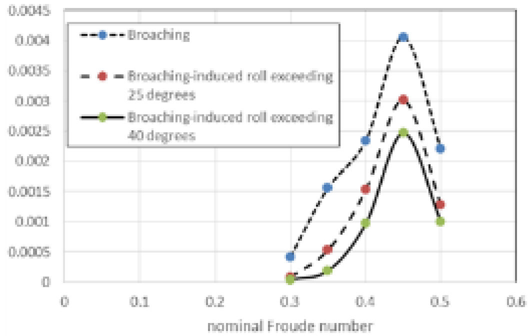

Figure 5.2.6. Probability per encountered wave of broaching associated with surf-riding vs. nominal Froude number for ONR flare topside vessel in the North Atlantic wave climate

5.3 Split-time/motion perturbation method

5.3.1 *Theoretical background for the application of extreme value theory*

5.3.1.1 The split-time method, also known as the motion perturbation method (MPM), and envelope peaks over threshold (EPOT) method are two extrapolation methods (Interim Guidelines, paragraph 3.5.5.4.1) based on the application of statistical extreme value theory. The text given in this section is meant to be used for familiarization with the principle of extreme value theory and should be considered as guidance for its practical application.

5.3.1.2 Extreme value theory describes statistical properties of a largest value in a sample of independent data points. It has been applied in engineering (e.g. flood management) and other areas. The central idea of the extreme value theory is that the distribution of the largest value in an independent data sample is different from the distribution of the sample. This idea can be illustrated with the following example:

- take a number of roll angle records;
- estimate the autocorrelation function (refer to paragraph 3.8.3);
- evaluate the decorrelation time (paragraph 3.8.7);
- extract independent roll angle data points by taking the points that are no closer to each other than the decorrelation time. This extraction makes several samples of independent roll angle data points (These independent roll angle data points have a distribution that can be estimated with a histogram, this distribution is further referred as "an underlying distribution"); and
- select the largest data point from each independent roll angle data sample. The outcome of this selection is the distribution of the largest data points (i.e. values) from each sample that is different than the underlying distribution.

5.3.1.3 For a sample with n data points, the distribution of the largest value in a sample is:

$$pdf_1(y|n) = pdf(y)(cdf(y))^{n-1}$$

where $pdf(y)$ and $cdf(y))$ are the probability density function (PDF) and the cumulative distribution function (CDF), respectively, of the underlying distribution. With an increase of the sample size, the distribution of the largest value tends to a universal limit that depends only on a small set of parameters characterizing the distribution of the sample data. This limit distribution is known as the Generalized Extreme Value Distribution (GEVD). The GEVD is defined by three parameters, a shape parameter ξ, a scale parameter σ, and location value μ and its CDF is:

$$\mathrm{cdf}_{GEV}(y) = \begin{cases} \exp\left(-\exp\left(-\frac{y-\mu}{\sigma}\right)\right) & \text{for } \xi = 0 \\ \exp\left(-\left(1+\xi\frac{y-\mu}{\sigma}\right)^{-(1/\xi)}\right) & \text{for } \xi \neq 0 \text{ and } \xi\frac{y-\mu}{\sigma} > -1 \\ 0 & \text{for } \xi > 0 \text{ and } \xi\frac{y-\mu}{\sigma} \leq -1 \\ 1 & \text{for } \xi < 0 \text{ and } \xi\frac{y-\mu}{\sigma} \leq -1 \end{cases} \tag{5.3.1}$$

The PDF of the GEVD is:

$$\mathrm{pdf}_{GEV}(y) = \begin{cases} \exp\left(-\frac{y-\mu}{\sigma}\right)\cdot\exp\left(-\exp\left(-\frac{y-\mu}{\sigma}\right)\right) & \text{for } \xi = 0 \\ \left(1+\xi\frac{y-u}{\sigma}\right)^{-(1+1/\xi)}\cdot\exp\left(-\left(1+\xi\frac{y-\mu}{\sigma}\right)^{-(1/\xi)}\right) & \text{for } \xi \neq 0 \text{ and } \xi\frac{y-\mu}{\sigma} > -1 \\ 0 & \text{otherwise} \end{cases} \tag{5.3.2}$$

The parameters ξ, σ and μ are found from data. Figures 5.3.1 and 5.3.2 illustrate this concept. The PDF of the largest value $pdf_1(y|n)$ is computed for an increasing volume of the sample from 10^1 to 10^7. Figure 5.3.1 shows the convergence with the $pdf(y)$ standard normal (where the mean value is 0 and standard deviation / variance is 1). Figure 5.3.2 uses the Rayleigh distribution for the illustration. The GEVD shape parameter ξ is known to be zero for both normal and Rayleigh distributions. The other GEVD parameters σ and μ, have the following relationship to the GEVD mean value E_{GEV} and variance V_{GEV}:

$$\sigma = \frac{\sqrt{6V_{GEV}}}{\pi} \ ; \mu = E_{GEV} - 0.57721\sigma \tag{5.3.3}$$

The value 0.57721 is known as the Euler–Mascheroni constant. The fitting is carried out by finding the mean value E_1 and the variance V_1 of the distribution of the largest value $pdf_1(y|n)$ and using these values instead of the E_{GEV} and the V_{GEV}, respectively:

$$E_{GEV} = E_1 = \int_{-\infty}^{\infty} y\cdot pdf_1(y|n)dy \ ; \quad V_{GEV} = V_1 = \int_{-\infty}^{\infty}(y-E_1)^2 pdf_1(y|n)dy \tag{5.3.4}$$

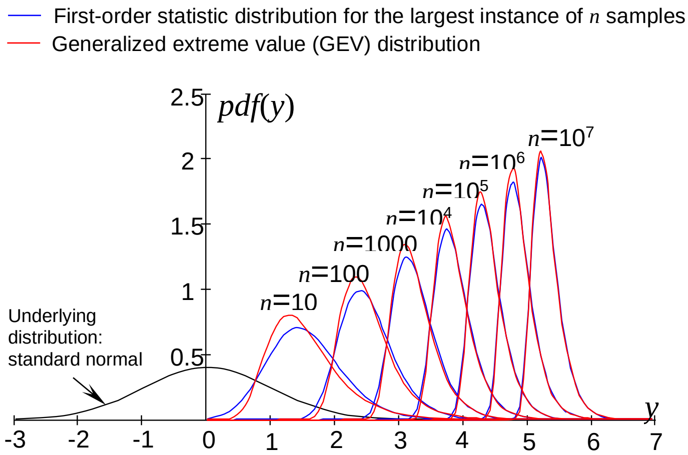

Figure 5.3.1 Conversion of the distribution of the largest value in a sample to a GEVD with an increasing number of samples, where the standard normal distribution is the underlying distribution

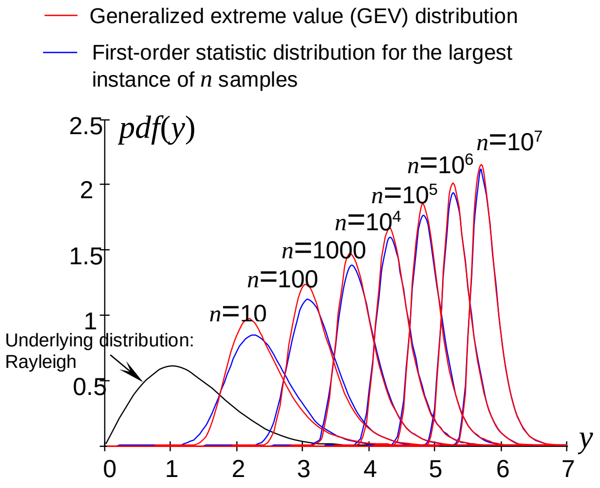

Figure 5.3.2 Conversion of the distribution of the largest value in a sample to the GEVD with an increasing number of samples where the Rayleigh distribution is the underlying distribution $\frac{x}{V_y}\exp\left(-\frac{x^2}{2V_y}\right)$: with $V_y = 1.0$

5.3.1.4 The statement in paragraph 5.3.1.3 is known as the first extreme value theorem or the Fisher-Tippett-Gnedenko theorem. It is proven by expressing a distribution of the largest value in a sample of independent identically distributed data points and showing that the limit of that distribution depends only on a small set of parameters that characterize the distribution of the sample data points.

5.3.1.5 Practical use of the GEVD involves collecting data, forming "blocks" from this data that may be considered independent, selecting the largest values from each block, fitting the GEVD with these block maxima data, and then estimating the shape (ξ), scale (σ) and location (μ) parameters.

5.3.1.6 In an effort to increase utilization of collected data (GEVD fitting uses only one data point from each block of data), it was proven that the GEVD can be approximated above a sufficiently large threshold u with a generalized Pareto distribution (GPD) as

$$\mathrm{cdf}(y) = \begin{cases} 1-\exp\left(-\frac{y-u}{\sigma}\right) & \text{for } \xi = 0 \\ 1-\left(1+\xi\frac{y-u}{\sigma}\right)^{-1/\xi} & \text{for } \xi \neq 0 \text{ and } \xi\frac{y-u}{\sigma} > -1 \\ 0 & \text{otherwise} \end{cases} \tag{5.3.5}$$

$$\mathrm{pdf}(y) = \begin{cases} \frac{1}{\sigma}\exp\left(-\frac{y-u}{\sigma}\right) & \text{for } \xi = 0 \\ \frac{1}{\sigma}\left(1+\xi\frac{y-u}{\sigma}\right)^{-(1+1/\xi)} & \text{for } \xi \neq 0 \text{ and } \xi\frac{y-u}{\sigma} > -1 \\ 0 & \text{otherwise} \end{cases} \tag{5.3.6}$$

5.3.1.7 The statement in paragraph 5.3.1.6 is known as the second extreme value theorem or the Pickands-Balkema-de Haan theorem. It is proven by consideration of the distribution in paragraph 5.3.1.3 under the condition that the random variable y exceeds the threshold u.

5.3.1.8 The practical use of the GPD involves the collection of data, selecting independent data points (de-clustering – using a similar procedure as that used in direct counting), searching for the location of the threshold, and then estimation of the shape and scale parameters from the de-clustered data points above the threshold.

5.3.1.9 The estimation of the shape and scale parameters can be performed with several methods. For example, one method (sometimes referred as the moment method) uses the mean value and variance of the GPD. For a given threshold u, the mean value E_{GPD} and the variance V_{GPD} are expressed as:

$$E_{GPD} = u + \frac{\sigma}{1-\xi} \quad \text{for } \xi < 1$$

$$V_{GPD} = \frac{\sigma^2}{(1-\xi)^2(1-2\xi)} \quad \text{for } \xi < \frac{1}{2} \qquad (5.3.7)$$

The mean value and the variance can be also estimated from the data directly. Then, the scale and shape parameters can be found, treating the formulae in this paragraph as a system of algebraic equations. Note that the mean value and variance of the GPD do not always exist, as the integrals $\int_0^\infty y \cdot \mathrm{pdf}(y)\, dy$ and $\int_0^\infty (y - E_{GPD})^2 \cdot \mathrm{pdf}(y) dy$ do not always converge for $\xi \geq 1$ and $\xi \geq 1/2$, respectively.

5.3.1.10 Another method is based on the maximum likelihood estimator (MLE). The idea of the MLE is to find such values of parameters that are "most likely" to fit the data. The data points that have been observed are the facts. At the same time, they are instances of a random variable. Because these particular values were observed, they are more likely to occur than others. This means that the probability of observing these particular values reaches a maximum when the correct parameters are used for distribution. Recall that a probability of observation of a certain value is $\mathrm{pdf}(y)dy$, where the likelihood function can be expressed through a product of these probabilities (as the data points were made independent through de-clustering). For a given threshold u, having N observations of random variable y, the likelihood is:

$$L(\xi, \sigma) = \prod_{i=1}^{N} \mathrm{pdf}(y_i; \xi, \sigma) \qquad i = 1, \dots, N \qquad (5.3.8)$$

The semicolon in the expression $\mathrm{pdf}(y_i; \xi, \sigma)$ means that a computation is carried out for the value y_i; while the scale and shape parameters values are ξ and σ, respectively. The parameters are estimated by maximizing the value of the likelihood function $L(\xi, \sigma)$. In practice this is made easier by taking the natural logarithm of the likelihood function, as the likelihoods usually are small values; also, products are transformed into sums, thus providing additional convenience and referred to as the log likelihood function:

$$\ell(\xi, \sigma) = \ln\big(L(\xi, \sigma)\big) = \sum_{i=1}^{N} \mathrm{pdf}(y_i; \xi, \sigma) \qquad (5.3.9)$$

5.3.1.11 To complete the GPD fit, a threshold needs to be found. Choosing a correct threshold is critical to ensuring the applicability of the GPD. If the threshold is too low, the fitted GPD is not an approximation of the tail, because the conditions of the second extreme value theorem have not been met. If the threshold is too high, too many data points will remain unused and the result will be less accurate. The second extreme value theorem states that the GPD can be used for an approximation of the tail of any distribution if the threshold is high enough. That means that above a certain threshold the GPD approximation must be invariant to the threshold. The simplest way to check this is to observe stabilization of the shape parameter estimate over a number of thresholds. Other methods are based on finding such a threshold that will minimize the difference between the observed data and fitted tail of the distribution.

5.3.1.12 Since the shape and scale parameters are estimated from data (which are random numbers), the estimated parameters are also random numbers. Their distribution can be approximated with a bivariate normal distribution, assuming that the deviations of the estimates from true values are caused by many different random reasons. This assumption allows the

Central Limit Theorem to be applied; this theorem is a standard technique used for the assessment of the uncertainty of estimation. The assumption of a normal distribution needs to be treated with certain caution, as it supports both negative and positive values, while the scale parameter is positive. To define the bivariate normal distribution, a covariance matrix of that bivariate normal distribution needs to be estimated. The estimation of a covariance matrix can be performed with the delta method, in which the minimization of the log likelihood function from paragraph 5.3.1.10 is considered to be a deterministic function of random variables. This function is linearized using a Taylor series expansion in which only the first-order terms are retained. A linear function of normally distributed arguments yields the following covariance matrix for the joint distribution of the scale ξ and shape σ parameter estimates:

$$C(\xi,\sigma) = \begin{pmatrix} V_\xi & r_{\xi\sigma}\sqrt{V_\xi V_\sigma} \\ r_{\xi\sigma}\sqrt{V_\xi V_\sigma} & V_\sigma \end{pmatrix} = -\begin{pmatrix} \frac{\partial^2 \ell(\xi,\sigma)}{\partial \xi^2} & \frac{\partial^2 \ell(\xi,\sigma)}{\partial \xi \partial \sigma} \\ \frac{\partial^2 \ell(\xi,\sigma)}{\partial \xi \partial \sigma} & \frac{\partial^2 \ell(\xi,\sigma)}{\partial \sigma^2} \end{pmatrix}^{-1} \qquad (5.3.10)$$

where V_ξ, V_σ are the variance of the estimated shape and scale parameters respectively; and $r_{\xi\sigma}$ is the correlation coefficient of the estimated shape and scale parameters. The confidence intervals for the shape and scale parameters can be evaluated using marginal normal distributions for the shape and scale estimates. These confidence intervals may be needed also for selecting the threshold u.

5.3.1.13 The shape parameter describes the type of tail: heavy, exponential or light, as shown in figure 5.3.3. (There is no universally accepted definition of either a heavy or light tail. Other sources may use heavy/light tail in a different context.) For example, the exponential tail ($\xi = 0$) describes the extreme values of a normal distribution. The heavy tail ($\xi > 0$) is above the exponential tail while the light tail ($\xi < 0$) is below it. Because the exponential tail is the smallest infinite tail, the light tail has a limit, which is its right boundary. The heavy tail is unbounded.

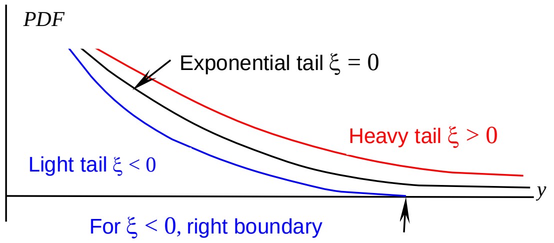

Figure 5.3.3 Types of tail

5.3.1.14 Using the GPD to extrapolate the probability of exceedance yields the conditional probability that the level of failure c has been exceeded if the threshold u has been exceeded:

$$\widehat{\mathrm{P}}(y > c) = 1 - \mathrm{cdf}(c) = \begin{cases} \exp\left(-\frac{y-u}{\hat{\sigma}}\right) & \text{for } \hat{\xi} = 0 \\ \left(1 + \frac{\hat{\xi}(y-u)}{\hat{\sigma}}\right)^{-\frac{1}{\hat{\xi}}} & \text{for } \hat{\xi} \neq 0 \text{ and } \frac{\hat{\xi}(y-u)}{\hat{\sigma}} > -1 \\ 0 & \text{for } \hat{\xi} \neq 0 \text{ and } \frac{\hat{\xi}(y-u)}{\hat{\sigma}} \leq -1 \end{cases} \qquad (5.3.11)$$

The symbol "hat" $\widehat{\ }$ indicates that the value is actually an estimate, i.e. a random quantity. The extrapolated stability failure rate of c can be estimated as:

$$\hat{r}(c) = \hat{r}(u)\widehat{\mathrm{P}}(y > c) \qquad (5.3.12)$$

where $\hat{r}(u)$ is a rate of exceedance of the threshold that is estimated with direct counting (see section 3 of this appendix for more description).

5.3.1.15 Since the extrapolated estimate is a random number, its uncertainty needs to be assessed in a form of confidence interval. For this purpose, the boundary method may be used where corresponding boundaries are multiplied. The confidence intervals of the estimated rate of exceedance of the threshold $\hat{r}(u)$ and the extrapolated estimate of the conditional probability of exceedance of the stability failure level $\hat{\mathrm{P}}(y > c)$ need to be computed for the confidence probability $\sqrt{1-\alpha}$.

$$\hat{r}_U(c; 1-\alpha) = \hat{r}_U(u; \sqrt{1-\alpha})\hat{\mathrm{P}}_U\left(y > c; \sqrt{1-\alpha}\right)$$
$$\hat{r}_L(c; 1-\alpha) = \hat{r}_L(u; \sqrt{1-\alpha})\hat{\mathrm{P}}_L\left(y > c; \sqrt{1-\alpha}\right) \quad (5.3.13)$$

The calculation of the boundaries of the confidence interval for direct counting is described in section 3 of this appendix.

5.3.1.16 The calculation of the boundaries of the confidence interval for the extrapolated estimate $\hat{\mathrm{P}}_{U,L}\left(y > c; \sqrt{1-\alpha}\right)$ can also be estimated with the boundary method using a bivariate distribution of estimates of the scale ξ and shape σ parameters, as discussed in 5.3.1.12. The application of the boundary method for the extrapolated estimate is known to produce a slightly conservative result. Alternatively, the distribution of the extrapolated estimate can be computed by treating the formula in paragraph 5.3.1.14 as a deterministic function of random arguments: the estimated scale and shape parameters bivariate distribution. Other methods exist and are described in technical literature.

5.3.1.17 The formula in paragraph 5.3.1.14 yields a zero-value result if the following conditions exist: $\hat{\xi}(c-u)/\hat{\sigma} \leq -1$; the right boundary has been encountered (see figure 5.3.1); and the failure level is beyond this right boundary. Because estimates of the scale and shape parameters are random quantities, the zero-value result is always possible. In the case of a zero-value result, the upper boundary of the confidence interval still may not be zero even if the estimate itself is zero. However, at the same time, if the upper boundary of the extrapolated estimate is zero, the result of extrapolation is zero.

5.3.1.18 The confidence interval of the extrapolated estimate in paragraph 5.3.1.15 may be large because the uncertainty is driven by two estimated parameters of the GPD distribution. At the same time, the application of the GPD is completely data-driven, i.e. it is not specific for any particular mode of failure. However, this universality may result in a large uncertainty and increase the requirements for the number of data points of the sample.

5.3.2 *Theoretical background for split-time / MPM method*

5.3.2.1 The split-time method, also known as the motion perturbation method (MPM), is one of the extrapolation methods mentioned in paragraph 3.5.5.4.1 of the Interim Guidelines. The split-time method is intended for estimating the probability of complex and rare physical phenomena in which the physics of the problem changes with the extreme response, such as that caused by stability failure in dead ship condition or pure loss of stability in stern-quartering and following waves. To account for changing physics and to reduce uncertainty, this extrapolation is performed for a specially computed metric, rather than the roll angle itself.

5.3.2.2 A stability failure of a stability-compliant ship in severe conditions cannot be observed during a simulation or set of simulations of reasonable length. Therefore, a special metric of failure likelihood is introduced. For a failure through motion to starboard, this metric is computed at the instant of up-crossing of an intermediate roll threshold u_s. The roll rate is perturbed until the failure through motion to starboard is observed, shown in figure 5.3.4. The difference between the roll rate at up-crossing $\dot{\varphi}_{U,i}$ and the roll rate when failure is observed $\dot{\varphi}_{S,i}$ is the metric, as this difference indicates "the distance to failure":

$$y_{S,i} = c + \dot{\varphi}_{U,i} - \dot{\varphi}_{S,i}\,; \quad c = 1\ \text{rad/s}\,; \quad i = 1, \ldots, N_U \qquad (5.3.14)$$

where N_U is the number of up-crossings and c is a dimensional location constant, for use with a failure threshold. The value 1 rad/s represents a level sufficiently large to be convenient in the calculations. The particular value of the dimensional location constant does affect the result of calculation.

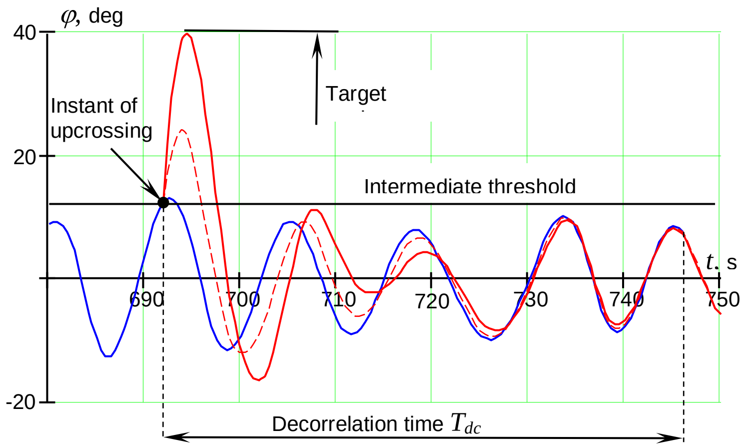

Figure 5.3.4 Motion perturbation for computing capsizing metric

5.3.2.3 Computation of the metric values, defined in paragraph 5.3.2.2 over a number of up-crossings creates a sample that can be used for extrapolation up to the level $c = 1\ \text{rad/s}$. An estimate of a conditional probability of exceedance of the level c under the condition of up-crossing of the intermediate threshold u_S: $\hat{P}(y_S \geq c |\ \varphi = u_s \cap\ \dot{\varphi} > 0\ )$ is used for the estimate of failure rate through motion to starboard $\hat{r}_S$ as

$$\hat{r}_S = \hat{r}_U \hat{P}(y_S \geq c \mid \varphi = u_s \cap\ \dot{\varphi} > 0\ ) \qquad (5.3.15)$$

where $\hat{r}_U$ is an estimate of the up-crossing rate of the intermediate threshold u_s, evaluated using direct counting; and the symbol ∩ means "and".

5.3.2.4 For failure through motion to port, the metric is computed at the instant of down-crossing of an intermediate roll threshold u_p. The roll rate is perturbed until the failure is observed. The difference between the roll rate at down-crossing $\dot{\varphi}_{D,i}$ and the roll rate when failure through motion to port is observed $\dot{\varphi}_{P,i}$ is the metric:

$$y_{P,i} = c + \left|\dot{\varphi}_{D,i}\right| - \left|\dot{\varphi}_{P,i}\right|\,; \quad c = 1\ \text{rad/s}\,; \quad i = 1, \ldots, N_D \qquad (5.3.16)$$

where N_D is the number of down-crossings.

5.3.2.5 The computation of the metric values, defined in paragraph 5.3.2.4 over a number of down-crossings creates a sample that can be used for an extrapolation up to the level $c = 1\ \text{rad/s}$. An estimate of a conditional probability of exceedance of the level c under the condition of down-crossing the intermediate threshold $\hat{P}(|y_P| \geq c \mid \varphi = u_p \cap \dot{\varphi} < 0)$ is used for the estimate of the failure rate through motion to port $\hat{r}_P$ as

$$\hat{r}_P = \hat{r}_D \hat{P}(|y_P| \geq c|\varphi = u_p \cap \dot{\varphi} < 0) \qquad (5.3.17)$$

where $\hat{r}_D$ is an estimate of the down-crossing rate of the intermediate threshold u_p, evaluated using direct counting.

5.3.2.6 The failure rate through motion to starboard or port is estimated as

$$\hat{r}_F = \hat{r}_S + \hat{r}_P \quad (5.3.18)$$

5.3.2.7 The metrics y_S and y_P are based on roll rate values at the instant of up-crossing or down-crossing. The non-linearities of roll motion, associated with roll rate are usually weak; distribution of roll rate is close to normal. Therefore, the distribution of roll rates at the instants of up-crossing or down-crossing follows closely to the Rayleigh[24] distribution and the tail is exponential.[25]

5.3.2.8 The application of the split-time/motion perturbation method does not depend on any information of non-linearity of roll motion because all the non-linear factors automatically are accounted for during the calculation of the metric. The method can handle unusual shapes of GZ curves and is capable of estimating the probability of capsizing.

5.3.3 *Description of split-time/motion perturbation method extrapolation procedure*

5.3.3.1 The input data for this extrapolation procedure is produced by a numerical simulation carried out as required by section 3.3 of the Interim Guidelines. The input data are presented in a form of a set of N_R records, each of which contains N_j instantaneous roll angles $\{\varphi_i\}_j$, roll rates $\{\dot{\varphi}_i\}_j$ (Note: The dot above the symbol means derivative with respect to time), motions and velocities in other degrees of freedom, each of which is computed at time instances $\{t_i\}_j$ using a constant time increment Δt. (An index inside the braces identifies a number of a value inside a record, an index after the braces identifies a number of a record in a set of records, N_R.)

$$\{\varphi_i\}_j;\ \ i = 1, \dots, N_j;\ \ j = 1, \dots, N_R. \quad (5.3.19)$$

5.3.3.2 The decorrelation time for roll motion, T_d, is evaluated as described in paragraphs 3.3 through 3.8 of appendix 4.

5.3.3.3 The intermediate threshold, u_s, for roll angles to starboard is established in order to achieve an average of 7 to 10 up-crossings for each 30 minutes of simulation time. The up-crossing of the threshold, u_s, is counted at each time when

$$\{\varphi_{i-1}\}_j < u_s \ and\ \{\varphi_i\}_j \geq u_s \ \ for\ u_s > 0 \quad (5.3.20)$$

5.3.3.4 The intermediate threshold, u_p, for roll angles to port is established in order to achieve an average of 7 to 10 down-crossings for each 30 minutes of simulation time. The down-crossing of the threshold, u_p, is counted at each time when

$$\{\varphi_{i-1}\}_j \geq u_p \ and\ \{\varphi_i\}_j < u_p \ \ for\ u_p < 0 \quad (5.3.21)$$

The additional steps of the procedure are described for roll angles to starboard only because the computations associated with port side roll angles are analogous.

5.3.3.5 The time instances of the up-crossings with linear interpolation are calculated using this equation:

$$\left\{T_{U,k}\right\}_j = \left\{t_{i-1} + \frac{t_i - t_{i-1}}{\varphi_i - \varphi_{i-1}}(u_s - \varphi_{i-1})\right\}_j \quad if\ \ (\varphi_{i-1} - u_s)(\varphi_i - u_s) < 0;\ \ k = 1, \dots, N_{Uj} \quad (5.3.22)$$

5.3.3.6 The value of the roll rate at the instant of each up-crossing with linear interpolation is calculated next:

[24] Leadbetter, M.R., Lindgren, G. and Rootzén, H. *Extremes and Related Properties of Random Sequences and Processes*. in: Springer Series in Statistics, Springer-Verlag, New York-Berlin, 1983.

[25] Coles, S. *An Introduction to Statistical Modeling of Extreme Values*. in: Springer Series in Statistics, Springer-Verlag London Ltd., London, 2001.

$$\left\{\dot{\varphi}_{0,k}\right\}_j = \left\{\dot{\varphi}_{i-1} + \frac{\dot{\varphi}_i - \dot{\varphi}_{i-1}}{t_i - t_{i-1}}(u_s - \varphi_{i-1})\right\}_j \quad if\ \ (\varphi_{i-1} - u_s)\,(\varphi_i - u_s) < 0;\ \ k = 1, \ldots, N_{Uj} \quad (5.3.23)$$

5.3.3.7 For each up-crossing and for all records, the evaluation of the MPM metric should be performed:

.1 the unperturbed solution is calculated starting from $\left\{T_{U,k}\right\}_j$ with the set of initial conditions $\left\{X_{0,k}\right\}_j$ at the time instance $\left\{T_{U,k}\right\}_j$. The duration of the unperturbed solution is recommended to be the largest among 30 natural roll periods, $1.5T_d$ or 300 s. The unperturbed solution should be verified to coincide with a portion of the original simulation following the up-crossing.

.2 The perturbed solution for $\dot{\varphi}_{p,k} = \dot{\varphi}_{0,k} + m\Delta\dot{\varphi},\ m = 1, 2, \ldots$ is calculated while keeping all other initial conditions from the set $\left\{X_{0,k}\right\}_j$. The values for $\Delta\dot{\varphi}$ that should be assumed are in the range of 0.001…0.0001 rad/s. The maximum angle achieved in the perturbed solution during the decorrelation time T_d should be recorded $\left\{\left(\varphi_{max,m}\right)_k\right\}_j$.

.3 Once the $\left\{\left(\varphi_{max,m}\right)_k\right\}_j \geq 40^0$ (or whatever roll angle is taken to be critical) is observed for $\dot{\varphi}_{p,k} = \dot{\varphi}_{0,k} + m\Delta\dot{\varphi}$, the critical roll rate is computed as

$$\dot{\varphi}_{C,k} = \dot{\varphi}_{0,k} + (m-1)\Delta\dot{\varphi}. \quad (5.3.24)$$

.4 The metric value for the k-th up-crossing at the j-th record is computed as

$$y_k = c + \dot{\varphi}_{0,k} - \dot{\varphi}_{C,k}\,;\ \ c = 1.0\,rad/s. \quad (5.3.25)$$

5.3.3.8 For all the metric values computed for each record y_k, a de-clustering is carried out using the following steps:

.1 The cluster is defined as a group of the metric values, y_k, corresponding to up-crossings that have occurred in time instances that are closer to each other than the decorrelation time T_d: $\{y_k\}_{k=b_q}^{k=f_q}, q = 1, 2, \ldots$, where b_q and f_q are indices of the beginning and the end of q-th cluster.

.2 The de-clustered values of the metric are determined as the maximum value within each cluster, $y1_q = \max\left(\{y_k\}_{k=b_q}^{k=f_q}\right)$.

5.3.3.9 The de-clustered values of the metric, $y1_q$, are considered independent, x_n, and are presented in a single record for fitting of an exponential tail for the distribution as explained in paragraph 5.3.2.7.[26]

$$x_n = \left\{y1_q\right\}_j; n = 1, \ldots, N_x \quad (5.3.26)$$

[26] Belenky, V., Weems, K., Pipiras, V. and Glotzer, D. (2018). *Extreme-value properties of the split-time metric*, Proc. 13th Intl. Conf. on Stability of Ships and Ocean Vehicles STAB 2018, Kobe, Japan.

5.3.3.10 The prediction error technique[27] is available for automatically finding the beginning of the distribution tail. Certain caution should be exercised while using automatic threshold finding algorithms, in general, because the sample data sets are subjects to random variation.

5.3.3.11 To use the prediction error technique, the metric values, x_n, are sorted in descending order

$$x1_n = \mathrm{sort}_{\mathrm{desc}}(x_n) \tag{5.3.27}$$

5.3.3.12 A starting index and a final index for the search for the beginning of the distribution tail, should be established. The interval for automatic search of the threshold should contain sufficiently large values for invoking extreme value properties. Also, there should be a sufficient amount of these large values for statistical methods to be numerically stable. For the typical data set, produced by MPM for moderate-to-high seas states, 2% largest values of the metric usually meet this requirement. However, if the number of data points fall significantly below 40, calculation of the error function may encounter difficulties. For the typical moderate-to-high data set, it is not reasonable to expect that extreme value properties can be used for the data below upper 20%. The range for automatic threshold search is initial set as

$$k_{beg} = \min(40, 0.02N_x); \quad k_{fin} = 0.2N_x \tag{5.3.28}$$

The range may be adjusted if the data set significantly differs from recommendations in 5.3.3.3.

5.3.3.13 The distribution tail of the MPM metric is approximated with conditional exponential distribution (exponential tail), see justification in paragraph 5.3.2.7. The pdf of the exponential tail is expressed as $(1/\beta)\exp(-x/\beta)$, where the scale parameter β equals to the mean value.

An estimate for the exponential tail scale parameter, $\hat{\beta}_k$, for the tail beginning at $x1_k$, is calculated:

$$\hat{\beta}_k = \frac{1}{k}\sum_{n=1}^{k}(x1_n - x1_k); \;\; k = k_{beg}, \ldots, k_{fin} \tag{5.3.29}$$

5.3.3.14 The determination of the beginning of the distribution tail is essentially finding how large a value should be to use extreme properties for practical calculation. When these properties can be used, approximated distribution tail fits well with the data. The prediction error technique uses the difference in natural logarithms of quantiles (inverse function for CDF). Averaged square of this difference lead to formulation of the error function for a particular threshold.

The error function for each candidate beginning of the distribution tail, $\hat{\Gamma}(k)$, is calculated:

$$\hat{\Gamma}(k) = \frac{1}{\hat{\beta}_k^2}\sum_{n=1}^{k}\left(\frac{k+1}{n} - 1\right)^{-1} \left(x1_n - x1_k + \hat{\beta}_k \log\left(\frac{n}{k+1}\right)\right)^2 + \frac{2}{k}\sum_{n=1}^{k}\left(\frac{k+1}{n} - 1\right)^{-1}\left(\log\left(\frac{n}{k+1}\right)\right)^2 - 1 \tag{5.3.30}$$

5.3.3.15 The beginning of the distribution tail, w, is the value of the metric value that corresponds to the index, $k1$, that corresponds to the minimum value of the error function, $\hat{\Gamma}(k)$.

$$k1 = k\left(\hat{\Gamma}(k) \to min\right); \;\; w = x1_{k1} \tag{5.3.31}$$

5.3.3.16 The values of the MPM metric are calculated at the instants of the up-crossing of the intermediate threshold u_s. Some of these values exceed the beginning of the distribution tail for the metric. The estimate of a rate of exceedance of the beginning of the distribution tail is

27 Mager, J., *Automatic threshold selection of the peaks over threshold method*, Master's Thesis, Technische Universitat Munchen, 2015.

used instead of the estimate of up-crossing of the intermediate threshold u_s , in paragraph 5.3.2.3 and, respectively:

$$\hat{r}_U = \frac{k1}{\Delta t \sum_{j=1}^{N_R} N_j} \tag{5.3.32}$$

5.3.3.17 The extrapolated estimate of the failure rate through the starboard heel angles is calculated using the exponential tail with the beginning at w (conditional exponential distribution for the random variables exceeding w):

$$\hat{r}_S = \hat{r}_U \exp\left(-(\mathrm{c} - w)/\hat{\beta}_{k1}\right) \tag{5.3.33}$$

5.3.3.18 The estimate of scale parameter, $\hat{\beta}_{k1}$ is essentially an estimate of a mean value (see 5.3.3.13). Given a sample $z_i; i = 1 \ldots N$, the standard deviation $\hat{\sigma}_E$ of a mean value estimate $\hat{E} = (1/N)\sum_{i=1}^{N} z_i$ can be found with the estimate of standard deviation $\hat{\sigma} = \left((1/N)\sum_{i=1}^{N}\left(z_i - \hat{E}\right)^2\right)^{1/2}$ as $\hat{\sigma}_E = \hat{\sigma}/\sqrt{N}$. The estimate of the standard deviation, $\hat{\sigma}_\beta$, of the scale parameter estimate, $\hat{\beta}_{k1}$, is calculated:

$$\hat{\sigma}_\beta = \frac{1}{k1}\sqrt{\sum_{n=1}^{k1}(x1_n - w)^2 - k1^2 \hat{\beta}_k^2} \tag{5.3.34}$$

5.3.3.19 Then, the estimate of the standard deviation of the rate of up-crossing through the beginning of the distribution tail, $\hat{r}_U$, is calculated as:

$$\hat{\sigma}_U = \frac{\sqrt{k1(1-\hat{r}_U \Delta t)}}{\Delta t \sum_{j=1}^{N_R} N_j} \approx \frac{\sqrt{k1}}{\Delta t \sum_{j=1}^{N_R} N_j} \tag{5.3.35}$$

5.3.3.20 A half non-dimensional confidence interval, $K_{\alpha 1}$, is calculated using the standard function for a normal standard quantile Q_N (i.e., a standard deviation equal to 1 with a mean value equal to zero) with a confidence probability 1 - α:

$$K_{\alpha 1} = Q_N\left(\frac{1+\sqrt{1-\alpha}}{2}\right) \tag{5.3.36}$$

5.3.3.21 The lower and upper boundaries of the confidence interval of the extrapolated estimate, $\hat{r}_{S,low}$ and $\hat{r}_{S,up}$, respectively, are calculated as:

$$\hat{r}_{S,low} = (\hat{r}_U - K_{\alpha 1}\hat{\sigma}_U)\exp\left(-(\mathrm{c} - w)/\left(\hat{\gamma}_{k1} - K_{\alpha 1}\hat{\sigma}_\beta\right)\right) \tag{5.3.37}$$

$$\hat{r}_{S,up} = (\hat{r}_U + K_{\alpha 1}\hat{\sigma}_U)\exp\left(-(\mathrm{c} - w)/\left(\hat{\gamma}_{k1} + K_{\alpha 1}\hat{\sigma}_\beta\right)\right) \tag{5.3.38}$$

5.3.3.22 The procedure for the estimation of the extrapolated failure rate with port roll angles differs only in the formula for the metric:

$$y_{P,i} = c + \left|\dot{\varphi}_{D,i}\right| - \left|\dot{\varphi}_{P,i}\right|;\;\; c = 1\ \mathrm{rad/s};\;\; i = 1, \ldots, N_D\ ] \tag{5.3.39}$$

5.3.3.23 The split-time/motion perturbation method can be applied for the excessive acceleration failure mode. The metric for the excessive acceleration failure mode is formulated on condition of exceedance of the target lateral acceleration.

5.3.4 *Example of application*

5.3.4.1 The extrapolation procedure is demonstrated for the ONR tumblehome topside ship. Table 5.3.1 shows the principal dimensions and environmental parameters for this design. To demonstrate the capabilities of the split-time method, capsizing event through the starboard was taken as a target for extrapolation. The target of extrapolation makes difference only for the metric calculation.

Table 5.3.1 Principal dimensions and environmental parameters			
Length BP, m	154	Significant wave height, m	9
Breadth, m	18	Mean zero-crossing period, s	14
Draught, m	5.5	Speed, knots	6
KG, m	7.5	Relative wave heading, deg	45

5.3.4.2 The extrapolation data sample consists of 86 half-hour records. The intermediate threshold was chosen at 12 degrees, resulting in 569 up-crossing events over 86 records. The de-clusterizing procedure produced 369 independent values of the metric, ranging from 0.597 rad/s to 0.993 rad/s.

5.3.4.3 For the choice of the threshold with the prediction error criterion, the mean squares prediction error function is shown in figure 5.3.5; other intermediate numerical results are given in table 5.3.2, and the final extrapolation results are shown in figure 5.3.6.

Table 5.3.2 Intermediate results of fitting exponential tail

Secondary threshold, u, rad/s	0.77
Available points	30
Parameter $\hat{\beta}$ rad/s	0.066
Variance of $\hat{\beta}$, (rad/s)^2	1.041e-4
Conditional extrapolated estimate $\widehat{P}(y > c)$	0.03
Rate exceedance of secondary threshold $\hat{r}_w$, s^{-1}	1.971e-4
Failure rate $\hat{r}$, s^{-1}	5.936e-6

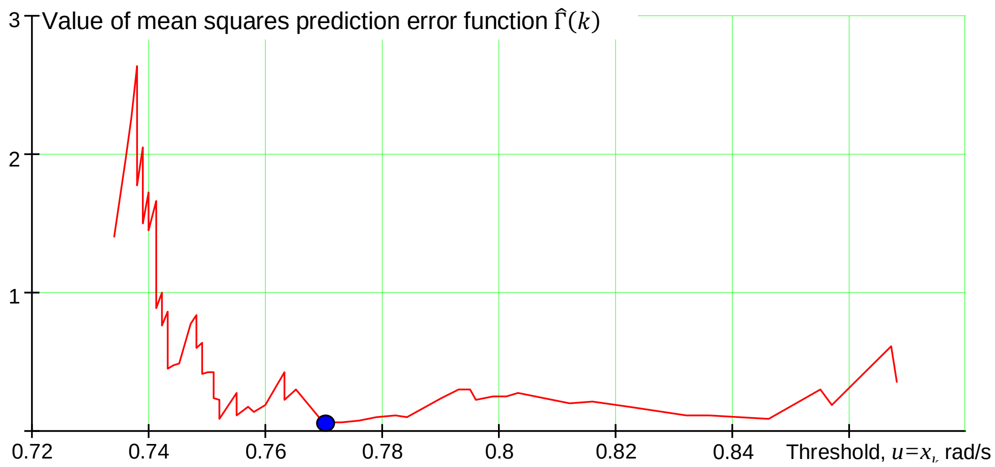

Figure 5.3.5 Mean squares prediction error function

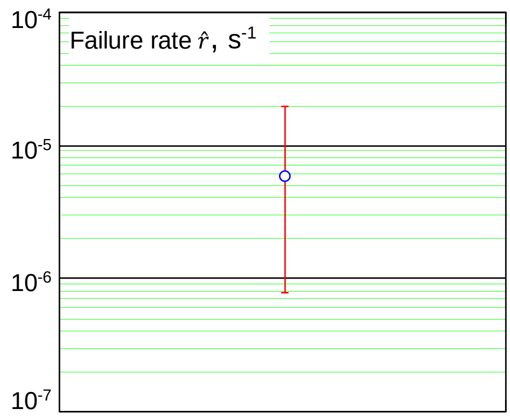

Figure 5.3.6 Results of extrapolation for exceedance of 40 degrees

5.4 Envelope peaks over threshold method for pure loss of stability and dead ship condition

5.4.1 *Theoretical background*

5.4.1.1 This section provides essential information concerning application and validation of the envelope peaks over threshold (EPOT) method, one of the statistical extrapolation methods included in the Interim Guidelines.

5.4.1.2 The stability failure modes for which the EPOT method is applicable include the dead ship condition and pure loss of stability. The applicability of the EPOT method may be extended to the parametric roll failure mode after adjustment of the de-clustering procedure and a proper statistical validation. EPOT is, in principle, also applicable to the excessive acceleration stability failure mode.

5.4.1.3 The basic idea of the peaks over threshold (POT) approach is to fit a generalized Pareto distribution (GPD) to the observed data above a particular threshold value of the response (e.g. above a certain roll angle). This idea is extended in this method as described below to become the EPOT method.
The mathematical background of the method is the second extreme value theorem, which states that the tail of an extreme value distribution can be approximated with a GPD above a "large enough" value.[28] See section 5.3.0 for the theoretical background for this method. A key feature of the POT extrapolation is that it can capture the non-linearity of the large amplitude response, such as that caused by the changes in the restoring moment in large roll angles and in waves.

5.4.1.4 However, the standard POT method is only applicable to independent data. The roll motions of a ship are not independent because they are correlated through the ship's inertia, the wave excitation, and the "memory" in the hydrodynamic forces. Therefore, the application of POT requires an extraction of independent points (or "de-clustering") from the roll motion data time history. Fitting an envelope to the roll motion time history, Figure 5.4.1, is a convenient way to de-cluster the data if the peaks of the envelope of the roll response are sufficiently far from each other to provide the necessary independence. The use of an envelope to de-cluster the roll motion provides the additional letter in the acronym of the method, so POT becomes EPOT – envelope peaks over threshold. An additional check may be necessary for

[28] Pickands, J. *Statistical inference using extreme order statistics,* The Annals of Statistics, Vol. 3, No.1, pp. 119-131, 1975.

application to parametric roll motion because the decorrelation time may be large. The time duration between the peaks of the envelope should not be less than the decorrelation time, which is estimated as described in section 3.8.

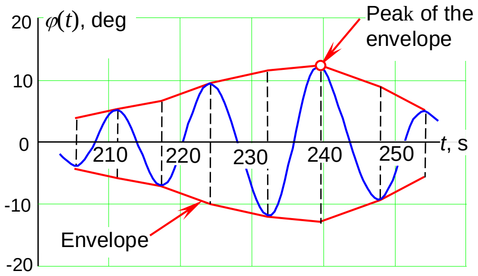

Figure 5.4.1 De-clustering using envelope

5.4.1.5 The uncertainty of the extrapolated estimate can be decreased by inclusion of physical considerations in a data-driven model. In particular, this can be done by assuming the type of the tail, based on the physics of non-linear roll motion as explained in paragraphs 5.4.1.6 - 5.4.1.14

5.4.1.6 The GZ curve of most ships features both a maximum GZ value near the midpoint of the range of stability and an angle of vanishing stability at which unstable equilibria appear. These GZ curve characteristics lead to a heavy tail after the angle of the maximum GZ curve, which switches to a light tail as the roll angle approaches and is close to the angle of vanishing stability. Figure 5.4.2[29] shows such a probability distribution function (pdf) that is computed for a dynamical system with piecewise linear restoring (the piecewise linear approximation of the GZ curve allows a closed-form solution for the tail of the distribution of the peaks and the instantaneous values of the roll angle).

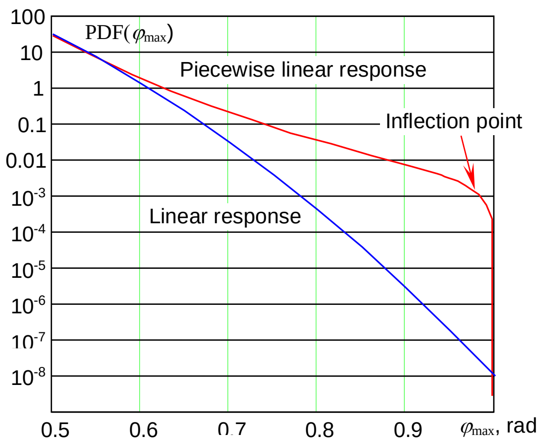

Figure 5.4.2 PDFs of peaks of linear response and piecewise linear restoring response

5.4.1.7 The roll angles associated with dynamic stability failures, are usually located around and beyond the angle of the maximum of the GZ curve. Therefore, the assumption of a heavy tail appears appropriate for extrapolation problems associated with dynamical stability failures. When the shape parameter indicates a heavy tail, $\xi > 0$, and threshold value $u = \sigma/\xi$, then the GPD is equivalent to a Pareto distribution with scale $y_m = u = \sigma/\xi$ and shape $\gamma = 1/\xi$:

$$\mathrm{pdf}(y) = \gamma \frac{y_m^\gamma}{y^{\gamma+1}} = \gamma \frac{u^\gamma}{y^{\gamma+1}} \qquad \mathrm{cdf}(y) = 1 - \left(\frac{y_m}{y}\right)^\gamma = 1 - \left(\frac{u}{y}\right)^\gamma \qquad (5.4.1)$$

Note that the Pareto distribution is a natural logarithm of an exponential distribution.

29 Belenky, V., Glotzer, D., Pipiras, V. and Sapsis, T. *Distribution tail structure and extreme value analysis of constrained piecewise linear oscillators*. Probabilistic Engineering Mechanics Vol. 57, pp. 1-13, 2019.

5.4.1.8 The conditional probability of exceedance of a target value y associated with dynamic stability failure is expressed as:

$$P(Y > y \mid Y > u) = (u/y)^{\gamma} = (y/u)^{-1/\xi} \qquad (5.4.2)$$

5.4.1.9 In equation (5.4.2), the threshold u (paragraph 5.4.1.8) is determined from the applicability considerations so that only one parameter needs to be fitted. Decreasing the number of parameters from two (in case the GPD is used) to one decreases the statistical uncertainty.

5.4.1.10 Caution should be exercised when approximating the tail for the excessive acceleration failure mode in the following areas:

.1 When using the GPD, a negative value of the shape parameter may indicate excessive uncertainty caused by insufficient data.[30]

.2 Using the Pareto distribution contains the assumption that the roll motions are in the vicinity of roll angles at which the GZ curve is at its maximum value.

.3 An exponential tail approximation (that uses the prediction error technique, see 5.3.3) may be used when roll angles are not expected to be the vicinity of maximum GZ curve.

5.4.2 *Description of the EPOT extrapolation procedure*

5.4.2.1 The input data for this extrapolation procedure is produced by a numerical simulation that is carried out as required in section 3.3 of the Interim Guidelines. The input data are presented in a form of a set of N_R records (referred to as an Ensemble), each of which contains N_j instantaneous roll angles $\{\varphi_i\}_j$, computed at time instances $\{t_i\}_j$ using a constant time increment Δt (a symbol given in braces identifies a record, an index inside the braces identifies a number of a value inside a record, and an index after the braces identifies a number of a record in a set of records):

$$\{\varphi_i\}_j;\ \ i = 1, \dots, N_j;\ \ j = 1, \dots, N_R. \qquad (5.4.3)$$

5.4.2.2 The ensemble-averaged mean value ($\hat{E}_{\varphi a}$) is estimated as:

$$\hat{E}_{\varphi a} = \frac{\sum_{j=1}^{N_R} \sum_{i=1}^{N_j} \{\varphi_i\}_j}{\sum_{j=1}^{N_R} N_j} \qquad (5.4.4)$$

5.4.2.3 The instantaneous roll angles of a set of roll records ($\{\varphi_{C,i}\}_j$) is centred relative to the estimate of the ensemble-averaged mean value:

$$\{\varphi_{C,i}\}_j = \{\varphi_i\}_j - \hat{E}_{\varphi a} \qquad (5.4.5)$$

5.4.2.4 The zero-crossing time instances ($\{T_{Z,q}\}_j$) are found with linear interpolation, for each record in the set, $N_{Z,j}$:

$$\{T_{Z,q}\}_j = \left\{ t_{i-1} - \frac{t_i - t_{i-1}}{\varphi_{Ci} - \varphi_{Ci-1}} \varphi_{Ci-1} \right\}_j \quad if \quad \varphi_{Ci-1}\varphi_{Ci} < 0;\ \ q = 1, \dots N_{Z,j} \qquad (5.4.6)$$

30 Pipiras, V. *Pitfalls of data-driven peaks-over-threshold analysis: Perspectives from extreme ship motion.* Probabilistic Engineering Mechanics, Vol. 60 103053 doi.org/10.1016/j.probengmech.2020.103053, 2020.

5.4.2.5 The values of an envelope are peaks that exist between two zero-crossing time instances ($\{\varphi_{e,q}\}_j$). These values are found as the maxima of the absolute values of the instantaneous roll angles between two adjacent zero-crossing time instances:

$$\{\varphi_{e,q}\}_j = \{\max(|\varphi_{Ci}|)\}_j \quad if \ \{T_{Z,q} < t_i \leq T_{Z,q+1}\}_j; \ q = 1, \ldots N_{Z,j} - 1 \tag{5.4.7}$$

5.4.2.6 The time instances, corresponding to the values of the envelope, ($\{t_{e,q}\}_j$), are recorded:

$$\{t_{e,q}\}_j; \ q = 1, \ldots N_{Z,j} - 1 \tag{5.4.8}$$

5.4.2.7 The ensemble-averaged mean value of the envelope ($\hat{E}_{\varphi,e}$) is estimated as:

$$\hat{E}_{\varphi,e} = \frac{\sum_{j=1}^{N_R}\sum_{q=1}^{N_{Zj}-1}\{\varphi_{e,q}\}_j}{\sum_{j=1}^{N_R}(N_{Zj}-1)} \tag{5.4.9}$$

5.4.2.8 The time at which the envelope crosses (or intersects) the ensemble-averaged mean value of the envelope, $\hat{E}_{\varphi,e}$, is called an envelope mean-crossing time instance $\{T_{e,m}\}_j$. and each record *j* contains certain number $N_{E,j}$ of such time instances. The values of these time instances $\{T_{e,m}\}_j$ are determined with linear interpolation for each of the $N_{E,j}$ time instances in each record *j* :

$$\{T_{e,m}\}_j = \left\{t_{e,q-1} + \frac{t_{e,q}-t_{e,q-1}}{\varphi_{e,q}-\varphi_{e,q-1}}\left(\hat{E}_{\varphi,e} - \varphi_{e,q-1}\right)\right\}_j; \ m = 1, \ldots, N_{E,j} \tag{5.4.10}$$

5.4.2.9 The values of the mean-crossing peaks of the envelope ($\{\varphi_{p,m}\}_j$) are found as the maxima of the envelope between two adjacent mean-crossing time instances, exceeding the estimated mean of the envelope (values of the envelope below $\hat{E}_{\varphi,e}$ are not considered)

$$\{\varphi_{p,m}\}_j = \{\max(\varphi_{e,q})\}_j \quad if \ \{T_{e,m} < T_{e,q} \leq T_{e,m+1} \text{ and } \varphi_{e,q} > \hat{E}_{\varphi,e}\}_j; \ m = 1, \ldots N_{E,j} - 1 \tag{5.4.11}$$

5.4.2.10 The peaks of the envelope are independent. They are presented in a single record and sorted in descending order to enable the use of the prediction error technique for threshold selection:[31]

$$Y_n = \mathrm{sort}_{\mathrm{desc}}\{\varphi_{p,m}\}_j; n = 1, \ldots, N_Y; \ N_Y = \sum_{j=1}^{N_R}(N_{E,j} - 1) \tag{5.4.12}$$

5.4.2.11 To search for the threshold, a beginning index (k_{beg}) and a final index (k_{fin}) should be established. The interval for automatic search of the threshold should contain sufficiently large values for invoking extreme value properties. Also, there should be sufficient amount of these large values for statistical methods to be numerically stable. For the typical data set, produced for EPOT in moderate-to-high seas states, the 2% largest envelope peak values usually meet this requirement. However, if the number of data points fall significantly below 40, the calculation of the error function may encounter difficulties. Experience has shown that, for the typical moderate-to-high seas data set, extreme value properties should not be used for the data below the upper 20%. The range for the automatic threshold search is initially set as:

$$k_{beg} = \min(40, 0{,}02N_Y); \quad k_{fin} = 0.2N_Y \tag{5.4.13}$$

5.4.2.12 The Hill's estimator for the shape parameter, ξ_k, is computed for each threshold, *k*:

$$\hat{\xi}_k = \frac{1}{k}\sum_{n=1}^{k}\log(Y_n/Y_k); \quad k = k_{beg}, \ldots, k_{fin} \tag{5.4.14}$$

---

31 Mager, J. *Automatic threshold selection of the peaks over threshold method*. Master's Thesis, Technische Universitat Munchen, 2015.

Hill's estimator is a standard technique for the estimation of the shape parameter for the Pareto distribution. Hill's estimator is based on the relation between the Pareto and exponential distributions (see paragraph 5.4.1.7). The estimate is essentially an average of the natural logarithm of data above the threshold (this can be compared to equation (5.3.15) in paragraph 5.3.3.14).

5.4.2.13 The determination of the beginning of the distribution tail is essentially finding the location at which a large value should be in order to use extreme properties of the distribution for practical calculation. When these properties can be used, the approximated distribution tail fits well with the data. The prediction error technique uses the difference in natural logarithms of quantiles (the inverse function for the cumulative function distribution (*cfd*). The averaged square of this difference leads to formulation of the error function for a particular threshold. The error function ($\hat{\Gamma}(k)$), is computed as:

$$\hat{\Gamma}(k) = \frac{1}{\hat{\xi}_k{}^2} \sum_{n=1}^{k} \frac{\left(\log(Y_{n-1}/Y_{k-1}) + \hat{\xi}_k \log(n/(k+1))\right)^2}{\left(\sum_{j=n}^{k} j^{-2}\right)} + \frac{2}{k} \sum_{n=1}^{k} \frac{(\log(n/(k+1)))^2}{\left(\sum_{j=n}^{k} j^{-2}\right)} - 1 \qquad (5.4.15)$$

5.4.2.14 The index, ($k1$), that corresponds to the minimum of the error function, ($\hat{\Gamma}(k)$), and the threshold, (k), corresponding to this index are determined as:

$$k1 = k\left(\hat{\Gamma}(k) \to min\right); \quad u = Y_{k1} \qquad (5.4.16)$$

5.4.2.15 The estimate of a rate of exceedance ($\hat{r}_u$) over the threshold, u, is calculated as*:*

$$\hat{r}_u = \frac{k1}{\Delta t \sum_{j=1}^{N_R} N_j} \qquad (5.4.17)$$

5.4.2.16 The extrapolated estimate of exceedance rate ($\hat{r}_c$) of the target value, c, is then calculated as:

$$\hat{r}_c = \hat{r}_u (c/u)^{-1/\hat{\xi}_{k1}} \qquad (5.4.18)$$

5.4.2.17 The estimate of the standard deviation of rate ($\hat{\sigma}_u$) of the exceedance, $\hat{r}_u$, is calculated as:

$$\hat{\sigma}_u = \frac{\sqrt{k1(1-\hat{r}_u \Delta t)}}{\Delta t \sum_{j=1}^{N_R} N_j} \approx \frac{\sqrt{k1}}{\Delta t \sum_{j=1}^{N_R} N_j} \qquad (5.4.19)$$

5.4.2.18 The estimate of the standard deviation ($\hat{\sigma}_\xi$) of the shape parameter, $\hat{\xi}_{k1}$, is calculated as a standard deviation for a mean value estimate (since Hill's estimator is a mean value of natural logarithms of data points, see paragraph 5.4.2.12):

$$\hat{\sigma}_\xi = \hat{\xi}_{k1}/\sqrt{k1} \qquad (5.4.20)$$

5.4.2.19 Because EPOT combines two estimates, each of which is computed with its confidence interval, the final result should be presented with the confidence probability $1-\alpha = 0.95$ and, for this reason, each component estimate is computed with the confidence probability $\sqrt{1-\alpha}$ as:

$$K_{\alpha 1} = Q_N\left(\frac{1+\sqrt{1-\alpha}}{2}\right) \qquad (5.4.21)$$

5.4.2.20 The boundaries of the confidence interval of the extrapolated estimate, ($\hat{r}_{c,low}$ and $\hat{r}_{c,up}$, respectively) are calculated as:

$$\hat{r}_{c,low} = (\hat{r}_u - K_{\alpha 1}\hat{\sigma}_u)(c/u)^{-1/\left(\hat{\xi}_{k1} - K_{\alpha 1}\hat{\sigma}_\xi\right)} \qquad (5.4.22)$$

$$\hat{r}_{c,up} = (\hat{r}_u + K_{\alpha 1}\hat{\sigma}_u)(c/u)^{-1/\left(\hat{\xi}_{k1} + K_{\alpha 1}\hat{\sigma}_\xi\right)} \qquad (5.4.23)$$

5.4.3 *Description of the extrapolation procedure and an example of its application*

5.4.3.1 The extrapolation procedure is demonstrated for the ONR tumblehome topside ship. Table 5.3.1 shows the principal dimensions and environmental parameters of this ship design.

5.4.3.2 The extrapolation data sample consists of 86 half-hour records, produced with a volume-based simulation tool. A portion of a sample record is shown in figure 5.4.3 and a fragment of the envelope for the de-clustering procedure is shown in figure 5.4.4. The objective is to estimate an exceedance rate for a roll angle of 40 degrees as given by the Interim Guidelines.

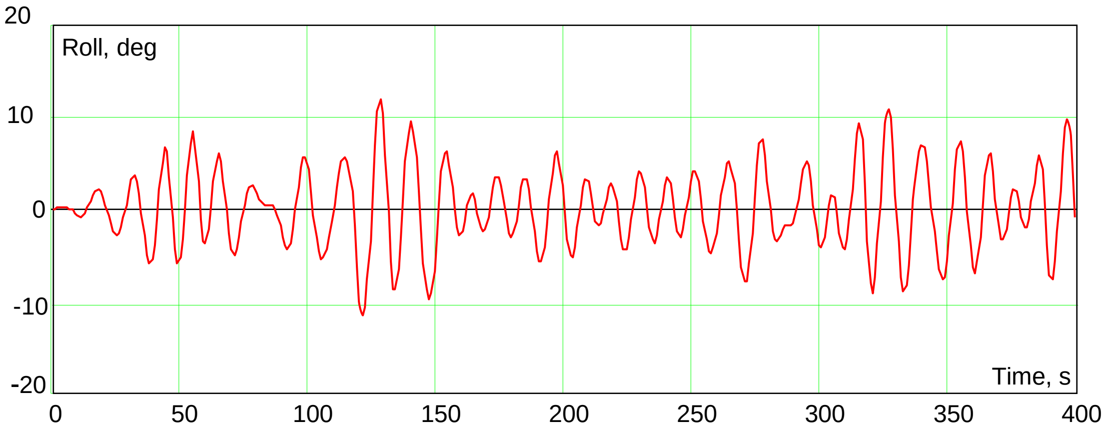

Figure 5.4.3 An example of roll record

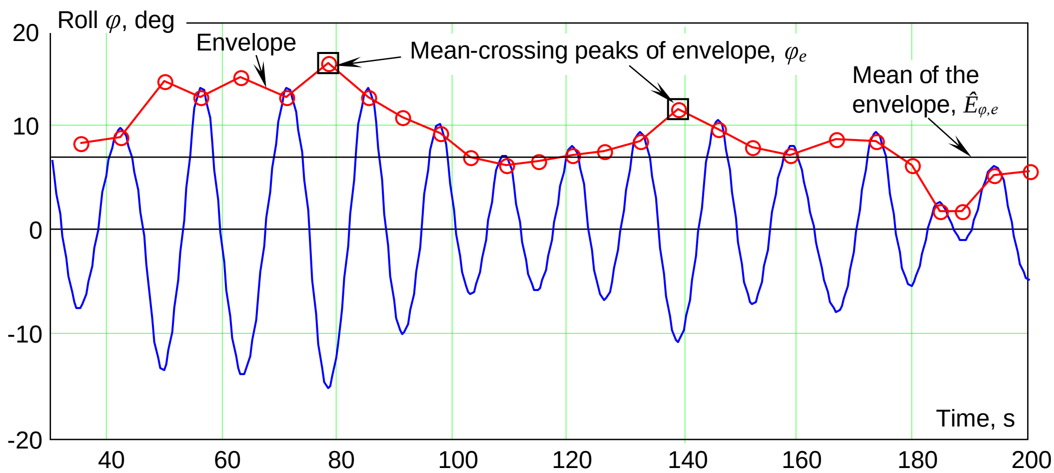

Figure 5.4.4 A fragment of the envelope and the procedure of de-clustering with mean-crossing peaks

5.4.3.3 The total number of data points after de-clustering is determined: $N_Y = 2619$. Per paragraph 5.4.2.11, the beginning and final index are evaluated as:

$$k_{beg} = \min(40, 0{,}02N_Y) = 40\,; \quad k_{fin} = 0.2N_Y = 522 \tag{5.4.24}$$

5.4.3.4 The threshold u is found by an index that corresponds to a minimum of the mean squared prediction error function that is computed per paragraph 5.4.2.13 and shown in figure 5.4.5:

Figure 5.4.5 The mean squares prediction error function

5.4.3.5 As described in paragraph 5.4.2.14, the index $k1$ corresponding to a minimum of the error function $\hat{\Gamma}(k)$ and the threshold are calculated as:

$$k1 = k\left(\hat{\Gamma}(k) \to min\right) = 446; \quad u = Y_{k1} = 17.37^0 \tag{5.4.25}$$

5.4.3.6 Per paragraph 5.4.2.15, the estimate of a rate of exceedance ($\hat{r}_u$) over the threshold, u, is calculated as:

$$\hat{r}_u = \frac{k1}{\Delta t \sum_{j=1}^{N_R} N_j} = 4.99 \cdot 10^{-4}\ 1/s \tag{5.4.26}$$

5.4.3.7 Per paragraph 5.4.2.12, the Hill estimator for the shape parameter, ξ_{k1}, is computed for the selected threshold:

$$\hat{\xi}_{k1} = \frac{1}{k1} \sum_{n=1}^{k1} \log(Y_n / Y_{k1}) = 0.161 \tag{5.4.27}$$

5.4.3.8 Per paragraph 5.4.2.16, the extrapolated estimate of the exceedance rate ($\hat{r}_c$) of the target value, $c = 40^0$, is then calculated as:

$$\hat{r}_c = \hat{r}_u (c/u)^{-1/\hat{\xi}_{k1}} = 2.76 \cdot 10^{-6}\ 1/s \tag{5.4.28}$$

5.4.3.9 Per paragraph 5.4.2.17, the estimate of the standard deviation of the rate ($\hat{\sigma}_u$) of the exceedance, $\hat{r}_u$, is calculated as:

$$\hat{\sigma}_u = \frac{\sqrt{k1(1-\hat{r}_u \Delta t)}}{\Delta t \sum_{j=1}^{N_R} N_j} \approx \frac{\sqrt{k1}}{\Delta t \sum_{j=1}^{N_R} N_j} = 5.73 \cdot 10^{-5} 1/s \tag{5.4.29}$$

5.4.3.10 Per paragraph 5.4.2.18, the estimate of the standard deviation ($\hat{\sigma}_\xi$) of the shape parameter, $\hat{\xi}_{k1}$, is calculated as:

$$\hat{\sigma}_\xi = \frac{\hat{\xi}_{k1}}{\sqrt{k1}} = 0.018 \tag{5.4.30}$$

5.4.3.11 As EPOT combines two estimates, each is computed with its confidence interval. In order to present the final result with the confidence probability $1 - \alpha 1 = \sqrt{1-\alpha} = 0.975$, each component estimate is computed with the confidence probability $1 - \alpha 1 = \sqrt{1-\alpha} = 0.975$. Per paragraph 5.4.2.19, a one-half non-dimensional confidence interval ($K_{\alpha 1}$) that uses a standard function for a normal standard quantile Q_N (i.e. a standard deviation = 1, with a zero mean) with confidence probability, $\alpha 1 = 0.975$, is calculated as:

$$K_{\alpha 1} = Q_N\left(\frac{1+\sqrt{1-\alpha}}{2}\right) = 2.236 \tag{5.4.31}$$

5.4.3.12 Per paragraph 5.4.2.20, the boundaries of the confidence interval of the extrapolated estimate, ($\hat{\lambda}_{c,low}$ and $\hat{\lambda}_{c,up}$, respectively) are calculated as:

$$\hat{r}_{c,low} = (\hat{r}_u - K_{\alpha 1}\hat{\sigma}_u)(c/u)^{-1/(\hat{\xi}_{k1} - K_{\alpha 1}\hat{\sigma}_\xi)} = 4.54 \cdot 10^{-7}\ 1/s \tag{5.4.32}$$

$$\hat{r}_{c,up} = (\hat{r}_u + K_{\alpha 1}\hat{\sigma}_u)(c/u)^{-1/(\hat{\xi}_{k1} + K_{\alpha 1}\hat{\sigma}_\xi)} = 9.00 \cdot 10^{-6}\ 1/s \tag{5.4.33}$$

The result of extrapolation for $c = 40^0$ with its confidence interval is shown in figure 5.4.6.

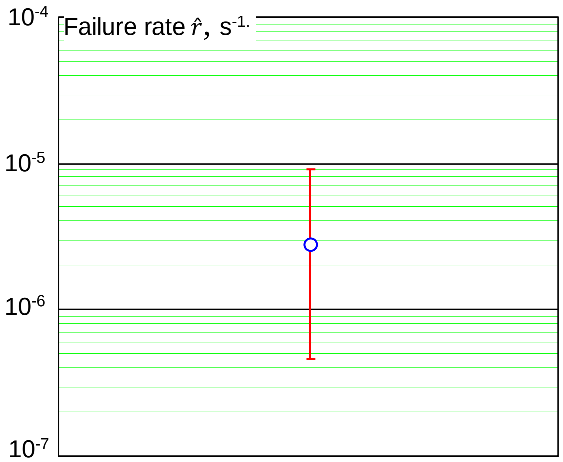

Figure 5.4.6 The results of an extrapolation for a target roll angle of 40 degrees

5.4.4 *Statistical validation*

5.4.4.1 Limited statistical validation of EPOT was carried out following the recommendations of paragraph 3.5.6 of the Interim Guidelines. According to the recommendation in paragraph 3.5.6.3, a reduced order mathematical model (volume-based 3-DOF calculations) was applied. This fast code creates very large samples of data in which large roll angles associated with rare failures are observable. The observations estimate a "true value" from direct counting.

5.4.4.2 A series of validation data sets was computed for the ONR tumblehome configuration with KG = 7.5 m, GM = 2.2 m. Simulations were performed with independent pseudo-random realizations of a seaway with a Bretschneider spectrum at a significant wave height 9 m, modal period 15 s and ship speed 6 knots. Table 5.4.1 shows other simulations parameters. Several maximum roll angles defining stability failure angles are examined.

Table 5.4.1 "True value" calculations

Heading, deg.	Total number of 30-min records	Number of targets	Largest target	Number of exceedances of largest target
15	570,000	5	20	14
22.5	200,000	7	27.5	16
30	200,000	13	45	9
37.5	200,000	15	60	7
45	690,000	15	70	8
60	600,000	15	70	12
90	690,000	9	37.5	12
135	690,000	3	20	6

5.4.4.3 The extrapolation procedure was applied to a series of small subsets of this large sample and the extrapolated estimates were compared with the "true value". Figure 5.4.7 shows an example comparison for a 45 degree heading (stern-quartering seas) and a target roll value of 45 degrees. Fifty extrapolation estimates are carried out, each computed from 100 hours of data. The main index of performance is the passing rate, which indicates the percentage of successful extrapolations. An extrapolation is considered successful if the confidence interval of the extrapolated exceedance rate includes the "true value". The example shown in figure 5.4.8 has 45 successful extrapolations, resulting in a passing rate of 90%.

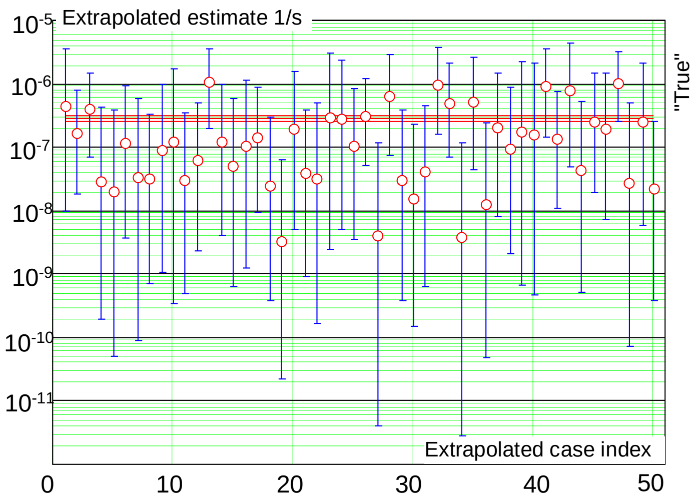

Figure 5.4.7 example of extrapolation validation for a heading of 45 degrees and target value of 45 degrees

5.4.4.4 Three validation tiers[32] are applied: extrapolation for one target value; extrapolation for all target values, and extrapolation for all operational and environmental conditions.

5.4.4.5 The tier 1 validation is a set of comparisons of extrapolated estimates with the true value, figure 5.4.7. The second tier considers all available target angles; the passing rates are shown in figure 5.4.8. An acceptable passing rate for 50 extrapolation data sets is from 0.88 to 1 (paragraph 3.5.6.7 of the Interim Guidelines). This variation of the passing rate can be explained by the natural variability of the statistical estimates. The extrapolations are acceptable for all targets excluding 50 and 60 degrees, for which the passing rates fell to 0.86. The average passing rate for the 45 degrees heading is 0.90, which is within the acceptable range.

32 Smith, T.C. *Validation Approach for Statistical Extrapolation.* Chapter 34 of *Contemporary Ideas on Ship Stability. Risk of Capsizing*, Belenky, V., Neves, M., Spyrou, K., Umeda, N., van Walree, F., eds., Springer, ISBN 978-3-030-00514-6, pp. 573-589, 2019.

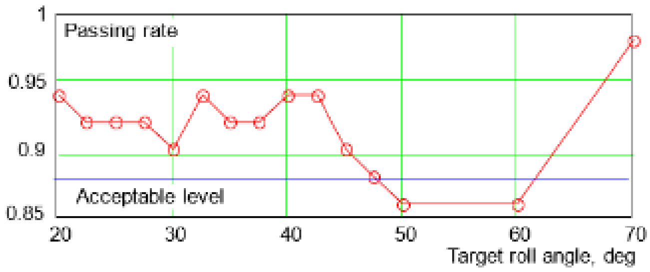

Figure 5.4.8 Passing rate for heading 45 degrees

5.4.4.6 The third tier of validation assesses the performance over all available conditions. The passing rates are shown in figure 5.4.9. Two lines are shown: one corresponds to an averaged passing rate over all target values, while the other corresponds to the smallest passing rate value encountered among all the target values. For 45 degrees heading, the latter corresponds to a minimum shown in figure 5.4.9. The extrapolation did not work for heading 135 degrees.

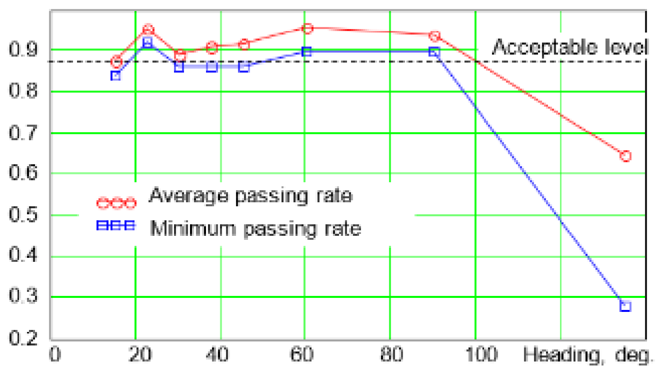

Figure 5.4.9 Passing rate for all headings

5.4.4.7 A validation at the heading of 135 degrees has a very likely failure due to insufficient data in the non-linear region. The average conservative distance (measure of practical statistical uncertainty) does not exceed an order of magnitude in terms of the exceedance rate. This performance seems to be sufficient to distinguish between realistic and distant chances of dynamic stability failure.

5.4.4.8 Overall, the validity of EPOT, except for the 135 degree heading, can be characterized as acceptable. The passing rate falls short of the required 0.88 for few cases, but not by much. The average passing rates exceed 0.88 for all cases except for the heading of 135 degrees.

5.5 Application of MPM and EPOT methods to full probabilistic assessment

5.5.1 A simplified sample of full probabilistic direct stability assessment was carried out for pure loss of stability failure mode using EPOT to estimate the exceedance rate of 40 degrees roll angle on either side of the ship and split-time method (motion perturbation method, MPM) to estimate capsizing rate to starboard only. Calculations were carried out for the principal dimensions and environmental parameters given in table 5.3.2. Primary focus of this example was feasibility of computational procedures rather than quantitative assessment. Thus, computations were performed for 3 DOF: heave, roll and pitch – surge was not included while required by the Interim Guidelines for the quantitative assessment.

5.5.2 Computations were carried out for a relatively coarse set of environmental and operation conditions. Speed varied from 0 to 10 knots, assuming that high speeds will not be practical in high sea states and lower sea states do not make a significant contribution towards the final results. The headings were 45, 90, 135, 225, 270 and 315 degrees. For computational speed, ship motions were evaluated with volume-based code, using body-non-linear formulation for Froude-Krylov and hydrostatic forces. The waves were long-crested, with the conditions defined in the wave scatter table from the Interim Guidelines There were total of 40 hours (80 records of 30 minutes duration) of simulation time histories generated for each combination of speed and heading.

5.5.3 For the consideration of computational speed and simplicity of this example, not all cells of the scatter diagram were used for calculations; interpolation was used between cells. Linear extrapolation was also used for the sea states with a mean zero-crossing period of 12.5 s; this is a conservative approach as those sea states do not contribute much to the final result. The calculations were not performed for the cells with zero statistical weight. Finally, calculations were limited by the sea states with significant wave height 5.5 m and above as no appreciable estimates were obtained for significant wave height 4.5 m and below, because contribution of these estimates are expected to be negligible, see tables 5.5.2 to 5.5.5.

5.5.4 The long-term results in table 5.5.1 were computed assuming an equal probability for all speeds and headings for all the weather (tables 5.5.2 to 5.5.5 show results per sea state). These results show very large values both for exceedance rate and capsizing rate compared to the standard rate $2.6 \cdot 10^{-8}$ (1/s) in the Interim Guidelines. Such large values could be expected because the ONR tumblehome configuration is known for its vulnerability for pure loss of stability.

Table 5.5.1 Assessment results for equal probability of speeds and headings

Estimate	rate, 1/s
estimate of exceedance rate of 40 degree	1.157e-7
Upper boundary of exceedance rate of 40 degree	2.079e-7
estimate of capsizing rate	1.434e-8
Upper boundary of capsizing rate	4.081e-8

5.5.5 Note that the average failure rate over all sea states and sailing conditions is dominated by a few sea states characterized by high steepness of waves, for which the estimates can be also obtained by direct counting.

Table 5.5.2 Estimate of exceedance rate of 40 degree roll, 1/s (columns are mean zero-crossing period in seconds, rows are significant wave heights in metres)

	5.5	6.5	7.5	8.5	9.5	10.5	11.5	12.5	13.5	14.5	15.5	16.5	17.5
5.5	5.44E-08	2.56E-08	1.20E-08	5.66E-09	2.66E-09	1.25E-09	6.53E-10	3.41E-10	1.78E-10	9.29E-11	4.85E-11	2.53E-11	1.32E-11
6.5	1.29E-06	4.61E-07	1.65E-07	5.90E-08	2.11E-08	7.56E-09	2.89E-09	1.11E-09	4.24E-10	1.62E-10	6.21E-11	2.38E-11	9.11E-12
7.5	0	6.88E-06	1.94E-06	5.49E-07	1.55E-07	4.37E-08	1.27E-08	3.69E-09	1.07E-09	3.10E-10	9.01E-11	2.62E-11	7.59E-12
8.5	0	7.04E-05	1.69E-05	4.04E-06	9.69E-07	2.32E-07	5.46E-08	1.29E-08	3.03E-09	7.12E-10	1.68E-10	3.94E-11	9.28E-12
9.5	0	0.000408	9.27E-05	2.10E-05	4.77E-06	1.08E-06	2.28E-07	4.82E-08	1.02E-08	2.14E-09	4.52E-10	9.55E-11	2.01E-11
10.5	0	0	0.000291	7.14E-05	1.75E-05	4.30E-06	9.20E-07	1.97E-07	4.21E-08	9.01E-09	1.93E-09	4.12E-10	8.82E-11
11.5	0	0	0.000579	0.000171	5.07E-05	1.50E-05	3.60E-06	8.63E-07	2.07E-07	4.97E-08	1.19E-08	2.86E-09	6.86E-10
12.5	0	0	0.000848	0.000326	0.000125	4.80E-05	1.38E-05	3.97E-06	1.14E-06	3.29E-07	9.46E-08	2.72E-08	7.83E-09
13.5	0	0	0	0.000551	0.000285	0.000147	5.24E-05	1.87E-05	6.67E-06	2.38E-06	8.49E-07	3.03E-07	1.08E-07
14.5	0	0	0	0.000694	0.000358	0.000185	6.60E-05	2.36E-05	8.40E-06	3.00E-06	1.07E-06	3.81E-07	0
15.5	0	0	0	0	0.000451	0.000233	8.31E-05	2.97E-05	1.06E-05	3.77E-06	1.35E-06	4.80E-07	0
16.5	0	0	0	0	0	0.000298	0.000105	3.73E-05	1.33E-05	4.75E-06	1.69E-06	0	0

Table 5.5.3. Estimate of upper boundary of exceedance rate of 40 degree roll, 1/s (columns are mean zero-crossing period in seconds, rows are significant wave heights in metres)

	5.5	6.5	7.5	8.5	9.5	10.5	11.5	12.5	13.5	14.5	15.5	16.5	17.5
5.5	1.32E-07	7.88E-08	4.71E-08	2.82E-08	1.69E-08	1.01E-08	5.31E-09	2.79E-09	1.47E-09	7.73E-10	4.07E-10	2.14E-10	1.13E-10
6.5	2.58E-06	1.14E-06	5.07E-07	2.24E-07	9.93E-08	4.40E-08	2.08E-08	9.84E-09	4.65E-09	2.20E-09	1.04E-09	4.93E-10	2.33E-10
7.5	0	1.39E-05	4.73E-06	1.61E-06	5.46E-07	1.86E-07	7.97E-08	3.42E-08	1.47E-08	6.31E-09	2.71E-09	1.16E-09	4.99E-10
8.5	0	0.000119	3.33E-05	9.35E-06	2.63E-06	7.37E-07	2.93E-07	1.16E-07	4.62E-08	1.83E-08	7.28E-09	2.89E-09	1.15E-09
9.5	0	0.000594	0.000154	3.98E-05	1.03E-05	2.67E-06	1.01E-06	3.81E-07	1.44E-07	5.44E-08	2.05E-08	7.76E-09	2.93E-09
10.5	0	0	0.000423	0.000116	3.16E-05	8.63E-06	3.21E-06	1.19E-06	4.45E-07	1.65E-07	6.16E-08	2.29E-08	8.52E-09
11.5	0	0	0.000763	0.000245	7.90E-05	2.54E-05	9.59E-06	3.61E-06	1.36E-06	5.14E-07	1.94E-07	7.30E-08	2.75E-08
12.5	0	0	0.00104	0.000423	0.000173	7.04E-05	2.74E-05	1.07E-05	4.15E-06	1.62E-06	6.29E-07	2.45E-07	9.53E-08
13.5	0	0	0	0.000657	0.000353	0.000189	7.68E-05	3.11E-05	1.26E-05	5.12E-06	2.08E-06	8.43E-07	3.42E-07
14.5	0	0	0	0.000828	0.000444	0.000238	9.66E-05	3.92E-05	1.59E-05	6.45E-06	2.62E-06	1.06E-06	0
15.5	0	0	0	0	0.000559	0.0003	0.000122	4.94E-05	2.00E-05	8.12E-06	3.29E-06	1.34E-06	0
16.5	0	0	0	0	0	0.000378	0.000153	6.21E-05	2.52E-05	1.02E-05	4.15E-06	0	0

Table 5.5.4 Capsize rate estimate, 1/s (columns are mean zero-crossing period in seconds, rows are significant wave heights in metres)

	5.5	6.5	7.5	8.5	9.5	10.5	11.5	12.5	13.5	14.5	15.5	16.5	17.5
5.5	5.58E-07	8.01E-08	1.15E-08	1.65E-09	2.37E-10	3.41E-11	7.71E-12	1.75E-12	3.95E-13	8.95E-14	2.03E-14	4.59E-15	1.04E-15
6.5	2.50E-06	3.58E-07	5.14E-08	7.39E-09	1.06E-09	1.52E-10	3.45E-11	7.81E-12	1.77E-12	4.00E-13	9.06E-14	2.05E-14	4.64E-15
7.5	0	1.60E-06	2.30E-07	3.30E-08	4.74E-09	6.81E-10	1.54E-10	3.49E-11	7.90E-12	1.79E-12	4.05E-13	9.17E-14	2.07E-14
8.5	0	4.24E-06	1.01E-06	2.42E-07	5.78E-08	1.38E-08	1.44E-09	1.51E-10	1.57E-11	1.64E-12	1.72E-13	1.79E-14	1.88E-15
9.5	0	1.13E-05	4.05E-06	1.45E-06	5.18E-07	1.85E-07	1.14E-08	6.97E-10	4.28E-11	2.63E-12	1.61E-13	9.89E-15	6.07E-16
10.5	0	0	1.37E-05	6.09E-06	2.72E-06	1.21E-06	6.65E-08	3.65E-09	2.01E-10	1.10E-11	6.06E-13	3.33E-14	1.83E-15
11.5	0	0	4.00E-05	1.90E-05	9.00E-06	4.27E-06	3.01E-07	2.13E-08	1.50E-09	1.06E-10	7.49E-12	5.28E-13	3.73E-14
12.5	0	0	0.000106	4.83E-05	2.20E-05	9.98E-06	1.15E-06	1.33E-07	1.53E-08	1.77E-09	2.04E-10	2.36E-11	2.72E-12
13.5	0	0	0	0.000111	4.59E-05	1.90E-05	4.04E-06	8.61E-07	1.83E-07	3.90E-08	8.30E-09	1.77E-09	3.76E-10
14.5	0	0	0	0.00014	5.78E-05	2.39E-05	5.09E-06	1.08E-06	2.31E-07	4.91E-08	1.05E-08	2.23E-09	0
15.5	0	0	0	0	7.28E-05	3.01E-05	6.41E-06	1.36E-06	2.90E-07	6.18E-08	1.32E-08	2.80E-09	0
16.5	0	0	0	0	0	3.79E-05	8.07E-06	1.72E-06	3.66E-07	7.78E-08	1.66E-08	0	0

Table 5.5.5 Upper boundary of capsize rate estimate, 1/s (columns are mean zero-crossing period in seconds, rows are significant wave heights in metres)

	5.5	6.5	7.5	8.5	9.5	10.5	11.5	12.5	13.5	14.5	15.5	16.5	17.5
5.5	1.26E-06	3.98E-07	1.26E-07	3.98E-08	1.26E-08	3.98E-09	6.42E-10	1.04E-10	1.67E-11	2.70E-12	4.35E-13	7.02E-14	1.13E-14
6.5	4.19E-06	1.33E-06	4.20E-07	1.33E-07	4.20E-08	1.33E-08	2.14E-09	3.46E-10	5.58E-11	9.00E-12	1.45E-12	2.34E-13	3.78E-14
7.5	0	4.43E-06	1.40E-06	4.43E-07	1.40E-07	4.43E-08	7.15E-09	1.15E-09	1.86E-10	3.00E-11	4.84E-12	7.82E-13	1.26E-13
8.5	0	1.05E-05	4.03E-06	1.55E-06	5.93E-07	2.27E-07	3.34E-08	4.91E-09	7.21E-10	1.06E-10	1.56E-11	2.29E-12	3.36E-13
9.5	0	2.48E-05	1.11E-05	4.93E-06	2.20E-06	9.82E-07	1.40E-07	1.99E-08	2.83E-09	4.03E-10	5.74E-11	8.17E-12	1.16E-12
10.5	0	0	2.79E-05	1.35E-05	6.52E-06	3.16E-06	4.85E-07	7.44E-08	1.14E-08	1.75E-09	2.70E-10	4.14E-11	6.36E-12
11.5	0	0	6.53E-05	3.22E-05	1.59E-05	7.85E-06	1.43E-06	2.59E-07	4.71E-08	8.56E-09	1.56E-09	2.83E-10	5.14E-11
12.5	0	0	0.000146	7.06E-05	3.41E-05	1.65E-05	3.77E-06	8.62E-07	1.97E-07	4.51E-08	1.03E-08	2.36E-09	5.39E-10
13.5	0	0	0	0.000148	6.85E-05	3.18E-05	9.43E-06	2.80E-06	8.30E-07	2.46E-07	7.31E-08	2.17E-08	6.44E-09
14.5	0	0	0	0.000186	8.63E-05	4.00E-05	1.19E-05	3.52E-06	1.05E-06	3.10E-07	9.20E-08	2.73E-08	0
15.5	0	0	0	0	0.000109	5.04E-05	1.49E-05	4.43E-06	1.32E-06	3.90E-07	1.16E-07	3.44E-08	0
16.5	0	0	0	0	0	6.34E-05	1.88E-05	5.58E-06	1.66E-06	4.92E-07	1.46E-07	0	0

5.6 Linear superposition method for excessive acceleration failure mode

5.6.1 *Description of method*

5.6.1.1 Linear superposition method is one of statistical extrapolation procedures that can be used for the direct stability assessment for the excessive acceleration failure mode if roll damping is modelled using the stochastically equivalent linearization technique.

5.6.1.2 With this method, the energy spectra of ship responses in irregular waves can be obtained by linear superposition using a product of the Response Amplitude Operators (RAOs) of ship responses with the wave energy spectrum.

5.6.1.3 The variance $[R_L(\mu)]^2$ of the lateral acceleration at a constant wave heading angle μ in irregular long-crested waves is obtained using sea wave elevation spectrum $S_{ZZ}(\omega)$ and RAO of the lateral acceleration $[A(\omega,\mu)]$ by the following equation:

$$R_L(\mu)^2 = \int_0^\infty S_{ZZ}(\omega) \cdot [A(\omega,\mu)]^2 d\omega \tag{5.6.1}$$

5.6.1.4 In short-crested irregular waves, this variance is calculated considering wave energy spreading function D with respect to the mean wave direction.

$$R_L(\mu)^2 = \int_{-\pi/2}^{\pi/2} \int_0^{\infty} S_{ZZ}(\omega) \cdot D(\omega, \chi) \cdot [A(\omega, \mu - \chi)]^2 d\omega \, d\chi \qquad (5.6.2)$$

5.6.1.5 Repeating such calculations for all relevant significant wave heights and zero-crossing wave periods for a specified wave heading and ship speed, the "short-term" and average "long-term" failure probabilities per encounter wave are calculated using the calculated variance of lateral acceleration in the same way as in level 2 vulnerability criterion for the excessive acceleration stability failure mode.

5.6.1.7 The average "long-term" stability failure rate, 1/s, can be calculated by

$$\bar{r} = -\ln(1 - p) / T_{\mathrm{e}} \qquad (5.6.3)$$

where p is the average "long-term" failure probability per encountered wave and T_{e} is the mean wave encounter period at a specified ship speed v_0, given by

$$T_e = \frac{T_w}{\left(1 - \frac{2\pi}{gT_w} v_0 \cos \chi\right)} \qquad (5.6.4)$$

where T_w is the mean wave period. In the case of full probabilistic assessment, T_w is mean value of zero-crossing wave period in North Atlantic.

5.6.1.8 The numerical method is validated in section 2.7 of this appendix. To validate the statistical extrapolation, table 5.6.1 compares the average "long-term" failure probability per encounter wave calculated with level 2 vulnerability criterion, the linear superposition method and time domain simulations. An example of validation was presented for a container ship, which is the same as section 2.7, and the modelling of short-crested irregular waves are also the same as in section 2.7. The time domain simulation tool used for comparison models ship motions in six degrees of freedom; hydrodynamic forces are calculated using the three-dimensional source distribution, considering memory effect. This tool showed sufficient accuracy for direct stability assessment for excessive acceleration failure mode in comparison with model tests. The average "long-term" failure probabilities per encounter wave calculated by the linear superposition method and time domain simulations are close to each other and consistent with respect to level 2 vulnerability criterion.

Table 5.6.1 Average "long-term" failure probabilities per encounter wave calculated with level 2 vulnerability criterion, linear superposition method and time domain simulations

Method:	Level 2	Linear superposition method	Time domain simulations
Average long-term failure probabilities per encounter wave	$5.35 \cdot 10^{-5}$	$2.02 \cdot 10^{-5}$	$1.68 \cdot 10^{-5}$

5.6.2 *Application example*

5.6.2.1 An example of application of the linear superposition method for the excessive acceleration stability failure mode concerns a container ship with the principal particulars in table 2.7.1.

5.6.2.2 The transfer functions of ship motions in waves were computed in frequency domain using the Salvesen-Tuck-Faltinsen method, based on strip theory. Details of the numerical method are given in section 2.7. The ship motions were calculated in five degrees of freedom; and hydrodynamic forces were calculated by a two-dimensional source distribution method. The roll damping coefficient was estimated from a roll decay model test. Short-crested irregular waves were employed, where the wave energy spectrum was the ITTC recommended unlimited fetch spectrum (1978) and the wave energy spreading was described by square of cosine function. The significant wave height and mean wave period correspond to wave scatter diagram of IACS Recommendation No.34 (Corr.1 Nov. 2001) (see the Interim Guidelines, Table 2.7.2.1.2).

5.6.2.3 Table 5.6.2 presents the short-term failure probability of exceedance of the lateral acceleration 9.81 m/s^2 in irregular short-crested beam waves at zero ship speed, calculated for significant wave heights and zero-crossing wave periods corresponding to the centres of the cells of IACS Recommendation No.34 (Corr.1 Nov. 2001) (see the Interim Guidelines, Table 2.7.2.1.2). The average "long-term" failure probability per encountered wave p is obtained by integrating the product of the short-term probability in a given sea state and the occurrence frequency of the sea state over the possible sea states in the assumed water area. The average "long-term" failure probability per encountered wave for this wave climate was calculated as $8.73 \cdot 10^{-6}$.

Table 5.6.2 Short-term probability of exceedance of lateral acceleration exceeding 9.81 m/s^2 in irregular short-crested beam waves

H_s \ T_z	T_z: average zero up-crossing wave periods [s]															
	3.5	4.5	5.5	6.5	7.5	8.5	9.5	10.5	11.5	12.5	13.5	14.5	15.5	16.5	17.5	18.5
0.5	0.00E+00	0.00E+00	0.00E+00	0.00E+00	0.00E+00	0.00E+00	0.00E+00	0.00E+00	0.00E+00	0.00E+00						
1.5		0.00E+00	0.00E+00	1.96E-155	5.04E-116	3.62E-115	3.30E-132	1.15E-162	2.61E-206	2.21E-264	0.00E+00	0.00E+00	0.00E+00			
2.5		3.53E-294	1.24E-116	2.03E-56	3.11E-42	6.33E-42	4.64E-48	5.03E-99	9.77E-75	1.21E-95	1.97E-122	6.01E-156	3.84E-197	4.48E-247		
3.5		2.41E-145	7.32E-60	3.85E-29	6.85E-22	9.56E-22	7.08E-25	1.80E-30	1.74E-38	3.74E-49	8.03E-63	6.39E-80	6.13E-101	2.05E-126	6.20E-157	
4.5			1.69E-36	6.47E-18	1.55E-13	1.92E-13	2.46E-15	1.02E-18	1.44E-23	5.07E-30	2.73E-38	1.24E-48	2.39E-61	9.25E-77	3.19E-95	
5.5			1.13E-24	3.11E-12	2.66E-09	3.08E-09	1.66E-10	9.01E-13	5.11E-16	2.45E-20	7.15E-26	6.50E-33	2.62E-41	1.26E-51	5.53E-64	1.22E-78
6.5			7.15E-18	5.77E-09	7.24E-07	8.04E-07	9.95E-08	2.38E-09	1.13E-11	9.10E-15	9.91E-19	1.09E-23	6.80E-30	3.81E-37	5.12E-46	1.84E-58
7.5				6.48E-07	2.44E-05	2.64E-05	5.50E-06	3.33E-07	5.98E-09	2.84E-11	3.00E-14	5.67E-18	1.50E-22	4.25E-28	9.56E-35	1.26E-42
8.5				1.52E-05	2.57E-04	2.73E-04	8.04E-05	9.05E-06	3.96E-07	6.16E-09	2.96E-11	3.74E-14	1.02E-17	4.89E-22	3.27E-27	2.39E-33
9.5				1.39E-04	1.34E-03	1.40E-03	5.27E-04	9.18E-05	7.49E-06	2.67E-07	3.73E-09	1.78E-11	2.50E-14	8.71E-18	6.27E-22	7.88E-27
10.5					4.44E-03	4.82E-03	2.07E-03	4.96E-04	6.37E-05	4.16E-06	1.26E-07	1.59E-09	7.33E-12	1.08E-14	4.40E-18	4.19E-22
11.5					1.09E-02	1.13E-02	5.80E-03	1.76E-03	3.16E-04	3.27E-05	1.77E-06	4.62E-08	5.22E-10	2.28E-12	3.40E-15	1.51E-18
12.5					2.19E-02	2.25E-02	1.28E-02	4.66E-03	1.10E-03	1.60E-04	1.35E-05	6.18E-07	1.39E-08	1.40E-10	5.67E-13	
13.5						3.86E-02	2.38E-02	1.00E-02	2.90E-03	5.56E-04	6.70E-05	4.75E-06	1.84E-07	3.56E-09	3.17E-11	
14.5						5.96E-02	3.92E-02	1.85E-02	6.31E-03	1.51E-03	2.41E-04	2.43E-05	1.45E-06	4.75E-08		
15.5							5.87E-02	3.04E-02	1.19E-02	3.39E-03	6.82E-04	9.16E-05	7.77E-06	3.90E-07		
16.5								4.59E-02	2.00E-02	6.62E-03	1.61E-03	2.73E-04	3.10E-05			

5.6.2.4 Figure 5.6.1 shows the average "long-term" probabilities of exceedance of the lateral acceleration 9.81 m/s^2 per encountered wave at zero ship speed for various wave headings from head to following waves. For uniform distribution of wave heading probabilities, the average "long-term" probability of exceedance of lateral acceleration 9.81 m/s^2 per encountered wave p is $2.33 \cdot 10^{-6}$. The average "long-term" stability failure rate r (1/s) is obtained using the average "long-term" probability per encountered wave p and mean wave encounter period T_e, as shown in eq. (5.6.3). Here, since the ship speed is zero, the expected value of the zero up-crossing wave period in the North Atlantic is used for T_e. The average "long-term" stability failure rate is $2.63 \cdot 10^{-7}$, which is larger than the standard of $2.6 \cdot 10^{-8}$ (1/s). Therefore, the ship is judged as unsafe to the excessive acceleration failure mode.

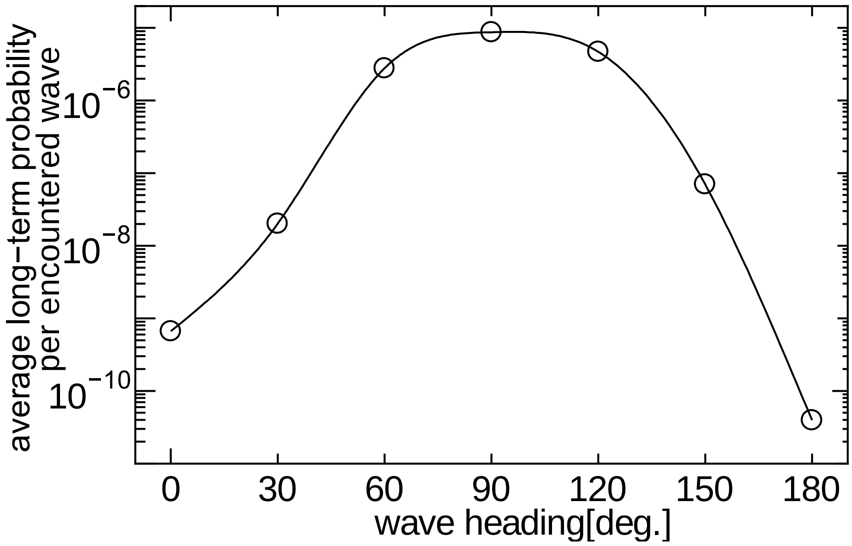

Figure 5.6.1 Average "long-term" probability of exceedance of lateral acceleration 9.81 m/s^2 per encountered wave depending on wave heading

6 Roll Damping

6.1 Calibration of roll damping in simulation codes

6.1.1 Paragraph 3.3.2.2 of the Interim Guidelines contains requirements for modelling roll damping. In that context, paragraph 3.3.2.2.1 indicates that roll decays may be used for the calibration of roll damping.

6.1.2 Most simulation codes internally compute the wave component of roll damping. Some simulation codes allow for directly computing roll damping contributions from different appendages (e.g. rudders, fins, bilge keels). These models, however, do not account for all effects associated with roll damping. Therefore, semi-empirical tuning damping parameters are also present in simulation codes for allowing calibration of roll damping. The scope of these semi-empirical tuning damping parameters is to account for those effects that are not explicitly addressed by specific numerical models available in the simulation code. Combining specific numerical models and tuning damping parameters with information from roll decay test data allows reasonable numerical simulations outside of the range of test parameters.

6.1.3 A calibration process is therefore generally carried out. The calibration process essentially corresponds to the modification of the tuning roll damping parameters in the simulation code in such a way that the numerically simulated roll decay is representative of the experimental roll decay.

6.1.4 Figure 6.1 shows an example comparison between experimental roll decays and simulated roll decays after tuning. Numerical and experimental data in the example figure are compared in terms of dimensionless linear equivalent roll damping coefficient ν_e as a function of the roll amplitude, for three different forward speeds.

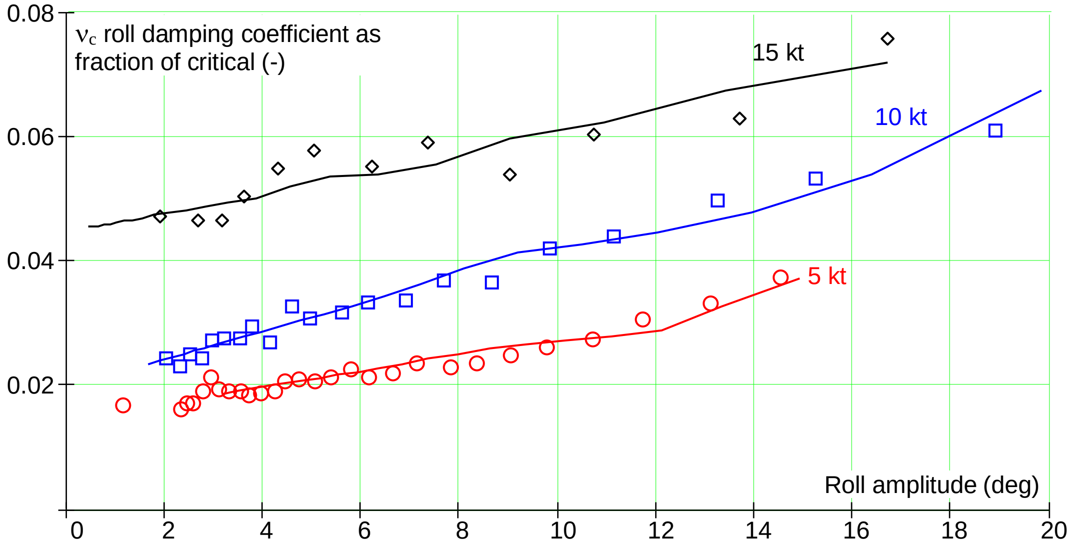

Figure 6.1 Example comparison of results from experimental roll decays (markers) and numerical roll decays after calibration (solid lines), for three different speeds.

7 Application examples of verification of failure modes

7.1 Parametric roll

7.1.1 Section 3.5.2 of the Interim Guidelines contains guidance on verification of the mode of failure. Per paragraph 3.5.2.1 of the Interim Guidelines, the objective is to examine whether the stability failure corresponding to the expected mode has been observed, provided that the numerical method has been validated for reproducing stability failure of the mode under examination. The judging criteria for the parametric roll are detailed in paragraph 3.5.2.3 of the Interim Guidelines. They suggest comparison of the period of roll motion to the local encounter period of waves. The roll period is expected to be close to the natural roll period at the observed amplitude see section 2.1 of this appendix. The roll period is expected to be close to twice the local wave encounter period.

7.1.2 Figure 7.1.1 shows the time history of roll motion for 5 minutes, from 400 s to 700 s (the initial transition is not shown). One can easily see 10 complete roll oscillations, making the observed roll period about 30 s. The natural roll frequency, corresponding to the considered loading condition with GM = 1.4 m, is about 0.21 rad/s; the corresponding natural roll period 29.9 s is very close to the visual estimate from figure 7.1.1.

7.1.3 Figure 7.1.2 shows time history of wave elevation at the position of the centre of gravity of the ship. Periods measured from this figure are essentially wave encounter periods. There are 23 full oscillations (counting by zero crossings), producing an encounter period about 13 s (actually, it is close to 13.9 s, calculated by the simulation code for this record). The ratio between the observed roll period and observed wave encounter period is about 2.3.

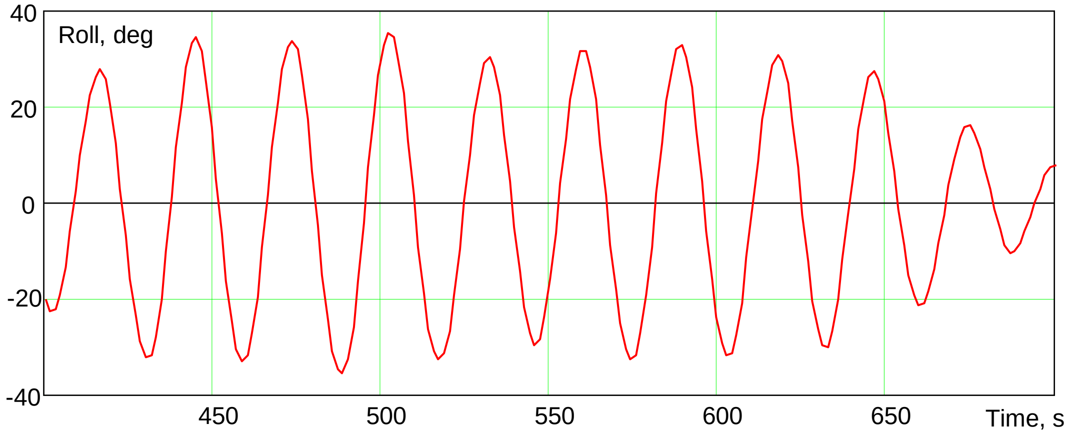

Figure 7.1.1 Verification of parametric roll: roll motion for heading 1° (almost following), speed 5 knots, significant wave height 3.5 m, mean zero-crossing period 8.5 s

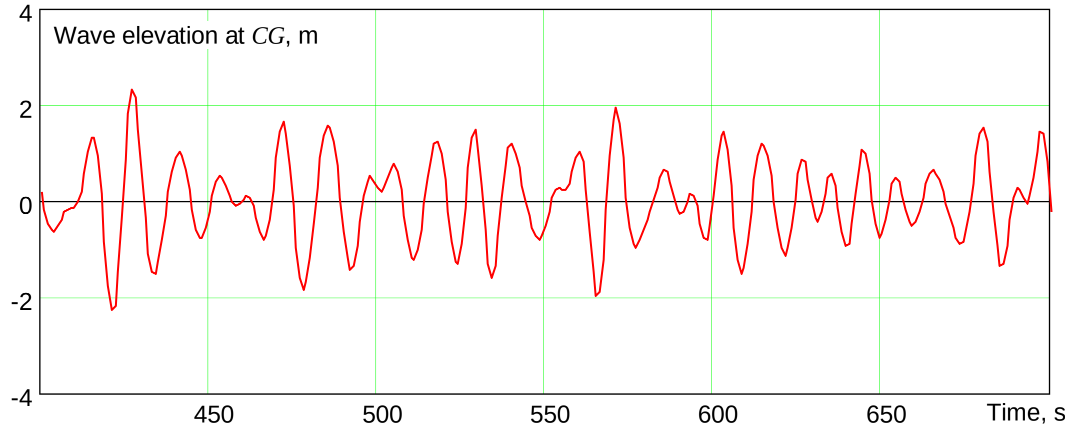

Figure 7.1.2 Verification of parametric roll: wave elevation at *CG* for heading 1° (almost following), speed 5 knots, significant wave height 3.5 m, mean zero-crossing period 8.5 s

7.1.4 This confirms that criteria from paragraph 3.5.2.3 of the Interim Guidelines are satisfied and stability failure can be positively verified as parametric roll.

7.1.5 Figure 7.1.3 shows another example of time record of large heel due to parametric roll from a model experiment of a 6,600 TEU container ship in short-crested irregular head waves of significant wave height 0.221 m and mean wave period 1.32 s. At the time of about 139 s, the roll amplitude exceeded 20 degrees, thus this is not a stability failure according to the Interim Guidelines but a kind of large heel incident. The local roll period including the time instance of large roll amplitude was 2.98 s, which was almost twice the local pitch period of 1.47 s and close to the natural roll period of 3.2 s. Thus, the procedure described in paragraph 3.5.2.3 of the Interim Guidelines suggests that this large heel incident can be judged as the result of parametric roll.

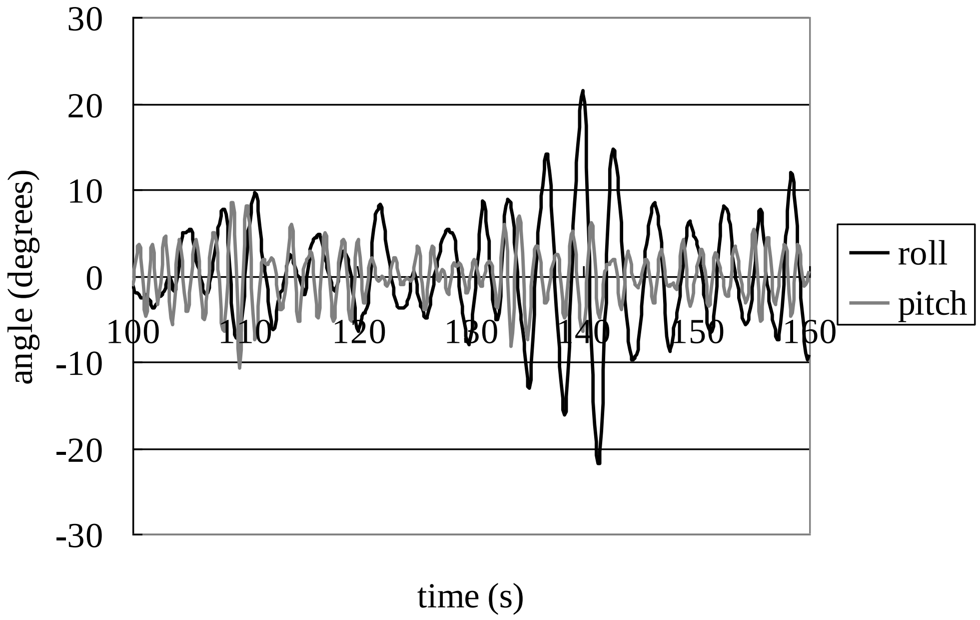

Figure 7.1.3 Time record of roll motion due to parametric roll from model experiment for 6,600 TEU container ship in short-crested irregular head waves

7.1.6 It is noted, however, that the analysis based on pitch motion as a proxy for the analysis based on wave elevation, due to its indirect nature, may lead to inaccurate interpretation of the occurring phenomenon. Therefore, it is advised, whenever possible, to base the analysis on the comparison of local roll behaviour and local wave characteristics, in accordance with paragraph 3.5.2.3 of the Interim Guidelines.

7.2 Pure loss of stability

7.2.1 An example of time record of stability failure due to pure loss of stability from a model experiment of the C11-class container ship in irregular long-crested stern-quartering waves is shown in figure 7.2.1. The significant wave height was 0.165 m, the mean wave period 1.295 s, and the nominal Froude number 0.35 and the specified autopilot course is -30 degrees from the wave direction. At the time of about 151 s, the roll angle exceeded 40 degrees so that it is a stability failure. Here the local roll period including the time instance of the stability failure is close to the local pitch period, which corresponds to the local wave encounter period. The local pitch period is about 4.4 s, which is much larger than the natural roll period of about 2 s. In addition, the stability failure occurred when the pitch up-crossed zero. This means a bow-upward movement as the ship is overtaken by waves, thus this up-crossing means a wave crest located amidship, when the metacentric height is smallest. Since the increase rate of the pitch angle near the wave crest is much smaller, the ship model spends longer time at the wave crest. Thus, the procedure described in paragraph 3.5.2.2 of the Interim Guidelines suggests that this stability failure can be judged as pure loss of stability.

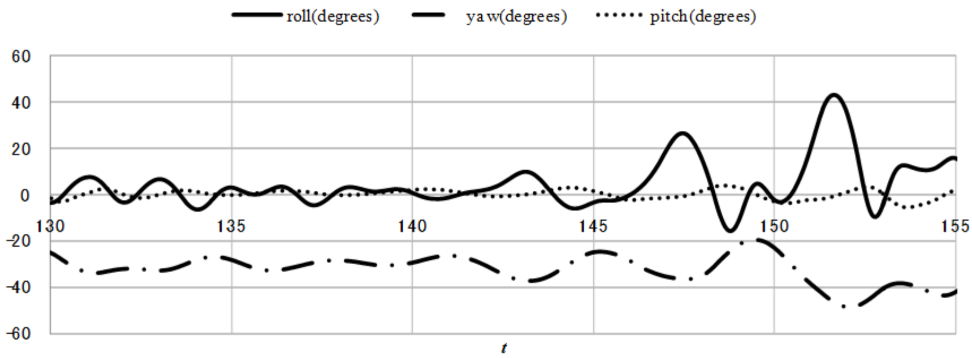

Figure 7.2.1 Time record of stability failure due to pure loss of stability from model experiment for C11-class container ship in irregular long-crested stern-quartering waves

7.2.2 It is noted, however, that the analysis based on pitch motion as a proxy for the analysis based on wave elevation, due to its indirect nature, may lead to inaccurate interpretation of the occurring phenomenon. Therefore, it is advised, whenever possible, to base the analysis on the comparison of local roll behaviour and local wave characteristics, in accordance with paragraph 3.5.2.2 of the Interim Guidelines.

7.3 Surf-riding/broaching

7.3.1 Figure 7.3.1 shows an example of a time record of stability failure due to broaching associated with surf-riding from a model experiment for the ONR flare topside vessel in irregular long-crested stern-quartering waves at significant wave height 0.207 m, mean wave period 1.627 s, the specified auto pilot course -15 degrees from the wave direction and nominal Froude number 0.44. At the time instance of about 19 s, the roll angle (φ) exceeded 30 degrees, which is not a stability failure according to the Interim Guidelines, but a kind of large heel incident. The rudder deflection (δ) reached the maximum angle to starboard but the angular velocity and angular acceleration in yaw (χ) increased in the direction of port turn. During the initial stage of course deviation, the pitch angle (θ) has an almost constant negative value, which indicates that the ship is temporarily surf-ridden at the wave downslope. Thus, the procedure described in paragraph 3.5.2.4 of the Interim Guidelines suggests that the reason of large heel can be judged as broaching.

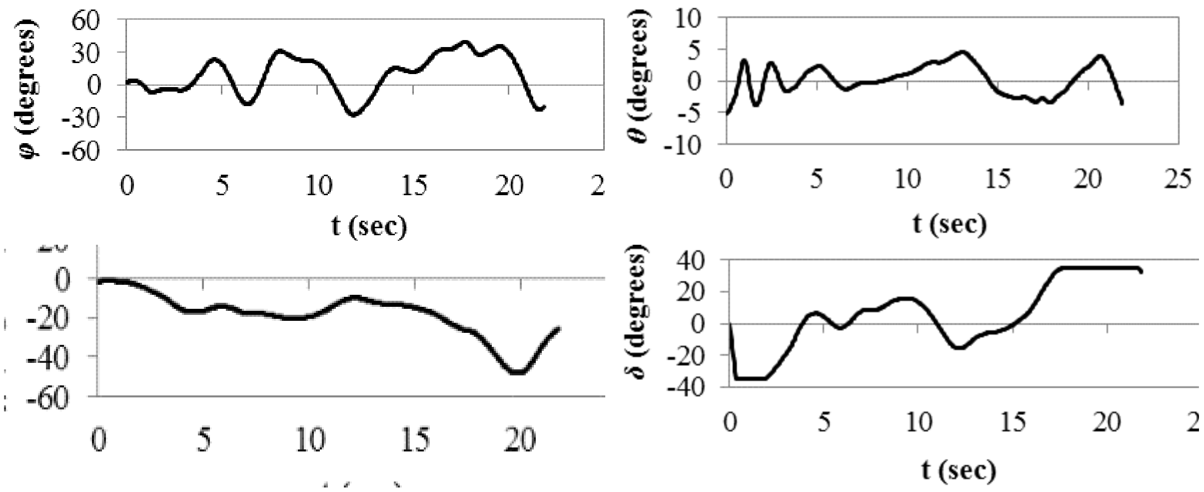

Figure 7.3.1 Time record of large heel due to broaching associated with surf-riding from model experiment for ONR flare topside vessel in irregular long-crested stern-quartering waves

7.4 Synchronous roll

7.4.1 Figure 7.4.1 shows an example of analysis of the relationship between the local roll period and local roll amplitude from a model experiment for a 246 m-long cruise ship in irregular long-crested beam waves with significant wave height 0.128 m (full scale: 10.5 m) and mean wave period 1.93 s at zero forward speed. The natural roll period of the model was 2.60 s. The diagram indicates that the ratio of the local roll period to the local heave period, which is equal to the local wave encounter period, is about 1 for larger local roll amplitudes. Thus, the procedure described in paragraph 3.5.2.5 of the Interim Guidelines suggests that larger heel angles can be judged as synchronous roll.

7.4.2 It is noted, however, that the analysis based on heave motion as a proxy for the analysis based on wave elevation, due to its indirect nature, may lead to inaccurate interpretation of the occurring phenomenon. Therefore, it is advised, whenever possible, to base the analysis on the comparison of local roll behaviour and local wave characteristics, in accordance with paragraph 3.5.2.5 of the Interim Guidelines.

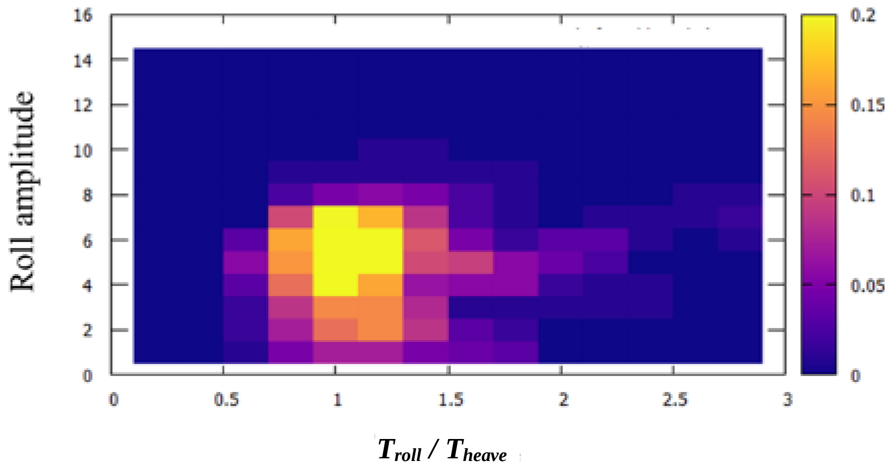

Figure 7.4.1 Local roll amplitude (degrees) vs. ratio of local roll period T_{roll} to local heave period T_{heave} from model test for 246 m-long cruise ship in irregular long-crested beam waves; yellow colour indicates large occurrence frequency

APPENDIX 5

Theoretical background, validation, and application examples for Guidelines on operational measures

1 Background information

1.1 Ships and loading conditions used in background studies

1.1.1 Five ships were used in the studies: a cruise vessel, a RoPax vessel and three container ships of 1700, 8400 and 14000 TEU capacity. For each ship, five loading conditions were selected: three loading conditions with small GM values (relevant for parametric roll, pure loss of stability and stability in dead ship condition) and two loading conditions with large GM values (relevant for excessive accelerations).

1.1.2 Table 1.1.1 summarizes the parameters of ships and loading conditions, and figure 1.1.1 shows examples of the calm-water righting lever curves for typical loading conditions with low metacentric height.

Table 1.1.1 Ships and loading conditions used in study

Ship	L_{BP}, m	B_{wl}, m	LC:	01	02	03	04	05
Cruise Vessel	230.9	32.2	draught, m	6.9				
			GM, m	1.5	2.0	2.5	3.25	3.75
RoPax Vessel	175.0	29.5	draught, m	5.5				
			GM, m	3.7	4.5	5.2	5.9	6.6
1700 TEU Container Ship	159.6	28.1	draught, m	9.5			5.5	
			GM, m	0.5	1.2	1.9	5.75	6.75
8400 TEU Container Ship	317.2	43.2	draught, m	13.93	14.44	14.48	11.36	
			GM, m	0.89	1.26	2.01	5.0	6.93
14000 TEU Container Ship	349.5	51.2	draught, m	14.5			8.5	
			GM, m	1.0	2.0	3.0	9.0	12.0

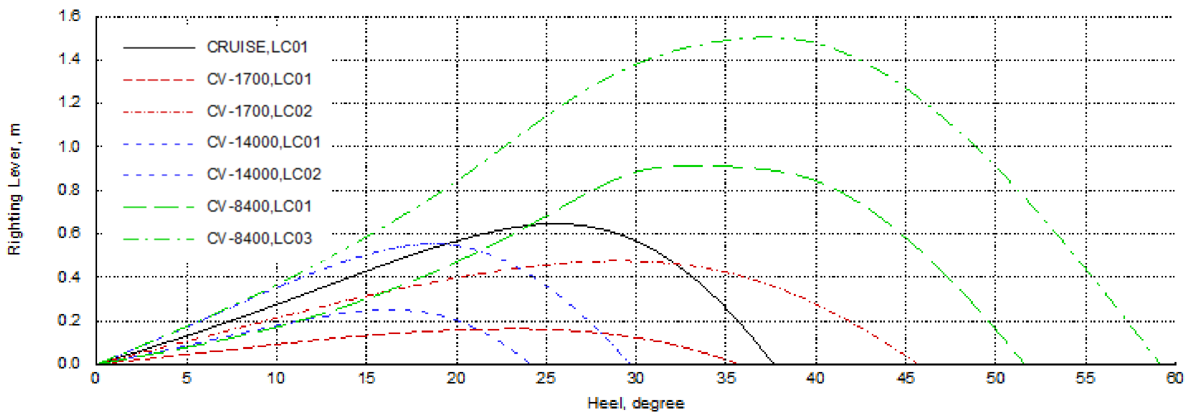

Figure 1.1.1 Calm-water righting lever curves for typical loading conditions with low GM

1.2 Preparation of operational measures

1.2.1 An important question is in what phase of ship life cycle operational measures should be provided, namely in design phase, in port before departure or directly en route:

.1 pre-computation in the design stage allows most comprehensive numerical tools and statistical procedures, qualified staff, dedicated hardware and a detailed check by the administration; a drawback is that the computations can be performed only for assumed input parameters, most importantly, standard seaway spectra;

.2 pre-computation before departure allows, in principle, using comprehensive numerical tools and statistical procedures together with qualified staff and dedicated hardware and, in addition, most accurate data about loading condition and the most actual weather forecast available. In principle, operational measures can be checked by the administration together with the weather forecast, but this requires a corresponding infrastructure. The drawback is a possibility of unforeseen delays in ship operation; and

.3 computations (on board or onshore) during operation allows using the most actual weather and loading condition data, but check by the administration is not possible. Besides, this approach requires significantly simplified numerical tools and statistical procedures, so that the advantage of more accurate weather data is to some degree compensated by the reduced accuracy of numerical tools and statistical procedures.

1.2.2 With any option, accurate weather forecast and corresponding operational measures should be ready in a sufficient time before a storm, e.g. three days, to allow for route change if safe operation in the foreseen storm is not possible. Note that operational limitations related to areas or routes and season do not require a weather forecast since they are prepared for a specified wave scatter table, whereas operational guidance and operational limitations related to maximum significant wave height require a weather forecast.

1.3 Preparation of operational guidance in design phase

1.3.1 A drawback of the pre-computation of operational guidance in the design stage is that it relies on assumed theoretical wave energy spectra and thus, deviation of real sea states from this assumption may lead to erroneous operational recommendations, especially in the cross sea when wind sea and swell have significantly different directions.

1.3.2 One relevant consideration is that the influence of swell is usually noticeable in small to moderate sea states and relatively small in strong storms, which are dominated by wind sea. Figure 1.3.1 compares theoretical relationship between wind speed and wave height of wind sea (solid line) in with hindcast data for two locations in North Atlantic (▲,▼), showing that influence of swell (indicated by the difference in wave height between the theoretical relationship and hindcast data at a given wind speed) is noticeable at small wave heights but becomes relatively insignificant in more severe storms. Figure 1.3.2, plotting the significant wave height of swell vs. the significant wave height of wind sea according to the same data, confirms this.

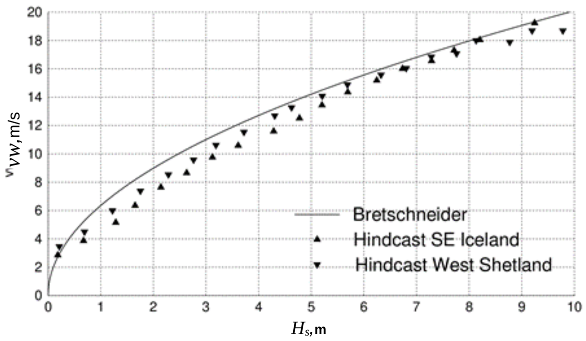

Figure 1.3.1 Theoretical relationship between wind speed (*y*- axis) and wave height (*x* axis), solid line, vs. hindcast for North Atlantic (▲,▼)

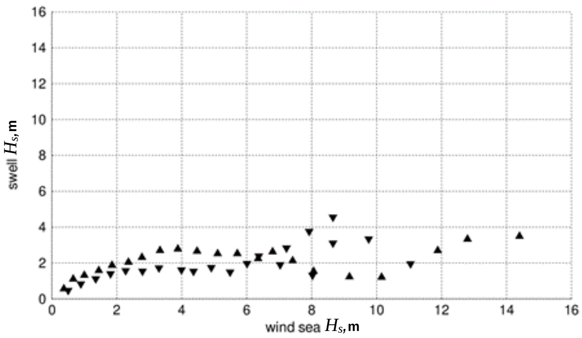

Figure 1.3.2 Significant wave height of swell (*y*- axis) plotted vs. significant wave height of wind sea (*x* axis) for hindcast data shown in figure 1.3.1

1.3.3 To verify this consideration, worldwide hindcast data from the ERA[33] Interim database were used to estimate the likelihood of severe cross sea. From data for one year (about 30 million entries), seaways were selected for which the angle between wind sea and swell was more than 80 degrees: for about 0.01% of all data, the heights of both wind sea and swell were more than 4 m; for about 0.001% of data more than 5 m, and for 0.0001% of data more than 6 m, i.e. the likelihood of a cross sea where both wind sea and swell are severe is negligible.

1.3.4 To check whether numerical simulations using theoretical wave energy spectra can be applied to approximate roll responses to complex measured wave energy spectra, several cross sea situations were selected from the ERA Interim database. For these situations, two questions were investigated: first, what influence the overlapping effect of wind sea and swell has, i.e. how much the combined response to the two separate (wind sea and swell) wave energy systems differs from the response to the total spectrum and, second, how large is the effect of the approximation of the real wave energy spectrum with a theoretical spectrum.

1.3.5 To answer these questions, numerical simulations of ship motions in irregular waves were performed for the selected situations for the following modes: first, for the measured wave energy spectrum, including wind sea and swell; second, for separate wave energy spectra of wind waves and swell, derived from the measured wave energy spectrum (the responses, i.e. the rate of stability failures, to these two separated spectra were summed); and third, for approximated wave energy spectra, separately for wind waves and swell. JONSWAP wave energy spectrum with the peak enhancement factor 3.3 and $\cos^2$ wave energy spreading with respect to the mean wave direction was used for approximation (the responses, i.e. the rate of stability failures, to the separate theoretical spectra were summed). In the definition of the separated wave energy spectra of wind sea and swell from the measurements, the significant wave height, mean period and mean direction of the wave energy spectrum, wind sea spectrum and swell spectrum were kept unchanged. The ship course was varied from 0 to 360 degrees every 10 degrees. Numerical simulations were performed for 200 realizations of each seaway until the first exceedance of 40 degrees roll angle.

1.3.6 This comparison was performed for all ships and loading conditions listed in table 1.1.1, at six forward speeds equally distributed between zero and full speed in calm water. Here, results are shown for two situations, table 1.3.1, for 1700 TEU container ship in loading condition LC01 and 14000 TEU container ship in loading conditions LC01 and LC02.

33 ERA is the abbreviation for ECMWF Reanalysis, where ECMWF is the abbreviation for European Centre for Medium-Range Weather Forecasts.

Table 1.3.1 Parameters of wave energy spectra for two situations

Situation	A	B
Significant wave height, m: total, wind sea, swell	9.8, 4.0, 8.9	8.7, 5.4, 6.8
Mean wave period, s: wind sea, swell	12.4, 10.9	9.0, 14.3
Mean wave propagation direction, deg: wind sea, swell, shift	60, 153, 93	213, 27, 186

1.3.7 The results in figure 1.3.3 (situation A) and figure 1.3.4 (situation B) show that the separate simulations for wave energy spectra of wind sea and swell and summing the resulting stability failure rates (compare the left and middle columns in figure 1.3.3 and 1.3.4) leads to slightly non-conservative results, whereas modelling of wind sea and swell systems using a theoretical spectrum leads to slightly conservative results (compare the middle and right columns in figures 1.3.3 and 1.3.4). The total effect due to both separate treatment of wind sea and swell and theoretical approximation of wave energy spectra for these wave systems is slightly conservative in situation A and slightly non-conservative in situation B.

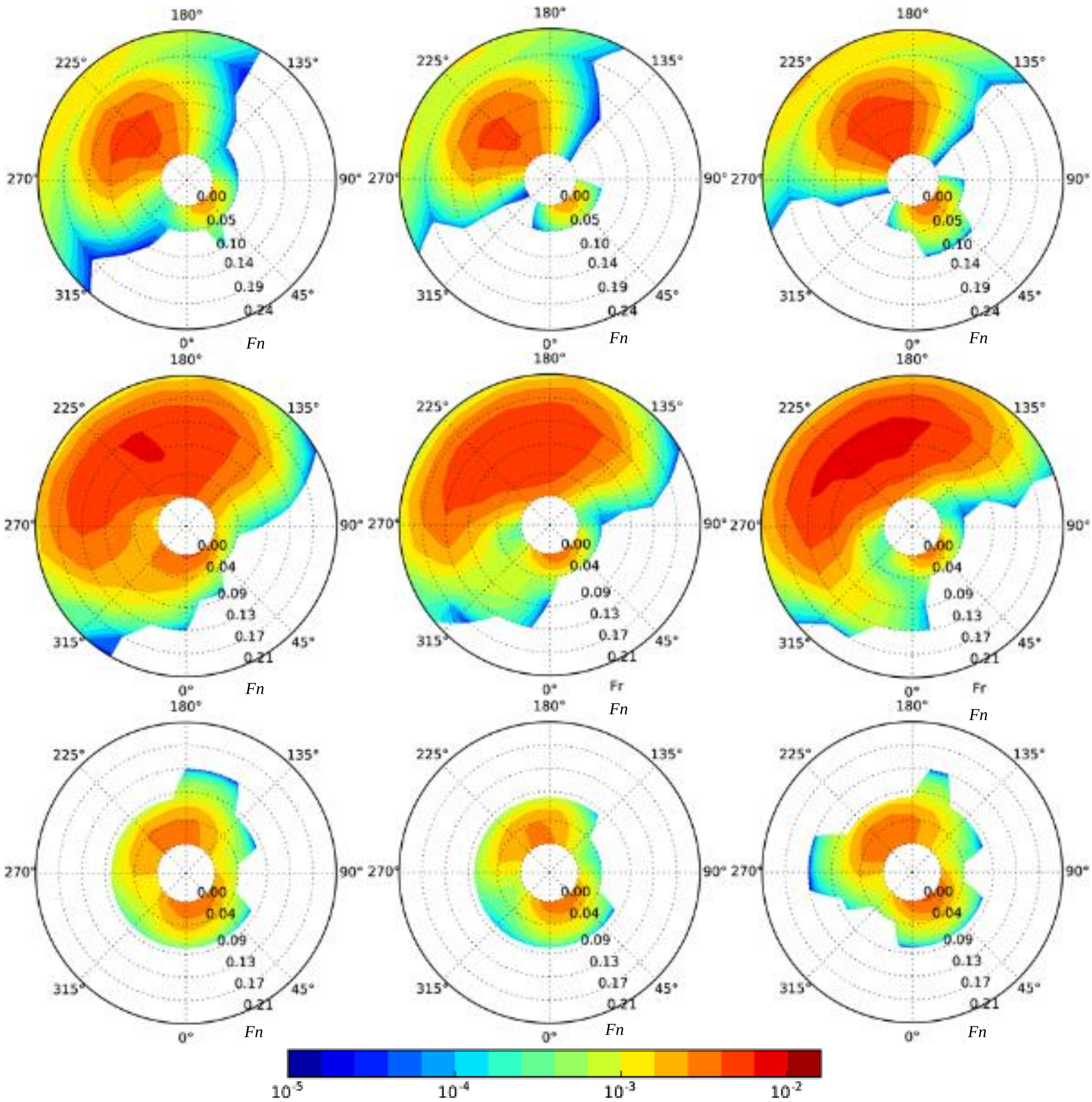

Figure 1.3.3 Situation A: colour plot of stability failure rate, 1/s, vs. *Fn* number (radial coordinate) and ship course (circumferential coordinate) for measured wave energy spectrum (left), summed rate for separate wind waves and swell wave energy spectra (middle) and summed rate for separate wind waves and swell wave energy spectra approximated with

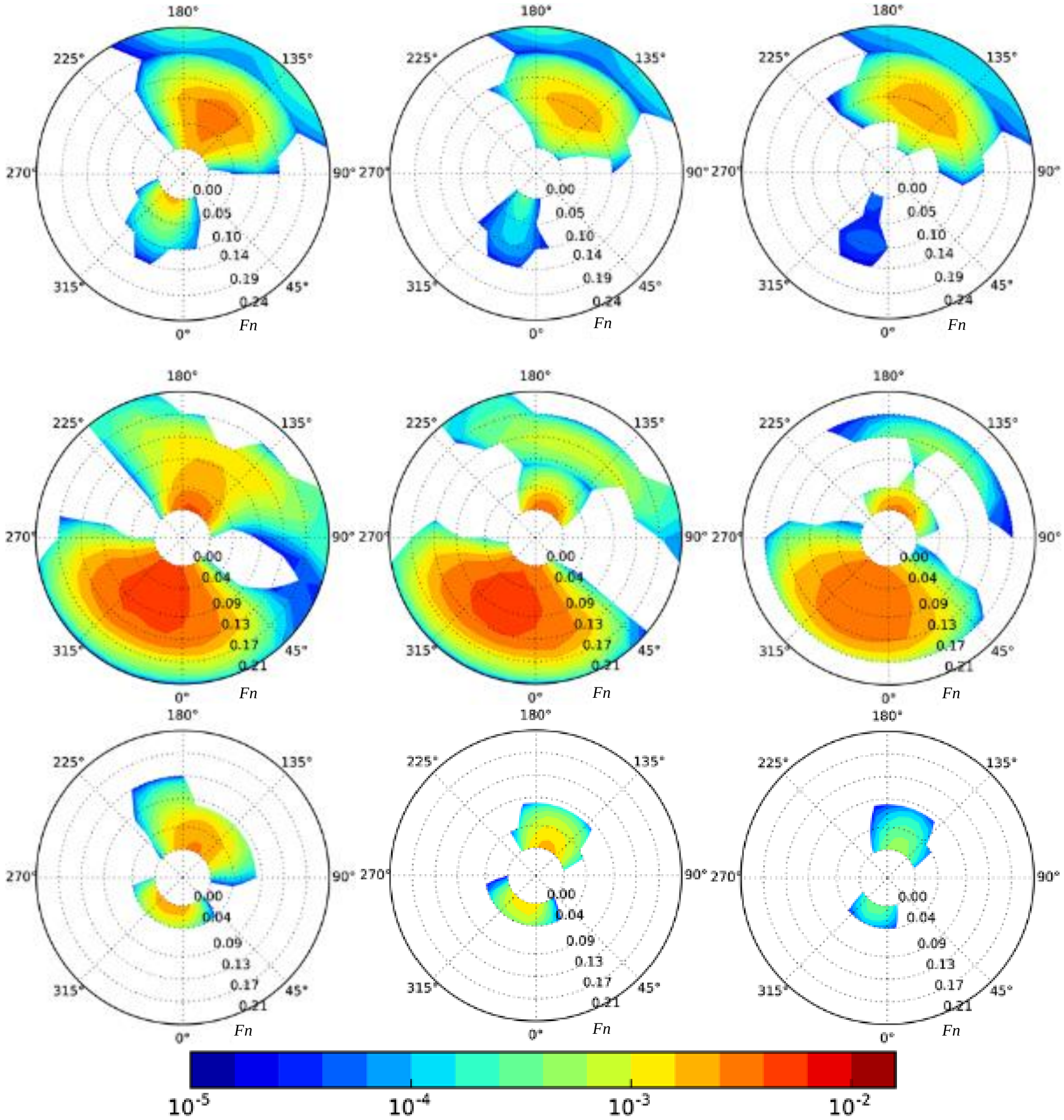

Figure 1.3.4 Situation B: colour plot of stability failure rate, 1/s, vs. *Fn* number (radial coordinate) and ship course (circumferential coordinate) for measured wave energy spectrum (left), summed rate for separate wind waves and swell wave energy spectra (middle) and summed rate for separate wind waves and swell wave energy spectra approximated with JONSWAP spectrum with γ = 3.3 and cos^2 wave energy spreading (right) for 1700 TEU container ship in LC01 (top) and 14000 TEU container ship in LC01 (middle) and LC02 (bottom)

JONSWAP spectrum with γ = 3.3 and cos^2 wave energy spreading (right) for 1700 TEU container ship in LC01 (top) and 14000 TEU container ship in LC01 (middle) and LC02 (bottom)

1.3.8 In all considered cases, theoretical modelling of wave systems and overlapping their effect by summing the failure rates corresponding to each of the systems leads to practically acceptable recommendations for a ship's forward speed and course, thus production and acceptance of operational guidance in design phase is considered an acceptable option.

1.4 Probabilistic operational guidance

1.4.1 To prepare a reference database, numerical simulations of motions in waves were conducted for each ship and each loading condition in table 1.1.1 at six forward speeds, equally distributed from zero to full speed in calm water, for all sea states (significant wave heights H_s and zero-crossing wave periods T_z) in the North Atlantic wave scatter table, IACS Recommendation No.34 (Corr.1 Nov. 2001), and for wave directions μ from 0 (following waves) to 180 (head waves) deg. every 10 deg. For each sailing condition (combination of forward speed and wave direction) and each sea state, numerical simulations were performed in multiple independent realizations of the same sea state for 2 hours or until the first exceedance event until 200 stability failures were encountered. Realizations of the same sea state were generated by random variation of frequencies, directions and phases of wave components composing the sea state.

1.4.2 Direct counting was used to define the time T_i to each stability failure; the expected time until stability failure was calculated by averaging over N=200 stability failures as

$$\hat{T} = (1/N)\sum_{i=1}^{N} T_i \qquad (1.4.1)$$

1.4.3 The maximum likelihood estimate $\hat{r}$ of stability failure rate was calculated as

$$\hat{r} = 1/\hat{T} \qquad (1.4.2)$$

1.4.4 For such combinations of sailing condition and sea state where the total simulation time of $3.4{\cdot}10^6$ hours was not sufficient to encounter 200 stability failures, a statistical extrapolation of stability failure rate over significant wave height from the sea states with greater significant wave heights was used.

1.4.5 Operational measures identify *unacceptable* (those that should be avoided) sailing conditions for each sea state in such a way that avoiding these conditions ensures the same safety level as the safety level provided by design assessment standards. For operational limitations, this requirement is straightforward since operational limitations represent design assessment procedures with changed environmental conditions. For operational guidance, the general principle is the same; however, to distinguish acceptable and unacceptable sailing conditions, a "short-term" criterion is required that can be defined for each situation (and compared with a corresponding "short-term" standard), whereas the safety level provided by operational guidance should be calculated over all situations (and compared with a "long-term" standard). For convenience, the "short-term" standard will be referred to as threshold.

1.4.6 Therefore, the safety level provided by operational guidance was computed as a function of a variable short-term acceptance threshold. Consistent with the discussion above, the safety level provided by operational guidance was defined as the average stability failure rate over all acceptable sailing conditions in all sea states (to investigate the dependency of results on the forward speed, different forward speeds were addressed first treated separately). The appropriate value of the short-term acceptance threshold was found from the requirement that this safety level is equal to the acceptance standard in the design assessment requirements.

$$w_{\mathrm{OG}} = \frac{\sum_{\mathrm{s},\mu} r(H_{\mathrm{s}}, T_{\mathrm{z}}, \mu, v_0) f_{\mathrm{OG}}(H_{\mathrm{s}}, T_{\mathrm{z}}, \mu)\Delta H_{\mathrm{s}} \Delta T_{\mathrm{z}} \Delta\mu}{\sum_{\mathrm{s},\mu} f_{\mathrm{OG}}(H_{\mathrm{s}}, T_{\mathrm{z}}, \mu)\Delta H_{\mathrm{s}} \Delta T_{\mathrm{z}} \Delta\mu} \qquad (1.4.3)$$

1.4.7 In eq. (1.4.3), w_{OG}, 1/s, is the average stability failure rate conditional on operational guidance, $f_{\mathrm{OG}}(H_{\mathrm{s}},T_{\mathrm{z}},\mu)$ is the conditional probability density of sea state with significant wave height H_s, zero-crossing period T_z and mean direction μ, set to zero if a combination (H_s, T_z, μ) is unacceptable and equal to $f_s(H_s, T_z) \cdot f_\mu(\mu)$ otherwise, and $r(H_s, T_z, \mu, v_0)$ is the average "short-term" stability failure rate, 1/s, in a specific sailing condition in a specific sea state. For research purposes, the total stability failure rate as well as contributions from various stability failure modes were calculated.

1.4.8 Two probabilistic "short-term" criteria were tested as candidates: the average stability failure rate r and the product $r \cdot f_s$. Figures 1.4.1(a-e) show the average stability failure rate w_{OG} (total and contributions from stability failure modes) vs. systematically varied short-term threshold of rf_s, and figures 1.4.2 (a-e) show corresponding dependencies for the systematically varied short-term threshold of r.

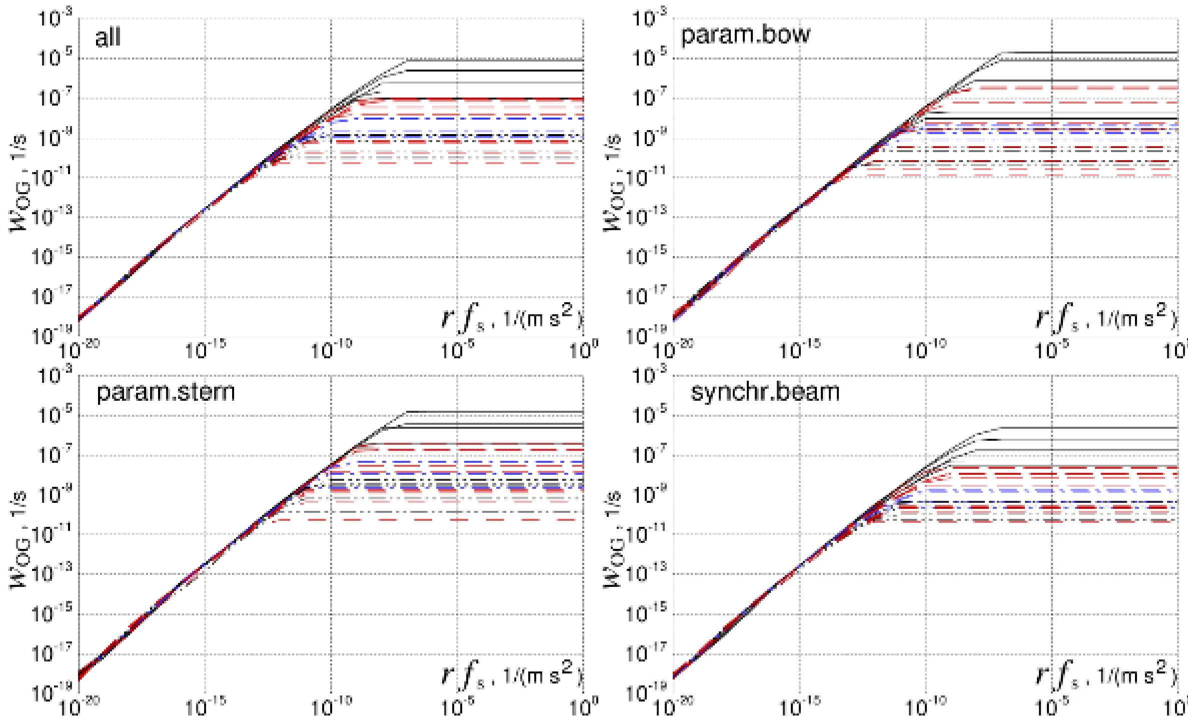

Figure 1.4.1.a. Average rate of stability failures w_{OG}, 1/s, for all failure modes (top left), parametric roll in bow (top right) and stern (bottom left) waves and synchronous roll, relevant for dead ship condition and excessive acceleration stability failures (bottom right) depending on rf_s-threshold, 1/(m·s^2) for cruise ship; types and colours of lines differentiate loading conditions, lines of the same type and colour correspond to various forward speeds for same loading condition

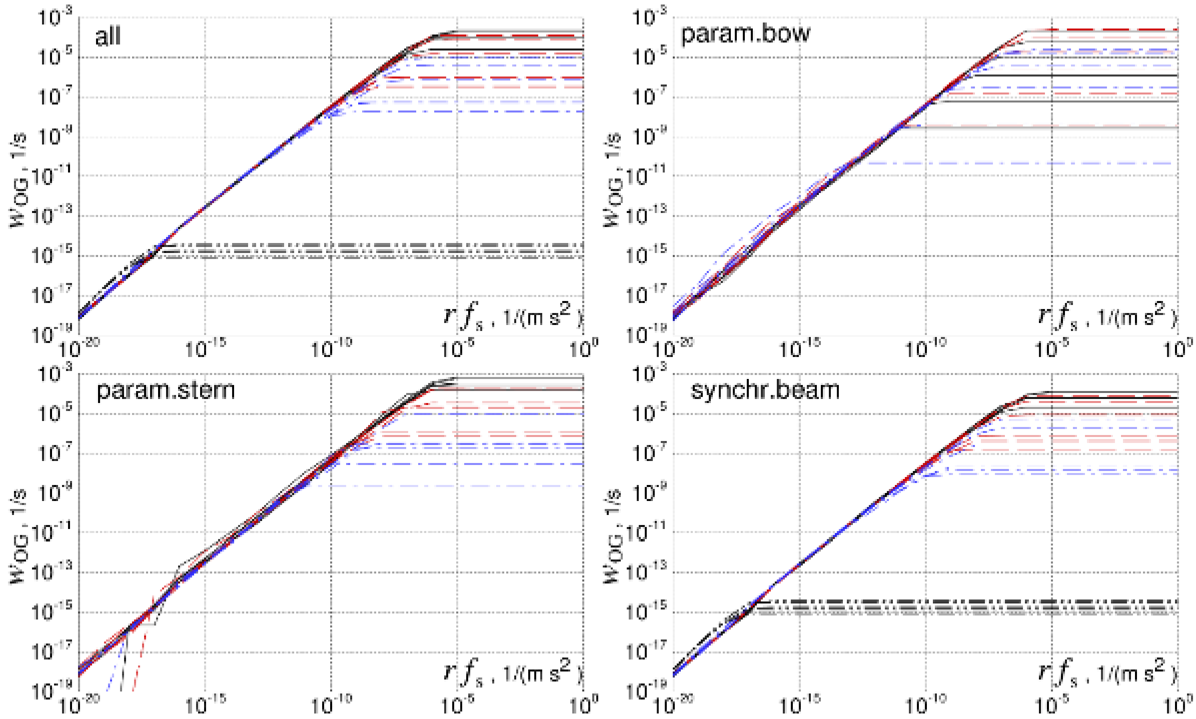

Figure 1.4.1.b. Same as Figure 1.4.1.a for 14000 TEU container ship

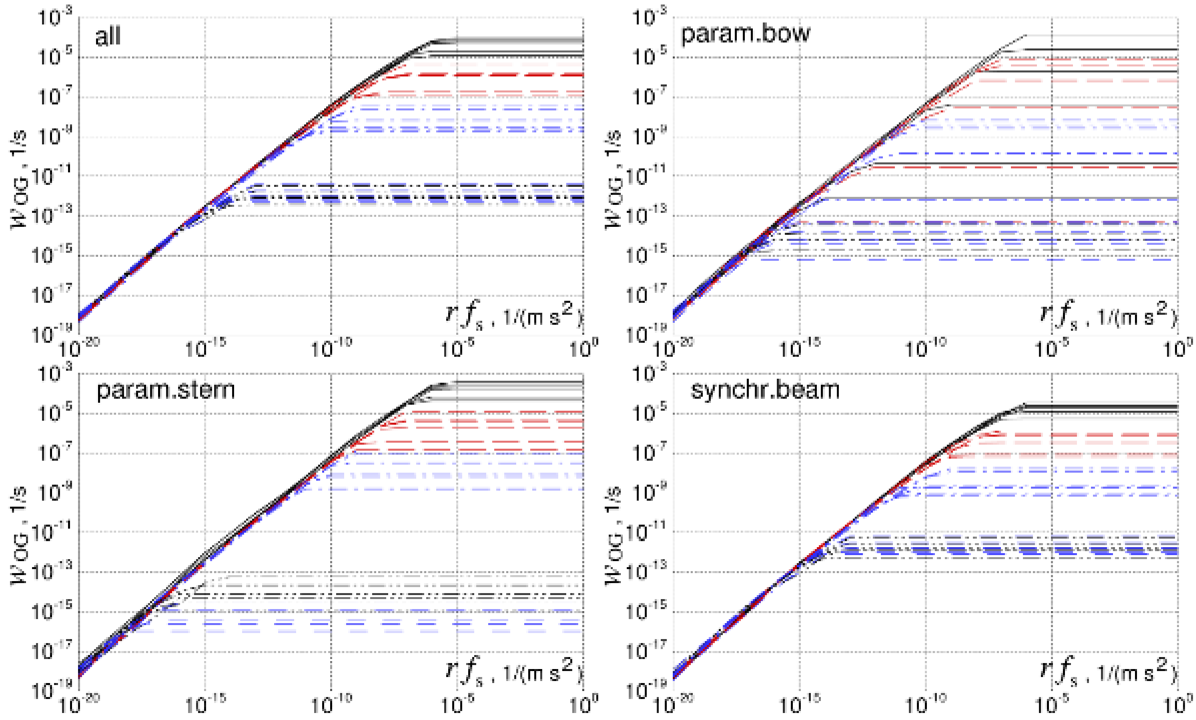

Figure 1.4.1.c. Same as Figure 1.4.1.a for 1700 TEU container ship

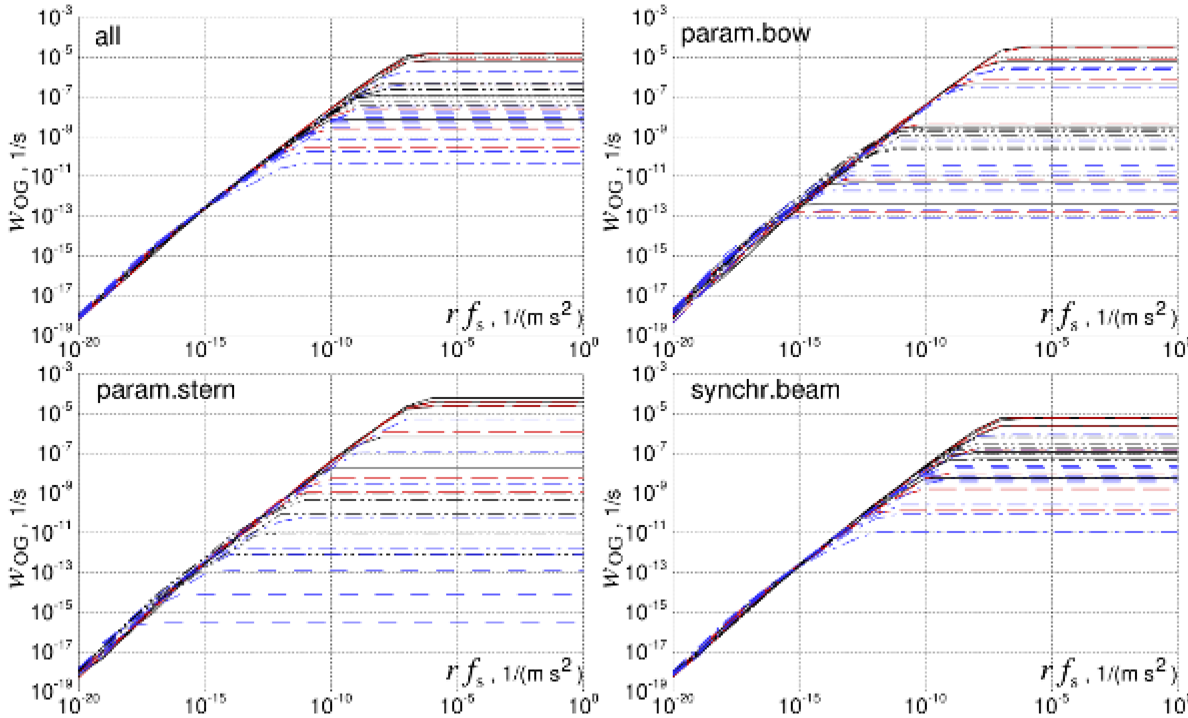

Figure 1.4.1.d. Same as Figure 1.4.1.a for 8400 TEU container ship

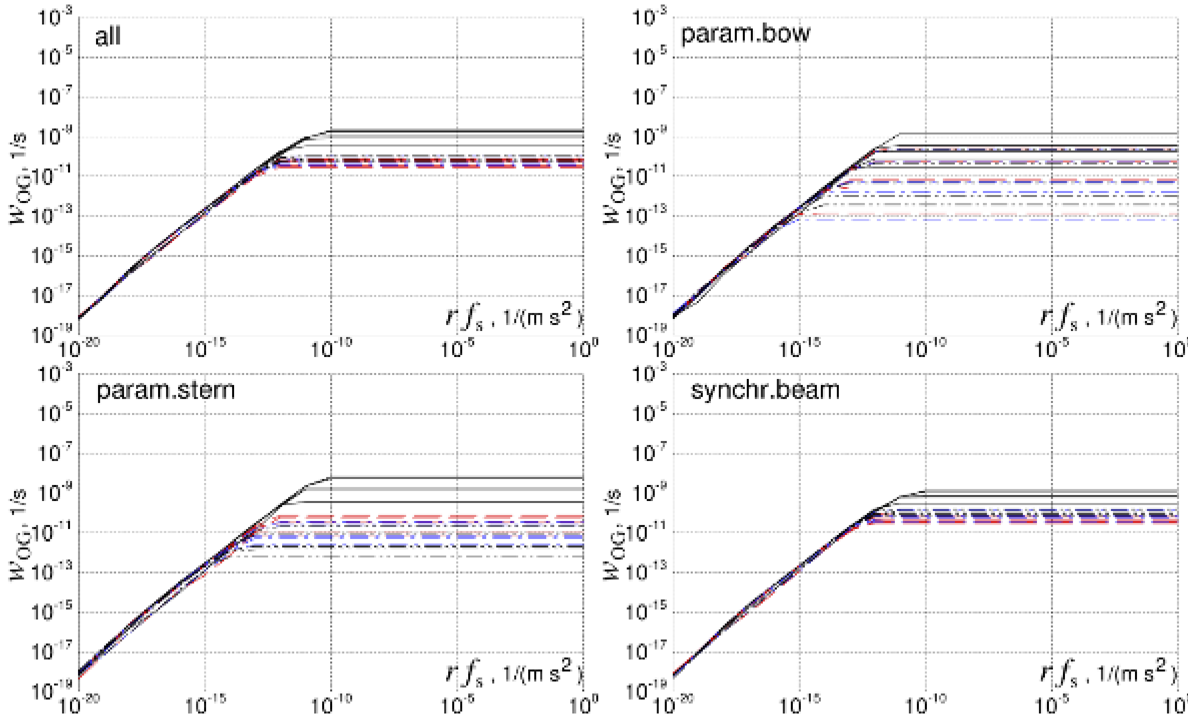

Figure 1.4.1.e. Same as figure 1.4.1.a for RoPax ship

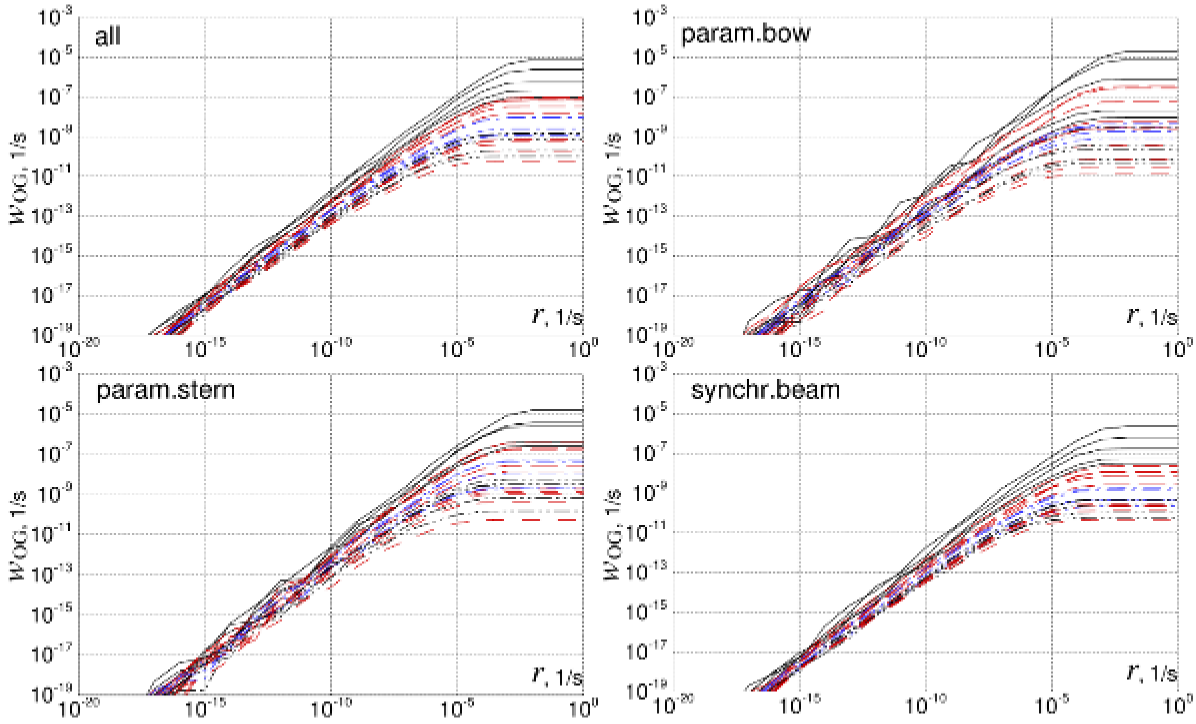

Figure 1.4.2.a. Average rate of stability failures w_{OG}, 1/s, for all failure modes (top left), parametric roll in bow (top right) and stern (bottom left) waves and synchronous roll, relevant for dead ship condition and excessive acceleration failure modes (bottom right) depending on *r*-threshold for cruise ship; types and colours of lines differentiate loading conditions, lines of the same type and colour correspond to various forward speeds for same loading condition

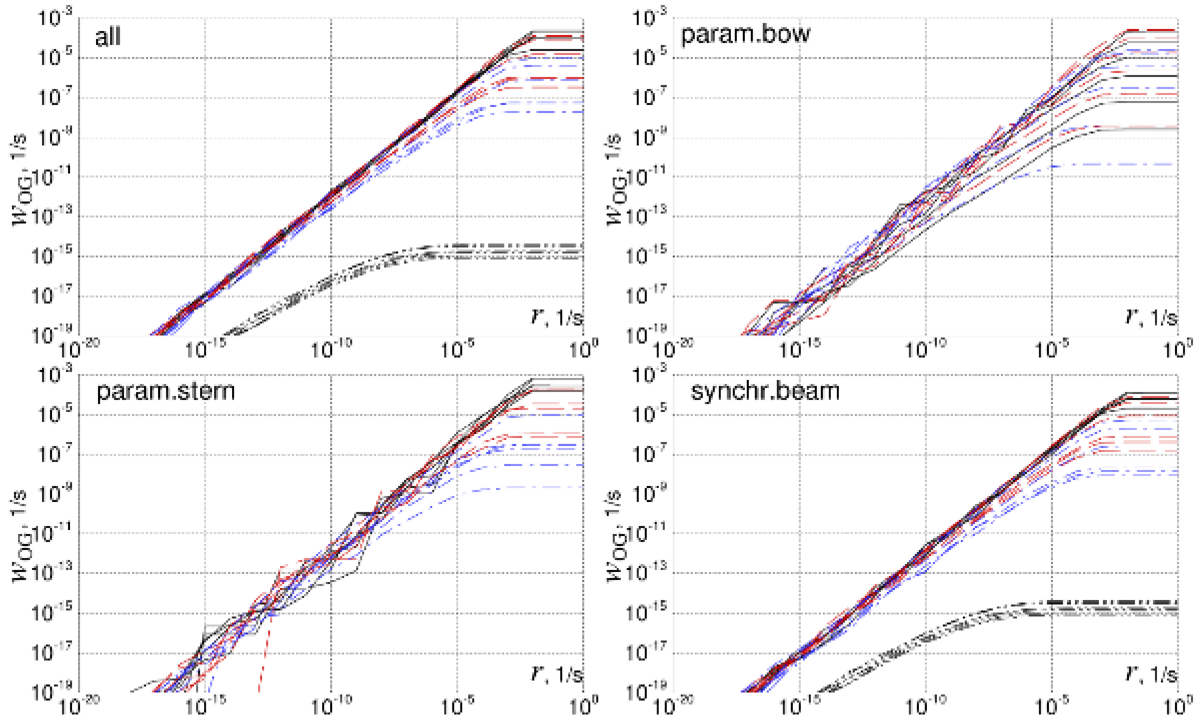

Figure 1.4.2.b. Same as in figure 1.4.2.a for 14000 TEU container ship

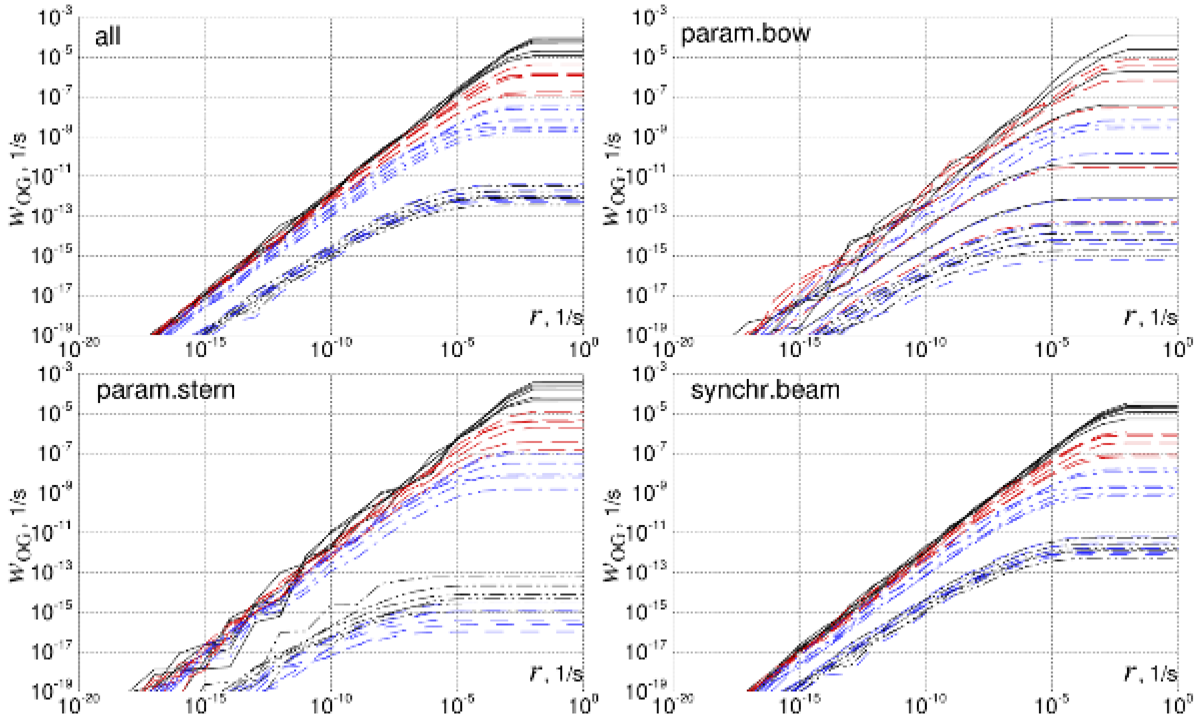

Figure 1.4.2.c. Same as in figure 1.4.2.a for 1700 TEU container ship

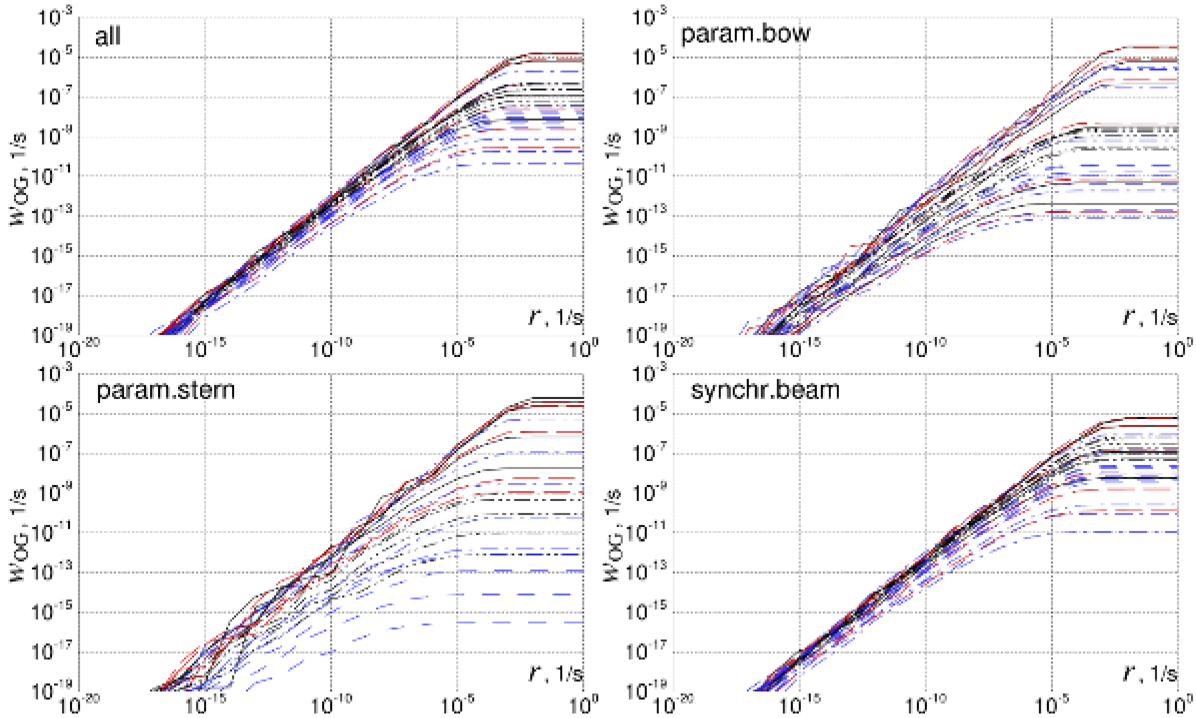

Figure 1.4.2.d. Same as in figure 1.4.2.a for 8400 TEU container ship

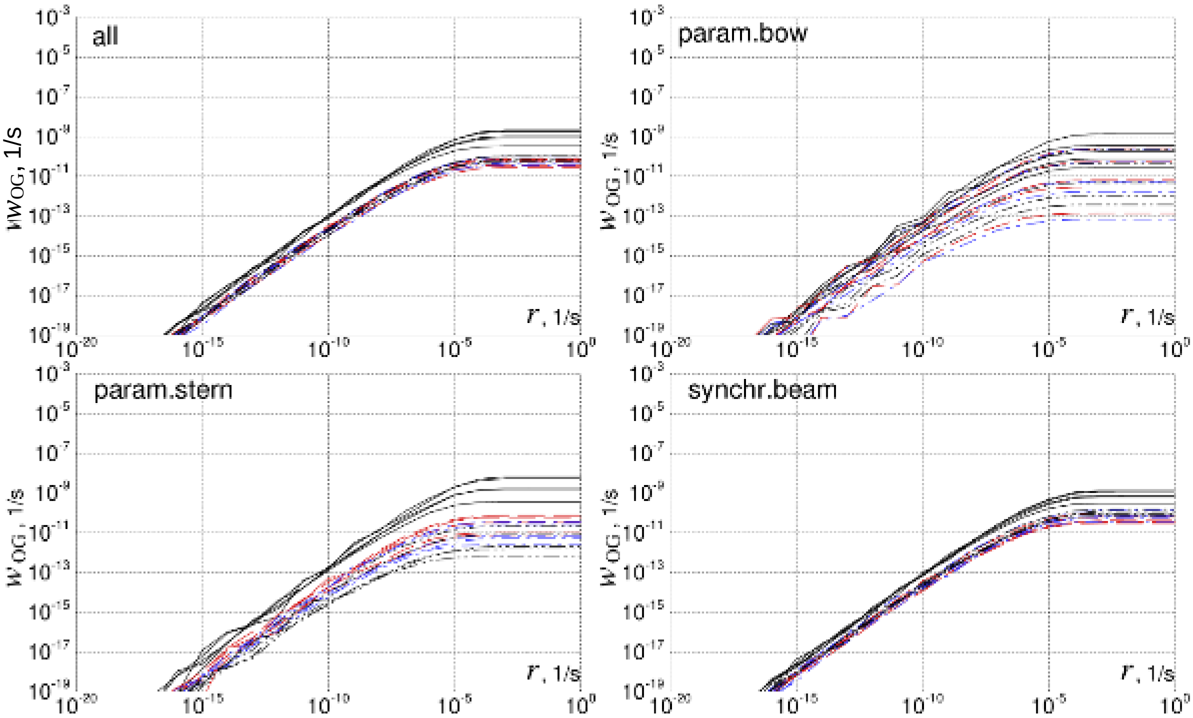

Figure 1.4.2.e. Same as in figure 1.4.2.a for RoPax ship

1.4.9 These results prove rf_s as a suitable criterion to be used for operational guidance since it leads to close dependencies of the long-term safety level w_{OG} on the rf_s-threshold for all ships, loading conditions and forward speeds until saturation (when further relaxation of the threshold does not change safety level anymore: at rf_s of about 10^{-5} 1/(m·s^2), the long-term safety level becomes saturated for all considered ships, loading conditions and forward speeds).

1.4.10 Using directly the stability failure rate r as a "short-term" criterion leads to some spreading of the safety level (at the same value of the short-term threshold) between forward speeds and loading conditions for the same ship and between ships, which means that using r as the "short-term" criterion for operational guidance will lead to spreading of the safety level provided by operational guidance between different ships and loading conditions.

1.4.11 An adequate "short-term" criterion should provide similar safety level for all ships and all loading and sailing conditions, i.e. not allow unsafe sailing conditions while not imposing unnecessary restrictions on safe sailing conditions. To check whether the proposed criteria satisfy these requirements, figure 1.4.3 (left) shows the results as a histogram of the total number of ships, loading conditions and forward speeds (normalized to 1) plotted against the resulting safety level w_{OG} for rf_s-criterion, and figure 1.4.4 shows the corresponding results for the r-criterion. Using the rf_s-criterion effectively removes cases with insufficient safety level, whereas cases that were safe enough without operational guidance are not influenced. As a result, all cases influenced by operational guidance achieve very close safety level. Using r as a criterion for operational guidance provides a similar, while slightly poorer, quality to using rf_s.

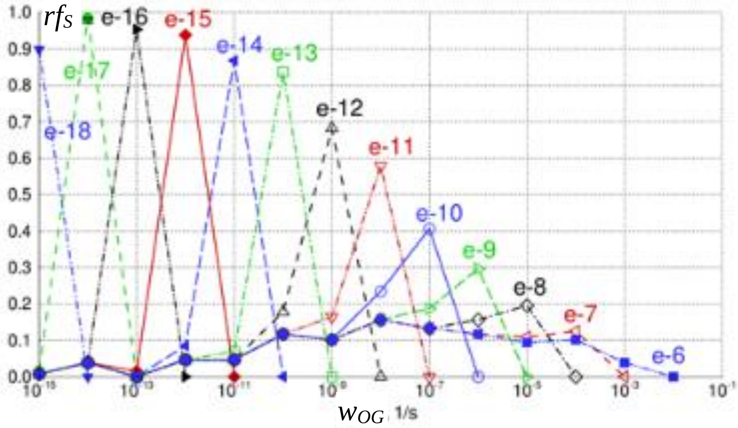

Figure 1.4.3 Number of ships, loading conditions and forward speeds normed on 1 having long-term safety level w_{OG}, 1/s (x-axis) for various rf_s-threshold values (indicated in plot)

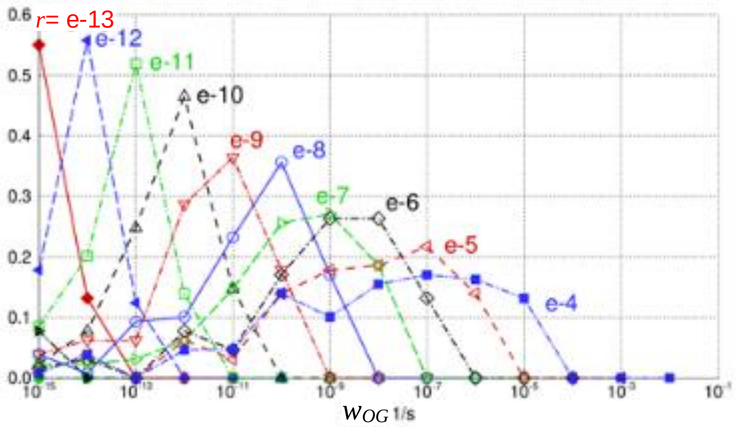

Figure 1.4.4 Number of ships, loading conditions and forward speeds normed on 1 having long-term safety level w_{OG}, 1/s (x- axis) for various r-threshold values (indicated in plot)

1.5 Deterministic operational guidance

1.5.1 Here, it was investigated whether operational guidance based on a non-probabilistic criterion is possible. Such operational guidance is simpler in production and acceptance than a probabilistic one. A drawback is, however, that deterministic operational guidance does not ensure consistent safety level across various ships, loading conditions and sailing conditions, thus it is difficult to ensure consistency with direct stability assessment.

1.5.2 A large inaccuracy of a deterministic operational guidance must be compensated by its excessive conservativeness (to keep a suitable safety level). Note, however, that an excessive conservativeness of operational guidance is a smaller problem than excessive conservativeness of direct stability assessment. Usually, operational practices are based on more conservative requirements than design assumptions anyway.

1.5.3 The approach is based on the same idea as in the probabilistic operational guidance, eq. (1.4.3), but instead of a probabilistic criterion (stability failure rate r or product rf_s above), a non-probabilistic criterion is used to differentiate between safe and unsafe sailing conditions. Studies on the development of deterministic direct stability assessment showed that among the compared non-probabilistic criteria, namely standard deviation of roll angle, average roll amplitude, significant roll amplitude and three-hour maximum roll amplitude, the latter provides the best results in direct stability assessment compared to the others; therefore, it was also used as a criterion in the deterministic operational guidance.

1.5.4 To compute the expected maximum three-hour roll amplitude, numerical simulations were carried out in 50 realizations of the same sea state; the realizations were generated by random variation of frequencies, directions and phases of harmonic components modelling seaway. A difficulty in the application of deterministic criteria is occurrence of capsizing in some realizations. In such cases, the maximum three-hour roll amplitude cannot be defined and thus, the mean three-hour maximum roll amplitude cannot be calculated. To indicate such cases in plots, mean -hour maximum roll amplitude is shown as 60 degrees in plots (since in situations where capsizing did not happen, mean 3-hour maximum roll amplitude never achieved 60 degrees).

1.5.5 Figures 1.5.1 (a-e) show the average "long-term" stability failure rate w_{OG} (total and due to various stability failure modes) vs. the systematically varied threshold of the mean three-hour maximum roll amplitude. The results indicate significant scatter of the dependencies of w_{OG} on the deterministic threshold between ships, loading conditions and forward speeds; saturation happens at about 30 degrees of mean three-hour maximum roll amplitude for all considered ships, loading conditions and forward speeds.

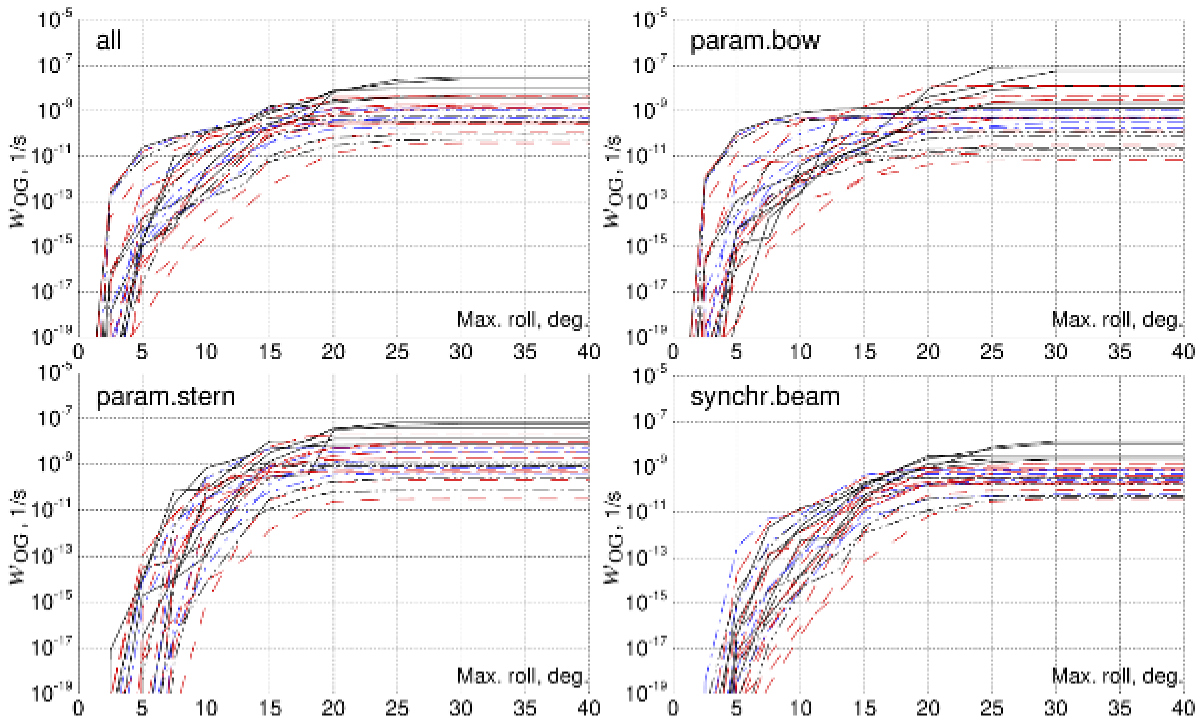

Figure 1.5.1.a. Average stability failure rate w_{OG}, 1/s, for all failure modes (top left), parametric roll in bow (top right) and stern (bottom left) waves and synchronous roll, relevant for dead ship condition and excessive acceleration failure modes, (bottom right) vs. threshold of mean three-hour maximum roll amplitude for cruise ship; line types and colours differentiate loading conditions, lines of the same type and colour correspond to various forward speeds

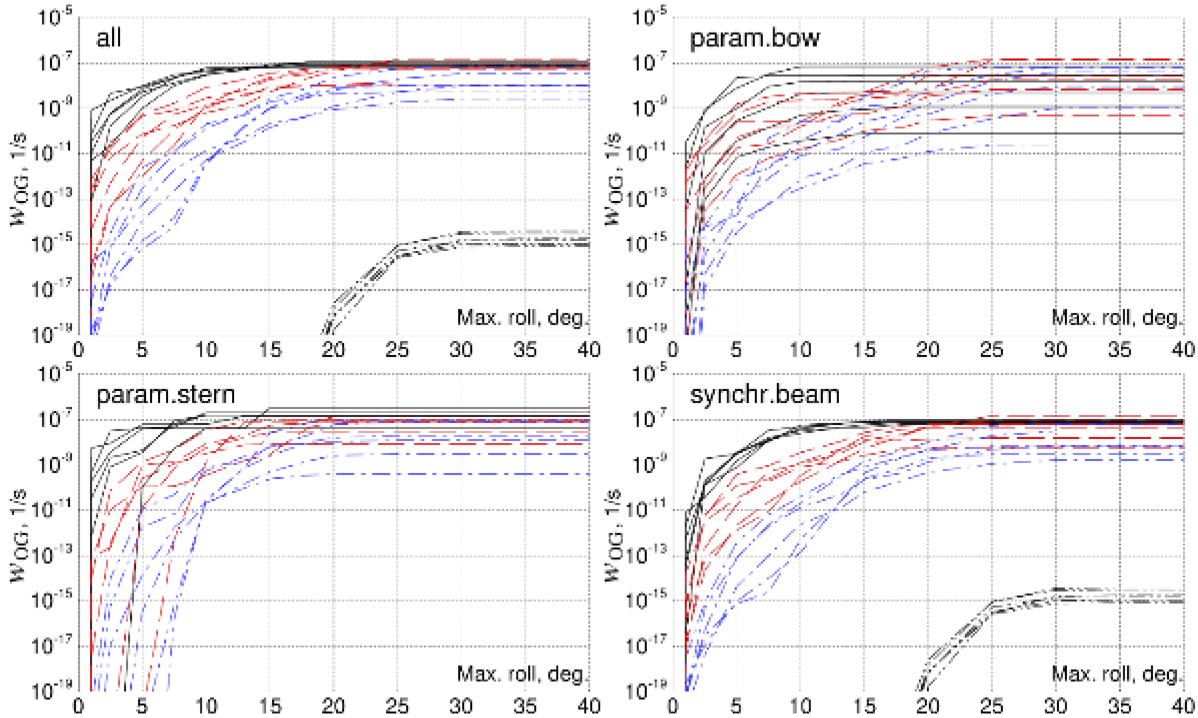

Figure 1.5.1.b. Same as in figure 1.5.1.a for 14000 TEU container ship

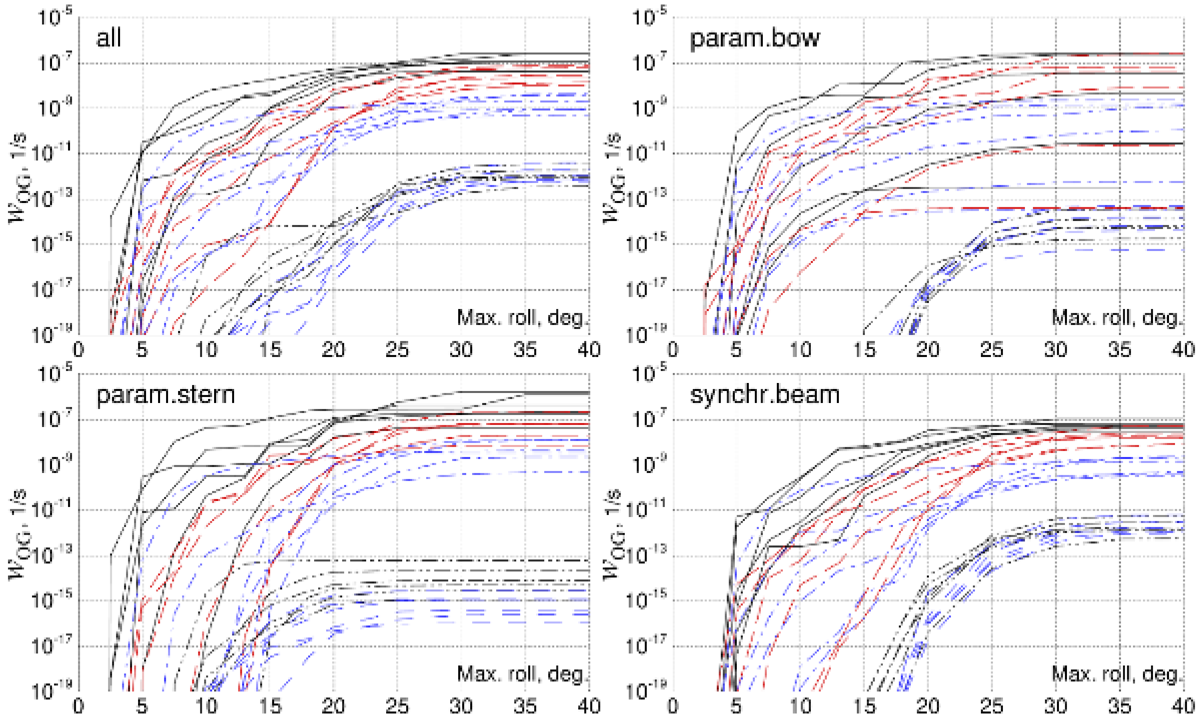

Figure 1.5.1.c. Same as in figure 1.5.1.a for 1700 TEU container ship

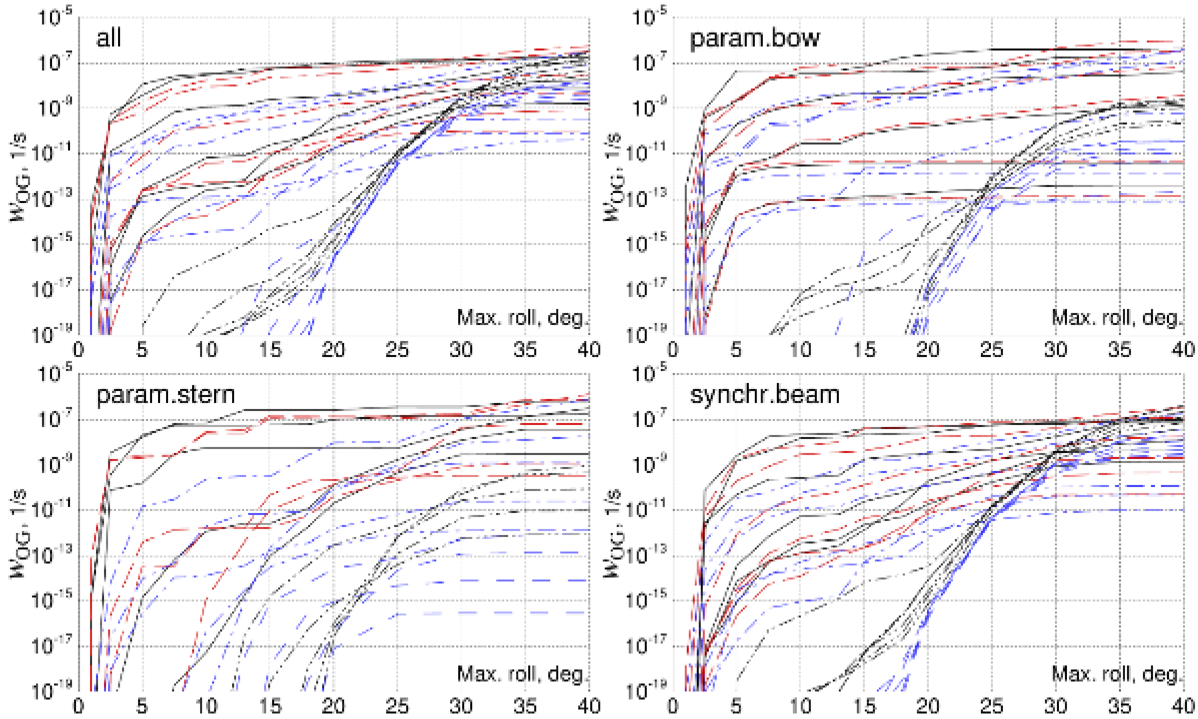

Figure 1.5.1.d. Same as in figure 1.5.1.a for 8400 TEU container ship

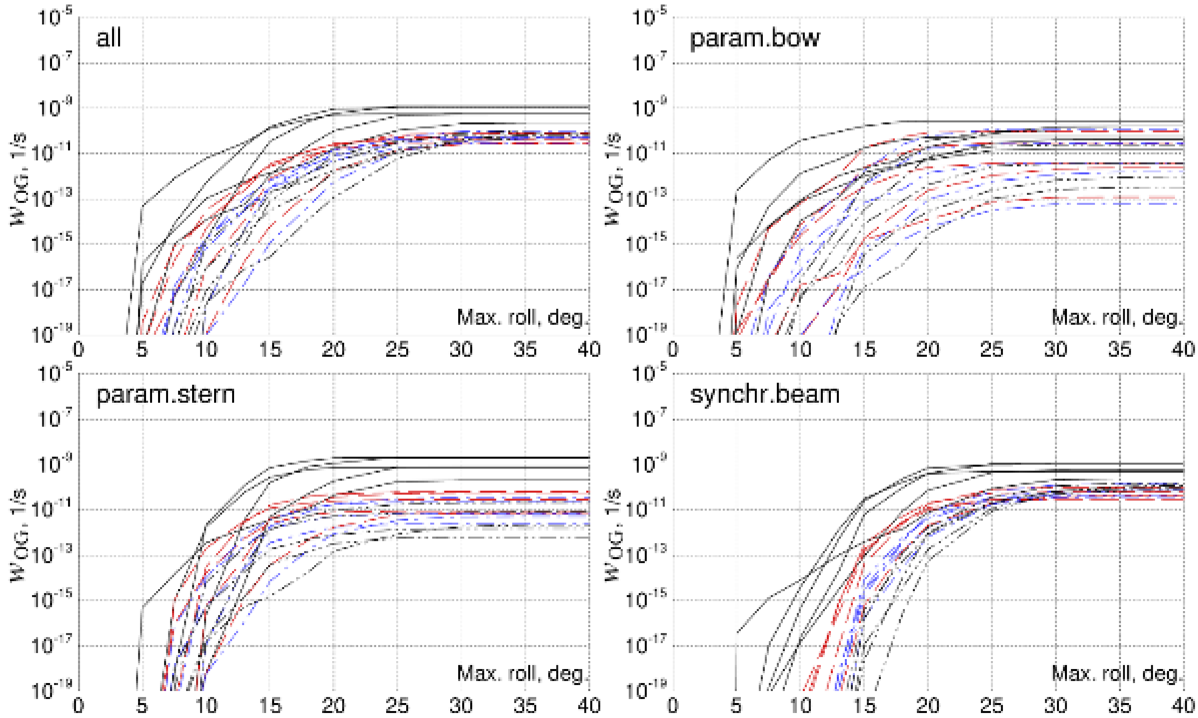

Figure 1.5.1.e. Same as in figure 1.5.1.a for RoPax ship

1.5.6 To check how deterministic operational guidance influences safety level of different ships and loading conditions at different forward speeds, figure 1.5.2 (left) shows histogram of the total number of ships, loading conditions and forward speeds normalized to 1, plotted against the achieved safety level w_{OG} for various values of the threshold for the mean three-hour maximum roll. Note that the results for the threshold values of 40 and 60 degrees are very similar (cases with 60 degrees maximum roll amplitude mean here such cases where at least one capsize happened in 50 simulations of three hours duration each).

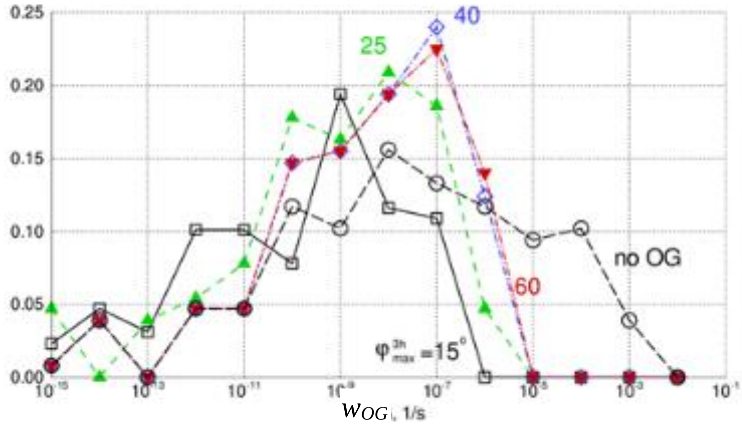

Figure 1.5.2 Total number of ships, loading conditions and forward speeds (normalized to 1) with long-term safety level w_{OG}, 1/s (x- axis) for various values (indicated in plot) of threshold of mean 3-hour maximum roll amplitude

1.5.7 The deterministic approach does not fully exclude cases with insufficient safety level: in fact, strengthening the threshold from 60 to 25 degrees little influences the mean "long-term" rate of stability failures at and below 10^{-7} 1/s. The safety level of all cases influenced by operational guidance is broadly spread.

1.6 Definition of thresholds

1.6.1 To differentiate between acceptable and unacceptable sailing conditions (combinations of forward speed and course) in each sea state, the "short-term" acceptance thresholds for rf_s, r and φ_{3h} are defined from the "long-term" standard (safety level) using the dependencies of the average "long-term" stability failure rate over all acceptable sailing conditions in all sea states on the short-term acceptance threshold described above.

1.6.2 Appendix 4 defines w_{OG}=2.6·10^{-8} 1/s as the required "long-term" standard (safety level). To derive the short-term thresholds, figures 1.6.1 (a-c) and table 1.6.1 show the "long-term" average stability failure rate w_{OG} (averaged over all speeds) depending on rf_s- (left), r- (middle) and φ_{3h}- (right) thresholds; the results indicate 10^{-10} 1/(m·s^2) and 10^{-6} 1/s as appropriate thresholds for rf_s and r, respectively.

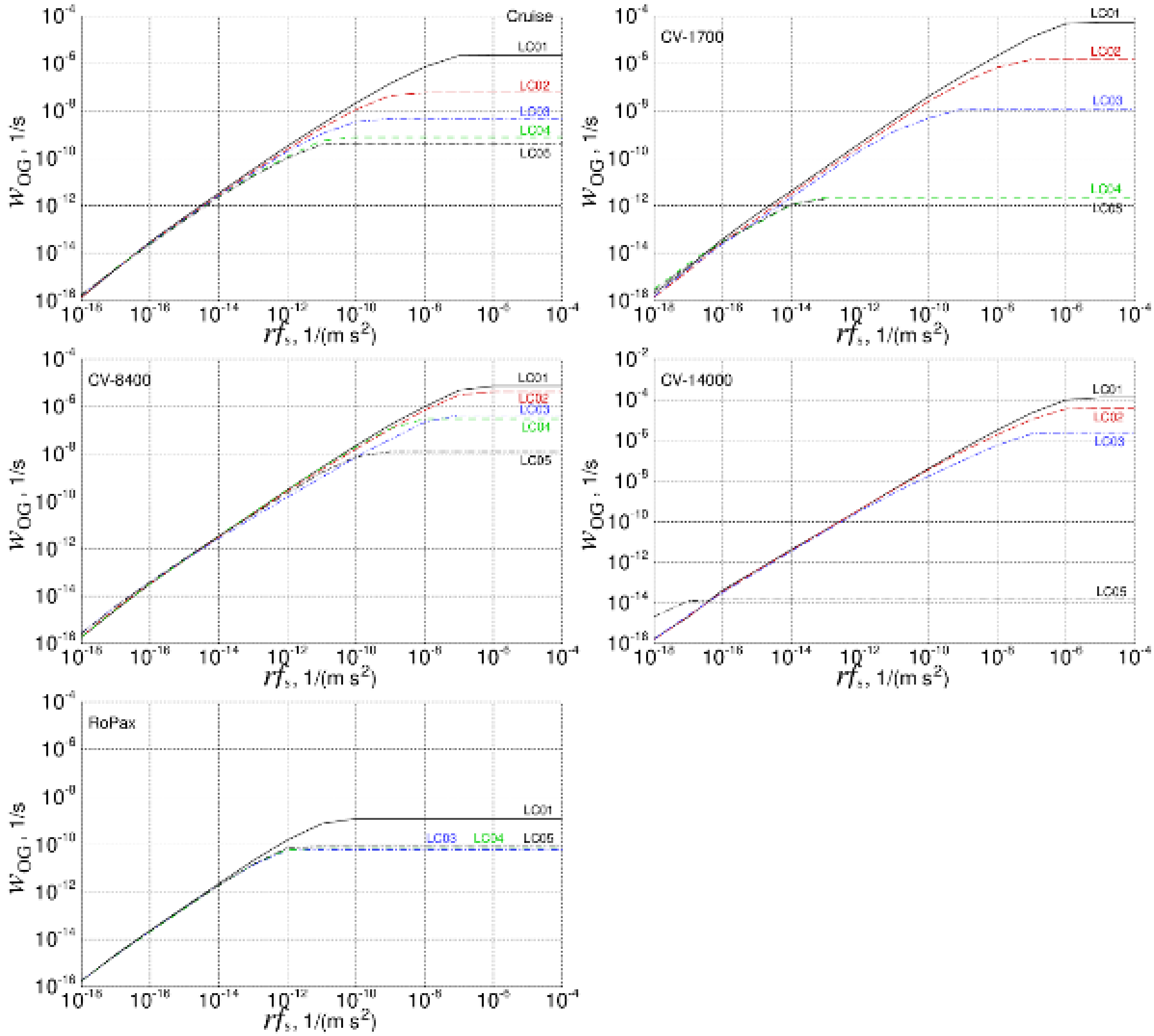

Figure 1.6.1.a. Average "long-term" stability failure rate w_{OG}, 1/s, averaged over all speeds, vs. "short-term" rf_s-threshold, 1/(m·s^2); each plot corresponds to one ship, each line corresponds to one loading condition

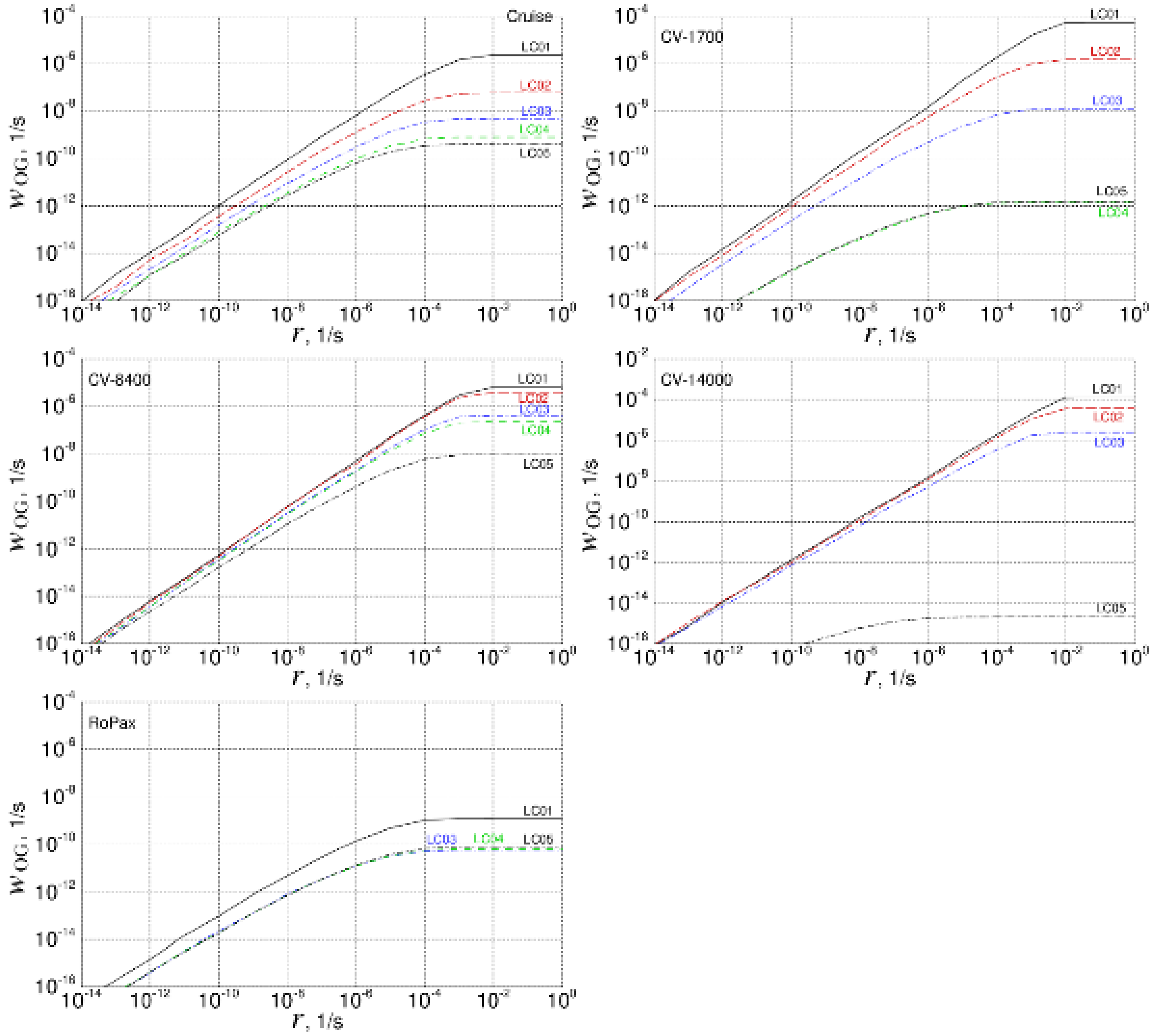

Figure 1.6.1.b. Average "long-term" stability failure rate w_{OG}, 1/s, averaged over all speeds, vs. "short-term" r-threshold, 1/s; each plot corresponds to one ship, each line corresponds to one loading condition

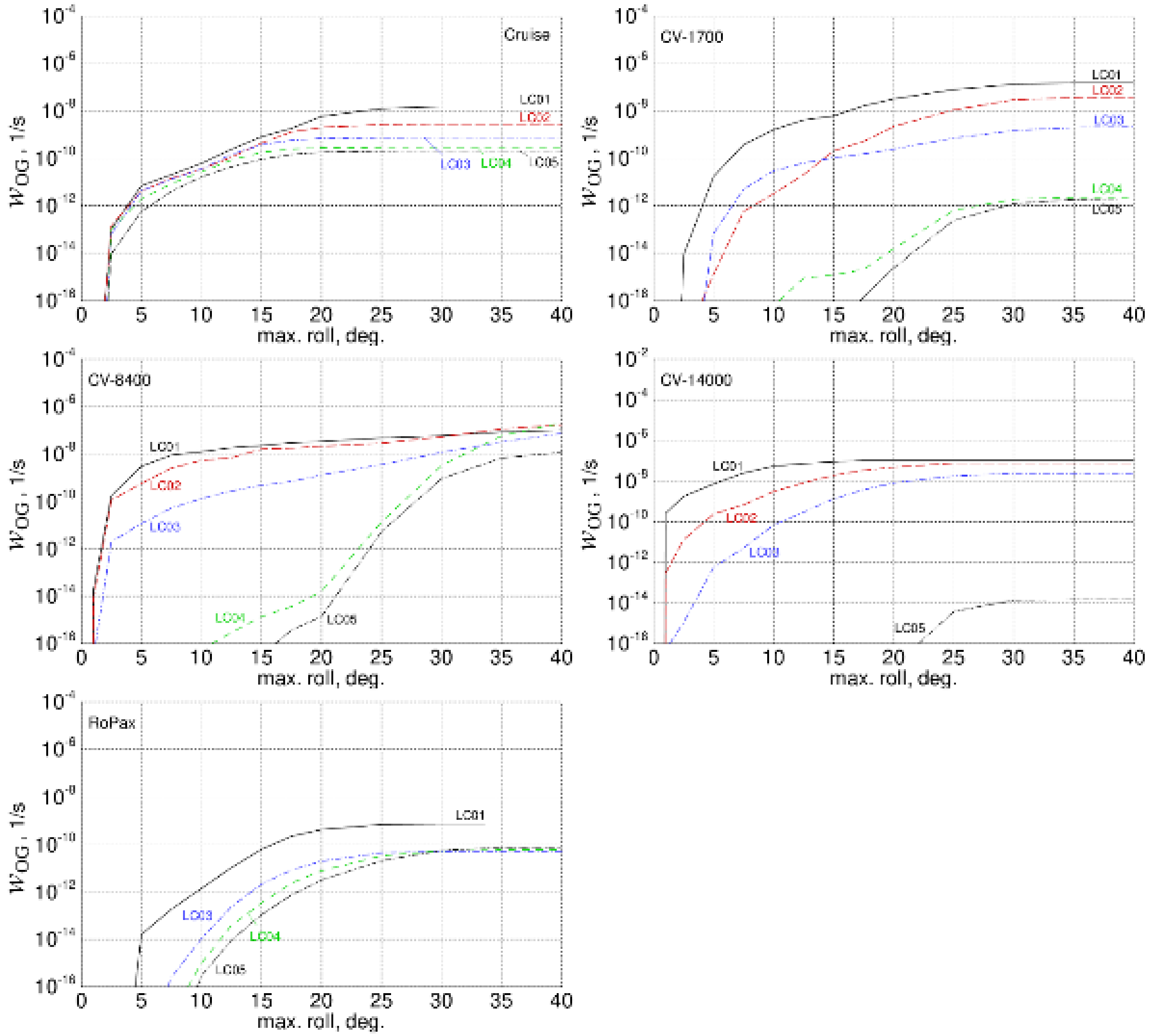

Figure 1.6.1.c. Average "long-term" stability failure rate w_{OG}, 1/s, averaged over all speeds, vs. "short-term" φ_{3h}-threshold, degree; each plot corresponds to one ship, each line corresponds to one loading condition

Table 1.6.1 Definition of short-term threshold for operational guidance

Ship	Loading condition	rf_s, 1/(m·s^2)	r, 1/s	φ_{3h},°
Cruise vessel	01	$1.3 \cdot 10^{-10}$	$4.7 \cdot 10^{-6}$	-
	02	$4.2 \cdot 10^{-10}$	$9.7 \cdot 10^{-5}$	-
1700 TEU container ship	01	$6.5 \cdot 10^{-11}$	$1.7 \cdot 10^{-6}$	20.7
	02	$1.1 \cdot 10^{-10}$	$5.9 \cdot 10^{-6}$	29.7
8400 TEU container ship	01	$1.2 \cdot 10^{-10}$	$5.2 \cdot 10^{-6}$	20.6
	02	$1.8 \cdot 10^{-10}$	$6.1 \cdot 10^{-6}$	23.6
	03	$5.4 \cdot 10^{-10}$	$1.6 \cdot 10^{-5}$	34.8
	04	$2.7 \cdot 10^{-10}$	$2.5 \cdot 10^{-5}$	33.6
CV-14000 container ship	01	$6.3 \cdot 10^{-11}$	$1.7 \cdot 10^{-6}$	7.7
	02	$7.1 \cdot 10^{-11}$	$2.1 \cdot 10^{-6}$	17.9
	03	$1.7 \cdot 10^{-10}$	$5.4 \cdot 10^{-6}$	-
Selection		10^{-10}	10^{-6}	s. text

1.6.3 To illustrate the difficulty of the definition of the required "short-term" threshold for the mean 3-hour maximum roll amplitude φ_{3h}, figure 1.6.2 shows some typical dependencies of the exceedance rate of certain roll amplitude on this amplitude. Such dependencies strongly depend on the form of the righting lever curve, stability failure mode and wave height, period and direction. These results indicate that the dependencies of the failure rate on roll amplitude can be unpredictable, therefore, some sort of extrapolation of failure rate over roll amplitude is in general impossible.

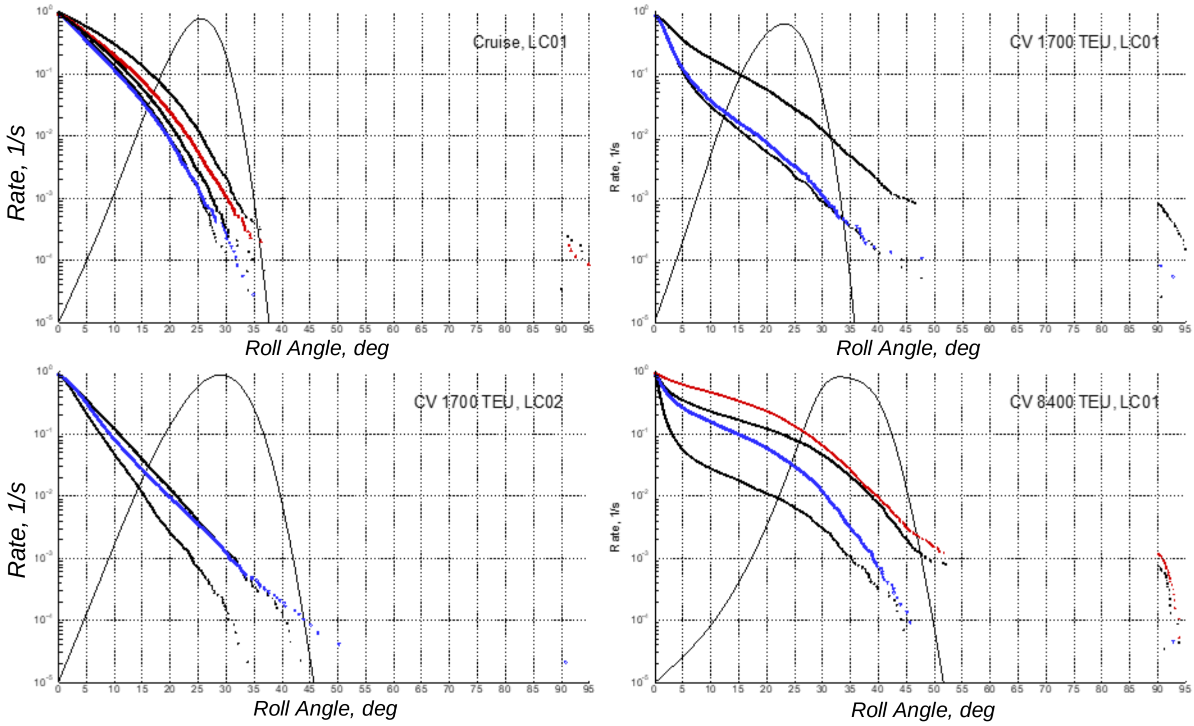

Figure 1.6.2. Exceedance rate (1/s, *y*- axis) of roll amplitudes shown along *x*- axis (degree) together with righting-lever curves in calm water for (top left to bottom right) cruise vessel in loading condition LC01 (parametric roll in head and following waves and synchronous roll in beam waves), 1700 TEU container ship in LC01 (parametric roll in head and following waves) and LC02 (synchronous roll in beam waves) and 8400 TEU container ship in LC01 (parametric roll in head and following waves)

1.6.4 One pragmatic alternative is to find a simple empirical formula for the φ_{3h}-threshold based on its relation with the safety level. Figure 1.6.1 (right) shows the "long-term" stability failure rate w_{OG}, averaged over all forward speeds, vs. short-term φ_{3h}-threshold for sample ships and loading conditions, and table 1.6.1 shows the resulting threshold values. Figure 1.6.3, comparing these values with the calm-water capsize heel angle, shows that the threshold can be approximated as half of the calm-water capsize heel angle (generally, as half of the heel angle defining stability failure). Although this definition appears not conservative in some cases, note that the results of probabilistic assessment used to define thresholds are conservative due to conservative extrapolation of stability failure rate over wave height. This does not matter for the definition of r- and rf_s-thresholds but influences the definition of φ_{3h}-threshold.

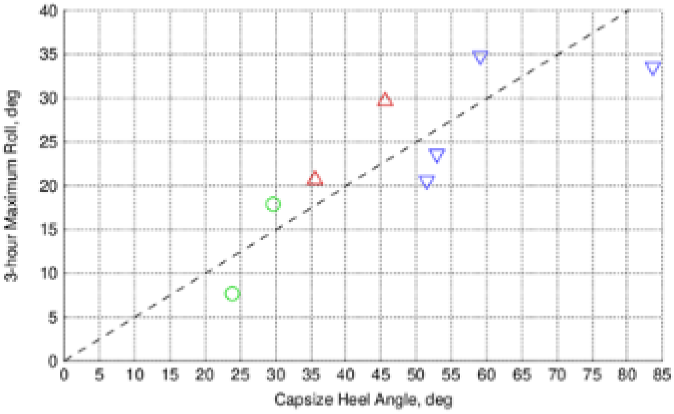

Figure 1.6.3 φ_{3h}-threshold vs. calm-water capsize heel angle

1.6.5 Another way is to use a relation following from the Rayleigh distribution of roll amplitudes, i.e. $\alpha \cdot \varphi_{3h} \le \varphi_{sf}$, where φ_{sf} defines stability failure, $\alpha = \{\ln(T/T_r) / \ln(T_{3h}/T_r)\}^{0.5}$ (but not less than 1), $T = f_s/10^{-10}$, T_r is the natural roll period and T_{3h} means three hours in seconds. Figure 1.6.4 shows that this approximation is suitable for synchronous roll in beam waves and conservative for parametric roll.

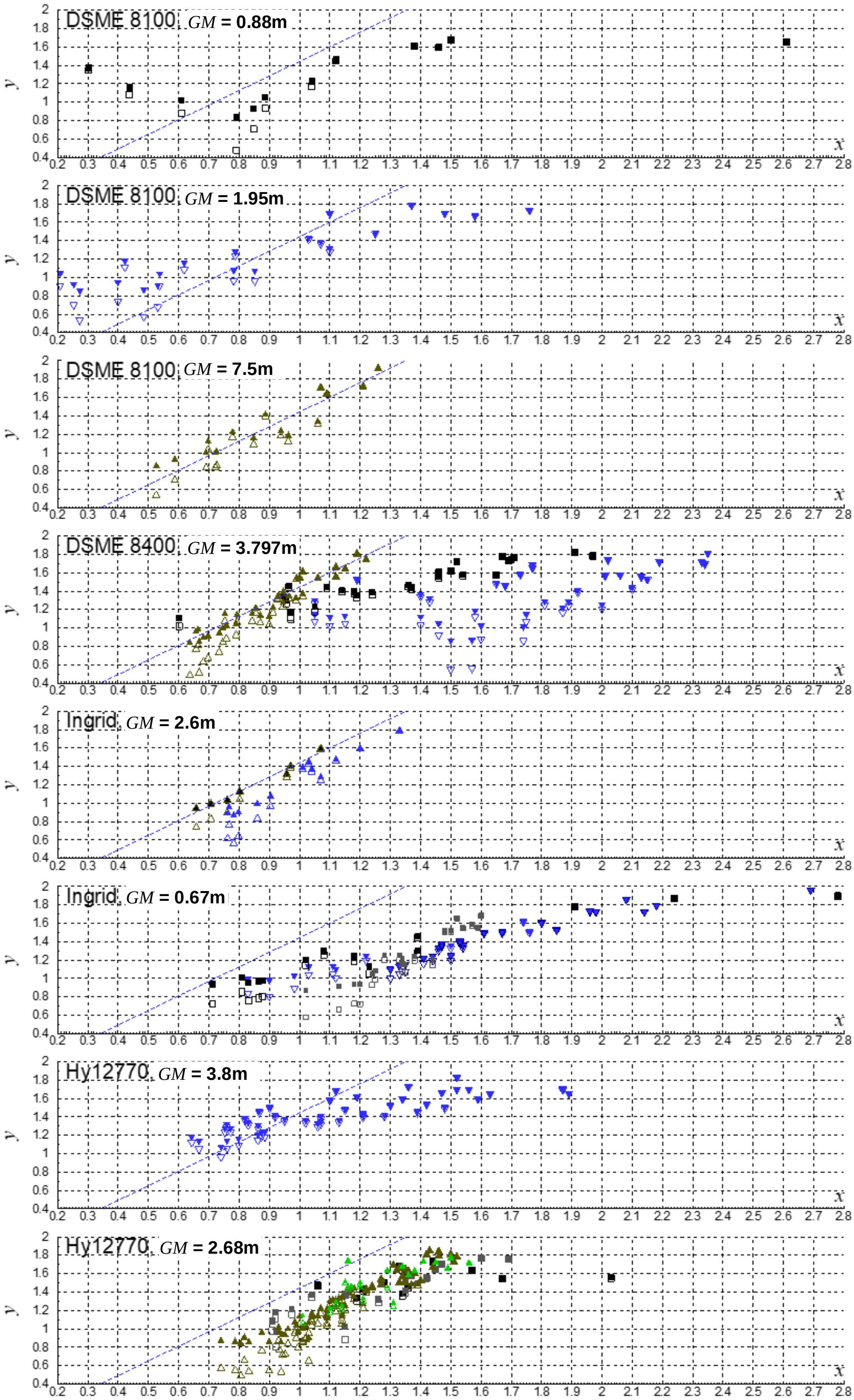

Figure 1.6.4 $\ln(-\ln r)$ vs. ln{φ_{3h} – φ)/σ_φ} for parametric roll in stern-quartering (■,□) and bow (▼,▽) waves and synchronous roll (▲,△); blue dashed lines show Rayleigh distribution

1.6.6 Figures 1.6.5 (a-c) show examples of mean 3-hour maximum roll amplitude, its double value and maximum 15-hour roll amplitude, defined from 15-hour simulations for several parametric and synchronous roll situations, vs. significant wave height; figures 1.6.6 (a-c) show corresponding results using factor α. The results indicate that doubling φ_{3h} produces slightly more conservative results than using factor α, and both provide the limiting significant wave height 1 m to 2 m less than that leading to capsizing in three hours.

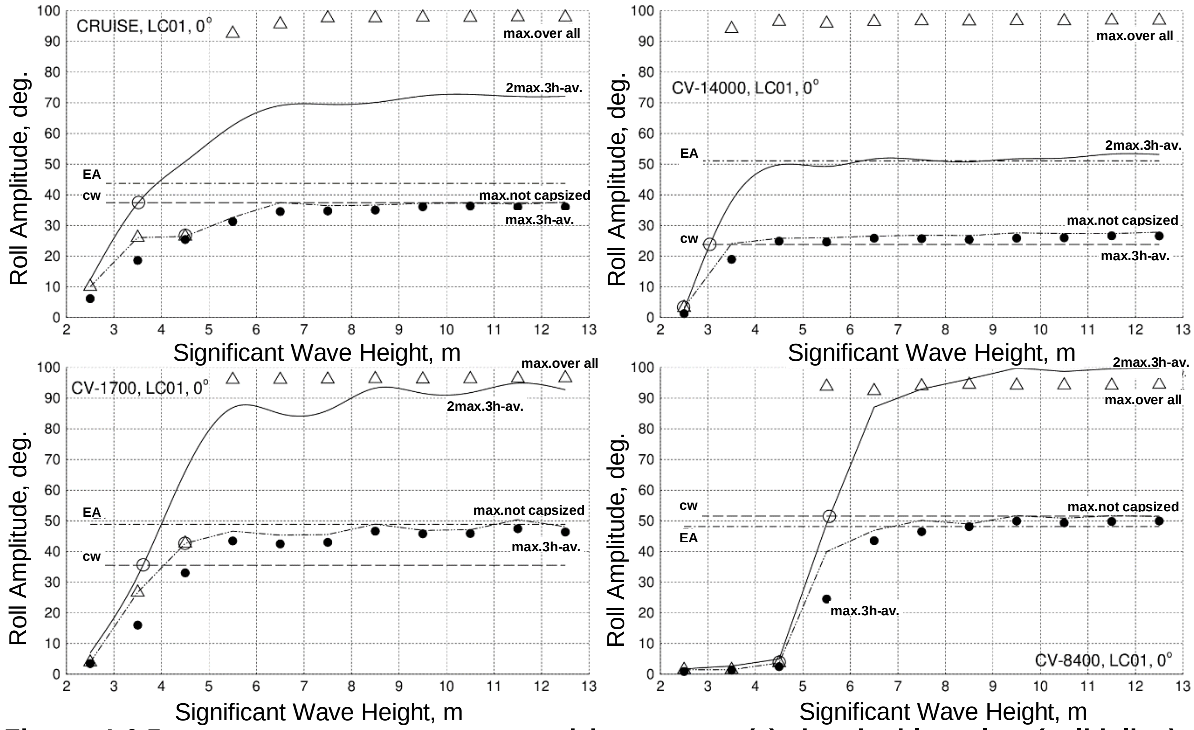

Figure 1.6.5.a. φ_{3h} defined excluding capsizing events (•), its double value (solid line), maximum 15-hour roll amplitude taking (△) and not taking (▽) into account capsizes and calm-water capsize heel angle (horizontal dashed line) vs. significant wave height for parametric roll in following waves for several ships and loading conditions

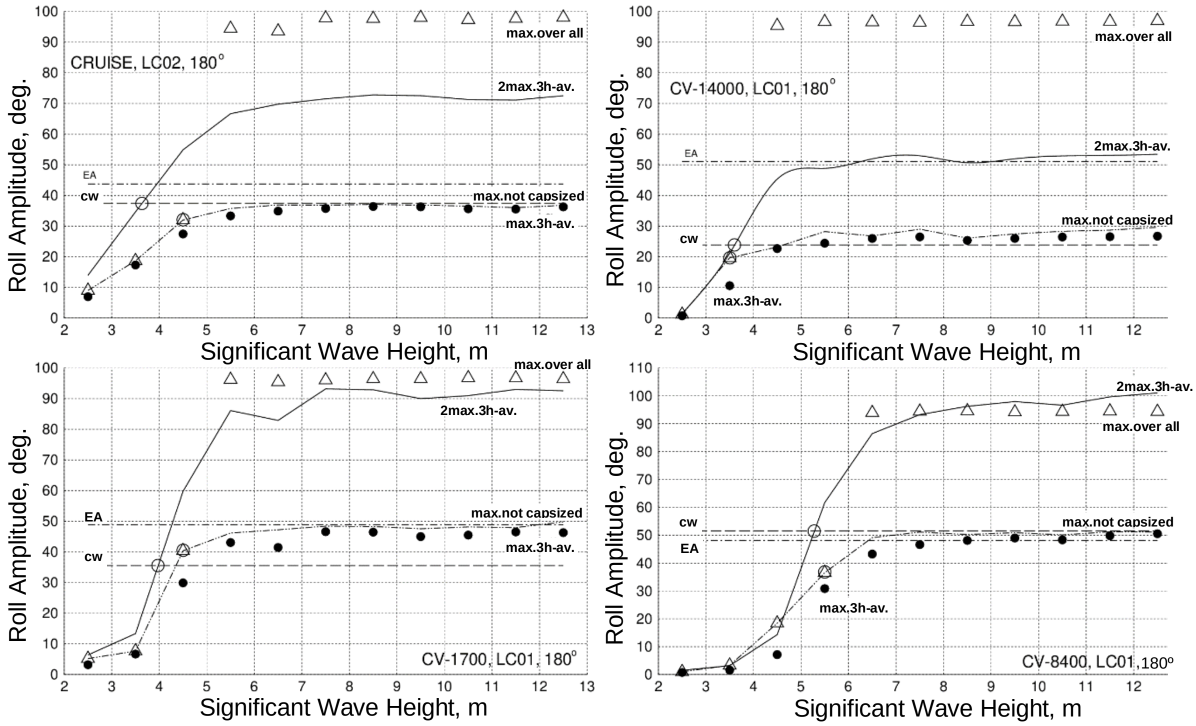

Figure 1.6. 5. b. Same as in figure 1.6.5.a for parametric roll in head waves

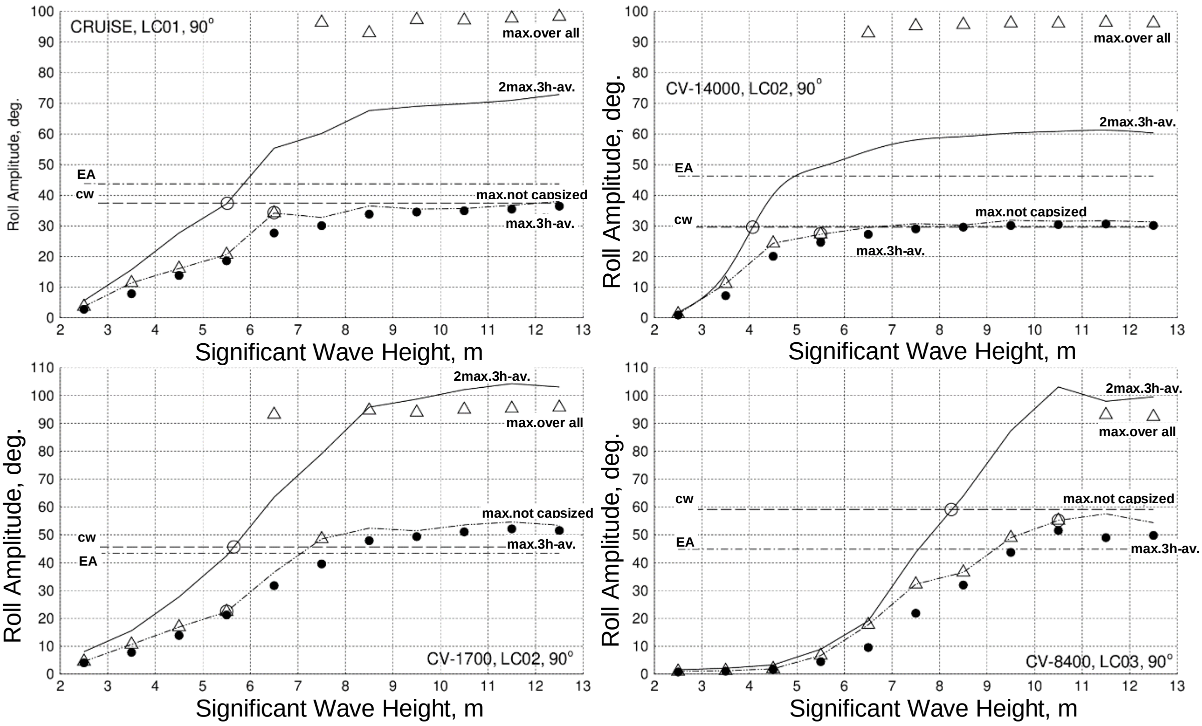

Figure 1.6.5.c. Same as in figure 1.6.5.a for synchronous roll in beam waves (relevant for dead ship condition and excessive acceleration failure modes)

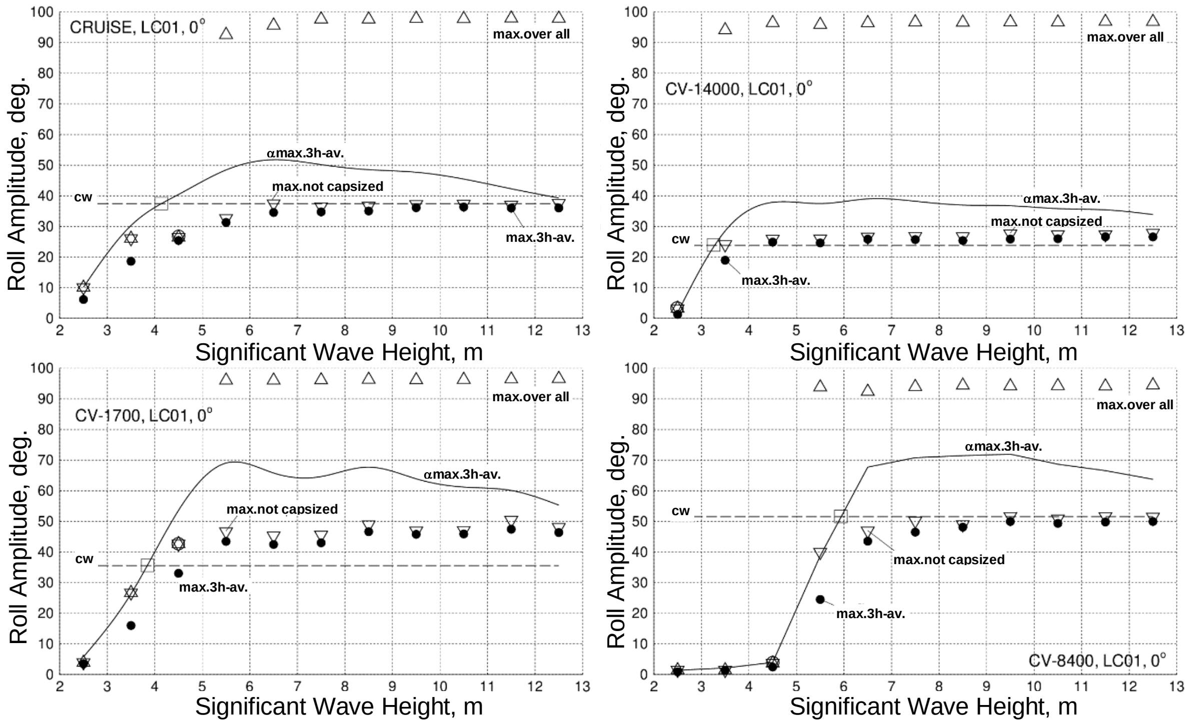

Figure 1.6.6.a. Mean three-hour maximum roll amplitude (●), its value multiplied with factor α (solid line), maximum roll amplitude taking (△) and not taking (▽) into account capsizes and calm-water capsize heel angle (horizontal dashed line) vs. significant wave height for parametric roll in following waves for several ships and loading conditions

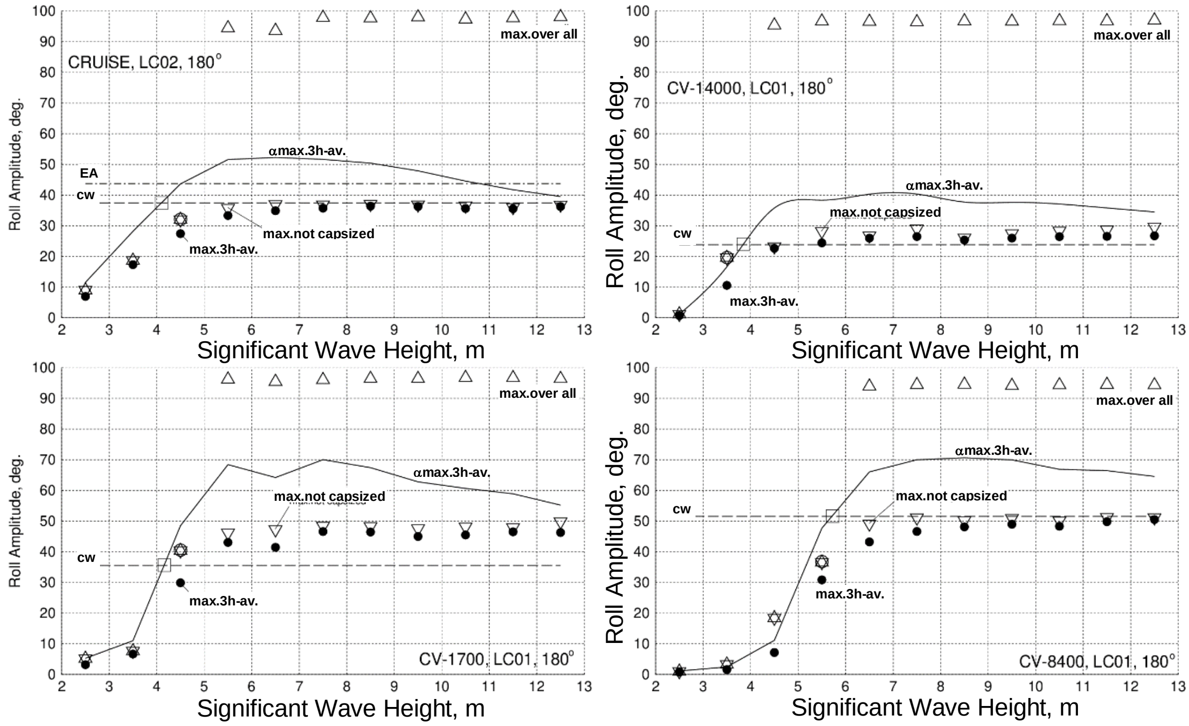

Figure 1.6.6.b. Same as in figure 1.6.6.a for parametric roll in head waves

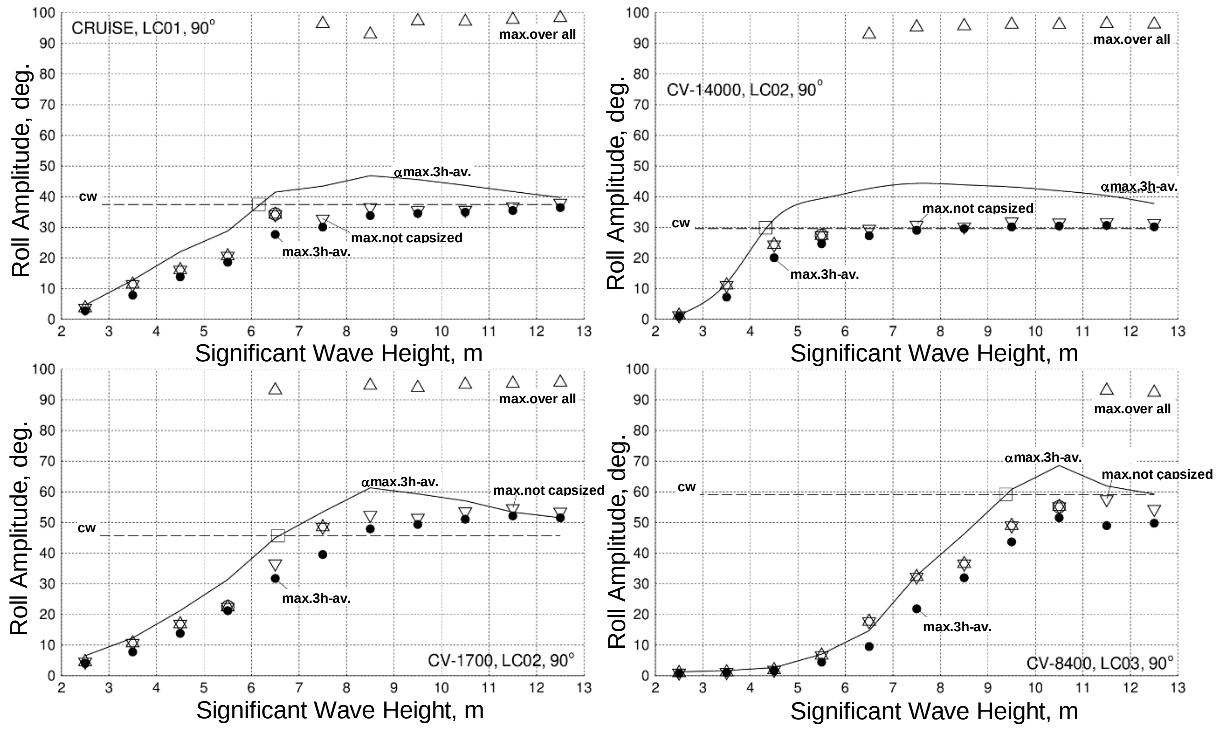

Figure 1.6.6.c. Same as in figure 1.6.6.a for synchronous roll in beam waves (relevant for dead ship condition and excessive acceleration failure modes)

1.6.7 Table 1.6.2 shows conservative and non-conservative errors, defined as percentage of the number of situations with conservative or non-conservative errors from the total number of situations, of deterministic operational guidance based on $2\varphi_{3h}$-criterion vs. probabilistic operational guidance based on r-criterion.

Table 1.6.2 Percentage of errors of deterministic operational guidance

Ship	Cruise	CV 1700 TEU		CV 8400 TEU	
LC	LC01	LC01	LC02	LC01	LC03
Non-conservative	2.4	1.6	2.5	3.5	2.1
Conservative	4.1	9.9	5.6	1.6	0.0

1.7 Simplified operational guidance

1.7.1 Operational guidance provides detailed recommendations regarding ship's forward speed and course and therefore, requires methods of the level corresponding to direct stability assessment. However, sometimes simpler conservative recommendations for the forward speed and course, provided by simpler means, such as level 1 or level 2 criteria, are sufficient for the shipowner and acceptable for the administration:

.1 for pure loss and surf-riding/broaching stability failure modes, operational limitation of the maximum acceptable significant wave height, defined with level 2 vulnerability assessment can be combined with the forward speed limit according to level 1 vulnerability criterion in following and stern-quartering seaways at greater significant wave heights; and

.2 for excessive accelerations, where the level 2 vulnerability assessment is performed at zero forward speed, forward speed effect can be added to level 2-based operational limitations in a conservative way.

1.7.2 Check 2 of level 2 parametric roll criterion provides dependency of roll motion on the forward speed; hence it is useful to check whether this dependency is sufficiently accurate for a simplified operational guidance. Here, the sensitivity of this criterion to changes in forward speed is compared with direct stability assessment.

1.7.3 According to an earlier version of the present criterion, a loading condition was considered not vulnerable to parametric roll stability failure mode if $C_2 = (1/7)\left\{\sum_{j=1}^{3} C_2^H(\mathrm{Fn_j}) + C_2^H(0) + \sum_{j=1}^{3} C_2^F(\mathrm{Fn}_j)\right\} < 0.06$, where $C_2^H(\mathrm{Fn}_j)$ and $C_2^F(\mathrm{Fn}_j)$ refer to sailing in head and following waves, respectively, at a Froude number Fn_j and are calculated for each of Fn_j as a sum over all N sea states of a scatter table as $C_2^{H,F} = \sum_{i=1}^{N} w_i c_i$; w_i is the normed probability of a sea state i, and c_i=1 when roll amplitude exceeds 25° and 0 otherwise.

1.7.4 To verify whether criteria $C_2^{H,F}$ can be used for forward speed recommendations, their dependency on the forward speed for all sample ships in all loading conditions was compared with the dependency on forward speed of the stability failure rate due to parametric roll obtained from direct stability assessment, separately in head (denoted as w_{PR}^H) and following (w_{PR}^F) waves. In the numerical simulations, roll damping was defined from roll decay model tests (for the three container ships and the cruise ship) and with the simplified Ikeda method (for the RoPax ship).

1.7.5 For comparison, 40, 25 and 15 degrees heel angles were used to define stability failure. Figures 1.7.1 (a-c) show w_{PR}^H (left y axis) and C_2^H (right y axis) vs. Froude number (x- axis) for 15 (left), 25 (middle) and 40 (right) degrees definitions for different loading conditions (differentiated with lines of the same type: those with symbols refer to direct assessment result w_{PR}^H and those without symbols to check 2 of level 2 result C_2^H) of sample ships (each ship corresponds to one row); figures 1.7.2 (a-c) show corresponding results for parametric roll in following waves.

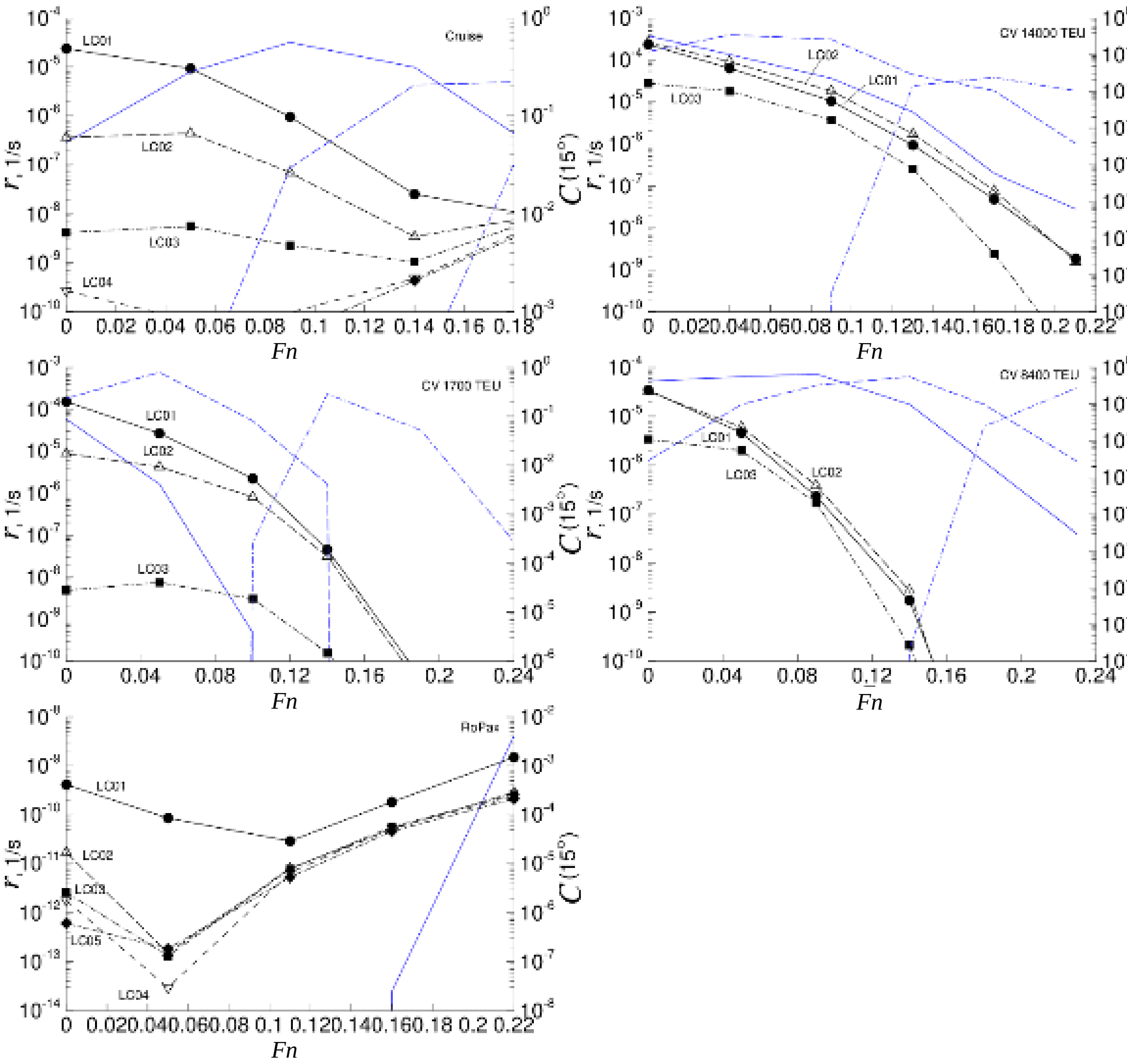

Figure 1.7.1.a. Parametric roll in head waves: direct assessment result $w_{\mathrm{PR}}^{\mathrm{H}}$ (left y- axis) and check 2 of level 2 result C_2^{H} (right axis) vs. Fn (x- axis) for 15 degrees definition of stability failure for all loading conditions; each line corresponds to one loading condition; black lines with symbols refer to $w_{\mathrm{PR}}^{\mathrm{H}}$, same type blue lines without symbols to C_2^{H}

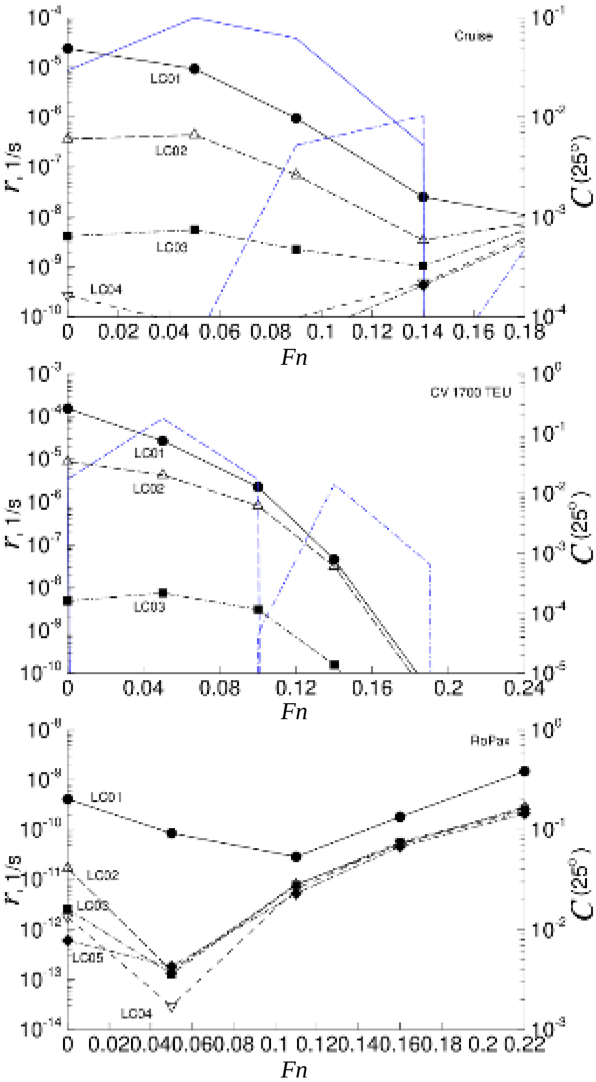

Figure 1.7.1.b. Same as in figure 1.7.1.a for 25 degrees definition of stability failure

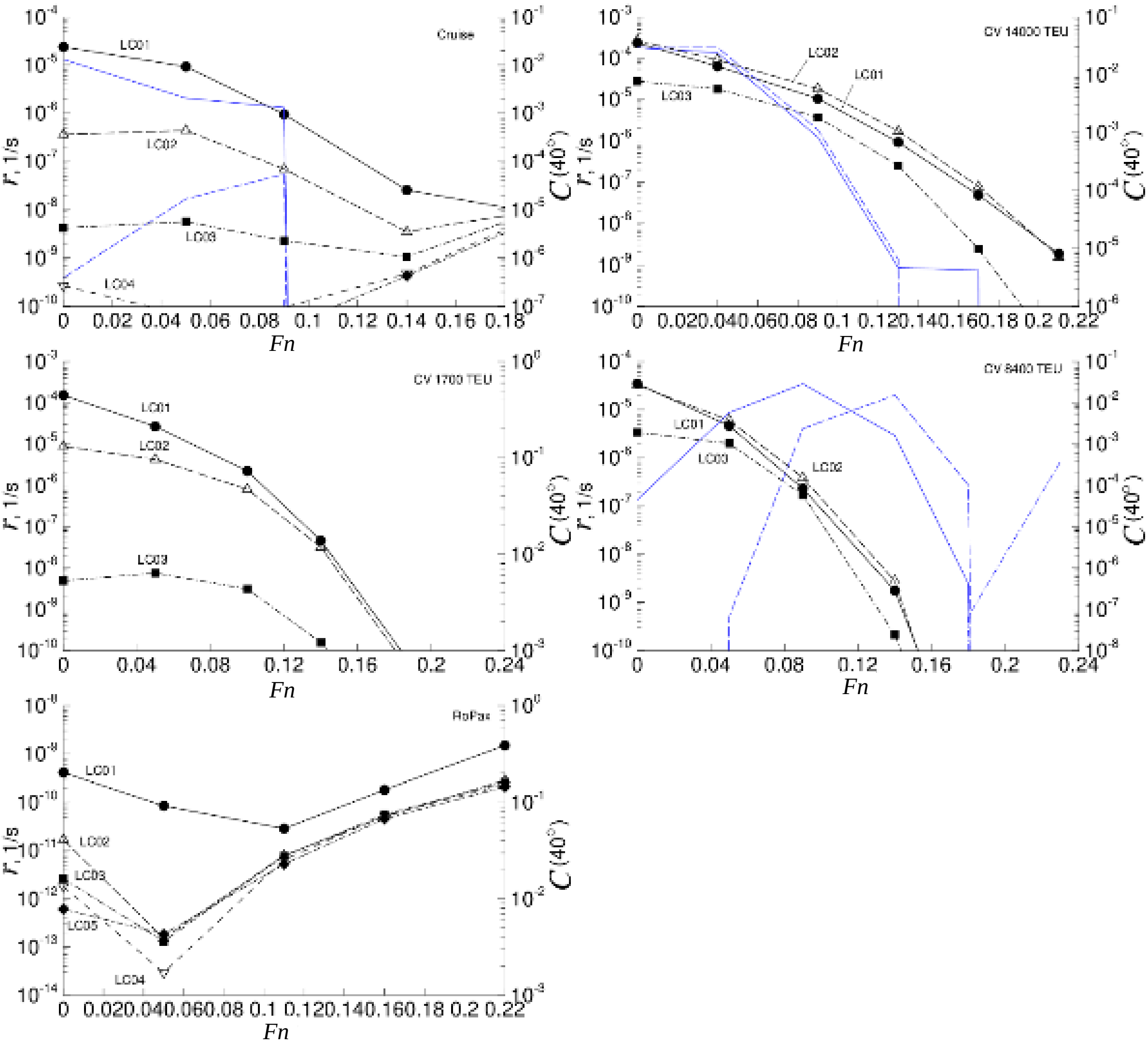

Figure 1.7.1.c. Same as in figure 1.7.1.a for 40 degrees definition of stability failure

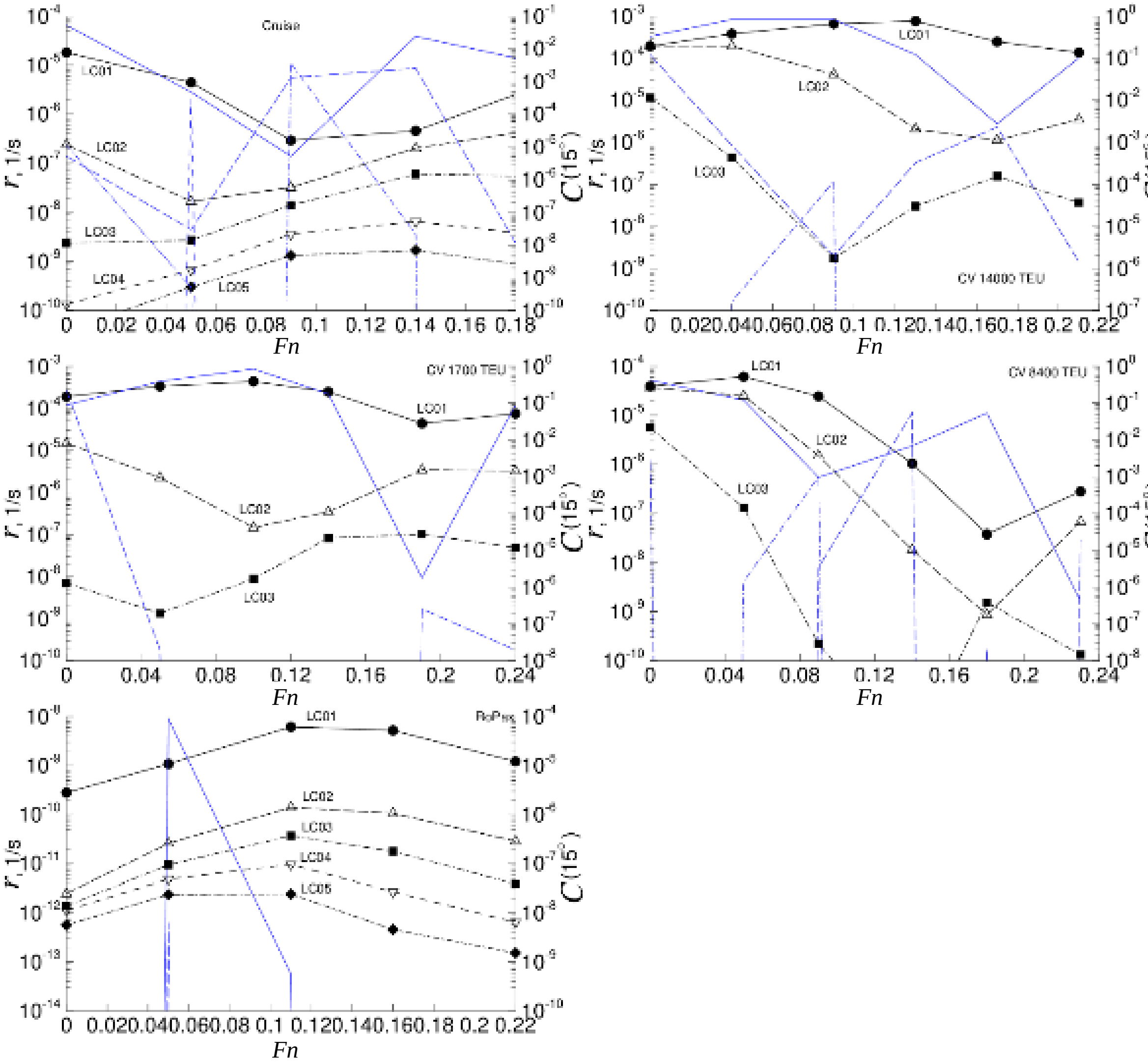

Figure 1.7.2.a. Parametric roll in following waves: results of direct assessment $w_{\mathrm{PR}}^{\mathrm{F}}$ (left y- axis) and check 2 of level 2 C_2^{F} (right y-axis) vs. Froude number (x- axis) for 15 degrees definition of stability failure for all loading conditions; each line corresponds to one loading condition: black lines with symbols refer to $w_{\mathrm{PR}}^{\mathrm{F}}$, same type blue lines without symbols to C_2^{F}

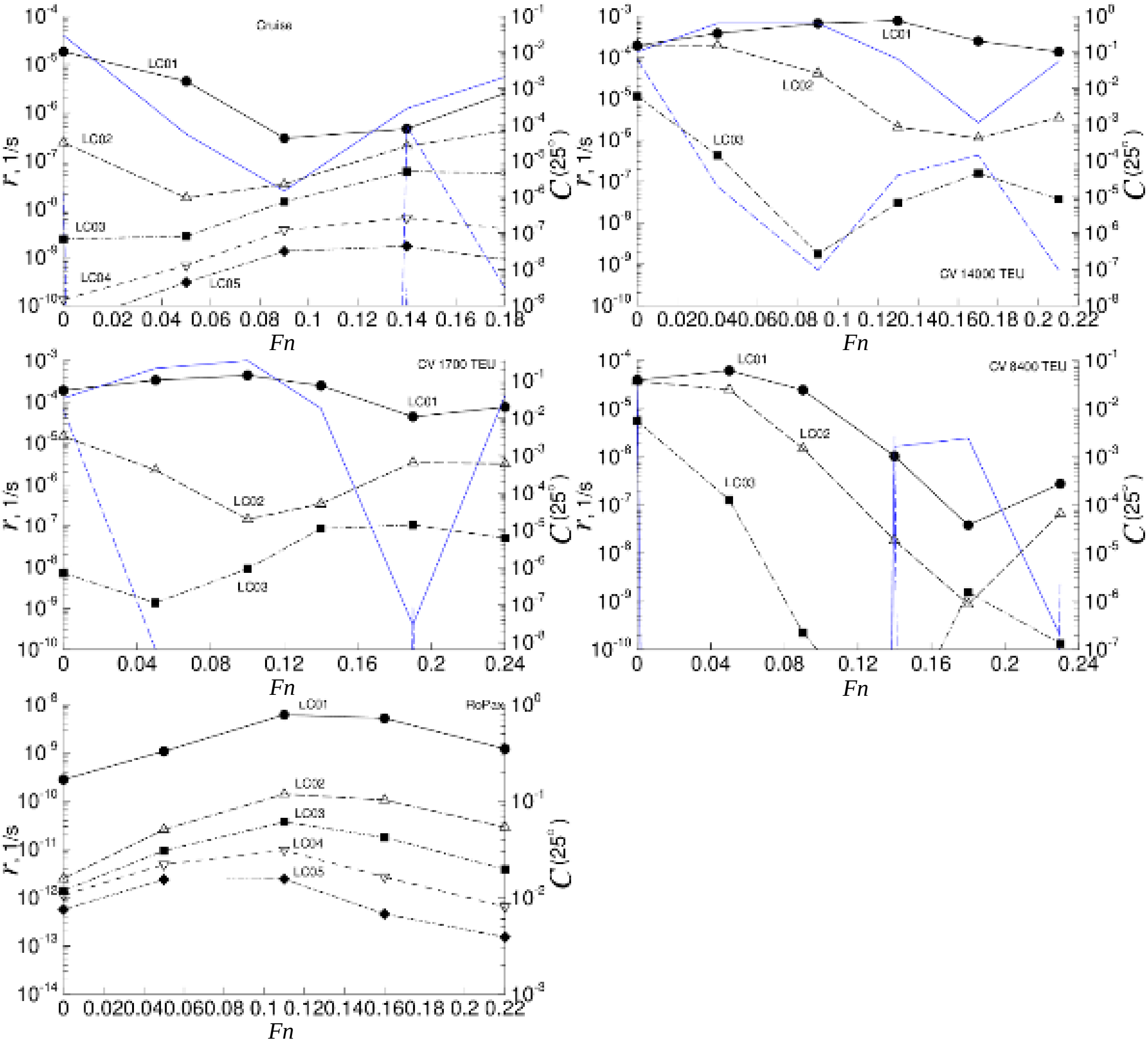

Figure 1.7.2.b. Same as in figure 1.7.2.a. for 25 degrees definition of stability failure

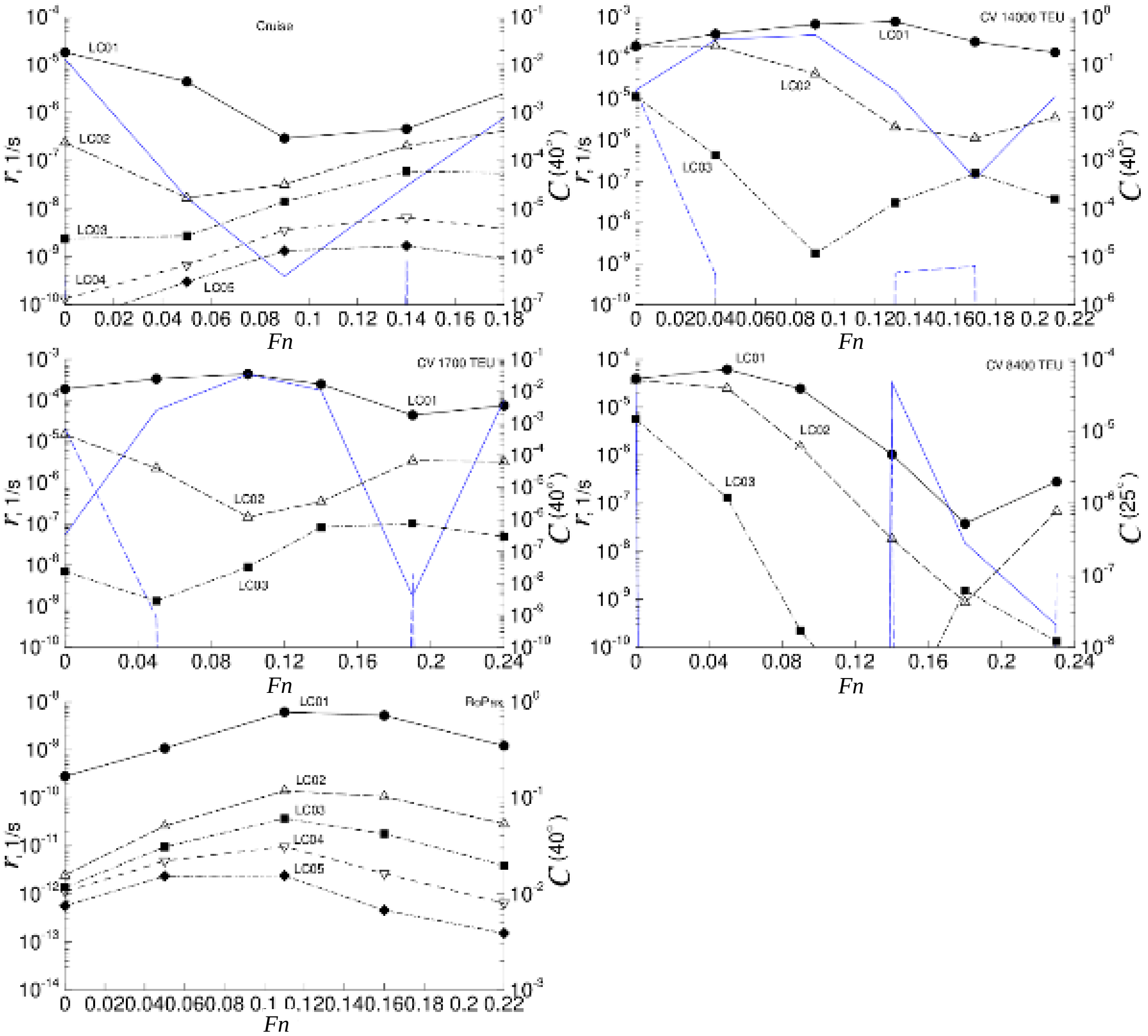

Figure 1.7.2.c. Same as in figure 1.7.2.a. for 40 degrees definition of stability failure

1.7.6 The results show that check 2 of level 2 parametric roll criterion produces in general good results at low *GM*. However, with increasing *GM*, the agreement worsens: this criterion indicates that large roll amplitudes move to higher forward speed or disappear, so that parametric roll becomes not dangerous any more at low forward speeds, whereas direct simulations indicate danger of parametric roll at low forward speeds (with the exception of RoPax, for which failure rate due to parametric roll is always very small). The agreement between check 2 of level 2 and direct simulation improves for 40° heel angle as failure definition instead of 25° and worsens for 15°.

1.7.7 To check the reason for this difference, figures 1.7.3 and 1.7.4 show failure rate due to parametric roll in head and following waves together with roll amplitude according to check 2 of level 2 depending on Froude number for 8400 TEU container ship, for which the differences between check 2 of level 2 and direct assessment in figures 1.7.1 and 1.7.2 are greatest, in three loading conditions with the smallest *GM* values at three significant wave heights and various mean wave periods. The figures show that the dependency of roll motion on forward speed differs between check 2 of level 2 and direct simulations.

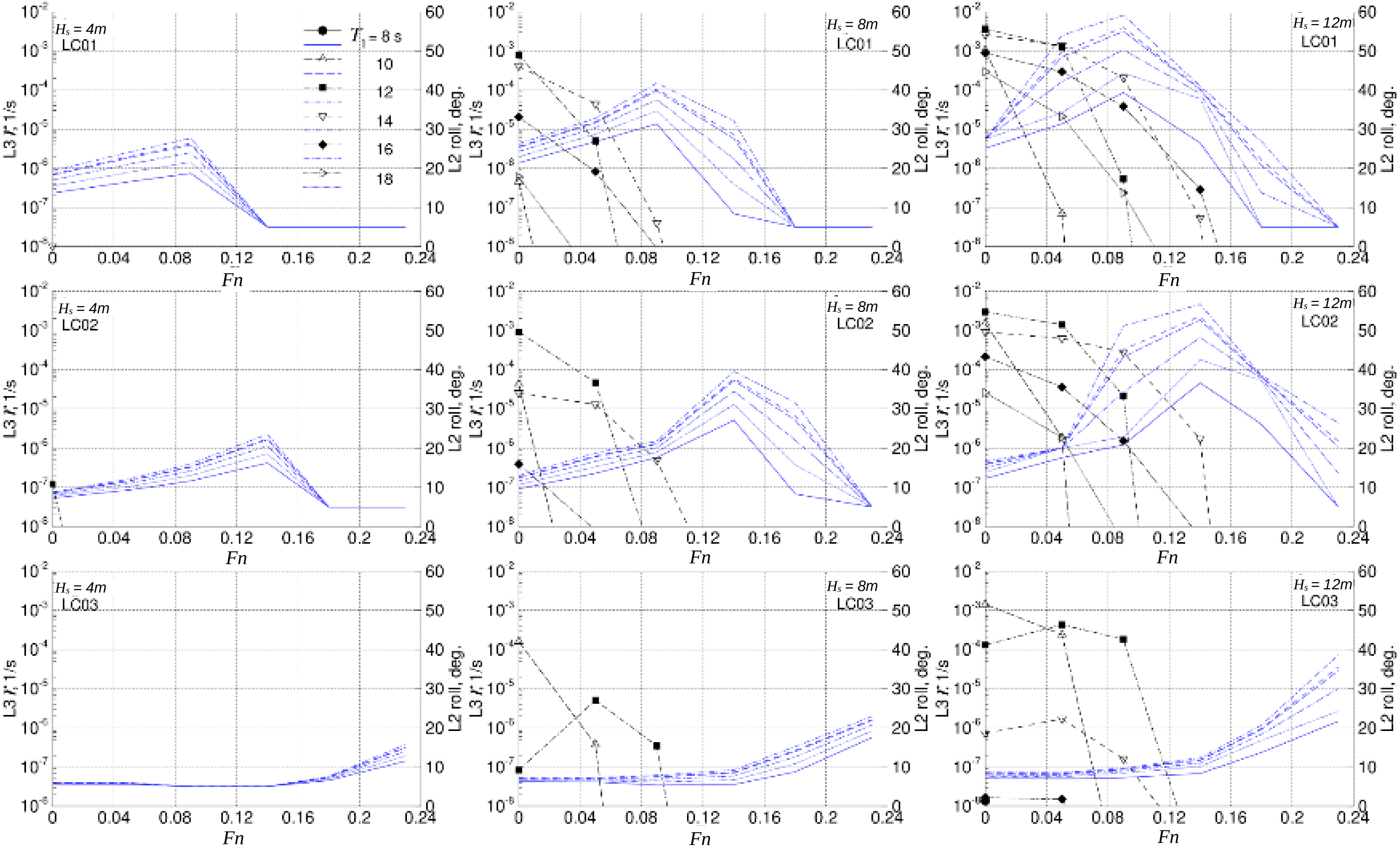

Figure 1.7.3. Failure rate due to parametric roll in head waves (left *y*- axis, black lines with symbols) and roll amplitude from check 2 of level 2 PR criterion (right *y* axis, blue lines without symbols) vs. Froude number (*x*- axis) for 8400 TEU container ship in three loading conditions (rows) at significant wave heights (columns) 4, 8 and 12 m; different lines correspond to different wave periods

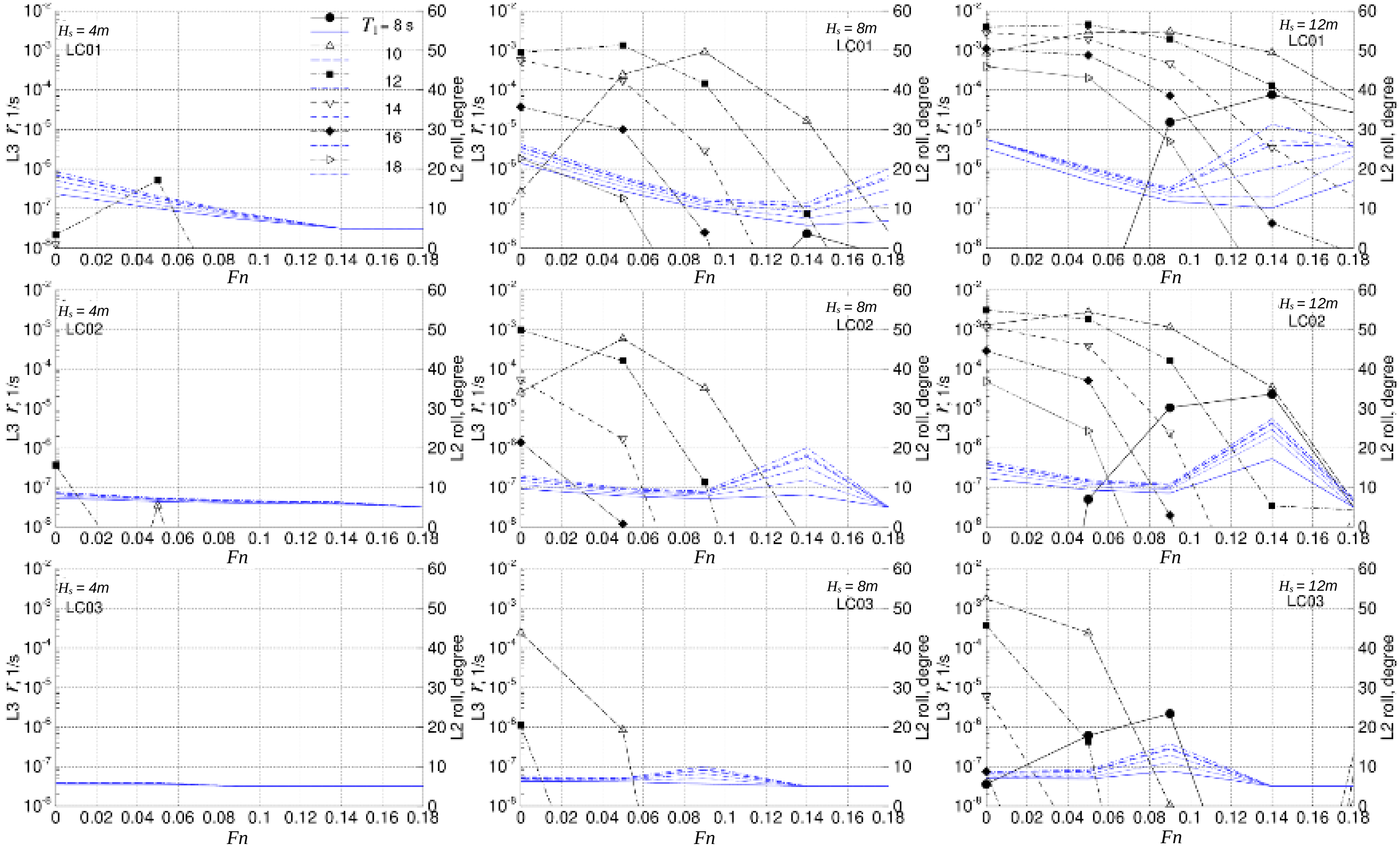

Figure 1.7.4 Failure rate due to parametric roll in following waves (left *y*- axis, black lines with symbols) and roll amplitude from check 2 of level 2 PR criterion (right *y* axis, blue lines without symbols) vs. Froude number (*x*- axis) for 8400 TEU container ship in three loading conditions (rows) at significant wave heights (columns) 4, 8 and 12 m; different lines correspond to different wave periods

1.7.8 These results mean that, first, using check 2 of level 2 parametric roll criterion to provide forward speed recommendations requires further validation and eventually improvement of this criterion and, second, that direct stability assessment for parametric roll in head waves can be conducted at zero (or as small as practicable) forward speed.

1.7.9 Model test results for the 8400 TEU container ship in figure 1.7.5 confirm that in irregular waves, low forward speeds are more critical for parametric roll in head waves than higher forward speeds, even when resonance condition suggests that higher forward speed should be more critical (compare with figure 1.7.6 which concerns parametric resonance in regular head waves for the same ship).

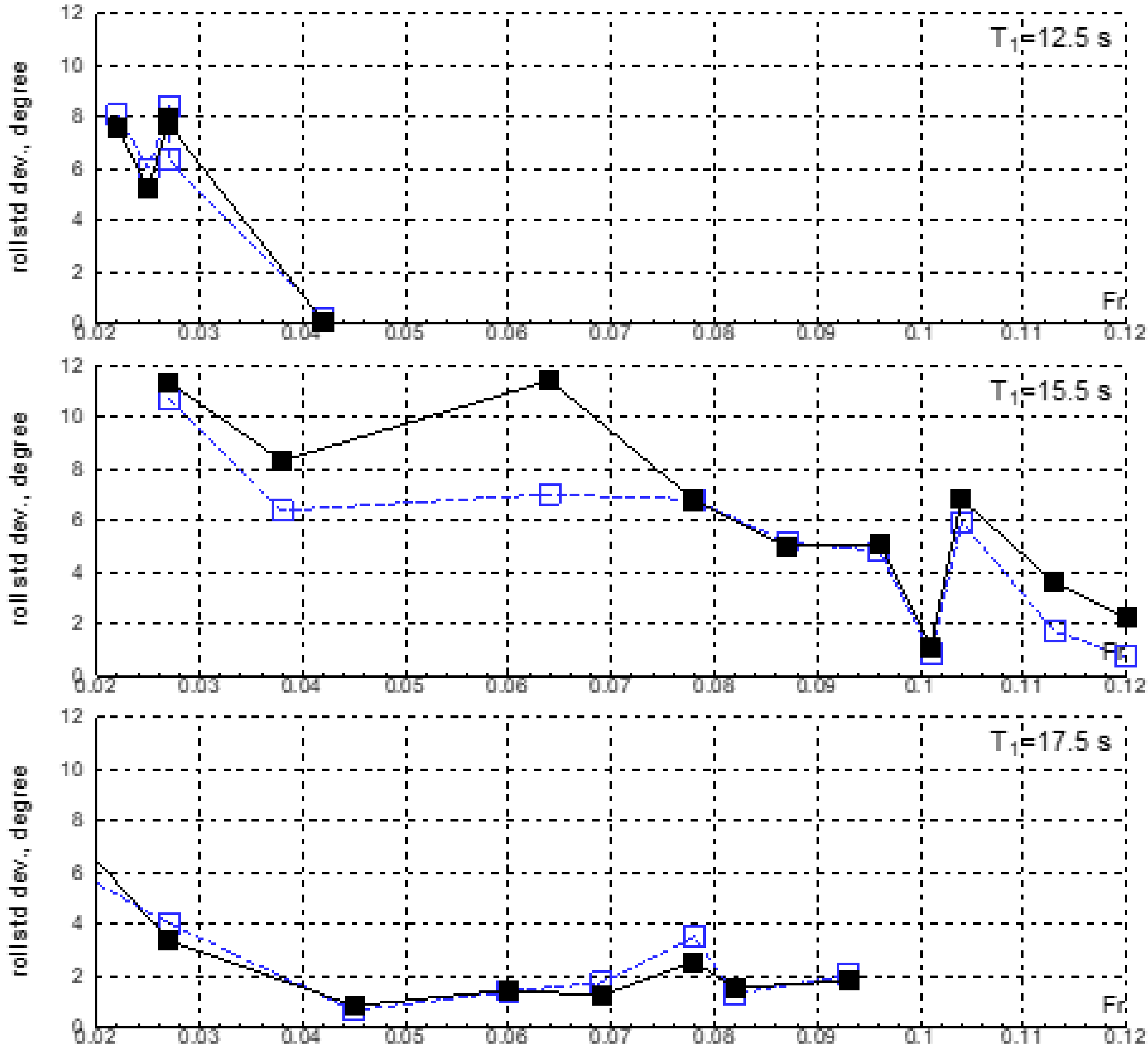

Figure 1.7.5 Measured (■) and computed (□) RMS of roll angle (*y*- axis) in irregular head waves vs. Froude number (*x*- axis) and wave period

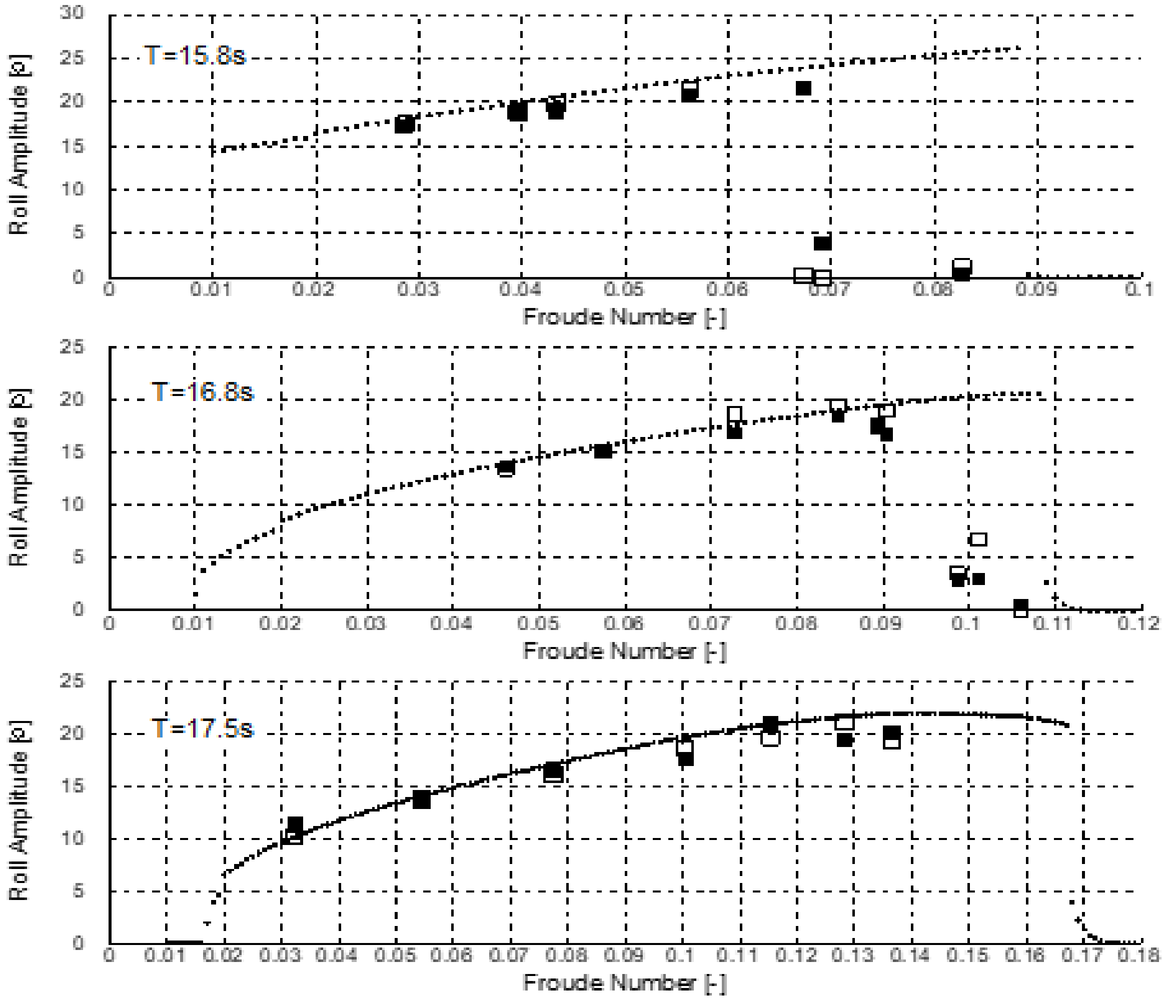

Figure 1.7.6 Measured (□,■) and computed (●) roll amplitude (*y*- axis) in regular head waves vs. Froude number (*x*- axis) and wave period

1.8 When operational measures are not suitable

1.8.1 Operational measures can reduce the average stability failure rate to any specified level; thus, any loading condition of any ship can be made "sufficiently safe" by application of sufficiently strict operational measures. However, if too many sailing conditions in too many sea states, especially in moderate sea states, should be excluded as unacceptable for some loading condition, it cannot be considered as sufficiently safe in routine practical operation. Therefore, if the total amount of acceptable sailing conditions becomes too small for some loading condition, it should not be considered as acceptable even when operational measures are provided. It follows from these considerations that a suitable criterion is desirable to distinguish such loading conditions for which operational measures are a possible solution from those which cannot be accepted even with operational measures. For this purpose, the total duration of acceptable sailing conditions in all relevant sea states, according to operational measures, as a percentage of the total operational life at sea is identified. Such a percentage is frequently referred to as operability, O, defined as

$$O = \sum_{\substack{\text{acceptable} \\ H_s, T_z, \mu, v_0}} f_s\left(H_s, T_z\right) f_\mu\left(\mu\right) f_{v_0}\left(v_0\right) \Delta H_s \Delta T_z \Delta\mu \Delta v_0 \qquad (1.8.1)$$

where μ is the wave heading, v_0 is the ship speed, H_s is the significant wave height, T_z is the mean zero-crossing period, and $f_S((H_s, T_z) f_\mu(\mu) f_{v0}(v_0))$ is the joint probability density function of the sailing condition (μ, v_0) and the sea state (H_s, T_z).

1.8.2 Similarly to other criteria, the threshold for operability can be defined from case studies. The operability O, corresponding to the "short-term" threshold of stability failure rate $r = 1.0 \cdot 10^{-6}$ 1/s for the five studied ships in all loading conditions is presented in table 1.8.1 (presented separately for different forward speeds, noting that RoRo vessel is not shown since it has an operability=1.0 at all speeds). The results in table 1.8.1 suggest that a minimum operability of 0.8 is an appropriate threshold because only one ship fails this requirement in two loading conditions (bold values): one loading condition (LC02) fails this requirement at zero forward speed and the other (LC01) also fails the weather criterion of the 2008 Intact Stability Code. The average operability over all forward speeds in table 1.8.2 exceeds 0.8 for all studied ships in all loading conditions. Moreover, the maximum significant wave height of about 4.4 m, which corresponds to an operability=0.8 in the North Atlantic, figure 1.8.1, confirms that this value is not too conservative. Therefore, the value 0.8 can be accepted as an appropriate operability standard to eliminate loading conditions for which operational guidance is not a suitable alternative.

Table 1.8.1 Operability (separately over forward speeds) corresponding to a short-term threshold of the stability failure rate r=1.0·10^{-6} 1/s for all studied ships and loading conditions

ship	Fr	LC01	LC02	LC03	LC04	LC05
1700 TEU CV	0.00	0.836	0.958	1.00	1.000	1.000
	0.05	0.852	0.983	1.000	1.000	1.000
	0.10	0.831	0.995	1.000	1.000	1.000
	0.14	0.855	0.996	0.999	1.000	1.000
	0.19	0.930	0.978	0.998	1.000	1.000
	0.24	0.905	0.976	1.000	1.000	1.000
8400 TEU CV	0.00	0.943	0.922	0.967	0.993	0.999
	0.05	0.946	0.946	0.991	0.993	0.999
	0.09	0.956	0.991	0.999	0.996	1.000
	0.14	0.993	1.000	1.000	0.997	1.000
	0.18	0.999	1.000	1.000	0.998	1.000
	0.23	0.996	0.999	1.000	0.999	1.000
14000 TEU CV	0.00	0.856	**0.760**	0.915	1.000	1.000
	0.04	0.861	0.811	0.957	1.000	1.000
	0.09	0.833	0.916	0.988	1.000	1.000
	0.13	**0.794**	0.985	0.998	1.000	1.000
	0.17	0.820	0.991	0.997	1.000	1.000
	0.21	0.872	0.981	0.999	1.000	1.000
Cruise Vessel	0.00	0.937	0.997	1.000	1.000	1.000
	0.05	0.970	0.998	1.000	1.000	1.000
	0.09	0.994	0.999	1.000	1.000	1.000
	0.14	0.997	0.999	0.999	1.000	1.000
	0.18	0.987	0.997	0.999	1.000	1.000

Table 1.8.2 Operability (average over all forward speeds) corresponding to a short-term threshold of the stability failure rate r=1.0·10^{-6} 1/s for all studied ships and loading conditions

Ship	Loading condition				
	LC01	LC02	LC03	LC04	LC05
Cruise Vessel	0.977	0.998	1.000	1.000	1.000
1700 TEU Container Ship	0.868	0.981	0.999	1.000	1.000
8400 TEU Container Ship	0.972	0.976	0.993	0.996	1.000
14000 TEU Container Ship	0.839	0.907	0.975	1.000	1.000

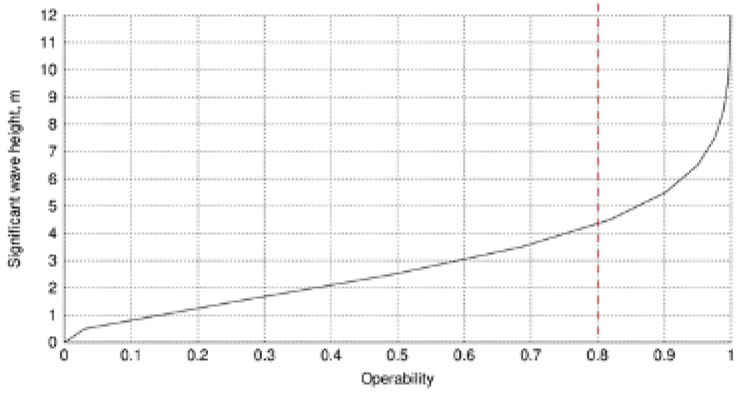

Figure 1.8.1. Maximum significant wave height vs. operability in North Atlantic wave climate

1.9 Influence of propulsion, steering and seakeeping

1.9.1 So far, propulsion and steering abilities of a ship, as well as seakeeping problems such as excessive vertical motions and accelerations and excessive loads at high forward speed in bow waves, have not been considered in design assessment and operational measures concerning dynamic stability. For some stability failure modes, this may lead to non-conservative errors in design assessment or misleading operational recommendations:

.1 for pure loss of stability and surf-riding/broaching stability failures, which are relevant in stern waves, consideration of propulsion and steering abilities and seakeeping problems is not critical for dynamic stability;

.2 for dead ship condition stability failure mode, relevant only at zero forward speed in beam seaway, such problems are also not critical;

.3 for excessive acceleration stability failures, forward speed in beam seaway rather moderately influences roll motion (due to decreasing roll damping with decreasing forward speed); this does not influence the design assessment (which is performed at zero forward speed) but has a moderate influence on operational guidance. A more important issue for operational guidance is the course-keeping ability in bow seaways: if the ship is not able to avoid excessive roll motions because it cannot steer into seaway, it is advisable to consider this in the operational guidance; and

.4 for parametric roll in bow waves, neglecting propulsion, steering and seakeeping abilities can lead to over-estimation of ship's safety in the design assessment (due to contributions from safe but unattainable ship's speed and course combinations) and to dangerous errors in terms of operational guidance (when attainable ship's speed and course combinations in a storm are unacceptable whereas all acceptable combinations are unattainable).

1.9.2 Figure 1.9.1 shows a colour plot of roll amplitude depending on forward speed and course together with the line of maximum attainable speed (solid black line) and line of maximum available steering effort (yellow dashed line) for the 8400 TEU container ship in three loading conditions: in bow waves, majority of forward speeds that lead to small roll motions are unattainable due to added resistance in seaway. Note that this observation is confirmed by experience: all parametric roll accidents in bow waves happened at low forward speeds.

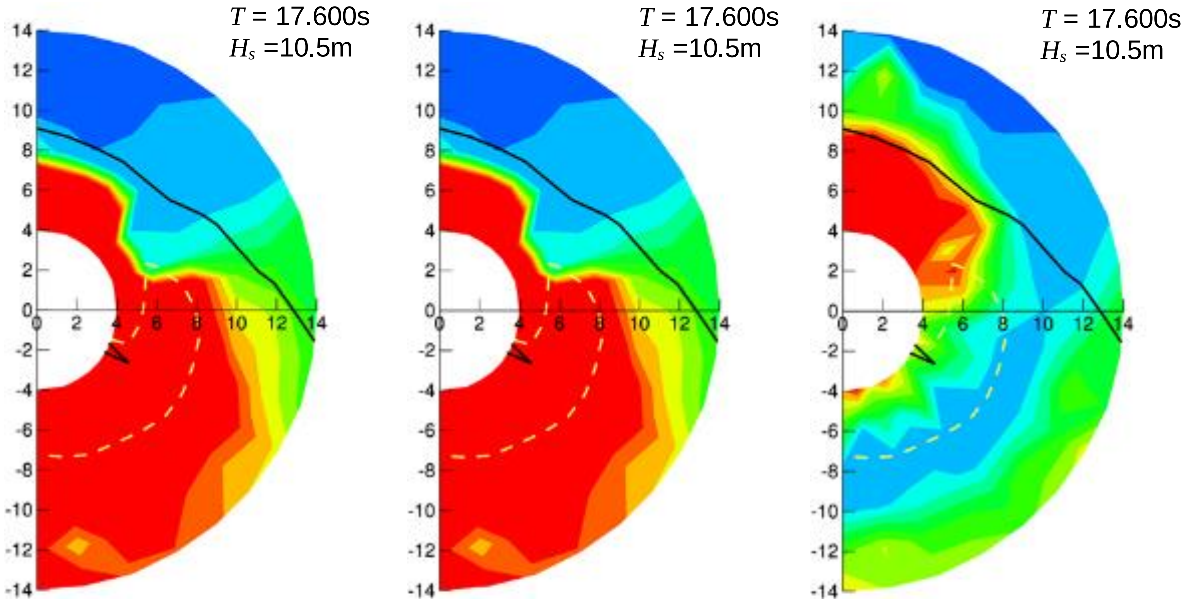

Figure 1.9.1 Colour plots of mean 3-hour maximum roll amplitude vs. forward speed (m/s, radial coordinate) and wave direction (circumferential coordinate, head waves at top) for 8400 TEU container ship in loading conditions (from left to right) LC01, LC02 and LC03 together with lines of maximum attainable speed (black solid) and maximum available steering effort (yellow dashed)

1.9.3 To estimate the influence of propulsion ability on parametric roll in head waves, average (over all significant wave heights and wave periods) rate of parametric roll stability failures in head waves was calculated with and without considering maximum attainable speed in head waves. In both cases, the forward speed was applied that minimizes the stability failure rate, but in the calculations accounting for propulsion ability, the range of speeds was restricted by the condition that the required engine power does not exceed the available power. Figure 1.9.2 shows the result as the stability failure rate considering speed limit plotted vs. the stability failure rate without considering speed limit.

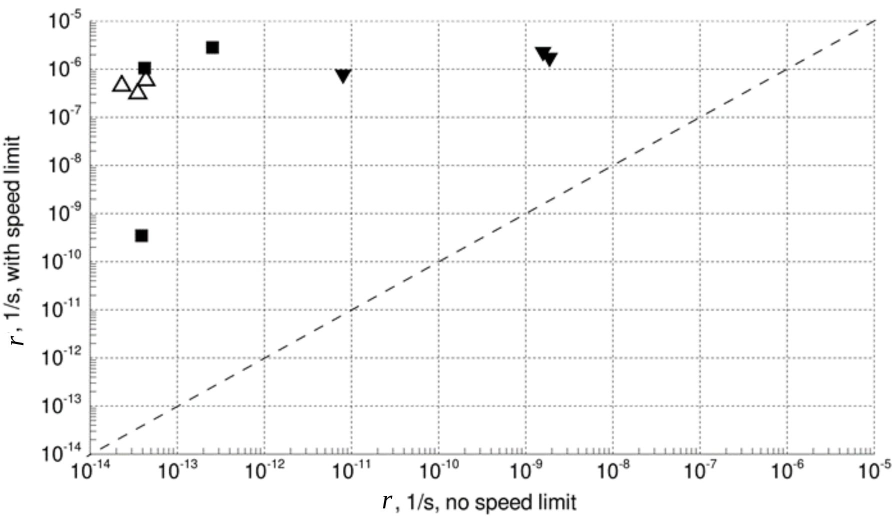

Figure 1.9.2 Rate of parametric roll stability failures in head waves considering (y axis) and not considering (x axis) attainable forward speed for three container ships (different symbols) in three loading conditions each

1.9.4 The results show that the stability failure rate increases by several orders of magnitude if propulsion ability is considered. This means that it is advisable to consider propulsion ability in operational guidance to prevent from misleading recommendations. The attainable forward speed can be defined from model tests or numerical computations; alternatively, simple empirical formulae can be established.

2 Application examples

2.1 Operational guidance based on DSA for parametric and synchronous roll

2.1.1 Operational guidance was prepared for all ships and loading conditions in table 1.1.1 by identifying unacceptable sailing conditions (v_0, μ) for each range of sea states (H_s, T_z) in the North Atlantic wave scatter table. Unacceptable sailing conditions for probabilistic operational guidance are those for which the upper boundary r_U of the 95%-confidence interval of the "short-term" stability failure rate exceeds standard 10^{-6} s^{-1}, while for deterministic operational guidance, those for which the mean three-hour maximum roll amplitude μ_{3h} or lateral acceleration amplitude a_{y3h} exceed $0.5{\cdot}40^o$ or $0.5{\cdot}g$, respectively.

2.1.2 For each assumed situation (H_s, T_z, v_0, μ), numerical simulations of ship motions were carried out in multiple independent sea state realizations produced by random variation of phases, frequencies and directions of wave components discretizing the wave energy spectrum. Transient hydrodynamic effects at the beginning of simulations were neutralized by switching off the counter of stability failures and simulation timer during initial transients.

2.1.3 For probabilistic operational guidance, each simulation was conducted for 2 hours' simulation time or until the first stability failure (exceedance of 40 degree roll angle or lateral acceleration g) if a stability failure occurred earlier, after which new simulation was conducted in another realization of the same sea state, until N=200 stability failures were encountered. After that, the upper boundary r_U of the 95%-confidence interval of stability failure rate was calculated as $r_U = 0.5r\chi^2_{1-0.05/2,2N}/N$, where $r = N/t_t$ and t_t is the total simulation time required to encounter 200 stability failures. For such assumed situations (H_s, T_z, v_0, μ) where a total simulation time of up to $3.4{\cdot}10^6$ hours was not enough to encounter 200 stability failures, extrapolation of stability failure rate over significant wave height was used (section 3.5.5.3 of the Interim Guidelines). For deterministic operational guidance, five 3-hour simulations were carried out for each assumed situation (H_s, T_z, v_0, μ); the mean 3-hour maximum roll amplitude φ_{3h} and mean 3-hour maximum lateral acceleration amplitude a_{y3h} were calculated as average values of the five 3-hour maxima from these simulations.

2.1.4 Table 2.1.1 shows the conservative estimate of the upper boundary of the 95%-confidence interval of the average "long-term" stability failure rate $\bar{r}_U$, calculated, according to the explanatory note to paragraph 3.5.3.2.1 of the Interim Guidelines, as the "long-term" weighted average of the upper boundaries of the 95%-confidence intervals of the "short-term" stability failure rate, for unrestricted service without operational guidance (i.e. result of full probabilistic direct stability assessment) and with operational guidance. The estimates of contributions to the total stability failure rate from principal parametric resonance in bow and stern waves and synchronous resonance in beam waves are also shown. Table 2.1.2 shows this upper boundary without and with operational guidance together with operability resulting from the use of operational guidance. The minimum operability over considered ships and loading conditions is 0.839, i.e. the ratio of the total duration of all unacceptable situations to the total operational time (0.161) does not exceed 0.2, i.e. all loading conditions can be considered as acceptable when operational guidance is used.

Table 2.1.1 "Long-term" weighted average $\bar{r}_U$, 1/s, of upper boundaries of 95%-confidence intervals of "short-term" stability failure rate for unrestricted service without and with operational guidance: total (ALL) and due to principal parametric resonance in bow (PRB) and stern (PRS) waves and synchronous resonance (SR) in beam waves

	LC	Without operational guidance				With operational guidance			
		ALL	PRB	PRS	SR	ALL	PRB	PRS	SR
Cruise	01	2.214e-6	8.157e-7	6.407e-7	4.013e-7	6.238e-9	1.254e-9	1.857e-9	2.526e-9
	02	5.706e-8	1.927e-8	2.220e-8	7.006e-9	1.219e-9	2.378e-10	4.218e-10	3.246e-10
	03	4.587e-9	3.979e-10	3.020e-9	5.323e-10	2.935e-10	3.409e-11	1.348e-10	7.222e-11
	04	7.582e-10	1.020e-10	3.617e-10	1.642e-10	8.980e-11	1.259e-11	3.661e-11	2.622e-11
	05	3.911e-10	8.124e-11	1.307e-10	1.091e-10	6.185e-11	1.065e-11	2.017e-11	1.940e-11
CV 1700	01	5.362e-5	3.802e-6	2.811e-5	1.230e-5	1.416e-8	1.030e-9	3.578e-9	7.741e-9
	02	1.432e-6	2.798e-7	5.527e-7	3.585e-7	5.493e-9	9.476e-10	1.269e-9	2.569e-9
	03	1.198e-8	3.048e-10	6.290e-9	3.390e-9	4.669e-10	3.027e-11	1.828e-10	1.907e-10
	04	1.388e-12	1.363e-15	2.032e-15	1.378e-12	4.789e-13	9.539e-16	1.795e-15	4.721e-13
	05	1.500e-12	1.748e-15	1.348e-16	1.490e-12	4.885e-13	1.145e-15	1.089e-16	4.829e-13
CV 8400	01	6.614e-6	8.859e-7	3.011e-6	1.592e-6	4.915e-9	4.709e-10	7.399e-10	2.388e-9
	02	3.907e-6	8.559e-7	1.462e-6	9.285e-7	3.677e-9	3.715e-10	5.542e-10	2.127e-9
	03	4.113e-7	1.162e-7	1.235e-7	1.088e-7	1.946e-9	3.250e-10	5.532e-10	8.926e-10
	04	2.303e-7	8.462e-11	2.130e-11	2.294e-7	1.803e-9	8.954e-12	3.407e-12	1.740e-9
	05	8.954e-9	9.143e-13	1.140e-14	8.943e-9	4.217e-10	3.395e-13	7.463e-15	4.193e-10
CV 14000	01	1.286e-4	6.742e-6	5.112e-5	4.936e-5	1.492e-8	1.236e-9	1.450e-9	1.067e-8
	02	3.645e-5	8.235e-6	9.367e-6	1.315e-5	1.203e-8	4.983e-10	3.051e-9	6.746e-9
	03	2.435e-6	1.015e-6	2.495e-7	7.956e-7	5.154e-9	1.030e-9	6.813e-10	2.603e-9
	04	5.306e-16	0.0	0.0	5.306e-16	5.103e-16	0.0	0.0	5.103e-16
	05	2.068e-15	0.0	0.0	2.068e-15	1.810e-15	0.0	0.0	1.810e-15
RoPax	01	1.223e-9	5.589e-11	4.300e-10	5.082e-10	1.365e-10	7.638e-12	4.040e-11	6.208e-11
	02	-	-	-	-	-	-	-	-
	03	5.493e-11	8.643e-12	5.055e-12	3.311e-11	1.286e-11	1.991e-12	1.478e-12	7.394e-12
	04	6.207e-11	8.255e-12	1.986e-12	4.578e-11	1.247e-11	1.692e-12	6.730e-13	8.774e-12
	05	7.839e-11	7.538e-12	8.646e-13	6.495e-11	1.348e-11	1.606e-12	2.868e-13	1.057e-11

Table 2.1.2. "Long-term" weighted average $\bar{r}_U$, 1/s, of upper boundaries of 95%-confidence intervals of "short-term" stability failure rate for unrestricted service without and with probabilistic operational guidance (corresponding to short-term threshold of stability failure rate $r_U = 10^{-6}$ 1/s) and operability due to use of operational guidance

Ship	Loading condition				
	01	02	03	04	05
Average "long-term" stability failure rate $\bar{r}_U$, 1/s, without using operational guidance					
Cruise Vessel	2.214e-6	5.706e-8	4.587e-9	7.582e-10	3.911e-10
1700 TEU Container Ship	5.362e-5	1.432e-6	1.198e-8	1.388e-12	1.500e-12
8400 TEU Container Ship	6.614e-6	3.907e-6	4.113e-7	2.303e-7	8.954e-9
14000 TEU Container Ship	1.286e-4	3.645e-5	2.435e-6	5.306e-16	2.068e-15
RoPax	1.223e-9	-	5.493e-11	6.207e-11	7.839e-11
"Long-term" weighted average $\bar{r}_U$, 1/s, due to using probabilistic operational guidance					
Cruise Vessel	6.238e-9	1.219e-9	2.935e-10	8.980e-11	6.185e-11
1700 TEU Container Ship	1.416e-8	5.493e-9	4.669e-10	4.789e-13	4.885e-13
8400 TEU Container Ship	4.915e-9	3.677e-9	1.946e-9	1.803e-9	4.217e-10
14000 TEU Container Ship	1.492e-8	1.203e-8	5.154e-9	5.103e-16	1.810e-15
RoPax	1.365e-10	-	1.286e-11	1.247e-11	1.348e-11
Operability due to using probabilistic operational guidance					
Cruise Vessel	0.977	0.998	1.000	1.000	1.000
1700 TEU Container Ship	0.868	0.981	0.999	1.000	1.000
8400 TEU Container Ship	0.972	0.976	0.993	0.996	1.000
14000 TEU Container Ship	0.839	0.907	0.975	1.000	1.000
RoPax	1.000	1.000	1.000	1.000	1.000

2.1.5 Figures 2.1.1(a and b) show examples of operational guidance in form of polar plots, showing unacceptable sailing situations (red) in selected sea states for loading condition LC01 of 1700 TEU and 8400 TEU container ships.

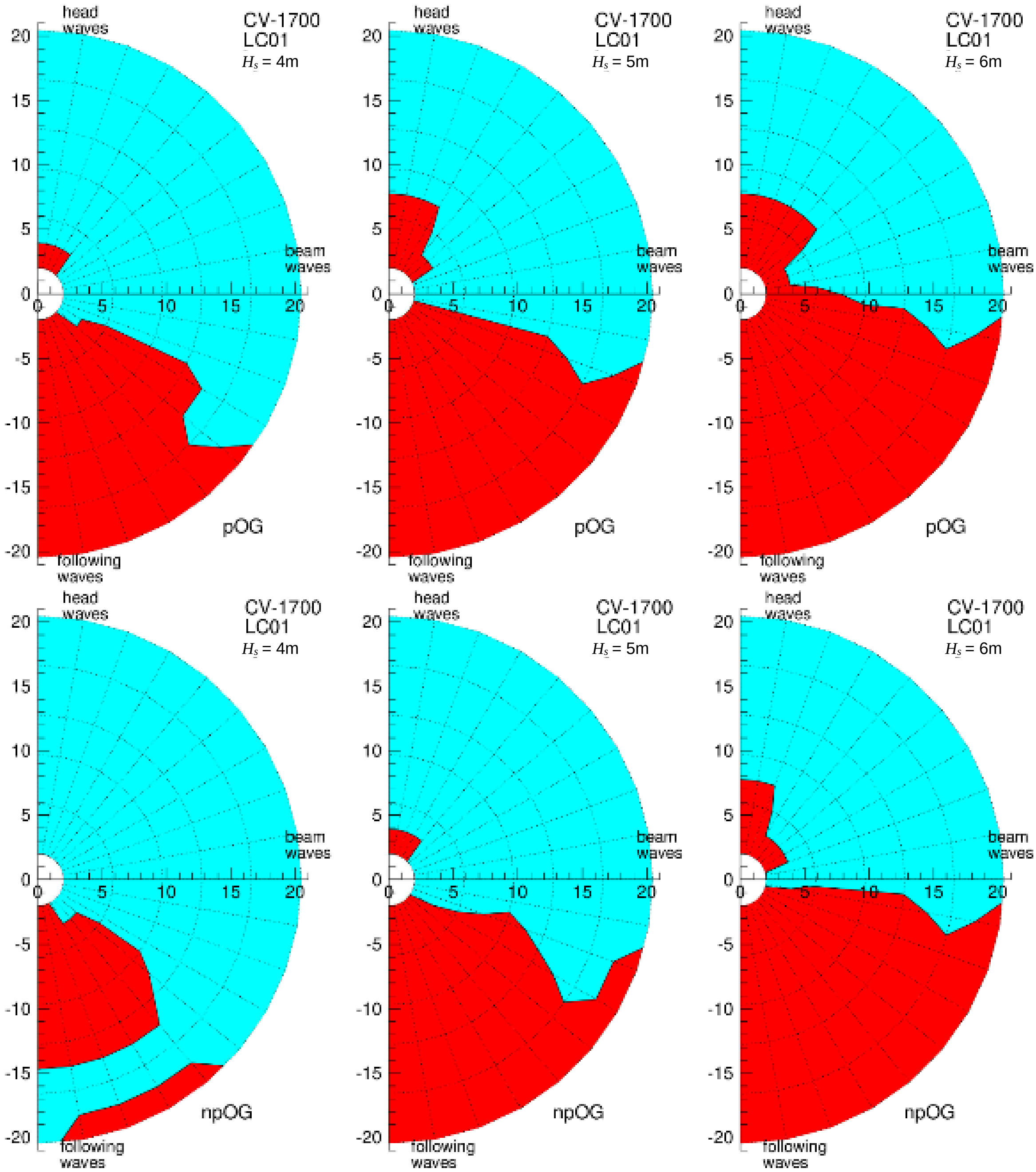

Figure 2.1.1.a. Examples of probabilistic (top) and deterministic (bottom) operational guidance in axes ship speed (knots, radial coordinate) - mean wave direction (circumferential coordinate) vs. significant wave height (columns) for 1700 TEU container ship

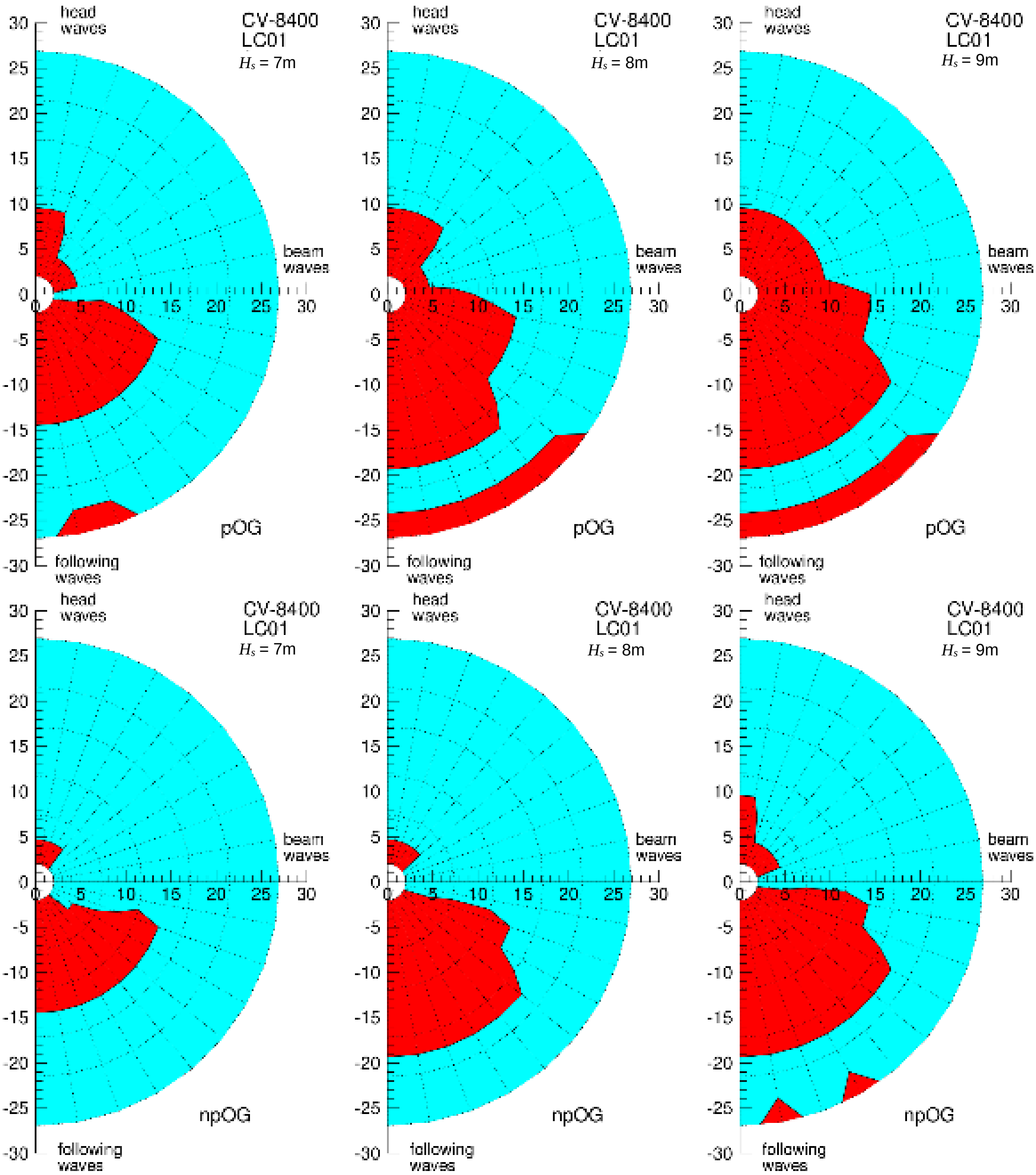

Figure 2.1.1.b. Same as in figure 2.1.1.a for 8400 TEU container ship

2.2 *Operational guidance for parametric roll*

2.2.1 An example for development of operational guidance for a C11 class containers ship is shown in figure 1.1 of appendix 2. Principal dimensions are given in table 1.2 of appendix 2, assuming that GM = 1.4 m.

2.2.2. Examples of operational guidance in figure 2.1.1 show only acceptable and non-acceptable combinations of speed and heading. Additional information on the proximity of the condition to the boundary between acceptable and unacceptable sailing conditions may be useful in operational decision-making. The additional information inside the zone of unacceptable sailing conditions may be useful in assisting for leaving this zone; additional information outside of this zone may serve as a warning.

2.2.3 As defined in paragraph 4.5.4.2 of the Interim guidelines, acceptable sailing conditions are those for which the upper boundary of the estimate of failure rate is less than 10^{-6} s^{-1}. Here, roll angle 40 degrees was used as the definition of stability failure, and the grading of danger of stability failure is shown with additional thresholds larger than 40 degrees. Additional thresholds of roll amplitudes less than 40 degrees are shown as a warning of approaching danger of stability failure.

2.2.4 The example of an augmented guidance is shown in figure 2.2.1 where multiple roll angle thresholds are used in addition to the threshold of 40 degrees. The thresholds 25, 30 and 35 degrees serve as waring and shown in yellow and orange colours; the thresholds 45, and 50 degrees are included to assist in return to acceptable sailing condition, thus are shown in different degrees of dark red colour.

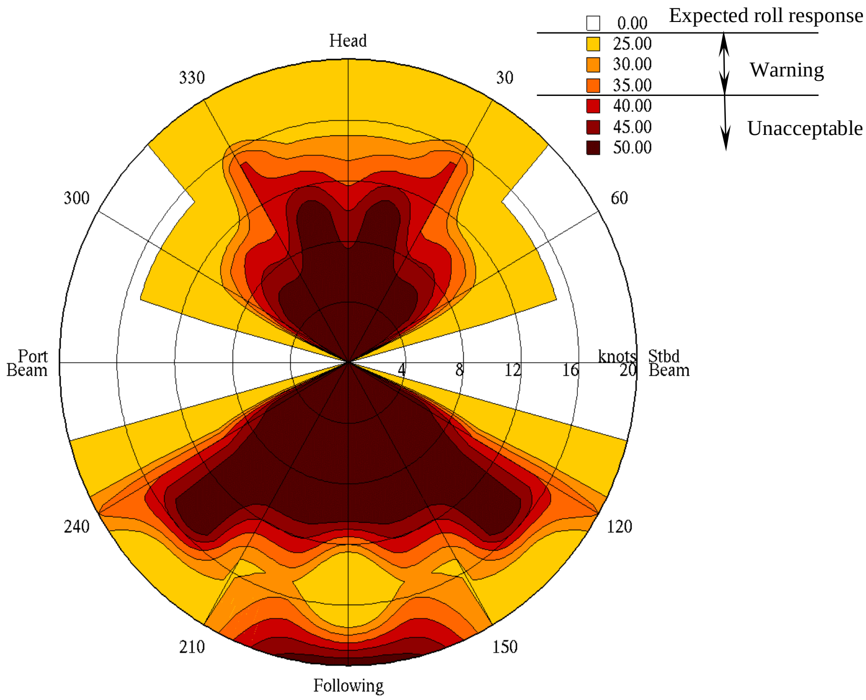

Figure 2.2.1. Sample operational guidance in form of polar plot for C11-class container ship at significant wave height 9 m, mean zero-crossing wave period 9.94 s, draught 11.5 m and GM=1.4 m

2.3 DSA-based operational limitations related to areas or routes and season

2.3.1 Examples of operational limitations related to areas or routes and season concern ships and loading conditions shown in table 1.1.1 and sample operational routes and seasons in table 2.3.1. Environmental conditions are specified by wave scatter tables according to IACS

Recommendation No.34 (Corr.1 Nov. 2001) (area 1) and Global Wave Statistics (areas 2 to 6).

Table 2.3.1. Routes and seasons used in examples of operational limitations

1	North Atlantic, IACS Recommendation No.34 (Corr.1 Nov. 2001) (annual average)
2	Representative worldwide route for Panamax container ships trade* (annual average)
3	Representative east-bound route for post-Panamax container ships trade** (annual average)
4	Same as 3, summer
5	Sample European route*** (annual average)
6	Same as 5, summer

* North Sea, Dover Strait, Biscay, North Atlantic, USA East Coast, Caribbean Sea, Panama Channel, West coast of North America, North Pacific Ocean, Japan East Coast, South China Sea

** North Sea, Dover Strait, Bay of Biscay, Gibraltar, Mediterranean Sea, Red Sea, North Indian Ocean, Strait of Malacca, South China Sea, Japan

*** Baltic Sea, Skagerrak, North Sea, Dover Strait, Biscay

2.3.2 Operational limitations were produced, according to section 4.5.1, by application of full probabilistic direct stability assessment (section 3.5.3.2 of Interim guidelines for direct stability assessment) to each ship, loading condition and sample route, using numerical simulations of ship motions at six forward speeds in waves of mean zero-crossing periods T_z and significant heights H_s covering the relevant scatter tables every 1.0 s and 1.0 m, respectively, and mean wave directions μ from 0 to 180° every 10°.

2.3.3 Numerical simulations of ship motions were performed in realizations of the same sea state by random variation of frequencies, directions and phases of wave components discretizing the wave energy spectrum. Each simulation was conducted for the simulation time of 2 hours or until the first stability failure (exceedance of 40° roll angle or lateral acceleration g) if it happened earlier, after which simulation was repeated in another realization, until $N=200$ stability failures were encountered. For such combinations (H_s, T_z, v_0, μ) for which the total simulation time of up to $3.4 \cdot 10^6$ hours was enough to encounter 200 stability failures, direct counting was used, namely, maximum likelihood estimate of stability failure rate was calculated as $r=N/t_t$, eq. (3.3.6), and the upper boundary of its 95%-confidence interval as $r_U = 0.5r\chi^2_{1-0.05/2,2N}/N$, eq. (3.3.9); otherwise extrapolation of stability failure rate over significant wave height was used.

2.3.4 A conservative estimate of the upper boundary $\bar{r}_U$ of the 95%-confidence interval of the average "long-term" stability failure rate was calculated as a weighted average over all combinations (H_s, T_z, v_0, μ) of the upper boundaries r_U of the 95%-confidence intervals of the "short-term" stability failure rate, see explanatory note to paragraph 3.5.3.2.1 of the Interim Guidelines, assuming uniform distributions of mean wave directions between 0 and 360° and ship forward speeds between zero and maximum service speed.

2.3.5 Table 2.3.2 shows the "long-term" weighted average $\bar{r}_U$ of the upper boundaries of the 95%-confidence intervals of the "short-term" stability failure rate for unrestricted operation (area 1) and specific routes and seasons (2 to 6, table 2.3.1); bold numbers indicate unacceptable loading conditions. For 64% of loading conditions, $\bar{r}_U$ decreases compared to unrestricted operation due to operational limitations, moreover, it decreases for 85% of relevant loading conditions, i.e. those for which change of route may influence acceptance decision. However, only one unacceptable loading condition of one ship changes to acceptable due to change of route, whereas the result is opposite for another loading condition. Thus, operational limitations related to areas or routes and season are less efficient than operational guidance (which rendered as acceptable all considered loading conditions for all considered ships, section 2.1), unless they are combined with other operational measures.

Table 2.3.2. "Long-term" weighted average $\bar{r}_U$ of upper boundaries of 95%-confidence intervals of "short-term" stability failure rate for areas or routes and seasons specified in table 2.2.1

Ship	LC	Areas or routes and seasons					
		1	2	3	4	5	6
Cruise	01	**2.214e-6**	**1.549e-6**	**5.125e-7**	**6.940e-7**	**5.154e-7**	**4.243e-7**
	02	**5.706e-8**	**1.114e-7**	**4.859e-8**	**6.461e-8**	**4.800e-8**	**2.702e-8**
	03	4.587e-9	1.025e-8	4.066e-9	5.798e-9	4.051e-9	1.911e-9
	04	7.582e-10	1.781e-9	5.266e-10	8.253e-10	5.456e-10	2.592e-10
	05	3.911e-10	1.085e-9	3.276e-10	5.103e-10	3.388e-10	1.611e-10
CV 1700	01	**5.362e-5**	**2.881e-5**	**1.117e-5**	**1.323e-5**	**1.118e-5**	**1.068e-5**
	02	**1.432e-6**	**1.950e-6**	**1.076e-6**	**1.226e-6**	**1.058e-6**	**7.199e-7**
	03	1.198e-8	**5.334e-8**	**3.686e-8**	**4.588e-8**	**3.567e-8**	1.555e-8
	04	1.388e-12	3.313e-11	2.290e-11	2.912e-11	2.140e-11	9.222e-12
	05	1.500e-12	5.260e-11	4.137e-11	5.220e-11	3.864e-11	1.589e-11
CV 8400	01	**6.614e-6**	**1.515e-6**	**3.156e-7**	**5.321e-7**	**3.306e-7**	**2.657e-7**
	02	**3.907e-6**	**1.006e-6**	**2.104e-7**	**3.526e-7**	**2.204e-7**	**1.839e-7**
	03	**4.113e-7**	**1.948e-7**	**4.685e-8**	**7.364e-8**	**4.865e-8**	**3.973e-8**
	04	**2.303e-7**	**6.816e-8**	1.383e-8	2.498e-8	1.484e-8	5.745e-9
	05	8.954e-9	6.772e-9	1.550e-9	2.681e-9	1.662e-9	7.203e-10
CV 14000	01	**1.286e-4**	**3.007e-5**	**6.692e-6**	**1.068e-5**	**6.922e-6**	**7.418e-6**
	02	**3.645e-5**	**9.328e-6**	**2.044e-6**	**3.307e-6**	**2.117e-6**	**2.117e-6**
	03	**2.435e-6**	**1.028e-6**	**2.541e-7**	**3.901e-7**	**2.618e-7**	**2.278e-7**
	04	5.306e-16	2.294e-20	5.613e-21	9.760e-21	6.113e-21	2.251e-21
	05	2.068e-15	9.388e-18	2.676e-18	4.343e-18	2.840e-18	1.257e-18
RoPax	01	1.223e-9	5.105e-9	2.119e-9	2.959e-9	2.093e-9	1.028e-9
	02	-	-	-	-	-	-
	03	5.493e-11	4.279e-10	1.937e-10	2.655e-10	1.886e-10	9.002e-11
	04	6.207e-11	6.398e-10	3.178e-10	4.254e-10	3.056e-10	1.435e-10
	05	7.839e-11	1.068e-9	5.942e-10	7.767e-10	5.647e-10	2.572e-10

2.4 DSA-based operational limitations related to maximum significant wave height

2.4.1 Operational limitations related to maximum significant wave height accept operation in sea states up to a specified maximum significant wave height. Sample operational limitations were developed for all ships and loading conditions in table 1.1.1 using the North Atlantic wave scatter table according to IACS Recommendation No.34 (Corr.1 Nov. 2001) (also shown in table 2.7.2.1.2), limited by a systematically varied maximum significant wave height with a step 1.0 m.

2.4.2 Operational limitations were produced, according to section 4.5.2 , by applying full probabilistic direct stability assessment (section 3.5.3.2) for each specified maximum significant wave height, using numerical simulations of ship motions at six forward speeds in waves of mean zero-crossing periods T_z and significant wave heights H_s covering all entries in the scatter table below the specified maximum significant wave height with steps 1.0 s and 1.0 m, respectively, and mean wave directions from 0 to 180° every 10°.

2.4.3 Numerical simulations of ship motions were performed in realizations of the same sea state by random variation of frequencies, directions and phases of wave components discretizing the wave energy spectrum. Each simulation was conducted for the simulation time of 2 hours or until the first stability failure (exceedance of 40° roll angle or lateral acceleration g) if it happened earlier, after which simulation was repeated in another realization, until $N = 200$ stability failures were encountered. Transient hydrodynamic effects at the start of simulations were neutralized by switching off the counter of stability failures and simulation timer during initial transients. For such combinations (H_s, T_z, v_0, μ), for which the total simulation time of $3.4 \cdot 10^6$ hours was enough to encounter 200 stability failures, direct counting was used: the maximum likelihood estimate of stability failure rate was calculated as $r = N / t_t$, eq. (3.3.6), and upper boundary of its 95%-confidence interval as $r_{\mathrm{U}} = 0.5r\chi^2_{1-0.05/2,2N}/N$, eq. (3.3.9); otherwise extrapolation of failure rate over significant wave height was used.

2.4.4 A conservative estimate of the upper boundary $\bar{r}_{\mathrm{U}}$ of the 95%-confidence interval of the average "long-term" stability failure rate was calculated as a weighted average, over all combinations (H_s, T_z, v_0, μ), of the upper boundaries r_{U} of the 95%-confidence intervals of the "short-term" stability failure rate, see explanatory note to paragraph 3.5.3.2.1, assuming uniform distributions of mean wave directions between 0 and 360° and ship forward speeds v_0 between zero and maximum service speed.

2.4.5 Figure 2.4.1 shows the "long-term" weighted average $\bar{r}_{\mathrm{U}}$ of the upper boundaries of the 95%-confidence intervals of the "short-term" stability failure rate (total and separately due to principal parametric resonance in bow and stern waves and synchronous roll in beam waves) and operability vs. the maximum significant wave height. Table 2.4.1 shows the maximum significant wave height at which the "long-term" weighted average of the upper boundaries of the 95%-confidence intervals of the 'short-term' stability failure rate is equal to the standard $2.6 \cdot 10^{-8}$ 1/s and the operability corresponding to this wave height.

Figure 2.4.1 (below):
"Long-term" weighted average $\bar{r}_{\mathrm{U}}$ of upper boundaries of 95%-confidence intervals of "short-term" stability failure rate (left y-axis): total (ALL, black solid lines) and due to principal parametric resonance in bow (PRB, red dashed lines) and stern (PRS, red dash-dot lines) waves and synchronous roll (SR, green dash-dot-dot lines) in beam waves and operability (right y-axis, blue dashed line marked O) vs. maximum significant wave height (x-axis) in North Atlantic wave climate

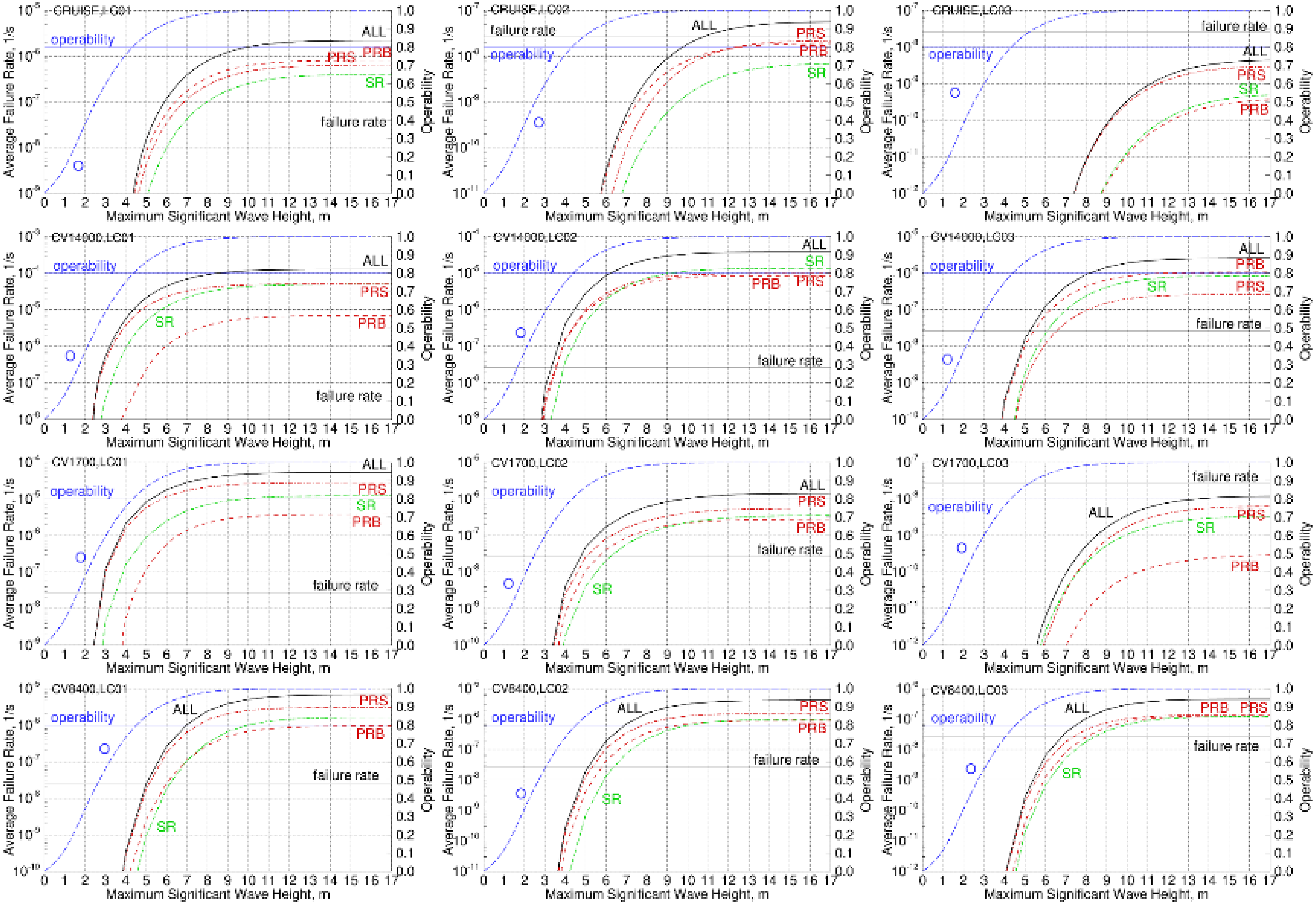
CRUISE,LC01
CRUISE,LC02
CRUISE,LC03
CV14000,LC01
CV14000,LC02
CV14000,LC03
CV1700,LC01
CV1700,LC02
CV1700,LC03
CV8400,LC01
CV8400,LC02
CV8400,LC03
operability
failure rate
ALL
PRS
PRB
SR
Average Failure Rate, 1/s
Operability
Maximum Significant Wave Height, m

Table 2.4.1. Maximum significant wave height at which "long-term" weighted average $\bar{r}_U$ of upper boundaries of 95%-confidence intervals of "short-term" stability failure rate does not exceed standard 2.6·10^{-8} 1/s ("unl." stands for "unlimited", meaning that limitation is not required) and corresponding operability (bold numbers indicates values less than 0.8) in North Atlantic wave climate

Ship ↓	Maximum significant wave height, m					Corresponding operability				
Loading conditions →	01	02	03	04	05	01	02	03	04	05
Cruise Vessel	5.266	10.763	unl.	unl.	unl.	0.883	0.999	1.0	1.0	1.0
1700 TEU CV	2.814	4.746	unl.	unl.	unl.	**0.557**	0.839	1.0	1.0	1.0
8400 TEU CV	5.009	5.111	6.796	9.576	unl.	0.850	0.858	0.951	0.994	1.0
14000 TEU CV	2.479	3.317	5.225	unl.	unl.	**0.476**	**0.639**	0.876	1.0	1.0
RoPax	unl.	unl.	unl.	unl.	unl.	1.0	1.0	1.0	1.0	1.0

2.4.6 Note that in the same wave climate, a probabilistic operational guidance allows achieving significantly greater operability than operational limitations related to maximum significant wave height, compare tables 2.1.2 and 2.4.1. Moreover, according to the results in table 2.1.2, the ratio of the total duration of all unacceptable situations to the total operational time does not exceed 0.2 for all considered loading conditions when operational guidance is used (which means that all considered loading conditions are acceptable if operational guidance is provided), whereas this ratio exceeds 0.2 (i.e. operability is less than 0.8) for three of the same loading conditions when operational limitations related to maximum significant wave height are used. This means that operational limitations related to maximum significant wave height are less efficient than operational guidance for the considered example applications.

2.5 Simplified operational guidance for surf-riding/broaching failure mode

2.5.1 The simplified operational guidance based on the methodology used for the vulnerability criteria for the surf-riding/broaching failure mode is provided in paragraph 4.5.6.2.4. The simplified operational guidance is based on indications from the Operational Diagram for the Master in MSC.1/Circ./707, which was used for practical application between 1996 and 2007 without actual problems reported. However, the simplified operational guidance based on level 2 vulnerability criterion specified in paragraph 4.5.6.2.4.2 requires validation and application examples.

2.5.2 For this purpose, the probabilistic indices based on paragraph 4.5.6.2.4.2, C_{HT}, equal to the conditional probability of surf-riding when the ship meets a wave, were calculated for several short-term sea states with different ship speeds and courses and compared with the broaching failure probability obtained with the critical wave method, which is equal to the conditional probability of large heel due to broaching associated with surf-riding when the ship meets a wave. The subject ship is an offshore research vessel, which is similar to a vessel lost in stern quartering waves at high forward speed; the sea states are based on those specified as the design situations in paragraphs 3.5.3.3.4 and 3.5.3.3.5. The tested ship speed ranges from 0.015 to 0.4 and the relative wave heading from 1 to 90 degrees.

2.5.3 Figures 2.5.1 and 2.5.2 indicate that the results of level 2 vulnerability criterion provide reasonably conservative estimate of the danger due to broaching in comparison with direct assessment for the considered sea states and sailing conditions, thus the simplified operational guidance based on level 2 vulnerability criterion specified in paragraph 4.5.6.2.4.2 is effective to assist the ship master to avoid dangerous situations. Note that such simplified operational guidance can be obtained as intermediate calculation data from the application of level 2 vulnerability criterion, thus no additional computational effort is required for the preparation of such simplified operational guidance.

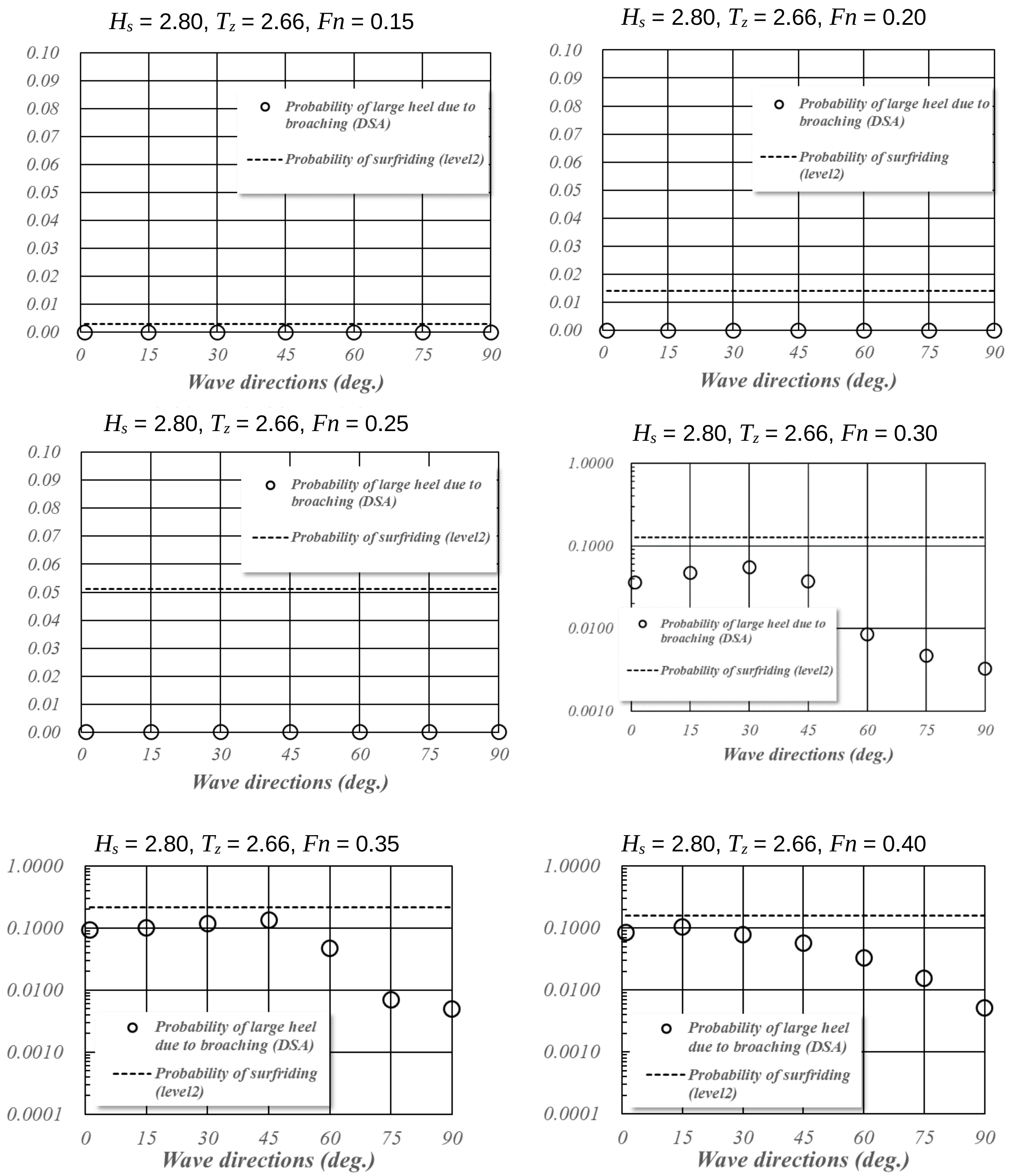

Figure 2.5.1 Comparison of level 2 criterion with failure probability computed with critical wave method in sea state with mean zero-crossing wave period 2.66 s (which corresponds to wavelength $1.0L$) and significant wave height 2.8 m from table 3.5.3.3

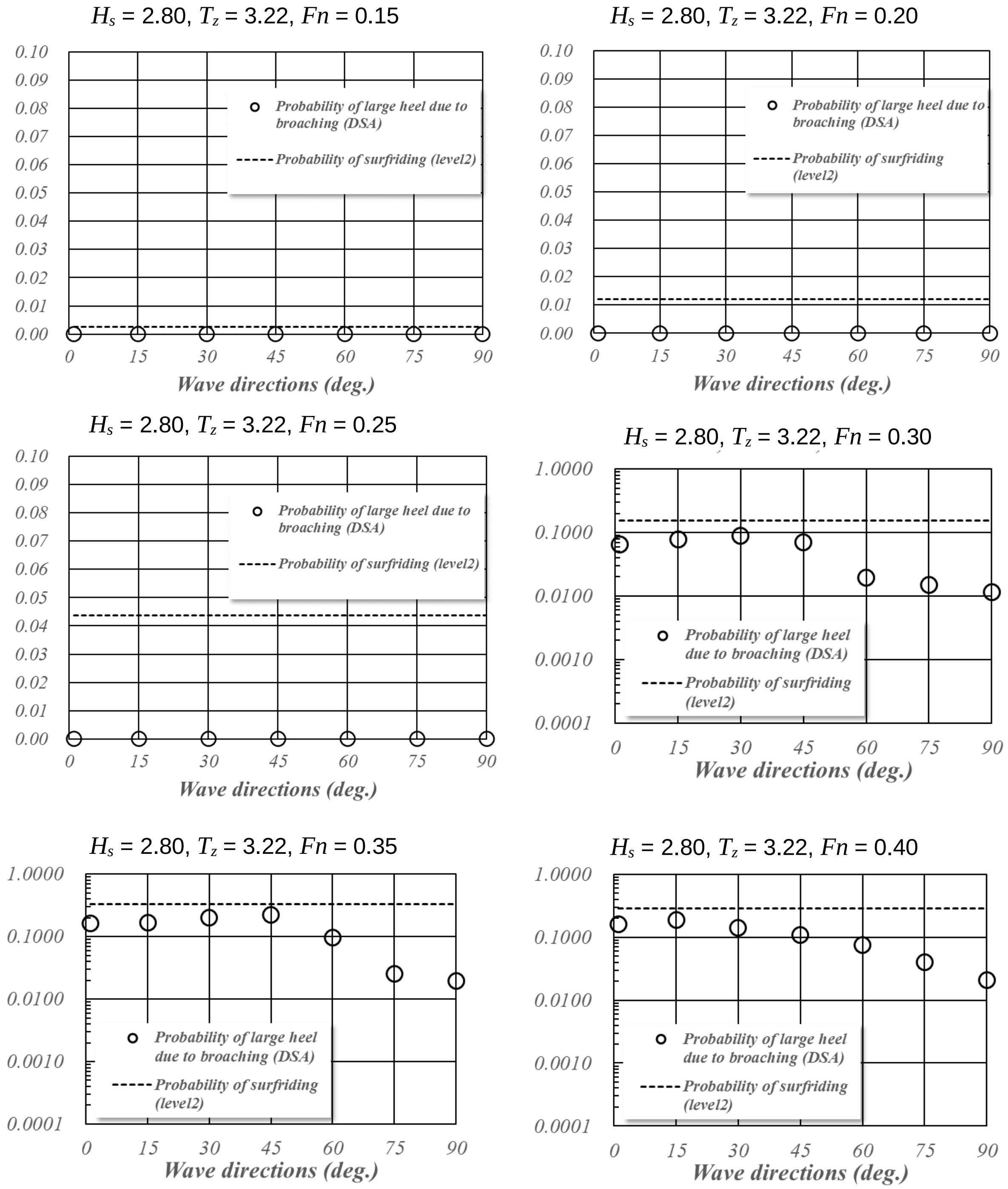

Figure 2.5.2. Comparison of level 2 criterion with failure probability computed with critical wave method in sea state with mean zero-crossing wave period 3.22 s (which corresponds to wavelength 1.5L) and significant wave height 2.8 m from table 3.5.3.3.5

2.6 Simplified operational guidance from level 2 vulnerability assessment for parametric roll

2.6.1 For the use of the simplified operational guidance for parametric rolling, which is defined in the paragraph 4.5.6.2.3 of the Interim Guidelines, it is essential to confirm the prediction accuracy of the method in the second check of the level 2 criterion for parametric rolling. This is because the operational guidance should be used for actual irregular waves while the method in the level 2 is based on the calculation in the equivalent regular waves.

Thus, the comparisons between the numerical results using the second check of the level 2 methodology and the existing experimental results in irregular waves are presented here.

2.6.2 The comparisons for the C11 class containership in head waves are shown in figures 2.6. 1-2. The simulation results to be used in the simplified operational guidance somewhat overestimate the experimental results[34] in irregular waves.

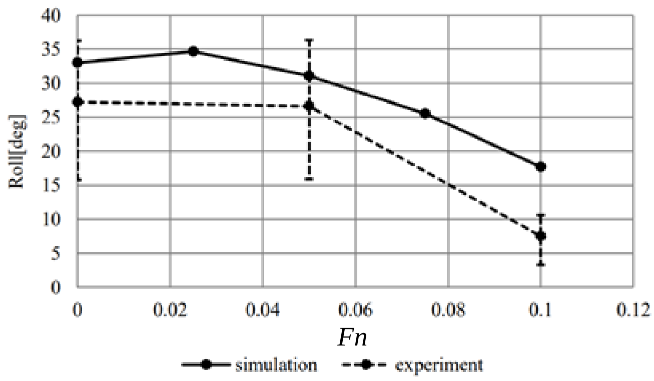

Figure 2.6. 1 Comparison in the roll amplitude between the simulation to be used for simplified guidance and the model experiment in irregular waves for the C11 class containership in head seas with the significant wave height of 7.82 m and the mean wave period of 9.99 s for different Froude numbers

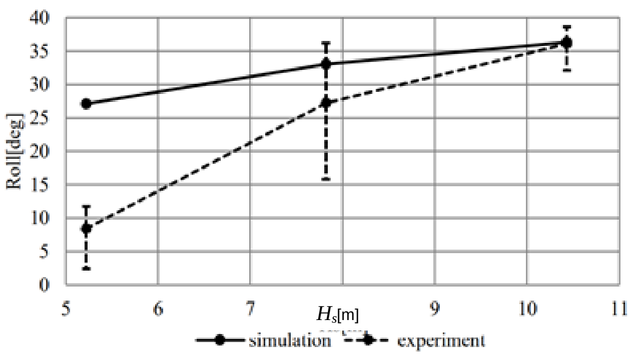

Figure 2.6.2 Comparison in the roll amplitude between the simulation to be used for simplified guidance and the model experiment in irregular waves for the C11 class containership in head seas with the mean wave period of 9.99 s and the Froude number of 0.0 for different significant wave heights

2.6.3 The comparison for the 150m-long containership in following waves is shown in figure 2.6.3. Here the roll angle of 80 degrees indicates capsizing. The reason for the frequent occurrence of capsizing due to parametric rolling is small metacentric height, which is critical to the 2008 Intact Stability Code and severest sea state in the oceans. In this case, also the

34 Hashimoto, H. and N. Umeda. *Prediction of Parametric Rolling in Irregular Head Waves.* Chapter 16 of Contemporary Ideas on Ship Stability. Risk of Capsizing, Belenky, V., Spyrou, K., van Walree F., Neves, M.A.S., and N. Umeda, eds., Springer, ISBN 978-3-030-00514-6, pp. 275-289, 2019.

simulation results to be used in the simplified operational guidance somewhat overestimate the experimental results[35] in irregular waves.

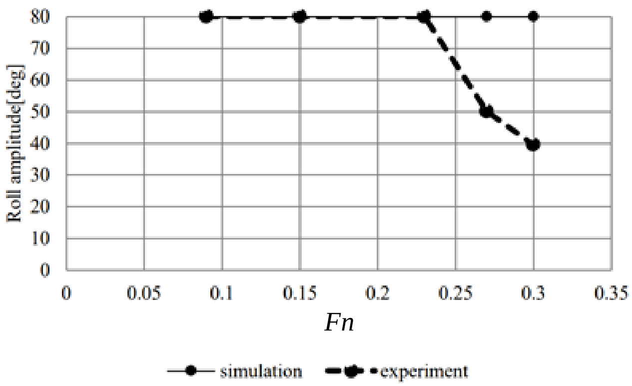

Figure 2.6.3 Comparison in the roll amplitude between the simulation to be used for simplified guidance and the model experiment in irregular waves for the 150m-long containership having the metacentric height of 0.15m in following seas with the significant wave height of 13.26 m and the mean wave period of 10.92 s for different Froude numbers

2.6.4 The comparison for the 192m-long PCTC in head waves is shown in figure 2.6.4. In this case, the simulation results to be used in the simplified operational guidance, which is labelled as "simulation 1" do not always overestimate the experimental results[36] in irregular waves. This is because the roll amplitude in regular waves does not always increase with the increasing the wave height, which is due to the increase of the mean of GM with the wave height. Roughly speaking, the amplitude of the GM variation is proportional to the wave height, while the mean of GM variation is proportional to the square of the wave height. Thus, sometimes the condition for parametric roll will not be met at a certain wave height or above. On the other hand, the roll amplitude in irregular waves normally increases with the increasing the wave height because of the spectrum of incident waves. To confirm this mechanism, the simulation ignoring the mean of GM variation is also shown as "simulation 2". As a result, the roll amplitude ignoring the mean of GM variation increases with the increasing wave height. This is a drawback of the simplified approach using the effective regular waves. Thus, the second check of the level 2 criterion requires to keep the maximum roll amplitude if the roll amplitude decreases with the increasing wave height in paragraph 3.5 of appendix 3. Therefore, the same procedure should be applied to the simplified operational guidance.

---

35 Umeda, N., M. Hamamoto, Y. Takaishi, Y. Chiba, A. Matsuda, W. Sera, S. Suzuki, K. J. Spyrou and K. Watanabe. *Model Experiments of Ship Capsize in Astern Seas*. Journal of the Society of Naval Architects of Japan, Vol.177, pp.207-217, Jun. 1995.

36 Umeda N., Hashimoto H., Tsukamoto I., Sogawa Y. *Estimation of Parametric Roll in Random Seaways*. In: Fossen T., Nijmeijer H. (eds) Parametric Resonance in Dynamical Systems. Springer, New York, NY, ISBN 978-1-4614-10423-0, pp: 45-59, 2012.

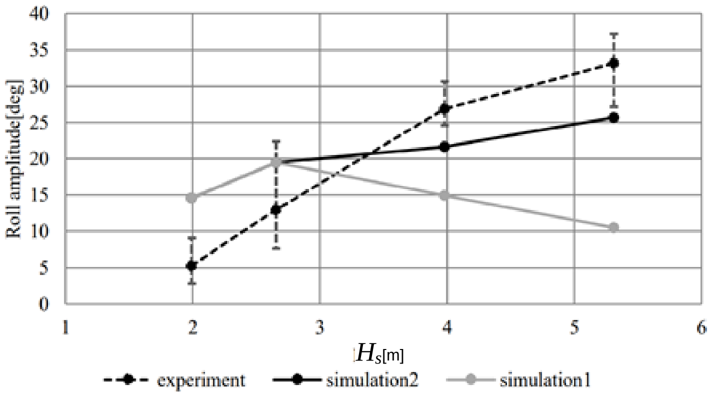

Figure 2.6.4 Comparison in the roll amplitude between the simulation to be used for simplified guidance and the model experiment in irregular waves for the 192m-long PCTC in head seas with the mean wave period of 9.76 s and the Froude number of 0.0 for different significant wave heights

2.6.5 In conclusion, if the requirement in paragraph 3.5 of appendix 3 is also taken into account, the calculation based on the second check of the level 2 criterion normally overestimates the model experiment. Since the numerical model used for the full operational guidance is required to be validated with model experiments, the simplified operational guidance for parametric rolling is expected to provide conservative estimates for the danger of parametric rolling in actual longitudinal seas. The remaining issue is the absence of the requirement for heading in the simplified guidance. However, the magnitude of parametric rolling in oblique waves can be reduced if the heading angle leaves from the longitudinal waves. Therefore, the safety level realized with the simplified operational guidance for parametric rolling is logically higher than that with full operational guidance.

2.7 Level 2-based operational limitations related to maximum wave height

2.7.1 A C11-class post-Panamax container ship was used as a sample ship; table 2.7.1 shows principal dimensions. This ship in the considered loading condition failed to pass check 1 and check 2 of vulnerability assessment for parametric roll, table 2.7.2. Therefore, operational measures were considered.

Table 2.7.1 Principal parameters of sample ship and loading condition

Length between perpendiculars, L_{BP}	262.0 m
Breadth, B	40.0 m
Draught, d	11.5 m
Total projected area of bilge keels, A_{BK}	30.6 m^2
Service speed, V_s	23.6 knots
Metacentric height, GM	1.965 m
Natural roll period, T_r	25.1 s

Table 2.7.2 Results of level 2 vulnerability check for parametric roll for sample ship

Value	Required value	Judgement
$C1$ = 0.4368	R_{PR0} = 0.06	fail
$C2$ = 0.02592	R_{PR1} = 0.025	fail

2.7.2 If level 2 vulnerability criterion for parametric roll is applied for the preparation of operational limitations, the corresponding procedure of the vulnerability check and the value of the standard should be used.

2.7.3 Operational limitations related to maximum significant wave height are developed for environmental conditions which are defined by cutting, at a specified significant wave height, the wave scatter table for a specified area or a specified route during a specified season and by corresponding modification of wind statistics.

2.7.4 The wave scatter table from level 2 vulnerability assessment for parametric roll was used, paragraph 2.5.3.4.2. Sea state probabilities up to specified significant wave heights were summed, as shown in table 2.7.3. Since the operability should be not less than 0.8 to apply operational limitations related to maximum significant wave height, the maximum significant wave height should exceed 5.0 m for the considered scatter table.

Table 2.7.3 Sum of sea state probabilities up to specified maximum significant wave height

Specified maximum H_s, m	Probability of occurrence	Sum
1.0	0.030504	0.03050
2.0	0.225754	0.25626
3.0	0.238104	0.49436
4.0	0.191277	0.68564
5.0	**0.132894**	**0.81853**
6.0	0.083281	0.90181
7.0	0.048063	0.94988
8.0	0.025862	0.97574
9.0	0.013087	0.98883
10.0	0.006262	0.99509
11.0	0.002848	0.99794
12.0	0.001236	0.99917
13.0	0.000511	0.99968
14.0	0.000205	0.99989
15.0	0.000077	0.99997
16.0	0.000028	0.99999
17.0	0.000009	1.00000

2.7.5 Check 2 of level 2 vulnerability criteria for parametric roll was used for the preparation of operational limitations. The results in table 2.7.4 indicate that the maximum operational significant wave height is 10.0 m for the considered loading condition. Since it is greater than 5.0 m, paragraph 2.7.4, operational limitations with the maximum operational significant wave height of 10.0 m can be applied.

Table 2.7.4 Vulnerability check with cut wave scatter diagrams

Specified H_s for cut-off, m	$C2$	Judgement
5.0	0.00858	pass
6.0	0.01509	pass
7.0	0.01892	pass
8.0	0.02194	pass
9.0	0.02391	pass
10.0	0.02496	pass
11.0	0.02551	fail
12.0	0.02575	fail
13.0	0.02585	fail
14.0	0.02590	fail
15.0	0.02591	fail
16.0	0.02592	fail
none	0.02592	fail

3 Wave cases for preparation of operational limitations using level 1 and level 2 vulnerability assessment

3.1 Wave cases and associated parameters for the preparation of operational limitations using level 1 and level 2 vulnerability assessment criteria should be defined in accordance with the procedure described in section 10 of appendix 3.

4 Supplementary information on preparation of simplified operational guidance for surf-riding/broaching failure mode

4.1 For predicting surf-riding/broaching, accurate estimation of the wave-induced surge force is indispensable. For level 2 vulnerability criterion for surf-riding/broaching in 2.6.3.4.5, the Froude-Krylov component is considered. The Froude-Krylov component alone normally overestimates the wave-induced surge force in situations relevant for surf-riding. This is because the diffraction component, which is the effect of hull disturbance on incident waves is not small. Thus, the diffraction effect may be considered for practical use.

4.2 The diffraction effect can be estimated with CFD or three-dimensional linear potential flow codes; for simplified operational guidance, the following empirical formula for f_{ij} can be used instead of that in paragraph 2.6.3.4.5 in MSC.1/Circ.1627 as an alternative to CFD or equivalent:

$$f_{ij} = 0.5\rho g \mu_x k_i H_{ij}\sqrt{Fc_i^2 + Fs_i^2} \qquad (4.1)$$

4.3 In eq. (4.1), the coefficient μ_x is defined using the following formulae based on experimental data for two container ships, a car carrier, a RoRo ship, a fishing vessel and two warships:

$$\begin{aligned} \mu_x &= 1.46\,C_b - 0.05 && \text{for} \quad C_\mathrm{m} < 0.86 \\ &= (5.76 - 5.00\,C_\mathrm{m})\,C_b - 0.05 && \text{for} \quad 0.86 \le C_\mathrm{m} < 0.94 \\ &= 1.06\,C_b - 0.05 && \text{for} \quad C_\mathrm{m} \ge 0.94 \end{aligned} \qquad (4.2)$$

where C_b is the block coefficient and C_m is the midship section coefficient.

APPENDIX 6

APPLICATION EXAMPLES OF TREATMENT OF LOADING CONDITIONS

Introduction

1 The application of vulnerability criteria should cover all loading conditions intended for the ship's operation. In this respect, GM, draught and trim should be appropriately considered. However, for the sake of simplicity, the application examples here cover only combinations of GM and draught. Specifically, matrix calculations have been carried out, where vulnerability criteria have been applied for each combination of GM and draught; and the roll period has been estimated in accordance with paragraph 2.7.1.2.

2 Paragraphs 2.2.1.3, 2.3.1.3, 2.4.1.3, 2.5.1.2 and 2.6.1.2 allow the use of direct stability assessment or operational measures as alternatives to the vulnerability criteria specified for each particular failure mode. Nevertheless, for demonstration purposes, the application examples stipulated here show only the results of probabilistic direct stability assessment and probabilistic operational measures for the parametric rolling and pure loss of stability failure modes. It is also noted that the verification of failure modes, according to section 3.5.2, has not been carried out for the reported example applications. Therefore, reported direct stability assessment results are conservative compared to those that would be obtained by applying section 3.5.2. Furthermore, for each example ship, results of the direct stability assessment are shown only for a typical draught. Examples of direct stability assessment for other loading conditions can be found in section 4.2 of appendix 4.

3 Since direct stability assessment requires significant computational efforts, the user may be guided by a sequential logic of application of the Interim Guidelines (section 1.1.3 therein). In this regard, direct stability assessment may be applied to the loading conditions that are indicated to be potentially vulnerable according to the vulnerability criteria for the relevant failure mode.

4 The numerical model used in the direct stability assessment should be validated based on paragraph 3.4.1.2 and the identified failure mode in the direct stability assessment should be the same as that used in the validation (see paragraph 3.5.2.1).

5 In these application examples, whenever the Weather Criterion is mentioned, the use of MSC.1/Circ.1200 is not taken into account. Thus, for the actual application, the possibility of its use could be considered in accordance with the provisions of part A, paragraphs 2.3.3 and 2.3.5 of the 2008 IS Code.

6 When comparing specific loading conditions with results from the assessment, GM values corrected for free surface effects should be used for the dead ship condition, pure loss of stability and parametric rolling failure modes (see paragraphs 2.2.1.7, 2.4.1.7 and 2.5.1.6, respectively); whereas GM values not corrected for free surface effects should be used for excessive acceleration failure mode (see paragraph 2.3.1.7).

7 In the matrix calculation shown in this appendix, red and blue colours indicate that the ship is "possibly vulnerable" and "acceptable" to the failure modes, respectively.

1 Examples of the treatment of loading conditions

1.1 Cruise ship

1.1.1 An existing cruise vessel with the length between perpendiculars 230.9 m and waterline breadth 32.2 m was used as an example.

1.1.2 The criteria from part A of the 2008 IS Code and the deterministic damage stability requirements in the SOLAS (as amended by resolutions in effect as on 1 July 2004) result in minimum *GM* dependencies on the draft shown in figure 1.1.1.

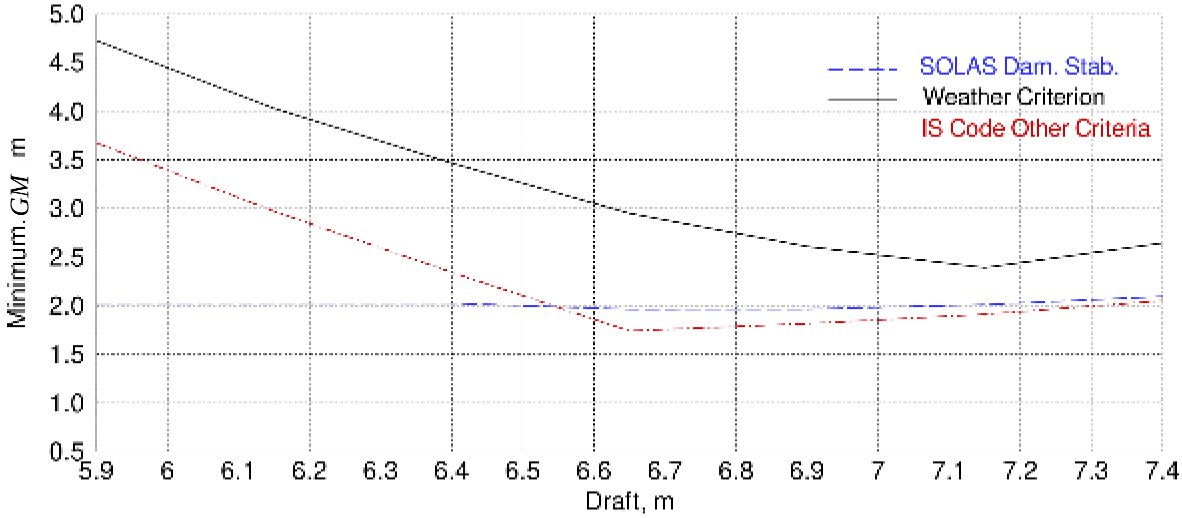

Figure 1.1.1. Minimum *GM* curves vs. draft according to the 2008 IS Code part A criteria and SOLAS damage stability requirements for cruise vessel

1.1.3 Figure 1.1.2 shows results of assessment with respect to level 1 and level 2 vulnerability criteria for parametric roll stability failure mode. Since it is sufficient to satisfy one of these three assessment options, these criteria do not suggest additional recommendations on the minimum *GM* for this vessel compared to the criteria from part A of the 2008 IS Code and SOLAS damage stability requirements because the mandatory criteria shown in figure 1.1.1 supersede those recommended in figure 1.1.2.

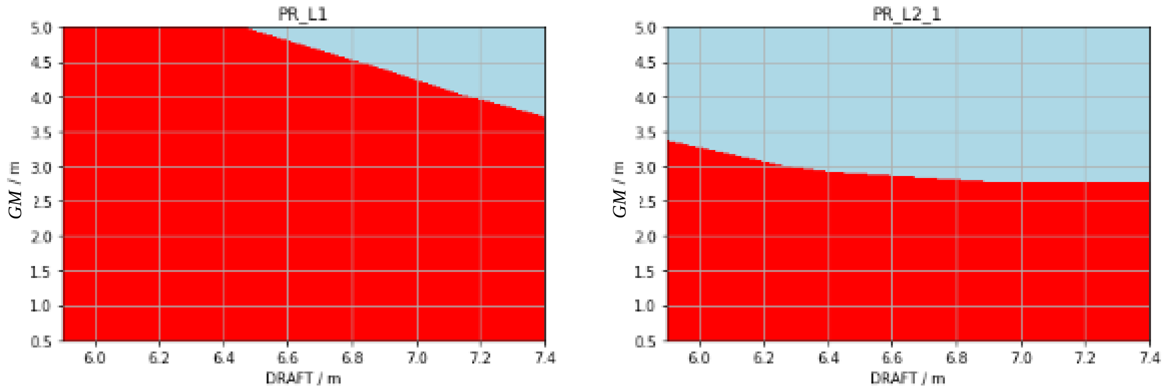

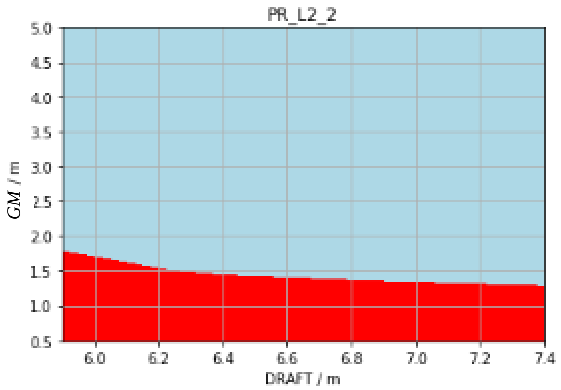

Figure 1.1.2 Result of level 1 (top left – PR_L1), level 2 check 1 (top right – PR_L2_1) and level 2 check 2 (bottom left – PR_L2_1) assessment for the parametric roll stability failure mode for cruise vessel

1.1.4 Assessment with respect to level 1 and level 2 vulnerability criteria for the pure loss of stability failure mode, figure 1.1.3, shows that the ship is vulnerable with respect to level 1 criterion in all combinations of draught and GM shown in figure 1.1.3. This failure mode does not suggest additional recommendations on the minimum GM for this vessel compared to the criteria from part A of the 2008 IS Code and SOLAS damage stability requirements.

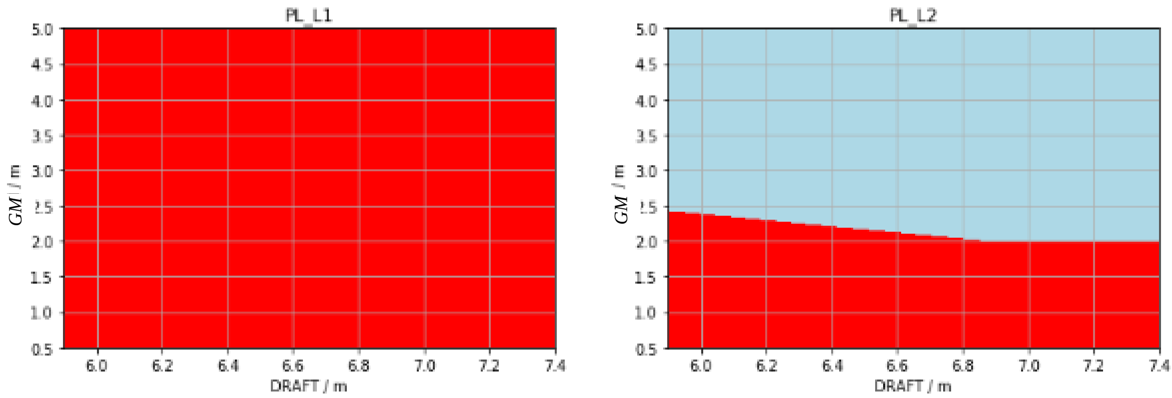

Figure 1.1.3 Results of level 1 and level 2 assessment for pure loss of stability failure mode for cruise vessel

1.1.5 Because the length of the vessel is greater than 200 m, an assessment with respect to the level 1 criterion for surf-riding/broaching indicates that the ship is not vulnerable to this stability failure mode in all loading conditions.

1.1.6 Since the natural roll period of the ship in the considered loading conditions is below (or only marginally above) 20 s, there is no difference between the Weather Criterion from part A of the 2008 IS Code and level 1 criterion for dead ship condition stability failure mode, figure 1.1.4. Application of level 2 criterion for dead ship condition stability failure mode does not suggest additional recommendations on the minimum *GM* value.

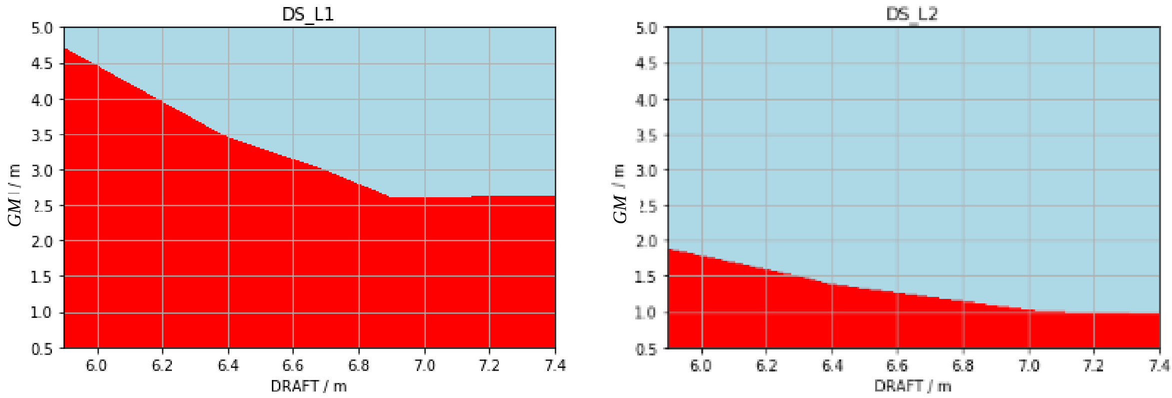

Figure 1.1.4. Results of level 1 and level 2 assessment for dead ship condition stability failure mode for cruise vessel, DS_L1 and DS_L2, respectively

1.1.7 The application of vulnerability criteria for the excessive acceleration stability failure mode leads to recommendations on the upper limit of *GM*. Figure 1.1.5 shows that level 2 allows significantly greater maximum *GM* values than level 1, which are also well above the *GM* range relevant in practice for this vessel. Users should note that the *GM* values associated with results of excessive acceleration criteria represent metacentric heights without correction for free surface.

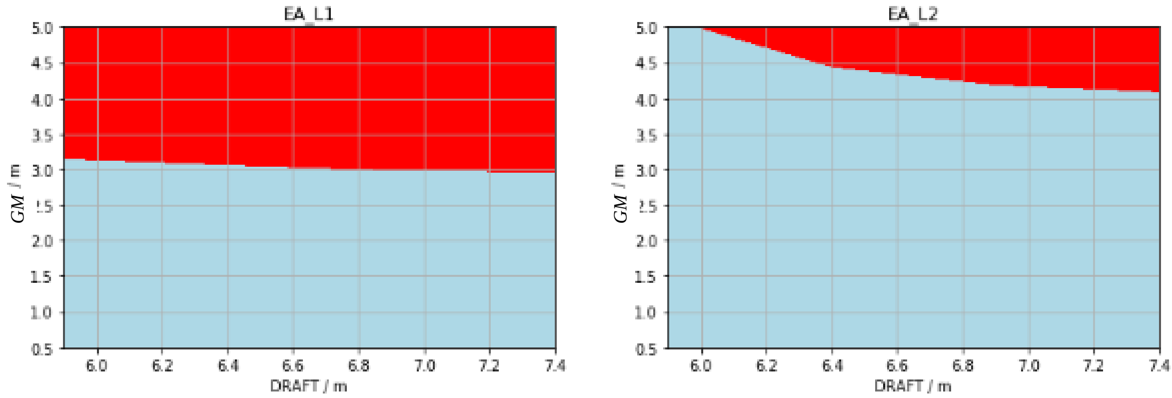

Figure 1.1.5. Results of level 1 and level 2 assessment for excessive acceleration stability failure mode for cruise vessel

1.1.8 For the considered cruise vessel, the second-generation intact stability criteria do not result in any additional recommendations relative to part A of the 2008 IS Code and the damage stability requirements of SOLAS on the minimum *GM* values (for the considered, practically relevant, range of draughts). Since the limiting criterion for the minimum *GM* values is the Weather Criterion, figure 1.1.6, and that the assessment for the level 2 criterion for the dead ship failure mode indicates lower minimum *GM* values, then the application of MSC.1/Circ.1200 may be utilized to evaluate revised minimum *GM* values. The vulnerability criteria for excessive accelerations impose additional limitations on the maximum *GM* values (however, these limitations are above the *GM* values relevant in practice).

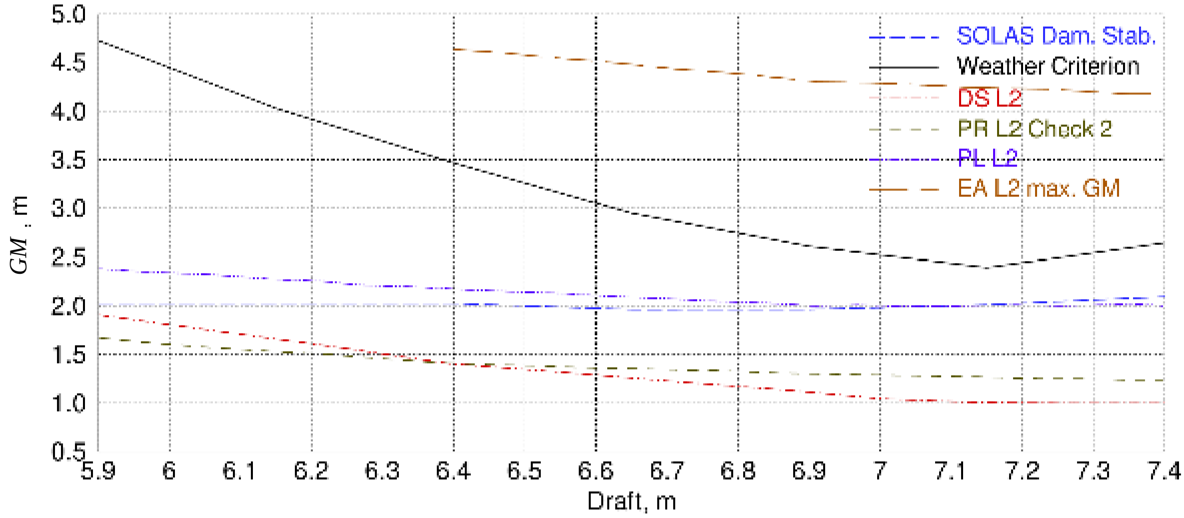

Figure 1.1.6. *GM* limits according to the 2008 IS Code part A, SOLAS damage stability requirements and second-generation intact stability criteria (including maximum *GM* according to excessive accelerations criterion) for cruise vessel

1.1.9 Six loading conditions at the practically most relevant draught 6.9 m and *GM* values 1.5, 2.0, 2.5, 3.25 and 3.75 m, table 4.1.1 of chapter 4 of appendix 4, were assessed using full probabilistic direct stability assessment. Figure 1.1.7 plots the conservative estimate of the upper boundary $\bar{r}_U$ of the 95%-confidence interval of the average "long-term" stability failure rate, calculated as the weighted average of the upper boundaries of the 95%-confidence intervals of the "short-term" stability failure rate (see explanatory note to paragraph 3.5.3.2.1 of the Interim Guidelines). The standard $2.6{\cdot}10^{-8}$ 1/s for $\bar{r}_U$ is satisfied for *GM* values above 2.158 m. This is greater than the minimum required *GM* from chapter 2 of MSC.1/Circ.1627 – vulnerability requirements (which indicates inconsistency between the vulnerability assessment and direct stability assessment for the considered ship and draught). However, the weather criterion requires greater minimum *GM* and, therefore, this consistency does not suggest any additional recommendations for the minimum *GM* value.

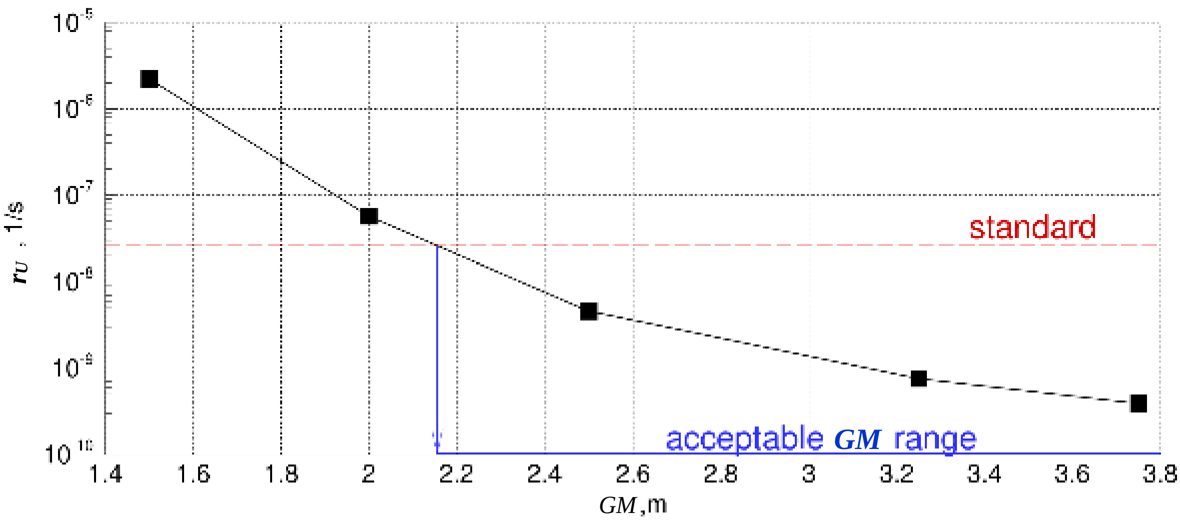

Figure 1.1.7. Conservative estimate of upper boundary $\bar{r}_U$ of 95%-confidence interval of average "long-term" stability failure rate vs. *GM* at draught 6.9 m for cruise vessel in comparison with acceptance standard $2.6{\cdot}10^{-8}$ 1/s and resulting acceptable *GM* range

1.1.10 Probabilistic operational guidance was prepared for the same loading conditions by identifying unacceptable sailing conditions (v_0,μ), i.e. sailing conditions for which the upper boundary of 95%-confidence interval of "short-term" stability failure rate exceeds acceptance standard 10^{-6} s^{-1}, for each sea state (H_s,T_z) in the North Atlantic wave scatter table. Figure 1.1.8 shows "long-term" weighted average $\bar{r}_U$ of upper boundaries of the 95%-confidence intervals of the "short-term" stability failure rate with and without using operational guidance together with the operability due to the use of operational guidance vs. GM. Since operability exceeds 0.8, operational guidance is an acceptable option for all considered loading conditions.

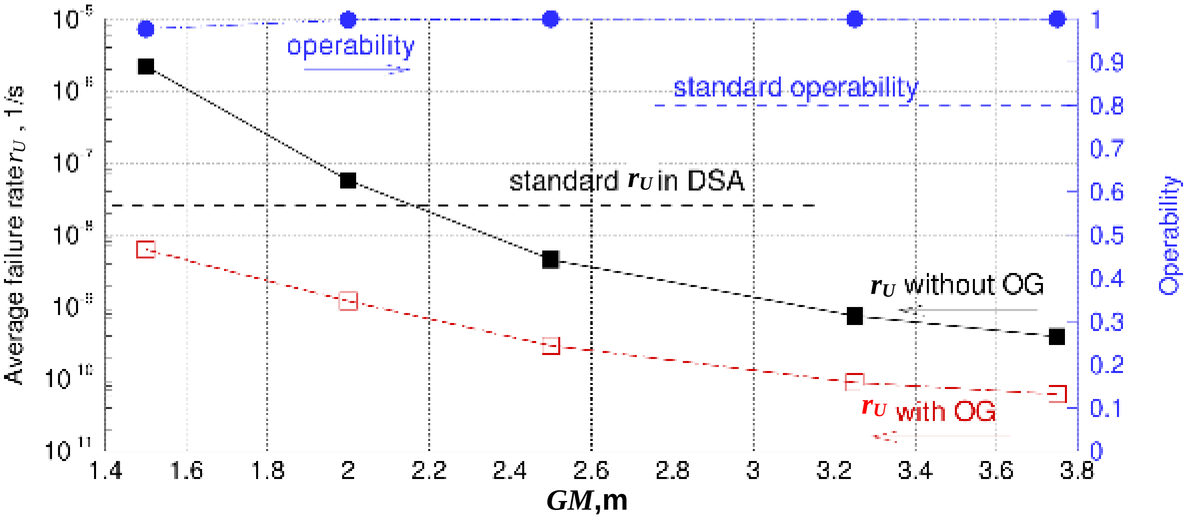

Figure 1.1.8. "Long-term" weighted average of upper boundaries of 95%-confidence intervals of "short-term" stability failure rate with and without OG and operability vs. GM at draught 6.9 m for cruise vessel

1.1.11 Examples of operational limitations related to areas or routes and season concern the same loading conditions for sample operational routes and seasons from table 2.2.1, chapter 2 of appendix 5. Table 1.1.1 shows the upper boundary $\bar{r}_U$ of the 95%-confidence interval of average "long-term" stability failure rate for unrestricted operation (area 1) and specific routes and seasons (areas 2 to 6); red colour indicates unacceptable loading conditions. The stability failure rate generally decreases for considered sample routes and seasons compared to unrestricted service but the reduction is insufficient to render the loading conditions that are unacceptable for unrestricted operation acceptable for considered specific routes and seasons.

Table 1.1.1. "Long-term" weighted average $\bar{r}_U$ of upper boundaries of 95%-confidence intervals of "short-term" stability failure rate for areas or routes and seasons specified in table 2.2.1, chapter 2 of appendix 5

LC	Areas or routes and seasons					
	1	2	3	4	5	6
01	2.214e-6	1.549e-6	5.125e-7	6.940e-7	5.154e-7	4.243e-7
02	5.706e-8	1.114e-7	4.859e-8	6.461e-8	4.800e-8	2.702e-8
03	4.587e-9	1.025e-8	4.066e-9	5.798e-9	4.051e-9	1.911e-9
04	7.582e-10	1.781e-9	5.266e-10	8.253e-10	5.456e-10	2.592e-10
05	3.911e-10	1.085e-9	3.276e-10	5.103e-10	3.388e-10	1.611e-10

1.1.12 Operational limitations related to maximum significant wave height were developed for loading conditions LC01, LC02 and LC03 for the North Atlantic wave scatter table, limited by a systematically varied maximum significant wave height with a step 1.0 m. Figure 1.1.9 shows the "long-term" weighted average $\bar{r}_U$ of the upper boundaries of the 95%-confidence intervals of the "short-term" stability failure rate and operability vs. maximum significant wave height. Table 1.1.2 shows the significant wave height at which $\bar{r}_U$ is equal to the standard 2.6·10^{-8} 1/s, together with operability corresponding to this wave height. Note that since operability exceeds 0.8, operational limitations related to maximum significant wave height is an acceptable option for all considered loading conditions, and that in the same wave climate, a probabilistic operational guidance allows achieving significantly greater operability than operational limitations related to maximum significant wave height, i.e. operational limitations related to maximum significant wave height are less efficient than operational guidance.

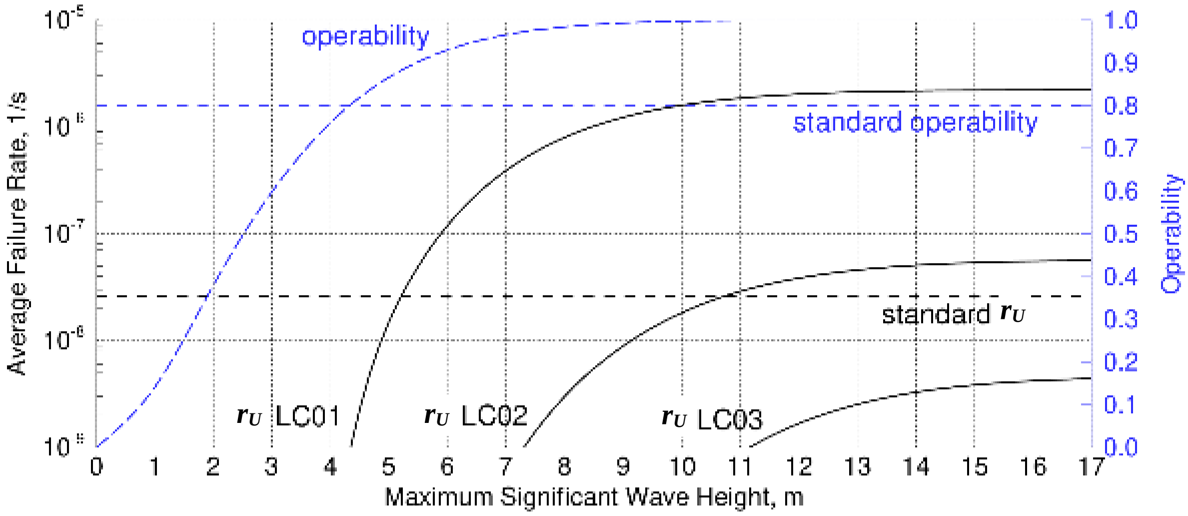

Figure 1.1.9. "Long-term" weighted average $\bar{r}_U$ of upper boundaries of 95%- confidence intervals of "short-term" stability failure rate (left *y*-axis, black solid line) and operability (right *y*-axis, blue dashed line) vs. maximum significant wave height (*x*-axis) in North Atlantic wave climate for cruise vessel

Table 1.1.2. Maximum significant wave height at which "long-term" weighted average $\bar{r}_U$ of upper boundaries of 95%-confidence intervals of "short-term" stability failure rate does not exceed standard 2.6·10^{-8} 1/s and corresponding operability in North Atlantic wave climate for cruise vessel

Loading condition	LC01	LC02	LC03
GM, m	1.5	2.0	2.5
Maximum significant wave height, m	5.266	10.763	unlimited
Corresponding operability	0.883	0.999	1.000

1.2 1700 TEU container ship

1.2.1 This example concerns a container ship with the length between perpendiculars 159.6 m and waterline breadth 28.1 m.

1.2.2 Figure 1.2.1 shows minimum *GM* values vs. draught according to the criteria from part A of the 2008 IS Code and damage stability requirements in SOLAS (as amended by resolution MSC.216(82)).

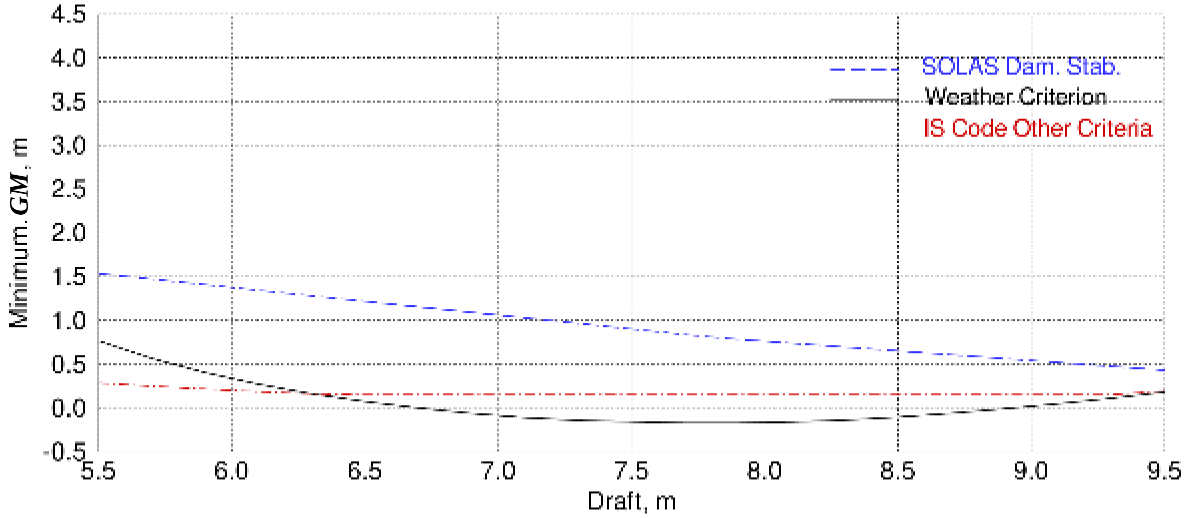

Figure 1.2.1. Minimum *GM* curves according to the 2008 IS Code part A criteria and SOLAS damage stability requirements for a 1700 TEU container ship

1.2.3 Figure 1.2.2 shows results of vulnerability assessment for parametric roll stability failure mode. Since it is sufficient to satisfy one of these three assessment options, they do not impose additional limitations on the minimum *GM* value compared to the criteria from part A of the 2008 IS Code and SOLAS damage stability requirements. Figure 1.2.3 shows assessment results with respect to vulnerability criteria for pure loss of stability failure mode. Assessment with respect to level 1 criterion for surf-riding/broaching indicates that since the operational Froude number of the vessel is less than 0.3, the vessel is not vulnerable to this stability failure mode in any of the considered loading conditions, therefore level 2 assessment was not performed. The assessment with respect to vulnerability criteria for dead ship condition, figure 1.2.4, shows that the ship is not vulnerable to this stability failure mode in all considered combinations of draught and *GM*.

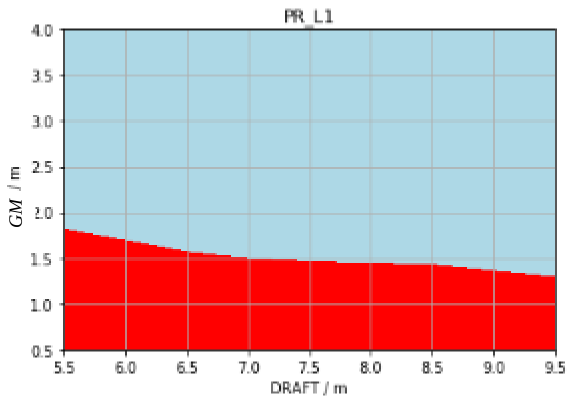

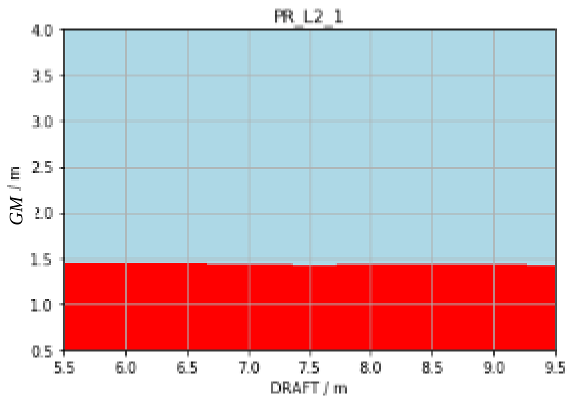

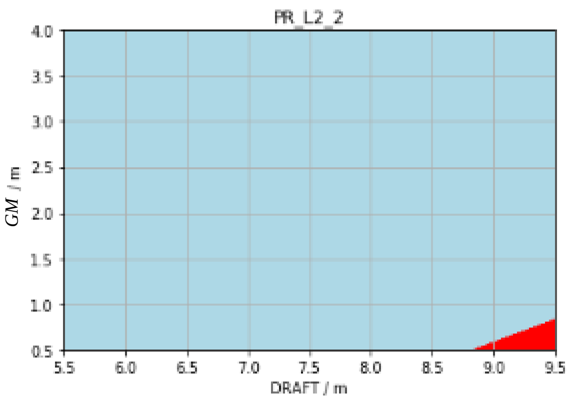

Figure 1.2.2 Results of level 1 (top left), level 2 check 1 (top right) and level 2 check 2 (bottom left) vulnerability assessment for parametric roll stability failure mode for 1700 TEU container ship

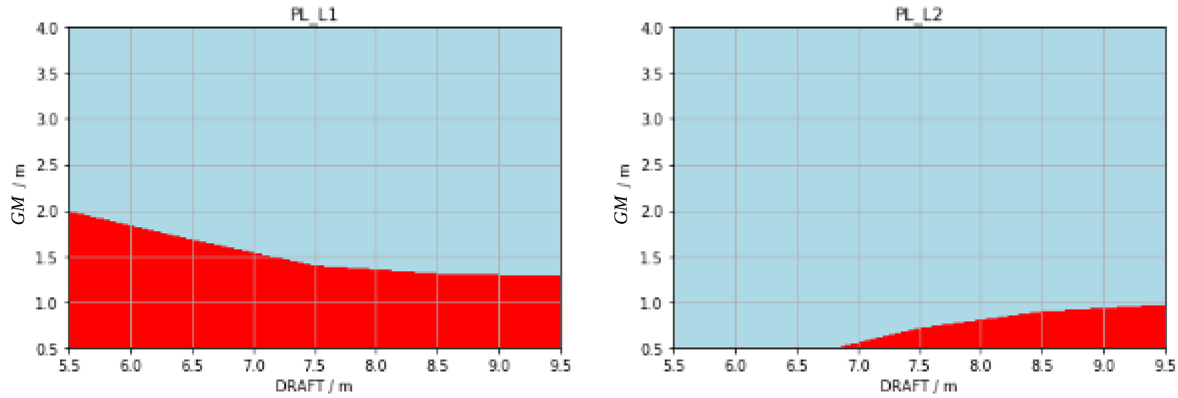

Figure 1.2.3. Results of assessment with respect to level 1 (left) and level 2 (right) vulnerability criteria for pure loss of stability failure mode for 1700 TEU container ship

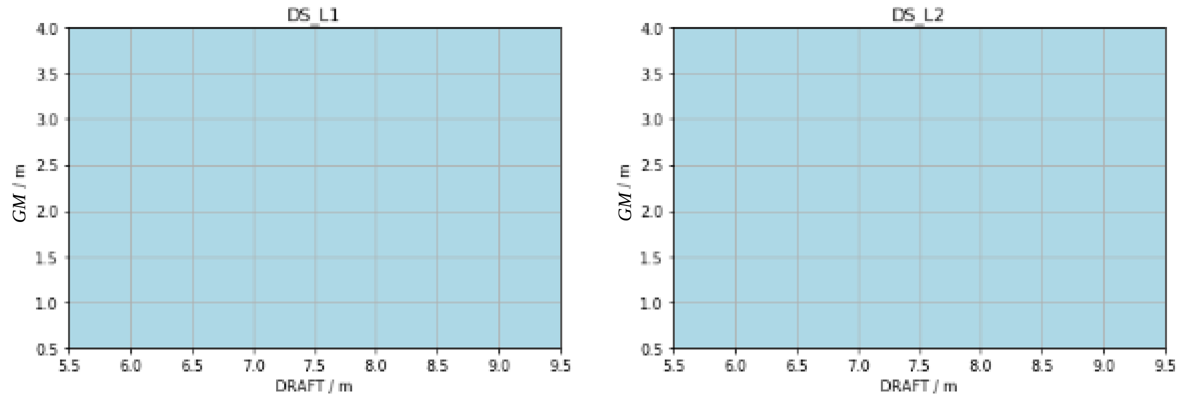

Figure 1.2.4 Results of application of level 1 (left) and level 2 (right) vulnerability criteria for dead ship condition stability failure mode for 1700 TEU container ship

1.2.4 Application of vulnerability criteria for excessive acceleration stability failure mode leads to recommendations on the upper limit of *GM*, shown in figure 1.2.5. Level 1 leads to a very restrictive maximum *GM* limit, which is slightly lifted by applying level 2 assessment. Note that the *GM* values associated with results of excessive acceleration criteria represent metacentric heights without correction for free surface.

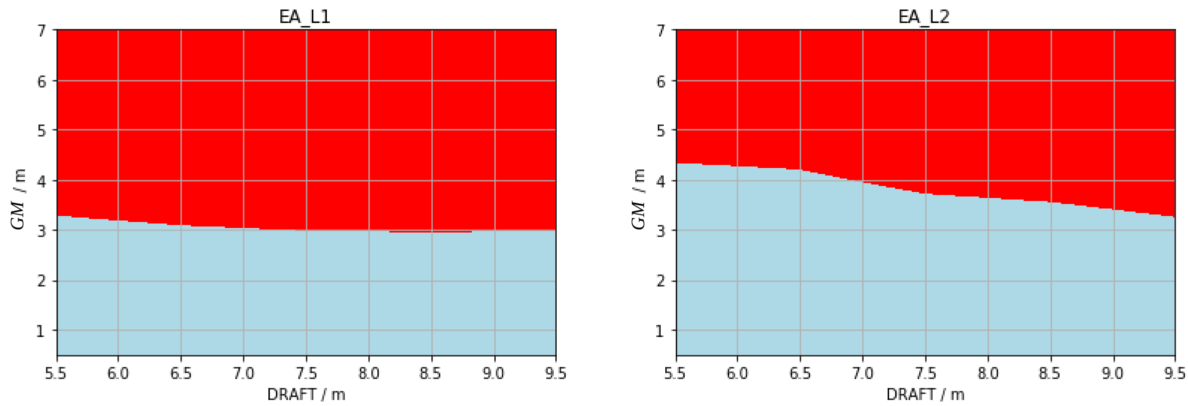

Figure 1.2.5. Results of level 1 and level 2 assessment for excessive acceleration stability failure mode for 1700 TEU container ship

1.2.5 The vulnerability assessment according to the second-generation intact stability criteria indicates for this ship additional limitations compared to the present requirements of part A of the 2008 IS Code and damage stability requirements of SOLAS on minimum acceptable GM values, as well as requirements on maximum acceptable GM values, figure 1.2.6. For draughts greater than 7.9 m, level 2 of pure loss of stability vulnerability assessment suggests increasing the minimum GM values compared to the damage stability requirements, whereas the maximum GM values are suggested to be limited by the vulnerability assessment for excessive acceleration stability failure mode. It is important to note that the GM values associated with results of excessive acceleration criteria represent metacentric heights without correction for free surface.

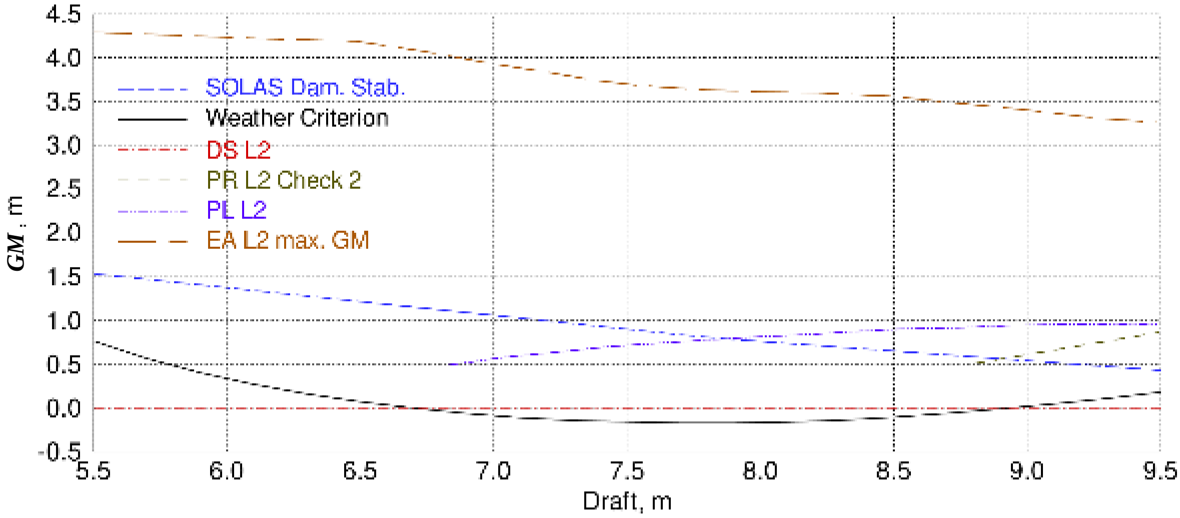

Figure 1.2.6. *GM* limits according to the 2008 IS Code part A, SOLAS damage stability requirements and vulnerability assessment of second-generation intact stability criteria (including maximum *GM* from excessive accelerations criterion) for 1700 TEU containership

1.2.6 For comparison, full probabilistic direct stability assessment was applied for three loading conditions with GM=0.5, 1.2 and 1.9 m at a typical loaded draught 9.5 m, table 4.1.1 of chapter 4 of appendix 4. Table 4.2.2 of chapter 4 of appendix 4 shows the resulting "long-term" weighted average $\bar{r}_U$ of the upper boundaries of the 95%-confidence intervals of the "short-term" stability failure rate, which is plotted in figure 1.2.7. The standard $2.6{\cdot}10^{-8}$ 1/s for $\bar{r}_U$ is satisfied for GM values greater than 1.788 m, which is larger than the required minimum GM values from the Weather Criterion and damage stability requirements. The direct stability assessment indicates the need to use a GM value higher than the one resulting from the level 2 vulnerability assessment for parametric roll stability failure mode for the considered ship and draught. Since the stability failure rate at small GM values is dominated by the parametric roll stability failure mode, operational measures may be utilized in such loading conditions (see the examples below).

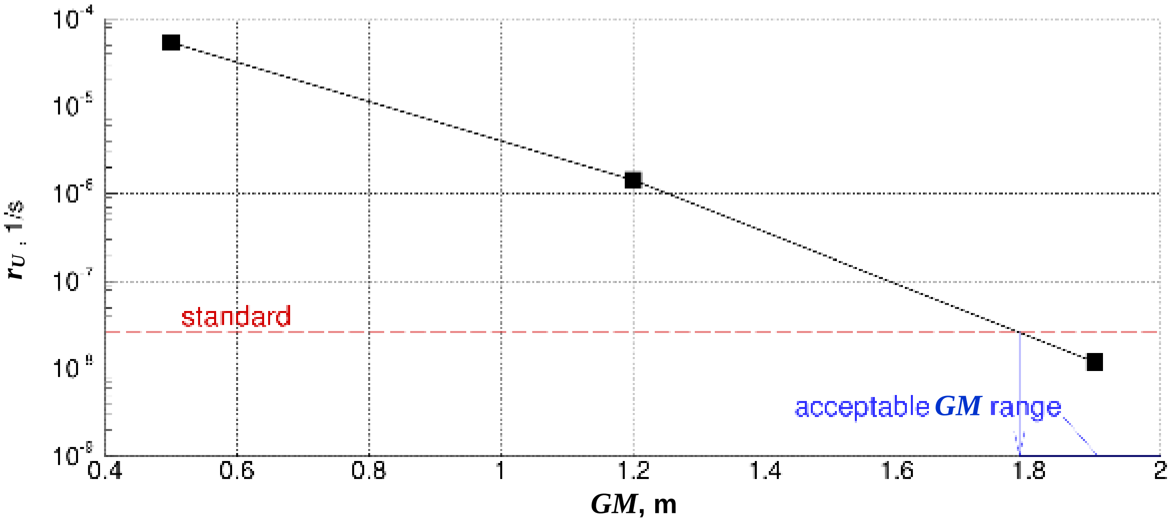

Figure 1.2.7. Computed conservative estimate of upper boundary $\bar{r}_U$ of 95%-confidence interval of average "long-term" stability failure rate vs. *GM* at draught 9.5 m for a 1700 TEU container ship compared with acceptance standard 2.6·10^{-8} 1/s and resulting acceptable *GM* range

1.2.7 Operational guidance was developed for loading conditions with draught 9.5 m and GM values 0.5, 1.2 and 1.9 m by identifying *unacceptable sailing conditions* (v_0, μ), i.e. those for which the upper boundary of 95%-confidence interval of "short-term" stability failure rate exceeds acceptance standard 10^{-6} s^{-1}, for each sea state (H_s, T_z) in the North Atlantic wave scatter table. Figure 1.2.8 shows the resulting computed "long-term" weighted average $\bar{r}_U$ of the upper boundaries of the 95%-confidence intervals of the "short-term" stability failure rate with and without operational guidance, together with the operability resulting from the use of operational guidance, depending on GM. Since operability exceeds 0.8 for all considered loading conditions, operational guidance is an acceptable option for all of them; note that the upper boundary $\bar{r}_U$ of the 95%-confidence interval of the average "long-term" stability failure rate reduces, due to the use of operational guidance, below the standard of the full probabilistic assessment 2.6·10^{-8} 1/s for all considered loading conditions.

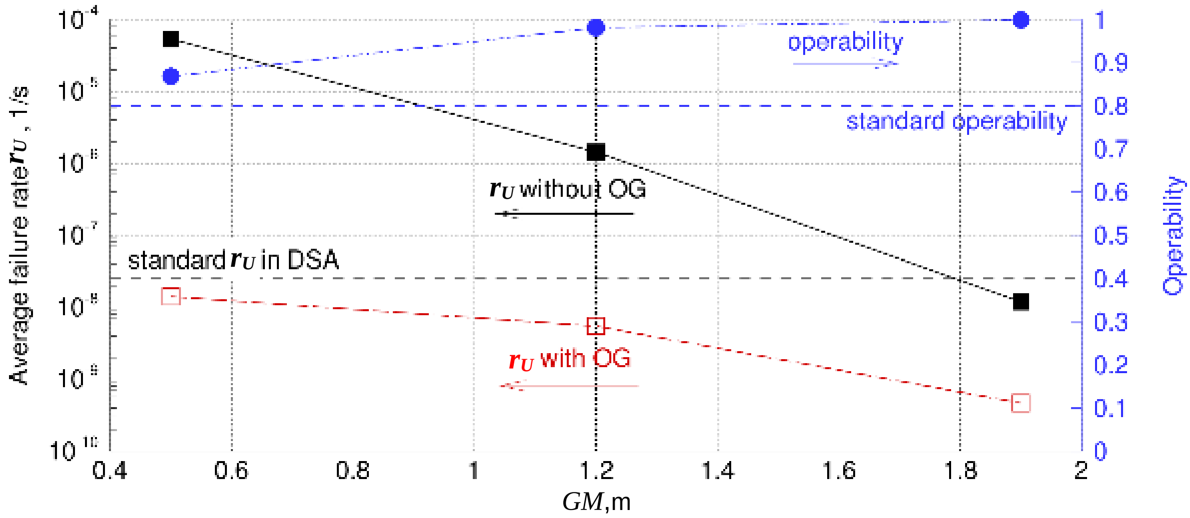

Figure 1.2.8. Computed "long-term" weighted average of upper boundaries of 95%-confidence interval of "short-term" stability failure rate (with and without operational guidance) and operability vs. *GM* at draught 9.5 m for 1700 TEU container ship

1.2.8 Examples of operational limitations related to areas or routes and season concern the same three loading conditions for the sample operational routes and seasons in table 2.2.1, chapter 2 of appendix 5. Table 1.2.1 shows the computed "long-term" weighted average $\bar{r}_U$ of the upper boundaries of the 95%-confidence intervals of the "short-term" stability failure rate for unrestricted operation (area 1) and specific routes and seasons (areas 2 to 6); the red colour indicates unacceptable loading conditions. Although the stability failure rate decreases compared to unrestricted service, this reduction is insufficient to render loading conditions LC01 and LC02 acceptable.

Table 1.2.1. "Long-term" weighted average $\bar{r}_U$ of upper boundaries of 95%-confidence intervals of "short-term" stability failure rate for 1700 TEU container ship; areas or routes and seasons per table 2.2.1, chapter 2 of appendix 5

LC	*GM*, m	Areas or routes and seasons					
		1	2	3	4	5	6
01	0.5	5.362e-5	2.881e-5	1.117e-5	1.323e-5	1.118e-5	1.068e-5
02	1.2	1.432e-6	1.950e-6	1.076e-6	1.226e-6	1.058e-6	7.199e-7
03	1.9	1.198e-8	5.334e-8	3.686e-8	4.588e-8	3.567e-8	1.555e-8

1.2.9 Operational limitations related to maximum significant wave height were developed for the same three loading conditions for the North Atlantic wave scatter table, limited by a systematically varied maximum significant wave height with a step 1.0 m. Figure 1.2.9 shows the resulting computed "long-term" weighted average $\bar{r}_U$ of the upper boundaries of the 95%-confidence intervals of the "short-term" stability failure rate and operability depending on the maximum significant wave height, and table 1.2.2 shows the significant wave height which corresponds to $\bar{r}_U$ matching the required standard $2.6 \cdot 10^{-8}$ 1/s, together with the operability corresponding to this wave height. Note that due to the use of the operational limitations related to maximum significant wave height, loading condition LC02 becomes acceptable (whereas loading condition LC01 remains unacceptable), whereas using operational guidance renders both loading conditions LC01 and LC02 acceptable, and that in the same wave climate, probabilistic operational guidance provides significantly greater operability than operational limitations related to maximum significant wave height, i.e. the latter are less efficient than operational guidance.

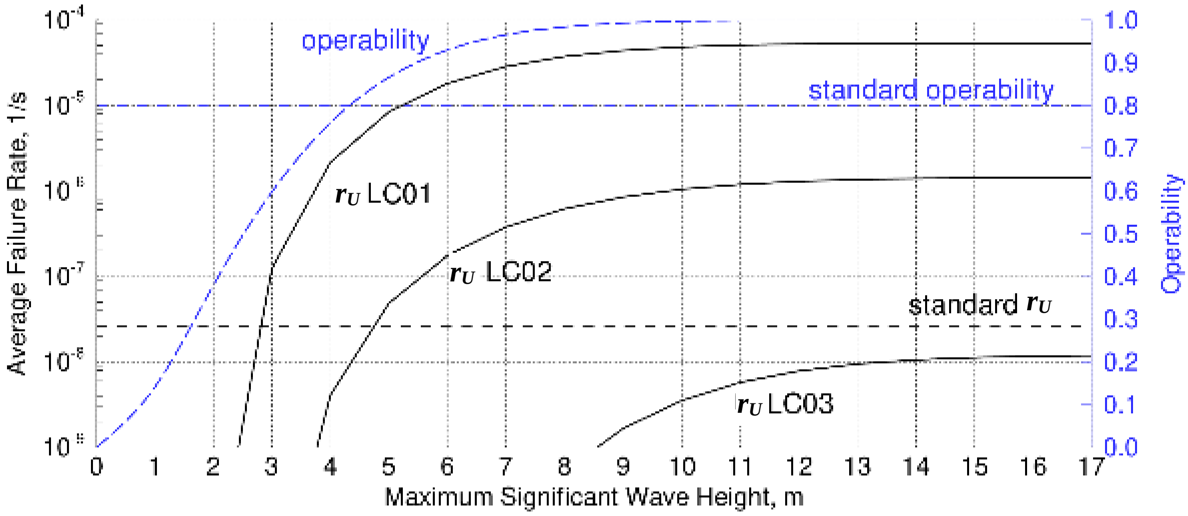

Figure 1.2.9. Computed "long-term" weighted average $\bar{r}_U$ of upper boundaries of 95%-confidence intervals of "short-term" stability failure rate (left *y*-axis, black solid line) and operability (right *y*-axis, blue dashed line) vs. maximum significant wave height (*x*-axis) in North Atlantic wave climate for 1700 TEU container ship

Table 1.2.2. Maximum significant wave height at which "long-term" weighted average $\bar{r}_U$ of upper boundaries of 95%-confidence intervals of "short-term" stability failure

rate satisfies acceptance standard 2.6·10^{-8} 1/s and corresponding operability in North Atlantic wave climate

Loading condition	01	02	03
Metacentric height, m	0.5	1.2	1.9
Maximum significant wave height, m	2.814	4.746	unlimited
Corresponding operability	0.557	0.839	1.0